Time-Dependent Radiation Transport Using the Staggered-Block Jacobi Method

by

Gregory Grant Davidson

A dissertation submitted in partial fulfillment
of the requirements for the degree of
Doctor of Philosophy
(Nuclear Engineering and Radiological Sciences and Scientific Computing)
in The University of Michigan
2010

Doctoral Committee:

Professor Edward W. Larsen, Chair
Professor William R. Martin
Professor James P. Holloway
Professor Bram Van Leer

To my parents, Steve and Judy Davidson

Acknowledgments

I would like to thank my advisor, Ed Larsen, for his guidance and patience throughout my time here at the University of Michigan, and especially in the course of this research. I would also like to thank the members of my committee, Bill Martin, James Holloway, and Bram van Leer for their assistance. I have also received technical assistance, as well as friendship, from many of my fellow graduate students. Space does not permit me to name everyone, but Troy Becker, Jesse Cheatham, and Seth Johnson were particularly influential.

I would also like to express my gratitude for the funding I received. This research was funded by the Department of Energy Computational Science Graduate Fellowship, the Continuum Dynamics (CCS-2) group at Los Alamos National Laboratory, and the Center for Radiation Shock Hydrodynamics (CRASH).

Finally, I would like thank my parents, Steve and Judy Davidson, for their continual love and support.

Table of Contents

List of Tables

Table

List of Figures

List of Appendices

Appendix

Abstract

The time-dependent radiation transport equation describes the dynamics of radiation traveling through and interacting with a background medium. These dynamics are important in a diversity of fields including nuclear reactor kinetics, stellar evolution, and inertial confinement fusion. Except for trivial problems, the transport equation must be solved numerically. This research is concerned with developing a new deterministic time discretization for numerical solutions of the radiation transport equation.

To preserve maximal parallelism, a deterministic transport method must maintain *locality*, meaning that the solution at a point in space is dependent only upon information that is locally available. Furthermore, computational efficiency requires that a method be *unconditionally stable*, meaning that it provides positive, physically permissible solutions for time steps of any length.

Existing unconditionally stable radiation transport methods require mesh sweeps, which make the methods non-local and inhibit their parallelism, thereby reducing their efficiency on large supercomputers. We present a new Staggered-Block Jacobi (SBJ) method, which produces unconditionally stable numerical solutions while maintaining locality.

The SBJ time discretization operates by forming *blocks* of cells. In one dimension, a block is composed of two cells. The incident information into the block is evaluated at the beginning of the time step. This decouples every block, and allows the solution in the blocks to be computed in parallel.

We apply the SBJ method to the linear diffusion and transport equations, as well as the linearized thermal radiation transport equations. We find that the SBJ time discretization, applied to the linear diffusion and transport equations, produces methods that are accurate and efficient when the particle wave advances about 20% of a cell per time step, i.e., where the time steps are small or the problem is optically thick. In the case of the thermal radiation transport equations, we find that the SBJ method is accurate and efficient whenever a time step length is chosen such that the error resulting from the linearization is small. The SBJ method should be more efficient than sweep-based methods for many problems of interest on massively parallel computers.

Chapter 1

Introduction

This dissertation is concerned with the development of a new computational radiation transport method called the Staggered-Block Jacobi method. Radiation transport considers the interaction of sub-atomic particles as they stream through and iteract with a background media. This process is described by the radiation transport equation, which can take a variety of forms depending upon the specifics of the problem in question. In this dissertation, we shall limit our investigation to the transport of electrically neutral particles, and we assume that the problems under consideration can be adequately described with one spatial dimension and no energy dependence. We make no assumptions, besides electrical neutrality, about what sort of particles are being transported until we get to Chapters 6 and 7, where we assume the radiation is photons. The computational issues in question are independent of the particles themselves. Typically, neutral particle radiation transport is concerned with neutrons, photons, and neutrinos. Neutron transport is particularly relevant to the field of nuclear engineering, and is important for nuclear reactor design and analysis, radiation shielding, nuclear criticality safety, and other topics. Photon transport is of interest in a variety of fields including medical imaging, stellar evolution, and inertial confinement fusion. Neutrino transport is used in the simulation of supernovae. All of these phenomena are described by one form or another of the radiation transport equation, which is itself a form of the more general Boltzmann transport equation [9], originally developed to describe the molecular dynamics of ideal gases. In the case of radiation transport, the equation has been adapted to describe the dynamics of subatomic particles.

In the radiation transport equations under consideration in this dissertation, many higher-order effects are ignored. The particle field is assumed to be sufficiently rarefied that particle-particle interactions may be neglected. Additionally, particle decay and the effects of gravity are considered negligible. The result is a seven-dimensional partial integro-differential equation. The mathematical complexity of the radiation transport equation

means that closed-form solutions may be found only for simplified problems. In general, the equation must be solved using numerical methods. Traditionally, the numerical techniques used to solve the radiation transport equation have fallen into two categories: *deterministic* methods, wherein the transport equation is discretized into a large set of algebraic equations which may then be solved using common numerical algebra routines, or *Monte Carlo*, in which the physics of the transport process itself is simulated using "virtual" particles on a computer. There are advantages and disadvantages to each approach. Deterministic methods tend to be less computationally expensive, but suffer from mathematical truncation errors and modeling errors, and, as we will discuss below, can have limited parallelism. Monte Carlo methods can be very computationally expensive and suffer from statistical errors, but are trivial to parallelize. Monte Carlo methods are generally most effective in source-detector problems, where the solution is not required everywhere in the problem domain, but only in a small region (the detector). In this case, variance reduction techniques are available that allow the Monte Carlo simulation to produce solutions with smaller statistical errors with fewer particles. However, in problems where the solution must be calculated everywhere (such as in nuclear reactor analysis or inertial confinement fusion problems), variance reduction techniques are much more limited. Recently, work has been done to create hybrid Monte Carlo-deterministic methods, where a coarse deterministic solution is used to reduce the variance of the Monte Carlo problem [36]. It is likely that efficient deterministic methods will continue to be necessary in the future.

Deterministic methods of the first-order form of the transport equation can themselves be broken into two major types, depending on how they discretize the angular variable. P_N methods discretize the angular variable by expanding it into a series of spherical harmonics moments. S_N methods discretize the angular variable using a quadrature rule. Both methods have advantages and disadvantages. The principle disadvantage of P_N methods is that they admit negative solutions (although work is ongoing in eliminating this defect [29]), while S_N methods can have "ray effects," or non-physical striations in the solution along the angular directions in the quadrature set [23]. Because negative particle densities, besides being unphysical, can break many advanced synthetic acceleration iterative methods needed to converge the scattering term, and can cause dramatic, catastrophic errors in thermal radiation transport problems, S_N has been the preferred angular discretization method, and is the angular discretization that we consider in this dissertation.

In practice, deterministic and Monte Carlo methods have proven to be too computationally expensive for many problems of interest. For these problems, the transport equation is often approximated by a diffusion equation. The diffusion approximation assumes a linearly anisotropic solution, and is accurate when the mean-free path and mean-free time of the

particle are short and the collisions are dominated by scattering. The diffusion equation is much easier to solve than the transport equation, and has become the primary workhorse of reactor physics and astrophysics codes. The motivation of this dissertation is to produce a deterministic transport method that is sufficiently efficient that it can replace diffusion codes for time dependent calculations.

1.1 Motivation of Research

In this research, we are primarily concerned with finding an accurate and efficient time discretization for the radiation transport equation with an S_N angular discretization. How the S_N equations are solved in practice is dependent, in part, on the time discretization used. Traditional time discretizations of differential equations come in three major types: implicit, fully-explicit, and Crank-Nicolson [25]. Consider the following partial differential equation

$$\frac{\partial}{\partial t}f(x,t)+\frac{\partial}{\partial x}f(x,t)+Af(x,t)=S\,, \tag{1.1}$$

where x is a spatial variable, t is the time variable, and $f(x,t)$ is the solution we seek. The quantities A and S may be considered, for simplicity, independent of space and time. Eq. (1.1) must also have an accompanying initial condition and boundary conditions, which we omit for simplicity. The first step in time discretizing Eq. (1.1) is to average it over an interval of time called a time step. If we assume a time step bounded by times t_k and t_{k+1}, and average Eq. (1.1) over the time step, we obtain

$$\frac{1}{\Delta t_{k+1}}\Big[f(x,t_{k+1})-f(x,t_k)\Big]+\frac{\mathrm{d}}{\mathrm{d}x}\bar{f}(x)+A\bar{f}(x)=S\,, \tag{1.2}$$

where $\Delta t_{k+1}=t_{k+1}-t_k$ is the length of the time step and $\bar{f}$(x) is the average of $f(x,t)$ over the time step.

Examining Eq. (1.2), we see that we have two unknowns, $f(x,t_{k+1})$ and $\bar{f}(x)$. The solution at the beginning of the time step, $f(x,t_k)$, is assumed to be known since it either came from an initial condition, or from a calculation at the previous time step. The second step in a time discretization is to assume a closure relationship that will eliminate $\bar{f}$(x). Different time discretizations use different closures. The fully-explicit time discretization assumes that the solution average over the time step is equal to the solution evaluated at the beginning of the time step, i.e.,

$$\bar{f}(x)=f(x,t_k)\,. \tag{1.3}$$

With this closure, we may write Eq. (1.2) as

$$f(x,t_{k+1}) = \left(1 - \Delta t_{k+1}\frac{\mathrm{d}}{\mathrm{d}x} - \Delta t_{k+1}A\right) f(x,t_k) + S. \tag{1.4}$$

Examining Eq. (1.4), we see that the solution at time t_{k+1} is only dependent upon $f(x,t_k)$, which is known. Therefore, $f(x,t_{k+1})$ may be calculated everywhere in the spatial domain simultaneously, i.e., the fully-explicit method yields solutions that are trivially parallel. Unfortunately, the fully-explicit method is known to be numerically unstable (i.e., it produces non-physical oscillations) for large time steps.

The implicit time discretization assumes that the solution average over the time step is equal to the solution evaluated at the end of the time step

$$\bar{f}(x) = f(x,t_{k+1}). \tag{1.5}$$

With this closure, Eq. (1.2) becomes

$$\left(\frac{1}{\Delta t_{k+1}} + \frac{\mathrm{d}}{\mathrm{d}x} + A\right) f(x,t_{k+1}) = \frac{1}{\Delta t_{k+1}} f(x,t_k) + S. \tag{1.6}$$

Eq. (1.6) is unconditionally stable. However, it is more difficult to solve than Eq. (1.4). The spatial derivative on the left side of Eq. (1.6) means that the solution at one point in space is dependent upon the solution at other points in space. In other words, the solution at time t_{k+1} is spatially coupled. In the context of implicit diffusion discretizations, this means that solving the diffusion equation requires finding the solution to a large, sparse system of equations. In the context of implicit S_N transport discretizations, this means that finding the solution requires mesh sweeps, and the scattering source must be iterated to convergence. Both mesh sweeps and sparse linear solvers inhibit the parallelism of the method. We describe mesh sweeps later in this chapter, and we discuss both mesh sweeps and iterations in detail in Chapter 3.

Finally, the Crank-Nicolson method assumes the closure

$$\bar{f}(x) = \frac{1}{2}\Big[f(x,t_{k+1}) + f(x,t_k)\Big]. \tag{1.7}$$

With this closure, Eq. (1.2) becomes

$$\left(\frac{1}{\Delta t_{k+1}} + \frac{1}{2}\frac{\partial}{\partial x} + \frac{A}{2}\right) f(x,t_{k+1}) = \left(\frac{1}{\Delta t_{k+1}} - \frac{1}{2}\frac{\partial}{\partial x} - \frac{A}{2}\right) f(x,t_k) + S. \tag{1.8}$$

Eq. (1.8) is oscillatory for large time steps, and is as difficult to solve as Eq. (1.6), meaning

that mesh sweeps are required in the context of the Crank-Nicolson discretized S_N equations. The advantage of the Crank-Nicolson method is that it is second-order accurate.

In practice, most time-dependent radiation transport codes use some version of the implicit, fully-explicit, or Crank-Nicolson time discretizations. The following is a sample of time-dependent S_N radiation transport codes and the time discretizations they use.

TIMEX

TIMEX is an older code developed at Los Alamos National Laboratory [17]. It uses an implicit time discretization, except that the in-group scattering and upscattering terms are treated explicitly. The group angular fluxes are then solved, starting with the highest energy group and proceeding to the thermal groups. Since the in-group scattering and upscattering terms are evaluated at the beginning of the time step, this method does not require source iteration, but does require mesh sweeps. Treating the in-group scattering and upscattering terms explicitly could be inaccurate for large time steps.

PARTISN

PARTISN is a major workhorse of the nuclear engineering community developed at Los Alamos National Laboratory [5]. It performs an implicit calculation for the first half of the time step, thus calculating a solution at the time step midpoint, using sweeps and iterations. After calculating the midpoint solution, it then extrapolates to the end of the time step using a Crank-Nicolson closure. PARTISN uses a negative flux fix-up scheme to prevent negative solutions, thereby mitigating oscillations caused by the extrapolation, but the implicit step requires mesh sweeps and iterations.

TDTORT

TDTORT is designed for reactor analysis [8], and uses the Improved Quasi-Static (IQS) method [14]. This method assumes that the angular flux in the reactor may be separated into a slowly-varying "shape" function $\psi(\mathbf{r},E,\Omega,t)$ and a quickly varying amplitude function $T(t)$, such that

$$\phi(\mathbf{r},E,\Omega,t) = T(t)\psi(\mathbf{r},E,\Omega,t)\,, \tag{1.9}$$

where $\mathbf{r}$ is the spatial position, E is the neutron energy, and Ω is the particle direction. The amplitude $T(t)$ is calculated using the point-kinetics equations, while $\psi(\mathbf{r},E,\Omega,t)$ is calculated using an implicit time discretization. The advantage of this approach is that larger time steps may be taken, provided the shape of the solution does not change rapidly in time. The disadvantage is that this method is nonlinear, requiring a nonlinear solver, and is limited to nuclear reactor analysis.

Other time dependent transport codes are SERANO, a thermal radiation transport code

under development at Los Alamos National Laboratory, which uses an implicit time discretization [35], AMTRAN, a linear transport code under development at Lawrence Livermore National Laboratory, which uses a Crank-Nicolson time discretization [7], and TETON, a thermal radiation transport code, also at Lawrence Livermore National Laboratory, which uses an implicit time discretization [7].

Implicit radiation transport methods operate using mesh sweeps, in which the transport operated is inverted for each mesh cell in each angle in the discrete ordinates set. For each angle, the cells must be considered in a particular order, called the sweep ordering. Because the cells must be solved in a particular order, the parallelism of sweep-based methods is limited. Sweeps will be described in detail in Chapter 3.

There have been efforts to find highly parallel sweep algorithms. One method is the KBA method [20], which is limited to rectangular grids. Other algorithms have been developed for unstructured grids [30]. However, these algorithms are generally designed for a modest number of processors. Ref. [30] considers up to 128 processors. In Ref. [6], Azmy found that the fraction of run time for a parallel S_N code consumed by network communication is significant only for small problems on small computers. On larger systems, the bottleneck is the algorithm itself, not the communication time. Azmy states that "...further advances in parallel performance requires exploring alternative solution algorithms beyond the mesh sweep algorithm that is perfectly suited for sequential architectures."

The inefficiencies inherent in the mesh sweep algorithm are likely to become more severe in the future, as the focus of new innovations in computer architecture continues to shift. Previously, computer processor manufacturers have focused on increasing the speed of the individual chips. However, as the processors have become smaller and faster, it has become increasingly difficult to continue to increase the performing power. As a result, the focus has moved to combining multiple "cores" (processing units) onto a single chip. Two and four core processors are now the norm on desktop computers. In the past, a typical computing cluster might be composed of hundreds or a few thousand processors. Today, large-scale computing is done on machines with hundreds of thousands of processors. The *IBM Roadrunner*, at Los Alamos National Laboratory, was the fastest computer in the world as of November 2008, with a total of 130,464 total cores [19]. As of the writing of this dissertation, the fastest computer in the world is *Jaguar* at Oak Ridge National Laboratory, with a total of 224,256 cores and a peak performance of 2.3 petaflops [34]. The *IBM Sequoia*, which is expected to come online at Livermore National Laboratory in 2011 will have 1.6 million cores [18].

At the SC09 conference, it was predicted that if advances in computers continue at the present rate, supercomputers a decade from now will be capable of exaflop performance and

have hundreds of millions of cores [32]. For this reason, it is increasingly important that transport methods scale well with the number of processors.

1.2 Proposed Work

The central research question for this dissertation is whether it is possible to find an unconditionally stable S_N radiation transport solver that does not require sweeps and satisfies the thick diffusion limit [1]. A transport problem is considered thick and diffusive when particles have short mean-free times and mean-free paths, and when collisions are dominated by scattering. As the subsequent chapters will demonstrate, the Staggered-Block Jacobi does satisfy these requirements. To our knowledge, this radiation transport solver is the only known solver that does not treat the transport operator implicitly, but still satisfies unconditional stability and produces non-oscillatory solutions. Because this method is a Jacobian method, it is trivial to parallelize, and should scale well with the number of processors. Additionally, unlike implicit S_N methods, it does not require acceleration techniques to efficiently solve the transport equations in the diffusion limit.

1.3 Thesis Synopsis

The following chapters in this dissertation are arranged as follows:

Chapter 2: Staggered-Block Jacobi Diffusion
This investigation of time discretizations begins with a study of the one-dimensional, monoenergetic diffusion equation. Because the diffusion equation has a simpler form than the transport equation, it provides a convenient starting point for examining the behavior of different time discretizations. We examine four time discretizations: fully-explicit, implicit, a possibly new semi-explicit discretization, and the SBJ diffusion discretization. A stability analysis of each of these methods shows that only the implicit and SBJ diffusion methods are unconditionally stable, and only the SBJ diffusion method also has trivial parallelism. We demonstrate the performance of these methods with numerical results.

Chapter 3: Derivation of the Staggered-Block Jacobi Transport Equations
To begin the investigation of the SBJ method applied to the linear transport equation, we derive implicit, fully-explicit, semi-explicit, and SBJ time discretizations with a linear discontinuous finite element spatial discretization of the S_N equations. We discuss the solution methodology of each of these methods. Additionally, we derive a global rebalance factor

for restoring global particle balance to the SBJ solution, and we discuss combining the SBJ transport method with stretched sweeps for improving the efficiency of the method in optically-thin regions.

Chapter 4: Asymptotic Analysis

In Chapter 4, we conduct an asymptotic analysis on the implicit, fully-explicit, semi-explicit and SBJ transport methods derived in Chapter 3. This analysis demonstrates that the implicit, fully-explicit, and SBJ transport methods limit to their diffusion analogs derived in Chapter 2, thereby allowing us to extrapolate the stability analysis made in Chapter 2 to the transport discretizations derived in Chapter 3. The semi-explicit transport method does not limit to the semi-explicit diffusion method, but rather to a discretization even less stable than the fully-explicit method.

Chapter 5: Linear Transport: Numerical Results

In this chapter, we demonstrate the numerical behavior of the implicit and SBJ transport methods derived in Chapter 3 and analyzed in Chapter 4. These results show that the SBJ transport method is accurate and efficient in optically-thick problems, or for small time steps, but is less accurate and efficient for large time steps or problems with optically-thin cells.

Chapter 6: Derivation of the Thermal Radiation Staggered-Block Jacobi Transport Equations

In Chapter 6, we consider the SBJ method applied to the IMC linearized thermal radiation transport equations. Therefore, we derive both the implicit and SBJ methods for the thermal radiation transport problem. We use an Implicit Monte Carlo (IMC) linearization on the grey equations, and then we proceed to use a similar angular and spatial discretization for the implicit and SBJ transport methods as was used for the linear problem in Chapter 3.

Chapter 7: Thermal Radiation Transport: Numerical Results

In Chapter 7, we show numerical results illustrating the implicit and SBJ IMC transport methods. These show that if a time step length is chosen such that the IMC linearization produces small errors, then the SBJ method is accurate and efficient.

Chapter 8: Conclusions and Future Work

Finally, in Chapter 8 we summarize the results from the previous chapters. We also propose future work for investigating the SBJ transport method, including implementing the SBJ method in higher spatial dimensions and multiple energy groups, and accelerating the SBJ transport method.

Chapter 2

Staggered-Block Jacobi Diffusion

To begin our study of the Staggered-Block Jacobi (SBJ) method, we first investigate an SBJ discretization of the diffusion equation. The diffusion equation is an approximation to the transport equation that is valid when the angular flux is approximately linearly anisotropic, the mean-free path and mean-free time of the particle are short, and the collision process is dominated by scattering. The diffusion equation has no angular dependence and is much easier to solve than the transport equation. Therefore, diffusion is often substituted for transport when the diffusion approximation is considered justified, or when the transport equation is simply too computationally expensive to apply to the problem of interest. Common examples of transport problems that are solved using the diffusion equation are full-core reactor analysis and stellar photon transport problems.

Because the diffusion equation is simpler than the transport equation, it is a good place to start an investigation of time discretizations. Many of the observations we make in this chapter regarding stability and numerical behavior of time discretizations for the diffusion equation extend to the more complicated but analogous time discretizations of the linear and thermal radiation transport equations we consider in later chapters. We begin by deriving the well-known fully-explicit and implicit node-centered diffusion discretizations. Analysis of the fully-explicit method shows that this method is *local*, meaning that at a given point in time every unknown in the spatial domain is decoupled from every other unknown. Therefore, each unknown in the spatial domain at a given point in time may be calculated independently, and thus the fully-explicit method is trivial to parallelize. However, a stability analysis shows that the fully-explicit method is not unconditionally stable and requires small time steps for physically correct solutions. The implicit method, by contrast, is unconditionally stable, but is non-local. Every unknown at a given point in time is coupled to every other unknown in the spatial domain. In practice, this means that a large, sparse linear system must be solved at every time step. This makes the implicit method more

difficult to parallelize, and the method does not scale well with the number of processors. These observations regarding the fully-explicit and implicit methods are well-known in the computational transport community (see Ref. [26], where the fully-explicit method is called the explicit method, and the implicit method is called the fully implicit method).

The comparative advantages of these two discretizations suggests a third discretization, which we call the semi-explicit method. To our knowledge, this semi-explicit method has not been studied previously. This method is an attempt to combine some of the advantages of the implicit method with the advantages of the fully-explicit method by evaluating the absorption term implicitly, while evaluating the leakage term explicitly. However, a stability analysis shows that this method fails to achieve unconditional stability.

Finally, we introduce the SBJ diffusion method, which, as far as we know, has not been previously investigated. This method is similar to the semi-explicit method, but has been altered to make it "more implicit." This alteration is sufficient to achieve unconditional stability while maintaining linear scaling. A formal definition of the SBJ method is deferred until Chapter 3, where it will be defined for the transport equation. For now, suffice it to say, the SBJ diffusion method discretizes the diffusion equation such that it is as "implicit" as possible while still maintaining locality. In Chapter 4, we conduct an asymptotic analysis of the SBJ transport method and show that the SBJ diffusion discretization examined here is analogous to the SBJ transport discretization in the thick diffusive limit.

The diffusion equation is a parabolic partial differential equation, and so is characterized by an infinite propagation speed. This means that every point in space is coupled to every other point. Therefore, non-local methods, such as the implicit method, which discretize the equations such that this spatial coupling is maintained, solve the equations in a way that is consistent with the underlying physics. Local methods, by contrast, in which every unknown is decoupled, solve the diffusion equation in a manner that is contrary to the underlying physics. For this reason, we expect that local methods will not be as accurate for large time steps as non-local methods, even if they are numerically stable. Nevertheless, because of their improved parallel scalability, it may be possible that local methods are superior to non-local methods for some problems.

The goal of this dissertation is to develop and test an accurate, local, and unconditionally stable transport discretization. The transport equation, which we examine in the remaining chapters of this dissertation, is hyperbolic, and therefore has a finite propagation speed, so local methods can still provide accurate solutions. However, the diffusion equation is a proper place to begin because it offers a simpler domain to start an investigation of the properties of time discretizations, and any stable and local transport discretization must satisfy a stable and local diffusion discretization in the thick diffusive limit. Motivated by

the SBJ diffusion method, we propose (in Chapter 3) an SBJ transport method, and later (in Chapter 4) we show that in the thick diffusion limit, the SBJ transport method limits to a slight variant of the SBJ diffusion method presented here.

Much of the material presented in this chapter is well-known, particularly the fully-explicit and implicit methods. Nevertheless, we present and analyze these methods in order to compare and contrast them with the new SBJ diffusion method, and to set the stage for presenting the new SBJ transport method.

2.1 Derivation of the Discretized Diffusion Equation

To derive the time-dependent, one-dimensional, mono-energetic diffusion equation, we begin by considering the time-dependent, one-dimensional, mono-energetic transport equation with isotropic scattering on a spatial domain spanning $0 \leq x \leq X$:

$$\frac{1}{v}\frac{\partial}{\partial t}\psi(x,\mu,t) + \mu\frac{\partial}{\partial x}\psi(x,\mu,t) + \Sigma_t(x)\psi(x,\mu,t) = \frac{\Sigma_s(x)}{2}\int_{-1}^{1}\psi(x,\mu',t)\,\mathrm{d}\mu' + \frac{1}{2}Q(x,t)\,, \qquad 0 \leq x \leq X\,, \quad -1 \leq \mu \leq 1\,, \quad t > 0\,, \quad (2.1)$$

where

$\psi(x,\mu,t)$ = angular flux [cm^{-2} s^{-1} cosine^{-1}],
v = particle velocity [cm/s],
μ = cosine of the particle direction with the x-axis,
$\Sigma_t(x)$ = total cross section [cm^{-1}],
$\Sigma_s(x)$ = isotropic scattering cross section [cm^{-1}],
$Q(x,t)$ = isotropic particle source [cm^{-3} s^{-1}].

The angular flux is the quantity we seek, and all other quantities in Eq. (2.1) may be considered known. The mono-energetic angular flux $\psi(x,\mu,t)$ is defined as

$$\psi(x,\mu,t)\,\mathrm{d}x\,\mathrm{d}\mu = vN(x,\mu,t)\,\mathrm{d}x\,\mathrm{d}\mu\,, \quad (2.2)$$

where $N(x,\mu,t)\,\mathrm{d}x\,\mathrm{d}\mu$ is the number of particles within volume $\mathrm{d}x$ about x, traveling within angles $\mathrm{d}\mu$ about angular cosine μ, at time t. Eq. (2.1) represents a balance equation in the (x,μ) phase space. On the left, the time derivative term represents the net rate of change of the number of particles in the phase space, the spatial derivative term is a leakage term representing the net particles streaming spatially out of the phase space, and the collision term represents the particles being removed from the phase space through nuclear collision.

On the right, the scattering term represents the particles entering the phase space by scattering from angular cosine μ' into μ, and $\frac{1}{2}Q(x,t)$ represents the particles introduced into the phase space from an isotropic particle source. This equation is accompanied by boundary conditions and an initial condition. For incident or vacuum boundary conditions, for the left boundary, we use

$$\psi(0,\mu,t) = \psi_L^b(\mu,t)\,, \qquad 0 < \mu \leq 1\,, \tag{2.3a}$$

and for the right boundary,

$$\psi(X,\mu,t) = \psi_R^b(\mu,t)\,, \qquad -1 \leq \mu < 0\,, \tag{2.3b}$$

where $\psi_L^b(\mu,t)$ and $\psi_R^b(\mu,t)$ are the specified incident angular fluxes for angular cosine μ and time t, for the left and right boundaries, respectively. For reflecting boundaries, we use

$$\psi(0,\mu,t) = \psi(0,\mu',t)\,, \qquad 0 < \mu \leq 1\,, \quad \mu' = -\mu\,, \tag{2.4a}$$

for the left boundary, and

$$\psi(X,\mu,t) = \psi(0,\mu',t)\,, \qquad -1 \leq \mu < 0\,, \quad \mu' = -\mu\,, \tag{2.4b}$$

for the right boundary. The initial condition is given by

$$\psi(x,\mu,0) = \psi^i(x,\mu)\,, \qquad 0 \leq x \leq X\,, \quad -1 \leq \mu \leq 1\,, \tag{2.5}$$

where $\psi^i(x,\mu)$ is a specified initial condition.

Calculating the zeroth and first angular moments of the transport equation by operating on Eq. (2.1) by $\int_{-1}^{1}(\cdot)\,\mathrm{d}\mu$ and $\int_{-1}^{1}\mu(\cdot)\,\mathrm{d}\mu$, we obtain

$$\frac{1}{v}\frac{\partial}{\partial t}\phi(x,t) + \frac{\partial}{\partial x}J(x,t) + \Sigma_a(x)\phi(x,t) = Q(x,t)\,, \tag{2.6a}$$

$$\frac{1}{v}\frac{\partial}{\partial t}J(x,t) + \frac{\partial}{\partial x}\Phi(x,t) + \Sigma_t(x)J(x,t) = 0\,, \tag{2.6b}$$

where

$\phi(x,t) = \displaystyle\int_{-1}^{1}\psi(x,\mu,t)\,\mathrm{d}\mu$ = scalar flux,

$J(x,t) = \displaystyle\int_{-1}^{1}\mu\,\psi(x,\mu,t)\,\mathrm{d}\mu$ = current,

$\Phi(x,t) = \displaystyle\int_{-1}^{1}\mu^2\psi(x,\mu,t)\,\mathrm{d}\mu$ = second-order flux moment.

The diffusion approximation is applied by setting

$$\frac{1}{v}\frac{\partial}{\partial t}J(x,t)=0\,, \tag{2.7a}$$

and

$$\frac{\partial}{\partial x}\Phi(x,t)=\frac{1}{3}\frac{\partial}{\partial x}\phi(x,t)\,. \tag{2.7b}$$

These approximations assume that the current changes slowly in time [13]

$$\frac{1}{J(x,t)}\frac{\partial}{\partial t}J(x,t)\ll v\Sigma_t(x)\,, \tag{2.8a}$$

and that the angular flux can be accurately represented as linearly anisotropic, i.e.,

$$\psi(x,\mu,t)\approx\frac{1}{2}\phi(x,t)+\frac{3}{2}\mu J(x,t)\,. \tag{2.8b}$$

These approximations are accurate in regions that are dominated by scattering and are optically-thick (short mean-free path and mean-free time).

Defining the diffusion coefficient

$$D(x)=\frac{1}{3\Sigma_t(x)}\,, \tag{2.9}$$

the diffusion equations, which result from Eqs. (2.6a)–(2.9), are

$$\frac{1}{v}\frac{\partial}{\partial t}\phi(x,t)+\frac{\partial}{\partial x}J(x,t)+\Sigma_a(x)\phi(x,t)=Q(x,t)\,, \tag{2.10a}$$

$$J(x,t)=-D(x)\frac{\partial}{\partial x}\phi(x,t)\,. \tag{2.10b}$$

In the case of reflecting boundaries, we set

$$J(0,t)=0\,,\qquad\text{left boundary}\,, \tag{2.11a}$$

and

$$J(X,t)=0\,,\qquad\text{right boundary}\,. \tag{2.11b}$$

In the case of incident boundaries, we use a Marshak boundary condition [13]

$$J_L^b(t)=\frac{1}{4}\phi(0,t)+\frac{1}{2}J(0,t)\,, \tag{2.12a}$$

and

$$J_R^b(t) = \frac{1}{4}\phi(X,t) - \frac{1}{2}J(X,t)\,, \tag{2.12b}$$

where $J_L^b(t)$ and $J_R^b(t)$ are the specified incident partial currents for the left and right boundaries, respectively, and are defined as

$$J_L^b(t) = \int_0^1 \mu\,\psi_L^b(\mu,t)\,\mathrm{d}\mu\,, \tag{2.13a}$$

and

$$J_R^b(t) = \int_{-1}^0 |\mu|\,\psi_R^b(\mu,t)\,\mathrm{d}\mu\,. \tag{2.13b}$$

The initial condition is specified as

$$\phi(x,0) = \phi^i(x) = \int_{-1}^1 \psi^i(x,\mu)\,\mathrm{d}\mu\,, \qquad 0 \le x \le X\,. \tag{2.14}$$

Eqs. (2.10), along with boundary conditions given by Eqs. (2.11) and (2.13), and the initial condition given by Eq. (2.14), represent time-dependent, one-dimensional, monoenergetic particle diffusion through a background medium. This simplified diffusion model provides a convenient way to test the efficacy of new numerical methods. We now begin discretizing this system of equations into a form appropriate for implementation on a computer.

2.1.1 Time Discretization

We now discretize Eqs. (2.10) in time. Consider a time grid with time step $k+1$ bounded

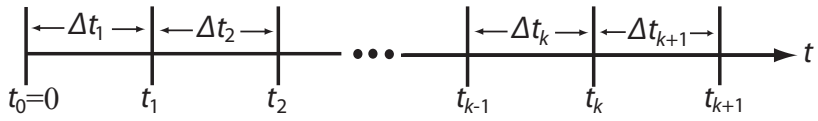

Figure 2.1 A Representative Time Grid

by times t_k and t_{k+1}, with $t_0 = 0$ and $\Delta t_{k+1} = t_{k+1} - t_k$, as shown in Figure 2.1. Averaging Eqs. (2.10) over time step $k+1$ by operating by $\frac{1}{\Delta t_{k+1}}\int_{t_k}^{t_{k+1}}(\cdot)\,\mathrm{d}t$ and defining

$$\bar{J}^{k+1}(x) = \frac{1}{\Delta t_{k+1}}\int_{t_k}^{t_{k+1}} J(x,t)\,\mathrm{d}t\,, \tag{2.15a}$$

$$\bar{\phi}^{k+1}(x) = \frac{1}{\Delta t_{k+1}} \int_{t_k}^{t_{k+1}} \phi(x,t)\,\mathrm{d}t\,, \tag{2.15b}$$

$$\phi^k(x) = \phi(x,t_k)\,, \tag{2.15c}$$

$$Q^{k+1}(x) = \frac{1}{\Delta t_{k+1}} \int_{t_k}^{t_{k+1}} Q(x,t)\,\mathrm{d}t\,, \tag{2.15d}$$

where $\bar{J}^{k+1}(x)$, $\bar{\phi}^{k+1}(x)$, and $Q^{k+1}(x)$ represent the average current, scalar flux, and particle source, respectively, over time step $k+1$, while $\phi^k(x)$ represents the scalar flux at time t_k. The time-averaged diffusion equations are

$$\frac{1}{v\Delta t_{k+1}}\left[\phi^{k+1}(x) - \phi^k(x)\right] + \frac{\mathrm{d}}{\mathrm{d}x}\bar{J}^{k+1}(x) + \Sigma_a(x)\bar{\phi}^{k+1}(x) = Q^{k+1}(x)\,, \tag{2.16a}$$

$$\bar{J}^{k+1}(x) = -D(x)\frac{\mathrm{d}}{\mathrm{d}x}\bar{\phi}^{k+1}(x)\,. \tag{2.16b}$$

Eqs. (2.16) are two equations with three unknowns, namely, $\bar{J}^{k+1}(x)$, $\bar{\phi}^{k+1}(x)$, and $\phi^{k+1}(x)$. The scalar flux at time t_k, $\phi^k(x)$, is considered known since it was either calculated during the previous time step, or if $k=0$, was specified by the initial condition. Because we may not solve for all three unknowns with only two equations, an approximation is required. Time discretizations are defined by how they approximate the time-averaged quantities $\bar{J}^{k+1}(x)$ and $\bar{\phi}^{k+1}(x)$.

For fully-explicit time discretizations, the time-averaged quantities are evaluated at the beginning of the time step, such that

$$\bar{\phi}^{k+1}(x) \approx \phi^k(x)\,, \tag{2.17a}$$

and

$$\bar{J}^{k+1}(x) \approx J^k(x) = J(x,t_k)\,. \tag{2.17b}$$

Then Eqs. (2.16) become

$$\frac{1}{v\Delta t_{k+1}}\left[\phi^{k+1}(x) - \phi^k(x)\right] + \frac{\mathrm{d}}{\mathrm{d}x}J^k(x) + \Sigma_a(x)\phi^k(x) = Q^{k+1}(x)\,, \tag{2.18a}$$

$$J^k(x) = -D(x)\frac{\mathrm{d}}{\mathrm{d}x}\phi^k(x)\,. \tag{2.18b}$$

For implicit time discretizations, the time-averaged quantities are evaluated at the end of the time step, such that

$$\bar{\phi}^{k+1}(x) \approx \phi^{k+1}(x)\,, \tag{2.19a}$$

and

$$\bar{J}^{k+1}(x) \approx J^{k+1}(x) = J(x, t_{k+1}) \,. \tag{2.19b}$$

Now Eqs. (2.16) become

$$\frac{1}{v\Delta t_{k+1}} \left[\phi^{k+1}(x) - \phi^{k}(x) \right] + \frac{\mathrm{d}}{\mathrm{d}x} J^{k+1}(x) + \Sigma_a(x) \phi^{k+1}(x) = Q^{k+1}(x) \,, \tag{2.20a}$$

$$J^{k+1}(x) = -D(x) \frac{\mathrm{d}}{\mathrm{d}x} \phi^{k+1}(x) \,. \tag{2.20b}$$

We can write both the implicit and fully-explicit time-discretized diffusion equations as

$$\frac{1}{v\Delta t_{k+1}} \left[\phi^{k+1}(x) - \phi^{k}(x) \right] + \frac{\mathrm{d}}{\mathrm{d}x} J^{k+\alpha}(x) + \Sigma_a(x) \phi^{k+\alpha}(x) = Q^{k+1}(x) \,, \tag{2.21a}$$

$$J^{k+\alpha}(x) = -D(x) \frac{\mathrm{d}}{\mathrm{d}x} \phi^{k+\alpha}(x) \,, \tag{2.21b}$$

where

$$\alpha = \begin{cases} 0: & \text{fully-explicit method} \,, \\ 1: & \text{implicit method} \,, \end{cases} \tag{2.22}$$

and with boundary conditions

$$J^{k}(0) = 0 \,, \qquad \text{left reflecting boundary} \,, \tag{2.23a}$$

$$J_L^{b,k} = \frac{1}{4} \phi^{k}(0) + \frac{1}{2} J^{k}(0) \,, \qquad \text{left incident boundary} \,, \tag{2.23b}$$

$$J^{k}(X) = 0 \,, \qquad \text{right reflecting boundary} \,, \tag{2.23c}$$

$$J_R^{b,k} = \frac{1}{4} \phi^{k}(X) - \frac{1}{2} J^{k}(X) \,, \qquad \text{right incident boundary} \,, \tag{2.23d}$$

and initial condition

$$\phi^{0}(x) = \phi^{i}(x) \,, \qquad 0 \leq x \leq X \,. \tag{2.24}$$

2.1.2 Spatial Discretization

We now discretize the spatial variable x in Eqs. (2.21). We have chosen to use a node-centered spatial discretization, named because the scalar flux unknowns are located at the mesh node positions. This discretization may be less common than the standard zone-centered spatial discretization, but has been chosen because it is analogous to the diffusion

limit of the linear discontinuous finite element transport discretization used in the remainder of this dissertation. Because the node-centered diffusion discretization is similar to the linear discontinuous transport discretization in the diffusion limit, many of the observations we will make in this chapter will be directly applicable to the transport discretizations we will derive in Chapter 3. In Chapter 4, we conduct an asymptotic analysis of the transport discretizations, and show how the linear discontinuous finite element transport discretizations behave like a node-centered diffusion discretization in the thick diffusive limit.

As already stated, for node-centered diffusion discretizations, the scalar flux unknowns are located at the mesh nodes. Consider a spatial grid spanning $0 \leq x \leq X$ divided into I cells, with cell i spanning $(x_{i-1/2}, x_{i+1/2})$, where $i = 1 \ldots I$, $x_{1/2} = 0$, and $x_{I+1/2} = X$, as shown in Figure 2.2. The center of cell i is located at x_i, and the left and right nodes

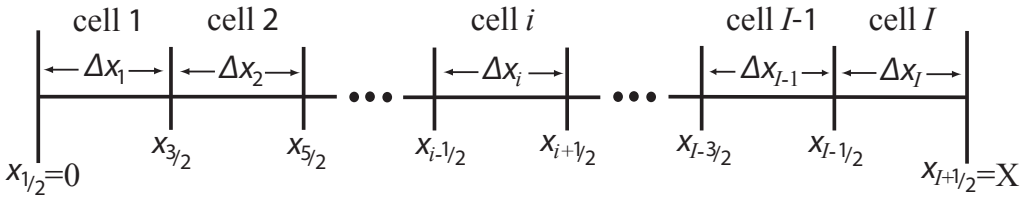

Figure 2.2 A Representative Spatial Grid

of cell i are located at $x_{i-1/2}$ and $x_{i+1/2}$, respectively. Therefore, the length of cell i is $\Delta x_i = x_{i+1/2} - x_{i-1/2}$. To derive the node-centered diffusion discretization, we first consider the domain interior. For the interior nodes, we integrate Eq. (2.21a) over the half-cells

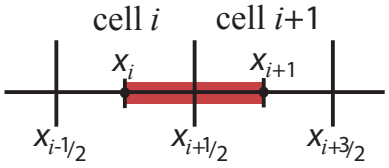

Figure 2.3 The Region of Integration about an Interior Node

adjacent to the node at $x_{i+1/2}$, as indicated in Figure 2.3. Therefore, operating on Eq. (2.21a) by $\int_{x_i}^{x_{i+1}} (\cdot)\,\mathrm{d}x$, we find

$$\frac{1}{v\Delta t_{k+1}}\left[\int_{x_i}^{x_{i+1}} \phi^{k+1}(x)\,\mathrm{d}x - \int_{x_i}^{x_{i+1}} \phi^{k}(x)\,\mathrm{d}x\right] + J^{k+\alpha}(x_{i+1}) - J^{k+\alpha}(x_i) + \int_{x_i}^{x_{i+1}} \Sigma_a(x)\phi^{k+\alpha}(x)\,\mathrm{d}x = \int_{x_i}^{x_{i+1}} Q^{k+1}(x)\,\mathrm{d}x. \quad (2.25)$$

The cell-centered currents $J^{k+\alpha}(x_{i+1})$ and $J^{k+\alpha}(x_i)$ are approximated as cell averages by operating on Eq. (2.21b) by $\frac{1}{\Delta x_{i+1}}\int_{x_{i+1/2}}^{x_{i+3/2}}(\cdot)\,\mathrm{d}x$ and $\frac{1}{\Delta x_i}\int_{x_{i-1/2}}^{x_{i+1/2}}(\cdot)\,\mathrm{d}x$ to acquire

$$J^{k+\alpha}(x_{i+1}) \approx J_{i+1}^{k+\alpha} = -\left(\frac{D_{i+1}}{\Delta x_{i+1}}\right)\left(\phi_{i+3/2}^{k+\alpha} - \phi_{i+1/2}^{k+\alpha}\right), \tag{2.26a}$$

$$J^{k+\alpha}(x_i) \approx J_i^{k+\alpha} = -\left(\frac{D_i}{\Delta x_i}\right)\left(\phi_{i+1/2}^{k+\alpha} - \phi_{i-1/2}^{k+\alpha}\right), \tag{2.26b}$$

where $J_i^{k+\alpha}$ and $J_{i+1}^{k+\alpha}$ are the cell-averaged currents for cells i and $i+1$, respectively, and we have defined

$$\phi_{i+1/2}^{k+\alpha} = \phi^{k+\alpha}(x_{i+1/2})\,. \tag{2.27}$$

We have also assumed that the diffusion coefficient, along with the absorption cross section and particle source are constant within a cell, i.e.,

$$D(x) = D_i\,, \qquad x_{i-1/2} < x < x_{i+1/2}\,, \tag{2.28a}$$

$$\Sigma_a(x) = \Sigma_{a,i}\,, \qquad x_{i-1/2} < x < x_{i+1/2}\,, \tag{2.28b}$$

$$Q^{k+1}(x) = Q_i^{k+1}\,, \qquad x_{i-1/2} < x < x_{i+1/2}\,. \tag{2.28c}$$

The absorption term is approximated as

$$\begin{aligned}\int_{x_i}^{x_{i+1}} \Sigma_a(x)\phi^{k+\alpha}(x)\,\mathrm{d}x &\approx \phi_{i+1/2}^{k+\alpha}\int_{x_i}^{x_{i+1}} \Sigma_a(x)\,\mathrm{d}x \\ &= \Sigma_{a,i+1/2}\Delta x_{i+1/2}\phi_{i+1/2}^{k+\alpha}\,,\end{aligned} \tag{2.29}$$

where we have defined

$$\Sigma_{a,i+1/2} = \frac{\Delta x_i\Sigma_{a,i} + \Delta x_{i+1}\Sigma_{a,i+1}}{\Delta x_i + \Delta x_{i+1}}\,, \tag{2.30}$$

and

$$\Delta x_{i+1/2} = \frac{\Delta x_i + \Delta x_{i+1}}{2}\,. \tag{2.31}$$

The source term is evaluated as

$$\int_{x_i}^{x_{i+1}} Q^{k+1}(x)\,\mathrm{d}x = Q_{i+1/2}^{k+1}\Delta x_{i+1/2}\,, \tag{2.32}$$

where

$$Q_{i+1/2}^{k+1} = \frac{\Delta x_i Q_i^{k+1} + \Delta x_{i+1}Q_{i+1}^{k+1}}{\Delta x_i + \Delta x_{i+1}}\,, \tag{2.33}$$

and the scalar flux integrals in the first term of Eq. (2.25) are approximated as

$$\int_{x_i}^{x_{i+1}} \phi^k(x)\,\mathrm{d}x \approx \phi^k_{i+1/2} \int_{x_i}^{x_{i+1}} \mathrm{d}x$$
$$= \phi^k_{i+1/2} \Delta x_{i+1/2}\,. \tag{2.34}$$

Therefore, the diffusion equations in the interior are

$$\frac{\Delta x_{i+1/2}}{v\Delta t_{k+1}}\left(\phi^{k+1}_{i+1/2} - \phi^k_{i+1/2}\right) + \left(J^{k+\alpha}_{i+1} - J^{k+\alpha}_i\right) + \left(\Sigma_{a,i+1/2}\Delta x_{i+1/2}\right)\phi^{k+\alpha}_{i+1/2}$$
$$= \Delta x_{i+1/2} Q^{k+1}_{i+1/2}\,, \qquad 1 \le i \le I-1\,, \tag{2.35a}$$

$$J^{k+\alpha}_i = -\left(\frac{D_i}{\Delta x_i}\right)\left(\phi^{k+\alpha}_{i+1/2} - \phi^{k+\alpha}_{i-1/2}\right). \tag{2.35b}$$

Figure 2.4 The Region of Integration for the Left (*left*) and Right (*right*) Boundaries

For the boundaries, we integrate Eq. (2.21a) over the half-cell adjacent to the boundaries, as shown in Figure 2.4. First, consider the left boundary. Operating on Eq. (2.21a) by $\int_{x_{1/2}}^{x_1}(\cdot)\,\mathrm{d}x$, we find

$$\frac{1}{v\Delta t_{k+1}}\left[\int_{x_{1/2}}^{x_1} \phi^{k+1}(x)\,\mathrm{d}x - \int_{x_{1/2}}^{x_1} \phi^k(x)\,\mathrm{d}x\right] + J^{k+\alpha}(x_1) - J^{k+\alpha}(x_{1/2})$$
$$+ \int_{x_{1/2}}^{x_1} \Sigma_a(x)\phi^{k+\alpha}(x)\,\mathrm{d}x = \int_{x_{1/2}}^{x_1} Q^{k+1}(x)\,\mathrm{d}x\,. \tag{2.36}$$

For a reflecting boundary, we set

$$J^{k+\alpha}(x_{1/2}) = J^{k+\alpha}_{1/2} = 0\,, \tag{2.37}$$

and for an incident or vacuum boundary, the current on the left boundary is approximated using a Marshak condition, to find

$$J^{k+\alpha}(x_{1/2}) = J^{k+\alpha}_{1/2} \approx 2J^{b,k+\alpha}_L - \frac{1}{2}\phi^{k+\alpha}_{1/2}\,. \tag{2.38}$$

Using the same approximations as before with the discretization in the domain interior, the diffusion discretization on the left boundary is

$$\frac{\Delta x_{1/2}}{v\Delta t_{k+1}}\left(\phi_{1/2}^{k+1}-\phi_{1/2}^{k}\right)+\left(J_{1}^{k+\alpha}-J_{1/2}^{k+\alpha}\right)+\left(\Sigma_{a,1/2}\Delta x_{1/2}\right)\phi_{1/2}^{k+\alpha}=\Delta x_{1/2}Q_{1/2}^{k+1}\,, \tag{2.39a}$$

$$J_{1/2}^{k+\alpha}=0\,, \qquad \text{left reflecting boundary}\,, \tag{2.39b}$$

$$J_{1/2}^{k+\alpha}=2J_{L}^{b,k+\alpha}-\frac{1}{2}\phi_{1/2}^{k+\alpha}\,, \qquad \text{left incident boundary}\,, \tag{2.39c}$$

$$J_{1}^{k+\alpha}=-\left(\frac{D_1}{\Delta x_1}\right)\left(\phi_{3/2}^{k+\alpha}-\phi_{1/2}^{k+\alpha}\right), \tag{2.39d}$$

where

$$\Delta x_{1/2}=\frac{\Delta x_1}{2}\,, \tag{2.40a}$$

$$\Sigma_{a,1/2}=\Sigma_{a,1}\,, \tag{2.40b}$$

$$Q_{1/2}^{k+1}=Q_{1}^{k+1}\,. \tag{2.40c}$$

Similarly, for the right boundary we find

$$\frac{\Delta x_{I+1/2}}{v\Delta t_{k+1}}\left(\phi_{I+1/2}^{k+1}-\phi_{I+1/2}^{k}\right)+\left(J_{I+1/2}^{k+\alpha}-J_{I}^{k+\alpha}\right)+\left(\Sigma_{a,I+1/2}\Delta x_{I+1/2}\right)\phi_{I+1/2}^{k+\alpha} = \Delta x_{I+1/2}Q_{I+1/2}^{k+1}\,, \tag{2.41a}$$

$$J_{I+1/2}^{k+\alpha}=0\,, \qquad \text{right reflecting boundary}\,, \tag{2.41b}$$

$$J_{I+1/2}^{k+\alpha}=\frac{1}{2}\phi_{I+1/2}^{k+\alpha}-2J_{R}^{b,k+\alpha}\,, \qquad \text{right incident boundary}\,, \tag{2.41c}$$

$$J_{I}^{k+\alpha}=-\left(\frac{D_I}{\Delta x_I}\right)\left(\phi_{I+1/2}^{k+\alpha}-\phi_{I-1/2}^{k+\alpha}\right), \tag{2.41d}$$

where

$$\Delta x_{I+1/2}=\frac{\Delta x_I}{2}\,, \tag{2.42a}$$

$$\Sigma_{a,I+1/2}=\Sigma_{a,I}\,, \tag{2.42b}$$

$$Q_{I+1/2}^{k+1}=Q_{I}^{k+1}\,. \tag{2.42c}$$

To summarize, the node-centered discretized diffusion equations are

$$\frac{\Delta x_{1/2}}{v\Delta t_{k+1}}\left(\phi_{1/2}^{k+1}-\phi_{1/2}^{k}\right)+\left(J_{1}^{k+\alpha}-J_{1/2}^{k+\alpha}\right)+\left(\Sigma_{a,1/2}\Delta x_{1/2}\right)\phi_{1/2}^{k+\alpha}=\Delta x_{1/2}Q_{1/2}^{k+1}\,, \quad (2.43a)$$

$$\frac{\Delta x_{i+1/2}}{v\Delta t_{k+1}}\left(\phi_{i+1/2}^{k+1}-\phi_{i+1/2}^{k}\right)+\left(J_{i+1}^{k+\alpha}-J_{i}^{k+\alpha}\right)+\left(\Sigma_{a,i+1/2}\Delta x_{i+1/2}\right)\phi_{i+1/2}^{k+\alpha} = \Delta x_{i+1/2}Q_{i+1/2}^{k+1}\,, \qquad 1\le i\le I-1\,, \quad (2.43b)$$

$$\frac{\Delta x_{I+1/2}}{v\Delta t_{k+1}}\left(\phi_{I+1/2}^{k+1}-\phi_{I+1/2}^{k}\right)+\left(J_{I+1/2}^{k+\alpha}-J_{I}^{k+\alpha}\right)+\left(\Sigma_{a,I+1/2}\Delta x_{I+1/2}\right)\phi_{I+1/2}^{k+\alpha} = \Delta x_{I+1/2}Q_{I+1/2}^{k+1}\,, \quad (2.43c)$$

where

$$J_{i}^{k+\alpha}=-\left(\frac{D_i}{\Delta x_i}\right)\left(\phi_{i+1/2}^{k+\alpha}-\phi_{i-1/2}^{k+\alpha}\right), \quad (2.44a)$$

$$J_{1/2}^{k+\alpha}=0\,, \qquad \text{left reflecting boundary}\,, \quad (2.44b)$$

$$J_{1/2}^{k+\alpha}=2J_{L}^{b,k+\alpha}-\frac{1}{2}\phi_{1/2}^{k+\alpha}\,, \qquad \text{left incident boundary}\,, \quad (2.44c)$$

$$J_{I+1/2}^{k+\alpha}=0\,, \qquad \text{right reflecting boundary}\,, \quad (2.44d)$$

$$J_{I+1/2}^{k+\alpha}=\frac{1}{2}\phi_{I+1/2}^{k+\alpha}-2J_{R}^{b,k+\alpha}\,, \qquad \text{right incident boundary}\,, \quad (2.44e)$$

and where

$$x_{i+1/2}=\begin{cases}\dfrac{\Delta x_1}{2}\,, & i=0\,,\\[2ex] \dfrac{\Delta x_i+\Delta x_{i+1}}{2}\,, & 1\le i\le I-1\,,\\[2ex] \dfrac{\Delta x_I}{2}\,, & i=I\,,\end{cases} \quad (2.45a)$$

$$\Sigma_{a,i+1/2}=\begin{cases}\Sigma_{a,1}\,, & i=0\,,\\[2ex] \dfrac{\Delta x_i\Sigma_{a,i}+\Delta x_{i+1}\Sigma_{a,i+1}}{\Delta x_i+\Delta x_{i+1}}\,, & 1\le i\le I-1\,,\\[2ex] \Sigma_{a,I}\,, & i=I\,,\end{cases} \quad (2.45b)$$

$$Q_{i+1/2}^{k+1} = \begin{cases} Q_1^{k+1}, & i = 0, \\ \dfrac{\Delta x_i Q_i^{k+1} + \Delta x_{i+1} Q_{i+1}^{k+1}}{\Delta x_i + \Delta x_{i+1}}, & 1 \le i \le I-1, \\ Q_I^{k+1}, & i = I, \end{cases} \tag{2.45c}$$

and

$$\alpha = \begin{cases} 0: & \text{fully-explicit method}, \\ 1: & \text{implicit method}, \end{cases} \tag{2.46}$$

and with the initial conditions

$$\phi_{1/2}^0 = \frac{1}{\Delta x_{1/2}} \int_{x_{1/2}}^{x_1} \phi^i(x)\,\mathrm{d}x, \tag{2.47a}$$

$$\phi_{i+1/2}^0 = \frac{1}{\Delta x_{i+1/2}} \int_{x_i}^{x_{i+1}} \phi^i(x)\,\mathrm{d}x, \qquad 1 \le i \le I-1, \tag{2.47b}$$

$$\phi_{I+1/2}^0 = \frac{1}{\Delta x_{I+1/2}} \int_{x_I}^{x_{I+1/2}} \phi^i(x)\,\mathrm{d}x. \tag{2.47c}$$

2.2 Analyzing the Behavior of the Implicit and Fully-Explicit Discretized Diffusion Methods

We next analyze the behavior of the implicit and fully-explicit discretized diffusion methods. This analysis shows that the implicit method is unconditionally stable, but it requires the solution of a large number of interdependent algebraic equations. The fully-explicit method, by contrast, is not unconditionally stable. However, each unknown in the fully-explicit method is independent. If each unknown in the method is independent, the method is *local*. Local methods have superior parallel scalability to non-local methods because each unknown in the problem may be calculated in parallel.

2.2.1 Locality of the Implicit and Fully-Explicit Discretized Diffusion Methods

Consider the discretized diffusion equations in the problem interior:

$$\frac{\Delta x_{i+1/2}}{v\Delta t_{k+1}}\left(\phi_{i+1/2}^{k+1}-\phi_{i+1/2}^{k}\right)+\left(J_{i+1}^{k+\alpha}-J_{i}^{k+\alpha}\right)+\left(\Sigma_{a,i+1/2}\Delta x_{i+1/2}\right)\phi_{i+1/2}^{k+\alpha} = \Delta x_{i+1/2}Q_{i+1/2}^{k+1}, \quad (2.48a)$$

$$J_{i}^{k+\alpha} = -\left(\frac{D_i}{\Delta x_i}\right)\left(\phi_{i+1/2}^{k+\alpha}-\phi_{i-1/2}^{k+\alpha}\right), \quad (2.48b)$$

where

$$\alpha = \begin{cases} 0: & \text{fully-explicit method}, \\ 1: & \text{implicit method}. \end{cases} \quad (2.49)$$

Substituting Eq. (2.48b) into Eq. (2.48a), we find

$$\frac{\Delta x_{i+1/2}}{v\Delta t_{k+1}}\left(\phi_{i+1/2}^{k+1}-\phi_{i+1/2}^{k}\right)-\left(\frac{D_{i+1}}{\Delta x_{i+1}}\right)\left(\phi_{i+3/2}^{k+\alpha}-\phi_{i+1/2}^{k+\alpha}\right)+\left(\frac{D_i}{\Delta x_i}\right)\left(\phi_{i+1/2}^{k+\alpha}-\phi_{i-1/2}^{k+\alpha}\right) + \left(\Sigma_{a,i+1/2}\Delta x_{i+1/2}\right)\phi_{i+1/2}^{k+\alpha} = \Delta x_{i+1/2}Q_{i+1/2}^{k+1}. \quad (2.50)$$

In the case of the fully-explicit method, $\alpha = 0$, and Eq. (2.50) can be written as

$$\frac{\Delta x_{i+1/2}}{v\Delta t_{k+1}}\left(\phi_{i+1/2}^{k+1}-\phi_{i+1/2}^{k}\right)-\left(\frac{D_{i+1}}{\Delta x_{i+1}}\right)\left(\phi_{i+3/2}^{k}-\phi_{i+1/2}^{k}\right)+\left(\frac{D_i}{\Delta x_i}\right)\left(\phi_{i+1/2}^{k}-\phi_{i-1/2}^{k}\right) + \left(\Sigma_{a,i+1/2}\Delta x_{i+1/2}\right)\phi_{i+1/2}^{k} = \Delta x_{i+1/2}Q_{i+1/2}^{k+1}. \quad (2.51)$$

Examining Eq. (2.51), we observe that the unknown scalar flux $\phi_{i+1/2}^{k+1}$ is only dependent upon the known particle source $Q_{i+1/2}^{k+1}$, the known mesh and material properties, and known scalar fluxes calculated from the previous time step. Therefore, we can solve directly for the new scalar flux at time t_{k+1} and find

$$\phi_{i+1/2}^{k+1} = \left(1-\Sigma_{a,i+1/2}v\Delta t_{k+1}\right)\phi_{i+1/2}^{k}+\left(\frac{v\Delta t_{k+1}}{\Delta x_{i+1/2}}\right)\left(\frac{D_{i+1}}{\Delta x_{i+1}}\right)\left(\phi_{i+3/2}^{k}-\phi_{i+1/2}^{k}\right) - \left(\frac{v\Delta t_{k+1}}{\Delta x_{i+1/2}}\right)\left(\frac{D_i}{\Delta x_i}\right)\left(\phi_{i+1/2}^{k}-\phi_{i-1/2}^{k}\right)+v\Delta t_{k+1}Q_{i+1/2}^{k+1}. \quad (2.52)$$

From Eq. (2.52), we can see that each unknown in the problem domain is independent and may be calculated in parallel. Though we will not demonstrate it here, the fully-explicit method is also local on the boundaries.

For the implicit method, we substitute $\alpha = 1$ into Eq. (2.50) and find

$$\frac{\Delta x_{i+1/2}}{v\Delta t_{k+1}}\left(\phi_{i+1/2}^{k+1}-\phi_{i+1/2}^{k}\right)-\left(\frac{D_{i+1}}{\Delta x_{i+1}}\right)\left(\phi_{i+3/2}^{k+1}-\phi_{i+1/2}^{k+1}\right)+\left(\frac{D_i}{\Delta x_i}\right)\left(\phi_{i+1/2}^{k+1}-\phi_{i-1/2}^{k+1}\right) + \left(\Sigma_{a,i+1/2}\Delta x_{i+1/2}\right)\phi_{i+1/2}^{k+1}=\Delta x_{i+1/2}Q_{i+1/2}^{k+1}. \quad (2.53)$$

Rearranging Eq. (2.53), we obtain

$$-\left(\frac{D_i}{\Delta x_i}\right)\phi_{i-1/2}^{k+1}+\left(\frac{\Delta x_{i+1/2}}{v\Delta t_{k+1}}+\frac{D_{i+1}}{\Delta x_{i+1}}+\frac{D_i}{\Delta x_i}+\Sigma_{a,i+1/2}\Delta x_{i+1/2}\right)\phi_{i+1/2}^{k+1} - \left(\frac{D_{i+1}}{\Delta x_{i+1}}\right)\phi_{i+3/2}^{k+1}=\left(\frac{\Delta x_{i+1/2}}{v\Delta t_{k+1}}\right)\phi_{i+1/2}^{k}+\Delta x_{i+1/2}Q_{i+1/2}^{k+1}. \quad (2.54)$$

Examining Eq. (2.54), we observe that the unknown scalar flux $\phi_{i+1/2}^{k+1}$ is dependent upon the unknown scalar fluxes $\phi_{i+3/2}^{k+1}$ and $\phi_{i-1/2}^{k+1}$. Therefore, solving for the unknown scalar fluxes at time t_{k+1} requires solving a tridiagonal system of equations. Because the unknown scalar fluxes are interdependent, the implicit method is not local, and the parallel scalability is limited.

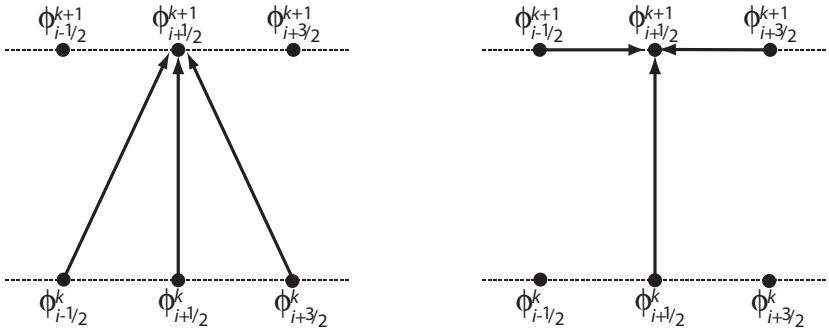

Figure 2.5 The Data Dependencies for the Fully-Explicit (*left*) and Implicit (*right*) Methods

In Figure 2.5, we graphically illustrate the data dependencies of the fully-explicit and implicit methods. For the fully-explicit method, the scalar flux $\phi_{i+1/2}^{k+1}$ is dependent upon the known scalar fluxes $\phi_{i-1/2}^{k}$, $\phi_{i+1/2}^{k}$, and $\phi_{i+3/2}^{k}$, as shown on the left side of Figure 2.5. Any method which has a data dependency like the one shown for the fully-explicit method is a local method. For the implicit method, the scalar flux $\phi_{i+1/2}^{k+1}$ is dependent upon the unknown scalar fluxes $\phi_{i-1/2}^{k+1}$ and $\phi_{i+3/2}^{k+1}$, as well as the known scalar flux $\phi_{i+1/2}^{k}$, as shown

on the right side of Figure 2.5.

We also note that, for local methods, because $\phi_{i+1/2}^{k+1}$ is dependent only upon information from the previous time step, this implies that local methods can advance an incident wave of particles at most one cell per time step. If the physical speed of the particle wave is greater than this limit, any local method will produce inaccurate solutions. We will demonstrate this property in the numerical results in Section 2.5.

2.2.2 Stability Analysis of Implicit and Fully-Explicit Diffusion

To conduct a stability analysis of the implicit and fully-explicit discretized diffusion methods, we begin with the discretized diffusion equation in the interior. We assume a homogeneous material with diffusion coefficient D and absorption cross section Σ_a, a uniform mesh with zone length Δx, and no source:

$$\frac{\Delta x}{v\Delta t_{k+1}}\left(\phi_{i+1/2}^{k+1}-\phi_{i+1/2}^{k}\right)-\frac{D}{\Delta x}\left(\phi_{i+3/2}^{k+\alpha}-2\phi_{i+1/2}^{k+\alpha}+\phi_{i-1/2}^{k+\alpha}\right)+\left(\Sigma_a\Delta x\right)\phi_{i+1/2}^{k+\alpha}=0\,, \quad (2.55)$$

where

$$\alpha=\begin{cases}0: & \text{fully-explicit}\,,\\ 1: & \text{implicit}\,.\end{cases} \quad (2.56)$$

Under the assumption of a homogeneous material, uniform mesh, and no fixed source, the Fourier modes are all independent. Therefore, we can represent the scalar flux with the so-called Fourier ansatz

$$\phi_{i+1/2}^{k}=\rho^{k}e^{\mathrm{i}\lambda x_{i+1/2}}\,, \quad (2.57)$$

where ρ is the amplification factor and λ represents the Fourier mode. For a method to be numerically stable, it must be the case that $|\rho|\leq 1$ for all λ. Substituting Eq. (2.57) into Eq. (2.55), we obtain

$$\begin{aligned}\frac{\Delta x}{v\Delta t_{k+1}}&\left(\rho^{k+1}e^{\mathrm{i}\lambda x_{i+1/2}}-\rho^{k}e^{\mathrm{i}\lambda x_{i+1/2}}\right)\\ &-\frac{D}{\Delta x}\left(\rho^{k+\alpha}e^{\mathrm{i}\lambda x_{i+3/2}}-2\rho^{k+\alpha}e^{\mathrm{i}\lambda x_{i+1/2}}+\rho^{k+\alpha}e^{\mathrm{i}\lambda x_{i-1/2}}\right)\\ &+\left(\Sigma_a\Delta x\right)\rho^{k+\alpha}e^{\mathrm{i}\lambda x_{i+1/2}}=0\,. \quad (2.58)\end{aligned}$$

Dividing by $\rho^{k}e^{\mathrm{i}\lambda x_{i+1/2}}$, we find

$$\frac{\Delta x}{v\Delta t_{k+1}}\left(\rho-1\right)-\frac{D}{\Delta x}\left(\rho^{\alpha}e^{\mathrm{i}\lambda\Delta x}-2\rho^{\alpha}+\rho^{\alpha}e^{-\mathrm{i}\lambda\Delta x}\right)+\left(\Sigma_a\Delta x\right)\rho^{\alpha}=0\,. \quad (2.59)$$

Using

$$\cos(\lambda\Delta x) = \frac{e^{\mathrm{i}\lambda\Delta x} + e^{-\mathrm{i}\lambda\Delta x}}{2}, \tag{2.60}$$

and rearranging, we have

$$\rho - 1 - \left[\frac{2Dv\Delta t_{k+1}}{(\Delta x)^2}\right]\Big[\cos(\lambda\Delta x) - 1\Big]\rho^{\alpha} + \Big[\Sigma_a v\Delta t_{k+1}\Big]\rho^{\alpha} = 0\,. \tag{2.61}$$

Stable solutions are guaranteed when $|\rho| \leq 1$. Next, we analyze Eq. (2.61) for the implicit and fully-explicit methods.

Implicit Method

Substituting $\alpha = 1$ into Eq. (2.61), we have

$$\rho - 1 - \left[\frac{2Dv\Delta t_{k+1}}{(\Delta x)^2}\right]\Big[\cos(\lambda\Delta x) - 1\Big]\rho + \Big[\Sigma_a v\Delta t_{k+1}\Big]\rho = 0\,. \tag{2.62}$$

Solving for ρ, we find

$$\rho = \frac{1}{1 + \Sigma_a v\Delta t_{k+1} + \left[\dfrac{2Dv\Delta t_{k+1}}{(\Delta x)^2}\right]\Big[1 - \cos(\lambda\Delta x)\Big]}\,. \tag{2.63}$$

Examining Eq. (2.63), we see that $|\rho| < 1$ for all λ. Therefore, the implicit method is unconditionally stable.

Fully-Explicit Method

For the fully-explicit method, we substitute $\alpha = 0$ into Eq. (2.61) and solve for ρ to find

$$\rho = \Big[1 - \Sigma_a v\Delta t_{k+1}\Big] + \left[\frac{2Dv\Delta t_{k+1}}{(\Delta x)^2}\right]\Big[\cos(\lambda\Delta x) - 1\Big]\,. \tag{2.64}$$

The range of $\cos(\lambda\Delta x)$ is $[-1, 1]$. Considering Eq. (2.64) when $\cos(\lambda\Delta x) = 1$, we have

$$\rho = 1 - \Sigma_a v\Delta t_{k+1}\,. \tag{2.65}$$

To satisfy $|\rho| \leq 1$, the time step length must satisfy

$$\Delta t_{k+1} \leq \frac{2}{\Sigma_a v}. \tag{2.66}$$

Examining Eq. (2.64) when $\cos(\lambda \Delta x) = -1$, we have

$$\rho = 1 - \Sigma_a v \Delta t_{k+1} - \frac{4Dv\Delta t_{k+1}}{(\Delta x)^2}. \tag{2.67}$$

From this we calculate the maximum time step length

$$\Delta t_{k+1} \leq \frac{2(\Delta x)^2}{v\left[\Sigma_a (\Delta x)^2 + 4D\right]}. \tag{2.68}$$

Eq. (2.68) is more restrictive than Eq. (2.66); therefore, it is the limiting time step condition. Any problem that violates the time step condition given in Eq. (2.68) will likely be numerically unstable and oscillatory.

To see the effects of numerical instability, consider a slab 1 cm thick divided into ten zones of equal length. The slab is filled with a homogeneous material with properties $\Sigma_a = 1$ cm^{-1} and $D = \frac{1}{3}$ cm, and the particle velocity is set at $v = 1$ cm/s. We place an incident partial current of $J_L^{b,k} = 10$ cm^{-2} s^{-1} on the left side of the slab, a vacuum on the right side, and we specify an initial condition of zero everywhere. The problem is marched forward in time for 10 s with a time step length of $\Delta t = 1$ s for both the implicit and fully-explicit methods. We also run a fine-mesh solution with $\Delta x = 0.01$ cm and a time step length of $\Delta t = 10^{-5}$ s. Using Eq. (2.68), we find that the stable, non-oscillatory condition for the fully-explicit method for this problem is $\Delta t = 0.014888$ s. Figure 2.6 shows the

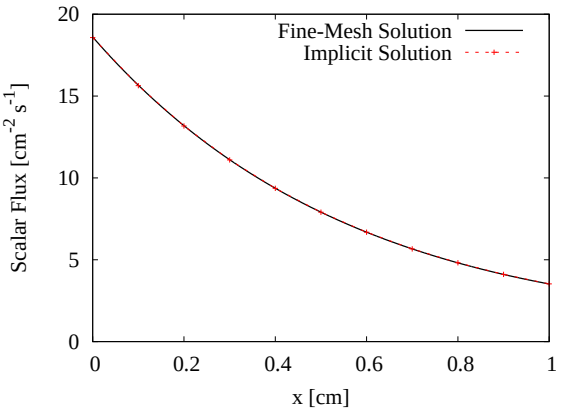

Figure 2.6 Implicit and Fine-Mesh Solutions

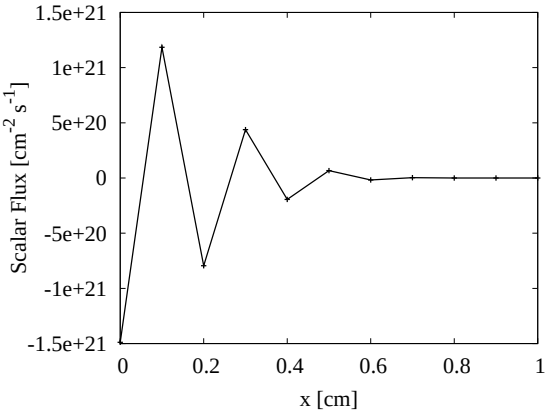

Figure 2.7 Unstable Fully-Explicit Solution

results for the implicit method (note that the fine-mesh solution and implicit solution are superimposed), and Figure 2.7 shows the results for the fully-explicit method. The implicit results are stable and accurate, whereas the fully-explicit results are unstable and oscillatory. If we decrease the time step for the fully-explicit method below the stability condition to $\Delta t = 0.01$ s, then the results become stable, as shown in Figure 2.8, where the fully-explicit and fine-mesh solutions are superimposed.

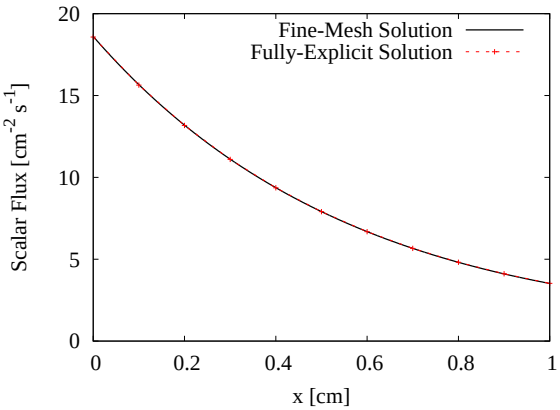

Figure 2.8 Stable Fully-Explicit and Fine-Mesh Solutions

Clearly, the existing methods are imperfect. The implicit method is unconditionally stable but lacks locality, thereby limiting its parallel scalability. The fully-explicit method is local but lacks unconditional stability. For problems of interest to the scientific community, the time step lengths required for stability with the fully-explicit method are often impractically short. Ideally, we would like to find a method that is both unconditionally stable and local.

2.3 The Semi-Explicit Diffusion Method

To find a method that is both unconditionally stable and local, we make the fully-explicit method more "implicit" by evaluating the absorption term at time t_{k+1} instead of at time t_k. The resulting semi-explicit method can be written as:

$$\frac{\Delta x_{1/2}}{v\Delta t_{k+1}}\left(\phi_{1/2}^{k+1}-\phi_{1/2}^{k}\right)+\left(J_{1}^{k}-J_{1/2}^{k}\right)+\left(\Sigma_{a,1/2}\Delta x_{1/2}\right)\phi_{1/2}^{k+1}=\Delta x_{1/2}Q_{1/2}^{k+1}\,, \qquad (2.69a)$$

$$\frac{\Delta x_{i+1/2}}{v\Delta t_{k+1}}\left(\phi_{i+1/2}^{k+1}-\phi_{i+1/2}^{k}\right)+\left(J_{i+1}^{k}-J_{i}^{k}\right)+\left(\Sigma_{a,i+1/2}\Delta x_{i+1/2}\right)\phi_{i+1/2}^{k+1}=\Delta x_{i+1/2}Q_{i+1/2}^{k+1},$$
$$1\leq i\leq I-1\,, \quad (2.69b)$$

$$\frac{\Delta x_{I+1/2}}{v\Delta t_{k+1}}\left(\phi_{I+1/2}^{k+1}-\phi_{I+1/2}^{k}\right)+\left(J_{I+1/2}^{k}-J_{I}^{k}\right)+\left(\Sigma_{a,I+1/2}\Delta x_{I+1/2}\right)\phi_{I+1/2}^{k+1}$$
$$=\Delta x_{I+1/2}Q_{I+1/2}^{k+1}\,, \quad (2.69c)$$

and

$$J_{i}^{k}=-\left(\frac{D_i}{\Delta x_i}\right)\left(\phi_{i+1/2}^{k}-\phi_{i-1/2}^{k}\right), \quad (2.70a)$$

$$J_{1/2}^{k}=0\,, \qquad \text{left reflecting boundary}\,, \quad (2.70b)$$

$$J_{1/2}^{k}=2J_{L}^{b,k}-\frac{1}{2}\phi_{1/2}^{k}\,, \qquad \text{left incident boundary}\,, \quad (2.70c)$$

$$J_{I+1/2}^{k}=0\,, \qquad \text{right reflecting boundary}\,, \quad (2.70d)$$

$$J_{I+1/2}^{k}=\frac{1}{2}\phi_{I+1/2}^{k}-2J_{R}^{b,k}\,, \qquad \text{right incident boundary}\,. \quad (2.70e)$$

This method has the same locality as the fully-explicit method. If it also has unconditional stability, then it will satisfy both our criteria.

2.3.1 Stability Analysis of the Semi-Explicit Method

Substituting Eq. (2.70a) into Eq. (2.69b), we find the semi-explicit diffusion equation in the interior. Assuming a homogeneous material with diffusion coefficient D and absorption cross section Σ_a, a uniform mesh with zone length Δx, and no source, we have

$$\frac{\Delta x}{v\Delta t_{k+1}}\left(\phi_{i+1/2}^{k+1}-\phi_{i+1/2}^{k}\right)-\frac{D}{\Delta x}\left(\phi_{i+3/2}^{k}-2\phi_{i+1/2}^{k}+\phi_{i-1/2}^{k}\right)+\left(\Sigma_a\Delta x\right)\phi_{i+1/2}^{k+1}=0\,. \quad (2.71)$$

Substituting in the Fourier ansatz

$$\phi_{i+1/2}^{k}=\rho^{k}e^{\mathrm{i}\lambda x_{i+1/2}}\,, \quad (2.72)$$

we find

$$\frac{\Delta x}{v\Delta t_{k+1}}\Big(\rho^{k+1}e^{\mathrm{i}\lambda x_{i+1/2}}-\rho^{k}e^{\mathrm{i}\lambda x_{i+1/2}}\Big)-\frac{D}{\Delta x}\Big(\rho^{k}e^{\mathrm{i}\lambda x_{i+3/2}}-2\rho^{k}e^{\mathrm{i}\lambda x_{i+1/2}}+\rho^{k}e^{\mathrm{i}\lambda x_{i-1/2}}\Big)$$
$$+\Big(\Sigma_a\Delta x\Big)\rho^{k+1}e^{\mathrm{i}\lambda x_{i+1/2}}=0\,. \quad (2.73)$$

Dividing by $\rho^{k}e^{\mathrm{i}\lambda x_{i+1/2}}$, we obtain

$$\frac{\Delta x}{v\Delta t_{k+1}}\Big(\rho-1\Big)-\frac{D}{\Delta x}\Big(e^{\mathrm{i}\lambda\Delta x}-2+e^{-\mathrm{i}\lambda\Delta x}\Big)+\Big(\Sigma_a\Delta x\Big)\rho=0\,. \quad (2.74)$$

Using

$$\cos(\lambda\Delta x)=\frac{e^{\mathrm{i}\lambda\Delta x}+e^{-\mathrm{i}\lambda\Delta x}}{2}\,, \quad (2.75)$$

we have

$$\frac{\Delta x}{v\Delta t_{k+1}}\Big[\rho-1\Big]-\frac{2D}{\Delta x}\Big[\cos(\lambda\Delta x)-1\Big]+\Big[\Sigma_a\Delta x\Big]\rho=0\,. \quad (2.76)$$

Solving for ρ, we find

$$\rho=\frac{1}{1+\Sigma_a v\Delta t_{k+1}}\left[1+\left(\frac{2Dv\Delta t_{k+1}}{(\Delta x)^2}\right)\Big(\cos(\lambda\Delta x)-1\Big)\right]\,. \quad (2.77)$$

Examining Eq. (2.77) when $\cos(\lambda\Delta x)=1$, we have

$$\rho=\frac{1}{1+\Sigma_a v\Delta t_{k+1}}\,. \quad (2.78)$$

In this case, $|\rho|\leq 1$. Examining Eq. (2.77) when $\cos(\lambda\Delta x)=-1$, we obtain

$$\rho=\frac{1}{1+\Sigma_a v\Delta t_{k+1}}\left[1-\frac{4Dv\Delta t_{k+1}}{(\Delta x)^2}\right]\,. \quad (2.79)$$

Examining Eq. (2.79) for when $\rho\leq 1$, we have

$$-4D\leq\Sigma_a\,(\Delta x)^2\,. \quad (2.80)$$

This condition is always satisfied. Examining Eq. (2.79) for when $\rho\geq -1$, we find

$$\Big[4D-\Sigma_a\,(\Delta x)^2\Big]v\Delta t_{k+1}\leq 2\,(\Delta x)^2\,. \quad (2.81)$$

If $\Sigma_a (\Delta x)^2 \geq 4D$, then this inequality is always true. However, if $\Sigma_a (\Delta x)^2 < 4D$, then we find that the stability condition for the semi-explicit method is

$$\Delta t_{k+1} \leq \frac{2(\Delta x)^2}{v\left[4D - \Sigma_a (\Delta x)^2\right]}, \qquad \text{if } \Sigma_a (\Delta x)^2 < 4D. \tag{2.82}$$

Thus, while the semi-explicit method is more robust than the fully-explicit method, it is not unconditionally stable. In particular, it is not stable in optically-thin problems with a fine mesh. Consider again a problem with a slab 1 cm thick, divided into ten cells of equal width, filled with a homogeneous material with properties $\Sigma_a = 1$ cm^{-1} and $D = \frac{1}{3}$ cm, and particle velocity of $v = 1$ cm/s. We specify an incident partial current of $J_L^{b,k} = 10$ cm^{-2} s^{-1} on the left boundary, a vacuum on the right boundary, and an initial condition of zero everywhere. For this problem, we find that $\Sigma_a (\Delta x)^2 < 4D$, so the semi-explicit method will not be unconditionally stable. The stability condition for this problem is $\Delta t \leq 0.01511335$ s. Running ten time steps of length $\Delta t = 1$ s, we find the unstable solution given in Figure 2.9. Reducing the time step length below the stability criterion to $\Delta t = 0.01$ s, we find the solution shown in Figure 2.10. While the semi-explicit method represents an improvement over the fully-explicit method, it fails to achieve both locality and unconditional stability.

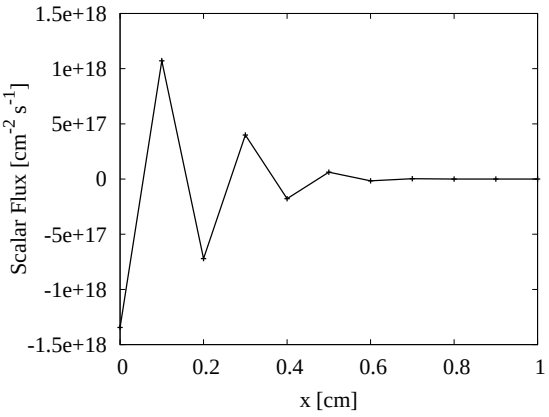

Figure 2.9 Unstable Semi-Explicit Solution

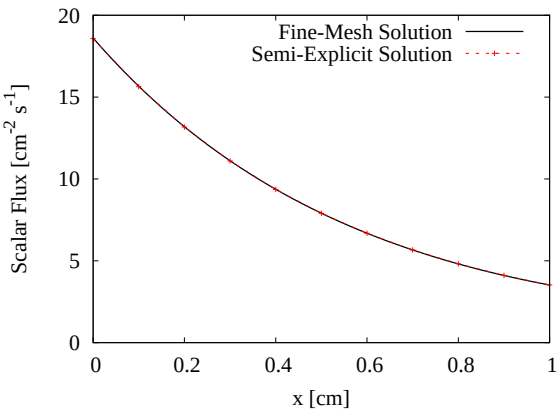

Figure 2.10 Stable Semi-Explicit Solution

2.4 The Staggered-Block Jacobi Discretization Method

In the previous section, we found that by making the absorption term in the fully-explicit method implicit, we could define a new semi-explicit method that has improved stability

while maintaining the locality of the fully-explicit method. However, the semi-explicit method is not unconditionally stable. The SBJ diffusion method continues this theme by making the central point in the leakage term implicit as well. Consider the semi-explicit equations derived in the previous section:

$$\frac{\Delta x_{1/2}}{v\Delta t_{k+1}}\left(\phi_{1/2}^{k+1}-\phi_{1/2}^{k}\right)+\left(J_{1}^{k}-J_{1/2}^{k}\right)+\left(\Sigma_{a,1/2}\Delta x_{1/2}\right)\phi_{1/2}^{k+1}=\Delta x_{1/2}Q_{1/2}^{k+1}\,, \tag{2.83a}$$

$$\frac{\Delta x_{i+1/2}}{v\Delta t_{k+1}}\left(\phi_{i+1/2}^{k+1}-\phi_{i+1/2}^{k}\right)+\left(J_{i+1}^{k}-J_{i}^{k}\right)+\left(\Sigma_{a,i+1/2}\Delta x_{i+1/2}\right)\phi_{i+1/2}^{k+1} = \Delta x_{i+1/2}Q_{i+1/2}^{k+1}\,, \qquad 1\le i\le I-1\,, \tag{2.83b}$$

$$\frac{\Delta x_{I+1/2}}{v\Delta t_{k+1}}\left(\phi_{I+1/2}^{k+1}-\phi_{I+1/2}^{k}\right)+\left(J_{I+1/2}^{k}-J_{I}^{k}\right)+\left(\Sigma_{a,I+1/2}\Delta x_{I+1/2}\right)\phi_{I+1/2}^{k+1} = \Delta x_{I+1/2}Q_{I+1/2}^{k+1}\,, \tag{2.83c}$$

and

$$J_{i}^{k}=-\left(\frac{D_i}{\Delta x_i}\right)\left(\phi_{i+1/2}^{k}-\phi_{i-1/2}^{k}\right), \tag{2.84a}$$

$$J_{1/2}^{k}=0\,, \qquad \text{left reflecting boundary}\,, \tag{2.84b}$$

$$J_{1/2}^{k}=2J_{L}^{b,k}-\frac{1}{2}\phi_{1/2}^{k}\,, \qquad \text{left incident boundary}\,, \tag{2.84c}$$

$$J_{I+1/2}^{k}=0\,, \qquad \text{right reflecting boundary}\,, \tag{2.84d}$$

$$J_{I+1/2}^{k}=\frac{1}{2}\phi_{I+1/2}^{k}-2J_{R}^{b,k}\,, \qquad \text{right incident boundary}\,. \tag{2.84e}$$

Substituting Eqs. (2.84) into Eqs. (2.83), we find

$$\frac{\Delta x_{1/2}}{v\Delta t_{k+1}}\left(\phi_{1/2}^{k+1}-\phi_{1/2}^{k}\right)-\left(\frac{D_1}{\Delta x_1}\right)\left(\phi_{3/2}^{k}-\phi_{1/2}^{k}\right)+\left(\Sigma_{a,1/2}\Delta x_{1/2}\right)\phi_{1/2}^{k+1}=\Delta x_{1/2}Q_{1/2}^{k+1}\,, \qquad \text{left reflecting boundary}\,, \tag{2.85a}$$

$$\frac{\Delta x_{1/2}}{v\Delta t_{k+1}}\left(\phi_{1/2}^{k+1}-\phi_{1/2}^{k}\right)-\left(\frac{D_1}{\Delta x_1}\right)\left(\phi_{3/2}^{k}-\phi_{1/2}^{k}\right)-\left(2J_{L}^{b,k}-\frac{1}{2}\phi_{1/2}^{k}\right)+\left(\Sigma_{a,1/2}\Delta x_{1/2}\right)\phi_{1/2}^{k+1}=\Delta x_{1/2}Q_{1/2}^{k+1}\,, \qquad \text{left incident boundary}\,, \tag{2.85b}$$

$$\frac{\Delta x_{i+1/2}}{v\Delta t_{k+1}}\left(\phi_{i+1/2}^{k+1}-\phi_{i+1/2}^{k}\right)-\left(\frac{D_{i+1}}{\Delta x_{i+1}}\right)\left(\phi_{i+3/2}^{k}-\phi_{i+1/2}^{k}\right)+\left(\frac{D_i}{\Delta x_i}\right)\left(\phi_{i+1/2}^{k}-\phi_{i-1/2}^{k}\right)$$
$$+\left(\Sigma_{a,i+1/2}\Delta x_{i+1/2}\right)\phi_{i+1/2}^{k+1}=\Delta x_{i+1/2}Q_{i+1/2}^{k+1},\qquad 1\le i\le I-1, \quad (2.85c)$$

$$\frac{\Delta x_{I+1/2}}{v\Delta t_{k+1}}\left(\phi_{I+1/2}^{k+1}-\phi_{I+1/2}^{k}\right)+\left(\frac{D_I}{\Delta x_I}\right)\left(\phi_{I+1/2}^{k}-\phi_{I-1/2}^{k}\right)+\left(\Sigma_{a,I+1/2}\Delta x_{I+1/2}\right)\phi_{I+1/2}^{k+1}$$
$$=\Delta x_{I+1/2}Q_{I+1/2}^{k+1},\qquad \text{right reflecting boundary}, \quad (2.85d)$$

$$\frac{\Delta x_{I+1/2}}{v\Delta t_{k+1}}\left(\phi_{I+1/2}^{k+1}-\phi_{I+1/2}^{k}\right)+\left(\frac{1}{2}\phi_{I+1/2}^{k}-2J_R^{b,k}\right)+\left(\frac{D_I}{\Delta x_I}\right)\left(\phi_{I+1/2}^{k}-\phi_{I-1/2}^{k}\right)$$
$$+\left(\Sigma_{a,I+1/2}\Delta x_{I+1/2}\right)\phi_{I+1/2}^{k+1}=\Delta x_{I+1/2}Q_{I+1/2}^{k+1},$$
$$\text{right incident boundary}. \quad (2.85e)$$

To define the SBJ diffusion method, we alter Eqs. (2.85) such that the central point in the leakage stencil is evaluated implicitly, i.e., at time t_{k+1}, as shown in Figure 2.11. Therefore,

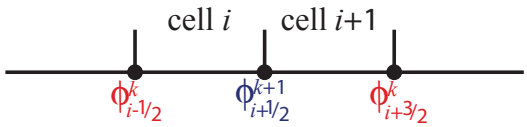

Figure 2.11 SBJ Diffusion Stencil in the Interior

the SBJ diffusion equations in the interior and with reflecting boundaries are

$$\frac{\Delta x_{1/2}}{v\Delta t_{k+1}}\left(\phi_{1/2}^{k+1}-\phi_{1/2}^{k}\right)-\left(\frac{D_1}{\Delta x_1}\right)\left(\phi_{3/2}^{k}-\phi_{1/2}^{k+1}\right)+\left(\Sigma_{a,1/2}\Delta x_{1/2}\right)\phi_{1/2}^{k+1}=\Delta x_{1/2}Q_{1/2}^{k+1},$$
$$\text{left reflecting boundary}, \quad (2.86a)$$

$$\frac{\Delta x_{i+1/2}}{v\Delta t_{k+1}}\left(\phi_{i+1/2}^{k+1}-\phi_{i+1/2}^{k}\right)-\left(\frac{D_{i+1}}{\Delta x_{i+1}}\right)\left(\phi_{i+3/2}^{k}-\phi_{i+1/2}^{k+1}\right)+\left(\frac{D_i}{\Delta x_i}\right)\left(\phi_{i+1/2}^{k+1}-\phi_{i-1/2}^{k}\right)$$
$$+\left(\Sigma_{a,i+1/2}\Delta x_{i+1/2}\right)\phi_{i+1/2}^{k+1}=\Delta x_{i+1/2}Q_{i+1/2}^{k+1},\qquad \text{interior}, \quad (2.86b)$$

$$\frac{\Delta x_{I+1/2}}{v\Delta t_{k+1}}\left(\phi_{I+1/2}^{k+1}-\phi_{I+1/2}^{k}\right)+\left(\frac{D_I}{\Delta x_I}\right)\left(\phi_{I+1/2}^{k+1}-\phi_{I-1/2}^{k}\right)+\left(\Sigma_{a,I+1/2}\Delta x_{I+1/2}\right)\phi_{I+1/2}^{k+1}$$
$$=\Delta x_{I+1/2}Q_{I+1/2}^{k+1},\qquad \text{right reflecting boundary}. \quad (2.86c)$$

Inspection of these equations shows that they have retained the locality of the fully-explicit and semi-explicit methods. For incident boundary conditions, we evaluate the two scalar

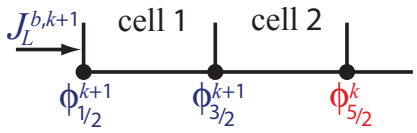

Figure 2.12 SBJ Diffusion Stencil for an Incident Boundary on the Left

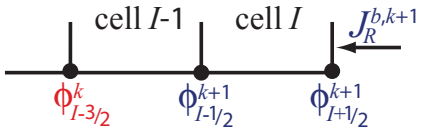

Figure 2.13 SBJ Diffusion Stencil for an Incident Boundary on the Right

fluxes adjacent to the boundary, as well as the boundary condition, at time t_{k+1}, as shown in Figures 2.12 and 2.13. Although this violates locality on the boundary, the violation has a minimal effect on the parallel scalability of the method. We use this stencil to be consistent with the SBJ transport method that we will derive in Chapter 3. Therefore, the SBJ diffusion equations on the left boundary with an incident boundary condition are

$$\frac{\Delta x_{1/2}}{v\Delta t_{k+1}}\left(\phi_{1/2}^{k+1}-\phi_{1/2}^{k}\right)-\left(\frac{D_1}{\Delta x_1}\right)\left(\phi_{3/2}^{k+1}-\phi_{1/2}^{k+1}\right)-\left(2J_L^{b,k+1}-\frac{1}{2}\phi_{1/2}^{k+1}\right)+\left(\Sigma_{a,1/2}\Delta x_{1/2}\right)\phi_{1/2}^{k+1}=\Delta x_{1/2}Q_{1/2}^{k+1}, \quad (2.87a)$$

$$\frac{\Delta x_{3/2}}{v\Delta t_{k+1}}\left(\phi_{3/2}^{k+1}-\phi_{3/2}^{k}\right)-\left(\frac{D_2}{\Delta x_2}\right)\left(\phi_{5/2}^{k}-\phi_{3/2}^{k+1}\right)+\left(\frac{D_1}{\Delta x_1}\right)\left(\phi_{3/2}^{k+1}-\phi_{1/2}^{k+1}\right)+\left(\Sigma_{a,3/2}\Delta x_{3/2}\right)\phi_{3/2}^{k+1}=\Delta x_{3/2}Q_{3/2}^{k+1}, \quad (2.87b)$$

and for the right incident boundary, we have

$$\frac{\Delta x_{I-1/2}}{v\Delta t_{k+1}}\left(\phi_{I-1/2}^{k+1}-\phi_{I-1/2}^{k}\right)-\left(\frac{D_I}{\Delta x_I}\right)\left(\phi_{I+1/2}^{k+1}-\phi_{I-1/2}^{k+1}\right)+\left(\frac{D_{I-1}}{\Delta x_{I-1}}\right)\left(\phi_{I-1/2}^{k+1}-\phi_{I-3/2}^{k}\right)+\left(\Sigma_{a,I-1/2}\Delta x_{I-1/2}\right)\phi_{I-1/2}^{k+1}=\Delta x_{I-1/2}Q_{I-1/2}^{k+1}, \quad (2.88a)$$

$$\frac{\Delta x_{I+1/2}}{v\Delta t_{k+1}}\left(\phi_{I+1/2}^{k+1}-\phi_{I+1/2}^{k}\right)+\left(\frac{1}{2}\phi_{I+1/2}^{k+1}-2J_R^{b,k+1}\right)+\left(\frac{D_I}{\Delta x_I}\right)\left(\phi_{I+1/2}^{k+1}-\phi_{I-1/2}^{k+1}\right)+\left(\Sigma_{a,I+1/2}\Delta x_{I+1/2}\right)\phi_{I+1/2}^{k+1}=\Delta x_{I+1/2}Q_{I+1/2}^{k+1}. \quad (2.88b)$$

The SBJ diffusion equations have retained the locality of the fully-explicit and semi-explicit methods, except on the boundaries, where we have compromised locality for consistency with SBJ transport. Indeed, this method is as "implicit" as a first-order diffusion discretization can be while still maintaining locality. If this method also possesses unconditional stability, then it will be a diffusion discretization that has both unconditional stability and locality. If it does not, then it is not possible to construct a first-order diffusion

discretization that possesses both unconditional stability and locality.

2.4.1 Stability Analysis of the SBJ Diffusion Method

As with the previous stability analyses, we consider the domain interior and a homogeneous material with diffusion coefficient D and absorption cross section Σ_a, a uniform mesh with zone length Δx, and no source. The SBJ diffusion equation can then be written as

$$\frac{\Delta x}{v\Delta t_{k+1}}\left(\phi_{i+1/2}^{k+1}-\phi_{i+1/2}^{k}\right)-\frac{D}{\Delta x}\left(\phi_{i+3/2}^{k}-2\phi_{i+1/2}^{k+1}+\phi_{i-1/2}^{k}\right)+\left(\Sigma_a\Delta x\right)\phi_{i+1/2}^{k+1}=0\,. \quad (2.89)$$

Substituting in the Fourier ansatz

$$\phi_{i+1/2}^{k}=\rho^k e^{\mathrm{i}\lambda x_{i+1/2}}\,, \quad (2.90)$$

we find

$$\frac{\Delta x}{v\Delta t_{k+1}}\left(\rho^{k+1}e^{\mathrm{i}\lambda x_{i+1/2}}-\rho^k e^{\mathrm{i}\lambda x_{i+1/2}}\right)-\frac{D}{\Delta x}\left(\rho^k e^{\mathrm{i}\lambda x_{i+3/2}}-2\rho^{k+1}e^{\mathrm{i}\lambda x_{i+1/2}}+\rho^k e^{\mathrm{i}\lambda x_{i-1/2}}\right)$$
$$+\left(\Sigma_a\Delta x\right)\rho^{k+1}e^{\mathrm{i}\lambda x_{i+1/2}}=0\,. \quad (2.91)$$

Dividing by $\rho^k e^{\mathrm{i}\lambda x_{i+1/2}}$, we obtain

$$\frac{\Delta x}{v\Delta t_{k+1}}\left(\rho-1\right)-\frac{D}{\Delta x}\left(e^{\mathrm{i}\lambda\Delta x}-2\rho+e^{-\mathrm{i}\lambda\Delta x}\right)+\left(\Sigma_a\Delta x\right)\rho=0\,. \quad (2.92)$$

Using

$$\cos(\lambda\Delta x)=\frac{e^{\mathrm{i}\lambda\Delta x}+e^{-\mathrm{i}\lambda\Delta x}}{2}\,, \quad (2.93)$$

we have

$$\frac{\Delta x}{v\Delta t_{k+1}}\left[\rho-1\right]-\frac{2D}{\Delta x}\left[\cos(\lambda\Delta x)-\rho\right]+\left[\Sigma_a\Delta x\right]\rho=0\,. \quad (2.94)$$

Solving for ρ, we obtain

$$\rho=\frac{(\Delta x)^2+2Dv\Delta t_{k+1}\cos(\lambda\Delta x)}{(\Delta x)^2\left(1+\Sigma_a v\Delta t_{k+1}\right)+2Dv\Delta t_{k+1}}\,. \quad (2.95)$$

Examining Eq. (2.95) we can see that $|\rho|\leq 1$ for all λ. Therefore, the SBJ diffusion method is unconditionally stable. However, according to Eq. (2.95), the method can become

oscillatory ($\rho < 0$) when

$$\Delta t_{k+1} > \frac{(\Delta x)^2}{2Dv}. \tag{2.96}$$

However, we can easily prove that this is not correct. Rearranging Eq. (2.89), we find

$$\left(\frac{\Delta x}{v\Delta t_{k+1}} + \frac{2D}{\Delta x} + \Sigma_a \Delta x\right) \phi_{i+1/2}^{k+1} = \left(\frac{\Delta x}{v\Delta t_{k+1}}\right) \phi_{i+1/2}^{k} + \frac{D}{\Delta x}\left(\phi_{i+3/2}^{k} + \phi_{i-1/2}^{k}\right). \tag{2.97}$$

Examining Eq. (2.97), and assuming physically permissible material properties and cell widths, we see that if the scalar flux at time t_k is non-negative, then the scalar flux at time t_{k+1} must be non-negative as well. Therefore, the method cannot be oscillatory. The discrepancy in the stability analysis is due to the Fourier ansatz being under-constrained. For the SBJ diffusion method, ρ may not be negative. Therefore, the SBJ diffusion method is both unconditionally stable and non-oscillatory.

Consider the same problem used to examine the stability of the implicit, fully-explicit, and semi-explicit methods, with a slab 1 cm thick divided into ten cells of equal length, filled with a homogeneous material with $\Sigma_a = 1$ cm^{-1} and $D = \frac{1}{3}$ cm, and particle velocity of $v = 1$ cm/s, with an incident partial current of $J_L^{b,k+1} = 10$ cm^{-2} s^{-1} on the left boundary and a vacuum on the right boundary. Running ten time steps of length $\Delta t = 1$ s, we find the results shown in Figure 2.14.

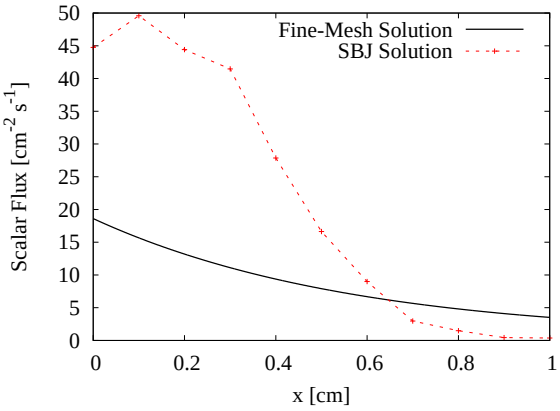

Figure 2.14 Stable Staggered-Block Jacobi Solution

Clearly, the SBJ diffusion result shown in Figure 2.14 is stable and non-oscillatory. However, it is not very accurate. Acquiring both locality and stability has come at the cost of accuracy. There is an additional drawback to the SBJ diffusion method—loss of particle

conservation. Consider again the SBJ diffusion equation in the interior:

$$\frac{\Delta x_{i+1/2}}{v\Delta t_{k+1}}\left(\phi_{i+1/2}^{k+1}-\phi_{i+1/2}^{k}\right)-\left(\frac{D_{i+1}}{\Delta x_{i+1}}\right)\left(\phi_{i+3/2}^{k}-\phi_{i+1/2}^{k+1}\right)+\left(\frac{D_i}{\Delta x_i}\right)\left(\phi_{i+1/2}^{k+1}-\phi_{i-1/2}^{k}\right)$$
$$+\left(\Sigma_{a,i+1/2}\Delta x_{i+1/2}\right)\phi_{i+1/2}^{k+1}=\Delta x_{i+1/2}Q_{i+1/2}^{k+1}. \quad (2.98)$$

Examining the leakage stencil (the second and third terms) in Eq. (2.98), we see that the central point of the stencil is evaluated at time t_{k+1} while the exterior points in the stencil are evaluated at time t_k. It is these terms that separate the SBJ diffusion method from the semi-explicit method shown in Section 2.3, and it is these terms that enables this method to have both locality and unconditional stability. However, because the scalar fluxes in these terms are not evaluated all at the same point in time, particles are no longer conserved. It is possible to restore *domain-wise* particle conservation (but not *cell-wise* conservation) using a rebalance method. It is also possible to improve the accuracy of the method using iterations. We discuss these topics next.

2.4.2 Restoring Particle Conservation for the SBJ Diffusion Equations

To derive a particle conservation rebalance factor, we consider the diffusion balance equation:

$$\frac{1}{v}\frac{\partial}{\partial t}\phi(x,t)+\frac{\partial}{\partial x}J(x,t)+\Sigma_a(x)\phi(x,t)=Q(x,t). \quad (2.99)$$

Operating by $\frac{1}{\Delta t_{k+1}}\int_{t_k}^{t_{k+1}}(\cdot)\,\mathrm{d}t$ and defining

$$\bar{\phi}^{k+1}(x)=\frac{1}{\Delta t_{k+1}}\int_{t_k}^{t_{k+1}}\phi(x,t)\,\mathrm{d}t, \quad (2.100a)$$

$$\bar{J}^{k+1}(x)=\frac{1}{\Delta t_{k+1}}\int_{t_k}^{t_{k+1}}J(x,t)\,\mathrm{d}t, \quad (2.100b)$$

and

$$Q^{k+1}(x)=\frac{1}{\Delta t_{k+1}}\int_{t_k}^{t_{k+1}}Q(x,t)\,\mathrm{d}t, \quad (2.100c)$$

we obtain

$$\frac{1}{v\Delta t_{k+1}}\left[\phi^{k+1}(x)-\phi^{k}(x)\right]+\frac{\mathrm{d}}{\mathrm{d}x}\bar{J}^{k+1}(x)+\Sigma_a(x)\bar{\phi}^{k+1}(x)=Q^{k+1}(x). \quad (2.101)$$

Then, integrating over the spatial domain by operating on Eq. (2.101) by $\int_0^X (\cdot)\,\mathrm{d}x$, and splitting the currents into incident and outgoing partial currents, we obtain

$$\frac{1}{v\Delta t_{k+1}}\left[\int_0^X \phi^{k+1}(x)\,\mathrm{d}x - \int_0^X \phi^{k}(x)\,\mathrm{d}x\right] + \left[\left(\bar{J}_R^{out,k+1} - \bar{J}_R^{b,k+1}\right) - \left(\bar{J}_L^{b,k+1} - \bar{J}_L^{out,k+1}\right)\right] + \int_0^X \Sigma_a(x)\bar{\phi}^{k+1}(x)\,\mathrm{d}x = \int_0^X Q^{k+1}(x)\,\mathrm{d}x, \quad (2.102)$$

where $\bar{J}_L^{out,k+1}$ and $\bar{J}_R^{out,k+1}$ are the time-averaged outgoing partial currents for the left and right boundaries, respectively, and $\bar{J}_L^{b,k+1}$ and $\bar{J}_R^{b,k+1}$ are the time-averaged incoming partial currents for the left and right boundaries, respectively. We treat the time-averaged scalar flux and partial current terms implicitly by evaluating them at time t_{k+1}:

$$\frac{1}{v\Delta t_{k+1}}\left[\int_0^X \phi^{k+1}(x)\,\mathrm{d}x - \int_0^X \phi^{k}(x)\,\mathrm{d}x\right] + \left[\left(J_R^{out,k+1} - J_R^{b,k+1}\right) - \left(J_L^{b,k+1} - J_L^{out,k+1}\right)\right] + \int_0^X \Sigma_a(x)\phi^{k+1}(x)\,\mathrm{d}x = \int_0^X Q^{k+1}(x)\,\mathrm{d}x. \quad (2.103)$$

The scalar flux, incident particle currents, and outgoing particle currents in Eq. (2.103) conserve particles because they satisfy the balance equation. Assuming that the scalar flux at time t_k and the incident partial currents satisfy particle conservation, we can define the conservative scalar flux at time t_{k+1} and the conservative outgoing partial currents in terms of the non-conservative quantities and a *rebalance factor* γ^{k+1}. Therefore, we define

$$\phi^{k+1}(x) = \gamma^{k+1}\phi^{nc,k+1}(x), \quad (2.104a)$$

$$J_L^{out,k+1} = \gamma^{k+1}J_L^{nc,out,k+1}, \quad (2.104b)$$

$$J_R^{out,k+1} = \gamma^{k+1}J_R^{nc,out,k+1}, \quad (2.104c)$$

where $\phi^{nc,k+1}(x)$, $J_L^{nc,out,k+1}$, and $J_R^{nc,out,k+1}$ are the non-conservative scalar flux, non-conservative outgoing partial current on the left boundary, and non-conservative outgoing partial current on the right boundary, respectively. Substituting Eqs. (2.104) into Eq. (2.103),

we find

$$\frac{1}{v\Delta t_{k+1}}\left[\gamma^{k+1}\int_0^X \phi^{nc,k+1}(x)\,\mathrm{d}x - \int_0^X \phi^{k}(x)\,\mathrm{d}x\right] + \left[\left(\gamma^{k+1}J_R^{nc,out,k+1} - J_R^{b,k+1}\right) - \left(J_L^{b,k+1} - \gamma^{k+1}J_L^{nc,out,k+1}\right)\right] + \gamma^{k+1}\int_0^X \Sigma_a(x)\phi^{nc,k+1}(x)\,\mathrm{d}x = \int_0^X Q^{k+1}(x)\,\mathrm{d}x. \quad (2.105)$$

Finally, we approximate the spatial integrals using sums over the spatial domain. Now Eq. (2.105) is written

$$\frac{1}{v\Delta t_{k+1}}\left[\gamma^{k+1}\sum_{i=0}^{I}\phi_{i+1/2}^{nc,k+1}\Delta x_{i+1/2} - \sum_{i=0}^{I}\phi_{i+1/2}^{k}\Delta x_{i+1/2}\right] + \left[\left(\gamma^{k+1}J_R^{nc,out,k+1} - J_R^{b,k+1}\right) - \left(J_L^{b,k+1} - \gamma^{k+1}J_L^{nc,out,k+1}\right)\right] + \gamma^{k+1}\sum_{i=0}^{I}\Sigma_{a,i+1/2}\phi_{i+1/2}^{nc,k+1}\Delta x_{i+1/2} = \sum_{i=0}^{I}Q_{i+1/2}^{k+1}\Delta x_{i+1/2}. \quad (2.106)$$

Solving for γ^{k+1}, we obtain

$$\gamma^{k+1} = \frac{A_\gamma^{k+1}}{B_\gamma^{k+1}}, \quad (2.107)$$

where

$$A_\gamma^{k+1} = \frac{1}{v\Delta t_{k+1}}\sum_{i=0}^{I}\phi_{i+1/2}^{k}\Delta x_{i+1/2} + \left(J_L^{b,k+1} + J_R^{b,k+1}\right) + \sum_{i=0}^{I}Q_{i+1/2}^{k+1}\Delta x_{i+1/2}, \quad (2.108a)$$

and

$$B_\gamma^{k+1} = \frac{1}{v\Delta t_{k+1}}\sum_{i=0}^{I}\phi_{i+1/2}^{nc,k+1}\Delta x_{i+1/2} + \left(J_L^{nc,out,k+1} + J_R^{nc,out,k+1}\right) + \sum_{i=0}^{I}\Sigma_{a,i+1/2}\phi_{i+1/2}^{nc,k+1}\Delta x_{i+1/2}. \quad (2.108b)$$

To conserve particles on the problem domain, γ^{k+1} is calculated at the end of each time step, and the scalar flux is scaled by γ^{k+1} at each grid point. We have not observed any loss of stability when using this rebalance method. In the numerical results we present in Section 2.5, we refer to the SBJ diffusion method without particle conservation as plain SBJ, and to the SBJ diffusion method with particle conservation as conservative SBJ.

2.4.3 Improving the Accuracy of SBJ Diffusion Using Iterations

The accuracy of the SBJ diffusion method can be improved by using iterations. By iterating on the scalar flux values lagged to time t_k in the leakage stencil, the SBJ diffusion method can be converged to the solution given by the implicit method. Iterations can also be used if cell-wise particle conservation is desired, since the implicit solution conserves particles in each cell. Writing the iterative SBJ diffusion equations, we have

$$\frac{\Delta x_{1/2}}{v\Delta t_{k+1}}\left(\phi_{1/2}^{(l+1),k+1}-\phi_{1/2}^{k}\right)-\left(\frac{D_1}{\Delta x_1}\right)\left(\phi_{3/2}^{(l),k+1}-\phi_{1/2}^{(l+1),k+1}\right) + \left(\Sigma_{a,1/2}\Delta x_{1/2}\right)\phi_{1/2}^{(l+1),k+1}=\Delta x_{1/2}Q_{1/2}^{k+1}\,,$$

left reflecting boundary, (2.109a)

$$\frac{\Delta x_{1/2}}{v\Delta t_{k+1}}\left(\phi_{1/2}^{(l+1),k+1}-\phi_{1/2}^{k}\right)-\left(\frac{D_1}{\Delta x_1}\right)\left(\phi_{3/2}^{(l+1),k+1}-\phi_{1/2}^{(l+1),k+1}\right) - \left(2J_L^{b,k+1}-\frac{1}{2}\phi_{1/2}^{(l+1),k+1}\right)+\left(\Sigma_{a,1/2}\Delta x_{1/2}\right)\phi_{1/2}^{(l+1),k+1}=\Delta x_{1/2}Q_{1/2}^{k+1}\,,$$

left incident boundary, (2.109b)

$$\frac{\Delta x_{3/2}}{v\Delta t_{k+1}}\left(\phi_{3/2}^{(l+1),k+1}-\phi_{3/2}^{k}\right)-\left(\frac{D_2}{\Delta x_2}\right)\left(\phi_{5/2}^{(l),k+1}-\phi_{3/2}^{(l+1),k+1}\right) + \left(\frac{D_1}{\Delta x_1}\right)\left(\phi_{3/2}^{(l+1),k+1}-\phi_{1/2}^{(l+1),k+1}\right)+\left(\Sigma_{a,3/2}\Delta x_{3/2}\right)\phi_{3/2}^{(l+1),k+1}=\Delta x_{3/2}Q_{1/2}^{k+1}\,,$$

left incident boundary, (2.109c)

$$\frac{\Delta x_{i+1/2}}{v\Delta t_{k+1}}\left(\phi_{i+1/2}^{(l+1),k+1}-\phi_{i+1/2}^{k}\right)-\left(\frac{D_{i+1}}{\Delta x_{i+1}}\right)\left(\phi_{i+3/2}^{(l),k+1}-\phi_{i+1/2}^{(l+1),k+1}\right) + \left(\frac{D_i}{\Delta x_i}\right)\left(\phi_{i+1/2}^{(l+1),k+1}-\phi_{i-1/2}^{(l),k+1}\right)+\left(\Sigma_{a,i+1/2}\Delta x_{i+1/2}\right)\phi_{i+1/2}^{(l+1),k+1}=\Delta x_{i+1/2}Q_{i+1/2}^{k+1}\,,$$

interior, (2.109d)

$$\frac{\Delta x_{I-1/2}}{v\Delta t_{k+1}}\left(\phi_{I-1/2}^{(l+1),k+1}-\phi_{I-1/2}^{k}\right)-\left(\frac{D_I}{\Delta x_I}\right)\left(\phi_{I+1/2}^{(l+1),k+1}-\phi_{I-1/2}^{(l+1),k+1}\right) + \left(\frac{D_{I-1}}{\Delta x_{I-1}}\right)\left(\phi_{I-1/2}^{(l+1),k+1}-\phi_{I-3/2}^{(l),k+1}\right)+\left(\Sigma_{a,I-1/2}\Delta x_{I-1/2}\right)\phi_{I-1/2}^{(l+1),k+1}=\Delta x_{I-1/2}Q_{I-1/2}^{k+1}\,,$$

right incident boundary, (2.109e)

$$\frac{\Delta x_{I+1/2}}{v\Delta t_{k+1}}\left(\phi_{I+1/2}^{(l+1),k+1}-\phi_{I+1/2}^{k}\right)+\left(\frac{1}{2}\phi_{I+1/2}^{(l+1),k+1}-2J_{R}^{b,k+1}\right)$$
$$+\left(\frac{D_I}{\Delta x_I}\right)\left(\phi_{I+1/2}^{(l+1),k+1}-\phi_{I-1/2}^{(l+1),k+1}\right)+\left(\Sigma_{a,I+1/2}\Delta x_{I+1/2}\right)\phi_{I+1/2}^{(l+1),k+1}=\Delta x_{I+1/2}Q_{I+1/2}^{k+1},$$

right incident boundary, (2.109f)

$$\frac{\Delta x_{I+1/2}}{v\Delta t_{k+1}}\left(\phi_{I+1/2}^{(l+1),k+1}-\phi_{I+1/2}^{k}\right)+\left(\frac{D_I}{\Delta x_I}\right)\left(\phi_{I+1/2}^{(l+1),k+1}-\phi_{I-1/2}^{(l),k+1}\right)$$
$$+\left(\Sigma_{a,I+1/2}\Delta x_{I+1/2}\right)\phi_{I+1/2}^{(l+1),k+1}=\Delta x_{I+1/2}Q_{I+1/2}^{k+1},$$

right reflecting boundary, (2.109g)

where l is the iteration index. The iterative scheme at a given time step is started by setting

$$\phi_{i+1/2}^{(0),k+1}=\phi_{i+1/2}^{k}. \tag{2.110}$$

Previously, we noted that local methods will advance particles one cell per time step. With the iteration method outlined here, particles may now advance one cell per iteration, thereby allowing the SBJ diffusion method to calculate accurate solutions to optically-thin problems with large time steps, although a large number of iterations may be required for such problems.

We have found that the most effective iteration procedure calculates and applies the rebalance factor that we derived in the previous section after each iteration. Therefore, the stated rebalance procedure not only maintains particle balance, but doubles as an acceleration method as well. For the numerical results presented in Section 2.5, we use the L_∞ error norm to choose when to cease iterations. However, as will be seen in the numerical results, false convergence becomes a concern in optically-thin problems where all of the zones are tightly coupled. Therefore, we protect against false convergence [2] by converging to

$$E_{L_\infty}^{(l+1),k+1}\leq\varepsilon_{L_\infty}\left(1-\rho^{(l+1),k+1}\right), \tag{2.111}$$

where $E_{L_\infty}^{(l+1),k+1}$ is the L_∞ error norm

$$E_{L_\infty}^{(l+1),k+1}=\max_i\left|\phi_{i+1/2}^{(l+1),k+1}-\phi_{i+1/2}^{(l),k+1}\right|, \tag{2.112}$$

ε_{L_∞} is a user-specified convergence criteria, and $\rho^{(l+1),k+1}$ is an estimate of the spectral

radius:

$$\rho^{(l+1),k+1} = \frac{\max\limits_i \left| \phi_{i+1/2}^{(l+1),k+1} - \phi_{i+1/2}^{(l),k+1} \right|}{\max\limits_i \left| \phi_{i+1/2}^{(l),k+1} - \phi_{i+1/2}^{(l-1),k+1} \right|} = \frac{E_{L_\infty}^{(l+1),k+1}}{E_{L_\infty}^{(l),k+1}} . \tag{2.113}$$

2.5 Numerical Results

We now present numerical results for five problems, illustrating the new Staggered-Block Jacobi diffusion method in comparison to the fully-explicit, semi-explicit, and implicit methods. In Section 2.5.1, we present a spatially flat solution and demonstrate the effectiveness of the particle conservation and iteration schemes, as well as the convergence of the SBJ diffusion method to the exact solution. In Sections 2.5.2 and 2.5.3, we examine the SBJ diffusion method in thick and thin media, respectively. In Section 2.5.4 we examine the behavior of the SBJ diffusion method in a variety of optical thicknesses, and in Section 2.5.5 we examine the SBJ diffusion method in heterogeneous media.

2.5.1 Diffusion Problem 1

For the first numerical problem, we consider a simple, homogeneous slab 1 cm in width with reflecting boundary conditions. The material is a pure absorber with diffusion coefficient $D = \frac{1}{3}$ cm. We use a particle source of $Q = 1$ cm^{-3} s^{-1} everywhere in the slab and set the particle velocity at $v = 1$ cm/s. Beginning this problem with an initial scalar flux of zero, the analytic diffusion solution for this problem is

$$\phi(t) = \left(\frac{Q}{v\Sigma_a} \right) \left(1 - \mathrm{e}^{-v\Sigma_a t} \right) . \tag{2.114}$$

The analytic solution at times $t = 1$, 2, 5, and 10 s is shown in Figure 2.15. Breaking the slab into ten zones of equal width and running the problem with the implicit method and a time step length of $\Delta t = 1$ s, we find the solutions shown in Figure 2.16. We see that the implicit method produces results that agree reasonably well with the analytic results, especially at later times, even for this very coarse time step.

Running the problem with the plain SBJ diffusion method, without particle conservation or iterations, produces the results shown in Figure 2.17. Here we see that the results of plain

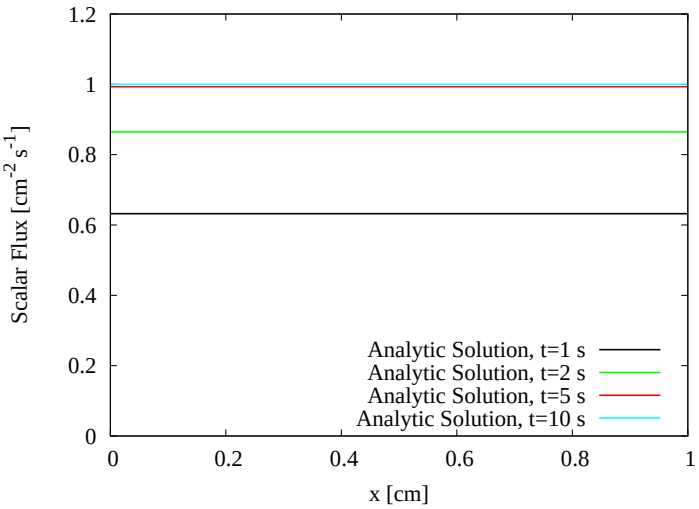

Figure 2.15 Diffusion Problem 1: Analytic Solution

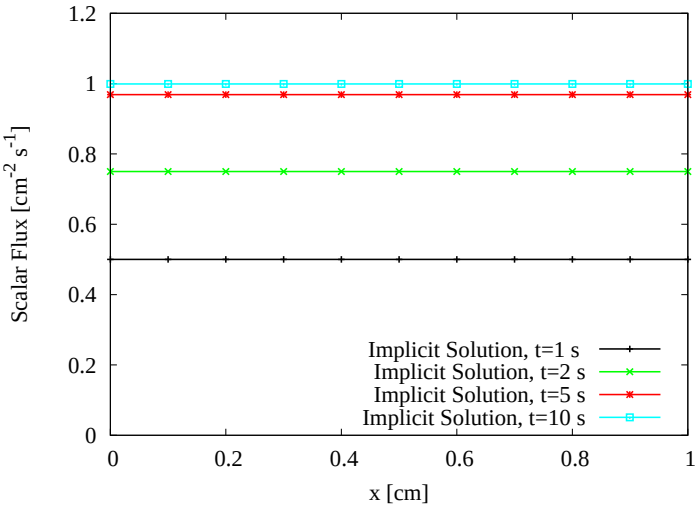

Figure 2.16 Diffusion Problem 1: Implicit Solution

SBJ are not accurate. Adding particle conservation improves the results significantly, to the point that they now match the implicit results; this is shown in Figure 2.18. We note, however, that this problem, because it is spatially flat, is particularly well-suited to a global rebalance. Such good results should not be expected with spatially-dependent solutions. We demonstrate the convergence of the iterative SBJ method (without rebalance) to the implicit results in Figure 2.19. Here, iterations were performed until the L_∞ norm converged to $\varepsilon_{L_\infty} = 10^{-6}$. To see the effectiveness of the iterations, we calculate the global, relative

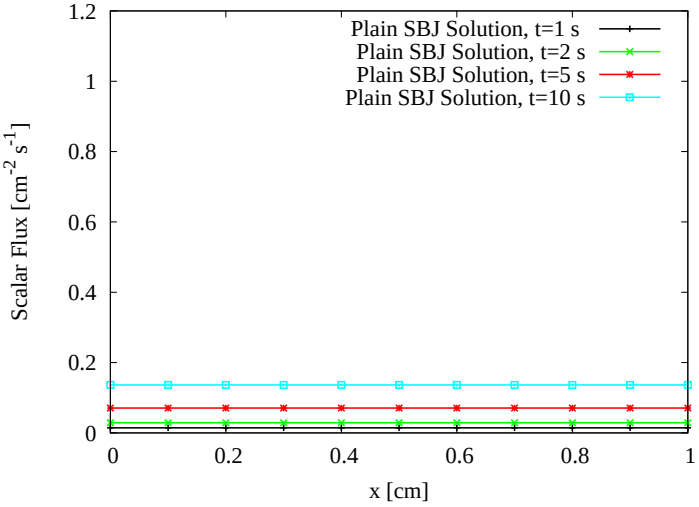

Figure 2.17 Diffusion Problem 1: Plain SBJ Solution

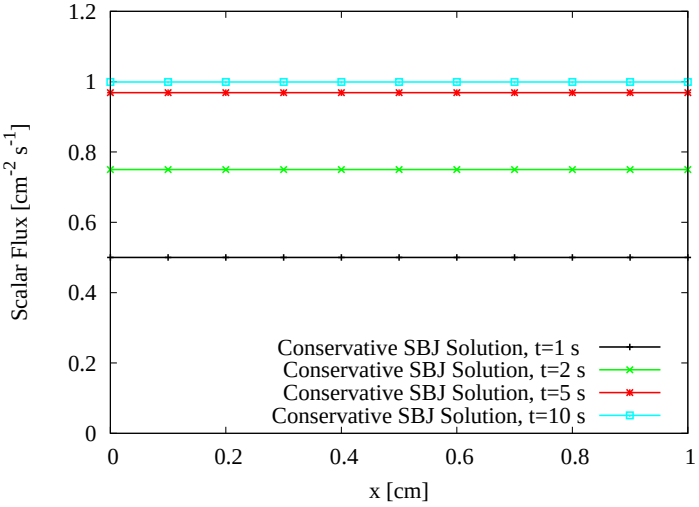

Figure 2.18 Diffusion Problem 1: SBJ Solution with Particle Conservation

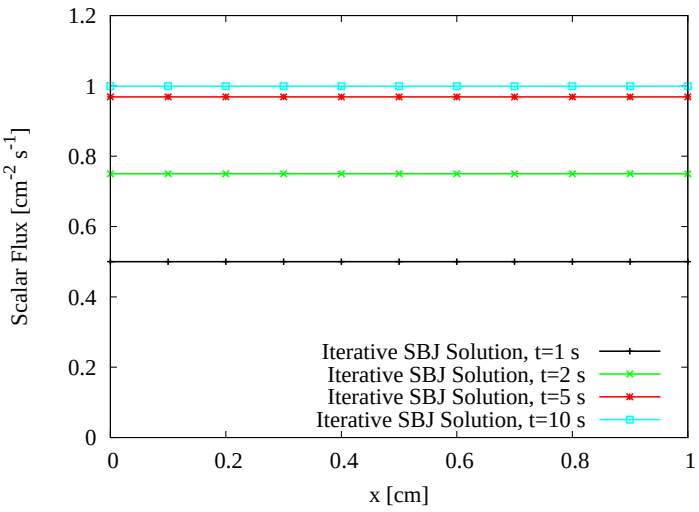

Figure 2.19 Diffusion Problem 1: SBJ Solution with Iterations

error versus the implicit result for a problem using

$$E = \frac{\sum_{i=0}^{I} \left| \frac{\phi_{i+1/2}^{\text{implicit}} - \phi_{i+1/2}^{SBJ}}{\phi_{i+1/2}^{\text{implicit}}} \right| \Delta x_{i+1/2}}{\sum_{i=0}^{I} \Delta x_{i+1/2}}. \tag{2.115}$$

In Figure 2.20, we see the global relative error for the SBJ diffusion solution versus the implicit solution for various numbers of iterations and at various simulation times, with a time step length of $\Delta t = 1$ s. We note that the solutions for $t = 5$ s and $t = 10$ s are superimposed.

Finally, we show how the SBJ diffusion method converges to the analytic solution as $\Delta t \to 0$. In Figure 2.21, we show the global relative error between the analytic solution and the implicit, fully-explicit, semi-explicit, and plain SBJ methods at $t = 1$ s for various time step lengths. We note that the solutions for the implicit, fully-explicit, and semi-explicit methods are superimposed for time step lengths of $\Delta t = 0.01$ s and smaller. Fully-explicit and semi-explicit solutions are not shown for $\Delta t = 1$ s because these methods are not stable for this time step length. We see that the SBJ diffusion method converges at the same rate (but with a larger constant) as the implicit, fully-explicit, and semi-explicit methods. The convergence is slightly slower in the $\Delta t = 1$ s to $\Delta t = 10^{-2}$ s range, likely because in this region the time step is too coarse to couple the zones together, and thus, the numerical

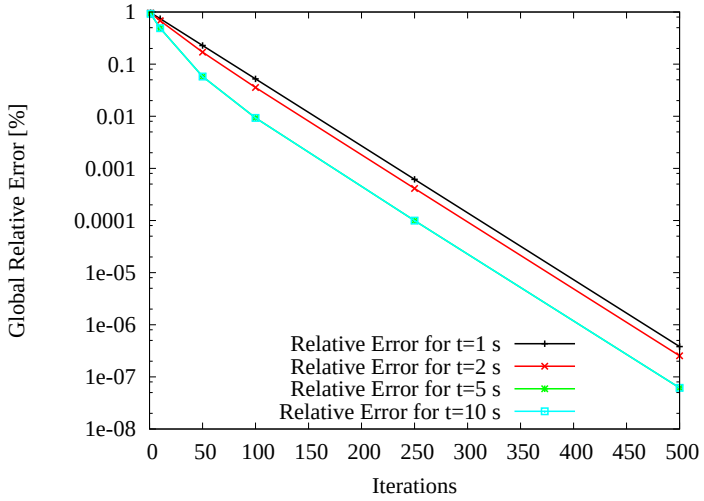

Figure 2.20 Diffusion Problem 1: Global Relative Error vs. Iterations

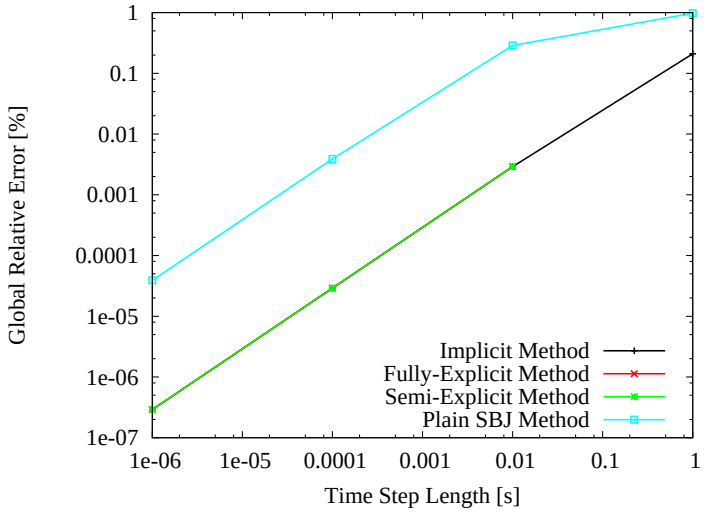

Figure 2.21 Diffusion Problem 1: Global Relative Error for Various Methods

solution is being solved in an inherently non-physical way. With smaller Δt, enough time steps elapse to more tightly couple the SBJ solution. The reason the SBJ solution (without particle conservation) is less accurate at every time step length is because of the inconsistent way that the SBJ method calculates the currents (with part of the current evaluated at time t_k and part at time t_{k+1}). Since the problem is spatially flat, the current should be zero everywhere, but because of this inconsistency, the current is not calculated to be zero for the SBJ diffusion method, as it is with the implicit, fully-explicit, and semi-explicit methods. Therefore, the SBJ diffusion method cannot be as accurate as these other methods without iterations. However, as we saw in Figure 2.18, rebalance can correct for these incorrect currents.

2.5.2 Diffusion Problem 2

We now test the SBJ diffusion method on a homogeneous, optically-thick problem. We consider a slab 1 cm wide, divided into 100 cells, filled with a purely scattering material with diffusion coefficient $D = \frac{1}{30{,}000}$ cm. With these properties, each cell is 100 mean-free paths thick. In the first cell we place a particle source of $Q = 1$ cm^{-3} s^{-1}, and no source elsewhere, and we use a particle velocity of $v = 1$ cm/s. The left boundary is reflecting, the right boundary is a vacuum, and the initial condition is zero everywhere. This problem was run for ten time steps with $\Delta t = 1$ s. A benchmark solution using $\Delta t = 10^{-8}$ s was also run. The results for the implicit, fully-explicit, and semi-explicit methods for the $x = [0,\ 0.1]$ region are shown in Figures 2.22, 2.23, and 2.24, respectively, and the results for the non-iterative SBJ diffusion method with and without particle conservation is shown in Figure 2.25.

In Appendix A.1, we derive a formula to estimate the location of the particle wave at a given time. For this problem, during the first time step, the particle wave advances $d_{RMS} = 0.0057735$ cm, or 0.57735 cell widths. Therefore, it is not surprising that the SBJ diffusion method is fairly accurate for this optically-thick problem, because in this problem the particle wave speed is slow and moves only a fraction of a cell width per time step. As a result, the "lagging" of the scalar fluxes on the outer points of the diffusion stencil is a reasonably good approximation, although the SBJ diffusion method is still not as accurate as the other methods. With iterations, we can converge the SBJ solution to the implicit solution. Figure 2.26 shows the number of iterations required to converge the SBJ solution to the implicit solution, with and without rebalance acceleration, and with $\varepsilon_{L_\infty} = 10^{-6}$.

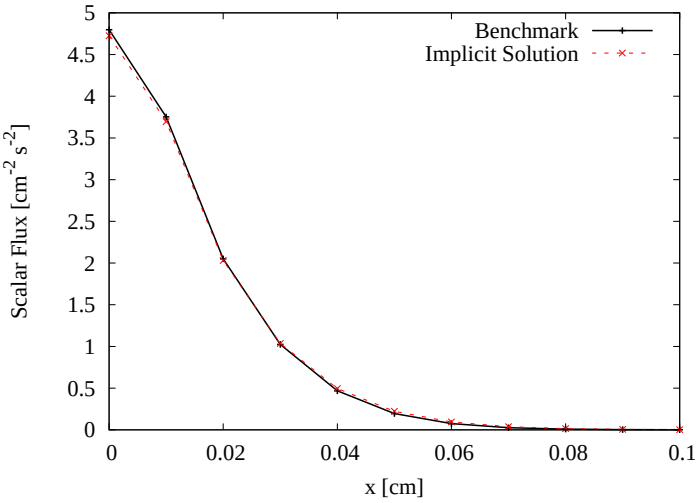

Figure 2.22 Diffusion Problem 2: Implicit Solution at $t = 10$ s

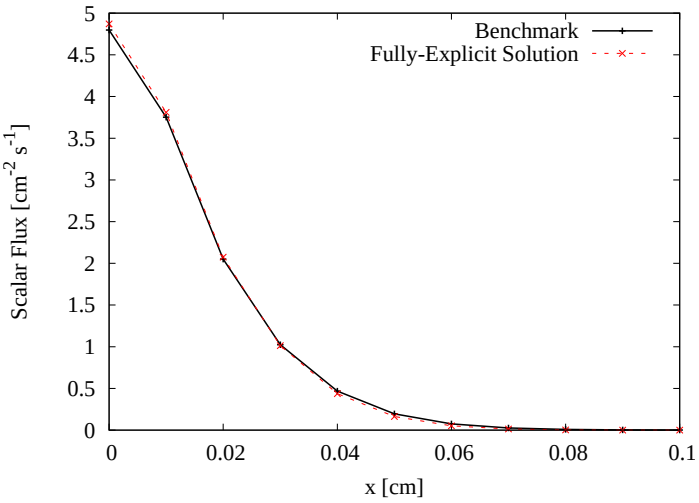

Figure 2.23 Diffusion Problem 2: Fully-Explicit Solution at $t = 10$ s

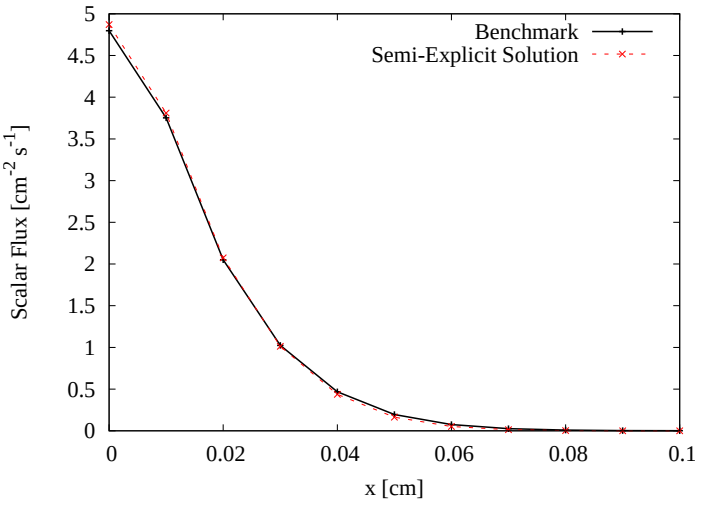

Figure 2.24 Diffusion Problem 2: Semi-Explicit Solution at $t = 10$ s

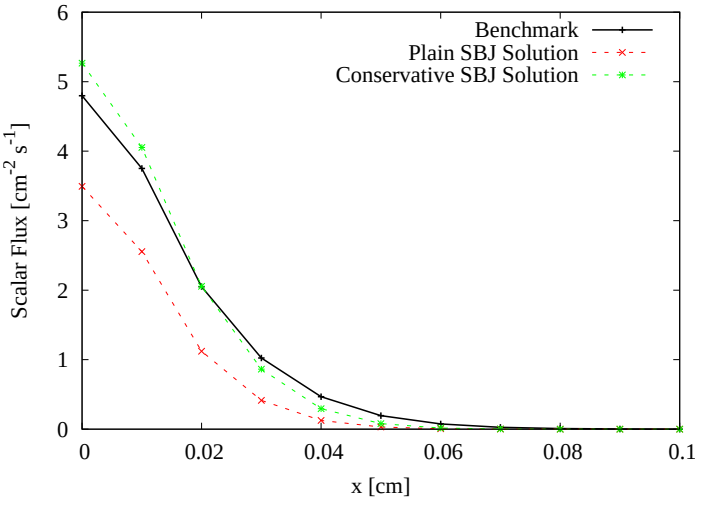

Figure 2.25 Diffusion Problem 2: SBJ Solutions at $t = 10$ s

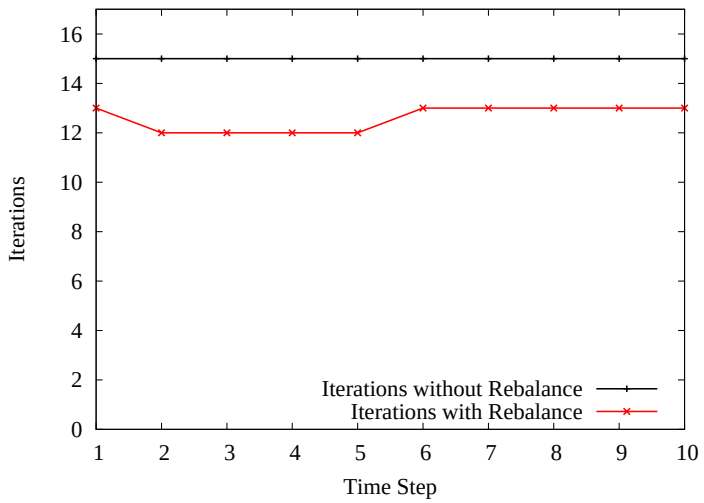

Figure 2.26 Diffusion Problem 2: Iterations Required for Convergence

2.5.3 Diffusion Problem 3

For the third test problem, we examine a homogeneous, optically-thin slab 1 cm wide, divided into 100 cells. The material is a pure scatterer with $D = \frac{1}{3}$ cm. A particle source of $Q = 10$ cm^{-3} s^{-1} is set in the first cell, with no source elsewhere. The left boundary is reflecting, the right boundary is a vacuum, the particle speed is set at $v = 1$ cm/s, and the initial condition is zero everywhere. We executed four time steps with $\Delta t = 0.25$ s. In Figure 2.27 we show the implicit solution and a benchmark solution that was run with a time step of $\Delta t = 2.5 \times 10^{-9}$ s. In Figure 2.28 we show the plain SBJ diffusion solution (which is zero almost everywhere, except near the left boundary), and in Figure 2.29 we show the conservative SBJ solution. We do not show a fully-explicit or semi-explicit solution for this problem because neither method is stable with the prescribed time step length.

We see that for optically-thin problems, the SBJ diffusion method is less accurate than before. Using the particle wave location equation from Appendix A.1, we find that during the first time step, the particle wave travels 0.288675 cm, or 28.8675 cell widths. Because the cells are optically-thin, they are more tightly coupled, and "local" methods, such as SBJ, are less accurate. We can also see that a global rebalance does not help make the solution more accurate, since the fundamental shape of the SBJ solution is incorrect. In Figure 2.30, we show the number of iterations required for the SBJ method to converge to the implicit solution, with and without rebalance, using $\varepsilon_{L_\infty} = 10^{-6}$. Optically-thin problems require many more iterations for convergence than optically-thick problems. However, rebalance acceleration has a major impact on the number of iterations required for this problem.

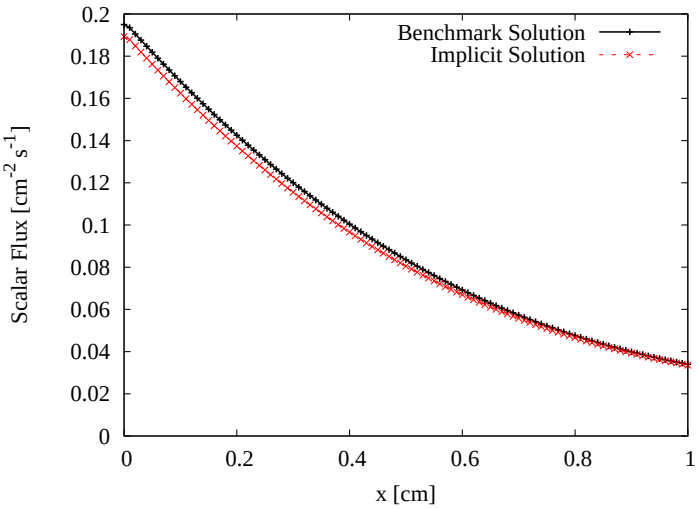

Figure 2.27 Diffusion Problem 3: Implicit Solution at $t = 1$ s

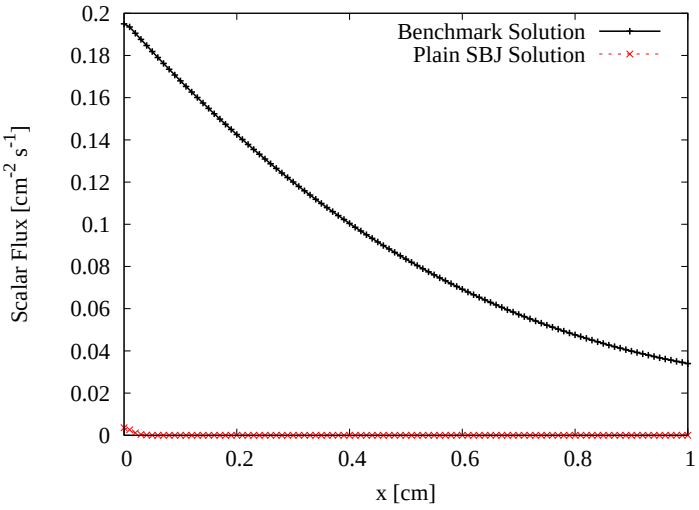

Figure 2.28 Diffusion Problem 3: Plain SBJ Solution at $t = 1$ s

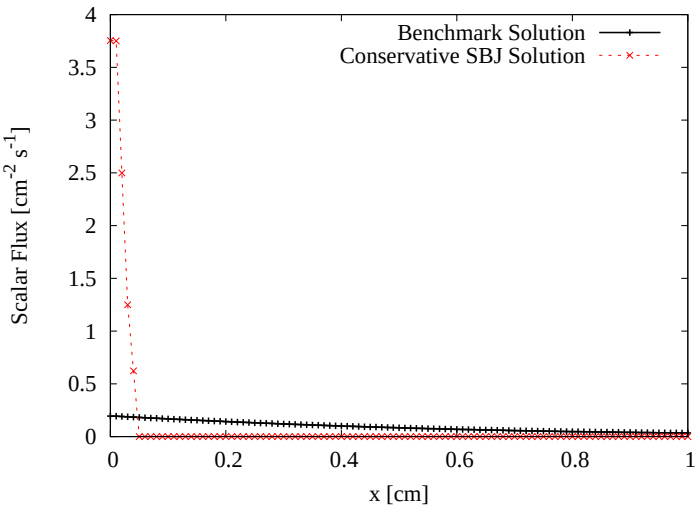

Figure 2.29 Diffusion Problem 3: Conservative SBJ Solution at $t = 1$ s

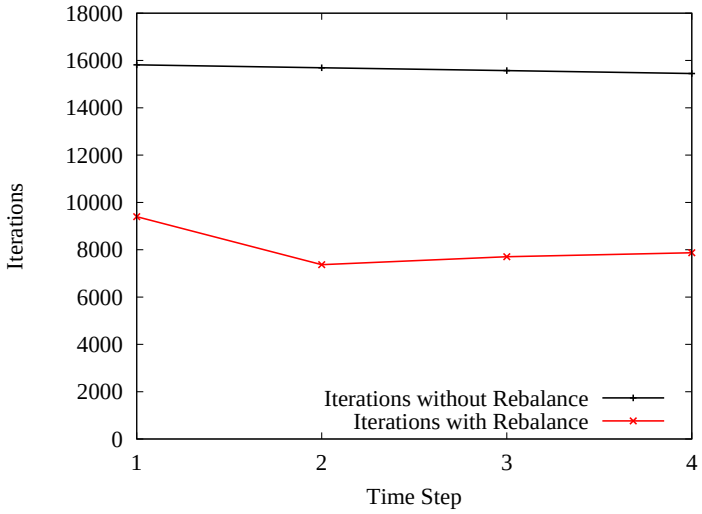

Figure 2.30 Diffusion Problem 3: Iterations for SBJ

2.5.4 Diffusion Problem 4

For the fourth numerical problem, we investigate how the SBJ diffusion method performs in systems with a variety of optical thicknesses. We now execute a series of problems, each on a slab 100 cm wide, divided into 100 cells. The material is purely scattering, with a total cross section of $\Sigma_t = 10^{\varepsilon}$ cm^{-1}, where ε varies from -3 to 3. We place a particle source of $Q = 10$ cm^{-3} s^{-1} in the first cell, and zero source elsewhere. The left boundary is reflecting, the right boundary is a vacuum, and the initial condition is zero everywhere. The particle velocity is set at $v = 1$ cm/s. We run ten time steps with $\Delta t = 1$ s. We also run a benchmark solution using the implicit method with a time step of $\Delta t = 10^{-8}$ s. We calculate the global relative L_1 error as

$$E_{L_1} = \frac{\sum_{i=0}^{I} \left| \phi_{i+1/2} - \phi_{i+1/2}^{benchmark} \right| \Delta x_{i+1/2}}{\sum_{i=0}^{I} \phi_{i+1/2}^{benchmark} \Delta x_{i+1/2}}. \tag{2.116}$$

Figure 2.31 shows the benchmark solutions on a semi-log plot. The optically-thin solutions are fairly flat, while the scalar flux in the optically-thick solutions decreases quickly. In

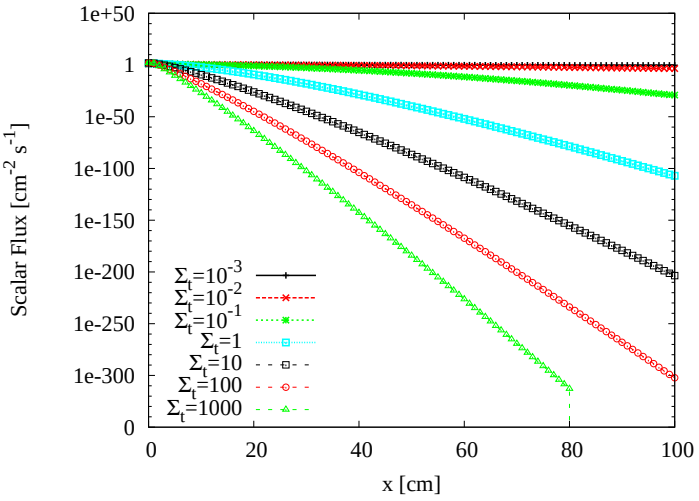

Figure 2.31 Diffusion Problem 4: Benchmark Solutions at $t = 10$ s

Figure 2.32 we show the errors for the implicit method at each optical thickness, and in Figure 2.33 we show the errors for the plain SBJ and conservative SBJ diffusion methods. In Figure 2.34 we show a close-up of the plain and conservative SBJ errors for the optically-thick problems. Here we see that the implicit method is quite accurate at all optical thicknesses. The SBJ diffusion method is inaccurate for optically-thin problems, and rebalance actually exacerbates the error in these problems. However, for optically-thick

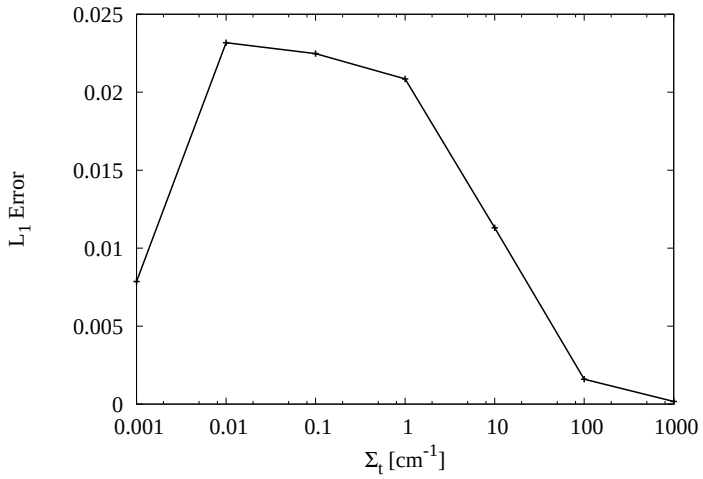

Figure 2.32 Diffusion Problem 4: Error in the Implicit Solutions

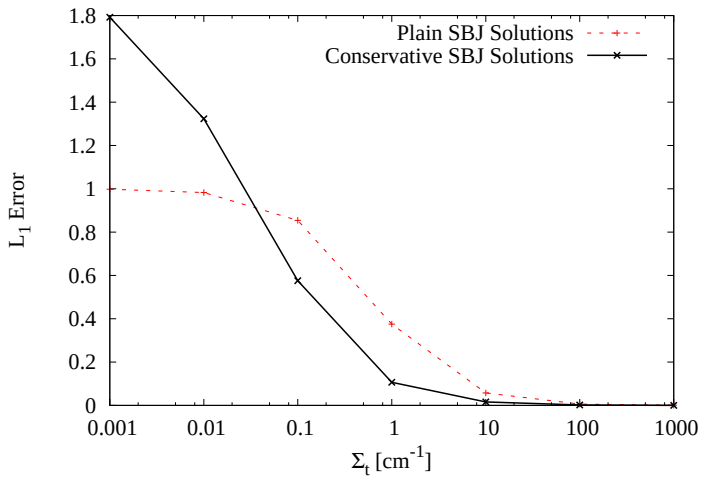

Figure 2.33 Diffusion Problem 4: Error in the Plain and Conservative SBJ Solutions

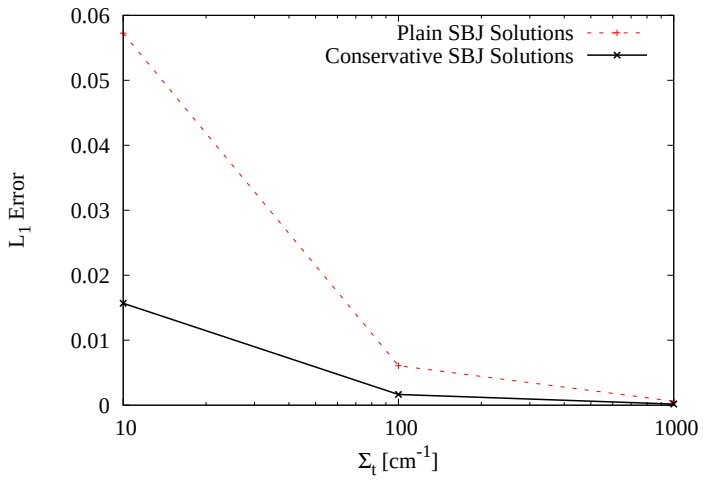

Figure 2.34 Diffusion Problem 4: Error in the SBJ Solutions for Optically-Thick Problems

problems, the SBJ diffusion method becomes fairly accurate, and particle conservation significantly improves the accuracy. The SBJ method with particle conservation is nearly as accurate as the implicit method for optically-thick problems.

Table 2.1 presents the distance the particle wave travels during the time step for each Σ_t, from the equations derived in Appendix A.1. Comparing the results in Table 2.1 with

Σ_t [cm^{-1}]	d_{RMS} [cm]	d_{RMS} [cell widths]
10^{-3}	18.257	18.257
10^{-2}	5.7735	5.7735
10^{-1}	1.8257	1.8257
10^{0}	0.57735	0.57735
10^{1}	0.18257	0.18257
10^{2}	0.057735	0.57735
10^{3}	0.018257	0.018257

Table 2.1 Diffusion Problem 4: Particle Wave Location After One Time Step

the results in Figures 2.33 and 2.34, we see that the error in the SBJ results becomes small when the particle wave moves 20% or less of a cell width per time step.

Table 2.2 presents the number of iterations required to converge the iterative SBJ diffusion method with and without rebalance, with a convergence criterion of $\varepsilon_{L_\infty} = 10^{-4}$. For optically-thin problems, a large number of iterations are required, but the number of iterations required to converge optically-thick problems is quite modest. In each case, rebalance reduces the number of iterations necessary. Comparing the results in Table 2.2 with

Σ_t [cm^{-1}]	Without Rebalance	With Rebalance
10^{-3}	4658	3371
10^{-2}	540	411
10^{-1}	67	53
10^{0}	12	11
10^{1}	5	5
10^{2}	4	3
10^{3}	3	3

Table 2.2 Diffusion Problem 4: Iterations Required for Convergence

Table 2.1, we see that the number of iterations required for convergence becomes modest when the particle wave advances 60% or less of a cell width per time step.

2.5.5 Diffusion Problem 5

For this final diffusion problem, we examine the behavior of the SBJ method in a heterogeneous system. We consider a slab 5 cm in width, composed of alternating purely scattering and purely absorbing regions, as shown in Figure 2.35. The red color represents

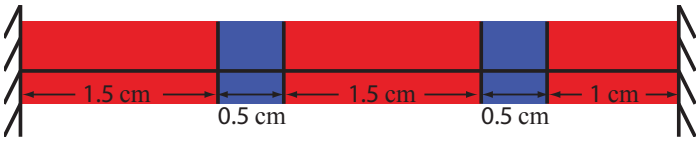

Figure 2.35 Diffusion Problem 5: Geometrical Layout of Materials

slabs of purely scattering material, and the blue color represents slabs of purely absorbing material. The system is divided into 50 cells. The purely scattering material has a total cross section of $\Sigma_t = 10^{\varepsilon}$ cm^{-1}, and the purely absorbing material has a total cross section of $\Sigma_t = 10^{-\varepsilon}$ cm^{-1}, where ε varies from 0 to 3. Therefore, as ε increases, the system becomes increasingly heterogeneous. The purely scattering material has a particle source of $Q = 1$ cm^{-3} s^{-1}, while the purely absorbing material has no source. The particle velocity is set at $v = 1$ cm/s. The left and right boundaries are reflecting, and the initial condition is zero everywhere. The problem was run with ten time steps of length $\Delta t = 1$ s. A benchmark solution with $\Delta t = 10^{-8}$ s was also run using the implicit method. The benchmark solutions are shown in Figure 2.36.

Figure 2.37 shows the implicit solutions, and here we see that the implicit solution

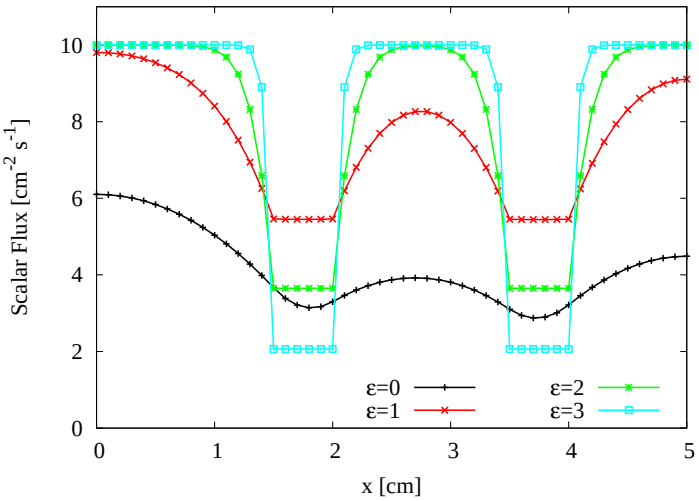

Figure 2.36 Diffusion Problem 5: Benchmark Solutions at $t = 10$ s

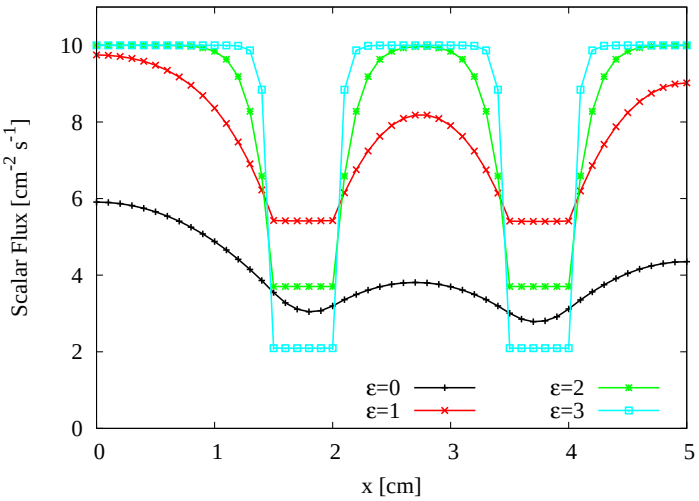

Figure 2.37 Diffusion Problem 5: Implicit Solution at $t = 10$ s

has good accuracy for every ε. Figures 2.38 and 2.39 show the SBJ solution without and with particle conservation, respectively. We can see that the locality of the SBJ diffusion

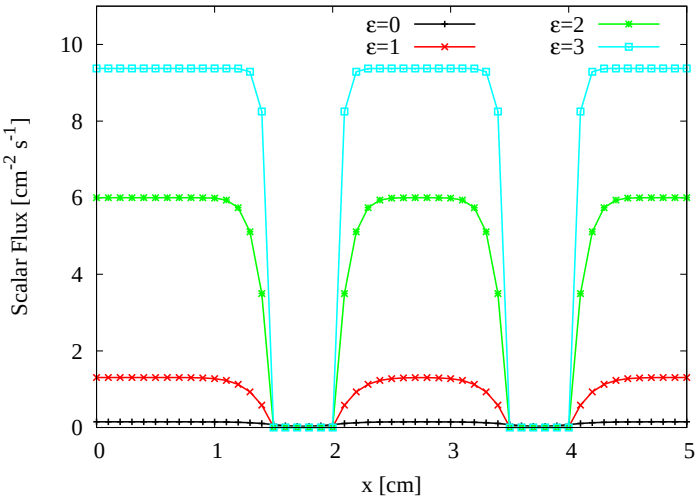

Figure 2.38 Diffusion Problem 5: Plain SBJ Solution at $t = 10$ s

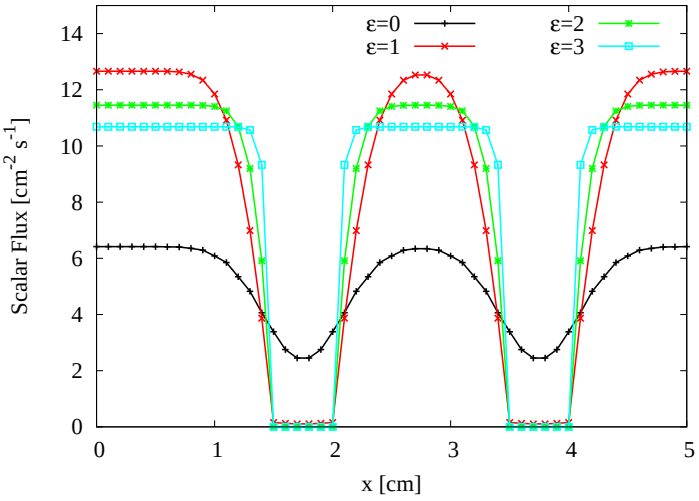

Figure 2.39 Diffusion Problem 5: Conservative SBJ Solution at $t = 10$ s

method causes an insufficient amount of coupling between the purely absorbing and purely scattering regions. The interface between the purely scattering and purely absorbing regions is too abrupt, and the solution is much too low in the purely absorbing regions because the SBJ diffusion method causes too few particles to diffuse into these regions. Adding particle conservation to the solutions "softens" the material interface, but the solution is still too small in the purely absorbing regions and too large in the purely scattering regions.

In Table 2.3 we show the number of iterations required to converge the SBJ solution to the implicit solution, with and without using rebalance acceleration, and with a convergence criterion of $\varepsilon_{L_\infty} = 10^{-4}$. We can see that as the problem becomes increasingly heterogeneous,

ε	Without Rebalance	With Rebalance
0	542	434
1	3010	380
2	39,284	307
3	n/a	336

Table 2.3 Diffusion Problem 5: Iterations Required for Convergence

the number of iterations required for convergence in the unaccelerated case increases. For $\varepsilon = 3$, we were unable to converge the solution with the given ε_{L_∞}, due to false convergence. This is because the estimate of the spectral radius $\rho^{(l+1),k+1}$ is inaccurate for small l. Reducing ε_{L_∞} to 10^{-6} required over half a million iterations to converge. However, with rebalance acceleration, the number of iterations required remains fairly steady, although hundreds of iterations are still required.

2.6 Summary

In summary, the fully-explicit method is *local*, meaning each unknown in the spatial domain at a given time step may be calculated independently, and thus, the fully-explicit method should scale nearly linearly with the number of processors, but the method requires a small time step length for stability. The implicit method, by contrast, is stable for any time step length, but is *non-local*, and thus more difficult to parallelize. We investigated a semi-explicit diffusion method, which treats the absorption term implicitly. This method is still local, is more stable than the fully-explicit method, and preserves particle balance, but it does not have unconditional stability. Finally, we investigated a new Staggered-Block Jacobi (SBJ) diffusion method, which retains the locality of the fully-explicit method, with the unconditional stability of the implicit method. However, the SBJ method has reduced accuracy for large time steps and fails to maintain particle conservation. We recovered global particle conservation using a rebalance procedure. We also found that we can use iterations to converge the SBJ diffusion method to the implicit solution.

In general, the SBJ diffusion method is accurate with a small number of iterations in optically-thick regions (where the particle wave advances slowly), but it requires a large number of iterations for accurate solutions in optically-thin regions. As we discussed in the

chapter introduction, the goal here is not necessarily to find a replacement for the implicit diffusion method, but rather to investigate the SBJ method in the context of diffusion, in order to set the stage for investigating the SBJ method in the more complicated context of linear and thermal radiation transport in later chapters.

It is possible, however, that with further research, the SBJ diffusion method could be a useful method for solving the diffusion equation. In particular, what is required is more advanced iteration acceleration techniques. A multigrid method [10] may be particularly useful for the SBJ diffusion method. Since the SBJ diffusion method is reasonably accurate for optically-thick regions, a multigrid method (which works by successively coarsening, and then refining the grid) could be particularly useful since the coarsened grids would be more optically-thick than the original grid. Thus, accurate solutions could be obtained with the SBJ diffusion method on the coarse grids, and these solutions could then be used to find accurate solutions on the original fine grid. Properly implemented, the multigrid method could maintain the parallelism of the SBJ diffusion method.

Chapter 3

Derivation of the Staggered-Block Jacobi Transport Equations

In the previous chapter, we investigated the Staggered-Block Jacobi (SBJ) method applied to a node-centered diffusion discretization. We did not give a formal definition of the SBJ transport method in that chapter, but rather stated that the SBJ diffusion method was analogous to the SBJ transport method in the diffusive limit. We found that the SBJ diffusion method is local and unconditionally stable. In this chapter, we present a formal definition of the Staggered-Block Jacobi transport method. First, however, we introduce the standard implicit time discretization of the transport equation. Therefore, we begin this chapter by discretizing the time-dependent, one-dimensional, mono-energetic transport equation. For completeness, we also derive and discuss the fully-explicit and semi-explicit methods in addition to the implicit method. We then give a formal definition of the SBJ transport method and show how the SBJ transport equations can be obtained by modifying the implicit equations.

In this study of the time-dependent, one-dimensional, mono-energetic transport equation, we employ a discrete ordinates angular discretization and a linear discontinuous finite element spatial discretization. The discrete ordinates method is an established method for discretizing the angular variable in the transport equation [26]. The linear discontinuous finite element method is also a well-established spatial discretization, and is known to give physically correct solutions in the diffusive limit [1].

3.1 S_N Angular Discretization

We consider the following time-dependent, one-dimensional, mono-energetic transport problem:

$$\frac{1}{v}\frac{\partial}{\partial t}\psi(x,\mu,t)+\mu\frac{\partial}{\partial x}\psi(x,\mu,t)+\Sigma_t(x)\psi(x,\mu,t)=\frac{\Sigma_s(x)}{2}\int_{-1}^{1}\psi(x,\mu',t)\,\mathrm{d}\mu'+Q(x,\mu,t)\,,$$
$$0\le x\le X\,,\quad -1\le\mu\le 1\,,\quad t>0\,, \tag{3.1a}$$

with boundary conditions

$$\psi(0,\mu,t)=\psi_L^b(\mu,t)\,,\qquad 0<\mu\le 1\,, \tag{3.1b}$$

$$\psi(X,\mu,t)=\psi_R^b(\mu,t)\,,\qquad -1\le\mu<0\,, \tag{3.1c}$$

where $\psi_L^b(\mu,t)$ and $\psi_R^b(\mu,t)$ are specified incident fluxes, or are defined by

$$\psi_L^b(\mu,t)=\psi(0,-\mu,t)\,,\qquad 0<\mu\le 1\,, \tag{3.1d}$$

$$\psi_R^b(\mu,t)=\psi(X,-\mu,t)\,,\qquad -1\le\mu<0\,, \tag{3.1e}$$

for reflecting boundaries. We also have a specified initial condition

$$\psi(x,\mu,0)=\psi^i(x,\mu)\,,\qquad 0\le x\le X\,,\quad -1\le\mu\le 1\,. \tag{3.1f}$$

We refer the reader to Section 2.1, where each term in Eq. (3.1) is defined. We note that in Section 2.1, an isotropic fixed source is assumed, but here we make no assumptions on the angular dependence of $Q(x,\mu,t)$.

The discrete ordinates angular discretization involves evaluating Eqs. (3.1) on a set of angles determined by a quadrature rule. Defining

$$\psi_n(x,t)=\psi(x,\mu_n,t)\,, \tag{3.2a}$$

and

$$Q_n(x,t)=Q(x,\mu_n,t)\,, \tag{3.2b}$$

we can approximate the scalar flux as

$$\begin{aligned}\phi(x,t) &= \int_{-1}^{1} \psi(x,\mu',t)\,\mathrm{d}\mu' \\ &\approx \sum_{n=1}^{N} \psi_n(x,t)\,\Delta_n\,,\end{aligned} \tag{3.3}$$

where $\{\mu_n, \Delta_n\}$ are the set of angular cosines and quadrature weights, respectively. Evaluating Eqs. (3.1) at angular cosine μ_n, we obtain

$$\frac{1}{v}\frac{\partial}{\partial t}\psi_n(x,t) + \mu_n\frac{\partial}{\partial x}\psi_n(x,t) + \Sigma_t(x)\psi_n(x,t) = \frac{\Sigma_s(x)}{2}\sum_{m=1}^{N}\psi_m(x,t)\,\Delta_m + Q_n(x,t)\,, \tag{3.4a}$$

$$\psi_n(0,t) = \psi^b_{n,L}(t)\,, \qquad 0 < \mu_n \leq 1\,, \tag{3.4b}$$

$$\psi_n(X,t) = \psi^b_{n,R}(t)\,, \qquad -1 \leq \mu_n < 0\,, \tag{3.4c}$$

$$\psi_n(x,0) = \psi^i_n(x)\,, \tag{3.4d}$$

where $\psi^b_{n,L}(t) = \psi^b_L(\mu_n,t)$, $\psi^b_{n,R}(t) = \psi^b_R(\mu_n,t)$, and $\psi^i_n(x) = \psi^i(x,\mu_n)$. Eqs. (3.4) are called the S_N equations.

3.2 Time Discretization

We now assume a time grid, with time step $k+1$ bounded by times t_k and t_{k+1}, with $\Delta t_{k+1} = t_{k+1} - t_k$ and time $t_0 = 0$, just like the time grid we introduced in Section 2.1.1. To discretize the time variable in Eqs. (3.4) we operate by $\frac{1}{\Delta t_{k+1}}\int_{t_k}^{t_{k+1}}(\cdot)\,\mathrm{d}t$. Defining

$$\bar{\psi}^{k+1}_n(x) = \frac{1}{\Delta t_{k+1}}\int_{t_k}^{t_{k+1}}\psi_n(x,t)\,\mathrm{d}t\,, \tag{3.5a}$$

$$Q^{k+1}_n(x) = \frac{1}{\Delta t_{k+1}}\int_{t_k}^{t_{k+1}}Q_n(x,t)\,\mathrm{d}t\,, \tag{3.5b}$$

$$\psi^k_n(x) = \psi_n(x,t_k)\,, \tag{3.5c}$$

$$\bar{\psi}^{b,k+1}_{n,L} = \frac{1}{\Delta t_{k+1}}\int_{t_k}^{t_{k+1}}\psi^b_{n,L}(t)\,\mathrm{d}t\,, \tag{3.5d}$$

$$\bar{\psi}^{b,k+1}_{n,R} = \frac{1}{\Delta t_{k+1}}\int_{t_k}^{t_{k+1}}\psi^b_{n,R}(t)\,\mathrm{d}t\,, \tag{3.5e}$$

the time-averaged S_N equations are

$$\frac{1}{v\Delta t_{k+1}}\left[\psi_n^{k+1}(x)-\psi_n^k(x)\right]+\mu_n\frac{\mathrm{d}}{\mathrm{d}x}\bar{\psi}_n^{k+1}(x)+\Sigma_t(x)\bar{\psi}_n^{k+1}(x) = \frac{\Sigma_s(x)}{2}\sum_{m=1}^{N}\bar{\psi}_m^{k+1}(x)\,\Delta_m+Q_n^{k+1}(x)\,, \quad (3.6a)$$

$$\bar{\psi}_n^{k+1}(0)=\bar{\psi}_{n,L}^{b,k+1}\,, \qquad 0<\mu_n\leq 1\,, \quad (3.6b)$$

$$\bar{\psi}_n^{k+1}(X)=\bar{\psi}_{n,R}^{b,k+1}\,, \qquad -1\leq\mu_n<0\,, \quad (3.6c)$$

$$\psi_n^0(x)=\psi_n^i(x)\,. \quad (3.6d)$$

In Eq. (3.6a), the angular flux at time t_k, $\psi_n^k(x)$, is considered known since it was either calculated during the previous time step, or if $k=0$, was specified by the initial condition. The time-averaged angular flux, $\bar{\psi}_n^{k+1}(x)$, and the angular flux at time t_{k+1}, $\psi_n^{k+1}(x)$, are both unknown. We cannot solve the single Eq. (3.6a) for both $\bar{\psi}_n^{k+1}(x)$ and $\psi_n^{k+1}(x)$. Therefore, we must close this system of equations by approximating the time-averaged angular flux. As with the diffusion discretizations derived in Chapter 2, time discretizations differ by how they approximate the time-averaged unknowns, and how this approximation is made dramatically affects the behavior of the method. Like with the diffusion discretizations, we begin with the standard implicit and fully-explicit methods, as well as, for completeness, a semi-explicit method analogous to the semi-explicit diffusion method introduced in Section 2.3.

3.2.1 Fully-Explicit Time Discretization

The fully-explicit time discretization approximates the time-averaged angular fluxes by evaluating them at the beginning of the time step, i.e.,

$$\bar{\psi}_n^{k+1}(x)\approx\psi_n^k(x)\,, \quad (3.7a)$$

$$\bar{\psi}_{n,L}^{b,k+1}\approx\psi_{n,L}^{b,k}\,, \quad (3.7b)$$

$$\bar{\psi}_{n,R}^{b,k+1}\approx\psi_{n,R}^{b,k}\,, \quad (3.7c)$$

where $\psi_{n,L}^{b,k} = \psi_{n,L}^{b}(t_k)$ and $\psi_{n,R}^{b,k} = \psi_{n,R}^{b}(t_k)$. Now the fully-explicit time-discretized S_N equations can be written

$$\frac{1}{v\Delta t_{k+1}}\left[\psi_n^{k+1}(x) - \psi_n^k(x)\right] + \mu_n \frac{\mathrm{d}}{\mathrm{d}x}\psi_n^k(x) + \Sigma_t(x)\psi_n^k(x) = \frac{\Sigma_s(x)}{2}\sum_{m=1}^{N}\psi_m^k(x)\,\Delta_m + Q_n^{k+1}(x)\,, \quad (3.8a)$$

$$\psi_n^k(0) = \psi_{n,L}^{b,k}\,, \qquad 0 < \mu_n \leq 1\,, \quad (3.8b)$$

$$\psi_n^k(X) = \psi_{n,R}^{b,k}\,, \qquad -1 \leq \mu_n < 0\,, \quad (3.8c)$$

$$\psi_n^0(x) = \psi_n^i(x)\,. \quad (3.8d)$$

3.2.2 Implicit Time Discretization

Implicit time discretizations approximate the time-averaged angular fluxes by evaluating them at the end of the time step

$$\bar{\psi}_n^{k+1}(x) \approx \psi_n^{k+1}(x)\,, \quad (3.9a)$$

$$\bar{\psi}_{n,L}^{b,k+1} \approx \psi_{n,L}^{b,k+1}\,, \quad (3.9b)$$

$$\bar{\psi}_{n,R}^{b,k+1} \approx \psi_{n,R}^{b,k+1}\,. \quad (3.9c)$$

The implicitly time-discretized S_N equations are

$$\frac{1}{v\Delta t_{k+1}}\left[\psi_n^{k+1}(x) - \psi_n^k(x)\right] + \mu_n \frac{\mathrm{d}}{\mathrm{d}x}\psi_n^{k+1}(x) + \Sigma_t(x)\psi_n^{k+1}(x) = \frac{\Sigma_s(x)}{2}\sum_{m=1}^{N}\psi_m^{k+1}(x)\,\Delta_m + Q_n^{k+1}(x)\,, \quad (3.10a)$$

$$\psi_n^{k+1}(0) = \psi_{n,L}^{b,k+1}\,, \qquad 0 < \mu_n \leq 1\,, \quad (3.10b)$$

$$\psi_n^{k+1}(X) = \psi_{n,R}^{b,k+1}\,, \qquad -1 \leq \mu_n < 0\,, \quad (3.10c)$$

$$\psi_n^0(x) = \psi_n^i(x)\,. \quad (3.10d)$$

3.2.3 Semi-Explicit Time Discretization

In Section 2.3, we found that a semi-explicit time discretization of the diffusion equations yielded a method that, while not unconditionally stable, has improved stability over the fully-explicit method. This method treated the absorption term implicitly and the leakage term explicitly. The semi-explicit time discretization for the transport equation is analogous, in that it treats the collision and scattering terms implicitly and the leakage term explicitly. Therefore, the semi-explicit time-discretized S_N equations are

$$\frac{1}{v\Delta t_{k+1}}\left[\psi_n^{k+1}(x)-\psi_n^k(x)\right]+\mu_n\frac{\mathrm{d}}{\mathrm{d}x}\psi_n^k(x)+\Sigma_t(x)\psi_n^{k+1}(x) = \frac{\Sigma_s(x)}{2}\sum_{m=1}^{N}\psi_m^{k+1}(x)\,\Delta_m+Q_n^{k+1}(x)\,, \quad (3.11a)$$

$$\psi_n^k(0)=\psi_{n,L}^{b,k}, \quad 0<\mu_n\leq 1\,, \quad (3.11b)$$

$$\psi_n^k(X)=\psi_{n,R}^{b,k}, \quad -1\leq\mu_n<0\,, \quad (3.11c)$$

$$\psi_n^0(x)=\psi_n^i(x)\,. \quad (3.11d)$$

3.2.4 Summary of the Time-Discretized S_N Methods

We can write the fully-explicit, semi-explicit, and implicit time-discretized S_N equations as

$$\frac{1}{v\Delta t_{k+1}}\left[\psi_n^{k+1}(x)-\psi_n^k(x)\right]+\mu_n\frac{\mathrm{d}}{\mathrm{d}x}\psi_n^{k+\alpha}(x)+\Sigma_t(x)\psi_n^{k+\beta}(x) = \frac{\Sigma_s(x)}{2}\sum_{m=1}^{N}\psi_m^{k+\beta}(x)\,\Delta_m+Q_n^{k+1}(x)\,, \quad (3.12a)$$

$$\psi_n^{k+\alpha}(0)=\psi_{n,L}^{b,k+\alpha}, \qquad 0<\mu_n\leq 1\,, \quad (3.12b)$$

$$\psi_n^{k+\alpha}(X)=\psi_{n,R}^{b,k+\alpha}, \qquad -1\leq\mu_n<0\,, \quad (3.12c)$$

$$\psi_n^0(x)=\psi_n^i(x)\,, \quad (3.12d)$$

where

$$\alpha=\begin{cases}0: & \text{fully-explicit and semi-explicit methods}\,,\\ 1: & \text{implicit method}\,,\end{cases} \quad (3.13a)$$

and

$$\beta = \begin{cases} 0: & \text{fully-explicit method}, \\ 1: & \text{semi-explicit and implicit methods}. \end{cases} \tag{3.13b}$$

3.3 Spatial Discretization

We now assume a spatial grid spanning $0 \leq x \leq X$, divided into I cells, with cell i bounded by nodes located at $x_{i-1/2}$ on the left and $x_{i+1/2}$ on the right. Cell i has a width of $\Delta x_i = x_{i+1/2} - x_{i-1/2}$, with $x_{1/2} = 0$ and $x_{I+1/2} = X$. This is identical to the spatial grid defined in Section 2.1.2. In this dissertation, we use the linear discontinuous finite element method (LDFEM) to discretize the S_N equations in space [1]. The finite element method is an established spatial discretization for finding weak variational solutions to partial differential equations. It operates according to the following algorithm:

1. Rearrange the partial differential equations to construct a residual
2. Calculate weighted averages of the residual, using some specified set of weight functions, and set the weighted averages equal to zero
3. Use the divergence theorem to eliminate any spatial derivatives of the unknown solution (or, in one dimension, integrate by parts)
4. Expand the solution as a linear superposition of basis functions.

Rearranging Eq. (3.12a) to form a residual, we find

$$R(x) = \frac{1}{v\Delta t_{k+1}}\left[\psi_n^{k+1}(x) - \psi_n^k(x)\right] + \mu_n \frac{\mathrm{d}}{\mathrm{d}x}\psi_n^{k+\alpha}(x) + \Sigma_t(x)\psi_n^{k+\beta}(x) - \frac{\Sigma_s(x)}{2}\sum_{m=1}^{N}\psi_m^{k+\beta}(x)\,\Delta_m - Q_n^{k+1}(x). \tag{3.14}$$

Multiplying the residual by a set of weight functions $w_{i,p}(x,y)$, where $p = 1 \ldots P$, which span the space of cell i, integrating over cell i, and setting these weighted averages of the

residual equal to zero, we have

$$\int_{x_{i-1/2}}^{x_{i+1/2}} R(x) w_{i,p}(x)\,\mathrm{d}x = \frac{1}{v\Delta t_{k+1}}\left[\int_{x_{i-1/2}}^{x_{i+1/2}} w_{i,p}(x)\psi_n^{k+1}(x)\,\mathrm{d}x - \int_{x_{i-1/2}}^{x_{i+1/2}} w_{i,p}(x)\psi_n^{k}(x)\,\mathrm{d}x\right] + \mu_n \int_{x_{i-1/2}}^{x_{i+1/2}} w_{i,p}(x)\frac{\mathrm{d}}{\mathrm{d}x}\psi_n^{k+\alpha}(x)\,\mathrm{d}x + \int_{x_{i-1/2}}^{x_{i+1/2}} \Sigma_t(x) w_{i,p}(x)\psi_n^{k+\beta}(x)\,\mathrm{d}x - \frac{1}{2}\sum_{m=1}^{N}\int_{x_{i-1/2}}^{x_{i+1/2}} \Sigma_s(x) w_{i,p}(x)\psi_m^{k+\beta}(x)\,\mathrm{d}x\Delta_m - \int_{x_{i-1/2}}^{x_{i+1/2}} w_{i,p}(x) Q_n^{k+1}(x)\,\mathrm{d}x = 0\,, \quad p = 1\ldots P. \tag{3.15}$$

Rearranging, we find

$$\frac{1}{v\Delta t_{k+1}}\left[\int_{x_{i-1/2}}^{x_{i+1/2}} w_{i,p}(x)\psi_n^{k+1}(x)\,\mathrm{d}x - \int_{x_{i-1/2}}^{x_{i+1/2}} w_{i,p}(x)\psi_n^{k}(x)\,\mathrm{d}x\right] + \mu_n \int_{x_{i-1/2}}^{x_{i+1/2}} w_{i,p}(x)\frac{\mathrm{d}}{\mathrm{d}x}\psi_n^{k+\alpha}(x)\,\mathrm{d}x + \int_{x_{i-1/2}}^{x_{i+1/2}} \Sigma_t(x) w_{i,p}(x)\psi_n^{k+\beta}(x)\,\mathrm{d}x = \frac{1}{2}\sum_{m=1}^{N}\int_{x_{i-1/2}}^{x_{i+1/2}} \Sigma_s(x) w_{i,p}(x)\psi_m^{k+\beta}(x)\,\mathrm{d}x\Delta_m + \int_{x_{i-1/2}}^{x_{i+1/2}} w_{i,p}(x) Q_n^{k+1}(x)\,\mathrm{d}x\,, \quad p = 1\ldots P. \tag{3.16}$$

Integrating by parts on the streaming term, we obtain

$$\frac{1}{v\Delta t_{k+1}}\left[\int_{x_{i-1/2}}^{x_{i+1/2}} w_{i,p}(x)\psi_n^{k+1}(x)\,\mathrm{d}x - \int_{x_{i-1/2}}^{x_{i+1/2}} w_{i,p}(x)\psi_n^{k}(x)\,\mathrm{d}x\right] + \mu_n\left[w_{i,p}(x_{i+1/2})\psi_n^{k+\alpha}(x_{i+1/2}) - w_{i,p}(x_{i-1/2})\psi_n^{k+\alpha}(x_{i-1/2})\right] - \mu_n \int_{x_{i-1/2}}^{x_{i+1/2}} \psi_n^{k+\alpha}(x)\frac{\mathrm{d}}{\mathrm{d}x} w_{i,p}(x)\,\mathrm{d}x + \int_{x_{i-1/2}}^{x_{i+1/2}} \Sigma_t(x) w_{i,p}(x)\psi_n^{k+\beta}(x)\,\mathrm{d}x = \frac{1}{2}\sum_{m=1}^{N}\int_{x_{i-1/2}}^{x_{i+1/2}} \Sigma_s(x) w_{i,p}(x)\psi_m^{k+\beta}(x)\,\mathrm{d}x\Delta_m + \int_{x_{i-1/2}}^{x_{i+1/2}} w_{i,p}(x) Q_n^{k+1}(x)\,\mathrm{d}x\,, \quad p = 1\ldots P. \tag{3.17}$$

Expanding the angular flux in cell i as a superposition of basis functions, i.e.,

$$\psi_n^k(x) = \sum_{s=1}^{S} \psi_{n,i,s}^k b_{i,s}(x)\,, \qquad s = 1\ldots S\,, \quad x_{i-1/2} < x < x_{i+1/2}\,, \tag{3.18}$$

we find

$$\begin{aligned}
\frac{1}{v\Delta t_{k+1}}&\left[\psi_{n,i,s}^{k+1}\int_{x_{i-1/2}}^{x_{i+1/2}} b_{i,s}(x)w_{i,p}(x)\,\mathrm{d}x - \psi_{n,i,s}^{k}\int_{x_{i-1/2}}^{x_{i+1/2}} b_{i,s}(x)w_{i,p}(x)\,\mathrm{d}x\right]\\
&\qquad+\mu_n\left[w_{i,p}(x_{i+1/2})\psi_n^{k+\alpha}(x_{i+1/2}) - w_{i,p}(x_{i-1/2})\psi_n^{k+\alpha}(x_{i-1/2})\right]\\
&-\mu_n\psi_{n,i,s}^{k+\alpha}\int_{x_{i-1/2}}^{x_{i+1/2}} b_{i,s}(x)\frac{\mathrm{d}}{\mathrm{d}x}w_{i,p}(x)\,\mathrm{d}x + \psi_{n,i.s}^{k+\beta}\int_{x_{i-1/2}}^{x_{i+1/2}}\Sigma_t(x)b_{i,s}(x)w_{i,p}(x)\,\mathrm{d}x\\
&=\frac{1}{2}\sum_{m=1}^{N}\psi_{m,i,s}^{k+\beta}\int_{x_{i-1/2}}^{x_{i+1/2}}\Sigma_s(x)b_{i,s}(x)w_{i,p}(x)\,\mathrm{d}x\Delta_m + \int_{x_{i-1/2}}^{x_{i+1/2}} w_{i,p}(x)Q_n^{k+1}(x)\,\mathrm{d}x,\\
&\qquad\qquad p=1\ldots P,\quad s=1\ldots S. \qquad (3.19)
\end{aligned}$$

Defining the following matrices:

$$\left[\underline{\underline{M_i}}\right]_{p,s} = \int_{x_{i-1/2}}^{x_{i+1/2}} b_{i,s}(x)w_{i,p}(x)\,\mathrm{d}x, \qquad (3.20a)$$

$$\left[\underline{\underline{L_i}}\right]_{p,s} = \int_{x_{i-1/2}}^{x_{i+1/2}} b_{i,s}(x)\frac{\mathrm{d}}{\mathrm{d}x}w_{i,p}(x)\,\mathrm{d}x, \qquad (3.20b)$$

$$\left[\underline{\underline{T_i}}\right]_{p,s} = \int_{x_{i-1/2}}^{x_{i+1/2}} \Sigma_t(x)b_{i,s}(x)w_{i,p}(x)\,\mathrm{d}x, \qquad (3.20c)$$

$$\left[\underline{\underline{S_i}}\right]_{p,s} = \int_{x_{i-1/2}}^{x_{i+1/2}} \Sigma_s(x)b_{i,s}(x)w_{i,p}(x)\,\mathrm{d}x, \qquad (3.20d)$$

and the angular flux vector

$$\left[\underline{\psi_{n,i}^{k}}\right]_s = \psi_{n,i,s}^{k}, \qquad (3.21a)$$

source vector

$$\left[\underline{\mathcal{Q}_{n,i}^{k+1}}\right]_p = \int_{x_{i-1/2}}^{x_{i+1/2}} w_{i,p}(x)Q_n^{k+1}(x)\,\mathrm{d}x, \qquad (3.21b)$$

and flux vector on the cell "sides"

$$\left[\underline{\psi_{n,i}^{k+\alpha,side}}\right]_p = w_{i,p}(x_{i+1/2})\psi_n^{k+\alpha}(x_{i+1/2}) - w_{i,p}(x_{i-1/2})\psi_n^{k+\alpha}(x_{i-1/2}), \qquad (3.21c)$$

then Eq. (3.19) may be written

$$\frac{1}{v\Delta t_{k+1}}\underline{\underline{M}}_i\left(\underline{\psi}_{n,i}^{k+1}-\underline{\psi}_{n,i}^{k}\right)+\mu_n\underline{\psi}_{n,i}^{k+\alpha,side}-\mu_n\underline{\underline{L}}_i\underline{\psi}_{n,i}^{k+\alpha}+\underline{\underline{T}}_i\underline{\psi}_{n,i}^{k+\beta} = \frac{1}{2}\underline{\underline{S}}_i\sum_{m=1}^{N}\underline{\psi}_{m,i}^{k+\beta}\Delta_m+\underline{\underline{\mathscr{Q}}}_{n,i}^{k+1}. \quad (3.22)$$

In finite-element literature, $\underline{\underline{M}}_i$ is called the mass matrix. Typically, $\underline{\underline{L}}_i$ is referred to as the leakage matrix. (Note that we have defined the leakage matrix with the opposite sign as in Ref. [1].)

For this research, we simplify our discretization by assuming that the cross sections are constant within a cell, i.e.,

$$\Sigma_t(x)=\Sigma_{t,i}\,,\qquad x_{i-1/2}<x<x_{i+1/2}\,, \quad (3.23a)$$

$$\Sigma_s(x)=\Sigma_{s,i}\,,\qquad x_{i-1/2}<x<x_{i+1/2}\,, \quad (3.23b)$$

and we expand the particle source as a superposition of the basis functions, such that

$$Q_n^{k+1}(x)=\sum_{s=1}^{S}Q_{n,i,s}^{k+1}b_{i,s}(x)\,. \quad (3.24)$$

Therefore,

$$\underline{\underline{T}}_i=\Sigma_{t,i}\underline{\underline{M}}_i\,, \quad (3.25a)$$

$$\underline{\underline{S}}_i=\Sigma_{s,i}\underline{\underline{M}}_i\,, \quad (3.25b)$$

and

$$\underline{\underline{\mathscr{Q}}}_{n,i}^{k+1}=\underline{\underline{M}}_i\underline{Q}_{n,i}^{k+1}\,, \quad (3.25c)$$

where

$$\left[\underline{Q}_{n,i}^{k+1}\right]_s=Q_{n,i,s}^{k+1}\,,\qquad x_{i-1/2}<x<x_{i+1/2}\,. \quad (3.26)$$

Then Eq. (3.22) can be written as

$$\frac{1}{v\Delta t_{k+1}}\underline{\underline{M}}_i\left(\underline{\psi}_{n,i}^{k+1}-\underline{\psi}_{n,i}^{k}\right)+\mu_n\underline{\psi}_{n,i}^{k+\alpha,side}-\mu_n\underline{\underline{L}}_i\underline{\psi}_{n,i}^{k+\alpha}+\Sigma_{t,i}\underline{\underline{M}}_i\underline{\psi}_{n,i}^{k+\beta} = \frac{\Sigma_{s,i}}{2}\underline{\underline{M}}_i\sum_{m=1}^{N}\underline{\psi}_{m,i}^{k+\beta}\Delta_m+\underline{\underline{M}}_i\underline{Q}_{n,i}^{k+1}. \quad (3.27)$$

Up to this point, we have derived the finite element transport equations without making any assumptions about the particular weight or basis functions. In this dissertation, we use a linear discontinuous finite element method, for which there are $S = 2$ basis functions per cell

$$b_{i,1}(x) = b_{i,L}(x) = \frac{x_{i+1/2} - x}{\Delta x_i}, \tag{3.28a}$$

$$b_{i,2}(x) = b_{i,R}(x) = \frac{x - x_{i-1/2}}{\Delta x_i}. \tag{3.28b}$$

These basis functions are shown in Figure 3.1. We also use Galerkin weighting, i.e., we set

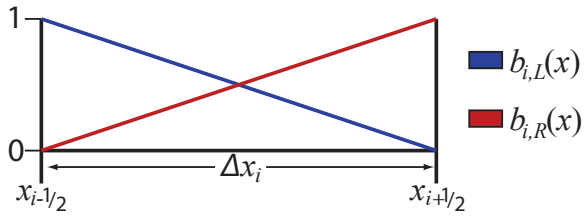

Figure 3.1 The Linear Discontinuous Basis Functions

the weight functions equal to the basis functions:

$$w_{i,1}(x) = w_{i,L}(x) = b_{i,L}(x), \tag{3.29a}$$

$$w_{i,2}(x) = w_{i,R}(x) = b_{i,R}(x). \tag{3.29b}$$

Therefore, we have two angular fluxes per cell,

$$\psi^k_{n,i,1} = \psi^k_{n,i,L}, \tag{3.30a}$$

$$\psi^k_{n,i,2} = \psi^k_{n,i,R}, \tag{3.30b}$$

located at the cell "corners," as shown in Figure 3.2, as well as two known sources per cell

$$Q^{k+1}_{n,i,1} = Q^{k+1}_{n,i,L}, \tag{3.31a}$$

$$Q^{k+1}_{n,i,2} = Q^{k+1}_{n,i,R}. \tag{3.31b}$$

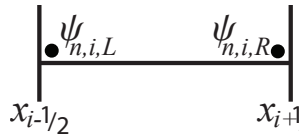

Figure 3.2 The Location of the Angular Flux Unknowns

Finally, examining Eq. (3.27), we see that we have two unknown angular flux vectors, $\underline{\psi}_{n,i}^{k+1}$ and $\underline{\psi}_{n,i}^{k+\alpha,side}$. We close this system by using an upstream closure, i.e., the angular fluxes on the sides of the cell are approximated by setting them equal to the "upstream" in-cell angular fluxes. We obtain

$$\psi_n^{k+\alpha}(x_{i-1/2}) = \psi_{n,i,L}^{k+\alpha,surf} = \begin{cases} \psi_{n,L}^{b,k+\alpha}, & \mu_n > 0, \quad i = 1, \\ \psi_{n,i-1,R}^{k+\alpha}, & \mu_n > 0, \quad 2 \le i \le I, \\ \psi_{n,i,L}^{k+\alpha}, & \mu_n < 0, \end{cases} \tag{3.32a}$$

$$\psi_n^{k+\alpha}(x_{i+1/2}) = \psi_{n,i,R}^{k+\alpha,surf} = \begin{cases} \psi_{n,i,R}^{k+\alpha}, & \mu_n > 0, \\ \psi_{n,i+1,L}^{k+\alpha}, & \mu_n < 0, \quad 1 \le i \le I-1, \\ \psi_{n,R}^{b,k+\alpha}, & \mu_n < 0, \quad i = I. \end{cases} \tag{3.32b}$$

Substituting Eqs. (3.32) and (3.29) into Eq. (3.21c) and defining

$$\underline{\underline{L}}_i^{surf} = \begin{bmatrix} -1 & 0 \\ 0 & 1 \end{bmatrix}, \tag{3.33a}$$

and

$$\underline{\psi}_{n,i}^{k+\alpha,surf} = \begin{bmatrix} \psi_{n,i,L}^{k+\alpha,surf} \\ \psi_{n,i,R}^{k+\alpha,surf} \end{bmatrix}, \tag{3.33b}$$

the cell-side angular flux vector may be written as

$$\underline{\psi}_{n,i}^{k+\alpha,side} = \underline{\underline{L}}_i^{surf} \underline{\psi}_{n,i}^{k+\alpha,surf}. \tag{3.34}$$

Typically, $\underline{\underline{L}}_i^{surf}$ is referred to as the surface matrix. Now Eq. (3.27) may be written

$$\frac{1}{v\Delta t_{k+1}}\underline{\underline{M}}_i\left(\underline{\psi}_{n,i}^{k+1}-\underline{\psi}_{n,i}^{k}\right)+\mu_n\underline{\underline{L}}_i^{surf}\underline{\psi}_{n,i}^{k+\alpha,surf}-\mu_n\underline{\underline{L}}_i\underline{\psi}_{n,i}^{k+\alpha}+\Sigma_{t,i}\underline{\underline{M}}_i\underline{\psi}_{n,i}^{k+\beta}$$
$$=\frac{\Sigma_{s,i}}{2}\underline{\underline{M}}_i\sum_{m=1}^{N}\underline{\psi}_{m,i}^{k+\beta}\,\Delta_m+\underline{\underline{M}}_i\underline{Q}_{n,i}^{k+1}\,, \quad (3.35a)$$

with initial condition

$$\underline{\psi}_{n,i}^{0}=\begin{bmatrix}\int_{x_{i-1/2}}^{x_{i+1/2}} w_{i,L}(x)\,\psi_n^i(x)\,\mathrm{d}x\\ \int_{x_{i-1/2}}^{x_{i+1/2}} w_{i,R}(x)\,\psi_n^i(x)\,\mathrm{d}x\end{bmatrix}. \quad (3.35b)$$

It remains to calculate the values of the integrals in the matrices. Substituting Eqs. (3.28) and (3.29) into Eqs. (3.20a) and (3.20b), we find

$$\underline{\underline{M}}_i=\frac{\Delta x_i}{6}\begin{bmatrix}2 & 1\\ 1 & 2\end{bmatrix}, \quad (3.36a)$$

and

$$\underline{\underline{L}}_i=\begin{bmatrix}-\frac{1}{2} & -\frac{1}{2}\\ \frac{1}{2} & \frac{1}{2}\end{bmatrix}. \quad (3.36b)$$

Often, the mass matrix is "lumped," or diagonalized. This reduces the spatial accuracy of the solutions, but gives improved numerical robustness [1]. The lumped mass matrix is

$$\underline{\underline{M}}_i^{lump}=\frac{\Delta x_i}{2}\begin{bmatrix}1 & 0\\ 0 & 1\end{bmatrix}. \quad (3.37)$$

The general mass matrix may be written

$$\underline{\underline{M}}_i=\frac{\Delta x_i}{6}\begin{bmatrix}2+\theta & 1-\theta\\ 1-\theta & 2+\theta\end{bmatrix}, \quad (3.38)$$

where

$$\theta=\begin{cases}0: & \text{unlumped method},\\ 1: & \text{lumped method}.\end{cases} \quad (3.39)$$

3.3.1 Solving the LDFEM Transport Equations

In this section, we briefly discuss how to solve the fully-explicit, semi-explicit, and implicit methods, and their locality (and therefore, their parallelism).

Fully-Explicit LDFEM Transport

Substituting $\alpha = \beta = 0$ into Eqs. (3.35a), we obtain the fully-explicit linear-discontinuous finite element transport equation

$$\frac{1}{v\Delta t_{k+1}}\underline{\underline{M}}_i\left(\underline{\psi}_{n,i}^{k+1} - \underline{\psi}_{n,i}^{k}\right) + \mu_n \underline{\underline{L}}_i^{surf}\underline{\psi}_{n,i}^{k,surf} - \mu_n \underline{\underline{L}}_i\underline{\psi}_{n,i}^{k} + \Sigma_{t,i}\underline{\underline{M}}_i\underline{\psi}_{n,i}^{k} = \frac{\Sigma_{s,i}}{2}\underline{\underline{M}}_i\sum_{m=1}^{N}\underline{\psi}_{m,i}^{k}\Delta_m + \underline{\underline{M}}_i\underline{Q}_{n,i}^{k+1}, \quad (3.40)$$

where

$$\psi_{n,i,L}^{k,surf} = \begin{cases} \psi_{n,L}^{b,k}, & \mu_n > 0, \quad i = 1, \\ \psi_{n,i-1,R}^{k}, & \mu_n > 0, \quad 2 \le i \le I, \\ \psi_{n,i,L}^{k}, & \mu_n < 0, \end{cases} \quad (3.41a)$$

$$\psi_{n,i,R}^{k,surf} = \begin{cases} \psi_{n,i,R}^{k}, & \mu_n > 0, \\ \psi_{n,i+1,L}^{k}, & \mu_n < 0, \quad 1 \le i \le I-1, \\ \psi_{n,R}^{b,k}, & \mu_n < 0, \quad i = I, \end{cases} \quad (3.41b)$$

and with the initial condition

$$\underline{\psi}_{n,i}^{0} = \begin{bmatrix} \int_{x_{i-1/2}}^{x_{i+1/2}} w_{i,L}(x)\psi_n^i(x)\,\mathrm{d}x \\ \int_{x_{i-1/2}}^{x_{i+1/2}} w_{i,R}(x)\psi_n^i(x)\,\mathrm{d}x \end{bmatrix}. \quad (3.42)$$

Eq. (3.40) may be solved directly for the unknown angular flux $\underline{\psi}_{n,i}^{k+1}$ to obtain

$$\underline{\psi}_{n,i}^{k+1} = \left(1 - \Sigma_{t,i}v\Delta t_{k+1}\right)\underline{\psi}_{n,i}^{k} - \mu_n v\Delta t_{k+1}\underline{\underline{M}}_i^{-1}\left(\underline{\underline{L}}_i^{surf}\underline{\psi}_{n,i}^{k,surf} - \underline{\underline{L}}_i\underline{\psi}_{n,i}^{k}\right) + \frac{\Sigma_{s,i}v\Delta t_{k+1}}{2}\sum_{m=1}^{N}\underline{\psi}_{m,i}^{k}\Delta_m + v\Delta t_{k+1}\underline{Q}_{n,i}^{k+1}. \quad (3.43)$$

In Section 2.2.1, we discussed how the fully-explicit node-centered diffusion discretization was *local*, which meant that every unknown is independent. Locality makes parallelism trivial, and allows a method to scale with the number of processors. Examining Eq. (3.43), we see that the fully-explicit transport equations are also local, both point-wise spatially (at a given point in space where an unknown angular flux resides, that unknown angular flux is independent from every other unknown angular flux in the spatial domain), and in angle (each angular flux at a given point in space is decoupled from the other angular fluxes at that spatial location). Therefore, this method has a large amount of parallelism that may be exploited. However, this method, like the fully-explicit diffusion method described in Section 2.1, is not unconditionally stable.

Semi-Explicit LDFEM Transport

Substituting $\alpha = 0$ and $\beta = 1$ into Eq. (3.35a), we obtain the semi-explicit linear discontinuous finite element transport equation

$$\frac{1}{v\Delta t_{k+1}}\underline{\underline{M}}_i\left(\underline{\psi}_{n,i}^{k+1} - \underline{\psi}_{n,i}^{k}\right) + \mu_n \underline{\underline{L}}_i^{surf}\underline{\psi}_{n,i}^{k,surf} - \mu_n \underline{\underline{L}}_i \underline{\psi}_{n,i}^{k} + \Sigma_{t,i}\underline{\underline{M}}_i\underline{\psi}_{n,i}^{k+1} = \frac{\Sigma_{s,i}}{2}\underline{\underline{M}}_i \sum_{m=1}^{N} \underline{\psi}_{m,i}^{k+1}\Delta_m + \underline{\underline{M}}_i\underline{Q}_{n,i}^{k+1}, \quad (3.44)$$

where

$$\psi_{n,i,L}^{k,surf} = \begin{cases} \psi_{n,L}^{b,k}, & \mu_n > 0, \quad i = 1, \\ \psi_{n,i-1,R}^{k}, & \mu_n > 0, \quad 2 \le i \le I, \\ \psi_{n,i,L}^{k}, & \mu_n < 0, \end{cases} \quad (3.45a)$$

$$\psi_{n,i,R}^{k,surf} = \begin{cases} \psi_{n,i,R}^{k}, & \mu_n > 0, \\ \psi_{n,i+1,L}^{k}, & \mu_n < 0, \quad 1 \le i \le I-1, \\ \psi_{n,R}^{b,k}, & \mu_n < 0, \quad i = I, \end{cases} \quad (3.45b)$$

and with the initial condition

$$\underline{\psi}_{n,i}^{0} = \begin{bmatrix} \int_{x_{i-1/2}}^{x_{i+1/2}} w_{i,L}(x)\psi_n^i(x)\,\mathrm{d}x \\ \int_{x_{i-1/2}}^{x_{i+1/2}} w_{i,R}(x)\psi_n^i(x)\,\mathrm{d}x \end{bmatrix}. \quad (3.46)$$

To solve Eq. (3.44), we must first solve for the unknown scalar flux at time t_{k+1}. Defining the scalar flux vector in cell i as

$$\underline{\phi}_i^k = \sum_{n=1}^{N} \underline{\psi}_{n,i}^k \Delta_n \,, \tag{3.47a}$$

and the current as

$$\underline{J}_i^k = \sum_{n=1}^{N} \mu_n \underline{\psi}_{n,i}^k \Delta_n \,, \tag{3.47b}$$

we operate on Eq. (3.44) by $\sum_{n=1}^{N}(\cdot)\Delta_n$ and solve for the scalar flux to find

$$\underline{\phi}_i^{k+1} = \left(\frac{1}{1+\Sigma_{a,i}v\Delta t_{k+1}}\right)\underline{\phi}_i^k - \left(\frac{v\Delta t_{k+1}}{1+\Sigma_{a,i}v\Delta t_{k+1}}\right)\underline{\underline{M}}_i^{-1}\left(\underline{\underline{L}}_i^{surf}\sum_{n=1}^{N}\mu_n\underline{\psi}_{n,i}^{k,surf}\Delta_n - \underline{\underline{L}}_i\underline{J}_i^k\right) + \left(\frac{v\Delta t_{k+1}}{1+\Sigma_{a,i}v\Delta t_{k+1}}\right)\sum_{n=1}^{N}\underline{Q}_{n,i}^{k+1}\Delta_n \,. \tag{3.48}$$

Now we solve Eq. (3.44) for the unknown angular flux $\underline{\psi}_{n,i}^{k+1}$, and obtain

$$\underline{\psi}_{n,i}^{k+1} = \left(\frac{1}{1+\Sigma_{t,i}v\Delta t_{k+1}}\right)\underline{\psi}_{n,i}^k - \mu_n\left(\frac{v\Delta t_{k+1}}{1+\Sigma_{t,i}v\Delta t_{k+1}}\right)\underline{\underline{M}}_i^{-1}\left(\underline{\underline{L}}_i^{surf}\underline{\psi}_{n,i}^{k,surf} - \underline{\underline{L}}_i\underline{\psi}_{n,i}^k\right) + \frac{\Sigma_{s,i}}{2}\left(\frac{v\Delta t_{k+1}}{1+\Sigma_{t,i}v\Delta t_{k+1}}\right)\underline{\phi}_i^{k+1} + \left(\frac{v\Delta t_{k+1}}{1+\Sigma_{t,i}v\Delta t_{k+1}}\right)\underline{Q}_{n,i}^{k+1} \,. \tag{3.49}$$

In the previous section, we observed that the fully-explicit transport method was local, which enables trivial parallelization. Examining Eqs. (3.48) and (3.49), we see that the semi-explicit method has point-wise spatial locality, but is not local in angle. Like the semi-explicit diffusion discretization described in Section 2.3, the semi-explicit method lacks unconditional stability.

Implicit LDFEM Transport

Substituting $\alpha = \beta = 1$ into Eq. (3.35a), we obtain the implicit linear discontinuous finite element transport equation

$$\frac{1}{v\Delta t_{k+1}}\underline{\underline{M}}_i\left(\underline{\psi}_{n,i}^{k+1} - \underline{\psi}_{n,i}^k\right) + \mu_n\underline{\underline{L}}_i^{surf}\underline{\psi}_{n,i}^{k+1,surf} - \mu_n\underline{\underline{L}}_i\underline{\psi}_{n,i}^{k+1} + \Sigma_{t,i}\underline{\underline{M}}_i\underline{\psi}_{n,i}^{k+1} = \frac{\Sigma_{s,i}}{2}\underline{\underline{M}}_i\sum_{m=1}^{N}\underline{\psi}_{m,i}^{k+1}\Delta_m + \underline{\underline{M}}_i\underline{Q}_{n,i}^{k+1} \,, \tag{3.50}$$

where

$$\psi_{n,i,L}^{k+1,surf} = \begin{cases} \psi_{n,L}^{b,k+1}, & \mu_n > 0, \quad i = 1, \\ \psi_{n,i-1,R}^{k+1}, & \mu_n > 0, \quad 2 \le i \le I, \\ \psi_{n,i,L}^{k+1}, & \mu_n < 0, \end{cases} \tag{3.51a}$$

$$\psi_{n,i,R}^{k+1,surf} = \begin{cases} \psi_{n,i,R}^{k+1}, & \mu_n > 0, \\ \psi_{n,i+1,L}^{k+1}, & \mu_n < 0, \quad 1 \le i \le I-1, \\ \psi_{n,R}^{b,k+1}, & \mu_n < 0, \quad i = I, \end{cases} \tag{3.51b}$$

and with the initial condition

$$\underline{\psi}_{n,i}^{0} = \begin{bmatrix} \int_{x_{i-1/2}}^{x_{i+1/2}} w_{i,L}(x)\psi_n^i(x)\,\mathrm{d}x \\ \int_{x_{i-1/2}}^{x_{i+1/2}} w_{i,R}(x)\psi_n^i(x)\,\mathrm{d}x \end{bmatrix}. \tag{3.52}$$

To solve these equations, we substitute Eqs. (3.51) into Eq. (3.50) and split the surface term into known (incident) and unknown components. For $\mu_n > 0$, we define

$$\begin{aligned} \underline{\psi}_{n,i}^{k+1,surf} &= \begin{bmatrix} \psi_{n,i,L}^{k+1,surf} \\ \psi_{n,i,R}^{k+1,surf} \end{bmatrix} \\ &= \begin{bmatrix} \psi_{n,i,L}^{k+1,inc} \\ \psi_{n,i,R}^{k+1} \end{bmatrix}, \end{aligned} \tag{3.53}$$

where the upstream closure is

$$\psi_{n,i,L}^{k+1,inc} = \begin{cases} \psi_{n,L}^{b,k+1}, & i = 1, \\ \psi_{n,i-1,R}^{k+1}, & 2 \le i \le I. \end{cases} \tag{3.54}$$

Therefore, defining

$$\underline{\underline{P}}_n = \begin{bmatrix} 0 & 0 \\ 0 & 1 \end{bmatrix}, \qquad \mu_n > 0, \tag{3.55a}$$

$$\underline{\underline{R}}_n = \begin{bmatrix} 1 & 0 \\ 0 & 0 \end{bmatrix}, \qquad \mu_n > 0, \tag{3.55b}$$

and

$$\underline{\psi}_{n,i}^{k+1,inc} = \begin{bmatrix} \psi_{n,i,L}^{k+1,inc} \\ \\ 0 \end{bmatrix}, \qquad \mu_n > 0, \tag{3.55c}$$

we can write the surface term as

$$\mu_n \underline{\underline{L}}_i^{surf} = \mu_n \underline{\underline{P}}_n \underline{\psi}_{n,i}^{k+1} - \mu_n \underline{\underline{R}}_n \underline{\psi}_{n,i}^{k+1,inc}. \tag{3.56}$$

Likewise, for $\mu_n < 0$ we have

$$\begin{aligned} \underline{\psi}_{n,i}^{k+1,surf} &= \begin{bmatrix} \psi_{n,i,L}^{k+1,surf} \\ \\ \psi_{n,i,R}^{k+1,surf} \end{bmatrix} \\ &= \begin{bmatrix} \psi_{n,i,L}^{k+1} \\ \\ \psi_{n,i,R}^{k+1,inc} \end{bmatrix}, \end{aligned} \tag{3.57}$$

where

$$\psi_{n,i,R}^{k+1,inc} = \begin{cases} \psi_{n,i+1,L}^{k+1}, & 1 \le i \le I-1, \\ \psi_{n,R}^{b,k+1}, & i = I. \end{cases} \tag{3.58}$$

Therefore, we define

$$\underline{\underline{P}}_n = \begin{bmatrix} -1 & 0 \\ \\ 0 & 0 \end{bmatrix}, \qquad \mu_n < 0, \tag{3.59a}$$

$$\underline{\underline{R}}_n = \begin{bmatrix} 0 & 0 \\ \\ 0 & -1 \end{bmatrix}, \qquad \mu_n < 0, \tag{3.59b}$$

and

$$\underline{\psi}_{n,i}^{k+1,inc} = \begin{bmatrix} 0 \\ \\ \psi_{n,i,R}^{k+1,inc} \end{bmatrix}, \qquad \mu_n < 0, \tag{3.59c}$$

and again Eq. (3.56) describes the surface term.

Now Eq. (3.50) can be written as

$$\begin{aligned} &\frac{1}{v\Delta t_{k+1}} \underline{\underline{M}}_i \left(\underline{\psi}_{n,i}^{k+1} - \underline{\psi}_{n,i}^{k} \right) + \mu_n \underline{\underline{P}}_n \underline{\psi}_{n,i}^{k+1} - \mu_n \underline{\underline{L}}_i \underline{\psi}_{n,i}^{k+1} + \Sigma_{t,i} \underline{\underline{M}}_i \underline{\psi}_{n,i}^{k+1} \\ &\qquad = \frac{\Sigma_{s,i}}{2} \underline{\underline{M}}_i \sum_{m=1}^{N} \underline{\psi}_{m,i}^{k+1} \Delta_m + \mu_n \underline{\underline{R}}_n \underline{\psi}_{n,i}^{k+1,inc} + \underline{\underline{M}}_i \underline{Q}_{n,i}^{k+1}. \end{aligned} \tag{3.60}$$

Rearranging, we obtain a dense (2×2) system of equations for the unknown angular flux in

each cell and for each quadrature angle:

$$\left[\left(\frac{1}{v\Delta t_{k+1}}+\Sigma_{t,i}\right)\underline{\underline{M}}_i+\mu_n\left(\underline{\underline{P}}_n-\underline{\underline{L}}_i\right)\right]\underline{\psi}_{n,i}^{k+1}=\frac{\Sigma_{s,i}}{2}\underline{\underline{M}}_i\sum_{m=1}^{N}\underline{\psi}_{m,i}^{k+1}\Delta_m+\mu_n\underline{\underline{R}}_n\underline{\psi}_{n,i}^{k+1,inc}+\underline{\underline{M}}_i\underline{Q}_{n,i}^{k+1}. \quad (3.61)$$

Examining Eq. (3.61), we see that the unknown angular flux at time t_{k+1} appears on both the left side of the equation and in the scattering term on the right. This equation can be solved by iterating over the scattering term. Writing Eq. (3.61) as an iterative scheme, we have

$$\left[\left(\frac{1}{v\Delta t_{k+1}}+\Sigma_{t,i}\right)\underline{\underline{M}}_i+\mu_n\left(\underline{\underline{P}}_n-\underline{\underline{L}}_i\right)\right]\underline{\psi}_{n,i}^{(l+1/2),k+1}=\frac{\Sigma_{s,i}}{2}\underline{\underline{M}}_i\underline{\phi}_i^{(l),k+1}+\mu_n\underline{\underline{R}}_n\underline{\psi}_{n,i}^{(l+1/2),k+1,inc}+\underline{\underline{M}}_i\underline{Q}_{n,i}^{k+1}, \quad (3.62a)$$

$$\underline{\phi}_i^{(l+1/2),k+1}=\sum_{n=1}^{N}\underline{\psi}_{n,i}^{(l+1/2),k+1}\Delta_n, \quad (3.62b)$$

$$\underline{\phi}_i^{(l+1),k+1}=\underline{\phi}_i^{(l+1/2),k+1}, \quad (3.62c)$$

where l is the iteration index. The iterative scheme described in Eqs. (3.62) is called source iteration, or sometimes Richardson iteration. It is known to converge slowly for diffusive problems [2], and so typically an acceleration scheme is used. In this dissertation, we employ the Modified Four-Step Diffusion Synthetic Acceleration (DSA) method [3]. See Appendix B.2 for a derivation of that method.

In order for the $\underline{\psi}_{n,i}^{(l+1/2),k+1,inc}$ vector on the right side of Eq. (3.62a) to be known, we must employ mesh sweeps to solve Eqs. (3.62) in each cell. The order that the cells are considered is dictated by the sign of μ_n. A mesh sweep operates by solving Eq. (3.62a) starting with the cell adjacent to the incident boundary for direction μ_n. The sweep proceeds along the direction of particle flow. Figures 3.3 and 3.4 describe the sweep algorithm for positive and negative μ_n in one dimension.

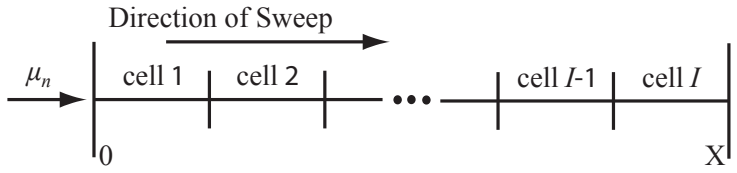

Figure 3.3 Sweep Ordering for Positive Angles

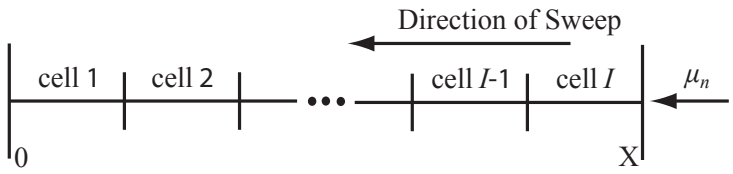

Figure 3.4 Sweep Ordering for Negative Angles

Mesh sweeps dictate that Eq. (3.62a) in each cell must be solved in a particular order. This sweep ordering limits the amount of parallelism that can be exploited. Therefore, although the implicit method, like the implicit diffusion method considered in Section 2.1, is unconditionally stable, its efficiency is reduced by the limited amount of parallelism available. We seek, instead, a method that has good parallel scalability, like the fully-explicit and semi-explicit transport methods, but also has unconditional stability, like the implicit method. We shall see next that the SBJ transport method satisfies this criteria.

3.4 Staggered-Block Jacobi Transport Method

In the previous section, we introduced the well-known fully-explicit and implicit linear-discontinuous transport methods, as well as a possibly new semi-explicit method. At this point, we present the formal definition of the new Staggered-Block Jacobi (SBJ) transport method, illustrated in one dimension in Figure 3.5. The concept behind the SBJ transport method is as follows: consider a *block*, which is composed of the two cells adjacent to a node (cell vertex). The incident flux on the block boundary is evaluated at time t_k (indicated

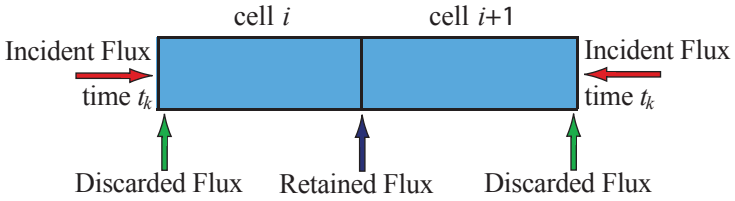

Figure 3.5 The Staggered-Block Jacobi Concept in One-Dimension

with red arrows in Figure 3.5). The full block-wise system of S_N equations is solved for the unknown angular fluxes within the block. The angular flux unknowns that are located at the block boundaries (indicated with green arrows) are discarded, while all other unknowns (indicated with the blue arrow) are retained. Blocks are staggered, such that an interior cell will be a member of two blocks. Therefore, an interior cell i is in a block with cell $i+1$, and

is also in another block with cell $i-1$.

In the description above, we have made no statements about the particular spatial discretization used. We believe that the SBJ transport method may be applied to any reasonable spatial discretization, although we make no claims about the stability of any scheme apart from the one we have studied. For this dissertation, we have used the linear discontinuous finite element spatial discretization. This method, applied to the SBJ concept, is illustrated in Figures 3.6 and 3.7. Solving the SBJ transport equations is a two-step process. *The*

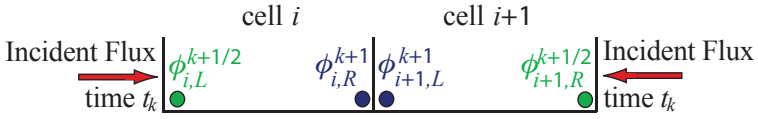

Figure 3.6 The LDFEM SBJ Transport Scalar Flux Stencil in the Interior

first step is calculating the unknown scalar fluxes in the block. The space-time stencil for this process is shown in Figure 3.6. Using the incident angular fluxes (indicated with the red arrows in Figure 3.6), lagged to time t_k, we may solve a 4×4 system of equations in the block to calculate the four unknown scalar fluxes. All four of these scalar fluxes are necessary in order to calculate the unknown angular fluxes in the block. However, after the angular fluxes have been calculated, the scalar fluxes adjacent to the exterior block boundary (shown in green in Figure 3.6) are discarded, while the scalar fluxes adjacent to the interior block boundary (shown in blue) are retained.

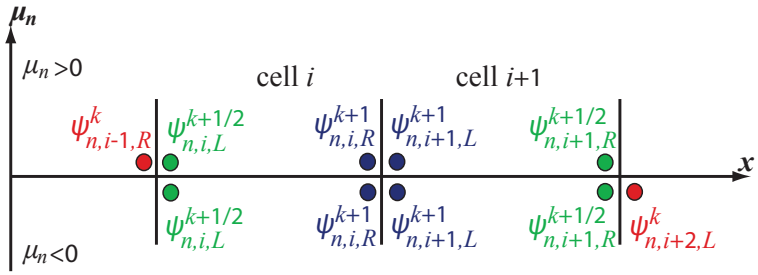

Figure 3.7 The LDFEM SBJ Transport Angular Flux Stencil in the Interior

The second step is calculating the unknown angular fluxes in the block. The space-time stencil for the angular flux calculation is shown in Figure 3.7. In this figure, for positive μ_n, the particles travel to the right, and the incident angular flux on the left side of the block is lagged to time t_k (indicated in red in Figure 3.7). The four unknown angular fluxes in the block are calculated for each discrete ordinate direction using the scalar fluxes in the block

that we calculated in the first step. The two angular fluxes adjacent to the block boundaries, $\psi_{n,i,L}^{k+1/2}$ and $\psi_{n,i+1,R}^{k+1/2}$, indicated in green in Figure 3.7, are discarded, while the two angular fluxes adjacent to the interior block boundary, $\psi_{n,i,R}^{k+1}$ and $\psi_{n,i+1,L}^{k+1}$, indicated in blue, are retained. For negative μ_n, the incident angular flux on the right side of the block is lagged to time t_k, and again the four unknown angular fluxes in the block interior are calculated. The angular fluxes adjacent to the exterior block boundaries are discarded, and the angular fluxes adjacent to the interior block boundary are retained. The reason for discarding the angular fluxes adjacent to the block boundary is explained in Chapter 4, where we perform an asymptotic analysis of the SBJ transport method, and show that discarding these angular fluxes is necessary for the method to acquire physically correct solutions in the asymptotic limit.

With respect to the problem boundaries, we handle reflecting boundaries with ghost cells, using the same stencil as is shown in Figures 3.6 and 3.7. Incident boundaries, however, are treated differently. In Figure 3.8, we show the space-time stencil for the scalar flux calculations on a left incident boundary. The incident angular flux on the left boundary

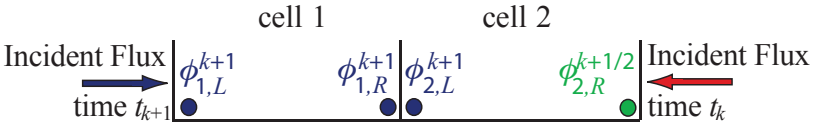

Figure 3.8 The LDFEM SBJ Transport Scalar Flux Stencil on a Left Incident Boundary

is evaluated at time t_{k+1}, and the scalar flux adjacent to the left boundary is evaluated at time t_{k+1}, and is retained. The incident angular flux from the problem interior on the right block boundary is lagged to time t_k, and the scalar flux adjacent to the right block boundary (shown in green in Figure 3.8) is discarded.

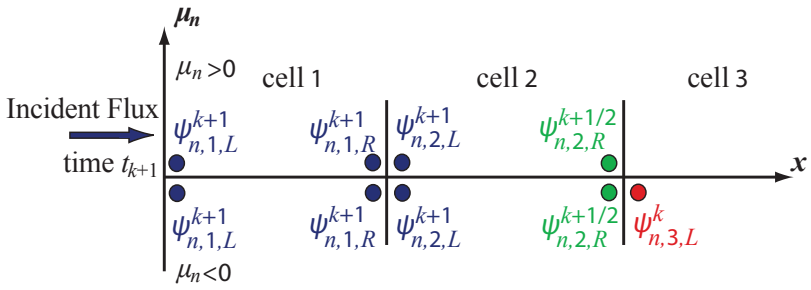

Figure 3.9 The LDFEM SBJ Transport Angular Flux Stencil on a Left Incident Boundary

In Figure 3.9, we show the space-time stencil for the angular flux calculations. For

positive μ_n, particles travel to the right, and the incident angular flux is evaluated using the boundary condition evaluated at time t_{k+1}. For negative μ_n, particles travel to the left, and the incident angular flux on the right side of the block is evaluated at time t_k. The angular flux adjacent to the left boundary is retained, while the angular flux adjacent to the right block boundary (shown in green in Figure 3.9) is discarded. The space-time stencils for the angular and scalar fluxes on a right incident boundary are analogous.

With the SBJ concept in mind, we now derive the SBJ linear discontinuous finite element equations. Consider an SBJ block composed of cells i and $i+1$. We begin by writing the implicit LDFEM equation, Eq. (3.50), only now we write a single equation for both cells i and $i+1$:

$$\frac{1}{v\Delta t_{k+1}}\underline{\underline{M}}_{i+1/2}\left(\underline{\psi}^{k+1}_{n,i+1/2}-\underline{\psi}^{k}_{n,i+1/2}\right)+\mu_n\underline{\underline{L}}^{surf}_{i+1/2}\underline{\psi}^{k+1,surf}_{n,i+1/2}-\mu_n\underline{\underline{L}}_{i+1/2}\underline{\psi}^{k+1}_{n,i+1/2}$$
$$+\underline{\underline{T}}_{i+1/2}\underline{\psi}^{k+1}_{n,i+1/2}=\frac{1}{2}\underline{\underline{S}}_{i+1/2}\sum_{m=1}^{N}\underline{\psi}^{k+1}_{m,i+1/2}\Delta_m+\underline{\underline{M}}_{i+1/2}\underline{Q}^{k+1}_{n,i+1/2}, \quad (3.63)$$

where

$$\underline{\psi}^{k+1}_{n,i+1/2}=\begin{bmatrix}\psi^{k+1}_{n,i,L} & \psi^{k+1}_{n,i,R} & \psi^{k+1}_{n,i+1,L} & \psi^{k+1}_{n,i+1,R}\end{bmatrix}^T, \quad (3.64a)$$

$$\underline{\psi}^{k+1,surf}_{n,i+1/2}=\begin{bmatrix}\psi^{k+1,surf}_{n,i,L} & \psi^{k+1,surf}_{n,i,R} & \psi^{k+1,surf}_{n,i+1,L} & \psi^{k+1,surf}_{n,i+1,R}\end{bmatrix}^T, \quad (3.64b)$$

$$\underline{Q}^{k+1}_{n,i+1/2}=\begin{bmatrix}Q^{k+1}_{n,i,L} & Q^{k+1}_{n,i,R} & Q^{k+1}_{n,i+1,L} & Q^{k+1}_{n,i+1,R}\end{bmatrix}^T. \quad (3.64c)$$

The matrices are defined as

$$\underline{\underline{M}}_{i+1/2}=\begin{bmatrix}\underline{\underline{M}}_i & \underline{\underline{0}}\\ \underline{\underline{0}} & \underline{\underline{M}}_{i+1}\end{bmatrix}$$
$$=\frac{1}{6}\begin{bmatrix}\Delta x_i\left(2+\theta\right) & \Delta x_i\left(1-\theta\right) & 0 & 0\\ \Delta x_i\left(1-\theta\right) & \Delta x_i\left(2+\theta\right) & 0 & 0\\ 0 & 0 & \Delta x_{i+1}\left(2+\theta\right) & \Delta x_{i+1}\left(1-\theta\right)\\ 0 & 0 & \Delta x_{i+1}\left(1-\theta\right) & \Delta x_{i+1}\left(2+\theta\right)\end{bmatrix}, \quad (3.65a)$$

$$\underline{\underline{T}}_{i+1/2} = \begin{bmatrix} \Sigma_{t,i}\underline{\underline{M}}_i & \underline{\underline{0}} \\ \underline{\underline{0}} & \Sigma_{t,i+1}\underline{\underline{M}}_{i+1} \end{bmatrix}$$

$$= \frac{1}{6}\begin{bmatrix} \Sigma_{t,i}\Delta x_i\Big(2+\theta\Big) & \Sigma_{t,i}\Delta x_i\Big(1-\theta\Big) & 0 & 0 \\ \Sigma_{t,i}\Delta x_i\Big(1-\theta\Big) & \Sigma_{t,i}\Delta x_i\Big(2+\theta\Big) & 0 & 0 \\ 0 & 0 & \Sigma_{t,i+1}\Delta x_{i+1}\Big(2+\theta\Big) & \Sigma_{t,i+1}\Delta x_{i+1}\Big(1-\theta\Big) \\ 0 & 0 & \Sigma_{t,i+1}\Delta x_{i+1}\Big(1-\theta\Big) & \Sigma_{t,i+1}\Delta x_{i+1}\Big(2+\theta\Big) \end{bmatrix}, \tag{3.65b}$$

$$\underline{\underline{S}}_{i+1/2} = \begin{bmatrix} \Sigma_{s,i}\underline{\underline{M}}_i & \underline{\underline{0}} \\ \underline{\underline{0}} & \Sigma_{s,i+1}\underline{\underline{M}}_{i+1} \end{bmatrix}$$

$$= \frac{1}{6}\begin{bmatrix} \Sigma_{s,i}\Delta x_i\Big(2+\theta\Big) & \Sigma_{s,i}\Delta x_i\Big(1-\theta\Big) & 0 & 0 \\ \Sigma_{s,i}\Delta x_i\Big(1-\theta\Big) & \Sigma_{s,i}\Delta x_i\Big(2+\theta\Big) & 0 & 0 \\ 0 & 0 & \Sigma_{s,i+1}\Delta x_{i+1}\Big(2+\theta\Big) & \Sigma_{s,i+1}\Delta x_{i+1}\Big(1-\theta\Big) \\ 0 & 0 & \Sigma_{s,i+1}\Delta x_{i+1}\Big(1-\theta\Big) & \Sigma_{s,i+1}\Delta x_{i+1}\Big(2+\theta\Big) \end{bmatrix}, \tag{3.65c}$$

where, as before

$$\theta = \begin{cases} 0: & \text{unlumped}, \\ 1: & \text{lumped}. \end{cases} \tag{3.66}$$

We have also defined

$$\underline{\underline{L}}^{surf}_{i+1/2} = \begin{bmatrix} \underline{\underline{L}}^{surf}_i & \underline{\underline{0}} \\ \underline{\underline{0}} & \underline{\underline{L}}^{surf}_{i+1} \end{bmatrix} = \begin{bmatrix} -1 & 0 & 0 & 0 \\ 0 & 1 & 0 & 0 \\ 0 & 0 & -1 & 0 \\ 0 & 0 & 0 & 1 \end{bmatrix}, \tag{3.67a}$$

and

$$\underline{\underline{L}}_{i+1/2} = \begin{bmatrix} \underline{\underline{L}}_i & \underline{\underline{0}} \\ \underline{\underline{0}} & \underline{\underline{L}}_{i+1} \end{bmatrix} = \begin{bmatrix} -\frac{1}{2} & -\frac{1}{2} & 0 & 0 \\ \frac{1}{2} & \frac{1}{2} & 0 & 0 \\ 0 & 0 & -\frac{1}{2} & -\frac{1}{2} \\ 0 & 0 & \frac{1}{2} & \frac{1}{2} \end{bmatrix}. \tag{3.67b}$$

We apply the SBJ concept to these equations by lagging the incident information to time t_k while the rest of the terms are evaluated at time t_{k+1}. Furthermore, we keep the angular flux values adjacent to the node in the block interior, labeling these unknowns with $k+1$ in the superscript, and discard the angular fluxes adjacent to the block boundary. The angular fluxes to be discarded are labeled with $k+1/2$ in the superscript. Therefore, we define

$$\underline{\hat{\psi}}^{k+1}_{n,i+1/2} = \begin{cases} \begin{bmatrix} \psi^{k+1}_{n,1,L} & \psi^{k+1}_{n,1,R} & \psi^{k+1}_{n,2,L} & \psi^{k+1/2}_{n,2,R} \end{bmatrix}^T, & \text{incident left boundary}, \\ \begin{bmatrix} \psi^{k+1/2}_{n,i,L} & \psi^{k+1}_{n,i,R} & \psi^{k+1}_{n,i+1,L} & \psi^{k+1/2}_{n,i+1,R} \end{bmatrix}^T, & \\ & \text{interior and reflecting boundaries}, \\ \begin{bmatrix} \psi^{k+1/2}_{n,I-1,L} & \psi^{k+1}_{n,I-1,R} & \psi^{k+1}_{n,I,L} & \psi^{k+1}_{n,I,R} \end{bmatrix}^T, & \text{incident right boundary}. \end{cases} \tag{3.68}$$

We also define the surface fluxes. For an incident boundary on the left, we define

$$\underline{\hat{\psi}}^{k+1,surf}_{n,3/2} = \begin{cases} \begin{bmatrix} \psi^{k+1}_{n,1,L} & \psi^{k+1}_{n,2,L} & \psi^{k+1}_{n,2,L} & \psi^{k}_{n,3,L} \end{bmatrix}^T, & \mu_n < 0, \\ \begin{bmatrix} \psi^{b,k+1}_{n,L} & \psi^{k+1}_{n,1,R} & \psi^{k+1}_{n,1,R} & \psi^{k+1/2}_{n,2,R} \end{bmatrix}^T, & \mu_n > 0, \end{cases} \tag{3.69a}$$

for the problem interior and reflecting boundaries, we define

$$\underline{\hat{\psi}}^{k+1,surf}_{n,i+1/2} = \begin{cases} \begin{bmatrix} \psi^{k+1/2}_{n,i,L} & \psi^{k+1}_{n,i+1,L} & \psi^{k+1}_{n,i+1,L} & \psi^{k}_{n,i+2,L} \end{bmatrix}^T, & \mu_n < 0, \\ \begin{bmatrix} \psi^{k}_{n,i-1,R} & \psi^{k+1}_{n,i,R} & \psi^{k+1}_{n,i,R} & \psi^{k+1/2}_{n,i+1,R} \end{bmatrix}^T, & \mu_n > 0, \end{cases} \tag{3.69b}$$

and for an incident boundary on the right, we define

$$\underline{\hat{\psi}}^{k+1,surf}_{n,I-1/2} = \begin{cases} \begin{bmatrix} \psi^{k+1/2}_{n,I-1,L} & \psi^{k+1}_{n,I,L} & \psi^{k+1}_{n,I,L} & \psi^{b,k+1}_{n,R} \end{bmatrix}^T, & \mu_n < 0, \\ \begin{bmatrix} \psi^{k}_{n,I-2,R} & \psi^{k+1}_{n,I-1,R} & \psi^{k+1}_{n,I-1,R} & \psi^{k+1}_{n,I,R} \end{bmatrix}^T, & \mu_n > 0. \end{cases} \tag{3.69c}$$

Now the SBJ equations are

$$\frac{1}{v\Delta t_{k+1}}\underline{\underline{M}}_{i+1/2}\left(\underline{\hat{\psi}}^{k+1}_{n,i+1/2}-\underline{\psi}^{k}_{n,i+1/2}\right)+\mu_n\underline{\underline{L}}^{surf}_{i+1/2}\underline{\hat{\psi}}^{k+1,surf}_{n,i+1/2}-\mu_n\underline{\underline{L}}_{i+1/2}\underline{\hat{\psi}}^{k+1}_{n,i+1/2}$$
$$+\underline{\underline{T}}_{i+1/2}\underline{\hat{\psi}}^{k+1}_{n,i+1/2}=\frac{1}{2}\underline{\underline{S}}_{i+1/2}\sum_{m=1}^{N}\underline{\hat{\psi}}^{k+1}_{m,i+1/2}\Delta_m+\underline{\underline{M}}_{i+1/2}\underline{Q}^{k+1}_{n,i+1/2}\,, \quad (3.70a)$$

with initial conditions

$$\underline{\psi}^{0}_{n,i+1/2}=\begin{bmatrix}\displaystyle\int_{x_{i-1/2}}^{x_{i+1/2}} w_{i,L}(x)\,\psi^{i}_{n}(x)\,\mathrm{d}x\\ \displaystyle\int_{x_{i-1/2}}^{x_{i+1/2}} w_{i,R}(x)\,\psi^{i}_{n}(x)\,\mathrm{d}x\\ \displaystyle\int_{x_{i+1/2}}^{x_{i+3/2}} w_{i+1,L}(x)\,\psi^{i}_{n}(x)\,\mathrm{d}x\\ \displaystyle\int_{x_{i+1/2}}^{x_{i+3/2}} w_{i+1,R}(x)\,\psi^{i}_{n}(x)\,\mathrm{d}x\end{bmatrix}. \quad (3.70b)$$

3.4.1 Solving the Staggered-Block Jacobi Equations

Because the incident angular flux in Eq. (3.70a) is lagged to time t_k, no sweeps are necessary to solve the SBJ equations. We break the surface term in Eq. (3.70a) into known (incident) and unknown components, as with the implicit method, by defining

$$\underline{\underline{P}}_n=\begin{cases}\begin{bmatrix}-1&0&0&0\\0&0&1&0\\0&0&-1&0\\0&0&0&0\end{bmatrix}, & \mu_n<0\,,\\ \begin{bmatrix}0&0&0&0\\0&1&0&0\\0&-1&0&0\\0&0&0&1\end{bmatrix}, & \mu_n>0\,,\end{cases} \quad (3.71a)$$

$$\underline{\underline{R}}_n = \begin{cases} \begin{bmatrix} 0 & 0 & 0 & 0 \\ 0 & 0 & 0 & 0 \\ 0 & 0 & 0 & 0 \\ 0 & 0 & 0 & -1 \end{bmatrix}, & \mu_n < 0\,, \\ \begin{bmatrix} 1 & 0 & 0 & 0 \\ 0 & 0 & 0 & 0 \\ 0 & 0 & 0 & 0 \\ 0 & 0 & 0 & 0 \end{bmatrix}, & \mu_n > 0\,, \end{cases} \tag{3.71b}$$

and also defining, for $\mu_n < 0$

$$\underline{\hat{\psi}}^{k,inc}_{n,i+1/2} = \begin{cases} \begin{bmatrix} 0 & 0 & 0 & \psi^k_{n,i+2,L} \end{bmatrix}^T, & 1 \le i \le I-2\,, \\ \begin{bmatrix} 0 & 0 & 0 & \psi^{b,k+1}_{n,R} \end{bmatrix}^T, & i = I-1\,, \end{cases} \tag{3.72a}$$

and for $\mu_n > 0$

$$\underline{\hat{\psi}}^{k,inc}_{n,i+1/2} = \begin{cases} \begin{bmatrix} \psi^{b,k+1}_{n,L} & 0 & 0 & 0 \end{bmatrix}^T, & i = 1\,, \\ \begin{bmatrix} \psi^k_{n,i-1,R} & 0 & 0 & 0 \end{bmatrix}^T, & 2 \le i \le I-1\,. \end{cases} \tag{3.72b}$$

Now the surface term in Eq. (3.70a) can be written

$$\mu_n \underline{\underline{L}}^{surf}_{i+1/2} \underline{\hat{\psi}}^{k+1,surf}_{n,i+1/2} = \mu_n \underline{\underline{P}}_n \underline{\hat{\psi}}^{k+1}_{n,i+1/2} - \mu_n \underline{\underline{R}}_n \underline{\hat{\psi}}^{k,inc}_{n,i+1/2}\,, \tag{3.73}$$

and Eq. (3.70a) can be rewritten as

$$\begin{aligned} \frac{1}{v\Delta t_{k+1}} \underline{\underline{M}}_{i+1/2} \left(\underline{\hat{\psi}}^{k+1}_{n,i+1/2} - \underline{\psi}^k_{n,i+1/2} \right) + \mu_n \underline{\underline{P}}_n \underline{\hat{\psi}}^{k+1}_{n,i+1/2} - \mu_n \underline{\underline{L}}_{i+1/2} \underline{\hat{\psi}}^{k+1}_{n,i+1/2} \\ + \underline{\underline{T}}_{i+1/2} \underline{\hat{\psi}}^{k+1}_{n,i+1/2} = \frac{1}{2} \underline{\underline{S}}_{i+1/2} \sum_{m=1}^{N} \underline{\hat{\psi}}^{k+1}_{m,i+1/2} \Delta_m + \mu_n \underline{\underline{R}}_n \underline{\hat{\psi}}^{k,inc}_{n,i+1/2} \\ + \underline{\underline{M}}_{i+1/2} \underline{Q}^{k+1}_{n,i+1/2}\,. \end{aligned} \tag{3.74}$$

Defining

$$\underline{\underline{U}}^{k+1}_{n,i+1/2} = \frac{1}{v\Delta t_{k+1}}\underline{\underline{M}}_{i+1/2} + \mu_n\left(\underline{\underline{P}}_n - \underline{\underline{L}}_{i+1/2}\right) + \underline{\underline{T}}_{i+1/2}\,, \tag{3.75}$$

and

$$\underline{\hat{\phi}}^{k+1}_{i+1/2} = \sum_{n=1}^{N} \underline{\hat{\psi}}^{k+1}_{n,i+1/2}\,\Delta_n\,, \tag{3.76}$$

and multiplying Eq. (3.74) by $\left(\underline{\underline{U}}^{k+1}_{n,i+1/2}\right)^{-1}$, we obtain

$$\begin{aligned}\underline{\hat{\psi}}^{k+1}_{n,i+1/2} = {} & \frac{1}{2}\left(\underline{\underline{U}}^{k+1}_{n,i+1/2}\right)^{-1}\underline{\underline{S}}_{i+1/2}\underline{\hat{\phi}}^{k+1}_{i+1/2} + \mu_n\left(\underline{\underline{U}}^{k+1}_{n,i+1/2}\right)^{-1}\underline{\underline{R}}_n\underline{\hat{\psi}}^{k,inc}_{n,i+1/2} \\ & + \frac{1}{v\Delta t_{k+1}}\left(\underline{\underline{U}}^{k+1}_{n,i+1/2}\right)^{-1}\underline{\underline{M}}_{i+1/2}\underline{\psi}^{k}_{n,i+1/2} + \left(\underline{\underline{U}}^{k+1}_{n,i+1/2}\right)^{-1}\underline{\underline{M}}_{i+1/2}\underline{Q}^{k+1}_{n,i+1/2}\,. \end{aligned} \tag{3.77}$$

Operating by $\sum_{n=1}^{N}(\cdot)\Delta_n$ and rearranging, we find

$$\begin{aligned}\left[\underline{\underline{I}} - \frac{1}{2}\sum_{n=1}^{N}\left(\underline{\underline{U}}^{k+1}_{n,i+1/2}\right)^{-1}\Delta_n\,\underline{\underline{S}}_{i+1/2}\right]\underline{\hat{\phi}}^{k+1}_{i+1/2} = {} & \sum_{n=1}^{N}\mu_n\left(\underline{\underline{U}}^{k+1}_{n,i+1/2}\right)^{-1}\underline{\underline{R}}_n\underline{\hat{\psi}}^{k,inc}_{n,i+1/2}\Delta_n \\ & + \frac{1}{v\Delta t_{k+1}}\sum_{n=1}^{N}\left(\underline{\underline{U}}^{k+1}_{n,i+1/2}\right)^{-1}\underline{\underline{M}}_{i+1/2}\underline{\psi}^{k}_{n,i+1/2}\Delta_n + \sum_{n=1}^{N}\left(\underline{\underline{U}}^{k+1}_{n,i+1/2}\right)^{-1}\underline{\underline{M}}_{i+1/2}\underline{Q}^{k+1}_{n,i+1/2}\,. \end{aligned} \tag{3.78}$$

To solve the SBJ transport equations, we first solve Eq. (3.78) for the scalar flux. This result is substituted into Eq. (3.77), and then the angular flux may be found. We emphasize that because the incident information is lagged to the previous time step, and is therefore known, every block in the problem is decoupled, and may be solved in parallel.

For the lumped SBJ method ($\theta = 1$), the SBJ transport method that we have presented in this section resembles the SBJ diffusion method we presented in Section 2.4 in the diffusive limit. This will be shown in an asymptotic analysis of the SBJ transport method in Chapter 4. Therefore, we anticipate that this SBJ transport method will be, like the SBJ diffusion method, unconditionally stable in the diffusive limit. We have found, empirically, that the SBJ transport method is also unconditionally stable away from the diffusive limit. That is, we have not yet found a problem for which the lumped SBJ transport method is not stable. This is not the case with the unlumped ($\theta = 0$) SBJ transport method. In that case, the SBJ transport method in the diffusive limit has a three-point removal stencil, rather than a one-point removal stencil as in the lumped case. Apparently, this three-point removal stencil is not unconditionally stable. Therefore, the numerical results we show in Chapter 5 will be

limited to the lumped case.

In addition to numerical stability, the SBJ transport method shares many other similar properties with the SBJ diffusion method investigated in Chapter 2. In particular, the SBJ transport method does not preserve particle balance and is inaccurate for optically-thin problems. Domain-wise particle balance can be restored using a rebalance procedure analogous to the rebalance method derived for the SBJ diffusion method in Section 2.4.2. This is presented in the following section. To improve accuracy, the lagged incident angular fluxes can be iterated; this is presented in Section 3.4.3. Accuracy can be improved in optically-thin regions by complementing the SBJ transport method with a single stretched sweep per time step; this is presented in Section 3.4.4.

3.4.2 Restoring Particle Conservation Using Rebalance

To calculate the particle conservation rebalance factor, we consider again the continuous, one-dimensional, mono-energetic transport equation with isotropic scattering, which represents a particle balance over the (x,μ) phase-space at time t:

$$\frac{1}{v}\frac{\partial}{\partial t}\psi(x,\mu,t)+\mu\frac{\partial}{\partial x}\psi(x,\mu,t)+\Sigma_t(x)\psi(x,\mu,t)=\frac{\Sigma_s(x)}{2}\int_{-1}^{1}\psi(x,\mu',t)\,\mathrm{d}\mu'+Q(x,\mu,t)\,. \tag{3.79}$$

Averaging Eq. (3.79) over a time step by operating with $\dfrac{1}{\Delta t_{k+1}}\displaystyle\int_{t_k}^{t_{k+1}}(\cdot)\,\mathrm{d}t$ and defining

$$\bar{\psi}^{k+1}(x,\mu)=\frac{1}{\Delta t_{k+1}}\int_{t_k}^{t_{k+1}}\psi(x,\mu,t)\,\mathrm{d}t\,, \tag{3.80a}$$

$$Q^{k+1}(x,\mu)=\frac{1}{\Delta t_{k+1}}\int_{t_k}^{t_{k+1}}Q(x,\mu,t)\,\mathrm{d}t\,, \tag{3.80b}$$

$$\psi^{k}(x,\mu)=\psi(x,\mu,t_k)\,, \tag{3.80c}$$

we obtain

$$\frac{1}{v\Delta t_{k+1}}\Big[\psi^{k+1}(x,\mu)-\psi^{k}(x,\mu)\Big]+\mu\frac{\partial}{\partial x}\bar{\psi}^{k+1}(x,\mu)+\Sigma_t(x)\bar{\psi}^{k+1}(x,\mu) = \frac{\Sigma_s(x)}{2}\int_{-1}^{1}\bar{\psi}^{k+1}(x,\mu')\,\mathrm{d}\mu'+Q^{k+1}(x,\mu)\,. \tag{3.81}$$

We can apply an implicit time discretization to this equation while maintaining particle balance. Therefore, we now have

$$\frac{1}{v\Delta t_{k+1}}\left[\psi^{k+1}(x,\mu)-\psi^{k}(x,\mu)\right]+\mu\frac{\partial}{\partial x}\psi^{k+1}(x,\mu)+\Sigma_t(x)\psi^{k+1}(x,\mu) = \frac{\Sigma_s(x)}{2}\int_{-1}^{1}\psi^{k+1}(x,\mu')\,\mathrm{d}\mu'+Q^{k+1}(x,\mu)\,. \quad (3.82)$$

We now integrate over the (x,μ) phase-space by operating on Eq. (3.82) with $\int_0^X\int_{-1}^1(\cdot)\,\mathrm{d}\mu\,\mathrm{d}x$ and define the current as

$$J^{k+1}(x)=\int_{-1}^{1}\mu\,\psi^{k+1}(x,\mu)\,\mathrm{d}\mu\,, \quad (3.83)$$

and obtain

$$\frac{1}{v\Delta t_{k+1}}\left[\int_0^X\phi^{k+1}(x)\,\mathrm{d}x-\int_0^X\phi^{k}(x)\,\mathrm{d}x\right]+\left[J^{k+1}(X)-J^{k+1}(0)\right]+\int_0^X\Sigma_a(x)\phi^{k+1}(x)\,\mathrm{d}x = \int_0^X\int_{-1}^1 Q^{k+1}(x,\mu)\,\mathrm{d}\mu\,\mathrm{d}x\,. \quad (3.84)$$

Splitting the current into incoming and outgoing partial currents, we have

$$\frac{1}{v\Delta t_{k+1}}\left[\int_0^X\phi^{k+1}(x)\,\mathrm{d}x-\int_0^X\phi^{k}(x)\,\mathrm{d}x\right]+\left[J_L^{out,k+1}+J_R^{out,k+1}\right]-\left[J_L^{b,k+1}+J_R^{b,k+1}\right] + \int_0^X\Sigma_a(x)\phi^{k+1}(x)\,\mathrm{d}x=\int_0^X\int_{-1}^1 Q^{k+1}(x,\mu)\,\mathrm{d}\mu\,\mathrm{d}x\,, \quad (3.85)$$

where $J_L^{out,k+1}$ and $J_R^{out,k+1}$ are the outgoing partial currents at time t_{k+1} for the left and right boundaries, respectively.

Eq. (3.85) represents a particle balance equation over the spatial domain $0\le x\le X$ and over all angles at time t_{k+1}. If we assume that the conservative angular flux is equal to the non-conservative angular flux multiplied by a rebalance factor, i.e.,

$$\psi^{k+1}(x,\mu)=\gamma^{k+1}\psi^{nc,k+1}(x,\mu)\,, \quad (3.86)$$

then the scalar flux and outgoing partial currents are also equal to the non-conservative scalar flux or outgoing partial currents multiplied by a rebalance factor. Therefore,

$$\phi^{k+1}(x)=\gamma^{k+1}\phi^{nc,k+1}(x)\,, \quad (3.87a)$$

$$J_L^{out,k+1} = \gamma^{k+1} J_L^{out,nc,k+1}, \tag{3.87b}$$

$$J_R^{out,k+1} = \gamma^{k+1} J_R^{out,nc,k+1}, \tag{3.87c}$$

where $\phi^{nc,k+1}(x)$ is the non-conservative scalar flux, $J_L^{out,nc,k+1}$ is the non-conservative outgoing partial current on the left boundary, and $J_R^{out,nc,k+1}$ is the non-conservative outgoing partial current on the right boundary. Substituting Eqs. (3.87) into Eq. (3.85), and solving for the rebalance factor γ^{k+1}, we find

$$\gamma^{k+1} = \frac{\frac{1}{v\Delta t_{k+1}} \int_0^X \phi^k(x)\,\mathrm{d}x + \left[J_L^{b,k+1} + J_R^{b,k+1}\right] + \int_0^X \int_{-1}^1 Q^{k+1}(x,\mu)\,\mathrm{d}\mu\,\mathrm{d}x}{\frac{1}{v\Delta t_{k+1}} \int_0^X \phi^{nc,k+1}(x)\,\mathrm{d}x + \left[J_L^{nc,out,k+1} + J_R^{nc,out,k+1}\right] + \int_0^X \Sigma_a(x)\phi^{nc,k+1}(x)\,\mathrm{d}x}. \tag{3.88}$$

Writing this in discretized form, we have

$$\gamma^{k+1} = \frac{\frac{1}{v\Delta t_{k+1}} \sum_{i=1}^I \phi_i^k \Delta x_i + \left[J_L^{b,k+1} + J_R^{b,k+1}\right] + \sum_{i=1}^I \sum_{n=1}^N Q_{n,i}^{k+1} \Delta_n \Delta x_i}{\frac{1}{v\Delta t_{k+1}} \sum_{i=1}^I \phi_i^{nc,k+1} \Delta x_i + \left[J_L^{nc,out,k+1} + J_R^{nc,out,k+1}\right] + \sum_{i=1}^I \Sigma_{a,i} \phi_i^{nc,k+1} \Delta x_i}, \tag{3.89}$$

where

$$\phi_i^k = \frac{\phi_{i,L}^k + \phi_{i,R}^k}{2}, \tag{3.90a}$$

$$\phi_i^{nc,k+1} = \frac{\phi_{i,L}^{nc,k+1} + \phi_{i,R}^{nc,k+1}}{2}, \tag{3.90b}$$

$$Q_{n,i}^{k+1} = \frac{Q_{n,i,L}^{k+1} + Q_{n,i,R}^{k+1}}{2}. \tag{3.90c}$$

After the rebalance factor γ^{k+1} has been calculated using Eq. (3.89), the conservative scalar flux may be calculated using Eq. (3.87a) and the conservative angular flux may be calculated using Eq. (3.86). This particle conservation rebalance factor may be applied at the end of a time step, where it ensures that the SBJ transport solution satisfies global particle conservation. Alternatively, if used as part of an iterative procedure (see the next section on the iterative SBJ transport method), wherein the rebalance factor is applied after every iteration, then the rebalance procedure doubles as an iteration acceleration method.

3.4.3 Improving Accuracy Using Iterations

The accuracy of the SBJ method can be improved by iterating the lagged incident angular fluxes on the boundaries of each block. Writing Eq. (3.70a) as an iterative method without rebalance, we have

$$\frac{1}{v\Delta t_{k+1}}\underline{\underline{M}}_{i+1/2}\left(\underline{\hat{\psi}}_{n,i+1/2}^{(l+1/2),k+1}-\underline{\psi}_{n,i+1/2}^{k}\right)+\mu_n\underline{\underline{L}}_{i+1/2}^{surf}\underline{\hat{\psi}}_{n,i+1/2}^{(l),k+1,surf}-\mu_n\underline{\underline{L}}_{i+1/2}\underline{\hat{\psi}}_{n,i+1/2}^{(l+1/2),k+1}$$
$$+\underline{\underline{T}}_{i+1/2}\underline{\hat{\psi}}_{n,i+1/2}^{(l+1/2),k+1}=\frac{1}{2}\underline{\underline{S}}_{i+1/2}\sum_{m=1}^{N}\underline{\hat{\psi}}_{m,i+1/2}^{(l+1/2),k+1}\Delta_m+\underline{\underline{M}}_{i+1/2}\underline{Q}_{n,i+1/2}^{k+1}, \quad (3.91a)$$

$$\underline{\hat{\psi}}_{n,i+1/2}^{(l+1),k+1}=\underline{\hat{\psi}}_{n,i+1/2}^{(l+1/2),k+1}, \quad (3.91b)$$

where l is the iteration index, and

$$\underline{\hat{\psi}}_{n,i+1/2}^{(l+1/2),k+1}=\begin{cases}\left[\psi_{n,1,L}^{(l+1/2),k+1} \quad \psi_{n,1,R}^{(l+1/2),k+1} \quad \psi_{n,2,L}^{(l+1/2),k+1} \quad \psi_{n,2,R}^{(l+1/2),k+1/2}\right]^T, \\ \qquad\qquad\qquad\qquad\qquad\qquad \text{left incident boundary}, \\ \left[\psi_{n,i,L}^{(l+1/2),k+1/2} \quad \psi_{n,i,R}^{(l+1/2),k+1} \quad \psi_{n,i+1,L}^{(l+1/2),k+1} \quad \psi_{n,i+1,R}^{(l+1/2),k+1/2}\right]^T, \\ \qquad\qquad\qquad\qquad\qquad\qquad \text{interior and reflecting boundaries}, \\ \left[\psi_{n,I-1,L}^{(l+1/2),k+1/2} \quad \psi_{n,I-1,R}^{(l+1/2),k+1} \quad \psi_{n,I,L}^{(l+1/2),k+1} \quad \psi_{n,I,R}^{(l+1/2),k+1}\right]^T, \\ \qquad\qquad\qquad\qquad\qquad\qquad \text{right incident boundary}.\end{cases} \quad (3.92)$$

The iterative surface flux vector is defined, for a left incident boundary, as

$$\underline{\hat{\psi}}_{n,3/2}^{(l),k+1,surf}=\begin{cases}\left[\psi_{n,1,L}^{(l+1/2),k+1} \quad \psi_{n,2,L}^{(l+1/2),k+1} \quad \psi_{n,2,L}^{(l+1/2),k+1} \quad \psi_{n,3,L}^{(l),k+1}\right]^T, & \mu_n<0, \\ \left[\psi_{n,L}^{b,k+1} \quad \psi_{n,1,R}^{(l+1/2),k+1} \quad \psi_{n,1,R}^{(l+1/2),k+1} \quad \psi_{n,2,R}^{(l+1/2),k+1/2}\right]^T, & \mu_n>0, \end{cases} \quad (3.93a)$$

for the interior and reflecting boundaries as

$$\underline{\hat{\psi}}_{n,i+1/2}^{(l),k+1,surf}=\begin{cases}\left[\psi_{n,i,L}^{(l+1/2),k+1/2} \quad \psi_{n,i+1,L}^{(l+1/2),k+1} \quad \psi_{n,i+1,L}^{(l+1/2),k+1} \quad \psi_{n,i+2,L}^{(l),k+1}\right]^T, & \mu_n<0, \\ \left[\psi_{n,i-1,R}^{(l/2),k+1} \quad \psi_{n,i,R}^{(l+1/2),k+1} \quad \psi_{n,i,R}^{(l+1/2),k+1} \quad \psi_{n,i+1,R}^{(l+1/2),k+1/2}\right]^T, & \mu_n>0, \end{cases} \quad (3.93b)$$

and for a right incident boundary as

$$\underline{\hat{\psi}}^{(l),k+1,surf}_{n,I-1/2} = \begin{cases} \begin{bmatrix} \psi^{(l+1/2),k+1/2}_{n,I-1,L} & \psi^{(l+1/2),k+1}_{n,I,L} & \psi^{(l+1/2),k+1}_{n,I,L} & \psi^{b,k+1}_{n,R} \end{bmatrix}^T, & \mu_n < 0\,, \\ \begin{bmatrix} \psi^{(l),k+1}_{n,I-2,R} & \psi^{(l+1/2),k+1}_{n,I-1,R} & \psi^{(l+1/2),k+1}_{n,I-1,R} & \psi^{(l+1/2),k+1}_{n,I,R} \end{bmatrix}^T, & \mu_n > 0\,. \end{cases} \tag{3.93c}$$

The initial conditions are

$$\underline{\psi}^0_{n,i+1/2} = \begin{bmatrix} \int_{x_{i-1/2}}^{x_{i+1/2}} w_{i,L}(x)\,\psi^i_n(x)\,\mathrm{d}x \\ \int_{x_{i-1/2}}^{x_{i+1/2}} w_{i,R}(x)\,\psi^i_n(x)\,\mathrm{d}x \\ \int_{x_{i+1/2}}^{x_{i+3/2}} w_{i+1,L}(x)\,\psi^i_n(x)\,\mathrm{d}x \\ \int_{x_{i+1/2}}^{x_{i+3/2}} w_{i+1,R}(x)\,\psi^i_n(x)\,\mathrm{d}x \end{bmatrix}. \tag{3.94}$$

The iteration procedure is begun by setting

$$\psi^{(0),k+1}_{n,i,L} = \psi^k_{n,i,L}\,, \tag{3.95a}$$

$$\psi^{(0),k+1}_{n,i,R} = \psi^k_{n,i,R}\,. \tag{3.95b}$$

Alternatively, we can use the rebalance procedure we derived in the previous section as an iterative acceleration scheme. In this case, the iterative procedure is

$$\frac{1}{v\Delta t_{k+1}}\underline{\underline{M}}_{i+1/2}\left(\underline{\hat{\psi}}^{(l+1/2),k+1}_{n,i+1/2} - \underline{\psi}^k_{n,i+1/2}\right) + \mu_n \underline{\underline{L}}^{surf}_{i+1/2}\underline{\hat{\psi}}^{(l),k+1,surf}_{n,i+1/2} - \mu_n \underline{\underline{L}}_{i+1/2}\underline{\hat{\psi}}^{(l+1/2),k+1}_{n,i+1/2}$$
$$+ \underline{\underline{T}}_{i+1/2}\underline{\hat{\psi}}^{(l+1/2),k+1}_{n,i+1/2} = \frac{1}{2}\underline{\underline{S}}_{i+1/2}\sum_{m=1}^{N}\underline{\hat{\psi}}^{(l+1/2),k+1}_{m,i+1/2}\,\Delta_m + \underline{\underline{M}}_{i+1/2}\underline{Q}^{k+1}_{n,i+1/2}\,, \tag{3.96a}$$

$$\underline{\hat{\psi}}^{(l+1),k+1}_{n,i+1/2} = \gamma^{(l+1),k+1}\,\underline{\hat{\psi}}^{(l+1/2),k+1}_{n,i+1/2}\,, \tag{3.96b}$$

where the rebalance factor $\gamma^{(l+1),k+1}$ is calculated using

$$\gamma^{(l+1),k+1} = \frac{A^{k+1}}{B^{(l+1),k+1}}\,, \tag{3.97}$$

where

$$A^{k+1} = \frac{1}{v\Delta t_{k+1}} \sum_{i=1}^{I} \phi_i^k \Delta x_i + \left[J_L^{b,k+1} + J_R^{b,k+1} \right] + \sum_{i=1}^{I} \sum_{n=1}^{N} Q_{n,i}^{k+1} \Delta_n \Delta x_i \,, \tag{3.98a}$$

$$B^{(l+1),k+1} = \frac{1}{v\Delta t_{k+1}} \sum_{i=1}^{I} \phi_i^{(l+1/2),k+1} \Delta x_i + \left[J_L^{(l+1/2),out,k+1} + J_R^{(l+1/2),out,k+1} \right] + \sum_{i=1}^{I} \Sigma_{a,i} \phi_i^{(l+1/2),k+1} \Delta x_i \,, \tag{3.98b}$$

and where

$$\phi_i^k = \frac{\phi_{i,L}^k + \phi_{i,R}^k}{2} \,, \tag{3.99a}$$

$$\phi_i^{(l+1/2),k+1} = \frac{\sum_{n=1}^{N} \left[\psi_{n,i,L}^{(l+1/2),k+1} + \psi_{n,i,R}^{(l+1/2),k+1} \right] \Delta_n}{2} \,, \tag{3.99b}$$

$$J_L^{(l+1/2),out,k+1} = \sum_{\mu_n<0} \mu_n \psi_{n,1,L}^{(l+1/2),k+1} \Delta_n \,, \tag{3.99c}$$

$$J_R^{(l+1/2),out,k+1} = \sum_{\mu_n>0} \mu_n \psi_{n,I,R}^{(l+1/2),k+1} \Delta_n \,, \tag{3.99d}$$

$$Q_{n,i}^{k+1} = \frac{Q_{n,i,L}^{k+1} + Q_{n,i,R}^{k+1}}{2} \,. \tag{3.99e}$$

Again the iteration procedure is begun by setting

$$\psi_{n,i,L}^{(0),k+1} = \psi_{n,i,L}^k \,, \tag{3.100a}$$

$$\psi_{n,i,R}^{(0),k+1} = \psi_{n,i,R}^k \,. \tag{3.100b}$$

3.4.4 Using Sweeps to Improve Accuracy in Optically-Thin Regions

In the numerical results for the SBJ diffusion method described in Section 2.5, we found that the method was fairly accurate in optically-thick regions, but inaccurate in optically-thin regions without a large number of iterations. This was due to the way the SBJ diffusion method lags incident information to the beginning of the time step. In optically-thin regions, where adjacent cells are tightly coupled, this lagging produces greater errors than in

optically-thick regions, where cells are not as tightly coupled. We show in the numerical results in Chapter 5 that this behavior holds for the SBJ transport method as well.

The implicit transport method, discussed in Section 3.3.1, is accurate and efficient for optically-thin or weakly-scattering problems, whereas optically-thick and diffusive problems require advanced iterative methods like the Modified Four-Step Diffusion Synthetic Acceleration method derived in Appendix B.2. In this way, the implicit and SBJ transport methods can be considered complementary. The implicit method is accurate and efficient in the optically-thin limit, while the SBJ method is accurate and efficient in the optically-thick limit. To see why the implicit method is accurate and efficient in the optically-thin limit, let us consider the iterative implicit LDFEM equation:

$$\frac{1}{v\Delta t_{k+1}}\underline{\underline{M}}_i\left(\underline{\psi}_{n,i}^{(l+1/2),k+1}-\underline{\psi}_{n,i}^{k}\right)+\mu_n\underline{\underline{L}}_i^{surf}\underline{\psi}_{n,i}^{(l+1/2),k+1,surf}-\mu_n\underline{\underline{L}}_i\underline{\psi}_{n,i}^{(l+1/2),k+1}$$
$$+\Sigma_{t,i}\underline{\underline{M}}_i\underline{\psi}_{n,i}^{(l+1/2),k+1}=\frac{\Sigma_{s,i}}{2}\underline{\underline{M}}_i\sum_{m=1}^{N}\underline{\psi}_{m,i}^{(l),k+1}\Delta_m+\underline{\underline{M}}_i\underline{Q}_{n,i}^{k+1}. \quad (3.101)$$

Typically, the implicit method sets $\underline{\psi}_{n,i}^{(0),k+1}=\underline{\psi}_{n,i}^{k}$. However, suppose we consider the first iteration ($l=0$), and suppose we set $\underline{\psi}_{n,i}^{(0),k+1}=0$. Then Eq. (3.101) resembles a purely absorbing problem, and the solution, $\underline{\psi}_{n,i}^{(1/2),k+1}$, represents the flux of particles that experience no collisions during time step $k+1$. Therefore, in a vacuum, $\underline{\psi}_{n,i}^{(1/2),k+1}$ represents the exact solution (except for truncation errors due to the discretizations). In this way, we can find the solution to the transport equation in the optically-thin limit using a single sweep per time step.

In reality, we can obtain improved solutions if, rather than setting $\underline{\psi}_{n,i}^{(0),k+1}=0$, we set $\underline{\psi}_{n,i}^{(0),k+1}=\underline{\psi}_{n,i}^{k}$. Therefore, the sweep equation is

$$\frac{1}{v\Delta t_{k+1}}\underline{\underline{M}}_i\left(\underline{\psi}_{n,i}^{sweep,k+1}-\underline{\psi}_{n,i}^{k}\right)+\mu_n\underline{\underline{L}}_i^{surf}\underline{\psi}_{n,i}^{sweep,k+1,surf}-\mu_n\underline{\underline{L}}_i\underline{\psi}_{n,i}^{sweep,k+1}$$
$$+\Sigma_{t,i}\underline{\underline{M}}_i\underline{\psi}_{n,i}^{sweep,k+1}=\frac{\Sigma_{s,i}}{2}\underline{\underline{M}}_i\sum_{m=1}^{N}\underline{\psi}_{m,i}^{k}\Delta_m+\underline{\underline{M}}_i\underline{Q}_{n,i}^{k+1}. \quad (3.102)$$

The solution, $\underline{\psi}_{n,i}^{sweep,k+1}$, no longer represents the uncollided flux at time t_{k+1}, but is much closer to the actual solution because it uses a much more accurate approximation of the scattering term.

The SBJ transport method with sweeps uses the angular flux produced by the sweep as the incident angular flux on each block. Therefore, rather than lagging the incident angular

fluxes to time t_k, we set, for $\mu_n < 0$

$$\underline{\hat{\psi}}^{k,inc}_{n,i+1/2} = \begin{cases} \begin{bmatrix} 0 & 0 & 0 & \psi^{sweep,k+1}_{n,i+2,L} \end{bmatrix}^T , & 1 \le i \le I-2 , \\ \begin{bmatrix} 0 & 0 & 0 & \psi^{b,k+1}_{n,R} \end{bmatrix}^T , & i = I-1 , \end{cases} \tag{3.103a}$$

and for $\mu_n > 0$

$$\underline{\hat{\psi}}^{k,inc}_{n,i+1/2} = \begin{cases} \begin{bmatrix} \psi^{b,k+1}_{n,L} & 0 & 0 & 0 \end{bmatrix}^T , & i = 1 , \\ \begin{bmatrix} \psi^{sweep,k+1}_{n,i-1,R} & 0 & 0 & 0 \end{bmatrix}^T , & 2 \le i \le I-1 . \end{cases} \tag{3.103b}$$

Alternatively, the solution to the sweep may be used as a starting guess for the iterative SBJ method

$$\psi^{(0),k+1}_{n,i,L} = \psi^{sweep,k+1}_{n,i,L} , \tag{3.104a}$$

$$\psi^{(0),k+1}_{n,i,R} = \psi^{sweep,k+1}_{n,i,R} . \tag{3.104b}$$

Stretching the Sweeps

As we show in the numerical results in Chapter 5, adding sweeps in this manner is only accurate in the optically-thin limit, and the SBJ transport method is only accurate in the optically-thick limit. This leaves a large intermediate region in which the SBJ transport method with sweeps is still inaccurate. We can mitigate this by "stretching" the sweep equation to maximize the mean-free path that particles travel. Rearranging Eq. (3.102), we find

$$\begin{aligned} \left(\frac{1}{v\Delta t_{k+1}} + \Sigma_{t,i} \right) \underline{\underline{M}}_i \underline{\psi}^{sweep,k+1}_{n,i} + \mu_n \underline{\underline{L}}^{surf}_i \underline{\psi}^{sweep,k+1,surf}_{n,i} - \mu_n \underline{\underline{L}}_i \underline{\psi}^{sweep,k+1}_{n,i} \\ = \frac{1}{v\Delta t_{k+1}} \underline{\underline{M}}_i \underline{\psi}^{k}_{n,i} + \frac{\Sigma_{s,i}}{2} \underline{\underline{M}}_i \sum_{m=1}^{N} \underline{\psi}^{k}_{m,i} \Delta_m + \underline{\underline{M}}_i \underline{Q}^{k+1}_{n,i} . \end{aligned} \tag{3.105}$$

Applying the standard diffusion stretching [1] to Eq. (3.105), we obtain

$$\begin{aligned} \left(\frac{\varepsilon}{v\Delta t_{k+1}} + \frac{\Sigma_{t,i}}{\varepsilon} \right) \underline{\underline{M}}_i \underline{\psi}^{sweep,k+1}_{n,i} + \mu_n \underline{\underline{L}}^{surf}_i \underline{\psi}^{sweep,k+1,surf}_{n,i} - \mu_n \underline{\underline{L}}_i \underline{\psi}^{sweep,k+1}_{n,i} \\ = \frac{\varepsilon}{v\Delta t_{k+1}} \underline{\underline{M}}_i \underline{\psi}^{k}_{n,i} + \frac{1}{2} \left(\frac{\Sigma_{t,i}}{\varepsilon} - \varepsilon \Sigma_{a,i} \right) \underline{\underline{M}}_i \sum_{m=1}^{N} \underline{\psi}^{k}_{m,i} \Delta_m + \varepsilon \underline{\underline{M}}_i \underline{Q}^{k+1}_{n,i} . \end{aligned} \tag{3.106}$$

The quantity $\left(\frac{\varepsilon}{v\Delta t_{k+1}} + \frac{\Sigma_{t,i}}{\varepsilon}\right)$ represents the inverse of the mean-free path. We would like to maximize the mean-free path (and therefore minimize this term). Defining

$$f(\varepsilon) = \frac{\varepsilon}{v\Delta t_{k+1}} + \frac{\Sigma_t}{\varepsilon}\,, \tag{3.107}$$

and calculating the derivative of $f(\varepsilon)$ as

$$f'(\varepsilon) = \frac{1}{v\Delta t_{k+1}} - \frac{\Sigma_t}{\varepsilon^2}\,, \tag{3.108}$$

we may obtain the ε for which $f(\varepsilon)$ is minimized by setting $f'(\varepsilon)$ equal to zero. The minimum ε is therefore

$$\varepsilon = \sqrt{v\Delta t_{k+1}\Sigma_t}\,. \tag{3.109}$$

Substituting Eq. (3.109) into Eq. (3.106) gives the maximally-stretched transport equation. By stretching the transport equation, we have altered the material properties in the transport problem in order to cause particles to travel farther than they normally would. In essence, we are reducing the mean-free-path so that the uncollided flux will more closely resemble the total flux for optically-thick problems. The stretched sweep solution can then be used as an improved initial guess for the iterative SBJ method.

It now remains to find a general expression for ε. We know

$$\varepsilon = \begin{cases} 1\,, & \text{optically-thin limit}\,, \\ \sqrt{v\Delta t_{k+1}\Sigma_t}\,, & \text{optically-thick limit}\,. \end{cases} \tag{3.110}$$

While there is no unique way to determine ε between these two limits, we have found good results with

$$\varepsilon_i^{k+1} = 1 + c^{\kappa}\sqrt{v\Delta t_{k+1}\Sigma_{t,i}}\left[1 - \mathrm{e}^{-\left(\chi v\Delta t_{k+1}\Sigma_{t,i}\right)}\right]\,, \tag{3.111}$$

where c is the scattering ratio, and κ and χ are user-specified parameters. We have used $\kappa = 24$ and $\chi = 0.07$ to obtain the numerical results we present in Chapter 5.

Figure 3.10 shows how Eq. (3.111) smoothly interpolates between a value of $\varepsilon = 1$ in the optically-thin limit to $\varepsilon = \sqrt{v\Delta t_{k+1}\Sigma_t}$ in the optically-thick limit for the purely scattering $(c = 1)$ case. Although this interpolation function is not perfect, it does not need to be since it is generally used as a starting guess for the iterative SBJ method, so that the number of iterations required for an accurate solution can be reduced.

To see the effects of stretching on the sweep solution, consider a homogeneous slab, 1 cm in length, of purely scattering material with $\Sigma_t = 10\ \mathrm{cm}^{-1}$, divided into 100 cells. In the

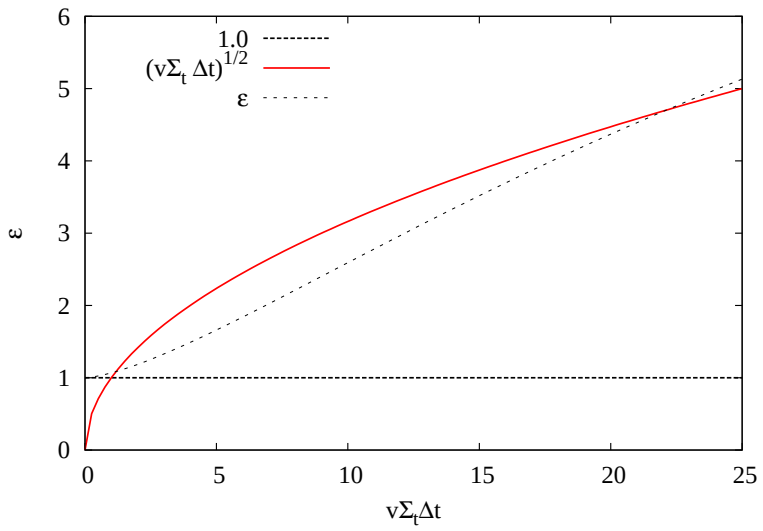

Figure 3.10 The ε Interpolation Function at Various Optical Thicknesses

first cell we place an isotropic source of strength $Q = 1$ cm^{-3} s^{-1}, with no source elsewhere. We set the particle velocity at $v = 1$ cm/s, and place a reflecting boundary condition on the left boundary, and a vacuum boundary condition on the right. The initial angular flux is zero. We executed a single time step of length $\Delta t = 1$ s, and also ran a benchmark calculation using the implicit method and time steps of length $\Delta t = 10^{-8}$ s. The resulting stretching parameter is $\varepsilon = 2.592$. In Figure 3.11 we show the scalar flux resulting from an unstretched sweep, a stretched sweep, and the benchmark solution. Here we see that the stretched sweep result is much closer to the benchmark result.

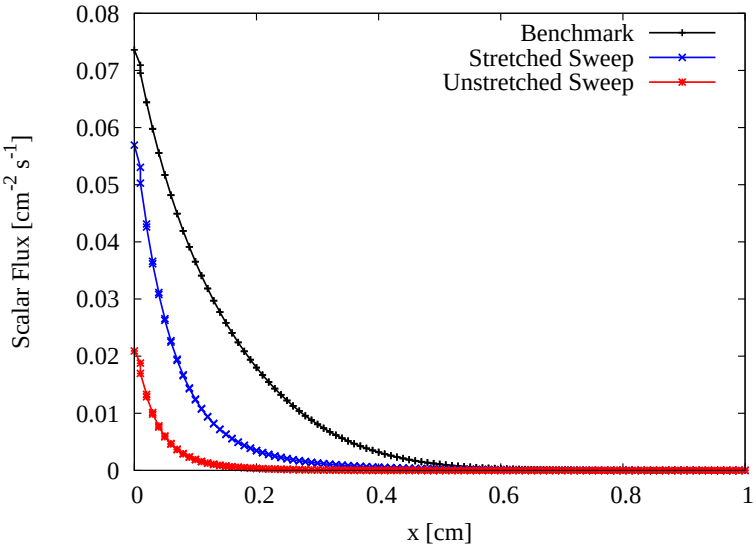

Figure 3.11 A Comparison Between Regular and Stretched Sweeps

Smoothing the Stretching Parameters

For heterogeneous problems, we have found that we can obtain improved results if we apply a smoothing technique to the stretching parameters. The smoothing technique we have used is

$$\acute{\varepsilon}_1^{k+1} = (1-\alpha)\varepsilon_1^{k+1} + \alpha\varepsilon_2^{k+1}\,, \tag{3.112a}$$

$$\acute{\varepsilon}_i^{k+1} = (1-\alpha)\varepsilon_i^{k+1} + \frac{\alpha}{2}\left(\varepsilon_{i-1}^{k+1} + \varepsilon_{i+1}^{k+1}\right), \qquad 2 \le i \le I-1\,, \tag{3.112b}$$

$$\acute{\varepsilon}_I^{k+1} = (1-\alpha)\varepsilon_I^{k+1} + \alpha\varepsilon_{I-1}^{k+1}\,, \tag{3.112c}$$

where ε_i^{k+1} is the unsmoothed stretching parameter calculated using Eq. (3.111), $\acute{\varepsilon}_i^{k+1}$ is the smoothed stretching parameters, and α is some specified smoothing parameter. For the heterogeneous problem we demonstrate in Section 5.5, we have used a smoothing parameter of $\alpha = 1/2$.

Angular Redistribution

Although the source iteration method iterates by converging on the scalar flux, the SBJ transport method iterates upon the angular flux. As a result, although the stretched sweeps produce an improved estimate of the scalar flux, the stretching can also produce a poor angular distribution of the particles. Knowing that as the material becomes increasingly

thick and diffusive, the angular flux should become more isotropic, we redistribute the angular flux using

$$\underline{\tilde{\psi}}_{n,i}^{sweep,k+1} = \underline{\psi}_{n,i}^{sweep,k+1} e^{A(1-\varepsilon)} + \frac{1}{2}\left(1 - e^{A(1-\varepsilon)}\right) \underline{\phi}_i^{sweep,k+1}, \tag{3.113}$$

where $\underline{\tilde{\psi}}_{n,i}^{sweep,k+1}$ is the angularly redistributed sweep solution, $\underline{\psi}_{n,i}^{sweep,k+1}$ is the sweep solution prior to the angular redistribution, $\underline{\phi}_i^{sweep,k+1}$ is the scalar flux from the sweep solution prior to the angular redistribution, and A is some specified parameter. For the numerical results we present in Chapter 5, we have used

$$A = 10c, \tag{3.114}$$

where c is the scattering ratio.

3.5 Summary

In this chapter we have introduced the well-known fully-explicit and implicit linear discontinuous finite element S_N transport methods. The fully-explicit method has both spatial and angular locality, making it easy to parallelize, but it lacks unconditional stability. The implicit method has unconditional stability, but requires mesh sweeps to solve, restricting the parallelism that can be exploited. For completeness, we also introduced the possibly new semi-explicit method. This method is also local, but it also lacks unconditional stability.

Finally, we introduced the new Staggered-Block Jacobi transport method. Like its diffusion analog introduced in Chapter 2, it has both unconditional stability and spatial locality. However, also like the SBJ diffusion method, the SBJ transport method lacks particle conservation, and, as we show in the numerical results in Chapter 5, it is also inaccurate in optically-thin regions. Domain-wise particle conservation can be restored using a rebalance procedure, and accuracy can be improved through the use of iterations and stretched sweeps.

Chapter 4

Asymptotic Analysis

In this chapter, we perform an asymptotic analysis of the various transport discretizations introduced in Chapter 3. This analysis will, first, demonstrate that the transport discretizations satisfy physically correct diffusion discretizations in the thick diffusive limit. If a transport discretization does not satisfy a physically correct diffusion discretization in the thick diffusive limit, it cannot be expected to provide physically correct solutions in that limit, unless the spatial cells are extremely small, i.e., smaller than one mean-free path in thickness. Second, the asymptotic analysis of the Staggered-Block Jacobi (SBJ) transport method will justify certain properties of the method, such as: a block must be composed of two cells (as opposed to one cell) in one dimension, and the angular fluxes adjacent to the exterior boundaries of the block must be discarded. The analysis will also demonstrate the relationship between the transport discretizations introduced in Chapter 3, and the diffusion discretizations introduced in Chapter 2. Namely, that the implicit, fully-explicit, and SBJ transport discretizations resemble the implicit, fully-explicit, and SBJ diffusion discretizations in the thick diffusive limit.

In this chapter, we follow the asymptotic analysis procedure outlined in Ref. [1], where it was performed on a general steady-state finite element transport discretization. First, in Section 4.1, we perform an asymptotic analysis of the continuous transport equation to derive a continuous diffusion equation. In Section 4.2, we present an asymptotic analysis of the implicit linear discontinuous finite element transport discretization, and in Section 4.3, we present an asymptotic analysis of the fully-explicit and semi-explicit linear discontinuous finite element transport discretizations. These three transport discretizations were derived in Section 3.3. Although the implicit and fully-explicit LDFEM transport methods are well-established, to our knowledge, the asymptotic analysis of these methods has not been published. Finally, in Section 4.4 we will present the asymptotic analysis of the SBJ transport method derived in Section 3.4.

4.1 Derivation of the Continuous Asymptotic Diffusion Equation

We begin by performing an asymptotic analysis of the continuous transport equation. This analysis will show that the solution of the transport equation, in the asymptotic limit, behaves to leading order according to a diffusion equation. Writing the one-dimensional, mono-energetic, time-dependent transport equation with isotropic scattering in the domain interior

$$\frac{1}{v}\frac{\partial}{\partial t}\psi(x,\mu,t)+\mu\frac{\partial}{\partial x}\psi(x,\mu,t)+\Sigma_t(x)\psi(x,\mu,t)=\frac{\Sigma_s(x)}{2}\int_{-1}^{1}\psi(x,\mu',t)\,\mathrm{d}\mu'+Q(x,\mu,t)\,, \tag{4.1}$$

we define the following asymptotic scalings:

$$\Sigma_t(x)=\frac{\sigma_t(x)}{\varepsilon}\,, \tag{4.2a}$$

$$\Sigma_a(x)=\varepsilon\sigma_a(x)\,, \tag{4.2b}$$

$$\Sigma_s(x)=\Sigma_t(x)-\Sigma_a(x)=\frac{\sigma_t(x)}{\varepsilon}-\varepsilon\sigma_a(x)\,, \tag{4.2c}$$

$$v=\frac{v'}{\varepsilon}\,, \tag{4.2d}$$

$$Q(x,\mu,t)=\varepsilon q(x,\mu,t)\,. \tag{4.2e}$$

Substituting Eqs. (4.2) into Eq. (4.1), we obtain

$$\begin{aligned}\frac{\varepsilon}{v'}\frac{\partial}{\partial t}\psi(x,\mu,t)+\mu\frac{\partial}{\partial x}\psi(x,\mu,t)+\frac{\sigma_t(x)}{\varepsilon}\psi(x,\mu,t)&\\ =\frac{1}{2}\left[\frac{\sigma_t(x)}{\varepsilon}-\varepsilon\sigma_a(x)\right]\int_{-1}^{1}\psi(x,\mu',t)\,\mathrm{d}\mu'+\varepsilon q(x,\mu,t)\,.&\end{aligned} \tag{4.3}$$

As ε vanishes, Eq. (4.3) describes an increasingly thick and diffusive transport problem. The source, $q(x,\mu,t)$, is scaled to maintain the infinite medium solution independent of ε.

Now we posit that $\psi(x,\mu,t)$ can be expanded as a power series in ε

$$\psi(x,\mu,t)=\psi^{(0)}(x,\mu,t)+\varepsilon\psi^{(1)}(x,\mu,t)+\varepsilon^2\psi^{(2)}(x,\mu,t)+O(\varepsilon^3)\,. \tag{4.4}$$

Substituting Eq. (4.4) into Eq. (4.3), we find

$$\begin{aligned}
&\frac{\varepsilon}{v'}\frac{\partial}{\partial t}\left[\psi^{(0)}(x,\mu,t)+\varepsilon\psi^{(1)}(x,\mu,t)+\varepsilon^2\psi^{(2)}(x,\mu,t)+O(\varepsilon^3)\right] \\
&\qquad+\mu\frac{\partial}{\partial x}\left[\psi^{(0)}(x,\mu,t)+\varepsilon\psi^{(1)}(x,\mu,t)+\varepsilon^2\psi^{(2)}(x,\mu,t)+O(\varepsilon^3)\right] \\
&\qquad+\frac{\sigma_t(x)}{\varepsilon}\left[\psi^{(0)}(x,\mu,t)+\varepsilon\psi^{(1)}(x,\mu,t)+\varepsilon^2\psi^{(2)}(x,\mu,t)+O(\varepsilon^3)\right] \\
&=\frac{1}{2}\left[\frac{\sigma_t(x)}{\varepsilon}-\varepsilon\sigma_a(x)\right]\int_{-1}^{1}\left[\psi^{(0)}(x,\mu',t)+\varepsilon\psi^{(1)}(x,\mu',t)+\varepsilon^2\psi^{(2)}(x,\mu',t)+O(\varepsilon^3)\right]\mathrm{d}\mu' \\
&\qquad+\varepsilon q(x,\mu,t)\,. \quad (4.5)
\end{aligned}$$

The asymptotic analysis proceeds by analyzing the equations of each order of ε in Eq. (4.5). Beginning with the $O(\varepsilon^{-1})$ terms in Eq. (4.5), we find

$$\sigma_t(x)\psi^{(0)}(x,\mu,t)=\frac{\sigma_t(x)}{2}\int_{-1}^{1}\psi^{(0)}(x,\mu',t)\,\mathrm{d}\mu'\,. \tag{4.6}$$

Solving for $\psi^{(0)}(x,\mu,t)$, we have

$$\psi^{(0)}(x,\mu,t)=\frac{1}{2}\int_{-1}^{1}\psi^{(0)}(x,\mu',t)\,\mathrm{d}\mu'=\frac{1}{2}\phi^{(0)}(x,t)\,, \tag{4.7}$$

where $\phi^{(0)}(x,t)$, the leading order scalar flux, is not yet determined. Therefore, the leading order angular flux is isotropic, and the total angular flux satisfies

$$\psi(x,\mu,t)=\frac{1}{2}\phi^{(0)}(x,t)+O(\varepsilon)\,. \tag{4.8}$$

Next, we analyze the $O(1)$ terms in Eq. (4.5) and find

$$\mu\frac{\partial}{\partial x}\psi^{(0)}(x,\mu,t)+\sigma_t(x)\psi^{(1)}(x,\mu,t)=\frac{\sigma_t(x)}{2}\int_{-1}^{1}\psi^{(1)}(x,\mu',t)\,\mathrm{d}\mu'\,. \tag{4.9}$$

Operating on Eq. (4.9) by $\int_{-1}^{1}\mu(\cdot)\,\mathrm{d}\mu$, we obtain

$$\frac{\partial}{\partial x}\int_{-1}^{1}\mu^2\psi^{(0)}(x,\mu,t)\,\mathrm{d}\mu+\sigma_t(x)\int_{-1}^{1}\mu\,\psi^{(1)}(x,\mu,t)\,\mathrm{d}\mu=0\,. \tag{4.10}$$

Defining the first-order current

$$J^{(1)}(x,t)=\int_{-1}^{1}\mu\,\psi^{(1)}(x,\mu,t)\,\mathrm{d}\mu\,, \tag{4.11}$$

and substituting Eq. (4.7) into Eq. (4.10), we solve for the first-order current to obtain

$$J^{(1)}(x,t) = -D(x)\frac{\partial}{\partial x}\phi^{(0)}(x,t)\,, \tag{4.12a}$$

where

$$D(x) = \frac{1}{3\sigma_t(x)} \tag{4.12b}$$

is the diffusion coefficient. Eqs. (4.12) represent Fick's Law.

Now we analyze the $O(\varepsilon)$ terms in Eq. (4.5) and find

$$\begin{aligned}\frac{1}{v'}\frac{\partial}{\partial t}\psi^{(0)}(x,\mu,t) + \mu\frac{\partial}{\partial x}\psi^{(1)}(x,\mu,t) + \sigma_t(x)\psi^{(2)}(x,\mu,t)& \\ = \frac{\sigma_t(x)}{2}\int_{-1}^{1}\psi^{(2)}(x,\mu',t)\,\mathrm{d}\mu' - \frac{\sigma_a(x)}{2}\int_{-1}^{1}\psi^{(0)}(x,\mu',t)\,\mathrm{d}\mu' + q(x,\mu,t)\,.&\end{aligned} \tag{4.13}$$

Operating on Eq. (4.13) by $\int_{-1}^{1}(\cdot)\,\mathrm{d}\mu$, we have

$$\frac{1}{v'}\frac{\partial}{\partial t}\phi^{(0)}(x,t) + \frac{\partial}{\partial x}J^{(1)}(x,t) = -\sigma_a(x)\phi^{(0)}(x,t) + \int_{-1}^{1}q(x,\mu,t)\,\mathrm{d}\mu\,. \tag{4.14}$$

Substituting Eqs. (4.12) into Eq. (4.14), we obtain

$$\frac{1}{v'}\frac{\partial}{\partial t}\phi^{(0)}(x,t) - \frac{\partial}{\partial x}\frac{1}{3\sigma_t(x)}\frac{\partial}{\partial x}\phi^{(0)}(x,t) + \sigma_a(x)\phi^{(0)}(x,t) = \int_{-1}^{1}q(x,\mu,t)\,\mathrm{d}\mu\,. \tag{4.15}$$

Substituting the unscaled variables in Eqs. (4.2) into Eq. (4.15), and multiplying by ε, we obtain the asymptotic diffusion equation

$$\frac{1}{v}\frac{\partial}{\partial t}\phi^{(0)}(x,t) - \frac{\partial}{\partial x}\frac{1}{3\Sigma_t(x)}\frac{\partial}{\partial x}\phi^{(0)}(x,t) + \Sigma_a(x)\phi^{(0)}(x,t) = \int_{-1}^{1}Q(x,\mu,t)\,\mathrm{d}\mu\,. \tag{4.16}$$

Eq. (4.16) is the familiar, one-dimensional, time-dependent diffusion equation. Therefore, in the thick diffusive limit, the solution to Eq. (4.1) satisfies

$$\psi(x,\mu,t) = \frac{1}{2}\phi^{(0)}(x,t) + O(\varepsilon)\,, \tag{4.17}$$

where $\phi^{(0)}(x,t)$ satisfies Eq. (4.16).

4.2 Asymptotic Analysis of the Implicit LDFEM Transport Method

In this section we perform an asymptotic analysis of the implicit linear discontinuous finite element transport method. We begin with the implicit linear discontinuous finite element transport equation

$$\frac{1}{v\Delta t_{k+1}}\underline{\underline{M}}_i\left(\underline{\psi}_{n,i}^{k+1}-\underline{\psi}_{n,i}^{k}\right)+\mu_n\underline{\underline{L}}_i^{surf}\underline{\psi}_{n,i}^{k+1,surf}-\mu_n\underline{\underline{L}}_i\underline{\psi}_{n,i}^{k+1}+\Sigma_{t,i}\underline{\underline{M}}_i\underline{\psi}_{n,i}^{k+1} = \frac{\Sigma_{s,i}}{2}\underline{\underline{M}}_i\sum_{m=1}^{N}\underline{\psi}_{m,i}^{k+1}\Delta_m+\underline{\underline{M}}_i\underline{Q}_{n,i}^{k+1}\,, \quad (4.18)$$

where

$$\underline{\psi}_{n,i}^{k}=\begin{bmatrix}\psi_{n,i,L}^{k} & \psi_{n,i,R}^{k}\end{bmatrix}^T\,, \quad (4.19a)$$

$$\underline{\psi}_{n,i}^{k+1,surf}=\begin{bmatrix}\psi_{n,i,L}^{k+1,surf} & \psi_{n,i,R}^{k+1,surf}\end{bmatrix}^T\,, \quad (4.19b)$$

and

$$\psi_{n,i,L}^{k+1,surf}=\begin{cases}\psi_{n,i,L}^{k+1}\,, & \mu_n<0\,,\\ \psi_{n,L}^{b,k+1}\,, & \mu_n>0\,, \quad i=1\,,\\ \psi_{n,i-1,R}^{k+1}\,, & \mu_n>0\,, \quad 2\le i\le I\,,\end{cases} \quad (4.19c)$$

$$\psi_{n,i,R}^{k+1,surf}=\begin{cases}\psi_{n,i+1,L}^{k+1}\,, & \mu_n<0\,, \quad 1\le i\le I-1\,,\\ \psi_{n,R}^{b,k+1}\,, & \mu_n<0\,, \quad i=I\,,\\ \psi_{n,i,R}^{k+1}\,, & \mu_n>0\,,\end{cases} \quad (4.19d)$$

and where $\psi_{n,L}^{b,k+1}$ and $\psi_{n,R}^{b,k+1}$ are the boundary conditions at time t_{k+1} for the left and right boundaries, respectively. For vacuum and incident boundaries, these boundary conditions are specified, whereas for reflecting boundaries, we have

$$\psi_{n,L}^{b,k+1}=\psi_{n',1,L}^{k+1}\,, \qquad \mu_n>0\,, \quad \mu_{n'}=-\mu_n\,, \quad (4.20a)$$

$$\psi_{n,R}^{b,k+1}=\psi_{n',I,R}^{k+1}\,, \qquad \mu_n<0\,, \quad \mu_{n'}=-\mu_n\,. \quad (4.20b)$$

We also have initial conditions

$$\underline{\psi}^0_{n,i} = \left[\int_{x_{i-1/2}}^{x_{i+1/2}} w_{i,L}(x)\, \psi^i_n(x)\, \mathrm{d}x \quad \int_{x_{i-1/2}}^{x_{i+1/2}} w_{i,R}(x)\, \psi^i_n(x)\, \mathrm{d}x \right]^T , \tag{4.21}$$

where $\psi^i_n(x)$ is a specified initial condition. The other terms in Eq. (4.18) are defined in Section 3.3 and will not be repeated here.

Now we introduce the following asymptotic scalings:

$$v = \frac{v'}{\varepsilon} , \tag{4.22a}$$

$$\Sigma_{t,i} = \frac{\sigma_{t,i}}{\varepsilon} , \tag{4.22b}$$

$$\Sigma_{a,i} = \varepsilon \sigma_{a,i} , \tag{4.22c}$$

$$\Sigma_{s,i} = \Sigma_{t,i} - \Sigma_{a,i} = \frac{\sigma_{t,i}}{\varepsilon} - \varepsilon \sigma_{a,i} , \tag{4.22d}$$

$$\underline{Q}^{k+1}_{n,i} = \varepsilon \underline{q}^{k+1}_{n,i} , \tag{4.22e}$$

where ε is some small parameter. Substituting Eqs. (4.22) into Eq. (4.18), we have the following fully discrete version of Eq. 4.3:

$$\begin{aligned} \frac{\varepsilon}{v' \Delta t_{k+1}} \underline{\underline{M}}_i \left(\underline{\psi}^{k+1}_{n,i} - \underline{\psi}^k_{n,i} \right) + \mu_n \underline{\underline{L}}^{surf}_i \underline{\psi}^{k+1,surf}_{n,i} - \mu_n \underline{\underline{L}}_i \underline{\psi}^{k+1}_{n,i} + \frac{\sigma_{t,i}}{\varepsilon} \underline{\underline{M}}_i \underline{\psi}^{k+1}_{n,i} \\ = \frac{1}{2} \left(\frac{\sigma_{t,i}}{\varepsilon} - \varepsilon \sigma_{a,i} \right) \underline{\underline{M}}_i \sum_{m=1}^{N} \underline{\psi}^{k+1}_{m,i} \Delta_m + \varepsilon \underline{\underline{M}}_i \underline{q}^{k+1}_{n,i} . \end{aligned} \tag{4.23}$$

As ε vanishes, Eq. (4.23) describes an increasingly thick and diffusive transport problem. Again, we posit that we can expand the unknown angular flux at time t_{k+1} as a power series in ε, such that

$$\underline{\psi}^{k+1}_{n,i} = \underline{\psi}^{k+1,(0)}_{n,i} + \varepsilon \underline{\psi}^{k+1,(1)}_{n,i} + \varepsilon^2 \underline{\psi}^{k+1,(2)}_{n,i} + O(\varepsilon^3) , \tag{4.24a}$$

$$\underline{\psi}^{k+1,surf}_{n,i} = \underline{\psi}^{k+1,surf,(0)}_{n,i} + \varepsilon \underline{\psi}^{k+1,surf,(1)}_{n,i} + \varepsilon^2 \underline{\psi}^{k+1,surf,(2)}_{n,i} + O(\varepsilon^3) . \tag{4.24b}$$

Therefore, for $\mu_n < 0$,

$$\psi_{n,i,L}^{k+1,surf} = \psi_{n,i,L}^{k+1,(0)} + \varepsilon\psi_{n,i,L}^{k+1,(1)} + \varepsilon^2\psi_{n,i,L}^{k+1,(2)} + O(\varepsilon^3)\,, \tag{4.25a}$$

$$\psi_{n,i,R}^{k+1,surf} = \begin{cases} \psi_{n,i+1,L}^{k+1,(0)} + \varepsilon\psi_{n,i+1,L}^{k+1,(1)} + \varepsilon^2\psi_{n,i+1,L}^{k+1,(2)} + O(\varepsilon^3)\,, & 1 \le i \le I-1\,, \\ \psi_{n,R}^{b,k+1}\,, & i = I\,, \end{cases} \tag{4.25b}$$

and for $\mu_n > 0$,

$$\psi_{n,i,L}^{k+1,surf} = \begin{cases} \psi_{n,L}^{b,k+1}\,, & i = 1\,, \\ \psi_{n,i-1,R}^{k+1,(0)} + \varepsilon\psi_{n,i-1,R}^{k+1,(1)} + \varepsilon^2\psi_{n,i-1,R}^{k+1,(2)} + O(\varepsilon^3)\,, & 2 \le i \le I\,, \end{cases} \tag{4.26a}$$

$$\psi_{n,i,R}^{k+1,surf} = \psi_{n,i,R}^{k+1,(0)} + \varepsilon\psi_{n,i,R}^{k+1,(1)} + \varepsilon^2\psi_{n,i,R}^{k+1,(2)} + O(\varepsilon^3)\,. \tag{4.26b}$$

Substituting Eq. (4.24) into Eq. (4.23), we obtain:

$$\begin{aligned} &\frac{\varepsilon}{v'\Delta t_{k+1}}\underline{\underline{M}}_i\left[\underline{\psi}_{n,i}^{k+1,(0)} + \varepsilon\underline{\psi}_{n,i}^{k+1,(1)} + \varepsilon^2\underline{\psi}_{n,i}^{k+1,(2)} + O(\varepsilon^3) - \underline{\psi}_{n,i}^{k}\right] \\ &\qquad + \mu_n\underline{\underline{L}}_i^{surf}\left[\underline{\psi}_{n,i}^{k+1,surf,(0)} + \varepsilon\underline{\psi}_{n,i}^{k+1,surf,(1)} + \varepsilon^2\underline{\psi}_{n,i}^{k+1,surf,(2)} + O(\varepsilon^3)\right] \\ &\qquad\qquad - \mu_n\underline{\underline{L}}_i\left[\underline{\psi}_{n,i}^{k+1,(0)} + \varepsilon\underline{\psi}_{n,i}^{k+1,(1)} + \varepsilon^2\underline{\psi}_{n,i}^{k+1,(2)} + O(\varepsilon^3)\right] \\ &\qquad\qquad + \frac{\sigma_{t,i}}{\varepsilon}\underline{\underline{M}}_i\left[\underline{\psi}_{n,i}^{k+1,(0)} + \varepsilon\underline{\psi}_{n,i}^{k+1,(1)} + \varepsilon^2\underline{\psi}_{n,i}^{k+1,(2)} + O(\varepsilon^3)\right] \\ &= \frac{1}{2}\left(\frac{\sigma_{t,i}}{\varepsilon} - \varepsilon\sigma_{a,i}\right)\underline{\underline{M}}_i\sum_{m=1}^{N}\left[\underline{\psi}_{m,i}^{k+1,(0)} + \varepsilon\underline{\psi}_{m,i}^{k+1,(1)} + \varepsilon^2\underline{\psi}_{m,i}^{k+1,(2)} + O(\varepsilon^3)\right]\Delta_m \\ &\qquad\qquad + \varepsilon\underline{\underline{M}}_i\underline{q}_{n,i}^{k+1}\,. \end{aligned} \tag{4.27}$$

We now analyze the terms of each power of ε in Eq. (4.27).

4.2.1 The $O(\varepsilon^{-1})$ Terms

Beginning with the $O(\varepsilon^{-1})$ terms in Eq. (4.27), we have

$$\sigma_{t,i}\underline{\underline{M}}_i\underline{\psi}_{n,i}^{k+1,(0)} = \frac{\sigma_{t,i}}{2}\underline{\underline{M}}_i\sum_{m=1}^{N}\underline{\psi}_{m,i}^{k+1,(0)}\Delta_m\,. \tag{4.28}$$

Assuming that $\underline{\underline{M}}_i$ is invertible, which is true for the linear discontinuous finite element discretization, we solve for $\underline{\psi}_{n,i}^{k+1,(0)}$ and find

$$\underline{\psi}_{n,i}^{k+1,(0)} = \frac{1}{2}\sum_{m=1}^{N} \underline{\psi}_{m,i}^{k+1,(0)} \Delta_m = \frac{1}{2}\underline{\phi}_i^{k+1,(0)}, \tag{4.29}$$

where $\underline{\phi}_i^{k+1,(0)}$, which is undetermined, is the leading order scalar flux at time t_{k+1} in cell i. Therefore, the leading order angular flux at time t_{k+1} is isotropic, and the angular flux at time t_{k+1} in the diffusion limit satisfies

$$\underline{\psi}_{n,i}^{k+1} = \frac{1}{2}\underline{\phi}_i^{k+1,(0)} + O(\varepsilon), \tag{4.30}$$

where again, $\underline{\phi}_i^{k+1,(0)}$ is not yet specified.

4.2.2 The $O(1)$ Terms

Next we examine the $O(1)$ terms in Eq. (4.27):

$$\mu_n \underline{\underline{L}}_i^{surf} \underline{\psi}_{n,i}^{k+1,surf,(0)} - \mu_n \underline{\underline{L}}_i \underline{\psi}_{n,i}^{k+1,(0)} + \sigma_{t,i} \underline{\underline{M}}_i \underline{\psi}_{n,i}^{k+1,(1)} = \frac{\sigma_{t,i}}{2} \underline{\underline{M}}_i \sum_{m=1}^{N} \underline{\psi}_{m,i}^{k+1,(1)} \Delta_m. \tag{4.31}$$

Operating on Eq. (4.31) by $\sum_{n=1}^{N}(\cdot)\Delta_n$, substituting in Eq. (4.29), and assuming that the quadrature set satisfies

$$\sum_{n=1}^{N} \Delta_n = \int_{-1}^{1} \mathrm{d}\mu = 2, \tag{4.32a}$$

and

$$\sum_{n=1}^{N} \mu_n \Delta_n = \int_{-1}^{1} \mu \, \mathrm{d}\mu = 0, \tag{4.32b}$$

we find

$$\underline{\underline{L}}_i^{surf} \sum_{n=1}^{N} \mu_n \underline{\psi}_{n,i}^{k+1,surf,(0)} \Delta_n = 0. \tag{4.33}$$

Eq. (4.33) represents a 2×2 system of algebraic equations. We first consider the problem interior. Substituting the upstream closures, Eqs. (4.25) and (4.26), into Eq. (4.33), and writing the two rows individually, we have

$$-\left(\sum_{\mu_n<0} \mu_n \psi_{n,i,L}^{k+1,(0)} \Delta_n + \sum_{\mu_n>0} \mu_n \psi_{n,i-1,R}^{k+1,(0)} \Delta_n \right) = 0, \tag{4.34a}$$

$$\left(\sum_{\mu_n<0} \mu_n \psi_{n,i+1,L}^{k+1,(0)} \Delta_n + \sum_{\mu_n>0} \mu_n \psi_{n,i,R}^{k+1,(0)} \Delta_n \right) = 0 . \tag{4.34b}$$

Substituting Eq. (4.29) into Eqs. (4.34), and assuming a symmetric quadrature set, for which

$$\sum_{\mu_n>0} \mu_n \Delta_n = - \sum_{\mu_n<0} \mu_n \Delta_n , \tag{4.35}$$

we find

$$\phi_{i,L}^{k+1,(0)} = \phi_{i-1,R}^{k+1,(0)} \equiv \phi_{i-1/2}^{k+1,(0)} , \tag{4.36a}$$

$$\phi_{i,R}^{k+1,(0)} = \phi_{i+1,L}^{k+1,(0)} \equiv \phi_{i+1/2}^{k+1,(0)} . \tag{4.36b}$$

Therefore, in the thick diffusive limit, the leading order scalar flux at time t_{k+1} is continuous across cell edges.

Considering an incident flux on the left boundary, substituting in the upstream closures, Eqs. (4.25) and Eqs. (4.26), and writing the first row of Eq. (4.33), we have

$$- \left(\sum_{\mu_n<0} \mu_n \psi_{n,1,L}^{k+1,(0)} \Delta_n + \sum_{\mu_n>0} \mu_n \psi_{n,L}^{b,k+1} \Delta_n \right) = 0 . \tag{4.37}$$

Substituting Eq. (4.29) into Eq. (4.37), and defining

$$\begin{aligned} \rho &= \sum_{\mu_n>0} \mu_n \Delta_n = - \sum_{\mu_n<0} \mu_n \Delta_n \\ &\approx \int_0^1 \mu \, \mathrm{d}\mu = \frac{1}{2} , \end{aligned} \tag{4.38}$$

we find

$$\phi_{1,L}^{k+1,(0)} \equiv \phi_{1/2}^{k+1,(0)} = \frac{2}{\rho} \sum_{\mu_n>0} \mu_n \psi_{n,L}^{b,k+1} \Delta_n , \qquad \text{left incident boundary} . \tag{4.39}$$

Likewise, for an incident boundary on the right, we find

$$\phi_{I,R}^{k+1,(0)} \equiv \phi_{I+1/2}^{k+1,(0)} = \frac{2}{\rho} \sum_{\mu_n<0} |\mu_n| \psi_{n,R}^{b,k+1} \Delta_n , \qquad \text{right incident boundary} . \tag{4.40}$$

Next, operating on Eq. (4.31) by $\sum_{n=1}^{N} \mu_n(\cdot) \Delta_n$, we find

$$\underline{\underline{L}}_i^{surf} \sum_{n=1}^{N} \mu_n^2 \underline{\psi}_{n,i}^{k+1,surf,(0)} \Delta_n - \underline{\underline{L}}_i \sum_{n=1}^{N} \mu_n^2 \underline{\psi}_{n,i}^{k+1,(0)} \Delta_n + \sigma_{t,i} \underline{\underline{M}}_i \sum_{n=1}^{N} \mu_n \underline{\psi}_{n,i}^{k+1,(1)} \Delta_n = 0 . \tag{4.41}$$

Substituting Eqs. (4.29) and (4.36) into Eq. (4.41), assuming that the quadrature set satisfies

$$\sum_{n=1}^{N} \mu_n^2 \Delta_n = \int_{-1}^{1} \mu^2 \, \mathrm{d}\mu = \frac{2}{3}, \tag{4.42}$$

and defining the first order current as

$$\underline{J}_i^{k+1,(1)} = \sum_{n=1}^{N} \mu_n \underline{\psi}_{n,i}^{k+1,(1)} \Delta_n, \tag{4.43}$$

we obtain

$$\underline{J}_1^{k+1,(1)} = -\frac{1}{\sigma_{t,1}} \underline{\underline{M}}_1^{-1} \left(\underline{\underline{L}}_1^{surf} \sum_{n=1}^{N} \mu_n^2 \underline{\psi}_{n,1}^{k+1,surf,(0)} \Delta_n - \frac{1}{3} \underline{\underline{L}}_1 \underline{\phi}_1^{k+1,(0)} \right), \tag{4.44a}$$

$$\underline{J}_i^{k+1,(1)} = -\frac{1}{3\sigma_{t,i}} \underline{\underline{M}}_i^{-1} \left(\underline{\underline{L}}_i^{surf} - \underline{\underline{L}}_i \right) \underline{\phi}_i^{k+1,(0)}, \qquad 2 \le i \le I-1, \tag{4.44b}$$

$$\underline{J}_I^{k+1,(1)} = -\frac{1}{\sigma_{t,I}} \underline{\underline{M}}_I^{-1} \left(\underline{\underline{L}}_I^{surf} \sum_{n=1}^{N} \mu_n^2 \underline{\psi}_{n,I}^{k+1,surf,(0)} \Delta_n - \frac{1}{3} \underline{\underline{L}}_I \underline{\phi}_I^{k+1,(0)} \right), \tag{4.44c}$$

where

$$\underline{J}_i^{k+1,(1)} = \begin{bmatrix} J_{i,L}^{k+1,(1)} & J_{i,R}^{k+1,(1)} \end{bmatrix}^T. \tag{4.45}$$

Substituting the upstream closures, Eqs. (4.25) and (4.26), and the definitions of the matrices, which we defined in Section 3.3, we evaluate the currents and find

$$J_{1,L}^{k+1,(1)} = -\frac{1}{3\sigma_{t,1}\Delta x_1 (1+2\theta)} \Big[(1+2\theta) \phi_{3/2}^{k+1,(0)} + (1-\theta) \phi_{1/2}^{k+1,(0)} - 6(2+\theta) \sum_{\mu_n > 0} \mu_n^2 \psi_{n,L}^{b,k+1} \Delta_n \Big], \quad \text{left incident boundary}, \tag{4.46a}$$

$$J_{1,R}^{k+1,(1)} = -\frac{1}{3\sigma_{t,1}\Delta x_1 (1+2\theta)} \Big[(1+2\theta) \phi_{3/2}^{k+1,(0)} - (2+\theta) \phi_{1/2}^{k+1,(0)} + 6(1-\theta) \sum_{\mu_n > 0} \mu_n^2 \psi_{n,L}^{b,k+1} \Delta_n \Big], \quad \text{left incident boundary}, \tag{4.46b}$$

$$J_{i,L}^{k+1,(1)} = J_{i,R}^{k+1,(1)} = -\frac{1}{3\sigma_{t,i}\Delta x_i}\left(\phi_{i+1/2}^{k+1,(0)} - \phi_{i-1/2}^{k+1,(0)}\right),$$

interior and reflecting boundaries, (4.46c)

$$J_{I,L}^{k+1,(1)} = -\frac{1}{3\sigma_{t,I}\Delta x_I(1+2\theta)}\Bigg[(2+\theta)\,\phi_{I+1/2}^{k+1,(0)} - (1+2\theta)\,\phi_{I-1/2}^{k+1,(0)} - 6(1-\theta)\sum_{\mu_n<0}\mu_n^2\psi_{n,R}^{b,k+1}\Delta_n\Bigg],$$

right incident boundary, (4.46d)

$$J_{I,R}^{k+1,(1)} = -\frac{1}{3\sigma_{t,I}\Delta x_I(1+2\theta)}\Bigg[-(1-\theta)\,\phi_{I+1/2}^{k+1,(0)} - (1+2\theta)\,\phi_{I-1/2}^{k+1,(0)} + 6(2+\theta)\sum_{\mu_n<0}\mu_n^2\psi_{n,R}^{b,k+1}\Delta_n\Bigg],$$

right incident boundary. (4.46e)

4.2.3 The $O(\varepsilon)$ Terms

The $O(\varepsilon)$ terms in Eq. (4.27) are

$$\frac{1}{v'\Delta t_{k+1}}\underline{\underline{M}}_i\left(\underline{\psi}_{n,i}^{k+1,(0)} - \underline{\psi}_{n,i}^{k}\right) + \mu_n\underline{\underline{L}}_i^{surf}\underline{\psi}_{n,i}^{k+1,surf,(1)} - \mu_n\underline{\underline{L}}_i\underline{\psi}_{n,i}^{k+1,(1)} + \sigma_{t,i}\underline{\underline{M}}_i\underline{\psi}_{n,i}^{k+1,(2)} = \frac{\sigma_{t,i}}{2}\underline{\underline{M}}_i\sum_{m=1}^{N}\underline{\psi}_{m,i}^{k+1,(2)}\Delta_m - \frac{\sigma_{a,i}}{2}\underline{\underline{M}}_i\sum_{m=1}^{N}\underline{\psi}_{m,i}^{k+1,(0)}\Delta_m + \underline{\underline{M}}_i\underline{q}_{n,i}^{k+1}. \quad (4.47)$$

Operating on Eq. (4.47) by $\sum_{n=1}^{N}(\cdot)\Delta_n$, we obtain

$$\frac{1}{v'\Delta t_{k+1}}\underline{\underline{M}}_i\left(\underline{\phi}_i^{k+1,(0)} - \underline{\phi}_i^{k}\right) + \underline{\underline{L}}_i^{surf}\sum_{n=1}^{N}\mu_n\underline{\psi}_{n,i}^{k+1,surf,(1)}\Delta_n - \underline{\underline{L}}_i\underline{J}_i^{k+1,(1)} + \sigma_{a,i}\underline{\underline{M}}_i\underline{\phi}_i^{k+1,(0)} = \underline{\underline{M}}_i\sum_{n=1}^{N}\underline{q}_{n,i}^{k+1}\Delta_n. \quad (4.48)$$

Writing each row of the 2×2 system described in Eq. (4.48), and substituting in Eq. (4.36), as well as the definitions of $\underline{\underline{M}}_i$, $\underline{\underline{L}}_i^{surf}$, and $\underline{\underline{L}}_i$, we have

$$\left[\frac{\Delta x_i\,(2+\theta)}{6v'\Delta t_{k+1}}\right]\left(\phi_{i-1/2}^{k+1,(0)}-\phi_{i,L}^{k}\right)+\left[\frac{\Delta x_i\,(1-\theta)}{6v'\Delta t_{k+1}}\right]\left(\phi_{i+1/2}^{k+1,(0)}-\phi_{i,R}^{k}\right)-\sum_{n=1}^{N}\mu_n\psi_{n,i,L}^{k+1,surf,(1)}\Delta_n$$
$$+\frac{1}{2}\left(J_{i,L}^{k+1,(1)}+J_{i,R}^{k+1,(1)}\right)+\left[\frac{\sigma_{a,i}\Delta x_i\,(2+\theta)}{6}\right]\phi_{i-1/2}^{k+1,(0)}+\left[\frac{\sigma_{a,i}\Delta x_i\,(1-\theta)}{6}\right]\phi_{i+1/2}^{k+1,(0)}$$
$$=\left[\frac{\Delta x_i\,(2+\theta)}{6}\right]\sum_{n=1}^{N}q_{n,i,L}^{k+1}\Delta_n+\left[\frac{\Delta x_i\,(1-\theta)}{6}\right]\sum_{n=1}^{N}q_{n,i,R}^{k+1}\Delta_n\,, \quad (4.49a)$$

$$\left[\frac{\Delta x_i\,(1-\theta)}{6v'\Delta t_{k+1}}\right]\left(\phi_{i-1/2}^{k+1,(0)}-\phi_{i,L}^{k}\right)+\left[\frac{\Delta x_i\,(2+\theta)}{6v'\Delta t_{k+1}}\right]\left(\phi_{i+1/2}^{k+1,(0)}-\phi_{i,R}^{k}\right)+\sum_{n=1}^{N}\mu_n\psi_{n,i,R}^{k+1,surf,(1)}\Delta_n$$
$$-\frac{1}{2}\left(J_{i,L}^{k+1,(1)}+J_{i,R}^{k+1,(1)}\right)+\left[\frac{\sigma_{a,i}\Delta x_i\,(1-\theta)}{6}\right]\phi_{i-1/2}^{k+1,(0)}+\left[\frac{\sigma_{a,i}\Delta x_i\,(2+\theta)}{6}\right]\phi_{i+1/2}^{k+1,(0)}$$
$$=\left[\frac{\Delta x_i\,(1-\theta)}{6}\right]\sum_{n=1}^{N}q_{n,i,L}^{k+1}\Delta_n+\left[\frac{\Delta x_i\,(2+\theta)}{6}\right]\sum_{n=1}^{N}q_{n,i,R}^{k+1}\Delta_n\,. \quad (4.49b)$$

Evaluating Eq. (4.49a) at cell $i+1$ and summing with Eq. (4.49b), and using the upstream closures, Eqs. (4.25) and (4.26), the first order surface terms cancel, and we find

$$\left[\frac{\Delta x_i\,(1-\theta)}{6v'\Delta t_{k+1}}\right]\left(\phi_{i-1/2}^{k+1,(0)}-\phi_{i,L}^{k}\right)+\left[\frac{\Delta x_i\,(2+\theta)}{6v'\Delta t_{k+1}}\right]\left(\phi_{i+1/2}^{k+1,(0)}-\phi_{i,R}^{k}\right)$$
$$+\left[\frac{\Delta x_{i+1}\,(2+\theta)}{6v'\Delta t_{k+1}}\right]\left(\phi_{i+1/2}^{k+1,(0)}-\phi_{i+1,L}^{k}\right)+\left[\frac{\Delta x_{i+1}\,(1-\theta)}{6v'\Delta t_{k+1}}\right]\left(\phi_{i+3/2}^{k+1,(0)}-\phi_{i+1,R}^{k}\right)$$
$$+\frac{1}{2}\left(J_{i+1,L}^{k+1,(1)}+J_{i+1,R}^{k+1,(1)}\right)-\frac{1}{2}\left(J_{i,L}^{k+1,(1)}+J_{i,R}^{k+1,(1)}\right)$$
$$+\left[\frac{\sigma_{a,i}\Delta x_i\,(1-\theta)}{6}\right]\phi_{i-1/2}^{k+1,(0)}+\left[\frac{(\sigma_{a,i+1}\Delta x_{i+1}+\sigma_{a,i}\Delta x_i)\,(2+\theta)}{6}\right]\phi_{i+1/2}^{k+1,(0)}$$
$$+\left[\frac{\sigma_{a,i+1}\Delta x_{i+1}\,(1-\theta)}{6}\right]\phi_{i+3/2}^{k+1,(0)}=\left[\frac{\Delta x_i\,(1-\theta)}{6}\right]\sum_{n=1}^{N}q_{n,i,L}^{k+1}\Delta_n$$
$$+\left[\frac{\Delta x_i\,(2+\theta)}{6}\right]\sum_{n=1}^{N}q_{n,i,R}^{k+1}\Delta_n+\left[\frac{\Delta x_{i+1}\,(2+\theta)}{6}\right]\sum_{n=1}^{N}q_{n,i+1,L}^{k+1}\Delta_n$$
$$+\left[\frac{\Delta x_{i+1}\,(1-\theta)}{6}\right]\sum_{n=1}^{N}q_{n,i+1,R}^{k+1}\Delta_n\,. \quad (4.50)$$

For a reflecting left boundary, we evaluate Eq. (4.49a) for cell 1, and use

$$\sum_{n=1}^{N}\mu_n\psi_{n,1,L}^{k+1,surf,(1)}\Delta_n=0\,, \quad (4.51)$$

and therefore, the diffusion equation on the left boundary for a reflecting boundary condition is

$$\left[\frac{\Delta x_1\,(2+\theta)}{6v'\Delta t_{k+1}}\right]\left(\phi_{1/2}^{k+1,(0)}-\phi_{1,L}^{k}\right)+\left[\frac{\Delta x_1\,(1-\theta)}{6v'\Delta t_{k+1}}\right]\left(\phi_{3/2}^{k+1,(0)}-\phi_{i,R}^{k}\right)$$
$$+\frac{1}{2}\left(J_{1,L}^{k+1,(1)}+J_{1,R}^{k+1,(1)}\right)+\left[\frac{\sigma_{a,1}\Delta x_1\,(2+\theta)}{6}\right]\phi_{1/2}^{k+1,(0)}+\left[\frac{\sigma_{a,1}\Delta x_1\,(1-\theta)}{6}\right]\phi_{3/2}^{k+1,(0)}$$
$$=\left[\frac{\Delta x_1\,(2+\theta)}{6}\right]\sum_{n=1}^{N}q_{n,1,L}^{k+1}\Delta_n+\left[\frac{\Delta x_1\,(1-\theta)}{6}\right]\sum_{n=1}^{N}q_{n,1,R}^{k+1}\Delta_n\,. \quad (4.52)$$

For a reflecting boundary on the right, we evaluate Eq. (4.49b) for cell I, and use

$$\sum_{n=1}^{N}\mu_n\psi_{n,I,R}^{k+1,surf,(1)}\Delta_n=0\,, \quad (4.53)$$

and therefore, the diffusion equation on the right boundary for a reflecting boundary condition is

$$\left[\frac{\Delta x_I\,(1-\theta)}{6v'\Delta t_{k+1}}\right]\left(\phi_{I-1/2}^{k+1,(0)}-\phi_{I,L}^{k}\right)+\left[\frac{\Delta x_I\,(2+\theta)}{6v'\Delta t_{k+1}}\right]\left(\phi_{I+1/2}^{k+1,(0)}-\phi_{I,R}^{k}\right)$$
$$-\frac{1}{2}\left(J_{I,L}^{k+1,(1)}+J_{I,R}^{k+1,(1)}\right)+\left[\frac{\sigma_{a,I}\Delta x_I\,(1-\theta)}{6}\right]\phi_{I-1/2}^{k+1,(0)}+\left[\frac{\sigma_{a,I}\Delta x_I\,(2+\theta)}{6}\right]\phi_{I+1/2}^{k+1,(0)}$$
$$=\left[\frac{\Delta x_I\,(1-\theta)}{6}\right]\sum_{n=1}^{N}q_{n,I,L}^{k+1}\Delta_n+\left[\frac{\Delta x_I\,(2+\theta)}{6}\right]\sum_{n=1}^{N}q_{n,I,R}^{k+1}\Delta_n\,. \quad (4.54)$$

4.2.4 Rescaling the Diffusion Equation

Substituting the currents in Eqs. (4.46) and the unscaled variables in Eq. (4.22) into Eqs. (4.50), (4.52), and (4.54), we have, together with Eqs. (4.39) and (4.40), the asymptotic diffusion equations for the implicit linear-discontinuous finite element transport discretization:

$$\phi_{1/2}^{k+1,(0)}=\frac{2}{\rho}\sum_{\mu_n>0}\mu_n\psi_{n,L}^{b,k+1}\Delta_n\,,\qquad\text{left incident boundary}\,, \quad (4.55a)$$

$$\left[\frac{\Delta x_1\left(1-\theta\right)}{6v\Delta t_{k+1}}\right]\left(\phi_{1/2}^{k+1,(0)}-\phi_{1,L}^{k}\right)+\left[\frac{\Delta x_1\left(2+\theta\right)}{6v\Delta t_{k+1}}\right]\left(\phi_{3/2}^{k+1,(0)}-\phi_{1,R}^{k}\right)$$
$$+\left[\frac{\Delta x_2\left(2+\theta\right)}{6v\Delta t_{k+1}}\right]\left(\phi_{3/2}^{k+1,(0)}-\phi_{2,L}^{k}\right)+\left[\frac{\Delta x_2\left(1-\theta\right)}{6v\Delta t_{k+1}}\right]\left(\phi_{5/2}^{k+1,(0)}-\phi_{2,R}^{k}\right)$$
$$-\frac{1}{3\Sigma_{t,2}\Delta x_2}\left(\phi_{5/2}^{k+1,(0)}-\phi_{3/2}^{k+1,(0)}\right)+\frac{1}{3\Sigma_{t,1}\Delta x_1}\left(\phi_{3/2}^{k+1,(0)}-\frac{1}{2}\phi_{1/2}^{k+1,(0)}-3\sum_{\mu_n>0}\mu_n^2\psi_{n,L}^{b,k+1}\Delta_n\right)$$
$$+\left[\frac{\Sigma_{a,1}\Delta x_1\left(1-\theta\right)}{6}\right]\phi_{1/2}^{k+1,(0)}+\left[\frac{\left(\Sigma_{a,2}\Delta x_2+\Sigma_{a,1}\Delta x_1\right)\left(2+\theta\right)}{6}\right]\phi_{3/2}^{k+1,(0)}$$
$$+\left[\frac{\Sigma_{a,2}\Delta x_2\left(1-\theta\right)}{6}\right]\phi_{5/2}^{k+1,(0)}=\left[\frac{\Delta x_1\left(1-\theta\right)}{6}\right]\sum_{n=1}^{N}Q_{n,1,L}^{k+1}\Delta_n+\left[\frac{\Delta x_1\left(2+\theta\right)}{6}\right]\sum_{n=1}^{N}Q_{n,1,R}^{k+1}\Delta_n$$
$$+\left[\frac{\Delta x_2\left(2+\theta\right)}{6}\right]\sum_{n=1}^{N}Q_{n,2,L}^{k+1}\Delta_n+\left[\frac{\Delta x_2\left(1-\theta\right)}{6}\right]\sum_{n=1}^{N}Q_{n,2,R}^{k+1}\Delta_n\,,$$

left incident boundary, (4.55b)

$$\left[\frac{\Delta x_1\left(2+\theta\right)}{6v\Delta t_{k+1}}\right]\left(\phi_{1/2}^{k+1,(0)}-\phi_{1,L}^{k,(0)}\right)+\left[\frac{\Delta x_1\left(1-\theta\right)}{6v\Delta t_{k+1}}\right]\left(\phi_{3/2}^{k+1,(0)}-\phi_{1,R}^{k,(0)}\right)$$
$$-\frac{1}{3\Sigma_{t,1}\Delta x_1}\left(\phi_{3/2}^{k+1,(0)}-\phi_{1/2}^{k+1,(0)}\right)+\left[\frac{\Sigma_{a,1}\Delta x_1\left(2+\theta\right)}{6}\right]\phi_{1/2}^{k+1,(0)}$$
$$+\left[\frac{\Sigma_{a,1}\Delta x_1\left(1-\theta\right)}{6}\right]\phi_{3/2}^{k+1,(0)}=\left[\frac{\Delta x_1\left(2+\theta\right)}{6}\right]\sum_{n=1}^{N}Q_{n,1,L}^{k+1}\Delta_n+\left[\frac{\Delta x_1\left(1-\theta\right)}{6}\right]\sum_{n=1}^{N}Q_{n,1,R}^{k+1}\Delta_n\,,$$

left reflecting boundary, (4.55c)

$$\left[\frac{\Delta x_i\left(1-\theta\right)}{6v\Delta t_{k+1}}\right]\left(\phi_{i-1/2}^{k+1,(0)}-\phi_{i,L}^{k}\right)+\left[\frac{\Delta x_i\left(2+\theta\right)}{6v\Delta t_{k+1}}\right]\left(\phi_{i+1/2}^{k+1,(0)}-\phi_{i,R}^{k}\right)$$
$$+\left[\frac{\Delta x_{i+1}\left(2+\theta\right)}{6v\Delta t_{k+1}}\right]\left(\phi_{i+1/2}^{k+1,(0)}-\phi_{i+1,L}^{k}\right)+\left[\frac{\Delta x_{i+1}\left(1-\theta\right)}{6v\Delta t_{k+1}}\right]\left(\phi_{i+3/2}^{k+1,(0)}-\phi_{i+1,R}^{k}\right)$$
$$-\frac{1}{3\Sigma_{t,i+1}\Delta x_{i+1}}\left(\phi_{i+3/2}^{k+1,(0)}-\phi_{i+1/2}^{k+1,(0)}\right)+\frac{1}{3\Sigma_{t,i}\Delta x_i}\left(\phi_{i+1/2}^{k+1,(0)}-\phi_{i-1/2}^{k+1,(0)}\right)$$
$$+\left[\frac{\Sigma_{a,i}\Delta x_i\left(1-\theta\right)}{6}\right]\phi_{i-1/2}^{k+1,(0)}+\left[\frac{\left(\Sigma_{a,i+1}\Delta x_{i+1}+\Sigma_{a,i}\Delta x_i\right)\left(2+\theta\right)}{6}\right]\phi_{i+1/2}^{k+1,(0)}$$
$$+\left[\frac{\Sigma_{a,i+1}\Delta x_{i+1}\left(1-\theta\right)}{6}\right]\phi_{i+3/2}^{k+1,(0)}=\left[\frac{\Delta x_i\left(1-\theta\right)}{6}\right]\sum_{n=1}^{N}Q_{n,i,L}^{k+1}\Delta_n+\left[\frac{\Delta x_i\left(2+\theta\right)}{6}\right]\sum_{n=1}^{N}Q_{n,i,R}^{k+1}\Delta_n$$
$$+\left[\frac{\Delta x_{i+1}\left(2+\theta\right)}{6}\right]\sum_{n=1}^{N}Q_{n,i+1,L}^{k+1}\Delta_n+\left[\frac{\Delta x_{i+1}\left(1-\theta\right)}{6}\right]\sum_{n=1}^{N}Q_{n,i+1,R}^{k+1}\Delta_n\,,$$

$$2\leq i\leq I-1\,,\quad(4.55\text{d})$$

$$\left[\frac{\Delta x_I\left(1-\theta\right)}{6v\Delta t_{k+1}}\right]\left(\phi_{I-1/2}^{k+1,(0)}-\phi_{I,L}^{k}\right)+\left[\frac{\Delta x_I\left(2+\theta\right)}{6v\Delta t_{k+1}}\right]\left(\phi_{I+1/2}^{k+1,(0)}-\phi_{I,R}^{k}\right)$$
$$+\frac{1}{3\Sigma_{t,I}\Delta x_I}\left(\phi_{I+1/2}^{k+1,(0)}-\phi_{I-1/2}^{k+1,(0)}\right)+\left[\frac{\Sigma_{a,I}\Delta x_I\left(1-\theta\right)}{6}\right]\phi_{I-1/2}^{k+1,(0)}+\left[\frac{\Sigma_{a,I}\Delta x_I\left(2+\theta\right)}{6}\right]\phi_{I+1/2}^{k+1,(0)}$$
$$=\left[\frac{\Delta x_I\left(1-\theta\right)}{6}\right]\sum_{n=1}^{N}Q_{n,I,L}^{k+1}\Delta_n+\left[\frac{\Delta x_I\left(2+\theta\right)}{6}\right]\sum_{n=1}^{N}Q_{n,I,R}^{k+1}\Delta_n\,,$$

right reflecting boundary, (4.55e)

$$\left[\frac{\Delta x_{I-1}\left(1-\theta\right)}{6v\Delta t_{k+1}}\right]\left(\phi_{I-3/2}^{k+1,(0)}-\phi_{I-1,L}^{k}\right)+\left[\frac{\Delta x_{I-1}\left(2+\theta\right)}{6v\Delta t_{k+1}}\right]\left(\phi_{I-1/2}^{k+1,(0)}-\phi_{I-1,R}^{k}\right)$$
$$+\left[\frac{\Delta x_I\left(2+\theta\right)}{6v\Delta t_{k+1}}\right]\left(\phi_{I-1/2}^{k+1,(0)}-\phi_{I,L}^{k}\right)+\left[\frac{\Delta x_I\left(1-\theta\right)}{6v\Delta t_{k+1}}\right]\left(\phi_{I+1/2}^{k+1,(0)}-\phi_{I,R}^{k}\right)$$
$$-\frac{1}{3\Sigma_{t,I}\Delta x_I}\left(\frac{1}{2}\phi_{I+1/2}^{k+1,(0)}-\phi_{I-1/2}^{k+1,(0)}+3\sum_{\mu_n<0}\mu_n^2\psi_{n,R}^{b,k+1}\Delta_n\right)$$
$$+\frac{1}{3\Sigma_{t,I-1}\Delta x_{I-1}}\left(\phi_{I-1/2}^{k+1,(0)}-\phi_{I-3/2}^{k+1,(0)}\right)+\left[\frac{\Sigma_{a,I-1}\Delta x_{I-1}\left(1-\theta\right)}{6}\right]\phi_{I-3/2}^{k+1,(0)}$$
$$+\left[\frac{\left(\Sigma_{a,I}\Delta x_I+\Sigma_{a,I-1}\Delta x_{I-1}\right)\left(2+\theta\right)}{6}\right]\phi_{I-1/2}^{k+1,(0)}+\left[\frac{\Sigma_{a,I}\Delta x_I\left(1-\theta\right)}{6}\right]\phi_{I+1/2}^{k+1,(0)}$$
$$=\left[\frac{\Delta x_{I-1}\left(1-\theta\right)}{6}\right]\sum_{n=1}^{N}Q_{n,I-1,L}^{k+1}\Delta_n+\left[\frac{\Delta x_{I-1}\left(2+\theta\right)}{6}\right]\sum_{n=1}^{N}Q_{n,I-1,R}^{k+1}\Delta_n$$
$$+\left[\frac{\Delta x_I\left(2+\theta\right)}{6}\right]\sum_{n=1}^{N}Q_{n,I,L}^{k+1}\Delta_n+\left[\frac{\Delta x_I\left(1-\theta\right)}{6}\right]\sum_{n=1}^{N}Q_{n,I,R}^{k+1}\Delta_n\,,$$

right incident boundary, (4.55f)

$$\phi_{I+1/2}^{k+1,(0)}=\frac{2}{\rho}\sum_{\mu_n<0}\left|\mu_n\right|\psi_{n,R}^{b,k+1}\Delta_n\,,\qquad\text{right incident boundary}.\quad(4.55g)$$

Eqs. (4.55) represent a physically-valid diffusion discretization. If we assume full-lumping ($\theta=1$), we obtain a node-centered implicit diffusion discretization similar to the implicit node-centered diffusion discretization we derived in Chapter 2. We will demonstrate this in the next section.

4.2.5 Examining the Implicit Asymptotic Diffusion Discretization

We now examine the relationship between Eqs. (4.55) and the implicit node-centered diffusion discretization examined in Chapter 2. Assuming a fully-lumped transport discretization ($\theta=1$), and assuming that the solution at time t_k is continuous across cell boundaries,

Eqs. (4.55) can be rewritten as:

$$\phi_{1/2}^{k+1,(0)} = \left(\frac{2}{\rho}\right) J_L^{b,k+1}, \qquad \text{left incident boundary}, \quad (4.56a)$$

$$\frac{\Delta x_{3/2}}{v\Delta t_{k+1}}\left(\phi_{3/2}^{k+1,(0)} - \phi_{3/2}^{k}\right) - \frac{D_2}{\Delta x_2}\left(\phi_{5/2}^{k+1,(0)} - \phi_{3/2}^{k+1,(0)}\right) + \frac{D_1}{\Delta x_1}\left(\phi_{3/2}^{k+1,(0)} - \frac{1}{2}\phi_{1/2}^{k+1,(0)} - 3\sum_{\mu_n>0}\mu_n^2\psi_{n,L}^{b,k+1}\Delta_n\right) + \left(\Sigma_{a,3/2}\Delta x_{3/2}\right)\phi_{3/2}^{k+1,(0)} = \Delta x_{3/2} Q_{3/2}^{k+1}, \qquad \text{left incident boundary}, \quad (4.56b)$$

$$\frac{\Delta x_{1/2}}{v\Delta t_{k+1}}\left(\phi_{1/2}^{k+1,(0)} - \phi_{1/2}^{k}\right) - \frac{D_1}{\Delta x_1}\left(\phi_{3/2}^{k+1,(0)} - \phi_{1/2}^{k+1,(0)}\right) + \left(\Sigma_{a,1/2}\Delta x_{1/2}\right)\phi_{1/2}^{k+1,(0)} = \Delta x_{1/2} Q_{1/2}^{k+1}, \qquad \text{left reflecting boundary}, \quad (4.56c)$$

$$\frac{\Delta x_{i+1/2}}{v\Delta t_{k+1}}\left(\phi_{i+1/2}^{k+1,(0)} - \phi_{i+1/2}^{k}\right) - \frac{D_{i+1}}{\Delta x_{i+1}}\left(\phi_{i+3/2}^{k+1,(0)} - \phi_{i+1/2}^{k+1,(0)}\right) + \frac{D_i}{\Delta x_i}\left(\phi_{i+1/2}^{k+1,(0)} - \phi_{i-1/2}^{k+1,(0)}\right) + \left(\Sigma_{a,i+1/2}\Delta x_{i+1/2}\right)\phi_{i+1/2}^{k+1,(0)} = \Delta x_{i+1/2} Q_{i+1/2}^{k+1}, \qquad 2 \le i \le I-1, \quad (4.56d)$$

$$\frac{\Delta x_{I+1/2}}{v\Delta t_{k+1}}\left(\phi_{I+1/2}^{k+1,(0)} - \phi_{I+1/2}^{k}\right) + \frac{D_I}{\Delta x_I}\left(\phi_{I+1/2}^{k+1,(0)} - \phi_{I-1/2}^{k+1,(0)}\right) + \left(\Sigma_{a,I+1/2}\Delta x_{I+1/2}\right)\phi_{I+1/2}^{k+1,(0)} = \Delta x_{I+1/2} Q_{I+1/2}^{k+1}, \qquad \text{right reflecting boundary}, \quad (4.56e)$$

$$\frac{\Delta x_{I-1/2}}{v\Delta t_{k+1}}\left(\phi_{I-1/2}^{k+1,(0)} - \phi_{I-1/2}^{k}\right) - \frac{D_I}{\Delta x_I}\left(\frac{1}{2}\phi_{I+1/2}^{k+1,(0)} - \phi_{I-1/2}^{k+1,(0)} + 3\sum_{\mu_n<0}\mu_n^2\psi_{n,R}^{b,k+1}\Delta_n\right) + \frac{D_{I-1}}{\Delta x_{I-1}}\left(\phi_{I-1/2}^{k+1,(0)} - \phi_{I-3/2}^{k+1,(0)}\right) + \left(\Sigma_{a,I-1/2}\Delta x_{I-1/2}\right)\phi_{I-1/2}^{k+1,(0)} = \Delta x_{I-1/2} Q_{I-1/2}^{k+1}, \qquad \text{right incident boundary}, \quad (4.56f)$$

$$\phi_{I+1/2}^{k+1,(0)} = \left(\frac{2}{\rho}\right) J_R^{b,k+1}, \qquad \text{right incident boundary}, \quad (4.56g)$$

where

$$J_L^{b,k+1} = \sum_{\mu_n>0}\mu_n\psi_{n,L}^{b,k+1}\Delta_n, \quad (4.57a)$$

$$J_R^{b,k+1} = \sum_{\mu_n<0} |\mu_n| \psi_{n,R}^{b,k+1} \Delta_n \,, \tag{4.57b}$$

$$D_i = \frac{1}{3\Sigma_{t,i}} \,, \tag{4.58}$$

and

$$\Delta x_{i+1/2} = \begin{cases} \dfrac{\Delta x_1}{2} \,, & i = 0 \,, \\ \dfrac{\Delta x_{i+1} + \Delta x_i}{2} \,, & 1 \leq i \leq I-1 \,, \\ \dfrac{\Delta x_I}{2} \,, & i = I \,, \end{cases} \tag{4.59a}$$

$$\Sigma_{a,i+1/2} = \begin{cases} \Sigma_{a,1} \,, & i = 0 \,, \\ \dfrac{\Sigma_{a,i+1}\Delta x_{i+1} + \Sigma_{a,i}\Delta x_i}{\Delta x_{i+1} + \Delta x_i} \,, & 1 \leq i \leq I-1 \,, \\ \Sigma_{a,I} \,, & i = I \,, \end{cases} \tag{4.59b}$$

$$Q_{i+1/2}^{k+1} = \begin{cases} \displaystyle\sum_{n=1}^{N} Q_{n,1,L}^{k+1} \Delta_n \,, & i = 0 \,, \\ \dfrac{\displaystyle\sum_{n=1}^{N} Q_{n,i,R}^{k+1} \Delta_n \Delta x_i + \sum_{n=1}^{N} Q_{n,i+1,L}^{k+1} \Delta_n \Delta x_{i+1}}{\Delta x_i + \Delta x_{i+1}} \,, & 1 \leq i \leq I-1 \,, \\ \displaystyle\sum_{n=1}^{N} Q_{n,I,R}^{k+1} \Delta_n \,, & i = I \,. \end{cases} \tag{4.59c}$$

Comparing Eqs. (4.56) with Eqs. (2.43) and (2.44), we see that the lumped implicit asymptotic diffusion equations are identical to the implicit node-centered diffusion equations in the interior and on reflecting boundaries, though the equations differ for the first two nodes on an incident boundary. Excepting this fairly slight difference, we expect the implicit transport solution to behave similarly to the implicit node-centered diffusion method in the thick diffusive limit.

To demonstrate the correctness of the asymptotic analysis, consider a homogeneous slab of material 1 cm in length, divided into 10 cells, with total cross section $\Sigma_t = \frac{1}{\varepsilon}$ cm^{-1} and absorption cross section $\Sigma_a = \varepsilon$ cm^{-1}, where we vary ε from 10^0 to 10^{-4}. We place an isotropic fixed source of strength $Q = \varepsilon$ cm^{-3} s^{-1} everywhere in the slab, and set the

particle velocity to $v = \frac{1}{\varepsilon}$ cm/s. The left boundary is a vacuum, and the right boundary is reflecting, and we use an S_{16} quadrature set. As $\varepsilon \to 0$, this problem converges to the diffusion problem:

$$\frac{\partial}{\partial t}\phi(x,t) - \frac{1}{3}\frac{\partial^2}{\partial x^2}\phi(x,t) + \phi(x,t) = 1\,, \tag{4.60a}$$

$$\phi(0,t) = 0\,, \tag{4.60b}$$

$$J(1,t) = 0\,. \tag{4.60c}$$

Setting an initial scalar flux of zero, and executing ten time steps with $\Delta t = 1$ s, we find the asymptotic diffusion result shown in Figure 4.1. In Figure 4.2, we show the convergence of the implicit transport method to the asymptotic diffusion solution as ε vanishes. We measure the difference between the asymptotic diffusion solution and the transport solution using an L_1 norm, i.e.,

$$L_1 \text{ Norm} = \frac{\sum_{i=1}^{I} \left| \phi_i^{k+1,transport} - \phi_i^{k+1,diffusion} \right| \Delta x_i}{\sum_{i=1}^{I} \Delta x_i}\,, \tag{4.61}$$

where $\phi_i^{k+1,transport}$ is the average transport scalar flux in cell i at time t_{k+1}, calculated using the implicit transport method, and $\phi_i^{k+1,diffusion}$ is the average diffusion scalar flux in cell i at

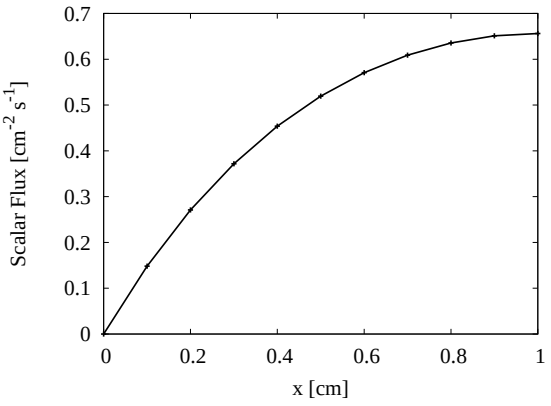

Figure 4.1 Asymptotic Implicit Diffusion Solution at $t = 10$ s

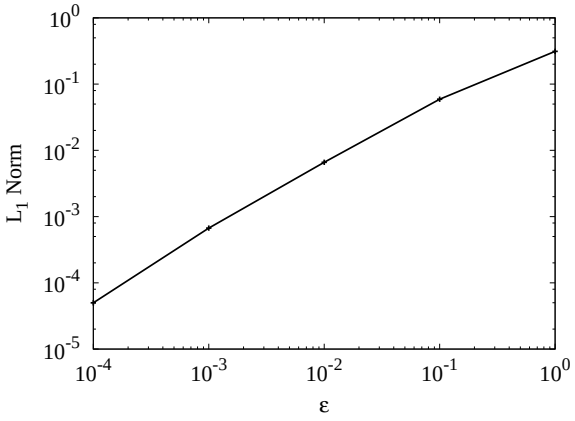

Figure 4.2 Convergence of the Implicit Transport Solution

time t_{k+1}, calculated using the implicit asymptotic diffusion equations. That the implicit LDFEM solution converges to the asymptotic diffusion solution as ε vanishes suggests that our asymptotic analysis is correct.

4.3 Asymptotic Analysis of the Fully- and Semi-Explicit LDFEM Transport Method

In this section we perform an asymptotic analysis of the fully- and semi-explicit linear discontinuous finite element transport methods. We begin with the fully- and semi-explicit linear discontinuous finite element transport equation:

$$\frac{1}{v\Delta t_{k+1}}\underline{\underline{M}}_i\left(\underline{\psi}_{n,i}^{k+1}-\underline{\psi}_{n,i}^{k}\right)+\mu_n\underline{\underline{L}}_i^{surf}\underline{\psi}_{n,i}^{k,surf}-\mu_n\underline{\underline{L}}_i\underline{\psi}_{n,i}^{k}+\Sigma_{t,i}\underline{\underline{M}}_i\underline{\psi}_{n,i}^{k+\beta}$$
$$=\frac{\Sigma_{s,i}}{2}\underline{\underline{M}}_i\sum_{m=1}^{N}\underline{\psi}_{m,i}^{k+\beta}\,\Delta_m+\underline{\underline{M}}_i\underline{Q}_{n,i}^{k+1}\,, \quad (4.62)$$

where

$$\underline{\psi}_{n,i}^{k}=\begin{bmatrix}\psi_{n,i,L}^{k} & \psi_{n,i,R}^{k}\end{bmatrix}^T\,, \quad (4.63a)$$

$$\underline{\psi}_{n,i}^{k,surf}=\begin{bmatrix}\psi_{n,i,L}^{k,surf} & \psi_{n,i,R}^{k,surf}\end{bmatrix}^T\,, \quad (4.63b)$$

and

$$\psi_{n,i,L}^{k,surf}=\begin{cases}\psi_{n,i,L}^{k}\,, & \mu_n<0\,,\\ \psi_{n,L}^{b,k}\,, & \mu_n>0\,, \quad i=1\,,\\ \psi_{n,i-1,R}^{k}\,, & \mu_n>0\,, \quad 2\le i\le I\,,\end{cases} \quad (4.63c)$$

$$\psi_{n,i,R}^{k,surf}=\begin{cases}\psi_{n,i+1,L}^{k}\,, & \mu_n<0\,, \quad 1\le i\le I-1\,,\\ \psi_{n,R}^{b,k}\,, & \mu_n<0\,, \quad i=I\,,\\ \psi_{n,i,R}^{k}\,, & \mu_n>0\,,\end{cases} \quad (4.63d)$$

and where $\psi_{n,L}^{b,k+1}$ and $\psi_{n,R}^{b,k+1}$ are the boundary conditions at time t_{k+1} for the left and right boundaries, respectively. For vacuum and incident boundaries, these boundary conditions are specified, whereas for reflecting boundaries, we use

$$\psi_{n,L}^{b,k}=\psi_{n',1,L}^{k}\,, \qquad \mu_n>0\,, \quad \mu_{n'}=-\mu_n\,, \quad (4.64a)$$

$$\psi_{n,R}^{b,k}=\psi_{n',I,R}^{k}\,, \qquad \mu_n<0\,, \quad \mu_{n'}=-\mu_n\,. \quad (4.64b)$$

We define

$$\beta = \begin{cases} 0: & \text{fully-explicit method}, \\ 1: & \text{semi-explicit method}, \end{cases} \tag{4.65}$$

and we also define initial conditions

$$\underline{\psi}_{n,i}^{0} = \left[\int_{x_{i-1/2}}^{x_{i+1/2}} w_{i,L}(x)\, \psi_n^i(x)\, \mathrm{d}x \quad \int_{x_{i-1/2}}^{x_{i+1/2}} w_{i,R}(x)\, \psi_n^i(x)\, \mathrm{d}x \right]^T, \tag{4.66}$$

where $\psi_n^i(x)$ is a specified initial condition. The other terms in Eq. (4.62) are defined in Section 3.3 and will not be repeated here.

We now apply the same asymptotic scalings used in the asymptotic analysis of the implicit linear discontinuous transport method. Substituting Eqs. (4.22) into Eq. (4.62), we have

$$\begin{aligned} \frac{\varepsilon}{v' \Delta t_{k+1}} \underline{\underline{M}}_i \left(\underline{\psi}_{n,i}^{k+1} - \underline{\psi}_{n,i}^{k} \right) + \mu_n \underline{\underline{L}}_i^{surf} \underline{\psi}_{n,i}^{k,surf} - \mu_n \underline{\underline{L}}_i \underline{\psi}_{n,i}^{k} + \frac{\sigma_{t,i}}{\varepsilon} \underline{\underline{M}}_i \underline{\psi}_{n,i}^{k+\beta} \\ = \frac{1}{2} \left(\frac{\sigma_{t,i}}{\varepsilon} - \varepsilon \sigma_{a,i} \right) \underline{\underline{M}}_i \sum_{m=1}^{N} \underline{\psi}_{m,i}^{k+\beta} \Delta_m + \varepsilon \underline{\underline{M}}_i \underline{q}_{n,i}^{k+1}. \end{aligned} \tag{4.67}$$

As ε vanishes, Eq. (4.67) describes an increasingly thick and diffusive transport problem. We expand the angular flux at both time t_k and t_{k+1} as a power series in ε, such that

$$\underline{\psi}_{n,i}^{k} = \underline{\psi}_{n,i}^{k,(0)} + \varepsilon \underline{\psi}_{n,i}^{k,(1)} + \varepsilon^2 \underline{\psi}_{n,i}^{k,(2)} + O(\varepsilon^3), \tag{4.68a}$$

$$\underline{\psi}_{n,i}^{k,surf} = \underline{\psi}_{n,i}^{k,surf,(0)} + \varepsilon \underline{\psi}_{n,i}^{k,surf,(1)} + \varepsilon^2 \underline{\psi}_{n,i}^{k,surf,(2)} + O(\varepsilon^3). \tag{4.68b}$$

Therefore, for $\mu_n < 0$,

$$\psi_{n,i,L}^{k,surf} = \psi_{n,i,L}^{k,(0)} + \varepsilon \psi_{n,i,L}^{k,(1)} + \varepsilon^2 \psi_{n,i,L}^{k,(2)} + O(\varepsilon^3), \tag{4.69a}$$

$$\psi_{n,i,R}^{k,surf} = \begin{cases} \psi_{n,i+1,L}^{k,(0)} + \varepsilon \psi_{n,i+1,L}^{k,(1)} + \varepsilon^2 \psi_{n,i+1,L}^{k,(2)} + O(\varepsilon^3), & 1 \le i \le I-1, \\ \psi_{n,R}^{b,k}, & i = I, \end{cases} \tag{4.69b}$$

and for $\mu_n > 0$,

$$\psi_{n,i,L}^{k,surf} = \begin{cases} \psi_{n,L}^{b,k}, & i = 1, \\ \psi_{n,i-1,R}^{k,(0)} + \varepsilon \psi_{n,i-1,R}^{k,(1)} + \varepsilon^2 \psi_{n,i-1,R}^{k,(2)} + O(\varepsilon^3), & 2 \le i \le I, \end{cases} \tag{4.70a}$$

$$\psi_{n,i,R}^{k,surf} = \psi_{n,i,R}^{k,(0)} + \varepsilon \psi_{n,i,R}^{k,(1)} + \varepsilon^2 \psi_{n,i,R}^{k,(2)} + O(\varepsilon^3). \tag{4.70b}$$

Substituting Eqs. (4.68) into Eq. (4.67), we obtain

$$\begin{aligned} \frac{\varepsilon}{v' \Delta t_{k+1}} \underline{\underline{M}}_i \Big[& \left(\underline{\psi}_{n,i}^{k+1,(0)} + \varepsilon \underline{\psi}_{n,i}^{k+1,(1)} + \varepsilon^2 \underline{\psi}_{n,i}^{k+1,(2)} \right) \\ & - \left(\underline{\psi}_{n,i}^{k,(0)} + \varepsilon \underline{\psi}_{n,i}^{k,(1)} + \varepsilon^2 \underline{\psi}_{n,i}^{k,(2)} \right) + O(\varepsilon^3) \Big] \\ & + \mu_n \underline{\underline{L}}_i^{surf} \left[\underline{\psi}_{n,i}^{k,surf,(0)} + \varepsilon \underline{\psi}_{n,i}^{k,surf,(1)} + \varepsilon^2 \underline{\psi}_{n,i}^{k,surf,(2)} + O(\varepsilon^3) \right] \\ & - \mu_n \underline{\underline{L}}_i \left[\underline{\psi}_{n,i}^{k,(0)} + \varepsilon \underline{\psi}_{n,i}^{k,(1)} + \varepsilon^2 \underline{\psi}_{n,i}^{k,(2)} + O(\varepsilon^3) \right] \\ & + \frac{\sigma_{t,i}}{\varepsilon} \underline{\underline{M}}_i \left[\underline{\psi}_{n,i}^{k+\beta,(0)} + \varepsilon \underline{\psi}_{n,i}^{k+\beta,(1)} + \varepsilon^2 \underline{\psi}_{n,i}^{k+\beta,(2)} + O(\varepsilon^3) \right] \\ = \frac{1}{2} & \left(\frac{\sigma_{t,i}}{\varepsilon} - \varepsilon \sigma_{a,i} \right) \underline{\underline{M}}_i \sum_{m=1}^{N} \left[\underline{\psi}_{m,i}^{k+\beta,(0)} + \varepsilon \underline{\psi}_{m,i}^{k+\beta,(1)} + \varepsilon^2 \underline{\psi}_{m,i}^{k+\beta,(2)} + O(\varepsilon^3) \right] \Delta_m \\ & + \varepsilon \underline{\underline{M}}_i \underline{q}_{n,i}^{k+1}. \end{aligned} \tag{4.71}$$

We now analyze the terms of each power of ε in Eq. (4.71).

4.3.1 The $O(\varepsilon^{-1})$ Terms

Beginning with the $O(\varepsilon^{-1})$ terms in Eq. (4.71), we have

$$\sigma_{t,i} \underline{\underline{M}}_i \underline{\psi}_{n,i}^{k+\beta,(0)} = \frac{\sigma_{t,i}}{2} \underline{\underline{M}}_i \sum_{m=1}^{N} \underline{\psi}_{m,i}^{k+\beta,(0)} \Delta_m. \tag{4.72}$$

Assuming that $\underline{\underline{M}}_i$ is invertible, which is true for the linear discontinuous finite element discretization, we solve for $\underline{\psi}_{n,i}^{k+\beta,(0)}$ and find

$$\underline{\psi}_{n,i}^{k+\beta,(0)} = \frac{1}{2} \sum_{m=1}^{N} \underline{\psi}_{m,i}^{k+\beta,(0)} \Delta_m = \frac{1}{2} \underline{\phi}_i^{k+\beta,(0)}. \tag{4.73}$$

Therefore, the leading order angular flux at time $t_{k+\beta}$ is isotropic, and the total angular flux at time $t_{k+\beta}$ in the diffusion limit satisfies

$$\underline{\psi}_{n,i}^{k+\beta} = \frac{1}{2}\underline{\phi}_i^{k+\beta,(0)} + O(\varepsilon)\,, \tag{4.74}$$

where $\underline{\phi}_i^{k+\beta,(0)}$ is not yet specified. Note that for the fully-explicit method ($\beta = 0$), Eq. (4.73) implies that the leading-order initial conditions must also be isotropic.

4.3.2 The $O(1)$ Terms

Next we examine the $O(1)$ terms in Eq. (4.71):

$$\mu_n \underline{\underline{L}}_i^{surf} \underline{\psi}_{n,i}^{k,surf,(0)} - \mu_n \underline{\underline{L}}_i \underline{\psi}_{n,i}^{k,(0)} + \sigma_{t,i} \underline{\underline{M}}_i \underline{\psi}_{n,i}^{k+\beta,(1)} = \frac{\sigma_{t,i}}{2} \underline{\underline{M}}_i \sum_{m=1}^{N} \underline{\psi}_{m,i}^{k+\beta,(1)} \Delta_m\,. \tag{4.75}$$

Operating on Eq. (4.75) by $\sum_{n=1}^{N}(\cdot)\Delta_n$, substituting in Eq. (4.73), and assuming that the quadrature set satisfies

$$\sum_{n=1}^{N} \Delta_n = \int_{-1}^{1} \mathrm{d}\mu = 2\,, \tag{4.76a}$$

and

$$\sum_{n=1}^{N} \mu_n \Delta_n = \int_{-1}^{1} \mu\, \mathrm{d}\mu = 0\,, \tag{4.76b}$$

we find

$$\underline{\underline{L}}_i^{surf} \sum_{n=1}^{N} \mu_n \underline{\psi}_{n,i}^{k,surf,(0)} \Delta_n = 0\,. \tag{4.77}$$

Eq. (4.77) represents a 2×2 system of algebraic equations. We first consider the problem interior. Substituting the upstream closures, Eqs. (4.69) and (4.70), into Eq. (4.77), and writing the two rows individually, we have

$$-\left(\sum_{\mu_n<0} \mu_n \psi_{n,i,L}^{k,(0)} \Delta_n + \sum_{\mu_n>0} \mu_n \psi_{n,i-1,R}^{k,(0)} \Delta_n \right) = 0\,, \tag{4.78a}$$

$$\left(\sum_{\mu_n<0} \mu_n \psi_{n,i+1,L}^{k,(0)} \Delta_n + \sum_{\mu_n>0} \mu_n \psi_{n,i,R}^{k,(0)} \Delta_n \right) = 0\,. \tag{4.78b}$$

For the fully-explicit method, we may substitute Eq. (4.73) into Eqs. (4.78), and assuming a symmetric quadrature set such that

$$\sum_{\mu_n>0} \mu_n \Delta_n = -\sum_{\mu_n<0} \mu_n \Delta_n \,, \tag{4.79}$$

we find

$$\phi_{i,L}^{k,(0)} = \phi_{i-1,R}^{k,(0)} \equiv \phi_{i-1/2}^{k,(0)} \,, \tag{4.80a}$$

$$\phi_{i,R}^{k,(0)} = \phi_{i+1,L}^{k,(0)} \equiv \phi_{i+1/2}^{k,(0)} \,. \tag{4.80b}$$

Therefore, in the thick diffusive limit, the leading order scalar flux at time t_k is continuous across cell edges. This also means that the initial conditions must be continuous to satisfy the diffusion limit.

Eqs. (4.80) must hold for a transport method to converge to a physically correct asymptotic diffusion discretization in the thick limit. In order for Eqs. (4.80) to hold for the semi-explicit method, we must require that Eq. (4.73) holds for the initial conditions, i.e., the initial conditions must be isotropic. We must also require that Eq. (4.80) holds for the initial conditions, i.e., the initial conditions must be continuous across cell edges.

We next consider an incident left boundary. Substituting the upstream closures, Eqs. (4.69) and Eqs. (4.70), into the first row of Eq. (4.77), we have

$$-\left(\sum_{\mu_n<0} \mu_n \psi_{n,1,L}^{k,(0)} \Delta_n + \sum_{\mu_n>0} \mu_n \psi_{n,L}^{b,k} \Delta_n \right) = 0 \,. \tag{4.81}$$

Substituting Eq. (4.73) into Eq. (4.81), and defining

$$\begin{aligned} \rho &= \sum_{\mu_n>0} \mu_n \Delta_n = -\sum_{\mu_n<0} \mu_n \Delta_n \\ &\approx \int_0^1 \mu \, \mathrm{d}\mu = \frac{1}{2} \,, \end{aligned} \tag{4.82}$$

we find

$$\phi_{1,L}^{k,(0)} \equiv \phi_{1/2}^{k,(0)} = \frac{2}{\rho} \sum_{\mu_n>0} \mu_n \psi_{n,L}^{b,k} \Delta_n \,, \qquad \text{left incident boundary} \,. \tag{4.83}$$

Likewise, for an incident right boundary, we find

$$\phi_{I,R}^{k,(0)} \equiv \phi_{I+1/2}^{k,(0)} = \frac{2}{\rho} \sum_{\mu_n<0} |\mu_n| \psi_{n,R}^{b,k} \Delta_n \,, \qquad \text{right incident boundary} \,. \tag{4.84}$$

Now, operating on Eq. (4.75) by $\sum_{n=1}^{N} \mu_n(\cdot)\Delta_n$, we find

$$\underline{\underline{L}}_i^{surf} \sum_{n=1}^{N} \mu_n^2 \underline{\psi}_{n,i}^{k,surf,(0)} \Delta_n - \underline{\underline{L}}_i \sum_{n=1}^{N} \mu_n^2 \underline{\psi}_{n,i}^{k,(0)} \Delta_n + \sigma_{t,i} \underline{\underline{M}}_i \sum_{n=1}^{N} \mu_n \underline{\psi}_{n,i}^{k+\beta,(1)} \Delta_n = 0 \,. \tag{4.85}$$

Substituting Eqs. (4.73) and (4.80) into Eq. (4.85), assuming that the quadrature set satisfies

$$\sum_{n=1}^{N} \mu_n^2 \Delta_n = \int_{-1}^{1} \mu^2 \, \mathrm{d}\mu = \frac{2}{3} \,, \tag{4.86}$$

and defining the first order current as

$$\underline{J}_i^{k+\beta,(1)} = \sum_{n=1}^{N} \mu_n \underline{\psi}_{n,i}^{k+\beta,(1)} \Delta_n \,, \tag{4.87}$$

we obtain

$$\underline{J}_1^{k+\beta,(1)} = -\frac{1}{\sigma_{t,1}} \underline{\underline{M}}_1^{-1} \left(\underline{\underline{L}}_1^{surf} \sum_{n=1}^{N} \mu_n^2 \underline{\psi}_{n,1}^{k,surf,(0)} \Delta_n - \frac{1}{3} \underline{\underline{L}}_1 \underline{\phi}_1^{k,(0)} \right) , \tag{4.88a}$$

$$\underline{J}_i^{k+\beta,(1)} = -\frac{1}{3\sigma_{t,i}} \underline{\underline{M}}_i^{-1} \left(\underline{\underline{L}}_i^{surf} - \underline{\underline{L}}_i \right) \underline{\phi}_i^{k,(0)} \,, \qquad 2 \le i \le I-1 \,, \tag{4.88b}$$

$$\underline{J}_I^{k+\beta,(1)} = -\frac{1}{\sigma_{t,I}} \underline{\underline{M}}_I^{-1} \left(\underline{\underline{L}}_I^{surf} \sum_{n=1}^{N} \mu_n^2 \underline{\psi}_{n,I}^{k,surf,(0)} \Delta_n - \frac{1}{3} \underline{\underline{L}}_I \underline{\phi}_I^{k,(0)} \right) . \tag{4.88c}$$

Substituting in the matrices and the upstream closures, and evaluating the currents, we find

$$J_{1,L}^{k+\beta,(1)} = -\frac{1}{3\sigma_{t,1}\Delta x_1 (1+2\theta)} \Bigg[(1+2\theta)\, \phi_{3/2}^{k,(0)} + (1-\theta)\, \phi_{1/2}^{k,(0)} - 6(2+\theta) \sum_{\mu_n>0} \mu_n^2 \psi_{n,L}^{b,k} \Delta_n \Bigg] \,, \quad \text{left incident boundary} \,, \tag{4.89a}$$

$$J_{1,R}^{k+\beta,(1)} = -\frac{1}{3\sigma_{t,1}\Delta x_1 (1+2\theta)} \Bigg[(1+2\theta)\, \phi_{3/2}^{k,(0)} - (2+\theta)\, \phi_{1/2}^{k,(0)} + 6(1-\theta) \sum_{\mu_n>0} \mu_n^2 \psi_{n,L}^{b,k} \Delta_n \Bigg] \,, \quad \text{left incident boundary} \,, \tag{4.89b}$$

$$J_{i,L}^{k+\beta,(1)} = J_{i,R}^{k+\beta,(1)} = -\frac{1}{3\sigma_{t,i}\Delta x_i}\left(\phi_{i+1/2}^{k,(0)} - \phi_{i-1/2}^{k,(0)}\right),$$

interior and reflecting boundaries, (4.89c)

$$J_{I,L}^{k+\beta,(1)} = -\frac{1}{3\sigma_{t,I}\Delta x_I\,(1+2\theta)}\Bigg[(2+\theta)\,\phi_{I+1/2}^{k,(0)} - (1+2\theta)\,\phi_{I-1/2}^{k,(0)} - 6\,(1-\theta)\sum_{\mu_n<0}\mu_n^2\,\psi_{n,R}^{b,k}\,\Delta_n\Bigg],$$

right incident boundary, (4.89d)

$$J_{I,R}^{k+\beta,(1)} = -\frac{1}{3\sigma_{t,I}\Delta x_I\,(1+2\theta)}\Bigg[-(1-\theta)\,\phi_{I+1/2}^{k,(0)} - (1+2\theta)\,\phi_{I-1/2}^{k,(0)} + 6\,(2+\theta)\sum_{\mu_n<0}\mu_n^2\,\psi_{n,R}^{b,k}\,\Delta_n\Bigg],$$

right incident boundary. (4.89e)

4.3.3 The $O(\varepsilon)$ Terms

The $O(\varepsilon)$ terms in Eq. (4.71) are

$$\frac{1}{v'\Delta t_{k+1}}\underline{\underline{M}}_i\left(\underline{\psi}_{n,i}^{k+1,(0)} - \underline{\psi}_{n,i}^{k,(0)}\right) + \mu_n\underline{\underline{L}}_i^{surf}\underline{\psi}_{n,i}^{k,surf,(1)} - \mu_n\underline{\underline{L}}_i\underline{\psi}_{n,i}^{k,(1)} + \sigma_{t,i}\underline{\underline{M}}_i\underline{\psi}_{n,i}^{k+\beta,(2)} = \frac{\sigma_{t,i}}{2}\underline{\underline{M}}_i\sum_{m=1}^{N}\underline{\psi}_{m,i}^{k+\beta,(2)}\,\Delta_m - \frac{\sigma_{a,i}}{2}\underline{\underline{M}}_i\sum_{m=1}^{N}\underline{\psi}_{m,i}^{k+\beta,(0)}\,\Delta_m + \underline{\underline{M}}_i\underline{q}_{n,i}^{k+1}. \quad (4.90)$$

Operating on Eq. (4.90) by $\sum_{n=1}^{N}(\cdot)\,\Delta_n$, we have

$$\frac{1}{v'\Delta t_{k+1}}\underline{\underline{M}}_i\left(\underline{\phi}_i^{k+1,(0)} - \underline{\phi}_i^{k,(0)}\right) + \underline{\underline{L}}_i^{surf}\sum_{n=1}^{N}\mu_n\underline{\psi}_{n,i}^{k,surf,(1)}\,\Delta_n - \underline{\underline{L}}_i\underline{J}_i^{k,(1)} + \sigma_{a,i}\underline{\underline{M}}_i\underline{\phi}_i^{k+\beta,(0)} = \underline{\underline{M}}_i\sum_{n=1}^{N}\underline{q}_{n,i}^{k+1}\,\Delta_n. \quad (4.91)$$

Eq. (4.91) represents a 2×2 system of equations. Writing each row out separately and substituting in Eq. (4.80) and the definitions of $\underline{\underline{M}}_i$, $\underline{\underline{L}}_i^{surf}$, and $\underline{\underline{L}}_i$, we have

$$\left[\frac{\Delta x_i\,(2+\theta)}{6v'\Delta t_{k+1}}\right]\left(\phi_{i-1/2}^{k+1,(0)}-\phi_{i-1/2}^{k,(0)}\right)+\left[\frac{\Delta x_i\,(1-\theta)}{6v'\Delta t_{k+1}}\right]\left(\phi_{i+1/2}^{k+1,(0)}-\phi_{i+1/2}^{k,(0)}\right)$$
$$-\sum_{n=1}^{N}\mu_n\psi_{n,i,L}^{k,surf,(1)}\,\Delta_n+\frac{1}{2}\left(J_{i,L}^{k,(1)}+J_{i,R}^{k,(1)}\right)+\left[\frac{\sigma_{a,i}\Delta x_i\,(2+\theta)}{6}\right]\phi_{i-1/2}^{k+\beta,(0)}$$
$$+\left[\frac{\sigma_{a,i}\Delta x_i\,(1-\theta)}{6}\right]\phi_{i+1/2}^{k+\beta,(0)}=\left[\frac{\Delta x_i\,(2+\theta)}{6}\right]\sum_{n=1}^{N}q_{n,i,L}^{k+1}\,\Delta_n$$
$$+\left[\frac{\Delta x_i\,(1-\theta)}{6}\right]\sum_{n=1}^{N}q_{n,i,R}^{k+1}\,\Delta_n\,, \quad (4.92a)$$

$$\left[\frac{\Delta x_i\,(1-\theta)}{6v'\Delta t_{k+1}}\right]\left(\phi_{i-1/2}^{k+1,(0)}-\phi_{i-1/2}^{k,(0)}\right)+\left[\frac{\Delta x_i\,(2+\theta)}{6v'\Delta t_{k+1}}\right]\left(\phi_{i+1/2}^{k+1,(0)}-\phi_{i+1/2}^{k,(0)}\right)$$
$$+\sum_{n=1}^{N}\mu_n\psi_{n,i,R}^{k,surf,(1)}\,\Delta_n-\frac{1}{2}\left(J_{i,L}^{k,(1)}+J_{i,R}^{k,(1)}\right)+\left[\frac{\sigma_{a,i}\Delta x_i\,(1-\theta)}{6}\right]\phi_{i-1/2}^{k+\beta,(0)}$$
$$+\left[\frac{\sigma_{a,i}\Delta x_i\,(2+\theta)}{6}\right]\phi_{i+1/2}^{k+\beta,(0)}=\left[\frac{\Delta x_i\,(1-\theta)}{6}\right]\sum_{n=1}^{N}q_{n,i,L}^{k+1}\,\Delta_n$$
$$+\left[\frac{\Delta x_i\,(2+\theta)}{6}\right]\sum_{n=1}^{N}q_{n,i,R}^{k+1}\,\Delta_n\,. \quad (4.92b)$$

We evaluate Eq. (4.92a) at cell $i+1$ and sum with Eq. (4.92b). Using the upstream closures, Eqs. (4.69) and (4.70), the first order surface terms cancel, and we find

$$\begin{aligned}
&\left[\frac{\Delta x_i\,(1-\theta)}{6v'\Delta t_{k+1}}\right]\left(\phi_{i-1/2}^{k+1,(0)}-\phi_{i-1/2}^{k,(0)}\right)+\left[\frac{(\Delta x_i+\Delta x_{i+1})\,(2+\theta)}{6v'\Delta t_{k+1}}\right]\left(\phi_{i+1/2}^{k+1,(0)}-\phi_{i+1/2}^{k,(0)}\right)\\
&\qquad+\left[\frac{\Delta x_{i+1}\,(1-\theta)}{6v'\Delta t_{k+1}}\right]\left(\phi_{i+3/2}^{k+1,(0)}-\phi_{i+3/2}^{k,(0)}\right)\\
&\qquad+\frac{1}{2}\left(J_{i+1,L}^{k,(1)}+J_{i+1,R}^{k,(1)}\right)-\frac{1}{2}\left(J_{i,L}^{k,(1)}+J_{i,R}^{k,(1)}\right)\\
&+\left[\frac{\sigma_{a,i}\Delta x_i\,(1-\theta)}{6}\right]\phi_{i-1/2}^{k+\beta,(0)}+\left[\frac{(\sigma_{a,i+1}\Delta x_{i+1}+\sigma_{a,i}\Delta x_i)\,(2+\theta)}{6}\right]\phi_{i+1/2}^{k+\beta,(0)}\\
&\qquad+\left[\frac{\sigma_{a,i+1}\Delta x_{i+1}\,(1-\theta)}{6}\right]\phi_{i+3/2}^{k+\beta,(0)}=\left[\frac{\Delta x_i\,(1-\theta)}{6}\right]\sum_{n=1}^{N}q_{n,i,L}^{k+1}\Delta_n\\
&\qquad+\left[\frac{\Delta x_i\,(2+\theta)}{6}\right]\sum_{n=1}^{N}q_{n,i,R}^{k+1}\Delta_n+\left[\frac{\Delta x_{i+1}\,(2+\theta)}{6}\right]\sum_{n=1}^{N}q_{n,i+1,L}^{k+1}\Delta_n\\
&\qquad+\left[\frac{\Delta x_{i+1}\,(1-\theta)}{6}\right]\sum_{n=1}^{N}q_{n,i+1,R}^{k+1}\Delta_n\,. \qquad (4.93)
\end{aligned}$$

For a reflecting left boundary, we evaluate Eq. (4.92a) for cell 1, and use

$$\sum_{n=1}^{N}\mu_n\psi_{n,1,L}^{k,surf,(1)}\Delta_n=0\,, \qquad (4.94)$$

and therefore, the diffusion equation on the left boundary for a reflecting boundary condition is

$$\begin{aligned}
&\left[\frac{\Delta x_1\,(2+\theta)}{6v'\Delta t_{k+1}}\right]\left(\phi_{1/2}^{k+1,(0)}-\phi_{1/2}^{k,(0)}\right)+\left[\frac{\Delta x_1\,(1-\theta)}{6v'\Delta t_{k+1}}\right]\left(\phi_{3/2}^{k+1,(0)}-\phi_{3/2}^{k,(0)}\right)\\
&\quad+\frac{1}{2}\left(J_{1,L}^{k,(1)}+J_{1,R}^{k,(1)}\right)+\left[\frac{\sigma_{a,1}\Delta x_1\,(2+\theta)}{6}\right]\phi_{1/2}^{k+\beta,(0)}+\left[\frac{\sigma_{a,1}\Delta x_1\,(1-\theta)}{6}\right]\phi_{3/2}^{k+\beta,(0)}\\
&\qquad=\left[\frac{\Delta x_1\,(2+\theta)}{6}\right]\sum_{n=1}^{N}q_{n,1,L}^{k+1}\Delta_n+\left[\frac{\Delta x_1\,(1-\theta)}{6}\right]\sum_{n=1}^{N}q_{n,1,R}^{k+1}\Delta_n\,. \qquad (4.95)
\end{aligned}$$

For a reflecting right boundary, we evaluate Eq. (4.92b) for cell I, and use

$$\sum_{n=1}^{N}\mu_n\psi_{n,I,R}^{k,surf,(1)}\Delta_n=0\,, \qquad (4.96)$$

and therefore, the diffusion equation on the right boundary for a reflecting boundary condi-

tion is

$$\left[\frac{\Delta x_I\left(1-\theta\right)}{6v'\Delta t_{k+1}}\right]\left(\phi_{I-1/2}^{k+1,(0)}-\phi_{I-1/2}^{k,(0)}\right)+\left[\frac{\Delta x_I\left(2+\theta\right)}{6v'\Delta t_{k+1}}\right]\left(\phi_{I+1/2}^{k+1,(0)}-\phi_{I+1/2}^{k,(0)}\right)$$
$$-\frac{1}{2}\left(J_{I,L}^{k,(1)}+J_{I,R}^{k,(1)}\right)+\left[\frac{\sigma_{a,I}\Delta x_I\left(1-\theta\right)}{6}\right]\phi_{I-1/2}^{k+\beta,(0)}+\left[\frac{\sigma_{a,I}\Delta x_I\left(2+\theta\right)}{6}\right]\phi_{I+1/2}^{k+\beta,(0)}$$
$$=\left[\frac{\Delta x_I\left(1-\theta\right)}{6}\right]\sum_{n=1}^{N}q_{n,I,L}^{k+1}\Delta_n+\left[\frac{\Delta x_I\left(2+\theta\right)}{6}\right]\sum_{n=1}^{N}q_{n,I,R}^{k+1}\Delta_n\,. \quad (4.97)$$

4.3.4 Rescaling the Diffusion Equation

Substituting the currents in Eqs. (4.89) and the unscaled variables in Eq. (4.22) into Eqs. (4.93), (4.95), and (4.97), and we have, together with Eqs. (4.83) and (4.84), the asymptotic diffusion equations for the fully- and semi-explicit linear discontinuous finite element transport discretizations:

$$\phi_{1/2}^{k+1,(0)}=\frac{2}{\rho}\sum_{\mu_n>0}\mu_n\psi_{n,L}^{b,k+1}\Delta_n\,,\qquad\text{left incident boundary}\,, \quad (4.98a)$$

$$\left[\frac{\Delta x_1\left(1-\theta\right)}{6v\Delta t_{k+1}}\right]\left(\phi_{1/2}^{k+1,(0)}-\phi_{1/2}^{k,(0)}\right)+\left[\frac{\left(\Delta x_1+\Delta x_2\right)\left(2+\theta\right)}{6v\Delta t_{k+1}}\right]\left(\phi_{3/2}^{k+1,(0)}-\phi_{3/2}^{k,(0)}\right)$$
$$+\left[\frac{\Delta x_2\left(1-\theta\right)}{6v\Delta t_{k+1}}\right]\left(\phi_{5/2}^{k+1,(0)}-\phi_{5/2}^{k,(0)}\right)-\frac{1}{3\Sigma_{t,2}\Delta x_2}\left(\phi_{5/2}^{k-\beta,(0)}-\phi_{3/2}^{k-\beta,(0)}\right)$$
$$+\frac{1}{3\Sigma_{t,1}\Delta x_1}\left(\phi_{3/2}^{k-\beta,(0)}-\frac{1}{2}\phi_{1/2}^{k-\beta,(0)}-3\sum_{\mu_n>0}\mu_n^2\psi_{n,L}^{b,k-\beta}\Delta_n\right)+\left[\frac{\Sigma_{a,1}\Delta x_1\left(1-\theta\right)}{6}\right]\phi_{1/2}^{k+\beta,(0)}$$
$$+\left[\frac{\left(\Sigma_{a,2}\Delta x_2+\Sigma_{a,1}\Delta x_1\right)\left(2+\theta\right)}{6}\right]\phi_{3/2}^{k+\beta,(0)}+\left[\frac{\Sigma_{a,2}\Delta x_2\left(1-\theta\right)}{6}\right]\phi_{5/2}^{k+\beta,(0)}$$
$$=\left[\frac{\Delta x_1\left(1-\theta\right)}{6}\right]\sum_{n=1}^{N}Q_{n,1,L}^{k+1}\Delta_n+\left[\frac{\Delta x_1\left(2+\theta\right)}{6}\right]\sum_{n=1}^{N}Q_{n,1,R}^{k+1}\Delta_n$$
$$+\left[\frac{\Delta x_2\left(2+\theta\right)}{6}\right]\sum_{n=1}^{N}Q_{n,2,L}^{k+1}\Delta_n+\left[\frac{\Delta x_2\left(1-\theta\right)}{6}\right]\sum_{n=1}^{N}Q_{n,2,R}^{k+1}\Delta_n\,,$$
$$\text{left incident boundary}\,, \quad (4.98b)$$

$$\left[\frac{\Delta x_1\,(2+\theta)}{6v\Delta t_{k+1}}\right]\left(\phi_{1/2}^{k+1,(0)}-\phi_{1/2}^{k,(0)}\right)+\left[\frac{\Delta x_1\,(1-\theta)}{6v\Delta t_{k+1}}\right]\left(\phi_{3/2}^{k+1,(0)}-\phi_{3/2}^{k,(0)}\right)$$
$$-\frac{1}{3\Sigma_{t,1}\Delta x_1}\left(\phi_{3/2}^{k-\beta,(0)}-\phi_{1/2}^{k-\beta,(0)}\right)+\left[\frac{\Sigma_{a,1}\Delta x_1\,(2+\theta)}{6}\right]\phi_{1/2}^{k+\beta,(0)}$$
$$+\left[\frac{\Sigma_{a,1}\Delta x_1\,(1-\theta)}{6}\right]\phi_{3/2}^{k+\beta,(0)}=\left[\frac{\Delta x_1\,(2+\theta)}{6}\right]\sum_{n=1}^{N}Q_{n,1,L}^{k+1}\Delta_n$$
$$+\left[\frac{\Delta x_1\,(1-\theta)}{6}\right]\sum_{n=1}^{N}Q_{n,1,R}^{k+1}\Delta_n\,,\qquad\text{left reflecting boundary}\,,\quad(4.98c)$$

$$\left[\frac{\Delta x_i\,(1-\theta)}{6v\Delta t_{k+1}}\right]\left(\phi_{i-1/2}^{k+1,(0)}-\phi_{i-1/2}^{k,(0)}\right)+\left[\frac{(\Delta x_i+\Delta x_{i+1})\,(2+\theta)}{6v\Delta t_{k+1}}\right]\left(\phi_{i+1/2}^{k+1,(0)}-\phi_{i+1/2}^{k,(0)}\right)$$
$$+\left[\frac{\Delta x_{i+1}\,(1-\theta)}{6v\Delta t_{k+1}}\right]\left(\phi_{i+3/2}^{k+1,(0)}-\phi_{i+3/2}^{k,(0)}\right)-\frac{1}{3\Sigma_{t,i+1}\Delta x_{i+1}}\left(\phi_{i+3/2}^{k-\beta,(0)}-\phi_{i+1/2}^{k-\beta,(0)}\right)$$
$$+\frac{1}{3\Sigma_{t,i}\Delta x_i}\left(\phi_{i+1/2}^{k-\beta,(0)}-\phi_{i-1/2}^{k-\beta,(0)}\right)+\left[\frac{\Sigma_{a,i}\Delta x_i\,(1-\theta)}{6}\right]\phi_{i-1/2}^{k+\beta,(0)}$$
$$+\left[\frac{(\Sigma_{a,i+1}\Delta x_{i+1}+\Sigma_{a,i}\Delta x_i)\,(2+\theta)}{6}\right]\phi_{i+1/2}^{k+\beta,(0)}+\left[\frac{\Sigma_{a,i+1}\Delta x_{i+1}\,(1-\theta)}{6}\right]\phi_{i+3/2}^{k+\beta,(0)}$$
$$=\left[\frac{\Delta x_i\,(1-\theta)}{6}\right]\sum_{n=1}^{N}Q_{n,i,L}^{k+1}\Delta_n+\left[\frac{\Delta x_i\,(2+\theta)}{6}\right]\sum_{n=1}^{N}Q_{n,i,R}^{k+1}\Delta_n$$
$$+\left[\frac{\Delta x_{i+1}\,(2+\theta)}{6}\right]\sum_{n=1}^{N}Q_{n,i+1,L}^{k+1}\Delta_n+\left[\frac{\Delta x_{i+1}\,(1-\theta)}{6}\right]\sum_{n=1}^{N}Q_{n,i+1,R}^{k+1}\Delta_n\,,$$
$$2\le i\le I-1\,,\quad(4.98d)$$

$$\left[\frac{\Delta x_I\,(1-\theta)}{6v\Delta t_{k+1}}\right]\left(\phi_{I-1/2}^{k+1,(0)}-\phi_{I,L}^{k,(0)}\right)+\left[\frac{\Delta x_I\,(2+\theta)}{6v\Delta t_{k+1}}\right]\left(\phi_{I+1/2}^{k+1,(0)}-\phi_{I,R}^{k,(0)}\right)$$
$$+\frac{1}{3\Sigma_{t,I}\Delta x_I}\left(\phi_{I+1/2}^{k-\beta,(0)}-\phi_{I-1/2}^{k-\beta,(0)}\right)+\left[\frac{\Sigma_{a,I}\Delta x_I\,(1-\theta)}{6}\right]\phi_{I-1/2}^{k+\beta,(0)}$$
$$+\left[\frac{\Sigma_{a,I}\Delta x_I\,(2+\theta)}{6}\right]\phi_{I+1/2}^{k+\beta,(0)}=\left[\frac{\Delta x_I\,(1-\theta)}{6}\right]\sum_{n=1}^{N}Q_{n,I,L}^{k+1}\Delta_n$$
$$+\left[\frac{\Delta x_I\,(2+\theta)}{6}\right]\sum_{n=1}^{N}Q_{n,I,R}^{k+1}\Delta_n\,,\qquad\text{right reflecting boundary}\,,\quad(4.98e)$$

$$\left[\frac{\Delta x_{I-1}(1-\theta)}{6v\Delta t_{k+1}}\right]\left(\phi_{I-3/2}^{k+1,(0)}-\phi_{I-3/2}^{k,(0)}\right)+\left[\frac{(\Delta x_{I-1}+\Delta x_I)(2+\theta)}{6v\Delta t_{k+1}}\right]\left(\phi_{I-1/2}^{k+1,(0)}-\phi_{I-1/2}^{k,(0)}\right)$$
$$+\left[\frac{\Delta x_I(1-\theta)}{6v\Delta t_{k+1}}\right]\left(\phi_{I+1/2}^{k+1,(0)}-\phi_{I+1/2}^{k,(0)}\right)$$
$$-\frac{1}{3\Sigma_{t,I}\Delta x_I}\left(\frac{1}{2}\phi_{I+1/2}^{k-\beta,(0)}-\phi_{I-1/2}^{k-\beta,(0)}+3\sum_{\mu_n<0}\mu_n^2\psi_{n,R}^{b,k-\beta}\Delta_n\right)$$
$$+\frac{1}{3\Sigma_{t,I-1}\Delta x_{I-1}}\left(\phi_{I-1/2}^{k-\beta,(0)}-\phi_{I-3/2}^{k-\beta,(0)}\right)+\left[\frac{\Sigma_{a,I-1}\Delta x_{I-1}(1-\theta)}{6}\right]\phi_{I-3/2}^{k+\beta,(0)}$$
$$+\left[\frac{(\Sigma_{a,I}\Delta x_I+\Sigma_{a,I-1}\Delta x_{I-1})(2+\theta)}{6}\right]\phi_{I-1/2}^{k+\beta,(0)}+\left[\frac{\Sigma_{a,I}\Delta x_I(1-\theta)}{6}\right]\phi_{I+1/2}^{k+\beta,(0)}$$
$$=\left[\frac{\Delta x_{I-1}(1-\theta)}{6}\right]\sum_{n=1}^{N}Q_{n,I-1,L}^{k+1}\Delta_n+\left[\frac{\Delta x_{I-1}(2+\theta)}{6}\right]\sum_{n=1}^{N}Q_{n,I-1,R}^{k+1}\Delta_n$$
$$+\left[\frac{\Delta x_I(2+\theta)}{6}\right]\sum_{n=1}^{N}Q_{n,I,L}^{k+1}\Delta_n+\left[\frac{\Delta x_I(1-\theta)}{6}\right]\sum_{n=1}^{N}Q_{n,I,R}^{k+1}\Delta_n,$$

right incident boundary, (4.98f)

$$\phi_{I+1/2}^{k+1,(0)}=\frac{2}{\rho}\sum_{\mu_n<0}|\mu_n|\psi_{n,R}^{b,k+1}\Delta_n. \qquad \text{right incident boundary.} \quad (4.98g)$$

4.3.5 Examining the Fully- and Semi-Explicit Asymptotic Diffusion Discretizations

We now examine the relationship between the fully-explicit and semi-explicit asymptotic diffusion equations just derived, and the fully-explicit and semi-explicit node-centered diffusion discretization we examined in Chapter 2. Assuming a fully-lumped transport discretization ($\theta=1$), Eqs. (4.98) can be rewritten as:

$$\phi_{1/2}^{k+1,(0)}=\frac{2}{\rho}J_L^{b,k+1}, \qquad \text{left incident boundary,} \quad (4.99a)$$

$$\frac{\Delta x_{3/2}}{v\Delta t_{k+1}}\left(\phi_{3/2}^{k+1,(0)}-\phi_{3/2}^{k,(0)}\right)-\frac{D_2}{\Delta x_2}\left(\phi_{5/2}^{k-\beta,(0)}-\phi_{3/2}^{k-\beta,(0)}\right)$$
$$+\frac{D_1}{\Delta x_1}\left(\phi_{3/2}^{k-\beta,(0)}-\frac{1}{2}\phi_{1/2}^{k-\beta,(0)}-3\sum_{\mu_n>0}\mu_n^2\psi_{n,L}^{b,k-\beta}\Delta_n\right)+\left(\Sigma_{a,3/2}\Delta x_{3/2}\right)\phi_{3/2}^{k+\beta,(0)}$$
$$=\Delta x_{3/2}Q_{3/2}^{k+1}, \qquad \text{left incident boundary,} \quad (4.99b)$$

$$\frac{\Delta x_{1/2}}{v\Delta t_{k+1}}\left(\phi_{1/2}^{k+1,(0)}-\phi_{1/2}^{k,(0)}\right)-\frac{D_1}{\Delta x_1}\left(\phi_{3/2}^{k-\beta,(0)}-\phi_{1/2}^{k-\beta,(0)}\right)+\left(\Sigma_{a,1/2}\Delta x_{1/2}\right)\phi_{1/2}^{k+\beta,(0)}$$
$$=\Delta x_{1/2}Q_{1/2}^{k+1}\,,\qquad\text{reflecting boundary}\,,\quad(4.99c)$$

$$\frac{\Delta x_{i+1/2}}{v\Delta t_{k+1}}\left(\phi_{i+1/2}^{k+1,(0)}-\phi_{i+1/2}^{k,(0)}\right)-\frac{D_{i+1}}{\Delta x_{i+1}}\left(\phi_{i+3/2}^{k-\beta,(0)}-\phi_{i+1/2}^{k-\beta,(0)}\right)$$
$$+\frac{D_i}{\Delta x_i}\left(\phi_{i+1/2}^{k-\beta,(0)}-\phi_{i-1/2}^{k-\beta,(0)}\right)+\left(\Sigma_{a,i+1/2}\Delta x_{i+1/2}\right)\phi_{i+1/2}^{k+\beta,(0)}=\Delta x_{i+1/2}Q_{i+1/2}^{k+1}\,,$$
$$2\le i\le I-1\,,\quad(4.99d)$$

$$\frac{\Delta x_{I+1/2}}{v\Delta t_{k+1}}\left(\phi_{I+1/2}^{k+1,(0)}-\phi_{I+1/2}^{k,(0)}\right)+\frac{D_I}{\Delta x_I}\left(\phi_{I+1/2}^{k-\beta,(0)}-\phi_{I-1/2}^{k-\beta,(0)}\right)+\left(\Sigma_{a,I+1/2}\Delta x_{I+1/2}\right)\phi_{I+1/2}^{k+\beta,(0)}$$
$$=\Delta x_{I+1/2}Q_{I+1/2}^{k+1}\,,\qquad\text{reflecting boundary}\,,\quad(4.99e)$$

$$\frac{\Delta x_{I-1/2}}{v\Delta t_{k+1}}\left(\phi_{I-1/2}^{k+1,(0)}-\phi_{I-1/2}^{k,(0)}\right)-\frac{D_I}{\Delta x_I}\left(\frac{1}{2}\phi_{I+1/2}^{k-\beta,(0)}-\phi_{I-1/2}^{k-\beta,(0)}+3\sum_{\mu_n<0}\mu_n^2\psi_{n,R}^{b,k-\beta}\Delta_n\right)$$
$$+\frac{D_{I-1}}{\Delta x_{I-1}}\left(\phi_{I-1/2}^{k-\beta,(0)}-\phi_{I-3/2}^{k-\beta,(0)}\right)+\left(\Sigma_{a,I-1/2}\Delta x_{I-1/2}\right)\phi_{I-1/2}^{k+\beta,(0)}$$
$$=\Delta x_{I-1/2}Q_{I-1/2}^{k+1}\,,\qquad\text{right incident boundary}\,,\quad(4.99f)$$

$$\phi_{I+1/2}^{k+1,(0)}=\frac{2}{\rho}J_R^{b,k+1}\,,\qquad\text{right incident boundary}\,,\quad(4.99g)$$

where

$$J_L^{b,k+1}=\sum_{\mu_n>0}\mu_n\psi_{n,L}^{b,k+1}\Delta_n\,,\quad(4.100a)$$

$$J_R^{b,k+1}=\sum_{\mu_n<0}|\mu_n|\psi_{n,R}^{b,k+1}\Delta_n\,,\quad(4.100b)$$

$$D_i=\frac{1}{3\Sigma_{t,i}}\,,\quad(4.101)$$

and

$$\Delta x_{i+1/2}=\begin{cases}\dfrac{\Delta x_1}{2}\,, & i=0\,,\\[2ex] \dfrac{\Delta x_{i+1}+\Delta x_i}{2}\,, & 1\le i\le I-1\,,\\[2ex] \dfrac{\Delta x_I}{2}\,, & i=I\,,\end{cases}\quad(4.102a)$$

$$\Sigma_{a,i+1/2} = \begin{cases} \Sigma_{a,1}\,, & i = 0\,, \\ \dfrac{\Sigma_{a,i+1}\Delta x_{i+1} + \Sigma_{a,i}\Delta x_i}{\Delta x_{i+1} + \Delta x_i}\,, & 1 \le i \le I-1\,, \\ \Sigma_{a,I}\,, & i = I\,, \end{cases} \tag{4.102b}$$

$$Q^{k+1}_{i+1/2} = \begin{cases} \displaystyle\sum_{n=1}^{N} Q^{k+1}_{n,1,L}\,\Delta_n\,, & i = 0\,, \\ \dfrac{\displaystyle\sum_{n=1}^{N} Q^{k+1}_{n,i,R}\,\Delta_n\,\Delta x_i + \sum_{n=1}^{N} Q^{k+1}_{n,i+1,L}\,\Delta_n\,\Delta x_{i+1}}{\Delta x_i + \Delta x_{i+1}}\,, & 1 \le i \le I-1\,, \\ \displaystyle\sum_{n=1}^{N} Q^{k+1}_{n,I,R}\,\Delta_n\,, & i = I\,, \end{cases} \tag{4.102c}$$

and

$$\beta = \begin{cases} 0: & \text{fully-explicit method}\,, \\ 1: & \text{semi-explicit method}\,. \end{cases} \tag{4.103}$$

Comparing the asymptotic diffusion equations, Eqs. (4.99), for the fully-explicit case ($\beta = 0$) with the fully-explicit node-centered diffusion equations, Eqs. (2.43) and (2.44), we see that the fully-explicit asymptotic diffusion equations are the same as the fully-explicit node-centered diffusion equations in the interior and for reflecting boundaries, but different for incident boundaries. Despite the difference between these equations on incident boundaries, we expect that the asymptotic diffusion equations should behave similarly to the node-centered diffusion equations. Therefore, the fully-explicit linear discontinuous transport discretization should behave similarly to the fully-explicit diffusion discretization in the thick diffusive limit. As we found in Section 2.2.2, the node-centered fully-explicit diffusion discretization is not unconditionally stable. Therefore, the fully-explicit LDFEM transport method will not be unconditionally stable in the thick limit either. Therefore, we will not consider this method further.

The semi-explicit asymptotic diffusion equations for the semi-explicit case ($\beta = 1$) are significantly different than the semi-explicit node-centered diffusion equations given in Eqs. (2.69) and (2.70), because the scalar fluxes in the leakage terms are evaluated at time t_{k-1} instead of at time t_k as in the node-centered diffusion discretization. We found in Chapter 2 that the semi-explicit node-centered diffusion discretization had improved stability over the fully-explicit discretization. However, in the case of the linear discontinuous transport discretizations, because the leakage terms are lagged by two time steps instead of one, we

expect that the semi-explicit transport method will be even less stable than the fully-explicit method. This illustrates the way that an asymptotic analysis can reveal how a seemingly reasonable transport discretization can limit to a poor diffusion discretization in the diffusion limit. Because this method lacks unconditional stability, we will not consider it further.

4.4 Asymptotic Analysis of the SBJ Method

In this section, we conduct an asymptotic analysis of the SBJ transport method. This analysis shows that the SBJ transport method limits to a physically correct diffusion discretization, similar to the SBJ diffusion discretization that we investigated in Chapter 2. To conduct this analysis, we begin with the SBJ transport equations derived in Chapter 3:

$$\frac{1}{v\Delta t_{k+1}}\underline{\underline{M}}_{i+1/2}\left(\underline{\hat{\psi}}^{k+1}_{n,i+1/2}-\underline{\psi}^{k}_{n,i+1/2}\right)+\mu_n\underline{\underline{L}}^{surf}_{i+1/2}\underline{\hat{\psi}}^{k+1,surf}_{n,i+1/2}-\mu_n\underline{\underline{L}}_{i+1/2}\underline{\hat{\psi}}^{k+1}_{n,i+1/2}$$
$$+\underline{\underline{T}}_{i+1/2}\underline{\hat{\psi}}^{k+1}_{n,i+1/2}=\frac{1}{2}\underline{\underline{S}}_{i+1/2}\sum_{m=1}^{N}\underline{\hat{\psi}}^{k+1}_{m,i+1/2}\Delta_m+\underline{\underline{M}}_{i+1/2}\underline{Q}^{k+1}_{n,i+1/2}. \quad (4.104)$$

In Chapter 3, we defined, for the domain interior and reflecting boundaries,

$$\underline{\hat{\psi}}^{k+1}_{n,i+1/2}=\begin{bmatrix}\psi^{k+1/2}_{n,i,L} & \psi^{k+1}_{n,i,R} & \psi^{k+1}_{n,i,L} & \psi^{k+1/2}_{n,i,R}\end{bmatrix}^T, \quad (4.105a)$$

$$\underline{\hat{\psi}}^{k+1,surf}_{n,i+1/2}=\begin{cases}\begin{bmatrix}\psi^{k+1/2}_{n,i,L} & \psi^{k+1}_{n,i+1,L} & \psi^{k+1}_{n,i+1,L} & \psi^{k}_{n,i+2,L}\end{bmatrix}^T, & \mu_n<0,\\ \begin{bmatrix}\psi^{k}_{n,i-1,R} & \psi^{k+1}_{n,i,R} & \psi^{k+1}_{n,i,R} & \psi^{k+1/2}_{n,i+1,R}\end{bmatrix}^T, & \mu_n>0.\end{cases} \quad (4.105b)$$

Reflecting boundaries for the SBJ transport method are implemented using ghost cells. For a left incident boundary, we defined

$$\underline{\hat{\psi}}^{k+1}_{n,3/2}=\begin{bmatrix}\psi^{k+1}_{n,1,L} & \psi^{k+1}_{n,1,R} & \psi^{k+1}_{n,2,L} & \psi^{k+1/2}_{n,2,R}\end{bmatrix}^T, \quad (4.106a)$$

$$\underline{\hat{\psi}}^{k+1,surf}_{n,3/2}=\begin{cases}\begin{bmatrix}\psi^{k+1}_{n,1,L} & \psi^{k+1}_{n,2,L} & \psi^{k+1}_{n,2,L} & \psi^{k}_{n,3,L}\end{bmatrix}^T, & \mu_n<0,\\ \begin{bmatrix}\psi^{b,k+1}_{n,L} & \psi^{k+1}_{n,1,R} & \psi^{k+1}_{n,1,R} & \psi^{k+1/2}_{n,2,R}\end{bmatrix}^T, & \mu_n>0,\end{cases} \quad (4.106b)$$

and for an incident boundary on the right, we defined

$$\underline{\hat{\psi}}_{n,I-1/2}^{k+1} = \left[\psi_{n,I-1,L}^{k+1/2} \quad \psi_{n,I-1,R}^{k+1} \quad \psi_{n,I,L}^{k+1} \quad \psi_{n,I,R}^{k+1}\right]^T, \tag{4.107a}$$

$$\underline{\hat{\psi}}_{n,I-1/2}^{k+1,surf} = \begin{cases} \left[\psi_{n,I-1,L}^{k+1/2} \quad \psi_{n,I,L}^{k+1} \quad \psi_{n,I,L}^{k+1} \quad \psi_{n,R}^{b,k+1}\right], & \mu_n < 0, \\ \left[\psi_{n,I-2,R}^{k} \quad \psi_{n,I-1,R}^{k+1} \quad \psi_{n,I-1,R}^{k+1} \quad \psi_{n,I,R}^{k+1}\right], & \mu_n > 0. \end{cases} \tag{4.107b}$$

We also defined the matrices

$$\underline{\underline{T}}_{i+1/2} = \begin{bmatrix} \Sigma_{t,i}\underline{\underline{M}}_i & 0 \\ 0 & \Sigma_{t,i+1}\underline{\underline{M}}_{i+1} \end{bmatrix}, \tag{4.108a}$$

and

$$\underline{\underline{S}}_{i+1/2} = \begin{bmatrix} \Sigma_{s,i}\underline{\underline{M}}_i & 0 \\ 0 & \Sigma_{s,i+1}\underline{\underline{M}}_{i+1} \end{bmatrix}. \tag{4.108b}$$

Additionally we define

$$\underline{\underline{A}}_{i+1/2} = \begin{bmatrix} \Sigma_{a,i}\underline{\underline{M}}_i & 0 \\ 0 & \Sigma_{a,i+1}\underline{\underline{M}}_{i+1} \end{bmatrix}. \tag{4.109}$$

The other matrices and vectors in Eq. (4.104) are defined in Section 3.4 and will not be repeated here.

Now we apply the usual asymptotic scalings:

$$v = \frac{v'}{\varepsilon}, \tag{4.110a}$$

$$\Sigma_{t,i} = \frac{\sigma_{t,i}}{\varepsilon}, \tag{4.110b}$$

$$\Sigma_{a,i} = \varepsilon\sigma_{a,i}, \tag{4.110c}$$

$$\Sigma_{s,i} = \Sigma_{t,i} - \Sigma_{a,i} = \frac{\sigma_{t,i}}{\varepsilon} - \varepsilon\sigma_{a,i}, \tag{4.110d}$$

$$\underline{Q}_{n,i+1/2}^{k+1} = \varepsilon\underline{q}_{n,i+1/2}^{k+1}, \tag{4.110e}$$

and we define the scaled matrices

$$\underline{\underline{T}}'_{i+1/2} = \begin{bmatrix} \sigma_{t,i}\underline{\underline{M}}_i & \underline{\underline{0}} \\ \underline{\underline{0}} & \sigma_{t,i+1}\underline{\underline{M}}_{i+1} \end{bmatrix} = \varepsilon \underline{\underline{T}}_{i+1/2}\,, \tag{4.111a}$$

$$\underline{\underline{A}}'_{i+1/2} = \begin{bmatrix} \sigma_{a,i}\underline{\underline{M}}_i & \underline{\underline{0}} \\ \underline{\underline{0}} & \sigma_{a,i+1}\underline{\underline{M}}_{i+1} \end{bmatrix} = \frac{1}{\varepsilon}\underline{\underline{A}}_{i+1/2}\,. \tag{4.111b}$$

Substituting Eqs. (4.110) and (4.111) into Eqs. (4.104), we have

$$\begin{aligned} \frac{\varepsilon}{v'\Delta t_{k+1}}\underline{\underline{M}}_{i+1/2}\left(\underline{\hat{\psi}}^{k+1}_{n,i+1/2} - \underline{\psi}^{k}_{n,i+1/2}\right) + \mu_n \underline{\underline{L}}^{surf}_{i+1/2}\underline{\hat{\psi}}^{k+1,surf}_{n,i+1/2} - \mu_n \underline{\underline{L}}_{i+1/2}\underline{\hat{\psi}}^{k+1}_{n,i+1/2} \\ + \frac{1}{\varepsilon}\underline{\underline{T}}'_{i+1/2}\underline{\hat{\psi}}^{k+1}_{n,i+1/2} = \frac{1}{2}\left(\frac{1}{\varepsilon}\underline{\underline{T}}'_{i+1/2} - \varepsilon\underline{\underline{A}}'_{i+1/2}\right)\sum_{m=1}^{N}\underline{\hat{\psi}}^{k+1}_{m,i+1/2}\Delta_m \\ + \varepsilon\underline{\underline{M}}_{i+1/2}\underline{q}^{k+1}_{n,i+1/2}\,. \end{aligned} \tag{4.112}$$

We posit that the angular fluxes at time t_{k+1} can be represented as a power-series in ε:

$$\underline{\hat{\psi}}^{k+1}_{n,i+1/2} = \underline{\hat{\psi}}^{k+1,(0)}_{n,i+1/2} + \varepsilon\underline{\hat{\psi}}^{k+1,(1)}_{n,i+1/2} + \varepsilon^2\underline{\hat{\psi}}^{k+1,(2)}_{n,i+1/2} + O(\varepsilon^3)\,, \tag{4.113a}$$

$$\underline{\hat{\psi}}^{k+1,surf}_{n,i+1/2} = \underline{\hat{\psi}}^{k+1,surf,(0)}_{n,i+1/2} + \varepsilon\underline{\hat{\psi}}^{k+1,surf,(1)}_{n,i+1/2} + \varepsilon^2\underline{\hat{\psi}}^{k+1,surf,(2)}_{n,i+1/2} + O(\varepsilon^3)\,. \tag{4.113b}$$

Therefore, the upstream closure expansions are, for $\mu_n < 0$,

$$\underline{\psi}^{k+1,surf,(0)}_{n,i+1/2} = \begin{cases} \left[\psi^{k+1,(0)}_{n,1,L} \quad \psi^{k+1,(0)}_{n,2,L} \quad \psi^{k+1,(0)}_{n,2,L} \quad \psi^{k}_{n,3,L}\right]^T, & i = 1\,, \\ \left[\psi^{k+1/2,(0)}_{n,i,L} \quad \psi^{k+1,(0)}_{n,i+1,L} \quad \psi^{k+1,(0)}_{n,i+1,L} \quad \psi^{k}_{n,i+2,L}\right]^T, & 2 \le i \le I-2\,, \\ \left[\psi^{k+1/2,(0)}_{n,I-1,L} \quad \psi^{k+1,(0)}_{n,I,L} \quad \psi^{k+1,(0)}_{n,I,L} \quad \psi^{b,k+1}_{n,R}\right]^T, & i = I-1\,, \end{cases} \tag{4.114a}$$

and

$$\underline{\psi}^{k+1,surf,(\eta)}_{n,i+1/2} = \begin{cases} \left[\psi^{k+1,(\eta)}_{n,1,L} \quad \psi^{k+1,(\eta)}_{n,2,L} \quad \psi^{k+1,(\eta)}_{n,2,L} \quad 0\right]^T, & i = 1\,, \\ \left[\psi^{k+1/2,(\eta)}_{n,i,L} \quad \psi^{k+1,(\eta)}_{n,i+1,L} \quad \psi^{k+1,(\eta)}_{n,i+1,L} \quad 0\right]^T, & 2 \le i \le I-2\,, \\ \left[\psi^{k+1/2,(\eta)}_{n,I-1,L} \quad \psi^{k+1,(\eta)}_{n,I,L} \quad \psi^{k+1,(\eta)}_{n,I,L} \quad 0\right]^T, & i = I-1\,, \end{cases} \tag{4.114b}$$

for $\eta > 0$. For $\mu_n > 0$, we have

$$\underline{\psi}_{n,i+1/2}^{k+1,surf,(0)} = \begin{cases} \begin{bmatrix} \psi_{n,L}^{b,k+1} & \psi_{n,1,R}^{k+1,(0)} & \psi_{n,1,R}^{k+1,(0)} & \psi_{n,2,R}^{k+1/2,(0)} \end{bmatrix}^T, & i = 1, \\ \begin{bmatrix} \psi_{n,i-1,R}^{k} & \psi_{n,i,R}^{k+1,(0)} & \psi_{n,i,R}^{k+1,(0)} & \psi_{n,i+1,R}^{k+1/2,(0)} \end{bmatrix}^T, & 2 \le i \le I-2, \\ \begin{bmatrix} \psi_{n,I-2,R}^{k} & \psi_{n,I-1,R}^{k+1,(0)} & \psi_{n,I-1,R}^{k+1,(0)} & \psi_{n,I,R}^{k+1,(0)} \end{bmatrix}^T, & i = I-1, \end{cases} \tag{4.115a}$$

and

$$\underline{\psi}_{n,i+1/2}^{k+1,surf,(\eta)} = \begin{cases} \begin{bmatrix} 0 & \psi_{n,1,R}^{k+1,(\eta)} & \psi_{n,1,R}^{k+1,(\eta)} & \psi_{n,2,R}^{k+1/2,(\eta)} \end{bmatrix}^T, & i = 1, \\ \begin{bmatrix} 0 & \psi_{n,i,R}^{k+1,(\eta)} & \psi_{n,i,R}^{k+1,(\eta)} & \psi_{n,i+1,R}^{k+1/2,(\eta)} \end{bmatrix}^T, & 2 \le i \le I-2, \\ \begin{bmatrix} 0 & \psi_{n,I-1,R}^{k+1,(\eta)} & \psi_{n,I-1,R}^{k+1,(\eta)} & \psi_{n,I,R}^{k+1,(\eta)} \end{bmatrix}^T, & i = I-1, \end{cases} \tag{4.115b}$$

for $\eta > 0$.

Substituting Eq. (4.113) into Eq. (4.112) we obtain

$$\begin{aligned} &\frac{\varepsilon}{\nu' \Delta t_{k+1}} \underline{\underline{M}}_{i+1/2} \left[\hat{\underline{\psi}}_{n,i+1/2}^{k+1,(0)} + \varepsilon \hat{\underline{\psi}}_{n,i+1/2}^{k+1,(1)} + \varepsilon^2 \hat{\underline{\psi}}_{n,i+1/2}^{k+1,(2)} + O(\varepsilon^3) - \underline{\psi}_{n,i+1/2}^{k} \right] \\ &\qquad + \mu_n \underline{\underline{L}}_{i+1/2}^{surf} \left[\hat{\underline{\psi}}_{n,i+1/2}^{k+1,surf,(0)} + \varepsilon \hat{\underline{\psi}}_{n,i+1/2}^{k+1,surf,(1)} + \varepsilon^2 \hat{\underline{\psi}}_{n,i+1/2}^{k+1,surf,(2)} + O(\varepsilon^3) \right] \\ &\qquad\qquad - \mu_n \underline{\underline{L}}_{i+1/2} \left[\hat{\underline{\psi}}_{n,i+1/2}^{k+1,(0)} + \varepsilon \hat{\underline{\psi}}_{n,i+1/2}^{k+1,(1)} + \varepsilon^2 \hat{\underline{\psi}}_{n,i+1/2}^{k+1,(2)} + O(\varepsilon^3) \right] \\ &\qquad\qquad + \frac{1}{\varepsilon} \underline{\underline{T}}'_{i+1/2} \left[\hat{\underline{\psi}}_{n,i+1/2}^{k+1,(0)} + \varepsilon \hat{\underline{\psi}}_{n,i+1/2}^{k+1,(1)} + \varepsilon^2 \hat{\underline{\psi}}_{n,i+1/2}^{k+1,(2)} + O(\varepsilon^3) \right] \\ &= \frac{1}{2} \left[\frac{1}{\varepsilon} \underline{\underline{T}}'_{i+1/2} - \varepsilon \underline{\underline{A}}'_{i+1/2} \right] \sum_{m=1}^{N} \left[\hat{\underline{\psi}}_{m,i+1/2}^{k+1,(0)} + \varepsilon \hat{\underline{\psi}}_{m,i+1/2}^{k+1,(1)} + \varepsilon^2 \hat{\underline{\psi}}_{m,i+1/2}^{k+1,(2)} + O(\varepsilon^3) \right] \Delta_m \\ &\qquad\qquad + \varepsilon \underline{\underline{M}}_{i+1/2} \underline{q}_{n,i+1/2}^{k+1}. \end{aligned} \tag{4.116}$$

The asymptotic analysis will proceed by analyzing terms of each order of ε in Eq. (4.116).

4.4.1 The $O(\varepsilon^{-1})$ Terms

Examining the $O(\varepsilon^{-1})$ terms in Eq. (4.116) we have

$$\underline{\underline{T}}'_{i+1/2} \hat{\underline{\psi}}_{n,i+1/2}^{k+1,(0)} = \frac{1}{2} \underline{\underline{T}}'_{i+1/2} \sum_{m=1}^{N} \hat{\underline{\psi}}_{m,i+1/2}^{k+1,(0)} \Delta_m. \tag{4.117}$$

Assuming that $\underline{\underline{T}}'_{i+1/2}$ is invertible (which is true for the linear discontinuous finite element discretization), we solve Eq. (4.117) for $\underline{\hat{\psi}}^{k+1,(0)}_{n,i+1/2}$ and find

$$\underline{\hat{\psi}}^{k+1,(0)}_{n,i+1/2} = \frac{1}{2}\sum_{m=1}^{N} \underline{\hat{\psi}}^{k+1,(0)}_{m,i+1/2}\Delta_m = \frac{1}{2}\underline{\hat{\phi}}^{k+1,(0)}_{i+1/2}\,. \tag{4.118}$$

From this, we see that the leading order SBJ angular flux is isotropic. Therefore, the angular flux satisfies

$$\underline{\hat{\psi}}^{k+1}_{n,i+1/2} = \frac{1}{2}\underline{\hat{\phi}}^{k+1,(0)}_{i+1/2} + O(\varepsilon)\,, \tag{4.119}$$

where $\underline{\hat{\phi}}^{k+1,(0)}_{i+1/2}$ is, as yet, undetermined.

4.4.2 The $O(1)$ Terms

Examining the $O(1)$ terms in Eq. (4.116), we find

$$\mu_n \underline{\underline{L}}^{surf}_{i+1/2}\underline{\hat{\psi}}^{k+1,surf,(0)}_{n,i+1/2} - \mu_n \underline{\underline{L}}_{i+1/2}\underline{\hat{\psi}}^{k+1,(0)}_{n,i+1/2} + \underline{\underline{T}}'_{i+1/2}\underline{\hat{\psi}}^{k+1,(1)}_{n,i+1/2} = \frac{1}{2}\underline{\underline{T}}'_{i+1/2}\sum_{m=1}^{N}\underline{\hat{\psi}}^{k+1,(1)}_{m,i+1/2}\Delta_m\,. \tag{4.120}$$

Operating on Eq. (4.120) by $\sum_{n=1}^{N}(\cdot)\Delta_n$, and assuming that the quadrature set satisfies

$$\sum_{n=1}^{N}\Delta_n = 2\,, \tag{4.121}$$

we find

$$\underline{\underline{L}}^{surf}_{i+1/2}\sum_{n=1}^{N}\mu_n\underline{\hat{\psi}}^{k+1,surf,(0)}_{n,i+1/2}\Delta_n - \underline{\underline{L}}_{i+1/2}\sum_{n=1}^{N}\mu_n\underline{\hat{\psi}}^{k+1,(0)}_{n,i+1/2}\Delta_n = 0\,. \tag{4.122}$$

Substituting Eq. (4.118) into Eq. (4.122), and assuming that the quadrature set is symmetric such that

$$\sum_{n=1}^{N}\mu_n\Delta_n = 0\,, \tag{4.123}$$

then Eq. (4.122) simplifies to

$$\underline{\underline{L}}^{surf}_{i+1/2}\sum_{n=1}^{N}\mu_n\underline{\hat{\psi}}^{k+1,surf,(0)}_{n,i+1/2}\Delta_n = 0\,. \tag{4.124}$$

We now consider Eq. (4.124) for the problem interior and reflecting boundaries. Substituting the upstream closures, Eqs. (4.114a) and (4.115a), and Eq. (4.118) into Eq. (4.124)

we obtain

$$\underline{\underline{L}}^{surf}_{i+1/2}\left(\begin{bmatrix} -\frac{\rho}{2}\phi_{i,L}^{k+1/2,(0)} \\ -\frac{\rho}{2}\phi_{i+1,L}^{k+1,(0)} \\ -\frac{\rho}{2}\phi_{i+1,L}^{k+1,(0)} \\ \sum_{\mu_n<0}\mu_n\psi_{n,i+2,L}^{k}\Delta_n \end{bmatrix}+\begin{bmatrix} \sum_{\mu_n>0}\mu_n\psi_{n,i-1,R}^{k}\Delta_n \\ \frac{\rho}{2}\phi_{i,R}^{k+1,(0)} \\ \frac{\rho}{2}\phi_{i,R}^{k+1,(0)} \\ \frac{\rho}{2}\phi_{i+1,R}^{k+1/2,(0)} \end{bmatrix}\right)=0\,, \tag{4.125}$$

where we have defined

$$\begin{aligned}\rho &= \sum_{\mu_n>0}\mu_n\Delta_n = -\sum_{\mu_n<0}\mu_n\Delta_n \\ &\approx \int_0^1 \mu\,\mathrm{d}\mu = \frac{1}{2}\,.\end{aligned} \tag{4.126}$$

From this we conclude

$$\phi_{i,L}^{k+1/2,(0)} = \frac{2}{\rho}\sum_{\mu_n>0}\mu_n\psi_{n,i-1,R}^{k}\Delta_n\,, \tag{4.127a}$$

$$\phi_{i+1,L}^{k+1,(0)} = \phi_{i,R}^{k+1,(0)} \equiv \phi_{i+1/2}^{k+1,(0)}\,, \tag{4.127b}$$

$$\phi_{i+1,R}^{k+1/2,(0)} = \frac{2}{\rho}\sum_{\mu_n<0}|\mu_n|\psi_{n,i+2,L}^{k}\Delta_n\,. \tag{4.127c}$$

For an incident boundary condition on the left boundary, we substitute the upstream closures and Eq. (4.118) into Eq. (4.124) and obtain

$$\underline{\underline{L}}^{surf}_{3/2}\left(\begin{bmatrix} -\frac{\rho}{2}\phi_{1,L}^{k+1,(0)} \\ -\frac{\rho}{2}\phi_{2,L}^{k+1,(0)} \\ -\frac{\rho}{2}\phi_{2,L}^{k+1,(0)} \\ \sum_{\mu_n<0}\mu_n\psi_{n,3,L}^{k}\Delta_n \end{bmatrix}+\begin{bmatrix} \sum_{\mu_n>0}\mu_n\psi_{n,L}^{b,k+1}\Delta_n \\ \frac{\rho}{2}\phi_{1,R}^{k+1,(0)} \\ \frac{\rho}{2}\phi_{1,R}^{k+1,(0)} \\ \frac{\rho}{2}\phi_{2,R}^{k+1/2,(0)} \end{bmatrix}\right)=0\,. \tag{4.128}$$

From this we find

$$\phi_{1,L}^{k+1,(0)} = \frac{2}{\rho}\sum_{\mu_n>0}\mu_n\psi_{n,L}^{b,k+1}\Delta_n \equiv \phi_{1/2}^{k+1,(0)}\,, \tag{4.129a}$$

$$\phi_{2,L}^{k+1,(0)} = \phi_{1,R}^{k+1,(0)} \equiv \phi_{3/2}^{k+1,(0)}, \tag{4.129b}$$

$$\phi_{2,R}^{k+1/2,(0)} = \frac{2}{\rho} \sum_{\mu_n<0} |\mu_n| \psi_{n,3,L}^{k} \Delta_n \,. \tag{4.129c}$$

Similarly, we calculate for an incident boundary condition on the right

$$\phi_{I-1,L}^{k+1/2,(0)} = \frac{2}{\rho} \sum_{\mu_n>0} \mu_n \psi_{n,I-2,R}^{k} \Delta_n \,, \tag{4.130a}$$

$$\phi_{I,L}^{k+1,(0)} = \phi_{I-1,R}^{k+1,(0)} \equiv \phi_{I-1/2}^{k+1,(0)}, \tag{4.130b}$$

$$\phi_{I,R}^{k+1,(0)} = \frac{2}{\rho} \sum_{\mu_n<0} |\mu_n| \psi_{n,R}^{b,k+1} \Delta_n \equiv \phi_{I+1/2}^{k+1,(0)} \,. \tag{4.130c}$$

Therefore, we have found

$$\phi_{1,L}^{k+1,(0)} = \phi_{1/2}^{k+1,(0)} = \frac{2}{\rho} \sum_{\mu_n>0} \mu_n \psi_{n,L}^{b,k+1} \Delta_n \,, \tag{4.131a}$$

$$\phi_{i+1,L}^{k+1,(0)} = \phi_{i,R}^{k+1,(0)} = \phi_{i+1/2}^{k+1,(0)}, \tag{4.131b}$$

$$\phi_{i,L}^{k+1/2,(0)} = \frac{2}{\rho} \sum_{\mu_n>0} \mu_n \psi_{n,i-1,R}^{k} \Delta_n \,, \tag{4.131c}$$

$$\phi_{i,R}^{k+1/2,(0)} = \frac{2}{\rho} \sum_{\mu_n<0} |\mu_n| \psi_{n,i+1,L}^{k} \Delta_n \,, \tag{4.131d}$$

$$\phi_{I,R}^{k+1,(0)} = \phi_{I+1/2}^{k+1,(0)} = \frac{2}{\rho} \sum_{\mu_n<0} |\mu_n| \psi_{n,R}^{b,k+1} \Delta_n \,. \tag{4.131e}$$

From Eq. (4.131b), we see that the leading order scalar flux in the problem interior is continuous across cell boundaries. Examining Eqs. (4.131c) and (4.131d), we now see why it is necessary to discard the angular and scalar fluxes adjacent to the boundaries of each block. These two equations indicate that the scalar fluxes adjacent to the outer boundaries of the block are "pinned" to time t_k, i.e., the leading order scalar fluxes (and therefore, the leading order angular fluxes) adjacent to the outer block boundaries are dependent only upon the incident flux on the block evaluated at time t_k. As a result, in the thick limit, the flux will not evolve in time on the block boundaries. Therefore, these angular fluxes must be discarded, and the blocks must be staggered.

Eqs. (4.131c) and (4.131d) also suggest an alternative Staggered-Block Jacobi method,

which we call the Modified Staggered-Block Jacobi method (MSBJ). In the modified method, the angular fluxes in the block adjacent to the block boundaries are evaluated at time t_k instead of at time t_{k+1}. The space-time stencil for the angular fluxes within a block for this method is shown in Figure 4.3. The MSBJ method has the same asymptotic diffusion limit as the SBJ method. An investigation of the MSBJ method is beyond the scope of this dissertation; however, we expect that this method is faster (because there are only two unknown angular fluxes per block, rather than four), but less accurate away from the thick limit. The MSBJ transport method may warrant future research.

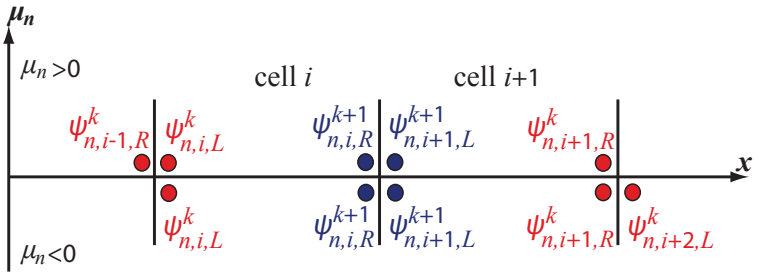

Figure 4.3 The Space-Time Stencil for the Modified Staggered-Block Jacobi Method in the Interior

Continuing with the asymptotic analysis, we now operate on Eq. (4.120) by $\sum_{n=1}^{N} \mu_n(\cdot)\Delta_n$ and obtain

$$\underline{\underline{L}}^{surf}_{i+1/2} \sum_{n=1}^{N} \mu_n^2 \underline{\hat{\psi}}^{k+1,surf,(0)}_{n,i+1/2} \Delta_n - \underline{\underline{L}}_{i+1/2} \sum_{n=1}^{N} \mu_n^2 \underline{\hat{\psi}}^{k+1,(0)}_{n,i+1/2} \Delta_n + \underline{\underline{T}}'_{i+1/2} \sum_{n=1}^{N} \mu_n \underline{\hat{\psi}}^{k+1,(1)}_{n,i+1/2} \Delta_n = 0 . \quad (4.132)$$

We define the first order SBJ current as

$$\underline{\hat{f}}^{k+1,(1)}_{i+1/2} = \sum_{n=1}^{N} \mu_n \underline{\hat{\psi}}^{k+1,(1)}_{n,i+1/2} \Delta_n , \quad (4.133)$$

such that

$$\underline{\hat{J}}_{i+1/2}^{k+1,(1)} = \begin{cases} \begin{bmatrix} J_{1,L}^{k+1,(1)} & J_{1,R}^{k+1,(1)} & J_{2,L}^{k+1,(1)} & J_{2,R}^{k+1/2,(1)} \end{bmatrix}^T, \\ \qquad\qquad\qquad\qquad i = 1\,, \quad \text{left incident boundary}\,, \\ \begin{bmatrix} J_{i,L}^{k+1/2,(1)} & J_{i,R}^{k+1,(1)} & J_{i+1,L}^{k+1,(1)} & J_{i+1,R}^{k+1/2,(1)} \end{bmatrix}^T, \\ \qquad\qquad\qquad\qquad \text{interior and reflecting boundaries}\,, \\ \begin{bmatrix} J_{I-1,L}^{k+1/2,(1)} & J_{I-1,R}^{k+1,(1)} & J_{I,L}^{k+1,(1)} & J_{I,R}^{k+1,(1)} \end{bmatrix}^T, \\ \qquad\qquad\qquad\qquad i = I-1\,, \quad \text{right incident boundary}\,. \end{cases} \tag{4.134}$$

Solving Eq. (4.132) for the first order current, we obtain

$$\underline{\hat{J}}_{i+1/2}^{k+1,(1)} = \left[\underline{\underline{T}}'_{i+1/2}\right]^{-1} \underline{\underline{L}}_{i+1/2} \sum_{n=1}^{N} \mu_n^2 \underline{\hat{\psi}}_{n,i+1/2}^{k+1,(0)} \Delta_n - \left[\underline{\underline{T}}'_{i+1/2}\right]^{-1} \underline{\underline{L}}_{i+1/2}^{surf} \sum_{n=1}^{N} \mu_n^2 \underline{\hat{\psi}}_{n,i+1/2}^{k+1,surf,(0)} \Delta_n\,. \tag{4.135}$$

Substituting Eqs. (4.118) into Eq. (4.135), and assuming the quadrature set satisfies

$$\sum_{n=1}^{N} \mu_n^2 \Delta_n = \int_{-1}^{1} \mu^2 \,\mathrm{d}\mu = \frac{2}{3}\,, \tag{4.136}$$

we have

$$\underline{\hat{J}}_{i+1/2}^{k+1,(1)} = -\frac{1}{3}\left[\underline{\underline{T}}'_{i+1/2}\right]^{-1} \left(\underline{\underline{L}}_{i+1/2}^{surf} \sum_{n=1}^{N} \mu_n^2 \underline{\hat{\psi}}_{n,i+1/2}^{k+1,surf,(0)} \Delta_n - \underline{\underline{L}}_{i+1/2} \underline{\hat{\phi}}_{i+1/2}^{k+1,(0)} \right). \tag{4.137}$$

Substituting in the definitions of the matrices, the upstream closures, Eqs. (4.114a) and (4.115a), and the continuity equations, Eqs. (4.131), we calculate the currents and find

$$\begin{aligned} J_{1,L}^{k+1,(1)} = &- \left[\frac{1}{3\sigma_{t,1}\Delta x_1\,(1+2\theta)}\right] \\ &\times \left[(1+2\theta)\,\phi_{3/2}^{k+1,(0)} + (1-\theta)\,\phi_{1/2}^{k+1,(0)} - 6\,(2+\theta) \sum_{\mu_n>0} \mu_n^2 \psi_{n,L}^{b,k+1} \Delta_n\right], \\ &\qquad\qquad\qquad\qquad \text{left incident boundary}\,, \end{aligned} \tag{4.138a}$$

$$J_{1,R}^{k+1,(1)} = -\left[\frac{1}{3\sigma_{t,1}\Delta x_1\left(1+2\theta\right)}\right]$$
$$\times\left[\left(1+2\theta\right)\phi_{3/2}^{k+1,(0)} - \left(2+\theta\right)\phi_{1/2}^{k+1,(0)} + 6\left(1-\theta\right)\sum_{\mu_n>0}\mu_n^2\psi_{n,L}^{b,k+1}\Delta_n\right],$$

left incident boundary, (4.138b)

$$J_{2,L}^{k+1,(1)} = -\left[\frac{1}{3\sigma_{t,2}\Delta x_2\left(1+2\theta\right)}\right]$$
$$\times\left[\left(2+\theta\right)\left(\frac{2}{\rho}\right)\sum_{\mu_n<0}|\mu_n|\psi_{n,3,L}^{k}\Delta_n - 6\left(1-\theta\right)\sum_{\mu_n<0}\mu_n^2\psi_{n,3,L}^{k}\Delta_n - \left(1+2\theta\right)\phi_{3/2}^{k+1,(0)}\right],$$

left incident boundary, (4.138c)

$$J_{2,R}^{k+1/2,(1)} = -\left[\frac{1}{3\sigma_{t,2}\Delta x_2\left(1+2\theta\right)}\right]$$
$$\times\left[-\left(1-\theta\right)\left(\frac{2}{\rho}\right)\sum_{\mu_n<0}|\mu_n|\psi_{n,3,L}^{k}\Delta_n + \left(2+\theta\right)\sum_{\mu_n<0}\mu_n^2\psi_{n,3,L}^{k}\Delta_n - \left(1+2\theta\right)\phi_{3/2}^{k+1,(0)}\right],$$

left incident boundary, (4.138d)

$$J_{i,L}^{k+1/2,(1)} = -\left[\frac{1}{3\sigma_{t,i}\Delta x_i\left(1+2\theta\right)}\right]$$
$$\times\left[\left(1+2\theta\right)\phi_{i+1/2}^{k+1,(0)} + \left(1-\theta\right)\left(\frac{2}{\rho}\right)\sum_{\mu_n>0}\mu_n\psi_{n,i-1,R}^{k}\Delta_n - 6\left(2+\theta\right)\sum_{\mu_n>0}\mu_n^2\psi_{n,i-1,R}^{k}\Delta_n\right],$$

interior and reflecting boundaries, (4.139a)

$$J_{i,R}^{k+1,(1)} = -\left[\frac{1}{3\sigma_{t,i}\Delta x_i\left(1+2\theta\right)}\right]$$
$$\times\left[\left(1+2\theta\right)\phi_{i+1/2}^{k+1,(0)} - \left(2+\theta\right)\left(\frac{2}{\rho}\right)\sum_{\mu_n>0}\mu_n\psi_{n,i-1,R}^{k}\Delta_n + 6\left(1-\theta\right)\sum_{\mu_n>0}\mu_n^2\psi_{n,i-1,R}^{k}\Delta_n\right],$$

interior and reflecting boundaries, (4.139b)

$$J_{i+1,L}^{k+1,(1)} = -\left[\frac{1}{3\sigma_{t,i+1}\Delta x_{i+1}\left(1+2\theta\right)}\right]$$
$$\times\left[\left(2+\theta\right)\left(\frac{2}{\rho}\right)\sum_{\mu_n<0}|\mu_n|\psi_{n,i+2,L}^{k}\Delta_n - 6\left(1-\theta\right)\sum_{\mu_n<0}\mu_n^2\psi_{n,i+2,L}^{k}\Delta_n - \left(1+2\theta\right)\phi_{i+1/2}^{k+1,(0)}\right],$$

interior and reflecting boundaries, (4.139c)

$$J_{i+1,R}^{k+1/2,(1)} = -\left[\frac{1}{3\sigma_{t,i+1}\Delta x_{i+1}\left(1+2\theta\right)}\right]$$
$$\times\left[-\left(1-\theta\right)\left(\frac{2}{\rho}\right)\sum_{\mu_n<0}\left|\mu_n\right|\psi_{n,i+2,L}^{k}\Delta_n+6\left(2+\theta\right)\sum_{\mu_n<0}\mu_n^2\psi_{n,i+2,L}^{k}\Delta_n-\left(1+2\theta\right)\phi_{i+1/2}^{k+1,(0)}\right],$$

interior and reflecting boundaries, (4.139d)

$$J_{I-1,L}^{k+1/2,(1)} = -\left[\frac{1}{3\sigma_{t,I-1}\Delta x_{I-1}\left(1+2\theta\right)}\right]$$
$$\times\left[\left(1+2\theta\right)\phi_{I-1/2}^{k+1,(0)}-6\left(2+\theta\right)\sum_{\mu_n>0}\mu_n^2\psi_{n,I-2,R}^{k}\Delta_n+\left(1-\theta\right)\left(\frac{2}{\rho}\right)\sum_{\mu_n>0}\mu_n\psi_{n,I-2,R}^{k}\Delta_n\right],$$

right incident boundary, (4.140a)

$$J_{I-1,R}^{k+1,(1)} = -\left[\frac{1}{3\sigma_{t,I-1}\Delta x_{I-1}\left(1+2\theta\right)}\right]$$
$$\times\left[\left(1+2\theta\right)\phi_{I-1/2}^{k+1,(0)}+6\left(1-\theta\right)\sum_{\mu_n>0}\mu_n^2\psi_{n,I-2,R}^{k}\Delta_n-\left(2+\theta\right)\left(\frac{2}{\rho}\right)\sum_{\mu_n>0}\mu_n^2\psi_{n,I-2,R}^{k}\Delta_n\right],$$

right incident boundary, (4.140b)

$$J_{I,L}^{k+1,(1)} = -\left[\frac{1}{3\sigma_{t,I}\Delta x_{I}\left(1+2\theta\right)}\right]$$
$$\times\left[\left(2+\theta\right)\phi_{I+1/2}^{k+1,(0)}-\left(1+2\theta\right)\phi_{I-1/2}^{k+1,(0)}-6\left(1-\theta\right)\sum_{\mu_n<0}\mu_n^2\psi_{n,R}^{b,k+1}\Delta_n\right],$$

right incident boundary, (4.140c)

$$J_{I,R}^{k+1,(1)} = -\left[\frac{1}{3\sigma_{t,I}\Delta x_{I}\left(1+2\theta\right)}\right]$$
$$\times\left[-\left(1-\theta\right)\phi_{I+1/2}^{k+1,(0)}-\left(1+2\theta\right)\phi_{I-1/2}^{k+1,(0)}+6\left(2+\theta\right)\sum_{\mu_n<0}\mu_n^2\psi_{n,R}^{b,k+1}\Delta_n\right],$$

right incident boundary. (4.140d)

4.4.3 The $O(\varepsilon)$ Terms

Examining the $O(\varepsilon)$ terms in Eq. (4.116), we have

$$\frac{1}{v'\Delta t_{k+1}}\underline{\underline{M}}_{i+1/2}\left[\underline{\hat{\psi}}^{k+1,(0)}_{n,i+1/2}-\underline{\psi}^{k}_{n,i+1/2}\right]+\mu_n\underline{\underline{L}}^{surf}_{i+1/2}\underline{\hat{\psi}}^{k+1,surf,(1)}_{n,i+1/2}-\mu_n\underline{\underline{L}}_{i+1/2}\underline{\hat{\psi}}^{k+1,(1)}_{n,i+1/2}$$
$$+\underline{\underline{T}}'_{i+1/2}\underline{\hat{\psi}}^{k+1,(2)}_{n,i+1/2}=\frac{1}{2}\underline{\underline{T}}'_{i+1/2}\sum_{m=1}^{N}\underline{\hat{\psi}}^{k+1,(2)}_{m,i+1/2}\Delta_m-\frac{1}{2}\underline{\underline{A}}'_{i+1/2}\sum_{m=1}^{N}\underline{\hat{\psi}}^{k+1,(0)}_{m,i+1/2}\Delta_m$$
$$+\underline{\underline{M}}_{i+1/2}\underline{q}^{k+1}_{n,i+1/2}. \quad (4.141)$$

Operating on Eq. (4.141) by $\sum_{n=1}^{N}(\cdot)\Delta_n$, we find

$$\frac{1}{v'\Delta t_{k+1}}\underline{\underline{M}}_{i+1/2}\left[\underline{\hat{\phi}}^{k+1,(0)}_{i+1/2}-\underline{\phi}^{k}_{i+1/2}\right]+\underline{\underline{L}}^{surf}_{i+1/2}\sum_{n=1}^{N}\mu_n\underline{\hat{\psi}}^{k+1,surf,(1)}_{n,i+1/2}\Delta_n-\underline{\underline{L}}_{i+1/2}\underline{\hat{J}}^{k+1,(1)}_{i+1/2}$$
$$+\underline{\underline{A}}'_{i+1/2}\underline{\hat{\phi}}^{k+1,(0)}_{i+1/2}=\underline{\underline{M}}_{i+1/2}\sum_{n=1}^{N}\underline{q}^{k+1}_{n,i+1/2}\Delta_n. \quad (4.142)$$

Eqs. (4.142) represents a 4×4 system of equations. We first consider Eq. (4.142) in the problem interior (and reflecting boundaries). Substituting in Eqs. (4.131b) and (4.139), and writing the second and third rows of Eq. (4.142), we have

$$\left[\frac{\Delta x_i(1-\theta)}{6v'\Delta t_{k+1}}\right]\left(\phi^{k+1/2,(0)}_{i,L}-\phi^{k}_{i,L}\right)+\left[\frac{\Delta x_i(2+\theta)}{6v'\Delta t_{k+1}}\right]\left(\phi^{k+1,(0)}_{i+1/2}-\phi^{k}_{i,R}\right)$$
$$+\sum_{\mu_n<0}\mu_n\psi^{k+1,(1)}_{n,i+1,L}\Delta_n+\sum_{\mu_n>0}\mu_n\psi^{k+1,(1)}_{n,i,R}\Delta_n$$
$$+\frac{1}{3\sigma_{t,i}\Delta x_i}\left[\phi^{k+1,(0)}_{i+1/2}-\frac{1}{\rho}\sum_{\mu_n>0}\mu_n\psi^{k}_{n,i-1,R}\Delta_n-3\sum_{\mu_n>0}\mu_n^2\psi^{k}_{n,i-1,R}\Delta_n\right]$$
$$+\left[\frac{\sigma_{a,i}\Delta x_i(1-\theta)}{6}\right]\phi^{k+1/2,(0)}_{i,L}+\left[\frac{\sigma_{a,i}\Delta x_i(2+\theta)}{6}\right]\phi^{k+1,(0)}_{i+1/2}$$
$$=\left[\frac{\Delta x_i(1-\theta)}{6}\right]\sum_{n=1}^{N}q^{k+1}_{n,i,L}\Delta_n+\left[\frac{\Delta x_i(2+\theta)}{6}\right]\sum_{n=1}^{N}q^{k+1}_{n,i,R}\Delta_n, \quad (4.143a)$$

$$\left[\frac{\Delta x_{i+1}(2+\theta)}{6v'\Delta t_{k+1}}\right]\left(\phi_{i+1/2}^{k+1,(0)}-\phi_{i+1,L}^{k}\right)+\left[\frac{\Delta x_{i+1}(1-\theta)}{6v'\Delta t_{k+1}}\right]\left(\phi_{i+1,R}^{k+1/2,(0)}-\phi_{i+1,R}^{k}\right)$$
$$-\sum_{\mu_n<0}\mu_n\psi_{n,i+1,L}^{k+1,(1)}\Delta_n-\sum_{\mu_n>0}\mu_n\psi_{n,i,R}^{k+1,(1)}\Delta_n$$
$$-\frac{1}{3\sigma_{t,i+1}\Delta x_{i+1}}\left[\frac{1}{\rho}\sum_{\mu_n<0}|\mu_n|\psi_{n,i+2,L}^{k}\Delta_n+\sum_{\mu_n<0}\mu_n^2\psi_{n,i+2,L}^{k}\Delta_n-\phi_{i+1/2}^{k+1,(0)}\right]$$
$$+\left[\frac{\sigma_{a,i+1}\Delta x_{i+1}(2+\theta)}{6}\right]\phi_{i+1/2}^{k+1,(0)}+\left[\frac{\sigma_{a,i+1}\Delta x_{i+1}(1-\theta)}{6}\right]\phi_{i+1,R}^{k+1/2,(0)}$$
$$=\left[\frac{\Delta x_{i+1}(2+\theta)}{6}\right]\sum_{n=1}^{N}q_{n,i+1,L}^{k+1}\Delta_n+\left[\frac{\Delta x_{i+1}(1-\theta)}{6}\right]\sum_{n=1}^{N}q_{n,i+1,R}^{k+1}\Delta_n\,. \quad (4.143b)$$

Substituting Eqs. (4.131c) and (4.131d) into Eqs. (4.143), we have

$$\left[\frac{\Delta x_i(1-\theta)}{6v'\Delta t_{k+1}}\right]\left(\frac{2}{\rho}\sum_{\mu_n>0}\mu_n\psi_{n,i-1,R}^{k}\Delta_n-\phi_{i,L}^{k}\right)+\left[\frac{\Delta x_i(2+\theta)}{6v'\Delta t_{k+1}}\right]\left(\phi_{i+1/2}^{k+1,(0)}-\phi_{i,R}^{k}\right)$$
$$+\sum_{\mu_n<0}\mu_n\psi_{n,i+1,L}^{k+1,(1)}\Delta_n+\sum_{\mu_n>0}\mu_n\psi_{n,i,R}^{k+1,(1)}\Delta_n$$
$$+\frac{1}{3\sigma_{t,i}\Delta x_i}\left[\phi_{i+1/2}^{k+1,(0)}-\frac{1}{\rho}\sum_{\mu_n>0}\mu_n\psi_{n,i-1,R}^{k}\Delta_n-3\sum_{\mu_n>0}\mu_n^2\psi_{n,i-1,R}^{k}\Delta_n\right]$$
$$+\left[\frac{\sigma_{a,i}\Delta x_i(1-\theta)}{6}\right]\left(\frac{2}{\rho}\sum_{\mu_n>0}\mu_n\psi_{n,i-1,R}^{k}\Delta_n\right)+\left[\frac{\sigma_{a,i}\Delta x_i(2+\theta)}{6}\right]\phi_{i+1/2}^{k+1,(0)}$$
$$=\left[\frac{\Delta x_i(1-\theta)}{6}\right]\sum_{n=1}^{N}q_{n,i,L}^{k+1}\Delta_n+\left[\frac{\Delta x_i(2+\theta)}{6}\right]\sum_{n=1}^{N}q_{n,i,R}^{k+1}\Delta_n\,, \quad (4.144a)$$

$$\left[\frac{\Delta x_{i+1}(2+\theta)}{6v'\Delta t_{k+1}}\right]\left(\phi_{i+1/2}^{k+1,(0)}-\phi_{i+1,L}^{k}\right)+\left[\frac{\Delta x_{i+1}(1-\theta)}{6v'\Delta t_{k+1}}\right]\left(\frac{2}{\rho}\sum_{\mu_n<0}|\mu_n|\psi_{n,i+2,L}^{k}\Delta_n-\phi_{i+1,R}^{k}\right)$$
$$-\sum_{\mu_n<0}\mu_n\psi_{n,i+1,L}^{k+1,(1)}\Delta_n-\sum_{\mu_n>0}\mu_n\psi_{n,i,R}^{k+1,(1)}\Delta_n$$
$$-\frac{1}{3\sigma_{t,i+1}\Delta x_{i+1}}\left[\frac{1}{\rho}\sum_{\mu_n<0}|\mu_n|\psi_{n,i+2,L}^{k}\Delta_n+\sum_{\mu_n<0}\mu_n^2\psi_{n,i+2,L}^{k}\Delta_n-\phi_{i+1/2}^{k+1,(0)}\right]$$
$$+\left[\frac{\sigma_{a,i+1}\Delta x_{i+1}(2+\theta)}{6}\right]\phi_{i+1/2}^{k+1,(0)}+\left[\frac{\sigma_{a,i+1}\Delta x_{i+1}(1-\theta)}{6}\right]\left(\frac{2}{\rho}\sum_{\mu_n<0}|\mu_n|\psi_{n,i+2,L}^{k}\Delta_n\right)$$
$$=\left[\frac{\Delta x_{i+1}(2+\theta)}{6}\right]\sum_{n=1}^{N}q_{n,i+1,L}^{k+1}\Delta_n+\left[\frac{\Delta x_{i+1}(1-\theta)}{6}\right]\sum_{n=1}^{N}q_{n,i+1,R}^{k+1}\Delta_n\,. \quad (4.144b)$$

By summing Eqs. (4.144), the first order surface terms cancel, and we obtain the scaled

asymptotic diffusion equation for the problem interior and on reflecting boundaries

$$\left[\frac{\Delta x_i(1-\theta)}{6v'\Delta t_{k+1}}\right]\left(\frac{2}{\rho}\sum_{\mu_n>0}\mu_n\psi^k_{n,i-1,R}\Delta_n-\phi^k_{i,L}\right)+\left[\frac{\Delta x_i(2+\theta)}{6v'\Delta t_{k+1}}\right]\left(\phi^{k+1,(0)}_{i+1/2}-\phi^k_{i,R}\right)$$
$$+\left[\frac{\Delta x_{i+1}(2+\theta)}{6v'\Delta t_{k+1}}\right]\left(\phi^{k+1,(0)}_{i+1/2}-\phi^k_{i+1,L}\right)+\left[\frac{\Delta x_{i+1}(1-\theta)}{6v'\Delta t_{k+1}}\right]\left(\frac{2}{\rho}\sum_{\mu_n<0}|\mu_n|\psi^k_{n,i+2,L}\Delta_n-\phi^k_{i+1,R}\right)$$
$$+\frac{1}{3\sigma_{t,i}\Delta x_i}\left[\phi^{k+1,(0)}_{i+1/2}-\frac{1}{\rho}\sum_{\mu_n>0}\mu_n\psi^k_{n,i-1,R}\Delta_n-3\sum_{\mu_n>0}\mu_n^2\psi^k_{n,i-1,R}\Delta_n\right]$$
$$-\frac{1}{3\sigma_{t,i+1}\Delta x_{i+1}}\left[\frac{1}{\rho}\sum_{\mu_n<0}|\mu_n|\psi^k_{n,i+2,L}\Delta_n+3\sum_{\mu_n<0}\mu_n^2\psi^k_{n,i+2,L}\Delta_n-\phi^{k+1,(0)}_{i+1/2}\right]$$
$$+\left[\frac{\sigma_{a,i}\Delta x_i(1-\theta)}{6}\right]\left(\frac{2}{\rho}\sum_{\mu_n>0}\mu_n\psi^k_{n,i-1,R}\Delta_n\right)+\left[\frac{\sigma_{a,i}\Delta x_i(2+\theta)}{6}\right]\phi^{k+1,(0)}_{i+1/2}$$
$$+\left[\frac{\sigma_{a,i+1}\Delta x_{i+1}(2+\theta)}{6}\right]\phi^{k+1,(0)}_{i+1/2}+\left[\frac{\sigma_{a,i+1}\Delta x_{i+1}(1-\theta)}{6}\right]\left(\frac{2}{\rho}\sum_{\mu_n<0}|\mu_n|\psi^k_{n,i+2,L}\Delta_n\right)$$
$$=\left[\frac{\Delta x_i(1-\theta)}{6}\right]\sum_{n=1}^{N}q^{k+1}_{n,i,L}\Delta_n+\left[\frac{\Delta x_i(2+\theta)}{6}\right]\sum_{n=1}^{N}q^{k+1}_{n,i,R}\Delta_n$$
$$+\left[\frac{\Delta x_{i+1}(2+\theta)}{6}\right]\sum_{n=1}^{N}q^{k+1}_{n,i+1,L}\Delta_n+\left[\frac{\Delta x_{i+1}(1-\theta)}{6}\right]\sum_{n=1}^{N}q^{k+1}_{n,i+1,R}\Delta_n\,. \quad (4.145)$$

Next we consider Eq. (4.142) for a left incident boundary. Substituting in Eqs. (4.138) and (4.131), and writing the second and third row of Eq. (4.142), we find

$$\left[\frac{\Delta x_1(1-\theta)}{6v'\Delta t_{k+1}}\right]\left(\phi^{k+1,(0)}_{1/2}-\phi^k_{1,L}\right)+\left[\frac{\Delta x_1(2+\theta)}{6v'\Delta t_{k+1}}\right]\left(\phi^{k+1,(0)}_{3/2}-\phi^k_{1,R}\right)$$
$$+\sum_{\mu_n<0}\mu_n\psi^{k+1,(1)}_{n,2,L}\Delta_n+\sum_{\mu_n>0}\mu_n\psi^{k+1,(1)}_{n,1,R}\Delta_n$$
$$+\frac{1}{3\sigma_{t,1}\Delta x_1}\left[\phi^{k+1,(0)}_{3/2}-\frac{1}{2}\phi^{k+1,(0)}_{1/2}-3\sum_{\mu_n>0}\mu_n^2\psi^{b,k+1}_{n,L}\Delta_n\right]$$
$$+\left[\frac{\sigma_{a,1}\Delta x_1(1-\theta)}{6}\right]\phi^{k+1,(0)}_{1/2}+\left[\frac{\sigma_{a,1}\Delta x_1(2+\theta)}{6}\right]\phi^{k+1,(0)}_{3/2}$$
$$=\left[\frac{\Delta x_1(1-\theta)}{6}\right]\sum_{n=1}^{N}q^{k+1}_{n,1,L}\Delta_n+\left[\frac{\Delta x_1(2+\theta)}{6}\right]\sum_{n=1}^{N}q^{k+1}_{n,1,R}\Delta_n\,, \quad (4.146a)$$

$$\left[\frac{\Delta x_2(2+\theta)}{6v'\Delta t_{k+1}}\right]\left(\phi_{3/2}^{k+1,(0)}-\phi_{2,L}^{k}\right)+\left[\frac{\Delta x_2(1-\theta)}{6v'\Delta t_{k+1}}\right]\left(\frac{2}{\rho}\sum_{\mu_n<0}|\mu_n|\psi_{n,3,L}^{k}\Delta_n-\phi_{2,R}^{k}\right)$$
$$-\sum_{\mu_n<0}\mu_n\psi_{n,2,L}^{k+1,(1)}\Delta_n-\sum_{\mu_n>0}\mu_n\psi_{n,1,R}^{k+1,(1)}\Delta_n$$
$$-\frac{1}{3\sigma_{t,2}\Delta x_2}\left[\frac{1}{\rho}\sum_{\mu_n<0}|\mu_n|\psi_{n,3,L}^{k}\Delta_n+3\sum_{\mu_n<0}\mu_n^2\psi_{n,3,L}^{k}\Delta_n-\phi_{3/2}^{k+1,(0)}\right]$$
$$+\left[\frac{\sigma_{a,2}\Delta x_2(2+\theta)}{6}\right]\phi_{3/2}^{k+1,(0)}+\left[\frac{\sigma_{a,2}\Delta x_2(1-\theta)}{6}\right]\left(\frac{2}{\rho}\sum_{\mu_n<0}|\mu_n|\psi_{n,3,L}^{k}\Delta_n\right)$$
$$=\left[\frac{\Delta x_2(2+\theta)}{6}\right]\sum_{n=1}^{N}q_{n,2,L}^{k+1}\Delta_n+\left[\frac{\Delta x_2(1-\theta)}{6}\right]\sum_{n=1}^{N}q_{n,2,R}^{k+1}\Delta_n\,. \quad (4.146b)$$

Summing Eqs. (4.146), the first order surface terms cancel, and we find the scaled asymptotic diffusion equation on a left incident boundary

$$\left[\frac{\Delta x_1(1-\theta)}{6v'\Delta t_{k+1}}\right]\left(\phi_{1/2}^{k+1,(0)}-\phi_{1,L}^{k}\right)+\left[\frac{\Delta x_1(2+\theta)}{6v'\Delta t_{k+1}}\right]\left(\phi_{3/2}^{k+1,(0)}-\phi_{1,R}^{k}\right)$$
$$+\left[\frac{\Delta x_2(2+\theta)}{6v'\Delta t_{k+1}}\right]\left(\phi_{3/2}^{k+1,(0)}-\phi_{2,L}^{k}\right)+\left[\frac{\Delta x_2(1-\theta)}{6v'\Delta t_{k+1}}\right]\left(\frac{2}{\rho}\sum_{\mu_n<0}|\mu_n|\psi_{n,3,L}^{k}\Delta_n-\phi_{2,R}^{k}\right)$$
$$+\frac{1}{3\sigma_{t,1}\Delta x_1}\left(\phi_{3/2}^{k+1,(0)}-\frac{1}{2}\phi_{1/2}^{k+1,(0)}-3\sum_{\mu_n>0}\mu_n^2\psi_{n,L}^{b,k+1}\Delta_n\right)$$
$$-\frac{1}{3\sigma_{t,2}\Delta x_2}\left(\frac{1}{\rho}\sum_{\mu_n<0}|\mu_n|\psi_{n,3,L}^{k}\Delta_n+3\sum_{\mu_n<0}\mu_n^2\psi_{n,3,L}^{k}\Delta_n-\phi_{3/2}^{k+1,(0)}\right)$$
$$+\left[\frac{\sigma_{a,1}\Delta x_1(1-\theta)}{6}\right]\phi_{1/2}^{k+1,(0)}+\left[\frac{\sigma_{a,1}\Delta x_1(2+\theta)}{6}\right]\phi_{3/2}^{k+1,(0)}$$
$$+\left[\frac{\sigma_{a,2}\Delta x_2(2+\theta)}{6}\right]\phi_{3/2}^{k+1,(0)}+\left[\frac{\sigma_{a,2}\Delta x_2(1-\theta)}{6}\right]\left(\frac{2}{\rho}\sum_{\mu_n<0}|\mu_n|\psi_{n,3,L}^{k}\Delta_n\right)$$
$$=\left[\frac{\Delta x_1(1-\theta)}{6}\right]\sum_{n=1}^{N}q_{n,1,L}^{k+1}\Delta_n+\left[\frac{\Delta x_1(2+\theta)}{6}\right]\sum_{n=1}^{N}q_{n,1,R}^{k+1}\Delta_n$$
$$+\left[\frac{\Delta x_2(2+\theta)}{6}\right]\sum_{n=1}^{N}q_{n,2,L}^{k+1}\Delta_n+\left[\frac{\Delta x_2(1-\theta)}{6}\right]\sum_{n=1}^{N}q_{n,2,R}^{k+1}\Delta_n\,. \quad (4.147)$$

Similarly, for a right incident boundary, we have

$$\begin{aligned}
&\left[\frac{\Delta x_{I-1}(1-\theta)}{6v'\Delta t_{k+1}}\right]\left(\frac{2}{\rho}\sum_{\mu>0}\psi^k_{n,I-2,R}\Delta_n-\phi^k_{I-1,L}\right)+\left[\frac{\Delta x_{I-1}(2+\theta)}{6v'\Delta t_{k+1}}\right]\left(\phi^{k+1,(0)}_{I-1/2}-\phi^k_{I-1,R}\right)\\
&\quad+\left[\frac{\Delta x_I(2+\theta)}{6v'\Delta t_{k+1}}\right]\left(\phi^{k+1,(0)}_{I-1/2}-\phi^k_{I,L}\right)+\left[\frac{\Delta x_I(1-\theta)}{6v'\Delta t_{k+1}}\right]\left(\phi^{k+1,(0)}_{I+1/2}-\phi^k_{I,R}\right)\\
&\quad+\frac{1}{3\sigma_{t,I-1}\Delta x_{I-1}}\left(\phi^{k+1,(0)}_{I-1/2}-\frac{1}{\rho}\sum_{\mu_n>0}\mu_n\psi^k_{n,I-2,R}\Delta_n-3\sum_{\mu_n>0}\mu_n^2\psi^k_{n,I-2,R}\Delta_n\right)\\
&\quad-\frac{1}{3\sigma_{t,I}\Delta x_I}\left(\frac{1}{2}\phi^{k+1,(0)}_{I+1/2}+3\sum_{\mu_n<0}\mu_n^2\psi^{b,k+1}_{n,R}\Delta_n-\phi^{k+1,(0)}_{I-1/2}\right)\\
&+\left[\frac{\sigma_{a,I-1}\Delta x_{I-1}(1-\theta)}{6}\right]\left(\frac{2}{\rho}\sum_{\mu>0}\psi^k_{n,I-2,R}\Delta_n\right)+\left[\frac{\sigma_{a,I-1}\Delta x_{I-1}(2+\theta)}{6}\right]\phi^{k+1,(0)}_{I-1/2}\\
&\quad+\left[\frac{\sigma_{a,I}\Delta x_I(2+\theta)}{6}\right]\phi^{k+1,(0)}_{I-1/2}+\left[\frac{\sigma_{a,I}\Delta x_I(1-\theta)}{6}\right]\phi^{k+1,(0)}_{I+1/2}\\
&\quad=\left[\frac{\Delta x_{I-1}(1-\theta)}{6}\right]\sum_{n=1}^{N}q^{k+1}_{n,I-1,L}\Delta_n+\left[\frac{\Delta x_{I-1}(2+\theta)}{6}\right]\sum_{n=1}^{N}q^{k+1}_{n,I-1,R}\Delta_n\\
&\quad\quad+\left[\frac{\Delta x_I(2+\theta)}{6}\right]\sum_{n=1}^{N}q^{k+1}_{n,I,L}\Delta_n+\left[\frac{\Delta x_I(1-\theta)}{6}\right]\sum_{n=1}^{N}q^{k+1}_{n,I,R}\Delta_n\,. \qquad (4.148)
\end{aligned}$$

4.4.4 Rescaling the SBJ Asymptotic Diffusion Equations

Substituting the unscaled variables in Eq. (4.110) into Eqs. (4.145), (4.147), and (4.148), together with Eqs. (4.131a) and (4.131e), we have the complete system of asymptotic diffusion equations for the SBJ transport method:

$$\phi^{k+1,(0)}_{1/2}=\frac{2}{\rho}\sum_{\mu_n>0}\mu_n\psi^{b,k+1}_{n,L}\Delta_n\,, \qquad \text{left incident boundary}\,, \quad (4.149a)$$

$$\left[\frac{\Delta x_1(1-\theta)}{6v\Delta t_{k+1}}\right]\left(\phi_{1/2}^{k+1,(0)}-\phi_{1,L}^{k}\right)+\left[\frac{\Delta x_1(2+\theta)}{6v\Delta t_{k+1}}\right]\left(\phi_{3/2}^{k+1,(0)}-\phi_{1,R}^{k}\right)$$
$$+\left[\frac{\Delta x_2(2+\theta)}{6v\Delta t_{k+1}}\right]\left(\phi_{3/2}^{k+1,(0)}-\phi_{2,L}^{k}\right)+\left[\frac{\Delta x_2(1-\theta)}{6v\Delta t_{k+1}}\right]\left(\frac{2}{\rho}\sum_{\mu_n<0}|\mu_n|\psi_{n,3,L}^{k}\Delta_n-\phi_{2,R}^{k}\right)$$
$$+\frac{1}{3\Sigma_{t,1}\Delta x_1}\left(\phi_{3/2}^{k+1,(0)}-\frac{1}{2}\phi_{1/2}^{k+1,(0)}-3\sum_{\mu_n>0}\mu_n^2\psi_{n,L}^{b,k+1}\Delta_n\right)$$
$$-\frac{1}{3\Sigma_{t,2}\Delta x_2}\left(\frac{1}{\rho}\sum_{\mu_n<0}|\mu_n|\psi_{n,3,L}^{k}\Delta_n+3\sum_{\mu_n<0}\mu_n^2\psi_{n,3,L}^{k}\Delta_n-\phi_{3/2}^{k+1,(0)}\right)$$
$$+\left[\frac{\Sigma_{a,1}\Delta x_1(1-\theta)}{6}\right]\phi_{1/2}^{k+1,(0)}+\left[\frac{\Sigma_{a,1}\Delta x_1(2+\theta)}{6}\right]\phi_{3/2}^{k+1,(0)}$$
$$+\left[\frac{\Sigma_{a,2}\Delta x_2(2+\theta)}{6}\right]\phi_{3/2}^{k+1,(0)}+\left[\frac{\Sigma_{a,2}\Delta x_2(1-\theta)}{6}\right]\left(\frac{2}{\rho}\sum_{\mu_n<0}|\mu_n|\psi_{n,3,L}^{k}\Delta_n\right)$$
$$=\left[\frac{\Delta x_1(1-\theta)}{6}\right]\sum_{n=1}^{N}Q_{n,1,L}^{k+1}\Delta_n+\left[\frac{\Delta x_1(2+\theta)}{6}\right]\sum_{n=1}^{N}Q_{n,1,R}^{k+1}\Delta_n$$
$$+\left[\frac{\Delta x_2(2+\theta)}{6}\right]\sum_{n=1}^{N}Q_{n,2,L}^{k+1}\Delta_n+\left[\frac{\Delta x_2(1-\theta)}{6}\right]\sum_{n=1}^{N}Q_{n,2,R}^{k+1}\Delta_n\,,\quad\text{left incident boundary}\,,\tag{4.149b}$$

$$\left[\frac{\Delta x_i(1-\theta)}{6\nu\Delta t_{k+1}}\right]\left(\frac{2}{\rho}\sum_{\mu_n>0}\mu_n\psi^k_{n,i-1,R}\Delta_n-\phi^k_{i,L}\right)+\left[\frac{\Delta x_i(2+\theta)}{6\nu\Delta t_{k+1}}\right]\left(\phi^{k+1,(0)}_{i+1/2}-\phi^k_{i,R}\right)$$
$$+\left[\frac{\Delta x_{i+1}(2+\theta)}{6\nu\Delta t_{k+1}}\right]\left(\phi^{k+1,(0)}_{i+1/2}-\phi^k_{i+1,L}\right)+\left[\frac{\Delta x_{i+1}(1-\theta)}{6\nu\Delta t_{k+1}}\right]\left(\frac{2}{\rho}\sum_{\mu_n<0}|\mu_n|\psi^k_{n,i+2,L}\Delta_n-\phi^k_{i+1,R}\right)$$
$$+\frac{1}{3\Sigma_{t,i}\Delta x_i}\left[\phi^{k+1,(0)}_{i+1/2}-\frac{1}{\rho}\sum_{\mu_n>0}\mu_n\psi^k_{n,i-1,R}\Delta_n-3\sum_{\mu_n>0}\mu_n^2\psi^k_{n,i-1,R}\Delta_n\right]$$
$$-\frac{1}{3\Sigma_{t,i+1}\Delta x_{i+1}}\left[\frac{1}{\rho}\sum_{\mu_n<0}|\mu_n|\psi^k_{n,i+2,L}\Delta_n+3\sum_{\mu_n<0}\mu_n^2\psi^k_{n,i+2,L}\Delta_n-\phi^{k+1,(0)}_{i+1/2}\right]$$
$$+\left[\frac{\Sigma_{a,i}\Delta x_i(1-\theta)}{6}\right]\left(\frac{2}{\rho}\sum_{\mu_n>0}\mu_n\psi^k_{n,i-1,R}\Delta_n\right)+\left[\frac{\Sigma_{a,i}\Delta x_i(2+\theta)}{6}\right]\phi^{k+1,(0)}_{i+1/2}$$
$$+\left[\frac{\Sigma_{a,i+1}\Delta x_{i+1}(2+\theta)}{6}\right]\phi^{k+1,(0)}_{i+1/2}+\left[\frac{\Sigma_{a,i+1}\Delta x_{i+1}(1-\theta)}{6}\right]\left(\frac{2}{\rho}\sum_{\mu_n<0}|\mu_n|\psi^k_{n,i+2,L}\Delta_n\right)$$
$$=\left[\frac{\Delta x_i(1-\theta)}{6}\right]\sum_{n=1}^{N}Q^{k+1}_{n,i,L}\Delta_n+\left[\frac{\Delta x_i(2+\theta)}{6}\right]\sum_{n=1}^{N}Q^{k+1}_{n,i,R}\Delta_n$$
$$+\left[\frac{\Delta x_{i+1}(2+\theta)}{6}\right]\sum_{n=1}^{N}Q^{k+1}_{n,i+1,L}\Delta_n+\left[\frac{\Delta x_{i+1}(1-\theta)}{6}\right]\sum_{n=1}^{N}Q^{k+1}_{n,i+1,R}\Delta_n\,,$$

interior and reflecting boundaries, (4.149c)

$$\left[\frac{\Delta x_{I-1}(1-\theta)}{6v\Delta t_{k+1}}\right]\left(\frac{2}{\rho}\sum_{\mu>0}\psi^k_{n,I-2,R}\Delta_n-\phi^k_{I-1,L}\right)+\left[\frac{\Delta x_{I-1}(2+\theta)}{6v\Delta t_{k+1}}\right]\left(\phi^{k+1,(0)}_{I-1/2}-\phi^k_{I-1,R}\right)$$
$$+\left[\frac{\Delta x_I(2+\theta)}{6v\Delta t_{k+1}}\right]\left(\phi^{k+1,(0)}_{I-1/2}-\phi^k_{I,L}\right)+\left[\frac{\Delta x_I(1-\theta)}{6v\Delta t_{k+1}}\right]\left(\phi^{k+1,(0)}_{I+1/2}-\phi^k_{I,R}\right)$$
$$+\frac{1}{3\Sigma_{t,I-1}\Delta x_{I-1}}\left(\phi^{k+1,(0)}_{I-1/2}-\frac{1}{\rho}\sum_{\mu_n>0}\mu_n\psi^k_{n,I-2,R}\Delta_n-3\sum_{\mu_n>0}\mu_n^2\psi^k_{n,I-2,R}\Delta_n\right)$$
$$-\frac{1}{3\Sigma_{t,I}\Delta x_I}\left(\frac{1}{2}\phi^{k+1,(0)}_{I+1/2}+3\sum_{\mu_n<0}\mu_n^2\psi^{b,k+1}_{n,R}\Delta_n-\phi^{k+1,(0)}_{I-1/2}\right)$$
$$+\left[\frac{\Sigma_{a,I-1}\Delta x_{I-1}(1-\theta)}{6}\right]\left(\frac{2}{\rho}\sum_{\mu>0}\psi^k_{n,I-2,R}\Delta_n\right)+\left[\frac{\Sigma_{a,I-1}\Delta x_{I-1}(2+\theta)}{6}\right]\phi^{k+1,(0)}_{I-1/2}$$
$$+\left[\frac{\Sigma_{a,I}\Delta x_I(2+\theta)}{6}\right]\phi^{k+1,(0)}_{I-1/2}+\left[\frac{\Sigma_{a,I}\Delta x_I(1-\theta)}{6}\right]\phi^{k+1,(0)}_{I+1/2}$$
$$=\left[\frac{\Delta x_{I-1}(1-\theta)}{6}\right]\sum_{n=1}^N Q^{k+1}_{n,I-1,L}\Delta_n+\left[\frac{\Delta x_{I-1}(2+\theta)}{6}\right]\sum_{n=1}^N Q^{k+1}_{n,I-1,R}\Delta_n$$
$$+\left[\frac{\Delta x_I(2+\theta)}{6}\right]\sum_{n=1}^N Q^{k+1}_{n,I,L}\Delta_n+\left[\frac{\Delta x_I(1-\theta)}{6}\right]\sum_{n=1}^N Q^{k+1}_{n,I,R}\Delta_n\,,\qquad\text{right incident boundary}\,, \tag{4.149d}$$

$$\phi^{k+1,(0)}_{I,R}=\phi^{k+1,(0)}_{I+1/2}=\frac{2}{\rho}\sum_{\mu_n<0}|\mu_n|\psi^{b,k+1}_{n,R}\Delta_n\,,\qquad\text{right incident boundary}\,. \tag{4.149e}$$

4.4.5 Examining the SBJ Asymptotic Diffusion Discretization

We now examing the SBJ asymptotic diffusion discretization and compare it to the node-centered SBJ diffusion discretization we investigated in Section 2.4. Writing Eqs. (4.149), assuming a lumped discretization ($\theta=1$), and assuming that the solution is isotropic and continuous at time t_k, the SBJ asymptotic diffusion equations simplify to

$$\phi^{k+1,(0)}_{1/2}=\left(\frac{2}{\rho}\right)J^{b,k+1}_L\,,\qquad\text{left incident boundary}\,, \tag{4.150a}$$

$$\left[\frac{\Delta x_{3/2}}{v\Delta t_{k+1}}\right]\left(\phi^{k+1,(0)}_{3/2}-\phi^k_{3/2}\right)+\frac{D_1}{\Delta x_1}\left(\phi^{k+1,(0)}_{3/2}-\frac{1}{2}\phi^{k+1,(0)}_{1/2}-3\sum_{\mu_n>0}\mu_n^2\psi^{b,k+1}_{n,L}\Delta_n\right)$$
$$-\frac{D_2}{\Delta x_2}\left(\phi^k_{5/2}-\phi^{k+1,(0)}_{3/2}\right)+\left(\Sigma_{a,3/2}\Delta x_{3/2}\right)\phi^{k+1,(0)}_{3/2}=\Delta x_{3/2}Q^{k+1}_{3/2}\,,$$
$$\text{left incident boundary}\,, \tag{4.150b}$$

$$\left[\frac{\Delta x_{i+1/2}}{v\Delta t_{k+1}}\right]\left(\phi_{i+1/2}^{k+1,(0)}-\phi_{i+1/2}^{k}\right)+\frac{D_i}{\Delta x_i}\left[\phi_{i+1/2}^{k+1,(0)}-\phi_{i-1/2}^{k}\right]$$
$$-\frac{D_{i+1}}{\Delta x_{i+1}}\left[\phi_{i+3/2}^{k}-\phi_{i+1/2}^{k+1,(0)}\right]+\left(\Sigma_{a,i+1/2}\Delta x_{i+1/2}\right)\phi_{i+1/2}^{k+1,(0)}=\Delta x_{i+1/2}Q_{i+1/2}^{k+1},$$
$$\text{interior and reflecting boundaries}, \quad (4.150c)$$

$$\left[\frac{\Delta x_{I-1/2}}{v\Delta t_{k+1}}\right]\left(\phi_{I-1/2}^{k+1,(0)}-\phi_{I-1,R}^{k}\right)+\frac{D_{I-1}}{\Delta x_{I-1}}\left(\phi_{I-1/2}^{k+1,(0)}-\phi_{I-3/2}^{k}\right)$$
$$-\frac{D_I}{\Delta x_I}\left(\frac{1}{2}\phi_{I+1/2}^{k+1,(0)}+3\sum_{\mu_n<0}\mu_n^2\psi_{n,R}^{b,k+1}\Delta_n-\phi_{I-1/2}^{k+1,(0)}\right)$$
$$+\left(\Sigma_{a,I-1/2}\Delta x_{I-1/2}\right)\phi_{I-1/2}^{k+1,(0)}=\Delta x_{I-1/2}Q_{I-1/2}^{k+1},$$
$$\text{right incident boundary}, \quad (4.150d)$$

$$\phi_{I,R}^{k+1,(0)}=\phi_{I+1/2}^{k+1,(0)}=\left(\frac{2}{\rho}\right)J_R^{b,k+1}, \qquad \text{right incident boundary}, \quad (4.150e)$$

where

$$J_L^{b,k+1}=\sum_{\mu_n>0}\mu_n\psi_{n,L}^{b,k+1}\Delta_n, \quad (4.151a)$$

$$J_R^{b,k+1}=\sum_{\mu_n<0}|\mu_n|\psi_{n,R}^{b,k+1}\Delta_n, \quad (4.151b)$$

$$D_i=\frac{1}{3\Sigma_{t,i}}, \quad (4.152)$$

and

$$\Delta x_{i+1/2}=\begin{cases}\dfrac{\Delta x_1}{2}, & i=0,\\ \dfrac{\Delta x_{i+1}+\Delta x_i}{2}, & 1\le i\le I-1,\\ \dfrac{\Delta x_I}{2}, & i=I,\end{cases} \quad (4.153a)$$

$$\Sigma_{a,i+1/2}=\begin{cases}\Sigma_{a,1}, & i=0,\\ \dfrac{\Sigma_{a,i+1}\Delta x_{i+1}+\Sigma_{a,i}\Delta x_i}{\Delta x_{i+1}+\Delta x_i}, & 1\le i\le I-1,\\ \Sigma_{a,I}, & i=I,\end{cases} \quad (4.153b)$$

$$Q_{i+1/2}^{k+1} = \begin{cases} \displaystyle\sum_{n=1}^{N} Q_{n,1,L}^{k+1} \Delta_n \,, & i = 0 \,, \\ \dfrac{\displaystyle\sum_{n=1}^{N} Q_{n,i,R}^{k+1} \Delta_n \Delta x_i + \sum_{n=1}^{N} Q_{n,i+1,L}^{k+1} \Delta_n \Delta x_{i+1}}{\Delta x_i + \Delta x_{i+1}} \,, & 1 \leq i \leq I-1 \,, \\ \displaystyle\sum_{n=1}^{N} Q_{n,I,R}^{k+1} \Delta_n \,, & i = I \,. \end{cases} \tag{4.153c}$$

Comparing Eqs. (4.150) with the node-centered SBJ diffusion equations we derived in Section 2.4, Eqs. (2.86), (2.87), and (2.88), we see that the asymptotic SBJ diffusion equations are the same as the node-centered SBJ equations in the interior, but different on the boundaries. This is similar to our findings with the implicit and fully-explicit methods. Therefore, we expect that the SBJ transport method will behave similarly to the SBJ diffusion method in the thick diffusive limit.

We next demonstrate the correctness of the SBJ transport asymptotic analysis numerically. Consider again a homogeneous slab of material 1 cm in length, divided into 10 cells, with total cross section $\Sigma_t = \frac{1}{\varepsilon}$ cm^{-1} and absorption cross section $\Sigma_a = \varepsilon$ cm^{-1}, where we vary ε from 10^0 to 10^{-4}. We place an isotropic fixed source of strength $Q = \varepsilon$ cm^{-3} s^{-1} everywhere in the slab, and set the particle velocity to $v = \frac{1}{\varepsilon}$ cm/s. The left boundary is a vacuum, and the right boundary is reflecting, and we use an S_{16} quadrature set. As ε vanishes, this problem converges to the diffusion problem

$$\frac{\partial}{\partial t}\phi(x,t) - \frac{1}{3}\frac{\partial^2}{\partial x^2}\phi(x,t) + \phi(x,t) = 1 \,, \tag{4.154a}$$

$$\phi(0,t) = 0 \,, \tag{4.154b}$$

$$J(1,t) = 0 \,. \tag{4.154c}$$

Setting an initial scalar flux of zero, and executing ten time steps with $\Delta t = 1$ s, we obtain the asymptotic diffusion result shown in Figure 4.4. In Figure 4.5, we show the convergence of the SBJ transport method to the asymptotic SBJ diffusion solution as ε vanishes. We measure the difference between the asymptotic diffusion solution and the transport solution

using an L_1 norm, i.e.,

$$L_1 \text{ Norm} = \frac{\sum_{i=1}^{I} \left| \phi_i^{k+1,transport} - \phi_i^{k+1,diffusion} \right| \Delta x_i}{\sum_{i=1}^{I} \Delta x_i}, \tag{4.155}$$

where $\phi_i^{k+1,transport}$ is the average transport scalar flux in cell i at time t_{k+1}, calculated using the SBJ transport method, and $\phi_i^{k+1,diffusion}$ is the average diffusion scalar flux in cell i at time t_{k+1}, calculated using the SBJ asymptotic diffusion equations. That the SBJ LDFEM

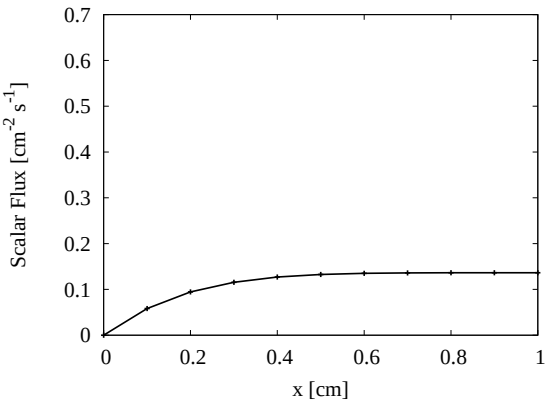

Figure 4.4 Asymptotic SBJ Diffusion Solution at $t = 10$ s

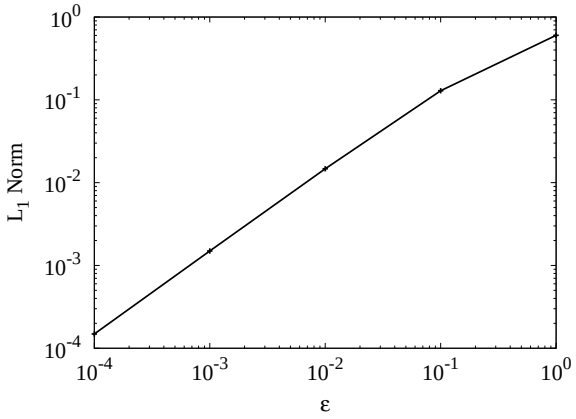

Figure 4.5 Convergence of the SBJ Transport Solution

solution converges to the asymptotic SBJ diffusion solution as ε vanishes suggests that our asymptotic analysis is correct.

4.5 Summary

In summary, we have derived the complete system of asymptotic diffusion equations for the implicit, fully-explicit, semi-explicit, and Staggered-Block Jacobi linear discontinuous finite element transport methods. In Section 4.2, we found that the implicit LDFEM transport method limits to a diffusion discretization that is identical to the implicit node-centered diffusion discretization, assuming isotropic and continuous initial conditions, in the problem interior and on reflecting boundaries. The implicit LDFEM method converges to a different diffusion equation on the first two nodes adjacent to an incident boundary. Likewise, we found in Section 4.3 that the fully-explicit LDFEM transport method limits to a diffusion

discretization that is identical to the node-centered fully-explicit diffusion discretization in the domain interior and on reflecting boundaries.

In Section 4.3, we found that the semi-explicit LDFEM transport method does not converge to the semi-explicit node-centered diffusion discretization in the thick diffusive limit. Instead, it converges to a diffusion discretization that lags the leakage terms to time t_{k-1}. As a result, while the semi-explicit node-centered diffusion method has improved stability over the fully-explicit method, the semi-explicit LDFEM transport method is less stable than the fully-explicit LDFEM transport method in the thick diffusive limit. It appears that there is no way to construct a first order time discretization of the LDFEM transport equations to produce an asymptotic diffusion limit equivalent to the node-centered semi-explicit diffusion discretization.

The asymptotic analysis of the SBJ transport method conducted in Section 4.4 shows that the SBJ transport method converges in the thick diffusive limit to the SBJ node-centered diffusion discretization. In the course of the asymptotic analysis, we observed that it is necessary to discard the angular fluxes adjacent to the outer boundaries of a block because these angular fluxes are pinned to the beginning of the time step and do not evolve forward in time properly. Based on this observation, we proposed the MSBJ method, which evaluates the angular fluxes adjacent to the outer boundaries of a block at time t_k instead of at time t_{k+1}. We believe the MSBJ method would be less accurate in optically-thin problems due to the additional lagging of the angular fluxes on the block boundaries. Therefore, we have neglected investigating this method.

Chapter 5

Linear Transport: Numerical Results

In this chapter, we present numerical results for the linear discontinuous finite element transport discretizations that we derived in Chapter 3 and analyzed in Chapter 4. These results show that the SBJ transport method is accurate and efficient for optically-thick problems, where the wave speed is slow, but can be inaccurate for optically-thin problems where the wave speed is fast. Iterations allow the SBJ transport method to converge to the implicit method, thus ensuring cell-wise particle conservation, but convergence can be slow for optically-thin problems.

In Section 5.1, we demonstrate the SBJ transport method on an optically-thick, purely scattering problem, and in Section 5.2, we demonstrate the SBJ transport method on an optically-thin purely scattering problem. In Section 5.3, we examine the SBJ transport method across a spectrum of optical thicknesses, and we also examine its iterative behavior. In Section 5.4, we examine the SBJ transport method for a series of problems with a scattering ratio of $c = 0.9$, and in Section 5.5, we test the SBJ transport method on a series of heterogeneous problems. Finally, in Section 5.6, we summarize our results. As discussed in Chapter 4, we expect the SBJ transport method to be unconditionally stable when using matrix lumping ($\theta = 1$), but not unconditionally stable otherwise. Therefore, for the numerical results presented in this chapter, we have assumed $\theta = 1$.

5.1 Transport Problem 1: Optically-Thick and Diffusive Problem

For the first numerical problem, we compare the accuracy of the SBJ transport method with the implicit method for an optically-thick and diffusive problem. We consider a slab 10 cm thick, divided into 100 cells, with a purely scattering material of total cross section

Σ_t =10,000 cm^{-1}. We place an incident isotropic flux of $\psi_{n,L}^{b,k+1} = 10$ cm^{-2} s^{-1} cosine^{-1} on the left boundary and a vacuum on the right boundary, and an initial condition of zero everywhere. The particle speed is v =1 cm/s and we use an S_{16} quadrature set. We run this problem to a final time of $t_f = 1000$ s, using time steps of length Δt =1 s, 10 s, 100 s, and 1000 s. Results for the implicit method are shown in Figure 5.1, for the plain SBJ transport method in Figure 5.2, and for the conservative SBJ transport method in Figure 5.3. As these

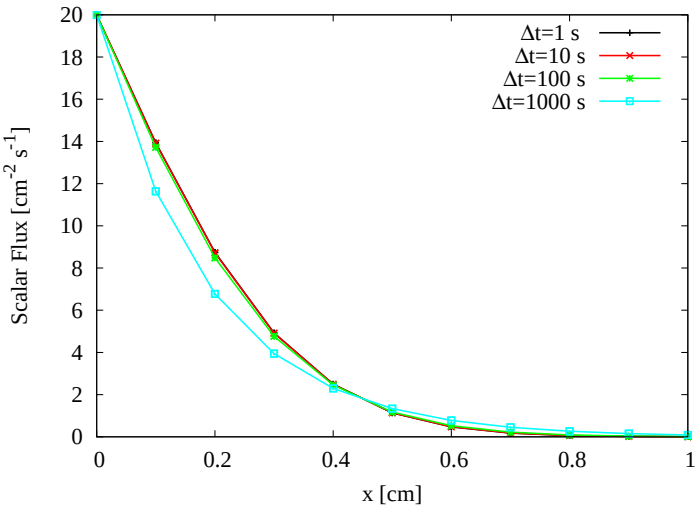

Figure 5.1 Transport Problem 1: Implicit Results at $t = 1000$ s

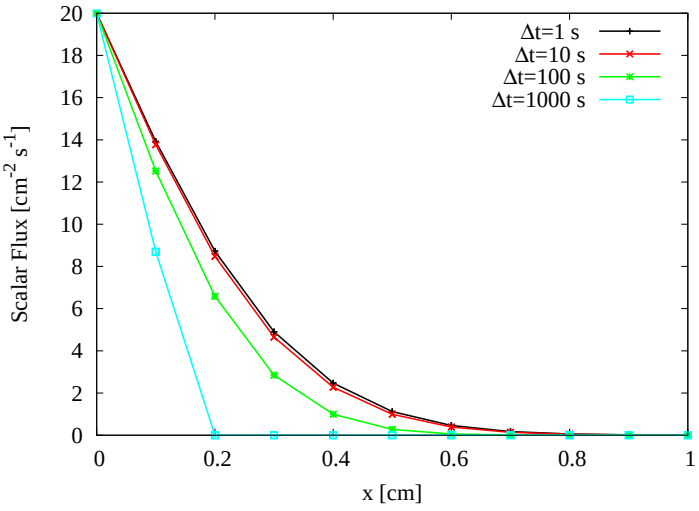

Figure 5.2 Transport Problem 1: Plain SBJ Results at $t = 1000$ s

figures show, the implicit result is accurate for every time step length except $\Delta t = 1000$ s. For very coarse time steps, Figure 5.1 demonstrates that the implicit method tends to transport

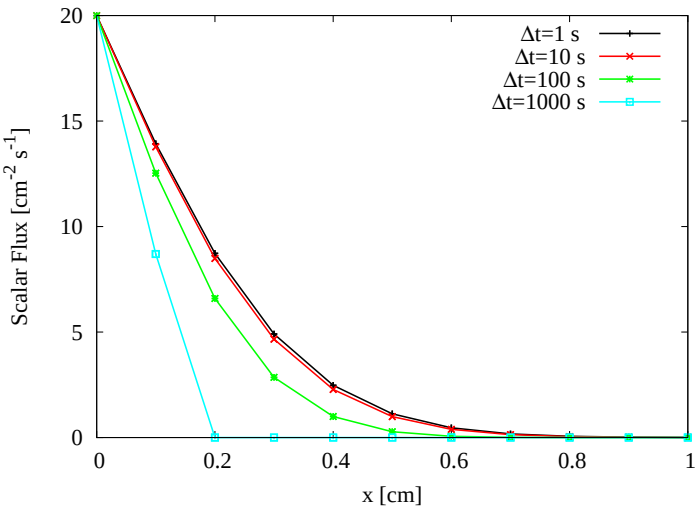

Figure 5.3 Transport Problem 1: Conservative SBJ Results at $t = 1000$ s

particles too deeply into the slab. The SBJ results are accurate for time step lengths of $\Delta t = 10$ s and $\Delta t = 1$ s, but are not accurate for longer time step lengths. Applying particle conservation makes little difference for this problem. In contrast to the implicit method, the SBJ transport method for coarse time steps tends to not transport the particles deeply enough into the slab.

Δt [s]	wave location [cm]	wave location [cell widths]
1	0.01	0.1
10	0.02	0.2
100	0.06	0.6
1000	0.18	1.8

Table 5.1 Transport Problem 1: Particle Wave Location at End of First Time Step

In Appendix A.2 we derive the equations necessary to calculate an estimate of the particle wave location. In Table 5.1 we show the wave location at the end of the first time step, for time steps of length $\Delta t = 1$ s, 10 s, 100 s, and 1000 s. The results in Table 5.1 indicate that the SBJ transport solution is accurate when the particle wave moves about 20% or less through a cell per time step. This is consistent with the diffusion results we found in Chapter 2.

5.2 Transport Problem 2: Optically-Thin Problem

For the second numerical problem, we demonstrate the SBJ transport method for an optically-thin, streaming problem. Consider a slab 1 cm in width, divided into 25 cells, and filled with a purely scattering material with cross section $\Sigma_t = 1$ cm^{-1}. We place an incident isotropic flux of $\psi_{n,L}^{b,k+1} = 1$ cm^{-2} s^{-1} cosine^{-1} on the left boundary, a vacuum on the right boundary, and an initial scalar flux of zero everywhere. The particle speed is $v = 1$ cm/s and we use an S_{16} quadrature set. We run this problem to a final time of $t_f = 4$ s, using time steps of length $\Delta t = 1$ s, 0.1 s, 0.01 s, and 0.001 s. Results for the implicit method are shown in Figure 5.4, for the plain SBJ transport method in Figure 5.5, and for the conservative SBJ transport method in Figure 5.6. Figure 5.4 shows that the implicit results are accurate for every time

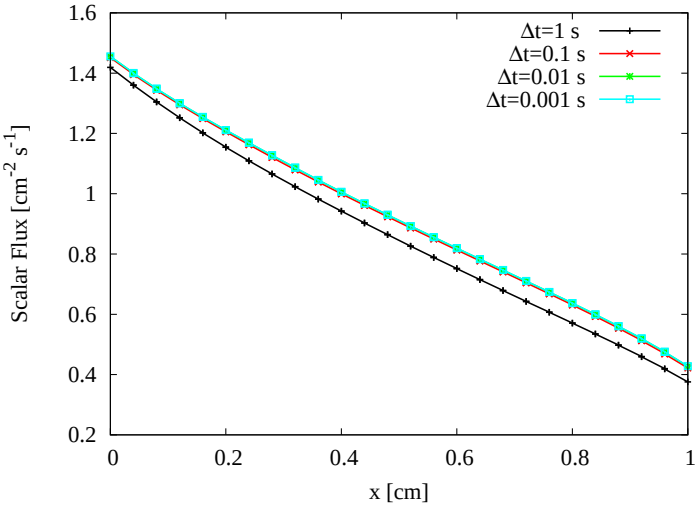

Figure 5.4 Transport Problem 2: Implicit Results at $t = 4$ s

step length except $\Delta t = 1$ s. Figure 5.5 shows that the SBJ transport results are accurate for time steps of length $\Delta t = 0.01$ s and $\Delta t = 0.001$ s. We can also see, in Figure 5.5, how the SBJ transport method imposes an artificial limit on the speed at which particles can flow through the problem per time step. This is necessarily true for all "local" methods. For $\Delta t = 1$ s, four time steps are performed. This allows particles to travel only five cells into the problem (two cells from the boundary for the first time step, one cell for each additional time step). In Figure 5.6, we see that the rebalance can significantly reduce the accuracy of the SBJ transport results when the method fails to capture the correct solution shape.

From the equations derived in Appendix A.2, we show in Table 5.2 the particle wave location after the first time step for various values of Δt. Again, we can see that as the distance the particle wave moves during a time step becomes small relative to the size of a

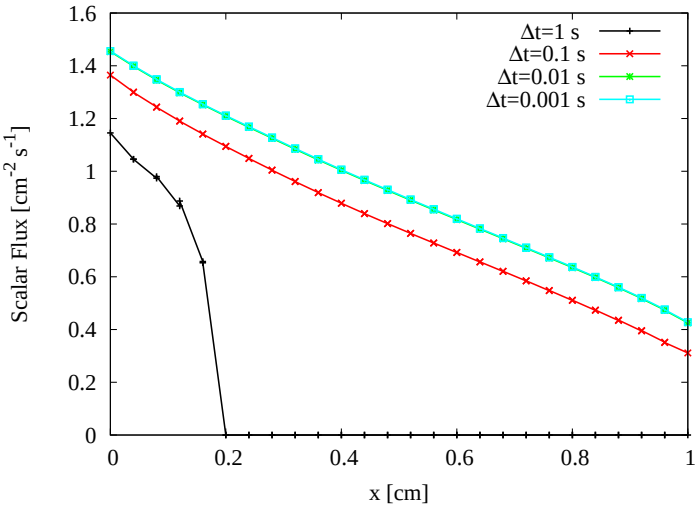

Figure 5.5 Transport Problem 2: Plain SBJ Results at $t = 4$ s

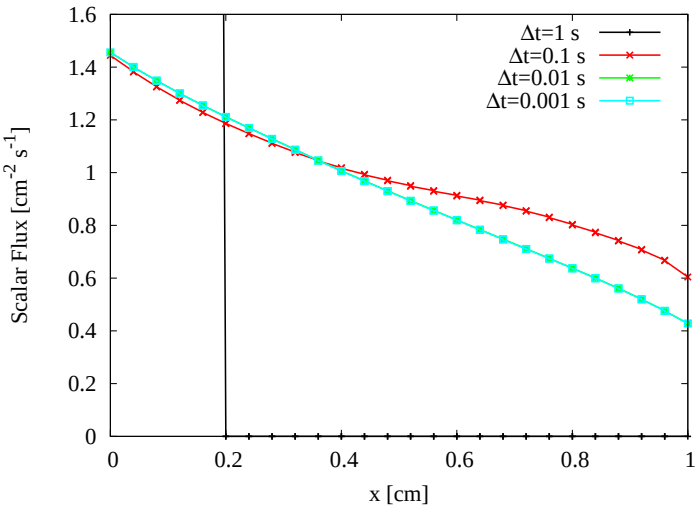

Figure 5.6 Transport Problem 2: Conservative SBJ Results at $t = 4$ s

Δt [s]	Wave Location [cm]	Wave Location [cell widths]
1	2.96783×10^{-1}	7.419575
0.1	3.29223×10^{-2}	0.8230575
0.01	3.32917×10^{-3}	0.08322925
0.001	3.33292×10^{-4}	0.0083323

Table 5.2 Transport Problem 2: Particle Wave Location at End of First Time Step

cell, the SBJ transport method becomes accurate.

5.3 Transport Problem 3: Various Homogeneous, Purely Scattering Slabs

In the previous two problems, we examined an optically-thick and an optically-thin problem, and we observed how the SBJ transport method converges as Δt is reduced such that the particle wave passes through a fraction of a cell per time step. In this problem, we generalize these results across a spectrum of optical thicknesses. Therefore, we consider a purely scattering slab of material 1 cm wide, divided into 100 cells. We run a series of problems, varying the total cross section as $\Sigma_t = 10^{\varepsilon}$ cm^{-1}, with $\varepsilon = -2 \ldots 6$. We place a reflecting boundary on the left and a vacuum boundary on the right, and an initial scalar flux of zero everywhere. In the first cell on the left, we place an isotropic source of $Q = 1$ cm^{-3} s^{-1}. We use an S_4 quadrature set, and execute a single time step of length $\Delta t = 1$ s using the implicit and SBJ transport methods. We compare these results to a benchmark calculation using the implicit method with a time step length of $\Delta t = 10^{-8}$ s. The benchmark results are shown in Figures 5.7 and 5.8. The "bumps" in the $\Sigma_t = 10^0$ cm^{-1} and $\Sigma_t = 10^{-2}$ cm^{-1} solutions in Figure 5.7 are due to ray effects.

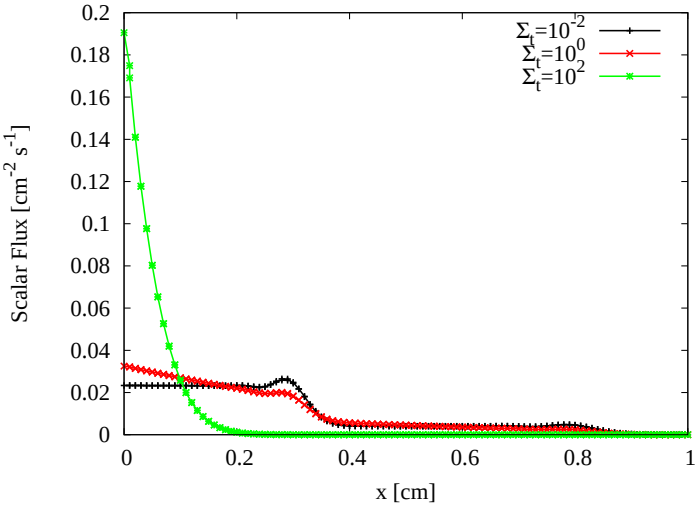

Figure 5.7 Transport Problem 3: Benchmark Results for the Optically-Thin Problems at $t = 1$ s

We analyze the implicit and SBJ transport results by calculating the relative L_1 error

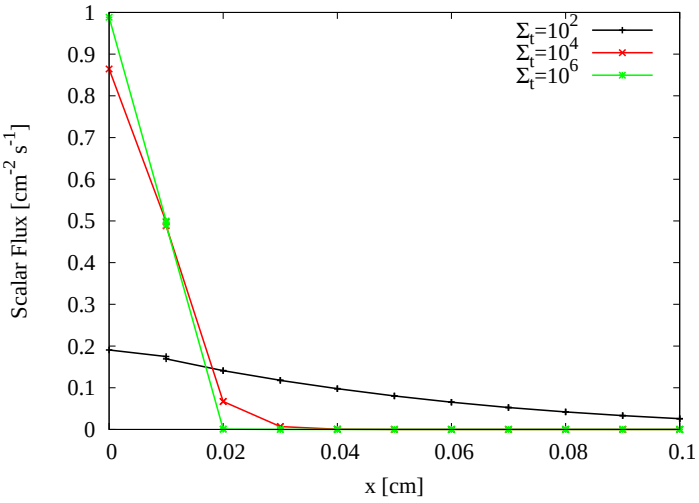

Figure 5.8 Transport Problem 3: Benchmark Results for the Optically-Thick Problems at $t = 1$ s

between the implicit or SBJ solutions and the benchmark solutions, using the definition

$$E_{L_1} = \frac{\sum_{i=1}^{I} \left| \phi_i^{k+1} - \phi_i^{k+1,benchmark} \right| \Delta x_i}{\sum_{i=1}^{I} \phi_i^{k+1,benchmark} \Delta x_i}, \tag{5.1}$$

where

$$\phi_i^{k+1} = \frac{\phi_{i,L}^{k+1} + \phi_{i,R}^{k+1}}{2}, \tag{5.2a}$$

and

$$\phi_i^{k+1,benchmark} = \frac{\phi_{i,L}^{k+1,benchmark} + \phi_{i,R}^{k+1,benchmark}}{2}. \tag{5.2b}$$

The L_1 error for the implicit, plain SBJ, and conservative SBJ transport methods is shown in Figures 5.9 and 5.10. We see from Figure 5.9 that the SBJ transport method is accurate for optically-thick problems (where the wave speed is slow), and inaccurate for optically-thin problems. From Figure 5.10 we see that conservation either improves or leaves mostly unchanged the accuracy of the results for the optically-thick problems, while dramatically reducing the accuracy for the optically-thin problems. These results conform to what we found for numerical problems 1 and 2.

Using the equations derived in Appendix A.2, we calculate the distance the particle wave travels during the time step versus Σ_t for these various problems. These results are presented in Table 5.3. Comparing the data in Table 5.3 with the results in Figures 5.9 and 5.10, we

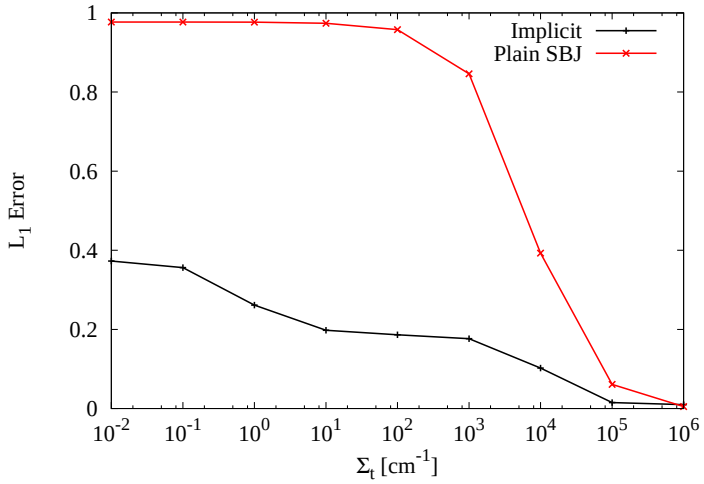

Figure 5.9 Transport Problem 3: L_1 Error for the Implicit and Plain SBJ Methods

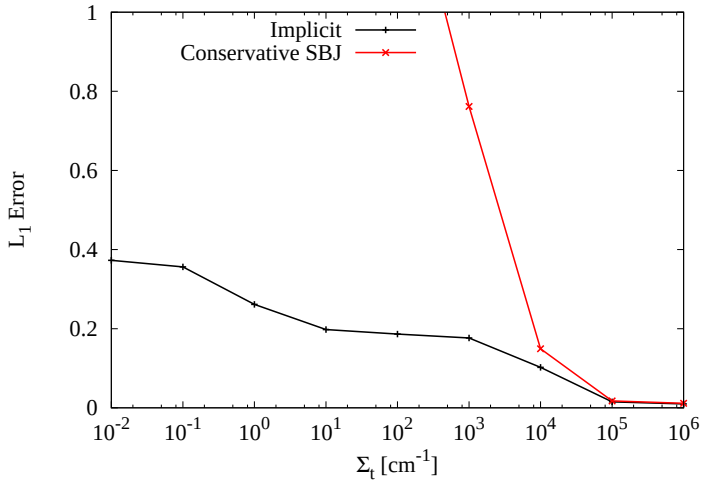

Figure 5.10 Transport Problem 3: L_1 Error for the Implicit and Conservative SBJ Methods

Σ_t [cm^{-1}]	Wave Location [cm]	Wave Location [cell widths]
10^6	5.7735×10^{-4}	0.0577
10^5	1.82572×10^{-3}	0.183
10^4	5.77293×10^{-3}	0.577
10^3	1.82392×10^{-2}	1.82
10^2	5.71606×10^{-2}	5.72
10^1	1.65328×10^{-1}	16.5
10^0	2.96783×10^{-1}	29.7
10^{-1}	3.29223×10^{-1}	32.9
10^{-2}	3.32917×10^{-1}	33.3

Table 5.3 Transport Problem 3: Particle Wave Location After the Time Step for Various Thicknesses

see that the SBJ transport method is accurate when the wave penetrates no more than about 20% of a cell width per time step (corresponding to $\Sigma_t = 10^5$ cm^{-1} for this problem). This matches the SBJ diffusion results we found in Chapter 2.

In Section 3.4.4, we introduced the idea of improving the accuracy of the SBJ transport method by coupling it to a sweep. The sweep captures the uncollided component of the solution for the time step. The L_1 error for the plain SBJ transport method with a sweep is shown in Figure 5.11, and the conservative SBJ transport with a sweep is shown in Figure 5.12. In Figures 5.11 and 5.12, we see that adding a sweep significantly reduces the error in the scalar flux for optically-thin problems, while maintaining the accuracy in

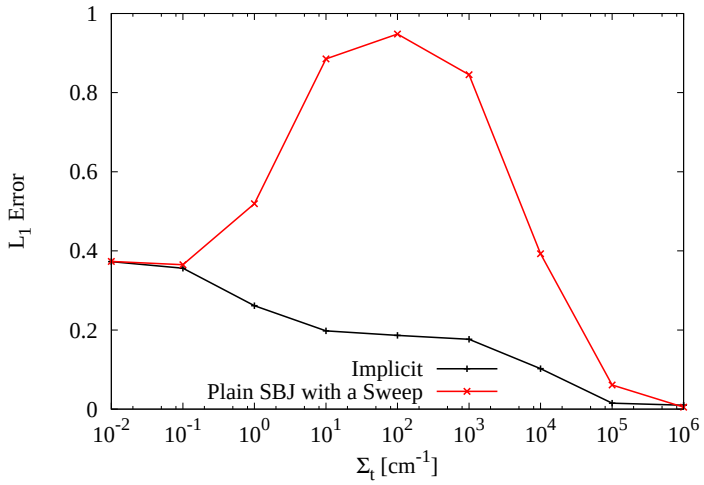

Figure 5.11 Transport Problem 3: L_1 Error for the Implicit and Plain SBJ with a Sweep Methods

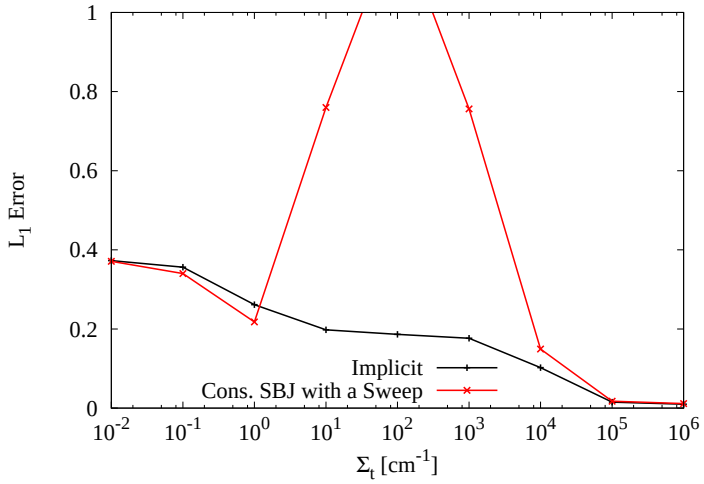

Figure 5.12 Transport Problem 3: L_1 Error for the Implicit and Conservative SBJ with a Sweep Methods

the optically-thick problems. However, the error is still large in intermediate thickness problems.

Finally, as discussed in Section 3.4.4, we can apply an asymptotic stretching and angular redistribution to the sweep. The results for the plain SBJ transport method with a stretched sweep is shown in Figure 5.13, and the results for the conservative SBJ transport method with a stretched sweep is shown in Figure 5.14. Comparing Figures 5.13 and 5.14 with Figures 5.11 and 5.12, respectively, we can see that the stretching significantly reduces the

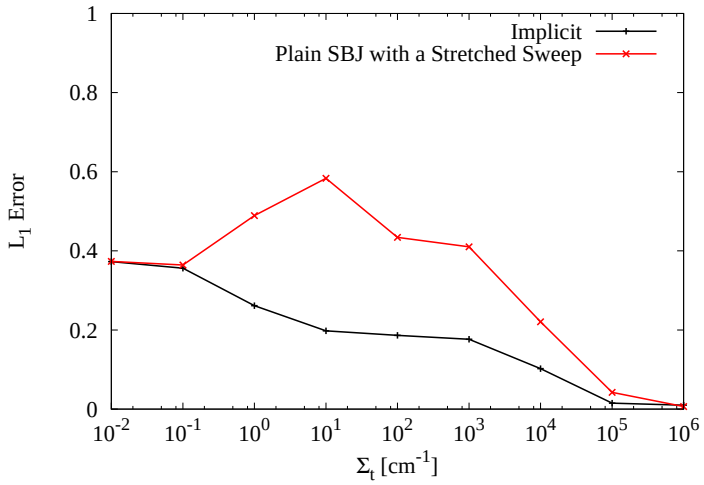

Figure 5.13 Transport Problem 3: L_1 Error for the Implicit and Plain SBJ with a Stretched Sweep Methods

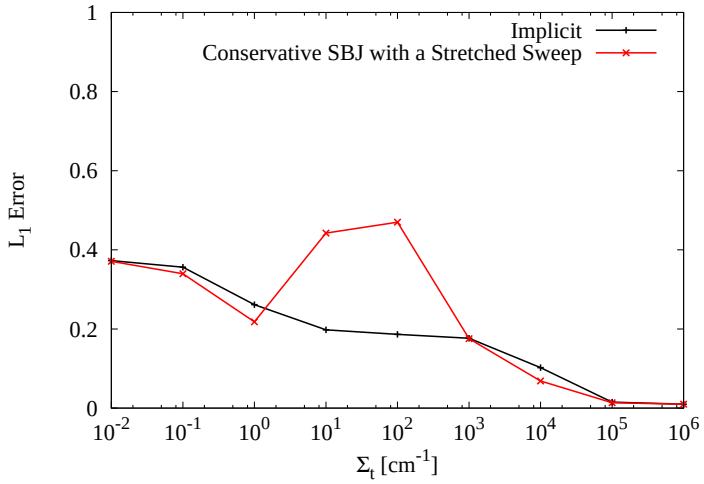

Figure 5.14 Transport Problem 3: L_1 Error for the Implicit and Conservative SBJ with a Stretched Sweep Methods

error in intermediate thickness problems.

In Section 3.4.3, we discussed using the SBJ transport method in an iterative scheme by iteratively updating the incident angular flux on each block. In so doing, we can converge the SBJ transport solution to the implicit solution for any time step length. This also ensures that the SBJ transport solution maintains cell-wise particle conservation, if that is deemed necessary. In Table 5.4, we show the number of iterations that the Modified Four-Step

Σ_t [cm^{-1}]	Implicit	Plain SBJ	Rebalanced SBJ
10^6	4	4	4
10^5	4	6	6
10^4	5	16	13
10^3	7	82	65
10^2	12	350	270
10^1	9	549	425
10^0	8	441	498
10^{-1}	6	294	697
10^{-2}	5	270	697

Table 5.4 Transport Problem 3: Number of Iterations Required for Convergence for the Implicit, Plain SBJ, and Conservative SBJ Methods

Diffusion Synthetic Acceleration (DSA) accelerated implicit method needs to converge to an L_2 error of 10^{-6}, along with the number of iterations used to converge the plain SBJ and rebalanced SBJ transport methods to the implicit solution, also with an L_2 error of 10^{-6}. We

derived the Modified Four-Step DSA method in Appendix B.2. We see in Table 5.4, that the SBJ transport method requires few iterations for optically-thick problems, but a large number of iterations to converge to the implicit result when the problems are optically thin. Rebalance reduces the number of iterations for thick and intermediate problems, but greatly increases the number of iterations for optically-thin problems. This conforms to the results in Figures 5.9 and Figures 5.10, where we found that rebalance improves the accuracy of thick problems, but degrades optically-thin problems. (Because rebalance degrades the optically-thin results, more iterations are required to converge.) It is worth noting that, though the number of iterations for optically-thin problems is large relative to the number of iterations required by the implicit method, a single SBJ iteration may be (depending upon the particular problem and the computer hardware) significantly faster than a single source iteration. The reason for this is that a single source iteration requires sweeping the entire mesh in every angle. A single SBJ iteration requires solving the SBJ equations in each block. However, because the blocks are decoupled, they may be solved in parallel. It may therefore be possible to execute several SBJ iterations in the time it takes to execute a single source iteration.

Therefore, we will pause here to offer some analysis of the respective speed (in mathematical operations) of the implicit method versus the SBJ transport method. Let M equal the number of operations required to solve a 2×2 matrix system. A mesh sweep requires the solution to a 2×2 matrix system in each cell for each angle in the quadrature set. Thus, the total computational expense for calculating the angular flux during a single mesh sweep is

$$C_{\psi}^{sweep} = MNI\,, \tag{5.3}$$

where N is the number of angles in the quadrature set and I is the number of cells in the problem. Calculating the scalar flux in each cell requires summing the product of the angular fluxes and the quadrature weights (two operations per angle). Therefore, with two scalar fluxes in each cell, the total cost of calculating the scalar flux in every cell during a mesh sweep is

$$C_{\phi}^{sweep} = 4NI\,. \tag{5.4}$$

The total computational cost of a single mesh sweep is

$$C^{sweep} = C_{\phi}^{sweep} + C_{\psi}^{sweep} = (M+4)NI\,. \tag{5.5}$$

We note that this underestimates the total computational cost of an iteration for the implicit method because it neglects the cost of the DSA.

For the SBJ method, we first calculate the scalar flux in each block, which involves solving a 4×4 system of equations. Since calculating dense matrix solutions is an $O(n^3)$ operation for an $n \times n$ matrix [24], we expect the total computational cost for calculating the scalar fluxes in $(I+1)$ blocks to be

$$C_{\phi}^{SBJ} = 8M(I+1)\,. \tag{5.6}$$

Calculating the angular fluxes requires the solution to a 2×2 system of equations (since the angular fluxes adjacent to the block boundaries are discarded, they need not be calculated) in each block and in each angle. Therefore, the computational cost for calculating all of the angular fluxes is

$$C_{\psi}^{SBJ} = MN(I+1)\,. \tag{5.7}$$

Therefore, the total computational cost of a single SBJ iteration is

$$C^{SBJ} = C_{\phi}^{SBJ} + C_{\psi}^{SBJ} = M(8+N)(I+1)\,. \tag{5.8}$$

The ratio between the SBJ computational cost and the implicit computational cost is

$$\begin{aligned} \frac{C^{SBJ}}{C^{sweep}} &= \frac{M(8+N)(I+1)}{(M+4)NI} \\ &= \left(\frac{M}{M+4}\right)\left(\frac{8+N}{N}\right)\left(\frac{I+1}{I}\right). \end{aligned} \tag{5.9}$$

Both M and N are small and I is large. Obviously, this does not include the cost of constructing the matrices, which is small for the implicit method, but $O(N)$ for the SBJ method because the matrix $\underline{\underline{A}}_{n,i+1/2}^{k+1}$ must be summed for every angular ordinate. Nevertheless, overall the difference in the computational costs between these two methods is modest. For a large parallel machine, the SBJ method must be faster than the implicit method because the expense of mathematical operations is negligible compared to the expense of cache misses and interprocessor communication. On modern hardware, the time required to perform a floating point operation is measured in hundreds of picoseconds, whereas DRAM memory latency is measured in tens of nanoseconds [16]. Therefore, methods that exhibit large amounts of spatial locality will have fewer cache misses, and improved performance, even if the number of mathematical operations is greater. The implicit method will suffer many more cache misses because mesh sweeps require striding across memory. Because modern hardware is virtually always bandwidth limited, as opposed to computationally limited, increased mathematical complexity is usually preferred if it leads to improved parallelism

and improved cache efficiency. Moreover, because the SBJ method is a Jacobian method, parallelism is trivial in comparison to the implicit method, and therefore load scheduling such that all processors are kept active is easily achieved. We believe that the SBJ transport method will be even more competitive in energy-dependent problems. We discuss this further in Chapter 8.

Since the fully-explicit transport method is also a local method, one might also consider whether it may be more efficient than the SBJ method. The answer is that it might, in fact, be preferable for optically-thin problems, but not for optically-thick problems. It is well-known that the fully-explicit method has a stability condition of $O(\frac{\Delta x}{v})$. Therefore, for this problem, a time step length of about $\Delta t = 0.01$ s would be required to preserve numerical stability, and a total of 100 time steps would be required to reach the final simulation time of $t_f = 1$ s. Since, at the end of each time step or iteration, the solution must be communicated to neighboring processors, the fully-explicit method would require 100 interprocessor communications. This exceeds the number of interprocessor communications needed by the SBJ method for $\Sigma_t = 10^3$ cm^{-1} and thicker problems, since, according to Table 5.4, fewer than 100 iterations are required to converge these problems. Since interprocessor communication is far more expensive than the mathematical operations themselves, the fully-explicit method will not be more efficient than the SBJ method for optically-thick problems.

Returning to the numerical results, we show, in Table 5.5, the number of iterations required to converge the plain and rebalanced SBJ transport methods when coupled with a sweep. The numbers in parenthesis indicate the difference in iterations between the

Σ_t [cm^{-1}]	Implicit	Plain SBJ with Sweep	Rebalanced SBJ with Sweep
10^6	4	4	4
10^5	4	6	6
10^4	5	16	13
10^3	7	82	65
10^2	12	350	264 (-6)
10^1	9	544 (-5)	281 (-144)
10^0	8	414 (-27)	401 (-97)
10^{-1}	6	254 (-40)	401 (-296)
10^{-2}	5	182 (-88)	301 (-396)

Table 5.5 Transport Problem 3: Number of Iterations Required for Convergence for the Implicit, Plain SBJ with Sweep, and Rebalanced SBJ with Sweep Methods (number in parenthesis indicates difference in iteration count versus SBJ without sweep)

SBJ method with and without sweeps. Here we see that the sweep reduces the number of iterations necessary to converge the optically-thin problems, while the rapid convergence of

the optically-thick problems is preserved.

Finally, in Tables 5.6 and 5.7, we show the number of iterations required to converge the plain and rebalanced SBJ transport methods when coupled to a stretched sweep, respectively.

Σ_t [cm^{-1}]	Implicit	Plain SBJ with Stretched Sweep
10^6	4	4
10^5	4	6
10^4	5	15 (-1)
10^3	7	78 (-4)
10^2	12	328 (-22)
10^1	9	524 (-20)
10^0	8	401 (-13)
10^{-1}	6	200 (-54)
10^{-2}	5	200 (+18)

Table 5.6 Transport Problem 3: Number of Iterations Required for Convergence for the Implicit and Plain SBJ with Stretched Sweep Methods (number in parenthesis indicates difference in iteration count versus plain SBJ with unstretched sweep)

Σ_t [cm^{-1}]	Implicit	Rebalanced SBJ with Stretched Sweep
10^6	4	3 (-1)
10^5	4	5 (-1)
10^4	5	12 (-1)
10^3	7	61 (-4)
10^2	12	255 (-9)
10^1	9	255 (-26)
10^0	8	398 (-3)
10^{-1}	6	401
10^{-2}	5	301

Table 5.7 Transport Problem 3: Number of Iterations Required for Convergence for the Implicit and Rebalanced SBJ with Stretched Sweep Methods (number in parenthesis indicates difference in iteration count versus rebalanced SBJ with unstretched sweep)

The numbers in parenthesis indicate the difference in the iteration count between the SBJ methods with stretched sweeps and with unstretched sweeps, with and without rebalance. We see that stretching the sweep provides a modest reduction in the number of iterations required for convergence, except for the $\Sigma_t = 10^{-2}$ cm^{-1} case without rebalance, where the stretched sweep causes a slight increase in the number of iterations required. Overall, stretching the sweep is a simple and straightforward way to improve the sweeps.

Comparing the number of iterations required for the SBJ transport method coupled to a

sweep, shown in Tables 5.5, 5.6, and 5.7, with the L_1 errors in Figures 5.11–5.14, we observe the curious result that, though the L_1 errors for the non-iterative SBJ coupled to a sweep are small for optically-thin problems, the number of iterations required for convergence is still large. There are two reasons for this. The first is that the L_1 errors represent the errors between the benchmark scalar flux and the SBJ scalar flux. However, after conducting a single sweep, though the particles may be close to their correct spatial distribution, the angular distribution is incorrect. This is important because it is the angular distribution (the angular flux) of the particles that is iterated upon in the SBJ transport method. This is mitigated somewhat by the angular redistribution method discussed in Section 3.4.4. Secondly, the number of iterations is large due to the unusual way that the SBJ transport method converges to the solution.

Because the blocks are decoupled, the solution tends to converge in "waves." In Figures 5.15 and 5.16, we show the solution to the $\Sigma_t = 100$ cm^{-1} problem for the rebalanced SBJ method coupled to an unstretched sweep, at iteration 10 and 50. Here we can see that an imperfect spatial and angular distribution of particles from the sweep creates an "error wave" that flows through the problem, moving one cell per time step. These waves can be exacerbated by rebalance. Multiple waves of this type move through the problem, and the iterations will not converge until the waves are either attenuated or travel out of the problem domain. Future work on acceleration techniques for the SBJ transport method should seek a way to dampen these waves.

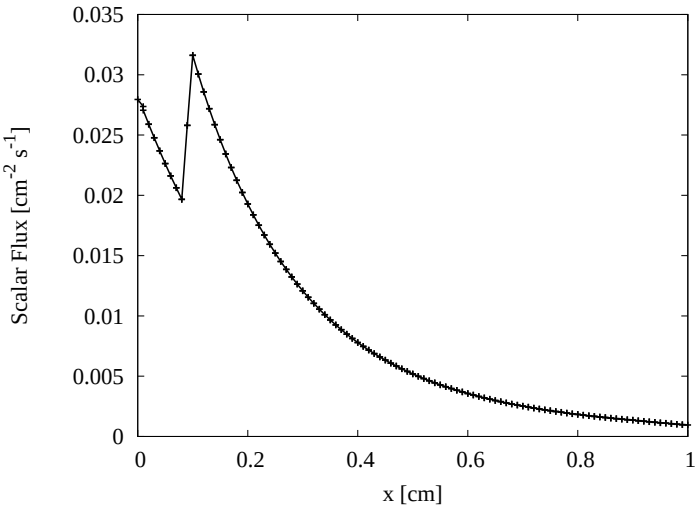

Figure 5.15 Transport Problem 3: SBJ Transport Error Wave at Iteration 10

Observing the L_1 errors from the implicit results, shown in Figure 5.9, we see that the implicit method produces results with small errors, relative to the benchmark calculations,

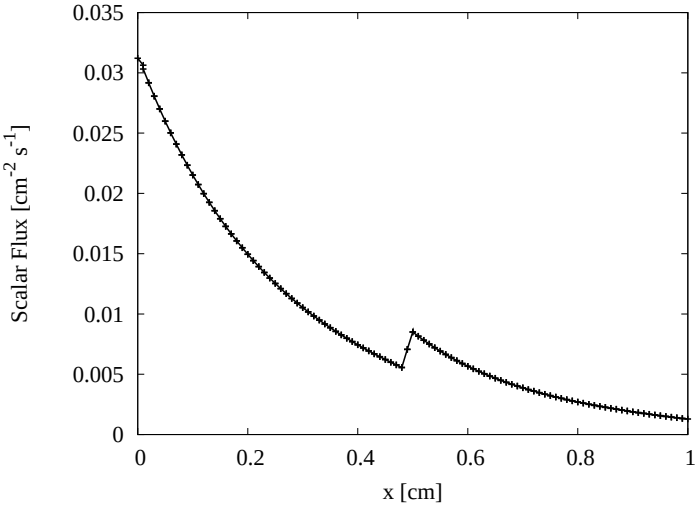

Figure 5.16 Transport Problem 3: SBJ Transport Error Wave at Iteration 50

for optically-thick problems, while the errors for optically-thin problems are relatively large (almost 40%). Therefore, we have not chosen a very "realistic" time step length ($\Delta t = 1$ s) for the optically-thin problems. Let us choose a time step length such that the implicit method produces L_1 errors around 10% compared to the benchmark solutions at $t = 1$ s. The time steps required are shown in Table 5.8. Here we have excluded $\Sigma_t = 10^4$ cm^{-1}, $\Sigma_t = 10^5$ cm^{-1}, and $\Sigma_t = 10^6$ cm^{-1}, since the implicit method produces errors of around 10% or less with the original time step length of $\Delta t = 1$ s.

Σ_t [cm^{-1}]	Time Step Length [s]	L_1 Error [%]
10^3	0.5	9.96
10^2	0.5	10.54
10^1	0.3333	8.06
10^0	0.1	9.18
10^{-1}	0.03333	10.07
10^{-2}	0.03333	10.74

Table 5.8 Transport Problem 3: Time Step Length Required for Approximately 10% L_1 Error for the Implicit Method

In Table 5.9, we show the wave location after the first time step for each of these problems. In Table 5.10, we show the number of iterations required to converge the SBJ transport method, with and without rebalance, for the time step requiring the most iterations, to an L_2 error of 10^{-6}. We show the same data for the SBJ transport method with unstretched sweeps,

Σ_t [cm^{-1}]	Time Step Length [s]	Wave Location [cm]	Wave Location [cell widths]
10^3	0.5	0.01288	1.288
10^2	0.5	0.04002	4.002
10^1	0.3333	0.07983	7.983
10^0	0.1	0.03292	3.292
10^{-1}	0.03333	0.01111	1.111
10^{-2}	0.03333	0.01111	1.111

Table 5.9 Transport Problem 3: Particle Wave Location After the First Time Step

Σ_t [cm^{-1}]	Implicit Method	Plain SBJ	Rebalanced SBJ
10^3	7	43	34
10^2	11	171	131
10^1	8	184	126
10^0	5	85	100
10^{-1}	4	29	31
10^{-2}	3	29	31

Table 5.10 Transport Problem 3: Number of Iterations for the 10% Error Runs, for the Implicit, Plain SBJ and Rebalanced SBJ Methods

Σ_t [cm^{-1}]	Implicit Method	Plain SBJ with Sweep	Rebalanced SBJ with Sweep
10^3	7	43	34
10^2	11	171	129 (-2)
10^1	8	180 (-4)	102 (-24)
10^0	5	58 (-27)	64 (-36)
10^{-1}	4	10 (-19)	10 (-21)
10^{-2}	3	4 (-25)	5 (-26)

Table 5.11 Transport Problem 3: Number of Iterations for the 10% Error Runs, for the Implicit, Plain SBJ with Sweep, and Rebalanced SBJ with Sweep Methods (number in parenthesis indicates difference in iteration count versus SBJ without sweep)

with and without rebalance, in Table 5.11. In this table, the numbers in parenthesis indicate the difference in the iteration count for the SBJ method with and without an unstretched mesh sweep. In Tables 5.12 and 5.13 we show the iteration counts for the SBJ transport method with a stretched sweep, with and without rebalance, respectively. In Tables 5.12 and

Σ_t [cm^{-1}]	Implicit Method	Plain SBJ with Stretched Sweep	
10^3	7	40	(-3)
10^2	11	159	(-12)
10^1	8	177	(-3)
10^0	5	60	(+2)
10^{-1}	4	10	
10^{-2}	3	4	

Table 5.12 Transport Problem 3: Number of Iterations for the 10% Error Runs, for the Implicit, Plain SBJ with Stretched Sweep, and Rebalanced SBJ with Stretched Sweep Methods (number in parenthesis indicates difference in iteration count versus plain SBJ with unstretched sweep)

Σ_t [cm^{-1}]	Implicit Method	Rebalanced SBJ with Stretched Sweep	
10^3	7	33	(-1)
10^2	11	129	
10^1	8	128	(+26)
10^0	5	65	(+1)
10^{-1}	4	10	
10^{-2}	3	5	

Table 5.13 Transport Problem 3: Number of Iterations for the 10% Error Runs, for the Implicit, Plain SBJ with Stretched Sweep, and Rebalanced SBJ with Stretched Sweep Methods (number in parenthesis indicates difference in iteration count versus rebalanced SBJ with unstretched sweep)

5.13, the numbers in parenthesis indicate the difference in iteration counts compared to the SBJ transport method with an unstretched sweep, with and without rebalance, respectively.

Comparing the results shown in Tables 5.10–5.13 with the wave locations shown in Table 5.9, *we again see that the SBJ transport method is reasonably efficient when the particle wave travels about one cell per time step*. As the wave speed increases to multiple cells per time step, the number of iterations required for convergence increases. Sweeps and rebalance help reduce the number of iterations required for most problems, but only modestly. However, for thin problems, the time step length required for accuracy coincides with the time step length required for efficiency. Intermediate thickness problems are still inefficient, however, and may require more advanced iteration acceleration techniques.

5.4 Transport Problem 4: Various Homogeneous $c = 0.9$ Slabs

In the previous problems, we considered purely scattering mediums. However, we also wish to know whether absorption alters the behavior of this method. Therefore, we consider a slab of material 1 cm wide, divided into 100 cells, with a scattering ratio of $c = 0.9$. We run a series of problems, varying the total cross section as $\Sigma_t = 10^{\varepsilon}$ cm^{-1}, with $\varepsilon = -2 \ldots 4$. We place a reflecting boundary on the left and a vacuum boundary on the right, and an initial scalar flux of zero everywhere. In the first cell on the left, we place an isotropic source of $Q = 1$ cm^{-3} s^{-1}. We use an S_4 quadrature set, and execute a single time step of length $\Delta t = 1$ s using the implicit and SBJ transport methods. We compare these results to a benchmark calculation using a time step length of $\Delta t = 10^{-8}$ s. The benchmark results are shown in Figures 5.17 and 5.18. Again, we note that the "bumps" in the optically-thin results are due to ray effects.

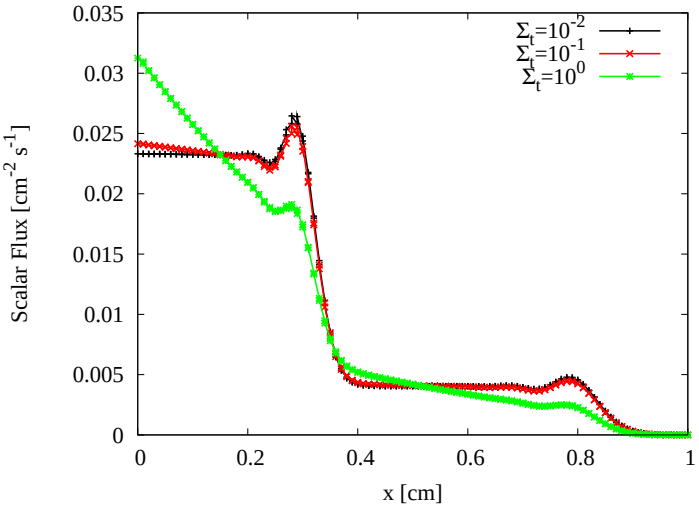

Figure 5.17 Transport Problem 4: Benchmark Results for Optically-Thin Problems

In Table 5.14, we show the wave location at the end of the time step for each of the problems under consideration, calculated from Appendix A.2.1. Comparing the values in Table 5.14 with those in Table 5.3 in Section 5.3, we see that absorption tends to decrease the particle wave speed for optically-thick problems, but has little effect on optically-thin problems. This is expected, since as a problem becomes increasingly absorptive a particle will travel less distance before being absorbed, and so the bulk wave speed is reduced. Therefore, we would generally expect the SBJ method to be more accurate and efficient as the scattering ratio is decreased.

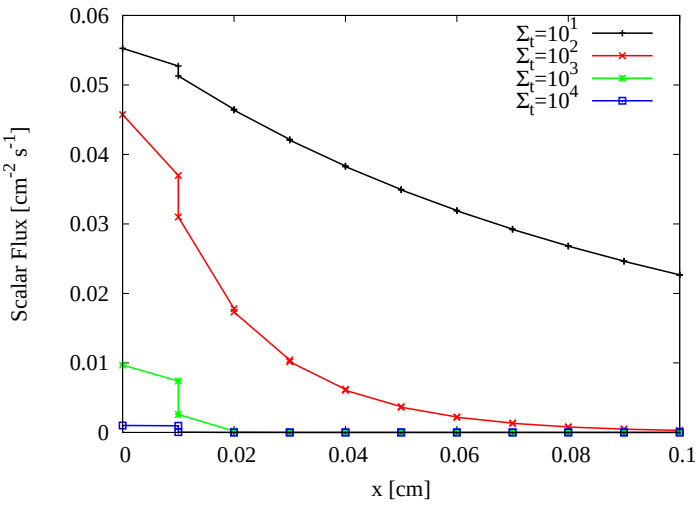

Figure 5.18 Transport Problem 4: Benchmark Results for Optically-Thick Problems

Σ_t [cm^{-1}]	Wave Location [cm]	Wave Location [cell widths]
10^4	0.0002582	0.02582
10^3	0.002582	0.2582
10^2	0.02581	2.581
10^1	0.1550	15.50
10^0	0.2964	29.64
10^{-1}	0.3292	32.92
10^{-2}	0.3329	33.29

Table 5.14 Transport Problem 4: Particle Wave Location at $t = 1$ s

In Figures 5.19 and 5.20, we show the L_1 error of the plain SBJ transport results, and the conservative SBJ transport results, along with the L_1 error for the implicit results. We note that, just as before with the purely scattering problems shown in Section 5.3, as the particle wave speed increases, the error in the SBJ transport solution increases as well. Moreover, while particle conservation improves the accuracy in optically-thick problems, it reduces the accuracy in optically-thin problems. This also conforms to the purely scattering results we found in Section 5.3.

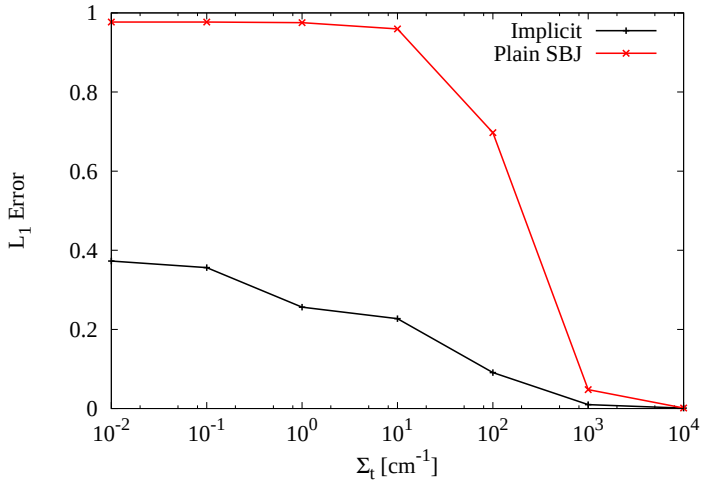

Figure 5.19 Transport Problem 4: L_1 Error for the Implicit and Plain SBJ Methods

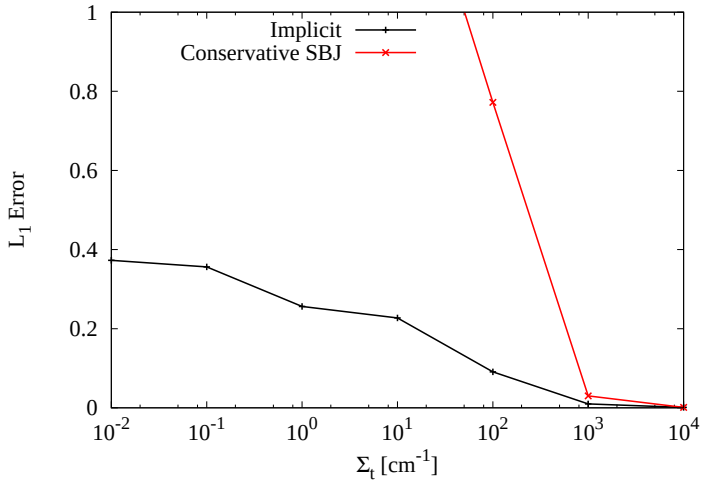

Figure 5.20 Transport Problem 4: L_1 Error for the Implicit and Conservative SBJ Methods

The L_1 error for the plain SBJ with an unstretched sweep, and the conservative SBJ with an unstretched sweep is shown in Figures 5.21 and 5.22. As before with the purely scattering problems, the sweep improves the accuracy of the scalar flux for optically-thin problems. Comparing these results to the results shown in Figures 5.11 and 5.12 in Section 5.3, we see that the sweep is less effective in the purely scattering problem than it is in this problem. This is because sweeps become more accurate as the scattering ratio is reduced, and captures the implicit solution exactly in the case of a purely absorbing problem.

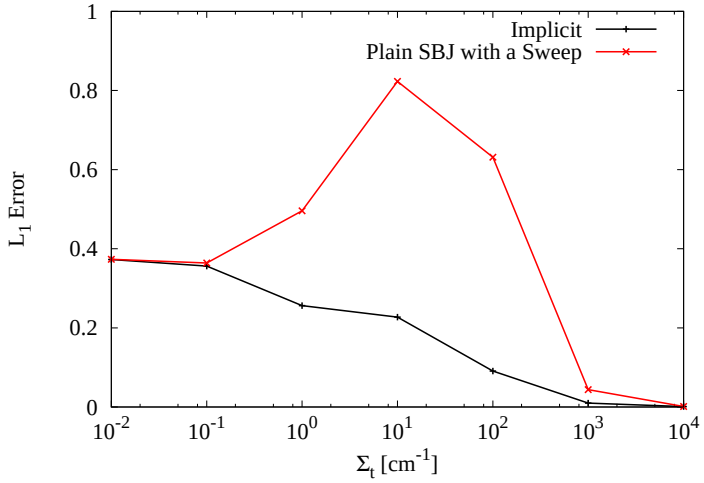

Figure 5.21 Transport Problem 4: L_1 Error for the Implicit and Plain SBJ with Sweep Methods

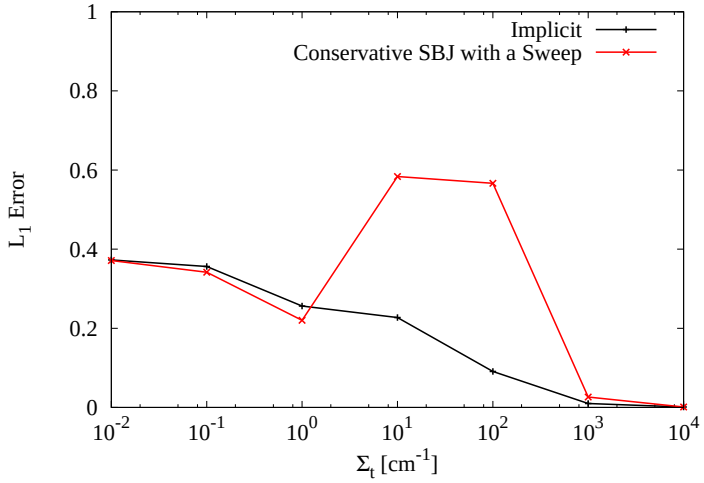

Figure 5.22 Transport Problem 4: L_1 Error for the Implicit and Conservative SBJ with Sweep Methods

The L_1 error for the plain SBJ with a stretched sweep, and the conservative SBJ with a

stretched sweep methods are shown in Figures 5.23 and 5.24. With these results, we see that the stretching has had only a marginal improvement over the unstretched sweep. Further refinements in the stretching parameters might improve these results.

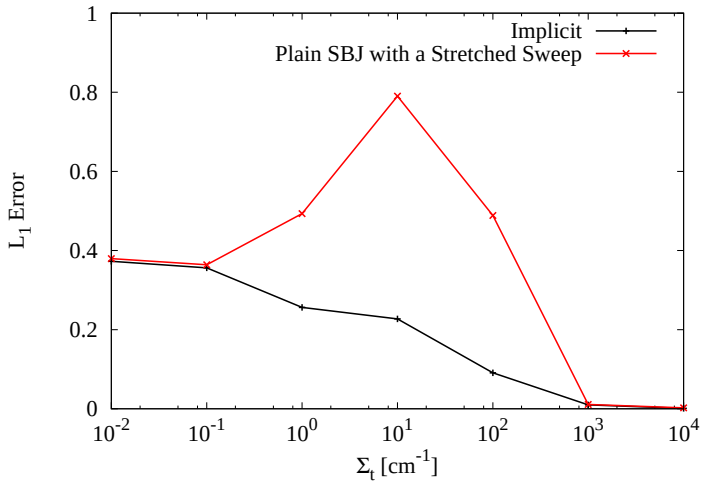

Figure 5.23 Transport Problem 4: L_1 Error for the Implicit and Plain SBJ with Stretched Sweep Methods

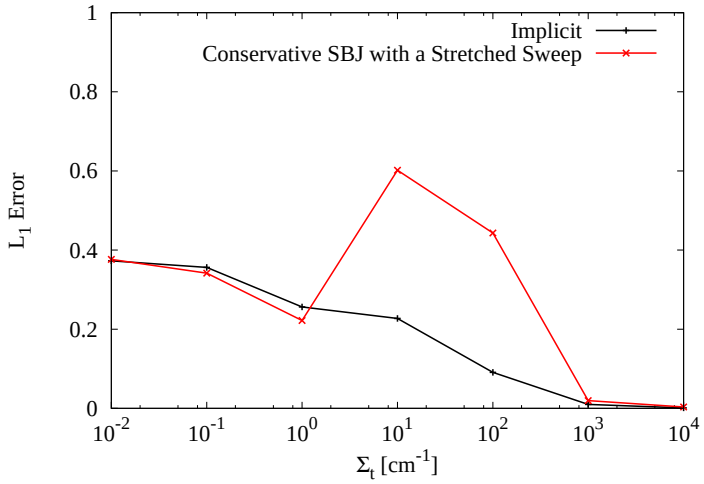

Figure 5.24 Transport Problem 4: L_1 Error for the Implicit and Conservative SBJ with Stretched Sweep Methods

In Tables 5.15–5.18 we show the number of iterations required to converge the SBJ transport method to the implicit results, using an L_2 convergence criteria of 10^{-6}, for the plain SBJ transport method, the SBJ transport method with an unstretched sweep, and the SBJ transport method with a stretched sweep, all with and without rebalance. Comparing

Σ_t [cm^{-1}]	Implicit	Plain SBJ	Rebalanced SBJ
10^4	3	2	2
10^3	5	4	4
10^2	10	34	26
10^1	8	278	199
10^0	8	406	498
10^{-1}	6	293	697
10^{-2}	5	267	697

Table 5.15 Transport Problem 4: Number of Iterations for the Plain and Rebalanced SBJ Methods

Σ_t [cm^{-1}]	Implicit	Plain SBJ with Sweep	Rebalanced SBJ with Sweep
10^4	3	2	2
10^3	5	4	4
10^2	10	33 (-1)	25 (-1)
10^1	8	273 (-5)	142 (-57)
10^0	8	377 (-29)	401 (-97)
10^{-1}	6	200 (-93)	401 (-296)
10^{-2}	5	180 (-87)	301 (-396)

Table 5.16 Transport Problem 4: Number of Iterations for the Plain SBJ with Sweep and Rebalanced SBJ Method with Sweep Methods (number in parenthesis indicates difference in iteration count versus SBJ without sweep)

Σ_t [cm^{-1}]	Implicit	Plain SBJ with Stretched Sweep
10^4	2	3 (+1)
10^3	5	4
10^2	10	32 (-1)
10^1	8	271 (-2)
10^0	8	375 (-2)
10^{-1}	6	199 (-1)
10^{-2}	5	180

Table 5.17 Transport Problem 4: Number of Iterations for the Plain SBJ with Stretched Sweep Method (number in parenthesis indicates difference in iteration count versus plain SBJ with unstretched sweep)

Σ_t [cm^{-1}]	Implicit	Rebalanced SBJ with Stretched Sweep	
10^4	2	3	(+1)
10^3	5	4	
10^2	10	24	(-1)
10^1	8	148	(-2)
10^0	8	397	(-2)
10^{-1}	6	401	(-1)
10^{-2}	5	301	

Table 5.18 Transport Problem 4: Number of Iterations for the Rebalanced SBJ Method with Stretched Sweep Method (number in parenthesis indicates difference in iteration count versus rebalanced SBJ with unstretched sweep)

the iteration counts in Tables 5.15–5.18 with the iteration counts in Tables 5.4–5.7 in Section 5.3, we find that the behavior of the method is similar to that of the $c = 1$ case shown in Section 5.3. Optically-thick problems converge in a small number of iterations, while optically-thin problems require larger numbers of iterations. Rebalance helps reduce the number of iterations in optically-thick problems, but it degrades performance in optically-thin problems. Sweeps reduce the number of iterations required for optically-thin problems by a modest amount. For these $c = 0.9$ problems, stretching has little effect. Overall, we find that absorption has little effect on the SBJ transport method, beyond reducing the particle wave speed.

5.5 Transport Problem 5: Heterogeneous Problems

For our final numerical result, we will examine the behavior of the SBJ transport method for a series of heterogeneous problems. We consider a slab 5 cm wide, divided into 50 cells. The slab is composed of two materials, a purely scattering material with a total cross

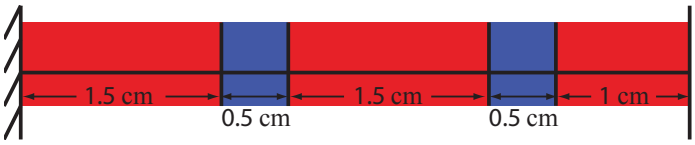

Figure 5.25 Transport Problem 5: Material Layout

section of $\Sigma_t = 10^{\varepsilon}$ cm^{-1}, and a purely absorbing material with a total cross section of $\Sigma_t = 10^{-\varepsilon}$ cm^{-1}, with $\varepsilon = 0 \ldots 3$, arranged as shown in Figure 5.25, where the scattering

material is represented in red and the absorbing material is represented in blue. We place an isotropic source of $Q = 1$ cm^{-3} s^{-1} in the scattering regions, and no source in the absorbing regions. We set the particle velocity at $v = 1$ cm/s, and we apply a reflecting boundary condition on the left, and a vacuum on the right. We also apply an initial scalar flux of zero everywhere. We executed ten time steps with a time step length of $\Delta t = 1$ s.

In Figures 5.26, 5.27, 5.28, and 5.29, we show the results at time $t = 10$ s for the implicit method for $\varepsilon = 0$, 1, 2, and 3, respectively, along with benchmark results created by using the implicit method with a time step length of $\Delta t = 10^{-8}$ s. From these results, we see that

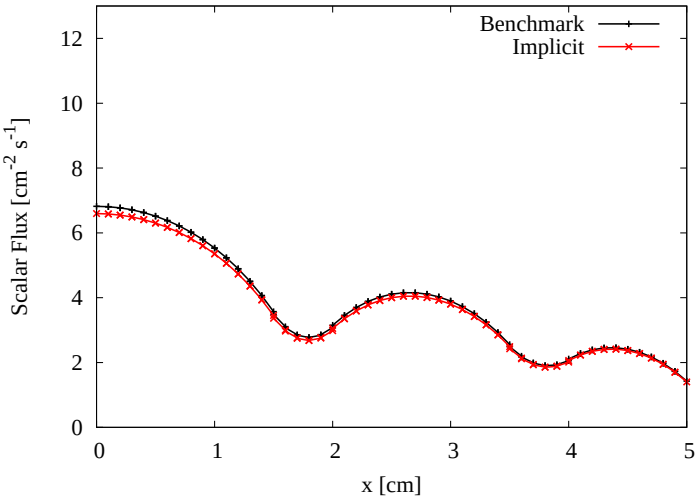

Figure 5.26 Transport Problem 5: Implicit Result for $\varepsilon = 0$ Problem at $t = 10$ s

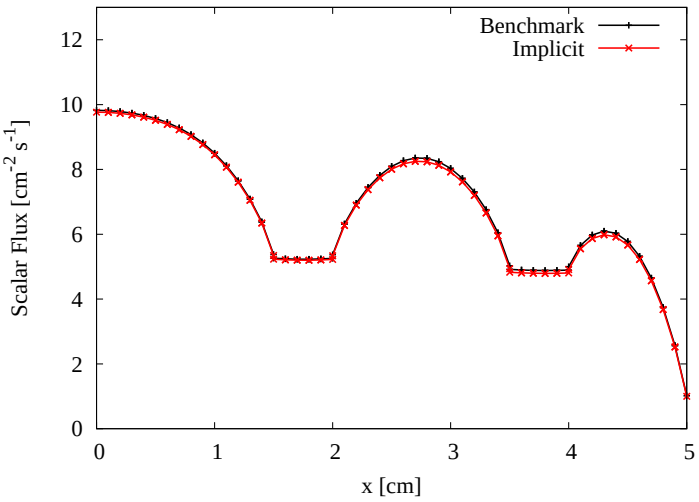

Figure 5.27 Transport Problem 5: Implicit Result for $\varepsilon = 1$ Problem at $t = 10$ s

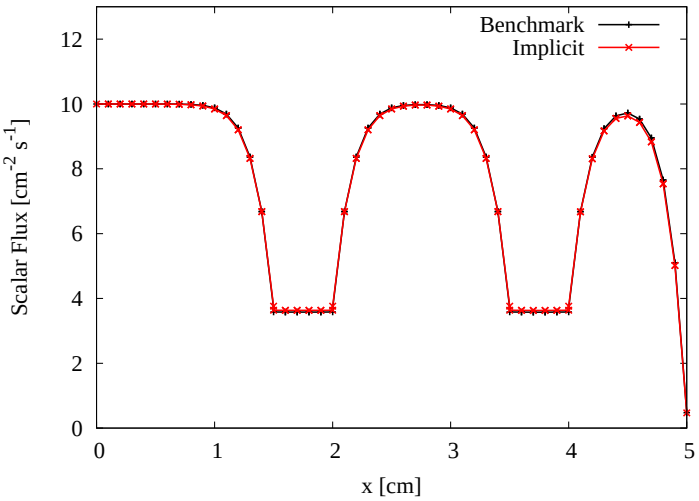

Figure 5.28 Transport Problem 5: Implicit Result for $\varepsilon = 2$ Problem at $t = 10$ s

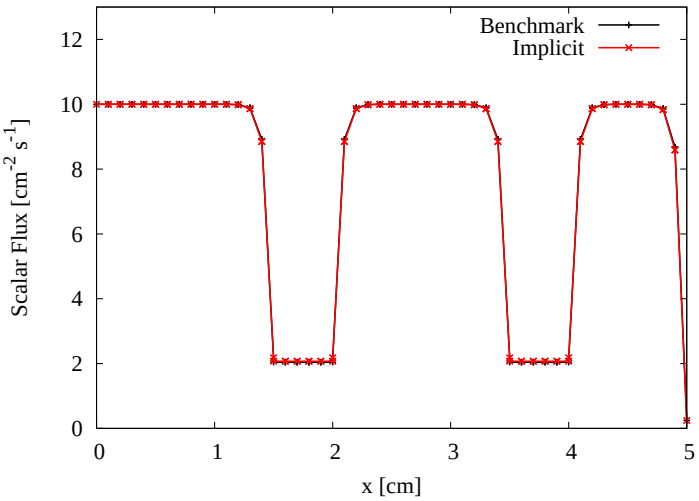

Figure 5.29 Transport Problem 5: Implicit Result for $\varepsilon = 3$ Problem at $t = 10$ s

the implicit method is fairly accurate for each of these problems, with accuracy least in the $\varepsilon = 0$ case, and greatest in the $\varepsilon = 3$ case.

In Figures 5.30–5.33 we show the results for the plain SBJ method for $\varepsilon = 0$, 1, 2, and 3, respectively. Examining these figures, we see that the SBJ transport method converges to

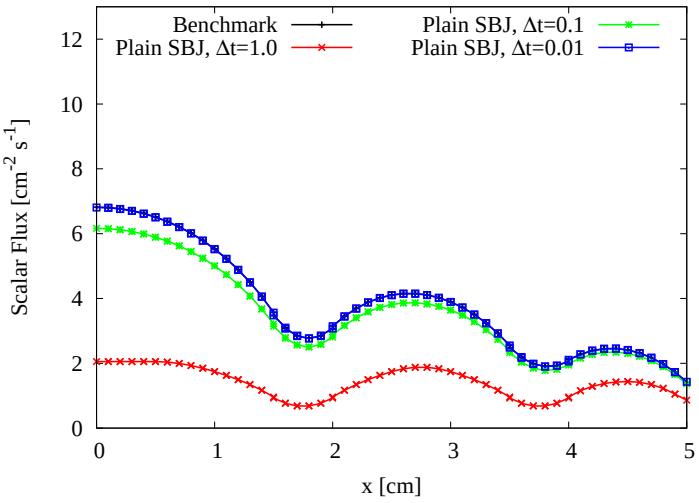

Figure 5.30 Transport Problem 5: Plain SBJ Result for $\varepsilon = 0$ Problem at $t = 10$ s

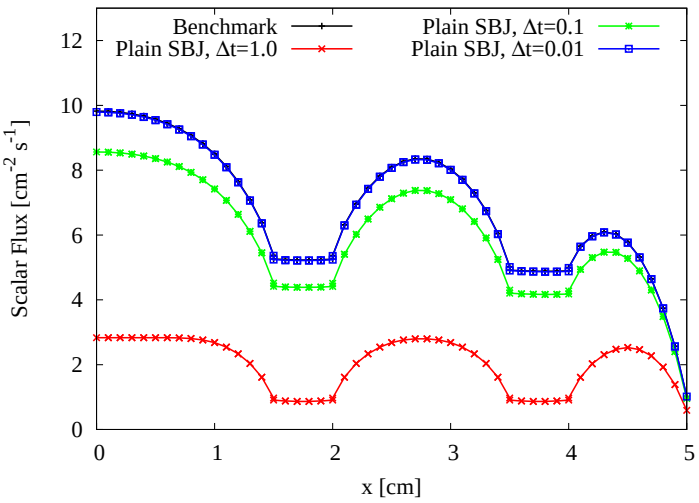

Figure 5.31 Transport Problem 5: Plain SBJ Result for $\varepsilon = 1$ Problem at $t = 10$ s

the benchmark solution for every ε when $\Delta t = 0.001$ s. For $\Delta t = 0.01$ s, the solution is fairly accurate in the most heterogeneous problems ($\varepsilon = 2$ and $\varepsilon = 3$), while being less accurate in the less heterogeneous problems. This is because the scattering material is more optically thick for larger ε, and therefore the wave speed is slower. Additionally, as ε becomes larger,

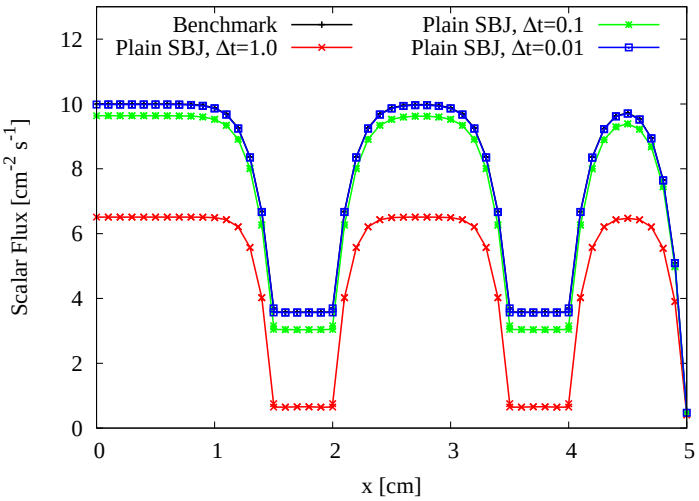

Figure 5.32 Transport Problem 5: Plain SBJ Result for $\varepsilon = 2$ Problem at $t = 10$ s

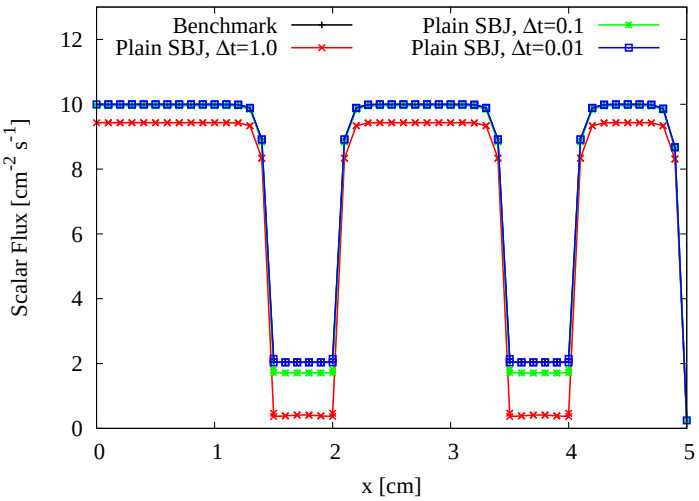

Figure 5.33 Transport Problem 5: Plain SBJ Result for $\varepsilon = 3$ Problem at $t = 10$ s

the amount of coupling between the scattering regions and absorbing regions becomes less, which also allows the SBJ transport method to produce more accurate results.

Results for the conservative SBJ transport method for $\varepsilon = 0$, 1, 2, and 3 are shown in Figures 5.34–5.37. Here we see that particle conservation significantly improves the

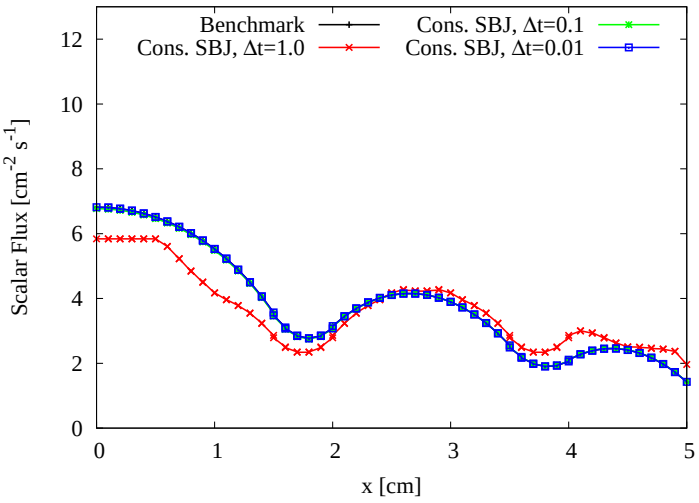

Figure 5.34 Transport Problem 5: Conservative SBJ Result for $\varepsilon = 0$ Problem at $t = 10$ s

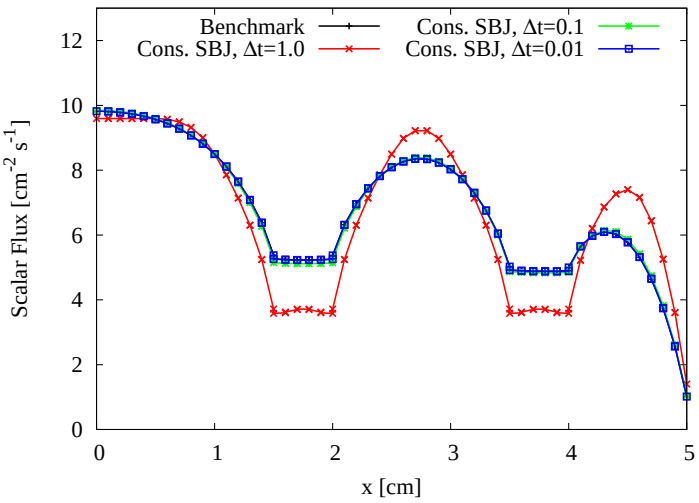

Figure 5.35 Transport Problem 5: Conservative SBJ Result for $\varepsilon = 1$ Problem at $t = 10$ s

accuracy of these results, such that the $\varepsilon = 0$ and $\varepsilon = 1$ problems, which were the least accurate for the plain SBJ case, are now converged with a time step of $\Delta t = 0.1$ s. Results for $\varepsilon = 2$ and $\varepsilon = 3$ are also improved. The reason that particle conservation works well for these problems is because the SBJ transport method is able to capture the basic shape of

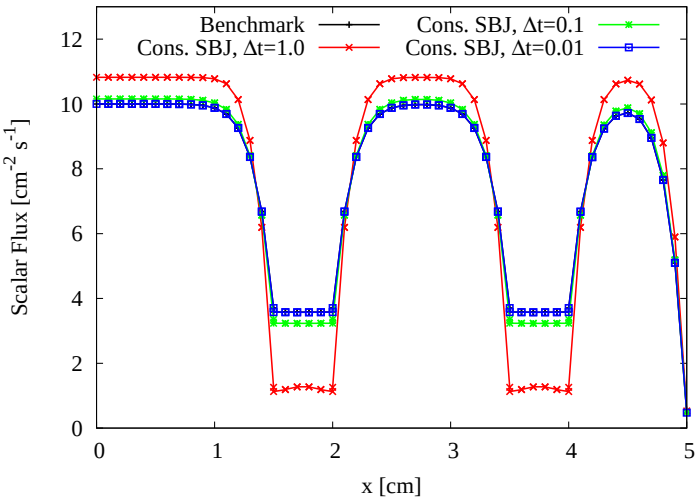

Figure 5.36 Transport Problem 5: Conservative SBJ Result for $\varepsilon = 2$ Problem at $t = 10$ s

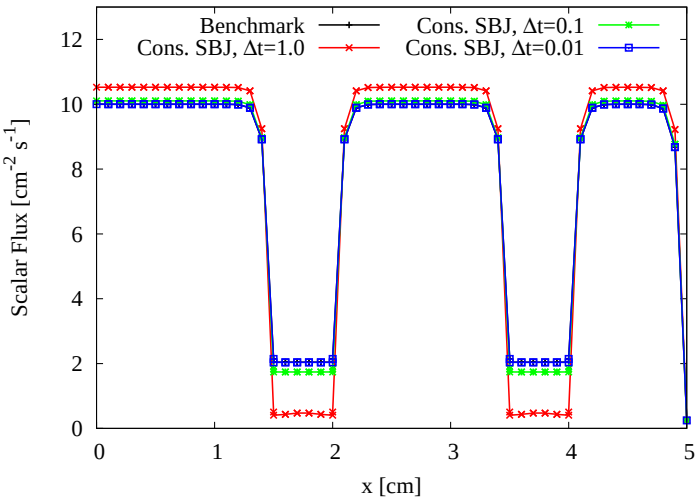

Figure 5.37 Transport Problem 5: Conservative SBJ Result for $\varepsilon = 3$ Problem at $t = 10$ s

the solution reasonably accurately. The conservation then ensures that the solution has the correct amplitude. This is in contrast with the problems shown previously, where a wave of particles was traveling through a slab, and the SBJ transport method could not move the particle wave with the correct speed. This resulted in an incorrect solution shape, which the particle conservation rebalance was unable to correct.

In Figures 5.38–5.41, we show the number of iterations required to converge the SBJ transport method (with and without stretched or unstretched sweeps), without rebalance, to the implicit solution, for an L_2 convergence criteria of 10^{-6}. Here we see that, for all of

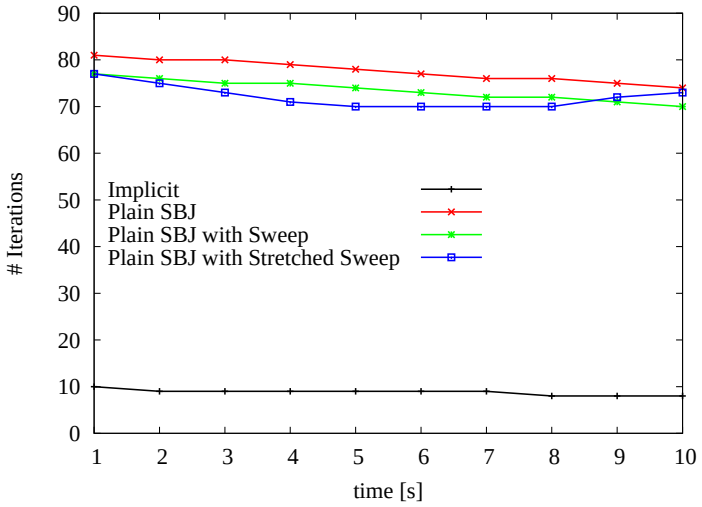

Figure 5.38 Transport Problem 5: Iterations for the Plain SBJ Method for the $\varepsilon = 0$ Problem

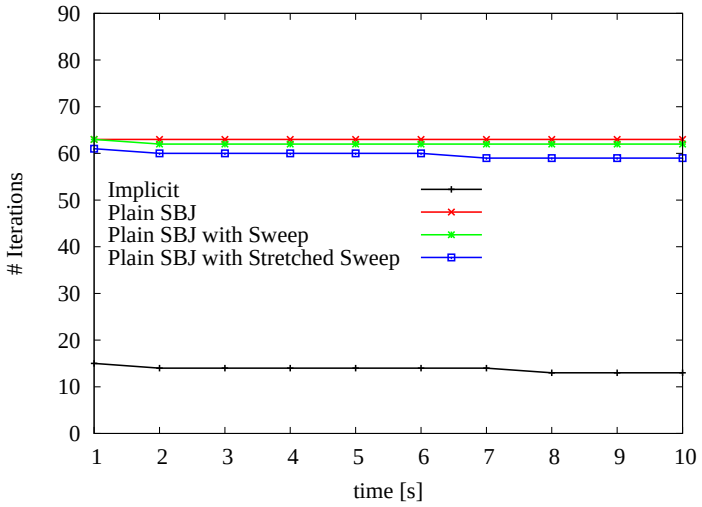

Figure 5.39 Transport Problem 5: Iterations for the Plain SBJ Method for the $\varepsilon = 1$ Problem

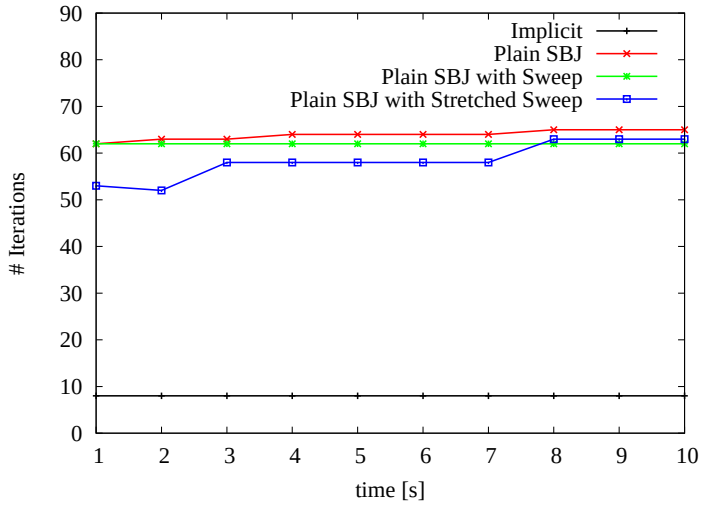

Figure 5.40 Transport Problem 5: Iterations for the Plain SBJ Method for the $\varepsilon = 2$ Problem

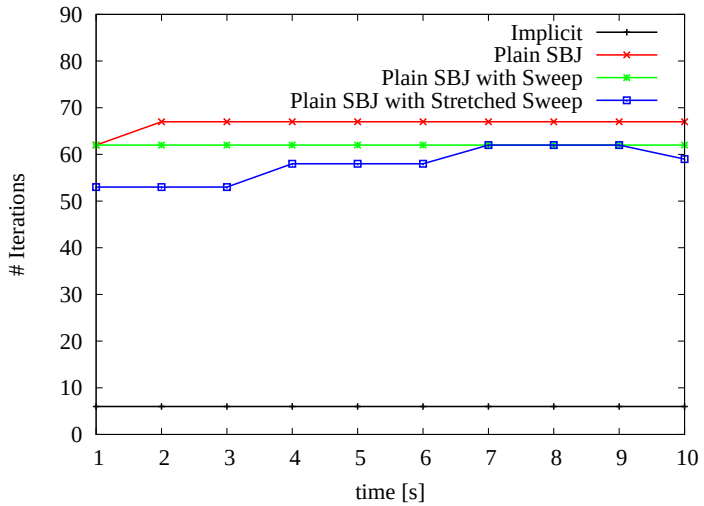

Figure 5.41 Transport Problem 5: Iterations for the Plain SBJ Method for the $\varepsilon = 3$ Problem

these problems, the number of iterations is constrained between about 50 and 80 iterations. Sweeps contribute a modest reduction in the number of iterations required, and stretching the sweep also causes a small improvement in the number of required iterations for most time steps.

In Figures 5.42–5.45, we show the number of iterations required to converge the SBJ transport method (with and without stretched or unstretched sweeps), with rebalance, to the implicit solution, for a convergence criteria of 10^{-6}. In these results, we find that the rebalance reduces the number of iterations compared to the unrebalanced results shown in

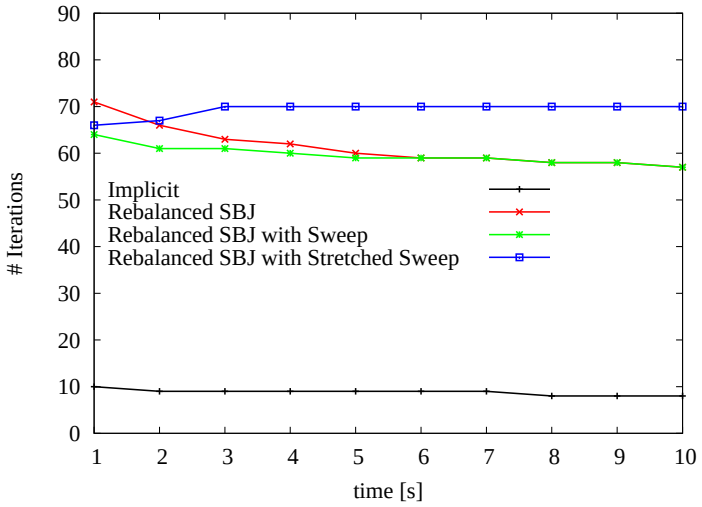

Figure 5.42 Transport Problem 5: Iterations for the Rebalanced SBJ Method for the $\varepsilon = 0$ Problem

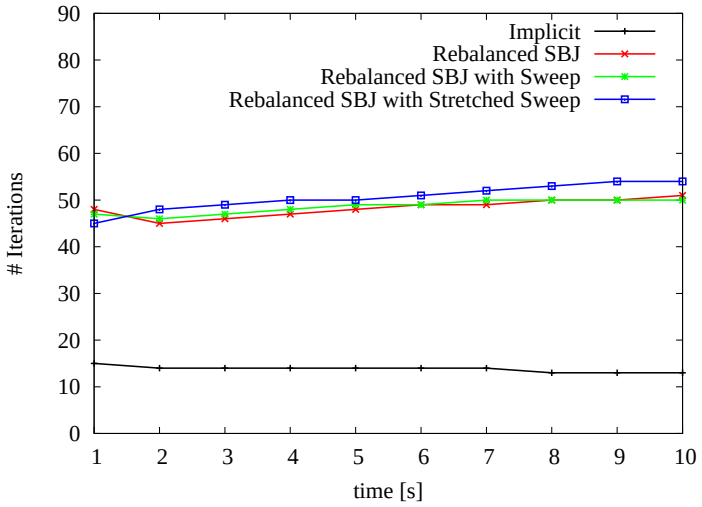

Figure 5.43 Transport Problem 5: Iterations for the Rebalanced SBJ Method for the $\varepsilon = 1$ Problem

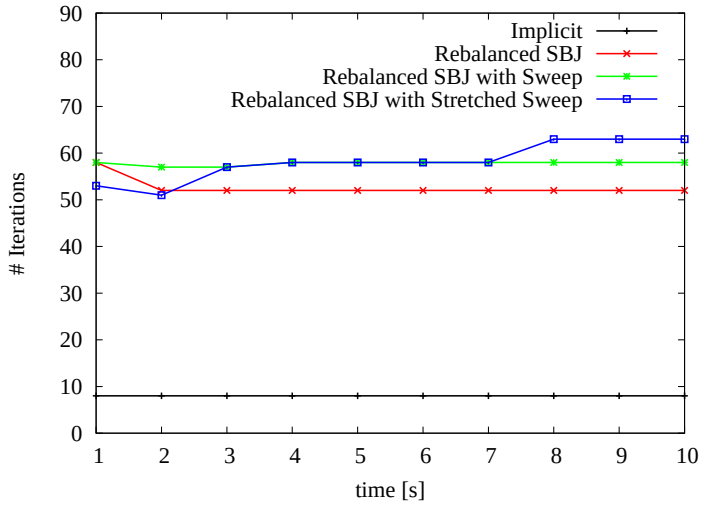

Figure 5.44 Transport Problem 5: Iterations for the Rebalanced SBJ Method for the $\varepsilon = 2$ Problem

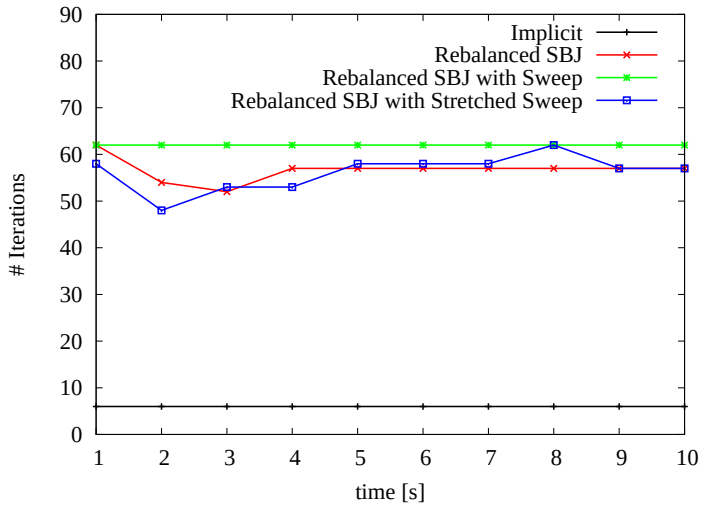

Figure 5.45 Transport Problem 5: Iterations for the Rebalanced SBJ Method for the $\varepsilon = 3$ Problem

Figures 5.38–5.45. Interestingly, for the rebalanced problems, sweeps increase the number of iterations required for convergence, although the increase is not large.

Overall, the number of iterations required for these problems are reasonably modest, although greater than the corresponding number of iterations required by the DSA accelerated implicit method. Research on more advanced acceleration techniques for the SBJ transport method could reduce the number of iterations required significantly. The number of iterations required by the SBJ transport method would be larger if the optically-thin regions spanned more cells, since it would then take more iterations to dampen any error waves moving through the problem.

5.6 Summary

In general, we have found that the SBJ transport method is accurate when the particle wave advances less than about 20% of a cell width per time step. We found in Section 5.3 that this corresponds to a reasonable time step length for optically-thin and optically-thick problems, but solving intermediate thickness problems with the SBJ transport method requires smaller time steps.

Alternatively, instead of reducing the time step length, we may instead iterate on the incident angular fluxes on each block. Using iterations converges the SBJ transport solution to the implicit solution, and guarantees cell-wise particle conservation, even if particle rebalance is not used. Iterations converge quickly when the wave advances less than about the width of a cell per time step. Faster wave speeds may require many more iterations. Rebalance helps reduce the number of iterations required for optically-thick problems, but can increase the number of iterations required to converge optically-thin problems.

Sweeps reduce the number of iterations required for convergence by a modest amount for most problems, and stretching the sweep can reduce the number of iterations further (if appropriate stretching parameters are chosen). Overall, the advantages of sweeps is modest, and may not outweigh the reduced parallelism. Nevertheless, mesh sweeps and the SBJ transport method are complementary, and there may be other ways to exploit this complementarity to produce methods with increased efficiency and accuracy.

Chapter 6

Derivation of the Thermal Radiation Staggered-Block Jacobi Transport Equations

In Chapters 3 through 5, we investigated the Staggered-Block Jacobi transport method in a linear S_N transport scheme. We found that the SBJ transport method is accurate and efficient in problems where the particle wave moves a fraction of a cell per time step, i.e., in problems where the time step length is short, or in optically-thick problems, where the wave speed is slow. This makes it complementary in some ways to the traditional sweep-based implicit method, which, without acceleration, is efficient in optically-thin or highly absorptive problems.

In this and the next chapter, we investigate the SBJ transport method applied to the grey thermal radiation transport (TRT) equations. This will demonstrate the efficacy of the SBJ transport method in a coupled physics context. With sweep-based methods, every cell is coupled to every other cell in the problem domain. Therefore, in order to find the solution to the transport equation in a single cell, the angular flux in every cell must be found. This is accomplished through sweeps and iterations. However, with the SBJ transport method, every block is decoupled from every other block, allowing the solution in each of the blocks to be calculated in parallel.

Since, with sweep-based methods, every cell is coupled to every other cell, it is difficult to directly couple other physics to the radiation transport. Direct coupling would require a very large system of equations to be solved simultaneously. Since this is often infeasible, the physics methods are typically decoupled through an operator split instead. Consider the following coupled physics problem:

$$\frac{1}{v}\frac{\partial \boldsymbol{\psi}}{\partial t} + \mathbf{L}\boldsymbol{\psi} = \mathbf{S}\boldsymbol{\phi} + \mathbf{V}u + Q\,, \tag{6.1a}$$

$$\frac{\partial u}{\partial t} + \mathbf{B}u = \mathbf{C}\psi + W\,. \tag{6.1b}$$

Eq. (6.1a) represents a radiation transport equation, where ψ is the angular radiation intensity or angular flux, and u is the solution to the coupled physics represented in Eq. (6.1b). Additionally, v is the radiation particle speed, $\mathbf{L}$ is the streaming-plus-collision operator, $\mathbf{S}$ is the scattering operator, $\mathbf{V}$ is some operator coupling u to the radiation, and Q is a source. Eq. (6.1b) is an equation describing some physics coupled to the radiation. Common possibilities include the solution to a material energy equation (in the case of thermal radiation transport problems), or perhaps the solution to the Navier-Stokes equations (in coupled radiation-thermal hydraulics problems), or some other physics of interest. The operator $\mathbf{B}$ represents some operator on u, $\mathbf{C}$ represents some operator coupling the radiation, and W is a source.

If we apply an implicit time discretization to Eqs. (6.1), we obtain

$$\frac{1}{v\Delta t_{k+1}}\left[\psi^{k+1} - \psi^{k}\right] + \mathbf{L}\psi^{k+1} = \mathbf{S}\phi^{k+1} + \mathbf{V}u^{k+1} + Q^{k+1}\,, \tag{6.2a}$$

$$\frac{1}{\Delta t_{k+1}}\left[u^{k+1} - u^{k}\right] + \mathbf{B}u^{k+1} = \mathbf{C}\psi^{k+1} + W^{k+1}\,. \tag{6.2b}$$

With this time discretization, Eqs. (6.2) represent two coupled equations for the two coupled unknowns ψ^{k+1} and u^{k+1}. However, because $\mathbf{L}$ contains a spatial derivative, ψ^{k+1} is spatially coupled throughout the problem domain. If either $\mathbf{V}$ or $\mathbf{B}$ also contains a spatial derivative, then u is also spatially coupled througout the problem domain, in which case we can not solve Eqs. (6.2) by mesh sweeps. This means that Eqs. (6.2) must be solved using a very large system of simultaneous equations, or by iterating.

Since these strategies are typically impractical, Eqs. (6.2) are modified using an operator split, wherein u in Eq. (6.2a) is lagged to the previous time step:

$$\frac{1}{v\Delta t_{k+1}}\left[\psi^{k+1} - \psi^{k}\right] + \mathbf{L}\psi^{k+1} = \mathbf{S}\phi^{k+1} + \mathbf{V}u^{k} + Q^{k+1}\,, \tag{6.3a}$$

$$\frac{1}{\Delta t_{k+1}}\left[u^{k+1} - u^{k}\right] + \mathbf{B}u^{k+1} = \mathbf{C}\psi^{k+1} + W^{k+1}\,. \tag{6.3b}$$

Because u^{k} in Eq. (6.3a) is known, Eq. (6.3a) may be solved using mesh sweeps. After ψ^{k+1} is calculated, it may be substituted into Eq. (6.3b) to calculate u^{k+1}. Operator splitting introduces an $O(\Delta t)$ error, and therefore may require small time steps.

With the SBJ transport method, every block is decoupled so there is no need to decouple the physics using operator splitting. Instead, the physics may be directly coupled and solved

simultaneously. Essentially, we have traded operator splitting for splitting $\mathbf{L}$ instead, by lagging the incident information on the boundaries of each block. Obviously, in order for the block to be decoupled in a multiphysics simulation, all of the incident information on each block must be lagged (i.e., if $\mathbf{B}$ contains a spatial derivative, the incident u on each block must also be lagged to the beginning of the time step). However, because the radiation physics will almost always have the shortest time scale, any choice of Δt which results in an accurate solution for the radiation physics should also give accurate solutions for any other physics that may be coupled to the radiation.

In this chapter, we consider coupled physics in the context of grey thermal radiation transport [31]. These problems concern a slab of material that radiates energy according to a Planck spectrum. As radiation flows through the material, it is absorbed, thereby raising the material temperature. The slab then re-emits radiation in a Planckian spectrum, cooling in the process. We consider this problem in the context of the grey approximation, wherein the frequency dependence of the radiation intensity has been integrated out.

This problem could be solved using operator splitting, but because of how tightly coupled the radiation intensity and material energy density are, this would require extremely small time steps. Instead, the physics are typically directly coupled. This direct coupling is simple in the case of the TRT equations because the material energy equation lacks a spatial derivative (i.e., there is no spatial derivative in $\mathbf{B}$ or $\mathbf{V}$, so u^{k+1} may be substituted directly into the transport equation). Therefore, this is an excellent starting point to study the direct coupling of physics for the SBJ transport method, since we may compare it to the traditional sweep-based approach, and use direct coupling for both.

In this chapter, we derive and discretize the grey thermal radiation transport equations, using the well-known implicit LDFEM S_N method, and the new Staggered-Block Jacobi LDFEM S_N method. In Section 6.1, we introduce the one-dimensional thermal radiation transport equations. In Section 6.2, we derive the grey equations from the frequency dependent one-dimensional thermal radiation equations. In Section 6.3, we derive the implicitly time-discretized, linear discontinuous finite element S_N thermal radiation transport equations. In Section 6.4, we modify the grey implicit TRT equations to find the grey SBJ TRT equations. In Section 6.5, we discuss the material models used in this dissertation, and in Section 6.6 we summarize. We present numerical results for the methods derived here in Chapter 7.

6.1 The Thermal Radiation Transport Equations

We begin with the one-dimensional, frequency-dependent, thermal radiation transport equations [31] without scattering on a spatial domain spanning $0 \leq x \leq X$:

$$\frac{1}{c}\frac{\partial}{\partial t}I(x,\mu,\nu,t)+\mu\frac{\partial}{\partial x}I(x,\mu,\nu,t)+\sigma_a(x,\nu,T)I(x,\mu,\nu,t)=2\pi\sigma_a(x,\nu,T)B(\nu,T) + Q_r(x,\mu,\nu,t)\,, \quad (6.4a)$$

$$c_v(x,T)\frac{\partial}{\partial t}T(x,t)=\int_0^\infty\int_{-1}^1\sigma_a(x,\nu',T)\Big[I(x,\mu',\nu',t)-2\pi B(\nu',T)\Big]\mathrm{d}\mu'\mathrm{d}\nu'+Q_m(x,t)\,, \quad (6.4b)$$

where

$I(x,\mu,\nu,t)=$ radiation intensity [keV cm^{-2} s^{-1} hz^{-1} cosine^{-1}],
$T(x,t)=$ material temperature [keV],
$c=$ speed of light $=3\times10^{10}$ cm/s,
$\mu=$ cosine of the particle direction with the x-axis,
$\nu=$ frequency [hz],
$\sigma_a(x,\nu,T)$ = absorption opacity [cm^{-1}],
$B(\nu,T)$ = Planck function [keV cm^{-2} s^{-1} hz^{-1}],
$Q_r(x,\mu,\nu,t)$ = radiation energy source [keV cm^3 s^{-1} hz^{-1}],
$c_v(x,T)$ = specific heat capacity [keV/(keV cm^3)]
$Q_m(x,t)$ = material heat source [keV cm^{-3} s^{-1}].

Eq. (6.4a) represents a radiation balance equation, with the left side representing loss terms and the right side representing source terms. Consider a phase space element $\mathrm{d}x\,\mathrm{d}\mu\,\mathrm{d}\nu$ about a point $(x,\,\mu,\,\nu)$. The first term represents the time rate-of-change of the radiation intensity in the phase space element. The second term represents the rate of spatial leakage out of the phase space element. The third term represents radiation absorption in the element. The first term on the right represents radiation emitted isotropically at frequency ν by the material at temperature T in the element, and finally, the second term on the right represents a particle source in the element. Likewise, Eq. (6.4b) represents a material energy balance equation. The term on the left represents the time rate-of-change in the material energy density in the element. The first term on the right represents gains in material energy density due to radiation absorption, and losses due to radiation emission in the element, and the last term on the right represents a material heat source within the element.

The radiation intensity is defined as

$$I(x,\mu,\nu,t)=ch\nu N(x,\mu,\nu,t)\,, \quad (6.5)$$

where $h = 4.135668 \times 10^{-18}$ keV s is the Planck constant and $N(x,\mu,\nu,t)\,\mathrm{d}x\,\mathrm{d}\mu\,\mathrm{d}\nu$ is the number of particles in $\mathrm{d}x$ about x, traveling within angles $\mathrm{d}\mu$ about angular cosine μ, in frequencies $\mathrm{d}\nu$ about ν, at time t. The material temperature is given in units of energy (keV). The relationship between the material temperature in keV and in Kelvin is

$$T = k_b T_K\,, \tag{6.6}$$

where $k_b = 8.6173423 \times 10^{-8}$ keV/K is the Boltzmann constant. Throughout the remainder of this dissertation the material temperature is defined in keV. The Planck function is defined as

$$B(\nu,T) = \frac{2h\nu^3}{c^2}\frac{1}{\mathrm{e}^{h\nu/T}-1}\,. \tag{6.7}$$

Eqs. (6.4) are accompanied by boundary and initial conditions. The boundary conditions for Eq. (6.4a) are

$$I(0,\mu,\nu,t) = I_L^b(\mu,\nu,t)\,, \qquad 0 < \mu \le 1\,, \tag{6.8a}$$

$$I(X,\mu,\nu,t) = I_R^b(\mu,\nu,t)\,, \qquad -1 \le \mu < 0\,, \tag{6.8b}$$

where $I_L^b(\mu,\nu,t)$ and $I_R^b(\mu,\nu,t)$ are specified incident angular intensities for the left and right boundaries, respectively, in the case of incident boundary conditions, or, in the case of reflecting boundary conditions, are

$$I_L^b(\mu,\nu,t) = I(0,-\mu,\nu,t)\,, \qquad 0 < \mu \le 1\,, \tag{6.9a}$$

$$I_R^b(\mu,\nu,t) = I(X,-\mu,\nu,t)\,, \qquad -1 \le \mu < 0\,. \tag{6.9b}$$

Initial conditions for Eqs. (6.4) are

$$I(x,\mu,\nu,0) = I^i(x,\mu,\nu)\,, \qquad 0 \le x \le X\,, \quad -1 \le \mu \le 1\,, \quad 0 \le \nu \le \infty\,, \tag{6.10a}$$

$$T(x,0) = T^i(x)\,, \qquad 0 \le x \le X\,, \tag{6.10b}$$

where $I^i(x,\mu,\nu)$ and $T^i(x)$ are specified initial angular intensities and initial temperatures, respectively.

At equilibrium, the relationship between $I(x,\mu,\nu,t)$ and $T(x,t)$ is

$$I^0(x,\mu,\nu) = 2\pi B(\nu,T^0)\,, \tag{6.11}$$

where T^0 is the equilibrium temperature and $I^0(x,\mu,\nu,t)$ is the equilibrium radiation inten-

sity. The equilibrium boundary conditions are

$$I_L^b(\mu,\nu) = I_R^b(\mu,\nu) = 2\pi B(\nu,T^0)\,. \tag{6.12}$$

6.2 The Grey Thermal Radiation Transport Equations

We now derive the grey thermal radiation transport (TRT) equations from Eqs. (6.4), (6.8), and (6.10a). The grey TRT equations represent Eqs. (6.4) and (6.8) integrated over all frequencies. To begin, we define the material energy density as

$$U_m(x,T) = \int_0^T c_v(x,T')\,\mathrm{d}T'\,, \tag{6.13}$$

and obtain

$$\frac{\partial}{\partial T}U_m(x,T) = c_v(x,T)\,. \tag{6.14}$$

Substituting Eq. (6.14) into Eq. (6.4b), we have

$$\frac{\partial}{\partial t}U_m(x,T) = \int_0^\infty \int_{-1}^1 \sigma_a(x,\nu',T)\Big[I(x,\mu',\nu',t) - 2\pi B(\nu',T)\Big]\mathrm{d}\mu'\mathrm{d}\nu' + Q_m(x,t)\,. \tag{6.15}$$

Integrating Eq. (6.4a) over all frequencies by operating by $\int_0^\infty(\cdot)\,\mathrm{d}\nu$, we find

$$\begin{aligned}\frac{1}{c}\frac{\partial}{\partial t}\int_0^\infty I(x,\mu,\nu,t)\,\mathrm{d}\nu + \mu\frac{\partial}{\partial x}\int_0^\infty I(x,\mu,\nu,t)\,\mathrm{d}\nu + \int_0^\infty \sigma_a(x,\nu,T)I(x,\mu,\nu,t)\,\mathrm{d}\nu \\ = 2\pi\int_0^\infty \sigma_a(x,\nu,T)B(\nu,T)\,\mathrm{d}\nu + \int_0^\infty Q_r(x,\mu,\nu,t)\,\mathrm{d}\nu\,.\end{aligned} \tag{6.16}$$

We define

$$\psi(x,\mu,t) = \int_0^\infty I(x,\mu,\nu,t)\,\mathrm{d}\nu\,, \tag{6.17a}$$

$$\sigma_P(x,T) = \frac{\int_0^\infty \sigma_a(x,\nu,T)B(\nu,T)\,\mathrm{d}\nu}{\int_0^\infty B(\nu,T)\,\mathrm{d}\nu}\,, \tag{6.17b}$$

and

$$Q_r(x,\mu,t) = \int_0^\infty Q_r(x,\mu,\nu,t)\,\mathrm{d}\nu\,, \tag{6.17c}$$

where $\psi(x,\mu,t)$ represents the grey radiation intensity, $\sigma_P(x,T)$ is the Planck opacity (i.e., the Planck spectrum-weighted frequency-integrated absorption opacity), and $Q_r(x,\mu,t)$ is the grey radiation source. Using

$$\int_0^\infty B(\nu,T)\,\mathrm{d}\nu = \frac{ca}{4\pi}T^4(x,t)\,, \tag{6.18}$$

where $a = 4.7215 \times 10^{-6}$ keV cm^{-3} K^{-4} is the radiation constant, and assuming that the frequency dependence of the radiation intensity is nearly Planckian, i.e.,

$$\int_0^\infty \sigma_a(x,\nu,T) I(x,\mu,\nu,t)\,\mathrm{d}\nu \approx \frac{\int_0^\infty \sigma_a(x,\nu,T) B(\nu,T)\,\mathrm{d}\nu}{\int_0^\infty B(\nu,T)\,\mathrm{d}\nu} \int_0^\infty I(x,\mu,\nu,t)\,\mathrm{d}\nu$$
$$= \sigma_P(x,T)\psi(x,\mu,t)\,, \tag{6.19}$$

then the frequency-integrated TRT equations can be written

$$\frac{1}{c}\frac{\partial}{\partial t}\psi(x,\mu,t) + \mu\frac{\partial}{\partial x}\psi(x,\mu,t) + \sigma_P(x,T)\psi(x,\mu,t) = \frac{ca\sigma_P(x,T)}{2}T^4(x,t) + Q_r(x,\mu,t)\,, \tag{6.20a}$$

$$\frac{\partial}{\partial t}U_m(x,T) + ca\sigma_P(x,T)T^4(x,t) = \sigma_P(x,T)\int_{-1}^{1}\psi(x,\mu,t)\,\mathrm{d}\mu + Q_m(x,t)\,. \tag{6.20b}$$

Finally, defining the radiation energy density

$$U_r(T) = aT^4(x,t)\,, \tag{6.21}$$

we obtain the grey thermal radiation equations:

$$\frac{1}{c}\frac{\partial}{\partial t}\psi(x,\mu,t) + \mu\frac{\partial}{\partial x}\psi(x,\mu,t) + \sigma_P(x,T)\psi(x,\mu,t) = \frac{c}{2}\sigma_P(x,T)U_r(T) + Q_r(x,\mu,t)\,, \tag{6.22a}$$

$$\frac{\partial}{\partial t}U_m(x,T) + c\sigma_P(x,T)U_r(T) = \sigma_P(x,T)\int_{-1}^{1}\psi(x,\mu,t)\,\mathrm{d}\mu + Q_m(x,t)\,. \tag{6.22b}$$

Operating on Eqs. (6.8) by $\int_0^\infty(\cdot)\,\mathrm{d}\nu$, we obtain the grey boundary conditions

$$\psi(0,\mu,t) = \psi_L^b(\mu,t)\,, \qquad 0 < \mu \le 1\,, \tag{6.23a}$$

$$\psi(X,\mu,t) = \psi_R^b(\mu,t)\,, \qquad -1 \le \mu < 0\,, \tag{6.23b}$$

where

$$\psi_L^b(\mu,t) = \int_0^\infty I_L^b(\mu,\nu,t)\,\mathrm{d}\nu\,, \tag{6.24a}$$

$$\psi_R^b(\mu,t) = \int_0^\infty I_R^b(\mu,\nu,t)\,\mathrm{d}\nu\,. \tag{6.24b}$$

Also operating on Eqs. (6.10a) by $\int_0^\infty(\cdot)\,\mathrm{d}\nu$, we obtain the grey radiation initial condition

$$\psi(x,\mu,0) = \psi^i(x,\mu) \qquad 0 \le x \le X\,, \quad -1 \le \mu \le 1\,, \tag{6.25}$$

where

$$\psi^i(x,\mu) = \int_0^\infty I^i(x,\mu,\nu)\,\mathrm{d}\nu\,. \tag{6.26}$$

6.3 Linearization and Discretization

In this section, we linearize and discretize the grey TRT equations. The most common linearization, and the linearization we will employ in this dissertation, is the *Implicit Monte Carlo* (IMC) linearization [15]. Despite its name, this linearization is not limited to Monte Carlo methods (nor is it fully implicit). In Section 6.3.1 we apply the IMC linearization and implicit time discretization to the grey TRT equations. In Section 6.3.2, we discretize the resulting equations in angle using the discrete ordinates method, and in Section 6.3.3, we apply the linear discontinuous finite element method.

6.3.1 IMC Linearization and Temporal Discretization

To begin, we define a relationship between $U_m(x,T)$ and $U_r(T)$:

$$\beta(x,t) = \frac{\partial U_r}{\partial U_m} = \frac{\mathrm{d}U_r}{\mathrm{d}T}\frac{\partial T}{\partial U_m} = \frac{4aT^3(x,t)}{c_v(x,t)}\,. \tag{6.27}$$

Substituting Eq. (6.27) into Eq. (6.22b), we eliminate $U_m(x,T)$ and obtain

$$\frac{1}{\beta(x,t)}\frac{\partial}{\partial t}U_r(T) + c\sigma_P(x,T)U_r(T) = \sigma_P(x,T)\int_{-1}^{1}\psi(x,\mu,t)\,\mathrm{d}\mu + Q_m(x,t)\,. \tag{6.28}$$

We note that Eqs. (6.22b) and (6.28) are, at this point, equivalent.

To proceed, we assume a time grid like that described in Figure 2.1 in Chapter 2, where a time step $k+1$ is bounded by times t_k and t_{k+1}, with $t_0 = 0$. We now average Eqs. (6.22) and (6.28) over time step $k+1$ by operating on them with $\frac{1}{\Delta t_{k+1}}\int_{t_k}^{t_{k+1}}(\cdot)\,\mathrm{d}t$. We obtain

$$\begin{aligned}\frac{1}{c\Delta t_{k+1}}\Big[\psi^{k+1}(x,\mu) - \psi^k(x,\mu)\Big] + \mu\frac{\partial}{\partial x}\big\langle\psi(x,\mu,t)\big\rangle^{k+1} + \big\langle\sigma_P[x,T(x,t)]\,\psi(x,\mu,t)\big\rangle^{k+1} \\ = \frac{c}{2}\big\langle\sigma_P[x,T(x,t)]U_r[T(x,t)]\big\rangle^{k+1} + Q_r^{k+1}(x,\mu)\,,\end{aligned} \tag{6.29a}$$

$$\frac{1}{\Delta t_{k+1}}\Big[U_m^{k+1}(x)-U_m^k(x)\Big]+c\big\langle\sigma_P(x,T)U_r[T(x,t)]\big\rangle^{k+1}$$
$$=\int_{-1}^{1}\big\langle\sigma_P[x,T(x,t)]\,\psi(x,\mu,t)\big\rangle^{k+1}\,\mathrm{d}\mu+Q_m^{k+1}(x)\,, \quad (6.29b)$$

$$\left\langle\frac{1}{\beta(x,t)}\frac{\partial}{\partial t}U_r[T(x,t)]\right\rangle^{k+1}+c\big\langle\sigma_P[x,T(x,t)]U_r[T(x,t)]\big\rangle^{k+1}$$
$$=\int_{-1}^{1}\big\langle\sigma_P[x,T(x,t)]\,\psi(x,\mu,t)\big\rangle^{k+1}\,\mathrm{d}\mu+Q_m^{k+1}(x)\,, \quad (6.29c)$$

where

$$\psi^k(x,\mu)=\psi(x,\mu,t_k)\,, \quad (6.30a)$$

$$T^k(x)=T(x,t_k)\,, \quad (6.30b)$$

$$U_m^k(x)=U_m[x,T^k(x)]\,, \quad (6.30c)$$

$$Q_r^{k+1}(x,\mu)=\frac{1}{\Delta t_{k+1}}\int_{t_k}^{t_{k+1}}Q_r(x,\mu,t)\,\mathrm{d}t\,, \quad (6.30d)$$

$$Q_m^{k+1}(x)=\frac{1}{\Delta t_{k+1}}\int_{t_k}^{t_{k+1}}Q_m(x,t)\,\mathrm{d}t\,, \quad (6.30e)$$

and where $\langle(\cdot)\rangle^{k+1}$ denotes an average over time step $k+1$. To apply the IMC linearization to these equations, we make the following three approximations. First, we lag the Planck opacity to time t_k. Therefore, defining

$$\sigma_P^k(x)=\sigma_P[x,T^k(x)]\,, \quad (6.31)$$

we write Eqs. (6.29) as

$$\frac{1}{c\Delta t_{k+1}}\Big[\psi^{k+1}(x,\mu)-\psi^k(x,\mu)\Big]+\mu\frac{\partial}{\partial x}\big\langle\psi(x,\mu,t)\big\rangle^{k+1}+\sigma_P^k(x)\big\langle\psi(x,\mu,t)\big\rangle^{k+1}$$
$$=\frac{c}{2}\sigma_P^k(x)\big\langle U_r[x,T(x,t)]\big\rangle^{k+1}+Q_r^{k+1}(x,\mu)\,, \quad (6.32a)$$

$$\frac{1}{\Delta t_{k+1}}\Big[U_m^{k+1}(x)-U_m^k(x)\Big]+c\sigma_P^k(x)\big\langle U_r[T(x,t)]\big\rangle^{k+1}$$
$$=\sigma_P^k(x)\int_{-1}^{1}\big\langle\psi(x,\mu,t)\big\rangle^{k+1}\,\mathrm{d}\mu+Q_m^{k+1}(x)\,, \quad (6.32b)$$

$$\left\langle \frac{1}{\beta(x,t)}\frac{\partial}{\partial t}U_r[T(x,t)] \right\rangle^{k+1} + c\sigma_P^k(x)\left\langle U_r[T(x,t)]\right\rangle^{k+1} = \sigma_P^k(x)\int_{-1}^{1}\left\langle \psi(x,\mu,t)\right\rangle^{k+1}\mathrm{d}\mu + Q_m^{k+1}(x)\,. \quad (6.32c)$$

The second approximation in the IMC linearization is to lag $\beta(x,t)$ to time t_k. Defining

$$\beta^k(x) = \beta(x,t_k)\,, \quad (6.33)$$

we write Eq. (6.32c) as

$$\frac{1}{\beta^k(x)\Delta t_{k+1}}\left[U_r^{k+1/2}(x) - U_r^k(x)\right] + c\sigma_P^k(x)\left\langle U_r[T(x,t)]\right\rangle^{k+1} = \sigma_P^k(x)\int_{-1}^{1}\left\langle \psi(x,\mu,t)\right\rangle^{k+1}\mathrm{d}\mu + Q_m^{k+1}(x)\,, \quad (6.34)$$

where

$$U_r^k(x) = U_r[T(x,t_k)]\,. \quad (6.35)$$

We note that after this step, Eqs. (6.32b) and (6.34) are no longer equivalent. In practice, this means that particle conservation will not be achieved if Eq. (6.34) is used to calculate the radiation energy density at the end of the time step, which is why we have denoted it with a $k+1/2$ in the superscript. Instead, Eqs. (6.32a) and (6.34) are used to calculate the radiation intensity at the end of the time step, Eq. (6.32b) is used to calculate the material energy density at the end of the time step, and then Eqs. (6.13) and (6.21) are used to calculate the temperature and radiation energy density at the end of the time step, respectively.

The third approximation in the IMC linearization is the following closure relationship between $\left\langle U_r[T(x,t)]\right\rangle^{k+1}$ and $U_r^{k+1/2}(x)$:

$$\left\langle U_r[T(x,t)]\right\rangle^{k+1} = \alpha U_r^{k+1/2}(x) - \big(1-\alpha\big)U_r^k(x)\,, \quad (6.36)$$

where α is a user-specified parameter. For stability, we must have $\frac{1}{2} \leq \alpha \leq 1$. This parameter controls how "implicitly" the time step-averaged radiation energy density $\left\langle U_r[T(x,t)]\right\rangle^{k+1}$ is treated, with unity being the most implicit, and by far the most common, choice (and the one we used throughout this dissertation). Rearranging Eq. (6.36), we obtain

$$U_r^{k+1/2}(x) - U_r^k(x) = \frac{\left\langle U_r[T(x,t)]\right\rangle^{k+1} - U_r^k(x)}{\alpha}\,. \quad (6.37)$$

Substituting Eq. (6.37) into Eq. (6.34), we find

$$\frac{1}{\alpha\beta^k(x)\Delta t_{k+1}}\Big[\big\langle U_r[T(x,t)]\big\rangle^{k+1} - U_r^k(x)\Big] + c\sigma_P^k(x)\big\langle U_r[T(x,t)]\big\rangle^{k+1} = \sigma_P^k(x)\int_{-1}^{1}\big\langle \psi(x,\mu,t)\big\rangle^{k+1}\,\mathrm{d}\mu + Q_m^{k+1}(x)\,. \quad (6.38)$$

Solving Eq. (6.38) for the time step-averaged radiation energy, we obtain

$$\big\langle U_r[T(x,t)]\big\rangle^{k+1} = f^k(x)U_r^k(x) + \left[\frac{1-f^k(x)}{c}\right]\int_{-1}^{1}\big\langle \psi(x,\mu,t)\big\rangle^{k+1}\,\mathrm{d}\mu + \left[\frac{1-f^k(x)}{c\sigma_P^k(x)}\right]Q_m^{k+1}(x)\,, \quad (6.39)$$

where

$$f^k(x) = \frac{1}{1+\alpha\Delta t_{k+1}\beta^k(x)c\sigma_P^k(x)} \quad (6.40)$$

is the *Fleck factor*.

Substituting Eq. (6.39) into Eqs. (6.32a) and (6.32b), we obtain the IMC equations:

$$\frac{1}{c\Delta t_{k+1}}\Big[\psi^{k+1}(x,\mu) - \psi^k(x,\mu)\Big] + \mu\frac{\partial}{\partial x}\big\langle \psi(x,\mu,t)\big\rangle^{k+1} + \sigma_P^k(x)\big\langle \psi(x,\mu,t)\big\rangle^{k+1} = \frac{\sigma_P^k(x)}{2}\Big[1-f^k(x)\Big]\int_{-1}^{1}\big\langle \psi(x,\mu',t)\big\rangle^{k+1}\,\mathrm{d}\mu' + \frac{c}{2}f^k(x)\sigma_P^k(x)U_r^k(x) + \left[\frac{1-f^k(x)}{2}\right]Q_m^{k+1}(x) + Q_r^{k+1}(x,\mu)\,, \quad (6.41a)$$

$$\frac{1}{\Delta t_{k+1}}\Big[U_m^{k+1}(x) - U_m^k(x)\Big] + cf^k(x)\sigma_P^k(x)U_r^k(x) = f^k(x)\sigma_P^k(x)\int_{-1}^{1}\big\langle \psi(x,\mu,t)\big\rangle^{k+1}\,\mathrm{d}\mu + f^k(x)Q_m^{k+1}(x)\,. \quad (6.41b)$$

We may now complete the time discretization of the IMC equations, Eqs. (6.41). In Section 6.4, we discuss the SBJ time discretization applied to Eqs. (6.41). For now however, we apply an implicit time discretization by approximating the average radiation intensity over the time step as equal to the radiation intensity at the end of time time step, i.e.,

$$\big\langle \psi(x,\mu,t)\big\rangle^{k+1} \approx \psi(x,\mu,t_{k+1}) = \psi^{k+1}(x,\mu)\,. \quad (6.42)$$

Now Eqs. (6.41) can be written

$$\frac{1}{c\Delta t_{k+1}}\Big[\psi^{k+1}(x,\mu)-\psi^{k}(x,\mu)\Big]+\mu\frac{\partial}{\partial x}\psi^{k+1}(x,\mu)+\sigma_P^k(x)\psi^{k+1}(x,\mu)$$
$$=\frac{\sigma_P^k(x)}{2}\Big[1-f^k(x)\Big]\int_{-1}^{1}\psi^{k+1}(x,\mu')\,\mathrm{d}\mu'+\frac{c}{2}f^k(x)\sigma_P^k(x)U_r^k(x)$$
$$+\left[\frac{1-f^k(x)}{2}\right]Q_m^{k+1}(x)+Q_r^{k+1}(x,\mu)\,, \quad (6.43a)$$

$$\frac{1}{\Delta t_{k+1}}\Big[U_m^{k+1}(x)-U_m^k(x)\Big]+cf^k(x)\sigma_P^k(x)U_r^k(x)=f^k(x)\sigma_P^k(x)\int_{-1}^{1}\psi^{k+1}(x,\mu)\,\mathrm{d}\mu$$
$$+f^k(x)Q_m^{k+1}(x)\,. \quad (6.43b)$$

The boundary conditions for Eq. (6.43a) are given by

$$\psi^{k+1}(0,\mu)=\psi_L^{b,k+1}(\mu)\,,\qquad 0<\mu\leq 1\,, \quad (6.44a)$$

$$\psi^{k+1}(X,\mu)=\psi_R^{b,k+1}(\mu)\,,\qquad -1\leq\mu<0\,, \quad (6.44b)$$

where

$$\psi_L^{b,k+1}(\mu)=\psi_L^{b}(\mu,t_{k+1})\,, \quad (6.45a)$$

$$\psi_R^{b,k+1}(\mu)=\psi_R^{b}(\mu,t_{k+1})\,. \quad (6.45b)$$

The initial conditions for Eqs. (6.43) are

$$\psi^{0}(x,\mu)=\psi^{i}(x,\mu)\,,\qquad 0\leq x\leq X\,,\quad -1\leq\mu\leq 1\,, \quad (6.46a)$$

$$U_r^0(x)=a\big[T^i(x)\big]^4\,,\qquad 0\leq x\leq X\,, \quad (6.46b)$$

$$U_m^0(x)=\int_0^{T^i(x)}c_v(x,T')\,\mathrm{d}T'\,,\qquad 0\leq x\leq X\,. \quad (6.46c)$$

Eqs. (6.43), together with the boundary conditions given in Eqs. (6.44) and the initial conditions given in Eqs. (6.46), represent the grey, implicit IMC TRT equations.

The solution algorithm for the IMC equations are as follows: at the beginning of the time step, the Planck cross section $\sigma_P(x,T)$ and $\beta(x,T)$ are calculated, using whichever material model is appropriate. These equations are given in Section 6.5. Then the angular intensity and material energy density at the end of the time step is calculated using Eqs. (6.43a) and (6.43b), respectively. The temperature at the end of the time step is calculated from

Eq. (6.13), using whatever definition of $c_v(x,T)$ is appropriate for the material model in equation. Finally, the radiation energy density at the end of the time step is calculated using Eq. (6.21).

6.3.2 Angular Discretization

We now apply the S_N approximation to Eqs. (6.43). This discretization is analogous to the S_N approximation we applied to the linear transport equation in Section 3.1. Assuming a Gauss-Legendre quadrature set $\{\mu_n, \Delta_n\}$, where μ_n are the angular cosines and Δ_n are the quadrature weights, we define

$$\psi_n^k(x) = \psi^k(x,\mu_n)\,, \tag{6.47a}$$

and

$$Q_{r,n}^{k+1}(x) = Q_r^{k+1}(x,\mu_n)\,, \tag{6.47b}$$

and have

$$\int_{-1}^{1} \psi^{k+1}(x,\mu)\,\mathrm{d}\mu \approx \sum_{n'=1}^{N} \psi_{n'}^{k+1}(x)\,\Delta_{n'}\,. \tag{6.48}$$

Substituting Eq. (6.48) into Eqs. (6.43), and evaluating Eq. (6.43a) at angle μ_n, we write the grey TRT S_N equations as

$$\begin{aligned}\frac{1}{c\Delta t_{k+1}}\left[\psi_n^{k+1}(x)-\psi_n^k(x)\right] &+ \mu_n\frac{\mathrm{d}}{\mathrm{d}x}\psi_n^{k+1}(x) + \sigma_P^k(x)\psi_n^{k+1}(x) \\ &= \frac{\sigma_P^k(x)}{2}\left[1-f^k(x)\right]\sum_{n'=1}^{N}\psi_{n'}^{k+1}(x)\,\Delta_{n'} + \frac{c}{2}f^k(x)\sigma_P^k(x)U_r^k(x) \\ &\qquad + \left[\frac{1-f^k(x)}{2}\right]Q_m^{k+1}(x) + Q_{r,n}^{k+1}(x)\,,\end{aligned} \tag{6.49a}$$

$$\begin{aligned}\frac{1}{\Delta t_{k+1}}\left[U_m^{k+1}(x)-U_m^k(x)\right] + cf^k(x)\sigma_P^k(x)U_r^k(x) &= f^k(x)\sigma_P^k(x)\sum_{n'=1}^{N}\psi_{n'}^{k+1}(x)\,\Delta_{n'} \\ &\qquad + f^k(x)Q_m^{k+1}(x)\,.\end{aligned} \tag{6.49b}$$

The boundary conditions for Eq. (6.49a) are

$$\psi_n^{k+1}(0) = \psi_{n,L}^{b,k+1}\,, \qquad 0 < \mu_n \leq 1\,, \tag{6.50a}$$

$$\psi_n^{k+1}(X) = \psi_{n,R}^{b,k+1}, \qquad -1 \leq \mu_n < 0, \tag{6.50b}$$

where

$$\psi_{n,L}^{b,k+1} = \psi_L^{k+1}(\mu_n), \tag{6.51a}$$

$$\psi_{n,R}^{b,k+1} = \psi_R^{k+1}(\mu_n). \tag{6.51b}$$

The initial condition for Eq. (6.49a) is

$$\psi_n^0(x) = \psi_n^i(x), \qquad 0 \leq x \leq X, \tag{6.52}$$

where

$$\psi_n^i(x) = \psi^i(x, \mu_n). \tag{6.53}$$

6.3.3 Spatial Discretization

We next apply the linear discontinuous finite element discretization to Eqs. (6.49). We refer the reader to Chapter 3 for a more detailed discussion of the linear discontinuous finite element method. We begin spatially discretizing Eq (6.49a) by rearranging it to form a residual:

$$\begin{aligned} R_I(x) = \frac{1}{c\Delta t_{k+1}}\left[\psi_n^{k+1}(x) - \psi_n^k(x)\right] + \mu_n \frac{\mathrm{d}}{\mathrm{d}x}\psi_n^{k+1}(x) + \sigma_P^k(x)\psi_n^{k+1}(x) \\ - \frac{\sigma_P^k(x)}{2}\left[1 - f^k(x)\right]\sum_{n'=1}^{N}\psi_{n'}^{k+1}(x)\Delta_{n'} - \frac{c}{2}f^k(x)\sigma_P^k(x)U_r^k(x) \\ - \left[\frac{1-f^k(x)}{2}\right]Q_m^{k+1}(x) - Q_{r,n}^{k+1}(x). \end{aligned} \tag{6.54}$$

We calculate weighted averages of Eq. (6.54) by multiplying by a set of weight functions $w_{i,p}(x)$, $p = 1 \ldots P$, integrating over cell i, and setting the weighted averages equal to zero.

After using integration-by-parts on the streaming term, we have

$$\begin{aligned}\int_{x_{i-1/2}}^{x_{i+1/2}} R_I(x)\,\mathrm{d}x = \frac{1}{c\Delta t_{k+1}}&\left[\int_{x_{i-1/2}}^{x_{i+1/2}} w_{i,p}(x)\,\psi_n^{k+1}(x)\,\mathrm{d}x - \int_{x_{i-1/2}}^{x_{i+1/2}} w_{i,p}(x)\,\psi_n^{k}(x)\,\mathrm{d}x\right]\\ &+\mu_n\left[w_{i,p}(x_{i+1/2})\,\psi_n^{k+1}(x_{i+1/2}) - w_{i,p}(x_{i-1/2})\,\psi_n^{k+1}(x_{i-1/2})\right]\\ &-\mu_n\int_{x_{i-1/2}}^{x_{i+1/2}} \psi_n^{k+1}(x)\frac{\mathrm{d}}{\mathrm{d}x}w_{i,p}(x)\,\mathrm{d}x + \int_{x_{i-1/2}}^{x_{i+1/2}} w_{i,p}(x)\,\sigma_P^k(x)\,\psi_n^{k+1}(x)\,\mathrm{d}x\\ &-\frac{1}{2}\int_{x_{i-1/2}}^{x_{i+1/2}} w_{i,p}(x)\,\sigma_P^k(x)\left[1-f^k(x)\right]\sum_{n'=1}^{N}\psi_{n'}^{k+1}(x)\,\Delta_{n'}\,\mathrm{d}x\\ &-\frac{c}{2}\int_{x_{i-1/2}}^{x_{i+1/2}} w_{i,p}(x)\,f^k(x)\,\sigma_P^k(x)\,U_r^k(x)\,\mathrm{d}x - \int_{x_{i-1/2}}^{x_{i+1/2}} w_{i,p}(x)\left[\frac{1-f^k(x)}{2}\right]Q_m^{k+1}(x)\,\mathrm{d}x\\ &-\int_{x_{i-1/2}}^{x_{i+1/2}} w_{i,p}(x)\,Q_{r,n}^{k+1}(x)\,\mathrm{d}x = 0\,, \qquad p = 1\ldots P\,. \quad (6.55)\end{aligned}$$

In this dissertation, we assume (just as in Chapter 3) that the functional form of the radiation intensity is spatially linear in each cell. We also assume that the temperature is piecewise constant in each cell. This is the typical functional form assumed for the temperature variable [4, 27], although there has been some recent work on spatially linear temperature distributions in each cell [28]. Nevertheless, most codes treat the temperature as constant in each cell. Additionally, thermal radiation transport codes are often coupled to hydrodynamics codes, and hydrodynamics methods treat the temperature as constant in a cell. As a consequence of the piecewise constant temperature distribution, the material energy density, radiation energy density, Planck cross section, Fleck factor, and $\beta^k(x)$ are also piecewise constant. We also assume that the temperature source $Q_m^{k+1}(x)$ is constant within a cell. Therefore, we define

$$T^k(x) = T_i^k\,, \qquad x_{i-1/2} < x < x_{i+1/2}\,, \quad (6.56a)$$

$$U_r^k(x) = U_{r,i}^k\,, \qquad x_{i-1/2} < x < x_{i+1/2}\,, \quad (6.56b)$$

$$U_m^k(x) = U_{m,i}^k\,, \qquad x_{i-1/2} < x < x_{i+1/2}\,, \quad (6.56c)$$

$$Q_m^k(x) = Q_{m,i}^k\,, \qquad x_{i-1/2} < x < x_{i+1/2}\,, \quad (6.56d)$$

$$\sigma_P^k(x) = \sigma_{P,i}^k\,, \qquad x_{i-1/2} < x < x_{i+1/2}\,, \quad (6.56e)$$

$$f^k(x) = f_i^k\,, \qquad x_{i-1/2} < x < x_{i+1/2}\,, \quad (6.56f)$$

$$c_v^k(x) = c_{v,i}^k\,, \qquad x_{i-1/2} < x < x_{i+1/2}\,, \tag{6.56g}$$

$$\beta^k(x) = \beta_i^k\,, \qquad x_{i-1/2} < x < x_{i+1/2}\,. \tag{6.56h}$$

Now we write Eq. (6.55) as

$$\begin{aligned}
&\frac{1}{c\Delta t_{k+1}}\Big[\int_{x_{i-1/2}}^{x_{i+1/2}} w_{i,p}(x)\psi_n^{k+1}(x)\,\mathrm{d}x - \int_{x_{i-1/2}}^{x_{i+1/2}} w_{i,p}(x)\psi_n^k(x)\,\mathrm{d}x\Big] \\
&\qquad + \mu_n\Big[w_{i,p}(x_{i+1/2})\psi_n^{k+1}(x_{i+1/2}) - w_{i,p}(x_{i-1/2})\psi_n^{k+1}(x_{i-1/2})\Big] \\
&\qquad - \mu_n\int_{x_{i-1/2}}^{x_{i+1/2}} \psi_n^{k+1}(x)\frac{\mathrm{d}}{\mathrm{d}x}w_{i,p}(x)\,\mathrm{d}x + \sigma_{P,i}^k\int_{x_{i-1/2}}^{x_{i+1/2}} w_{i,p}(x)\psi_n^{k+1}(x)\,\mathrm{d}x \\
&= \frac{1}{2}\sigma_{P,i}^k\Big[1-f_i^k\Big]\sum_{n'=1}^{N}\int_{x_{i-1/2}}^{x_{i+1/2}} w_{i,p}(x)\psi_{n'}^{k+1}(x)\,\mathrm{d}x\Delta_{n'} + \frac{c}{2}f_i^k\sigma_{P,i}^k U_{r,i}^k\int_{x_{i-1/2}}^{x_{i+1/2}} w_{i,p}(x)\,\mathrm{d}x \\
&\qquad + \left[\frac{1-f_i^k}{2}\right]Q_{m,i}^{k+1}\int_{x_{i-1/2}}^{x_{i+1/2}} w_{i,p}(x)\,\mathrm{d}x + \int_{x_{i-1/2}}^{x_{i+1/2}} w_{i,p}(x)Q_{r,n}^{k+1}(x)\,\mathrm{d}x\,.
\end{aligned} \tag{6.57}$$

Next, we approximate the angular flux and particle source as a superposition of the linear discontinuous basis functions:

$$\psi_n^k(x) = b_{i,L}(x)\psi_{n,i,L}^k + b_{i,R}(x)\psi_{n,i,R}^k\,, \qquad x_{i-1/2} < x < x_{i+1/2}\,, \tag{6.58a}$$

$$Q_{r,n}^{k+1}(x) = b_{i,L}(x)Q_{r,n,i,L}^{k+1} + b_{i,R}(x)Q_{r,n,i,L}^{k+1}\,, \qquad x_{i-1/2} < x < x_{i+1/2}\,, \tag{6.58b}$$

where

$$b_{i,L}(x) = \frac{x_{i+1/2}-x}{\Delta x_i}\,, \tag{6.59a}$$

$$b_{i,R}(x) = \frac{x-x_{i-1/2}}{\Delta x_i}\,. \tag{6.59b}$$

We also assume Galerkin weighting, such that

$$w_{i,1}(x) = w_{i,L}(x) = b_{i,L}(x)\,, \tag{6.60a}$$

$$w_{i,2}(x) = w_{i,R}(x) = b_{i,R}(x)\,. \tag{6.60b}$$

We found, in Chapter 4, that the SBJ transport method limits to the unconditionally stable SBJ diffusion discretization in the case of full matrix lumping. Therefore, we assume full matrix lumping in the implicit and SBJ discretizations of the grey TRT equations, and write

Eq. (6.57) as

$$\frac{1}{c\Delta t_{k+1}}\underline{\underline{M}}_i\left(\underline{\psi}_{n,i}^{k+1}-\underline{\psi}_{n,i}^{k}\right)+\mu_n\underline{\underline{L}}_i^{surf}\underline{\psi}_{n,i}^{k+1,edge}-\mu_n\underline{\underline{L}}_i\underline{\psi}_{n,i}^{k+1}+\sigma_{P,i}^{k}\underline{\underline{M}}_i\underline{\psi}_{n,i}^{k+1}$$
$$=\frac{\sigma_{P,i}^{k}}{2}\left[1-f_i^k\right]\underline{\underline{M}}_i\sum_{n'=1}^{N}\underline{\psi}_{n',i}^{k+1}\Delta_{n'}+\frac{c}{2}f_i^k\sigma_{P,i}^{k}\underline{\underline{M}}_i\underline{U}_{r,i}^{k}+\left[\frac{1-f_i^k}{2}\right]\underline{\underline{M}}_i\underline{Q}_{m,i}^{k+1}+\underline{\underline{M}}_i\underline{Q}_{r,n,i}^{k+1}\,, \quad (6.61)$$

where the matrices are defined as

$$\underline{\underline{M}}_i=\frac{\Delta x_i}{2}\begin{bmatrix}1 & 0\\ 0 & 1\end{bmatrix}\,, \quad (6.62a)$$

$$\underline{\underline{L}}_i=\begin{bmatrix}-\frac{1}{2} & -\frac{1}{2}\\ \frac{1}{2} & \frac{1}{2}\end{bmatrix}\,, \quad (6.62b)$$

$$\underline{\underline{L}}_i^{surf}=\begin{bmatrix}-1 & 0\\ 0 & 1\end{bmatrix}\,, \quad (6.62c)$$

and the vectors are defined as

$$\underline{\psi}_{n,i}^{k}=\begin{bmatrix}\psi_{n,i,L}^{k} & \psi_{n,i,R}^{k}\end{bmatrix}^T\,, \quad (6.63a)$$

$$\underline{\psi}_{n,i}^{k+1,edge}=\begin{bmatrix}\psi_{n}^{k+1}(x_{i-1/2}) & \psi_{n}^{k+1}(x_{i+1/2})\end{bmatrix}^T\,, \quad (6.63b)$$

$$\underline{U}_{r,i}^{k}=\begin{bmatrix}U_{r,i}^{k} & U_{r,i}^{k}\end{bmatrix}^T\,, \quad (6.63c)$$

$$\underline{Q}_{m,i}^{k+1}=\begin{bmatrix}Q_{m,i}^{k+1} & Q_{m,i}^{k+1}\end{bmatrix}^T\,, \quad (6.63d)$$

$$\underline{Q}_{r,n,i}^{k+1}=\begin{bmatrix}Q_{r,n,i,L}^{k+1} & Q_{r,n,i,R}^{k+1}\end{bmatrix}^T\,. \quad (6.63e)$$

We close this equation using the upstream closures

$$\psi_n^{k+1}(x_{i-1/2})\approx\psi_{n,i,L}^{k+1,surf}=\begin{cases}\psi_{n,i,L}^{k+1}\,, & \mu_n<0\,,\\ \psi_{n,L}^{b,k+1}\,, & \mu_n>0\,, \quad i=1\,,\\ \psi_{n,i-1,R}^{k+1}\,, & \mu_n>0\,, \quad 2\le i\le I\,,\end{cases} \quad (6.64a)$$

$$\psi_n^{k+1}(x_{i+1/2}) \approx \psi_{n,i,R}^{k+1,surf} = \begin{cases} \psi_{n,i+1,L}^{k+1}, & \mu_n < 0, \quad 1 \le i \le I-1, \\ \psi_{n,R}^{b,k+1}, & \mu_n < 0, \quad i = I, \\ \psi_{n,i,R}^{k+1}, & \mu_n > 0, \end{cases} \tag{6.64b}$$

and define

$$\underline{\psi}_{n,i}^{k+1,surf} = \begin{bmatrix} \psi_{n,i,L}^{k+1,surf} & \psi_{n,i,R}^{k+1,surf} \end{bmatrix}^T . \tag{6.65}$$

Now Eq. (6.61) becomes

$$\begin{aligned} &\frac{1}{c\Delta t_{k+1}} \underline{\underline{M}}_i \left(\underline{\psi}_{n,i}^{k+1} - \underline{\psi}_{n,i}^{k} \right) + \mu_n \underline{\underline{L}}_i^{surf} \underline{\psi}_{n,i}^{k+1,surf} - \mu_n \underline{\underline{L}}_i \underline{\psi}_{n,i}^{k+1} + \sigma_{P,i}^k \underline{\underline{M}}_i \underline{\psi}_{n,i}^{k+1} \\ &= \frac{\sigma_{P,i}^k}{2} \left[1 - f_i^k \right] \underline{\underline{M}}_i \sum_{n'=1}^{N} \underline{\psi}_{n',i}^{k+1} \Delta_{n'} + \frac{c}{2} f_i^k \sigma_{P,i}^k \underline{\underline{M}}_i \underline{U}_{r,i}^k + \left[\frac{1 - f_i^k}{2} \right] \underline{\underline{M}}_i \underline{Q}_{m,i}^{k+1} + \underline{\underline{M}}_i \underline{Q}_{r,n,i}^{k+1} . \end{aligned} \tag{6.66}$$

We also have an initial condition given by

$$\underline{\psi}_{n,i}^0 = \begin{bmatrix} \int_{x_{i-1/2}}^{x_{i+1/2}} w_{i,L}(x) \psi_n^i(x) \, \mathrm{d}x \\ \int_{x_{i-1/2}}^{x_{i+1/2}} w_{i,R}(x) \psi_n^i(x) \, \mathrm{d}x \end{bmatrix} . \tag{6.67}$$

Comparing Eq. (6.66) with Eq. (3.50), which was derived in Chapter 3, we see that the grey IMC LDFEM transport equation has a similar form to the linear implicit LDFEM transport equation, though with different cross sections and sources. The first term on the right is called the pseudo-scattering term, since it is mathematically similar to the scattering term in the linear implicit LDFEM equations. Just as in the case of linear transport, this term must be iterated to convergence, and Eq. (6.66) must be solved using mesh sweeps.

To spatially discretize Eq. (6.43b) we average over a cell by operating by $\frac{1}{\Delta x_i} \int_{x_{i-1/2}}^{x_{i+1/2}} (\cdot) \, \mathrm{d}x$, and obtain

$$\frac{1}{\Delta t_{k+1}} \left[U_{m,i}^{k+1} - U_{m,i}^k \right] + c f_i^k \sigma_{P,i}^k U_{r,i}^k = \frac{f_i^k \sigma_{P,i}^k}{2} \sum_{n'=1}^{N} \left(\psi_{n',i,L}^{k+1} + \psi_{n',i,R}^{k+1} \right) \Delta_{n'} + f_i^k(x) Q_{m,i}^{k+1} , \tag{6.68}$$

with initial conditions

$$T_i^0 = \frac{1}{\Delta x_i} \int_{x_{i-1/2}}^{x_{i+1/2}} T^i(x) \, \mathrm{d}x , \tag{6.69a}$$

$$U_{m,i}^0 = \int_0^{T_i^0} c_{v,i}(T') \, \mathrm{d}T' , \tag{6.69b}$$

$$U_{r,i}^0 = a \left(T_i^0 \right)^4 . \tag{6.69c}$$

Eqs. (6.66) and (6.68), together with the upsteam closures, Eqs. (6.64), and the initial conditions, Eqs. (6.67) and (6.69), represent the grey, implicit linear discontinuous finite element IMC equations.

6.3.4 Solving the Implicit Grey Equations

Solving the grey linear discontinuous finite element IMC equations proceeds in several steps. The first step is to solve Eq. (6.66) for the grey radiation intensity, $\underline{\psi}_{n,i}^{k+1}$. As we already stated, this equation must be solved using mesh sweeps, and the pseudo-scattering term must be iterated to convergence. To solve Eqs. (6.66), we start by writing the streaming term as

$$\mu_n \underline{\underline{L}}_i^{surf} \underline{\psi}_{n,i}^{k+1,surf} = \mu_n \underline{\underline{P}}_n \underline{\psi}_{n,i}^{k+1} - \mu_n \underline{\underline{R}}_n \underline{\psi}_{n,i}^{k+1,inc}, \tag{6.70}$$

where

$$\underline{\underline{P}}_n = \begin{cases} \begin{bmatrix} -1 & 0 \\ 0 & 0 \end{bmatrix}, & \mu_n < 0, \\ \begin{bmatrix} 0 & 0 \\ 0 & 1 \end{bmatrix}, & \mu_n > 0, \end{cases} \tag{6.71a}$$

$$\underline{\underline{R}}_n = \begin{cases} \begin{bmatrix} 0 & 0 \\ 0 & -1 \end{bmatrix}, & \mu_n < 0, \\ \begin{bmatrix} 1 & 0 \\ 0 & 0 \end{bmatrix}, & \mu_n > 0, \end{cases} \tag{6.71b}$$

and

$$\underline{\psi}_{n,i}^{k+1,inc} = \begin{cases} \begin{bmatrix} 0 & \psi_{n,i,R}^{k+1,inc} \end{bmatrix}^T, & \mu_n < 0, \\ \begin{bmatrix} \psi_{n,i,L}^{k+1,inc} & 0 \end{bmatrix}^T, & \mu_n > 0, \end{cases} \tag{6.72}$$

where

$$\psi_{n,i,L}^{k+1,inc} = \begin{cases} \psi_{n,L}^{b,k+1}, & i = 1, \\ \psi_{n,i-1,R}^{k+1}, & 2 \leq i \leq I, \end{cases} \tag{6.73a}$$

$$\psi_{n,i,R}^{k+1,inc} = \begin{cases} \psi_{n,i+1,L}^{k+1}, & 1 \le i \le I-1, \\ \psi_{n,R}^{b,k+1}, & i = I. \end{cases} \tag{6.73b}$$

Then, Eq. (6.66) may be written as

$$\left[\left(\frac{1}{c\Delta t_{k+1}} + \sigma_{P,i}^k\right)\underline{\underline{M}}_i + \mu_n\left(\underline{\underline{P}}_n - \underline{\underline{L}}_i\right)\right]\underline{\psi}_{n,i}^{k+1} = \frac{\sigma_{P,i}^k}{2}\left[1 - f_i^k\right]\underline{\underline{M}}_i \sum_{n'=1}^{N} \underline{\psi}_{n',i}^{k+1}\,\Delta_{n'}$$
$$+ \frac{1}{c\Delta t_{k+1}}\underline{\underline{M}}_i\underline{\psi}_{n,i}^k + \mu_n\underline{\underline{R}}_n\underline{\psi}_{n,i}^{k+1,inc} + \frac{c}{2}f_i^k\sigma_{P,i}^k\underline{\underline{M}}_i\underline{U}_{r,i}^k + \left[\frac{1-f_i^k}{2}\right]\underline{\underline{M}}_i\underline{Q}_{m,i}^{k+1} + \underline{\underline{M}}_i\underline{Q}_{r,n,i}^{k+1}. \tag{6.74}$$

In order for the $\underline{\psi}_{n,i}^{k+1,inc}$ vector on the right side of Eq. (6.74) to be known, we use mesh sweeps to solve Eq. (6.74) in each cell. See Section 3.3.1 for a description of mesh sweeps.

Just as with the linear implicit method, we must use iterations to converge the pseudo-scattering term in Eq. (6.74). Writing Eq. (6.74) as an iterative method, we have

$$\left[\left(\frac{1}{c\Delta t_{k+1}} + \sigma_{P,i}^k\right)\underline{\underline{M}}_i + \mu_n\left(\underline{\underline{P}}_n - \underline{\underline{L}}_i\right)\right]\underline{\psi}_{n,i}^{(l+1/2),k+1} = \frac{\sigma_{P,i}^k}{2}\left[1 - f_i^k\right]\underline{\underline{M}}_i\underline{\phi}_i^{(l),k+1}$$
$$+ \frac{1}{c\Delta t_{k+1}}\underline{\underline{M}}_i\underline{\psi}_{n,i}^k + \mu_n\underline{\underline{R}}_n\underline{\psi}_{n,i}^{(l+1/2),k+1,inc} + \frac{c}{2}f_i^k\sigma_{P,i}^k\underline{\underline{M}}_i\underline{U}_{r,i}^k + \left[\frac{1-f_i^k}{2}\right]\underline{\underline{M}}_i\underline{Q}_{m,i}^{k+1}$$
$$+ \underline{\underline{M}}_i\underline{Q}_{r,n,i}^{k+1}, \tag{6.75a}$$

$$\underline{\phi}_i^{(l+1/2),k+1} = \sum_{n=1}^{N} \underline{\psi}_{n,i}^{(l+1/2),k+1}\,\Delta_n, \tag{6.75b}$$

$$\underline{\phi}_i^{(l+1),k+1} = \underline{\phi}_i^{(l+1/2),k+1}, \tag{6.75c}$$

where l is the iteration index and $\underline{\phi}_i^{(l),k+1}$ is the grey scalar intensity. The iterative scheme described in Eqs. (6.75) is called source iteration, and is known to converge slowly when the time steps are large. In this dissertation, we have used the Modified Four-Step Diffusion Synthetic Accereration (DSA) method [3]. See Appendix B.3 for a derivation of that method applied to the grey IMC equations.

The second step in solving the grey IMC LDFEM equations, after calculating the grey radiation intensity at the end of the time step, is to calculate the new material energy density. Solving Eq. (6.68) for $U_{m,i}^{k+1}$, we obtain

$$U_{m,i}^{k+1} = U_{m,i}^k - c\Delta t_{k+1}\sigma_{P,i}^k f_i^k U_{r,i}^k + \frac{\Delta t_{k+1}\sigma_{P,i}^k f_i^k}{2}\sum_{n'=1}^{N}\left(\psi_{n',i,L}^{k+1} + \psi_{n',i,R}^{k+1}\right)\Delta_{n'} + \Delta t_{k+1} f_i^k Q_{m,i}^{k+1}. \tag{6.76}$$

Finally, the new temperature and radiation energy are calculated using

$$U_{m,i}^{k+1} = \int_0^{T^{k+1}} c_{v,i}(T')\,\mathrm{d}T', \tag{6.77a}$$

$$U_{r,i}^{k+1} = a\left(T_i^{k+1}\right)^4. \tag{6.77b}$$

6.4 The Grey SBJ Method

In the previous section we derived the equations for the well-known grey IMC linear discontinuous finite element. In this section, we apply the SBJ method to the IMC LDFEM equations. To review, the SBJ method operates (in one dimension) by lagging the incident angular intensity on a two-cell block to the beginning of the time step. With this approximation, the four unknown angular and scalar intensities in the two-cell system may be calculated. The unknowns adjacent to the outer block boundaries are discarded, while the unknowns adjacent to the cell boundary in the block interior are retained. Reflecting boundaries are simulated using ghost cells. On an incident boundary, the boundary condition is evaluated at the end of the time step, and the unknowns adjacent to the problem boundary are retained. A more in-depth description of the SBJ transport method is provided in Section 3.4.

Writing Eq. (6.66) for a block, and modifying the equation according to the SBJ method, we obtain

$$\begin{aligned}\frac{1}{c\Delta t_{k+1}}\underline{\underline{M}}_{i+1/2}\left(\underline{\hat{\psi}}_{n,i+1/2}^{k+1} - \underline{\psi}_{n,i+1/2}^{k}\right) + \mu_n \underline{\underline{L}}_{i+1/2}^{surf}\underline{\hat{\psi}}_{n,i+1/2}^{k+1,surf} - \mu_n \underline{\underline{L}}_{i+1/2}\underline{\hat{\psi}}_{n,i+1/2}^{k+1} \\ + \underline{\underline{M}}_{i+1/2}^{P,k}\underline{\hat{\psi}}_{n,i+1/2}^{k+1} = \frac{1}{2}\left(\underline{\underline{M}}_{i+1/2}^{P,k} - \underline{\underline{M}}_{i+1/2}^{f,P,k}\right)\sum_{n'=1}^{N}\underline{\hat{\psi}}_{n',i+1/2}^{k+1}\Delta_{n'} + \frac{c}{2}\underline{\underline{M}}_{i+1/2}^{f,P,k}\underline{U}_{r,i+1/2}^{k} \\ + \frac{1}{2}\left(\underline{\underline{M}}_{i+1/2} - \underline{\underline{M}}_{i+1/2}^{f,k}\right)\underline{Q}_{m,i+1/2}^{k+1} + \underline{\underline{M}}_{i+1/2}\underline{Q}_{r,n,i+1/2}^{k+1},\end{aligned} \tag{6.78}$$

where the matrices are defined as

$$\underline{\underline{M}}_{i+1/2} = \begin{bmatrix}\underline{\underline{M}}_i & \underline{\underline{0}} \\ \underline{\underline{0}} & \underline{\underline{M}}_{i+1}\end{bmatrix} = \begin{bmatrix}\frac{\Delta x_i}{2} & 0 & 0 & 0 \\ 0 & \frac{\Delta x_i}{2} & 0 & 0 \\ 0 & 0 & \frac{\Delta x_{i+1}}{2} & 0 \\ 0 & 0 & 0 & \frac{\Delta x_{i+1}}{2}\end{bmatrix}, \tag{6.79a}$$

$$\underline{\underline{M}}^{P,k}_{i+1/2} = \begin{bmatrix} \sigma^k_{P,i}\underline{\underline{M}}_i & \underline{\underline{0}} \\ \underline{\underline{0}} & \sigma^k_{P,i+1}\underline{\underline{M}}_{i+1} \end{bmatrix}$$

$$= \begin{bmatrix} \frac{\sigma^k_{P,i}\Delta x_i}{2} & 0 & 0 & 0 \\ 0 & \frac{\sigma^k_{P,i}\Delta x_i}{2} & 0 & 0 \\ 0 & 0 & \frac{\sigma^k_{P,i+1}\Delta x_{i+1}}{2} & 0 \\ 0 & 0 & 0 & \frac{\sigma^k_{P,i+1}\Delta x_{i+1}}{2} \end{bmatrix}, \tag{6.79b}$$

$$\underline{\underline{M}}^{f,P,k}_{i+1/2} = \begin{bmatrix} f^k_i\sigma^k_{P,i}\underline{\underline{M}}_i & \underline{\underline{0}} \\ \underline{\underline{0}} & f^k_{i+1}\sigma^k_{P,i+1}\underline{\underline{M}}_{i+1} \end{bmatrix}$$

$$= \begin{bmatrix} \frac{f^k_i\sigma^k_{P,i}\Delta x_i}{2} & 0 & 0 & 0 \\ 0 & \frac{f^k_i\sigma^k_{P,i}\Delta x_i}{2} & 0 & 0 \\ 0 & 0 & \frac{f^k_{i+1}\sigma^k_{P,i+1}\Delta x_{i+1}}{2} & 0 \\ 0 & 0 & 0 & \frac{f^k_{i+1}\sigma^k_{P,i+1}\Delta x_{i+1}}{2} \end{bmatrix}, \tag{6.79c}$$

$$\underline{\underline{M}}^{f,k}_{i+1/2} = \begin{bmatrix} f^k_i\underline{\underline{M}}_i & \underline{\underline{0}} \\ \underline{\underline{0}} & f^k_{i+1}\underline{\underline{M}}_{i+1} \end{bmatrix} = \begin{bmatrix} \frac{f^k_i\Delta x_i}{2} & 0 & 0 & 0 \\ 0 & \frac{f^k_i\Delta x_i}{2} & 0 & 0 \\ 0 & 0 & \frac{f^k_{i+1}\Delta x_{i+1}}{2} & 0 \\ 0 & 0 & 0 & \frac{f^k_{i+1}\Delta x_{i+1}}{2} \end{bmatrix}, \tag{6.79d}$$

$$\underline{\underline{L}}^{surf}_{i+1/2} = \begin{bmatrix} \underline{\underline{L}}^{surf}_{i} & \underline{\underline{0}} \\ \underline{\underline{0}} & \underline{\underline{L}}^{surf}_{i+1} \end{bmatrix} = \begin{bmatrix} -1 & 0 & 0 & 0 \\ 0 & 1 & 0 & 0 \\ 0 & 0 & -1 & 0 \\ 0 & 0 & 0 & 1 \end{bmatrix}, \tag{6.79e}$$

$$\underline{\underline{L}}_{i+1/2} = \begin{bmatrix} \underline{\underline{L}}_{i} & \underline{\underline{0}} \\ \underline{\underline{0}} & \underline{\underline{L}}_{i+1} \end{bmatrix} = \begin{bmatrix} -\frac{1}{2} & -\frac{1}{2} & 0 & 0 \\ \frac{1}{2} & \frac{1}{2} & 0 & 0 \\ 0 & 0 & -\frac{1}{2} & -\frac{1}{2} \\ 0 & 0 & \frac{1}{2} & \frac{1}{2} \end{bmatrix}. \tag{6.79f}$$

The vectors in Eq. (6.78) are defined as

$$\underline{\hat{\psi}}^{k+1}_{n,i+1/2} = \begin{cases} \begin{bmatrix} \psi^{k+1}_{n,1,L} & \psi^{k+1}_{n,1,R} & \psi^{k+1}_{n,2,L} & \psi^{k+1/2}_{n,2,R} \end{bmatrix}^T, & \text{incident left boundary}, \\ \begin{bmatrix} \psi^{k+1/2}_{n,i,L} & \psi^{k+1}_{n,i,R} & \psi^{k+1}_{n,i+1,L} & \psi^{k+1/2}_{n,i+1,R} \end{bmatrix}^T, & \\ & \text{interior and reflecting boundaries}, \\ \begin{bmatrix} \psi^{k+1/2}_{n,I-1,L} & \psi^{k+1}_{n,I-1,R} & \psi^{k+1}_{n,I,L} & \psi^{k+1}_{n,I,R} \end{bmatrix}^T, & \text{incident right boundary}, \end{cases} \tag{6.80a}$$

$$\underline{\psi}^{k}_{n,i+1/2} = \begin{bmatrix} \psi^{k}_{n,i,L} & \psi^{k}_{n,i,R} & \psi^{k}_{n,i+1,L} & \psi^{k}_{n,i+1,R} \end{bmatrix}^T, \tag{6.80b}$$

$$\underline{U}^{k}_{r,i+1/2} = \begin{bmatrix} U^{k}_{r,i} & U^{k}_{r,i} & U^{k}_{r,i+1} & U^{k}_{r,i+1} \end{bmatrix}^T, \tag{6.80c}$$

$$\underline{Q}^{k+1}_{m,i+1/2} = \begin{bmatrix} Q^{k+1}_{m,i} & Q^{k+1}_{m,i} & Q^{k+1}_{m,i+1} & Q^{k+1}_{m,i+1} \end{bmatrix}^T, \tag{6.80d}$$

$$\underline{Q}^{k+1}_{r,n,i+1/2} = \begin{bmatrix} Q^{k+1}_{r,n,i,L} & Q^{k+1}_{r,n,i,R} & Q^{k+1}_{r,n,i+1,L} & Q^{k+1}_{r,n,i+1,R} \end{bmatrix}^T. \tag{6.80e}$$

We also define the surface angular intensity vector in Eq. (6.78). For an incident boundary

on the left, we define

$$\underline{\hat{\psi}}_{n,3/2}^{k+1,surf} = \begin{cases} \begin{bmatrix} \psi_{n,1,L}^{k+1} & \psi_{n,2,L}^{k+1} & \psi_{n,2,L}^{k+1} & \psi_{n,3,L}^{k} \end{bmatrix}^T, & \mu_n < 0, \\ \begin{bmatrix} \psi_{n,L}^{b,k+1} & \psi_{n,1,R}^{k+1} & \psi_{n,1,R}^{k+1} & \psi_{n,2,R}^{k+1/2} \end{bmatrix}^T, & \mu_n > 0, \end{cases} \tag{6.81a}$$

for the problem interior and reflecting boundaries, we define

$$\underline{\hat{\psi}}_{n,i+1/2}^{k+1,surf} = \begin{cases} \begin{bmatrix} \psi_{n,i,L}^{k+1/2} & \psi_{n,i+1,L}^{k+1} & \psi_{n,i+1,L}^{k+1} & \psi_{n,i+2,L}^{k} \end{bmatrix}^T, & \mu_n < 0, \\ \begin{bmatrix} \psi_{n,i-1,R}^{k} & \psi_{n,i,R}^{k+1} & \psi_{n,i,R}^{k+1} & \psi_{n,i+1,R}^{k+1/2} \end{bmatrix}^T, & \mu_n > 0, \end{cases} \tag{6.81b}$$

and for a right incident boundary, we define

$$\underline{\hat{\psi}}_{n,I-1/2}^{k+1,surf} = \begin{cases} \begin{bmatrix} \psi_{n,I-1,L}^{k+1/2} & \psi_{n,I,L}^{k+1} & \psi_{n,I,L}^{k+1} & \psi_{n,R}^{b,k+1} \end{bmatrix}^T, & \mu_n < 0, \\ \begin{bmatrix} \psi_{n,I-2,R}^{k} & \psi_{n,I-1,R}^{k+1} & \psi_{n,I-1,R}^{k+1} & \psi_{n,I,R}^{k+1} \end{bmatrix}^T, & \mu_n > 0. \end{cases} \tag{6.81c}$$

Just as in the linear SBJ transport method presented in Section 3.4, the grey SBJ TRT method can be solved without sweeps. We discuss how to solve the grey SBJ equations in the next section. Like the linear SBJ transport method, the grey SBJ TRT method is not conservative. To conserve energy on the problem domain, we use a global rebalance. This is derived in Section 6.4.2. Finally, we can improve the accuracy of the grey SBJ transport method using iterations, which we derive in Section 6.4.3.

6.4.1 Solving the Grey SBJ Transport Equations

In this section we discuss how to solve Eq. (6.78). To begin, we split the surface term into known and unknown components:

$$\mu_n \underline{\underline{L}}_{i+1/2}^{surf} \underline{\hat{\psi}}_{n,i+1/2}^{k+1,surf} = \mu_n \underline{\underline{\hat{P}}}_n \underline{\hat{\psi}}_{n,i+1/2}^{k+1} - \mu_n \underline{\underline{\hat{R}}}_n \underline{\hat{\psi}}_{n,i+1/2}^{k,inc}, \tag{6.82}$$

where the matrices $\underline{\underline{\hat{P}}}_n$ and $\underline{\underline{\hat{R}}}_n$ are defined as

$$\underline{\underline{\hat{P}}}_n = \begin{cases} \begin{bmatrix} -1 & 0 & 0 & 0 \\ 0 & 0 & 1 & 0 \\ 0 & 0 & -1 & 0 \\ 0 & 0 & 0 & 0 \end{bmatrix}, & \mu_n < 0\,, \\ \begin{bmatrix} 0 & 0 & 0 & 0 \\ 0 & 1 & 0 & 0 \\ 0 & -1 & 0 & 0 \\ 0 & 0 & 0 & 1 \end{bmatrix}, & \mu_n > 0\,, \end{cases} \tag{6.83a}$$

$$\underline{\underline{\hat{R}}}_n = \begin{cases} \begin{bmatrix} 0 & 0 & 0 & 0 \\ 0 & 0 & 0 & 0 \\ 0 & 0 & 0 & 0 \\ 0 & 0 & 0 & -1 \end{bmatrix}, & \mu_n < 0\,, \\ \begin{bmatrix} 1 & 0 & 0 & 0 \\ 0 & 0 & 0 & 0 \\ 0 & 0 & 0 & 0 \\ 0 & 0 & 0 & 0 \end{bmatrix}, & \mu_n > 0\,, \end{cases} \tag{6.83b}$$

and we have also defined, for $\mu_n < 0$,

$$\underline{\hat{\psi}}^{k,inc}_{n,i+1/2} = \begin{cases} \begin{bmatrix} 0 & 0 & 0 & \psi^k_{n,i+2,L} \end{bmatrix}^T, & 1 \le i \le I-2\,, \\ \begin{bmatrix} 0 & 0 & 0 & \psi^{b,k+1}_{n,R} \end{bmatrix}^T, & i = I-1\,, \end{cases} \tag{6.84a}$$

and for $\mu_n > 0$,

$$\underline{\hat{\psi}}^{k,inc}_{n,i+1/2} = \begin{cases} \begin{bmatrix} \psi^{b,k+1}_{n,L} & 0 & 0 & 0 \end{bmatrix}^T , & i = 1 , \\ \begin{bmatrix} \psi^{k}_{n,i-1,R} & 0 & 0 & 0 \end{bmatrix}^T , & 2 \le i \le I-1 . \end{cases} \tag{6.84b}$$

Now Eq. (6.78) may be rearranged and written as

$$\begin{aligned} \left[\frac{1}{c\Delta t_{k+1}} \underline{\underline{M}}_{i+1/2} + \mu_n \left(\underline{\underline{\hat{P}}}_n - \underline{\underline{L}}_{i+1/2} \right) + \underline{\underline{M}}^{P,k}_{i+1/2} \right] \underline{\hat{\psi}}^{k+1}_{n,i+1/2} &= \frac{1}{c\Delta t_{k+1}} \underline{\underline{M}}_{i+1/2} \underline{\psi}^{k}_{n,i+1/2} \\ + \frac{1}{2} \left(\underline{\underline{M}}^{P,k}_{i+1/2} - \underline{\underline{M}}^{f,P,k}_{i+1/2} \right) \sum_{n'=1}^{N} \underline{\hat{\psi}}^{k+1}_{n',i+1/2} \Delta_{n'} + \mu_n \underline{\underline{\hat{R}}}_n \underline{\hat{\psi}}^{k,inc}_{n,i+1/2} + \frac{c}{2} \underline{\underline{M}}^{f,P,k}_{i+1/2} \underline{U}^{k}_{r,i+1/2} \\ + \frac{1}{2} \left(\underline{\underline{M}}_{i+1/2} - \underline{\underline{M}}^{f,k}_{i+1/2} \right) \underline{Q}^{k+1}_{m,i+1/2} + \underline{\underline{M}}_{i+1/2} \underline{Q}^{k+1}_{r,n,i+1/2} . \end{aligned} \tag{6.85}$$

Defining

$$\underline{\underline{A}}^{k+1}_{n,i+1/2} = \frac{1}{c\Delta t_{k+1}} \underline{\underline{M}}_{i+1/2} + \mu_n \left(\underline{\underline{\hat{P}}}_n - \underline{\underline{L}}_{i+1/2} \right) + \underline{\underline{M}}^{P,k}_{i+1/2} , \tag{6.86}$$

and multiplying Eq. (6.85) by $\left(\underline{\underline{A}}^{k+1}_{n,i+1/2} \right)^{-1}$, we obtain

$$\begin{aligned} \underline{\hat{\psi}}^{k+1}_{n,i+1/2} &= \frac{1}{c\Delta t_{k+1}} \left(\underline{\underline{A}}^{k+1}_{n,i+1/2} \right)^{-1} \underline{\underline{M}}_{i+1/2} \underline{\psi}^{k}_{n,i+1/2} \\ + \frac{1}{2} \left(\underline{\underline{A}}^{k+1}_{n,i+1/2} \right)^{-1} \left(\underline{\underline{M}}^{P,k}_{i+1/2} - \underline{\underline{M}}^{f,P,k}_{i+1/2} \right) \sum_{n'=1}^{N} \underline{\hat{\psi}}^{k+1}_{n',i+1/2} \Delta_{n'} + \mu_n \left(\underline{\underline{A}}^{k+1}_{n,i+1/2} \right)^{-1} \underline{\underline{\hat{R}}}_n \underline{\hat{\psi}}^{k,inc}_{n,i+1/2} \\ + \frac{c}{2} \left(\underline{\underline{A}}^{k+1}_{n,i+1/2} \right)^{-1} \underline{\underline{M}}^{f,P,k}_{i+1/2} \underline{U}^{k}_{r,i+1/2} + \frac{1}{2} \left(\underline{\underline{A}}^{k+1}_{n,i+1/2} \right)^{-1} \left(\underline{\underline{M}}_{i+1/2} - \underline{\underline{M}}^{f,k}_{i+1/2} \right) \underline{Q}^{k+1}_{m,i+1/2} \\ + \left(\underline{\underline{A}}^{k+1}_{i+1/2} \right)^{-1} \underline{\underline{M}}_{i+1/2} \underline{Q}^{k+1}_{r,n,i+1/2} . \end{aligned} \tag{6.87}$$

Operating on Eq. (6.87) by $\sum_{n=1}^{N} (\cdot) \Delta_n$ and defining the scalar intensity

$$\underline{\hat{\phi}}^{k+1}_{i+1/2} = \sum_{n=1}^{N} \underline{\hat{\psi}}^{k+1}_{n,i+1/2} \Delta_n , \tag{6.88}$$

we obtain

$$\begin{aligned}
&\left[\underline{\underline{I}} - \frac{1}{2}\sum_{n=1}^{N}\left(\underline{\underline{A}}_{n,i+1/2}^{k+1}\right)^{-1}\Delta_n\left(\underline{\underline{M}}_{i+1/2}^{P,k} - \underline{\underline{M}}_{i+1/2}^{f,P,k}\right)\right]\underline{\hat{\phi}}_{i+1/2}^{k+1} \\
&\quad = \frac{1}{c\Delta t_{k+1}}\sum_{n=1}^{N}\left(\underline{\underline{A}}_{n,i+1/2}^{k+1}\right)^{-1}\underline{\underline{M}}_{i+1/2}\underline{\psi}_{n,i+1/2}^{k}\Delta_n + \sum_{n=1}^{N}\mu_n\left(\underline{\underline{A}}_{n,i+1/2}^{k+1}\right)^{-1}\underline{\underline{\hat{R}}}_n\underline{\hat{\psi}}_{n,i+1/2}^{k,inc}\Delta_n \\
&\qquad\qquad + \frac{c}{2}\left[\sum_{n=1}^{N}\left(\underline{\underline{A}}_{n,i+1/2}^{k+1}\right)^{-1}\Delta_n\right]\underline{\underline{M}}_{i+1/2}^{f,P,k}\underline{U}_{r,i+1/2}^{k} \\
&\qquad\qquad + \frac{1}{2}\left[\sum_{n=1}^{N}\left(\underline{\underline{A}}_{n,i+1/2}^{k+1}\right)^{-1}\Delta_n\right]\left(\underline{\underline{M}}_{i+1/2} - \underline{\underline{M}}_{i+1/2}^{f,k}\right)\underline{Q}_{m,i+1/2}^{k+1} \\
&\qquad\qquad\qquad + \sum_{n=1}^{N}\left(\underline{\underline{A}}_{n,i+1/2}^{k+1}\right)^{-1}\underline{\underline{M}}_{i+1/2}\underline{Q}_{r,n,i+1/2}^{k+1}\Delta_n\,. \quad (6.89)
\end{aligned}$$

Solving the grey SBJ transport equations consists of first solving Eq. (6.89) for the grey SBJ scalar intensity $\underline{\hat{\phi}}_{i+1/2}^{k+1}$. This may then be substituted into Eq. (6.87), and the grey SBJ angular intensity $\underline{\hat{\psi}}_{n,i+1/2}^{k+1}$ may be calculated.

After the angular intensity has been calculated, we calculate the new material energy density using Eq. (6.76), the new temperature using Eq. (6.77a), and the new radiation energy density using Eq. (6.77b).

6.4.2 Restoring Particle Conservation Using Rebalance

Just as in the case of the linear SBJ transport method, as well as the SBJ diffusion method discussed in Chapter 2, the grey SBJ TRT method does not conserve particles. We can obtain *domain-wise* particle conservation using a global rebalance. To calculate the global rebalance factor, we return to Eq. (6.43a):

$$\begin{aligned}
&\frac{1}{c\Delta t_{k+1}}\left[\psi^{k+1}(x,\mu) - \psi^{k}(x,\mu)\right] + \mu\frac{\partial}{\partial x}\psi^{k+1}(x,\mu) + \sigma_P^k(x)\psi^{k+1}(x,\mu) \\
&\qquad = \frac{\sigma_P^k(x)}{2}\left[1 - f^k(x)\right]\int_{-1}^{1}\psi^{k+1}(x,\mu')\,\mathrm{d}\mu' + \frac{c}{2}f^k(x)\sigma_P^k(x)U_r^k(x) \\
&\qquad\qquad + \left[\frac{1-f^k(x)}{2}\right]Q_m^{k+1}(x) + Q_r^{k+1}(x,\mu)\,. \quad (6.90)
\end{aligned}$$

Operating on Eq. (6.90) by $\int_{-1}^{1}(\cdot)\,\mathrm{d}\mu$, we find

$$\frac{1}{c\Delta t_{k+1}}\left[\phi^{k+1}(x)-\phi^{k}(x)\right]+\frac{\mathrm{d}}{\mathrm{d}x}F^{k+1}(x)+f^{k}(x)\sigma_{P}^{k}(x)\phi^{k+1}(x)=cf^{k}(x)\sigma_{P}^{k}(x)U_{r}^{k}(x)$$
$$+\left[1-f^{k}(x)\right]Q_{m}^{k+1}(x)+\int_{-1}^{1}Q_{r}^{k+1}(x,\mu)\,\mathrm{d}\mu\,, \quad (6.91)$$

where

$$F^{k+1}(x)=\int_{-1}^{1}\mu\,\psi^{k+1}(x,\mu)\,\mathrm{d}\mu\,, \quad (6.92)$$

is the radiation flux.

Integrating over the spatial domain by operating on Eq. (6.91) with $\int_{0}^{X}(\cdot)\,\mathrm{d}x$, we obtain

$$\frac{1}{c\Delta t_{k+1}}\left[\int_{0}^{X}\phi^{k+1}(x)\,\mathrm{d}x-\int_{0}^{X}\phi^{k}(x)\,\mathrm{d}x\right]+\left[F_{L}^{out,k+1}+F_{R}^{out,k+1}\right]-\left[F_{L}^{b,k+1}+F_{R}^{b,k+1}\right]$$
$$+\int_{0}^{X}f^{k}(x)\sigma_{P}^{k}(x)\phi^{k+1}(x)\,\mathrm{d}x=c\int_{0}^{X}f^{k}(x)\sigma_{P}^{k}(x)U_{r}^{k}(x)\,\mathrm{d}x+\int_{0}^{X}\left[1-f^{k}(x)\right]Q_{m}^{k+1}(x)\,\mathrm{d}x$$
$$+\int_{0}^{X}\int_{-1}^{1}Q_{r}^{k+1}(x,\mu)\,\mathrm{d}\mu\,\mathrm{d}x\,, \quad (6.93)$$

where

$$F_{L}^{out,k+1}=\int_{-1}^{0}\mu\,\psi^{k+1}(0,\mu)\,\mathrm{d}\mu\,, \quad (6.94a)$$

$$F_{R}^{out,k+1}=\int_{0}^{1}\mu\,\psi^{k+1}(X,\mu)\,\mathrm{d}\mu\,, \quad (6.94b)$$

are the radiation fluxes out of the left and right boundaries, respectively, at time t_{k+1}, and

$$F_{L}^{b,k+1}=\int_{0}^{1}\mu\,\psi_{L}^{b,k+1}(\mu)\,\mathrm{d}\mu\,, \quad (6.95a)$$

$$F_{R}^{b,k+1}=\int_{-1}^{0}\mu\,\psi_{R}^{b,k+1}(\mu)\,\mathrm{d}\mu\,, \quad (6.95b)$$

are the incident radiation fluxes on the left and right boundaries, respectively, at time t_{k+1}.

Eq. (6.93) represents a radiation energy balance equation over the spatial domain $0\le x\le X$ and over all angles at time t_{k+1}. Just as in the linear SBJ transport rebalance method described in Section 3.4.2, we assume that the conservative angular intensity is equal to the non-conservative angular intensity multiplied by a rebalance factor, i.e.,

$$\psi^{k+1}(x,\mu)=\gamma^{k+1}\psi^{nc,k+1}(x,\mu)\,. \quad (6.96)$$

Therefore, the scalar intensity and outgoing radiation fluxes are also equal to the non-

conservative scalar intensity or non-conservative outgoing radiation fluxes multiplied by a rebalance factor:

$$\phi^{k+1}(x) = \gamma^{k+1}\phi^{nc,k+1}(x)\,, \tag{6.97a}$$

$$F_L^{out,k+1} = \gamma^{k+1}F_L^{out,nc,k+1}\,, \tag{6.97b}$$

$$F_R^{out,k+1} = \gamma^{k+1}F_R^{out,nc,k+1}\,, \tag{6.97c}$$

where $\phi^{nc,k+1}(x)$ is the non-conservative scalar intensity, $F_L^{out,k+1}$ is the non-conservative outgoing radiation flux on the left boundary, and $F_R^{out,k+1}$ is the non-conservative outgoing radiation flux on the right boundary. Substituting Eqs. (6.97) into Eq. (6.93) and solving for the rebalance factor, we obtain

$$\gamma^{k+1} = \frac{A^{k+1}}{B^{k+1}}\,, \tag{6.98}$$

where

$$A^{k+1} = \frac{1}{c\Delta t_{k+1}}\int_0^X \phi^k(x)\,\mathrm{d}x + \left[F_L^{b,k+1} + F_R^{b,k+1}\right] + \int_0^X \left[1 - f^k(x)\right]Q_m^{k+1}(x)\,\mathrm{d}x + \int_0^X\int_{-1}^1 Q^{k+1}(x,\mu)\,\mathrm{d}\mu\,\mathrm{d}x\,, \tag{6.99a}$$

$$B^{k+1} = \frac{1}{c\Delta t_{k+1}}\int_0^X \phi^{nc,k+1}(x)\,\mathrm{d}x + \left[F_L^{nc,out,k+1} + F_R^{nc,out,k+1}\right] + \int_0^X f^k(x)\sigma_P^k(x)\phi^{nc,k+1}(x)\,\mathrm{d}x\,. \tag{6.99b}$$

Writing Eqs. (6.99) in discretized form, we have

$$A^{k+1} = \frac{1}{c\Delta t_{k+1}}\sum_{i=1}^I \phi_i^k\,\Delta x_i + \left(F_L^{b,k+1} + F_R^{b,k+1}\right) + \sum_{i=1}^I \left(1 - f_i^k\right)Q_{m,i}^{k+1}\,\Delta x_i + \sum_{i=1}^I\sum_{n=1}^N Q_{r,n,i}^{k+1}\,\Delta_n\,\Delta x_i\,, \tag{6.100a}$$

$$B^{k+1} = \frac{1}{c\Delta t_{k+1}}\sum_{i=1}^I \phi_i^{nc,k+1}\,\Delta x_i + \left(F_L^{nc,out,k+1} + F_R^{nc,out,k+1}\right) + \sum_{i=1}^I f_i^k\sigma_{P,i}^k\phi_i^{nc,k+1}\,\Delta x_i\,, \tag{6.100b}$$

where

$$\phi_i^k = \frac{\phi_{i,L}^k + \phi_{i,R}^k}{2}\,, \tag{6.101a}$$

$$\phi_i^{nc,k+1} = \frac{\phi_{i,L}^{nc,k+1} + \phi_{i,R}^{nc,k+1}}{2}, \tag{6.101b}$$

$$Q_{r,n,i}^{k+1} = \frac{Q_{r,n,i,L}^{k+1} + Q_{r,n,i,R}^{k+1}}{2}, \tag{6.101c}$$

and where

$$F_L^{b,k+1} = \sum_{\mu_n>0} \psi_{n,L}^{b,k+1} \Delta_n, \tag{6.102a}$$

$$F_R^{b,k+1} = \sum_{\mu_n<0} \psi_{n,R}^{b,k+1} \Delta_n, \tag{6.102b}$$

$$F_L^{nc,out,k+1} = \sum_{\mu_n<0} \psi_{n,1,L}^{nc,k+1} \Delta_n, \tag{6.102c}$$

$$F_R^{nc,out,k+1} = \sum_{\mu_n>0} \psi_{n,I,R}^{nc,k+1} \Delta_n. \tag{6.102d}$$

6.4.3 Improving Accuracy Using Iterations

As is demonstrated in the numerical results in Chapter 7, we can improve the accuracy of the grey SBJ TRT method by iterating on the incident angular intensity on each block. The equations for the iterative grey SBJ TRT method without rebalance are

$$\begin{aligned}
&\frac{1}{c\Delta t_{k+1}} \underline{\underline{M}}_{i+1/2} \left(\underline{\hat{\psi}}_{n,i+1/2}^{(l+1/2),k+1} - \underline{\psi}_{n,i+1/2}^{k} \right) + \mu_n \underline{\underline{L}}_{i+1/2}^{surf} \underline{\hat{\psi}}_{n,i+1/2}^{(l),k+1,surf} - \mu_n \underline{\underline{L}}_{i+1/2} \underline{\hat{\psi}}_{n,i+1/2}^{(l+1/2),k+1} \\
&+ \underline{\underline{M}}_{i+1/2}^{P,k} \underline{\hat{\psi}}_{n,i+1/2}^{(l+1/2),k+1} = \frac{1}{2} \left(\underline{\underline{M}}_{i+1/2}^{P,k} - \underline{\underline{M}}_{i+1/2}^{f,P,k} \right) \sum_{n'=1}^{N} \underline{\hat{\psi}}_{n',i+1/2}^{(l+1/2),k+1} \Delta_{n'} + \frac{c}{2} \underline{\underline{M}}_{i+1/2}^{f,P,k} \underline{U}_{r,i+1/2}^{k} \\
&\qquad + \frac{1}{2} \left(\underline{\underline{M}}_{i+1/2} - \underline{\underline{M}}_{i+1/2}^{f,k} \right) \underline{Q}_{m,i+1/2}^{k+1} + \underline{\underline{M}}_{i+1/2} \underline{Q}_{r,n,i+1/2}^{k+1},
\end{aligned} \tag{6.103a}$$

$$\underline{\hat{\psi}}_{n,i+1/2}^{(l+1),k+1} = \underline{\hat{\psi}}_{n,i+1/2}^{(l+1/2),k+1}, \tag{6.103b}$$

where l is the iteration index, and

$$\underline{\hat{\psi}}_{n,i+1/2}^{(l+1/2),k+1} = \begin{cases} \left[\psi_{n,1,L}^{(l+1/2),k+1} \quad \psi_{n,1,R}^{(l+1/2),k+1} \quad \psi_{n,2,L}^{(l+1/2),k+1} \quad \psi_{n,2,R}^{(l+1/2),k+1/2}\right]^T, \\ \qquad\qquad\qquad\qquad\qquad\qquad \text{incident left boundary}, \\ \left[\psi_{n,i,L}^{(l+1/2),k+1/2} \quad \psi_{n,i,R}^{(l+1/2),k+1} \quad \psi_{n,i+1,L}^{(l+1/2),k+1} \quad \psi_{n,i+1,R}^{(l+1/2),k+1/2}\right]^T, \\ \qquad\qquad\qquad\qquad\qquad\qquad \text{interior and reflecting boundaries}, \\ \left[\psi_{n,I-1,L}^{(l+1/2),k+1/2} \quad \psi_{n,I-1,R}^{(l+1/2),k+1} \quad \psi_{n,I,L}^{(l+1/2),k+1} \quad \psi_{n,I,R}^{(l+1/2),k+1}\right]^T, \\ \qquad\qquad\qquad\qquad\qquad\qquad \text{incident right boundary}. \end{cases} \tag{6.104}$$

For a left incident boundary, we define

$$\underline{\hat{\psi}}_{n,3/2}^{(l),k+1,surf} = \begin{cases} \left[\psi_{n,1,L}^{(l+1/2),k+1} \quad \psi_{n,2,L}^{(l+1/2),k+1} \quad \psi_{n,2,L}^{(l+1/2),k+1} \quad \psi_{n,3,L}^{(l),k+1}\right]^T, & \mu_n < 0, \\ \left[\psi_{n,L}^{b,k+1} \quad \psi_{n,1,R}^{(l+1/2),k+1} \quad \psi_{n,1,R}^{(l+1/2),k+1} \quad \psi_{n,2,R}^{(l+1/2),k+1/2}\right]^T, & \mu_n > 0, \end{cases} \tag{6.105a}$$

for the problem interior and reflecting boundaries, we define

$$\underline{\hat{\psi}}_{n,i+1/2}^{(l),k+1,surf} = \begin{cases} \left[\psi_{n,i,L}^{(l+1/2),k+1/2} \quad \psi_{n,i+1,L}^{(l+1/2),k+1} \quad \psi_{n,i+1,L}^{(l+1/2),k+1} \quad \psi_{n,i+2,L}^{(l),k+1}\right]^T, & \mu_n < 0, \\ \left[\psi_{n,i-1,R}^{(l),k+1} \quad \psi_{n,i,R}^{(l+1/2),k+1} \quad \psi_{n,i,R}^{(l+1/2),k+1} \quad \psi_{n,i+1,R}^{(l+1/2),k+1/2}\right]^T, & \mu_n > 0, \end{cases} \tag{6.105b}$$

and for a right incident boundary, we define

$$\underline{\hat{\psi}}_{n,I-1/2}^{(l),k+1,surf} = \begin{cases} \left[\psi_{n,I-1,L}^{(l+1/2),k+1/2} \quad \psi_{n,I,L}^{(l+1/2),k+1} \quad \psi_{n,I,L}^{(l+1/2),k+1} \quad \psi_{n,R}^{b,k+1}\right]^T, & \mu_n < 0, \\ \left[\psi_{n,I-2,R}^{(l),k+1} \quad \psi_{n,I-1,R}^{(l+1/2),k+1} \quad \psi_{n,I-1,R}^{(l+1/2),k+1} \quad \psi_{n,I,R}^{(l+1/2),k+1}\right]^T & \mu_n > 0. \end{cases} \tag{6.105c}$$

Alternatively, we can use the rebalance method derived in the previous section as an acceleration method. The equations for the iterative grey SBJ TRT method with rebalance

are

$$\frac{1}{c\Delta t_{k+1}}\underline{\underline{M}}_{i+1/2}\left(\underline{\hat{\psi}}_{n,i+1/2}^{(l+1/2),k+1}-\underline{\psi}_{n,i+1/2}^{k}\right)+\mu_n\underline{\underline{L}}_{i+1/2}^{surf}\underline{\hat{\psi}}_{n,i+1/2}^{(l),k+1,surf}-\mu_n\underline{\underline{L}}_{i+1/2}\underline{\hat{\psi}}_{n,i+1/2}^{(l+1/2),k+1}$$
$$+\underline{\underline{M}}_{i+1/2}^{P,k}\underline{\hat{\psi}}_{n,i+1/2}^{(l+1/2),k+1}=\frac{1}{2}\left(\underline{\underline{M}}_{i+1/2}^{P,k}-\underline{\underline{M}}_{i+1/2}^{f,P,k}\right)\sum_{n'=1}^{N}\underline{\hat{\psi}}_{n',i+1/2}^{(l+1/2),k+1}\Delta_{n'}+\frac{c}{2}\underline{\underline{M}}_{i+1/2}^{f,P,k}\underline{U}_{r,i+1/2}^{k}$$
$$+\frac{1}{2}\left(\underline{\underline{M}}_{i+1/2}-\underline{\underline{M}}_{i+1/2}^{f,k}\right)\underline{Q}_{m,i+1/2}^{k+1}+\underline{\underline{M}}_{i+1/2}\underline{Q}_{r,n,i+1/2}^{k+1}\,, \quad (6.106a)$$

$$\underline{\hat{\psi}}_{n,i+1/2}^{(l+1),k+1}=\gamma^{(l+1),k+1}\underline{\hat{\psi}}_{n,i+1/2}^{(l+1/2),k+1}\,, \quad (6.106b)$$

where

$$\gamma^{(l+1),k+1}=\frac{A^{k+1}}{B^{(l+1/2),k+1}}\,, \quad (6.107)$$

and

$$A^{k+1}=\frac{1}{c\Delta t_{k+1}}\sum_{i=1}^{I}\phi_i^k\,\Delta x_i+\left(F_L^{b,k+1}+F_R^{b,k+1}\right)+\sum_{i=1}^{I}\left(1-f_i^k\right)Q_{m,i}^{k+1}\,\Delta x_i$$
$$+\sum_{i=1}^{I}\sum_{n=1}^{N}Q_{r,n,i}^{k+1}\,\Delta_n\,\Delta x_i\,, \quad (6.108a)$$

$$B^{(l+1/2),k+1}=\frac{1}{c\Delta t_{k+1}}\sum_{i=1}^{I}\phi_i^{(l+1/2),k+1}\,\Delta x_i+\left(F_L^{(l+1/2),out,k+1}+F_R^{(l+1/2),out,k+1}\right)$$
$$+\sum_{i=1}^{I}f_i^k\sigma_{P,i}^k\phi_i^{(l+1/2),k+1}\,\Delta x_i\,, \quad (6.108b)$$

and where

$$\phi_i^k=\frac{\phi_{i,L}^k+\phi_{i,R}^k}{2}\,, \quad (6.109a)$$

$$\phi_i^{(l+1/2),k+1}=\frac{\sum_{n=1}^{N}\left[\psi_{n,i,L}^{(l+1/2),k+1}+\psi_{n,i,R}^{(l+1/2),k+1}\right]\Delta_n}{2}\,, \quad (6.109b)$$

$$Q_{r,n,i}^{k+1}=\frac{Q_{r,n,i,L}^{k+1}+Q_{r,n,i,R}^{k+1}}{2}\,, \quad (6.109c)$$

and

$$F_L^{b,k+1}=\sum_{\mu_n>0}\psi_{n,L}^{b,k+1}\,\Delta_n\,, \quad (6.110a)$$

$$F_R^{b,k+1}=\sum_{\mu_n<0}\psi_{n,R}^{b,k+1}\,\Delta_n\,, \quad (6.110b)$$

$$F_L^{(l+1/2),out,k+1} = \sum_{\mu_n<0} \psi_{n,1,L}^{(l+1/2),k+1} \Delta_n \,, \tag{6.110c}$$

$$F_R^{(l+1/2),out,k+1} = \sum_{\mu_n>0} \psi_{n,I,R}^{(l+1/2),k+1} \Delta_n \,. \tag{6.110d}$$

6.5 Material Models

In this dissertation, we use two material models. For the Su-Olson benchmark problem presented in Section 7.1, we use the Su-Olson material model, which we present in Section 6.5.1. For the other numerical results, shown in Sections 7.2 and 7.3, we use the ideal gas model, which we present in Section 6.5.2.

6.5.1 Su-Olson Material Model

For the Su-Olson benchmark problem presented in Section 7.1, we use the Su-Olson material model [33]. In this model, we have

$$\sigma_a(x,\nu,T) = \sigma_a(x) \,, \tag{6.111}$$

and the heat capacity satisfies

$$c_v(x,T) = \alpha(x) T^3 \,, \tag{6.112}$$

where $\alpha(x)$ is a user-specified parameter. Therefore

$$\beta(x) = 4a\alpha(x) \,. \tag{6.113}$$

6.5.2 Ideal Gas Material Model

For the results presented in Sections 7.2 and 7.3, we will use the ideal gas material model. In this model, we have [22]

$$\sigma_a(x,\nu,T) = \frac{\gamma_a(x)}{(h\nu)^3} \left(1 - e^{-h\nu/T(x,t)}\right) \,, \tag{6.114}$$

where $\gamma_a(x)$ is a user-specified parameter, and we have a user-specified, temperature-independent heat capacity

$$c_v(x,T) = c_v(x) \,. \tag{6.115}$$

The Planck cross section for this model is then

$$\begin{aligned}\sigma_P(x,t) &= \frac{\int_0^\infty \sigma_a(x,\nu,T)B(\nu,T)\,\mathrm{d}\nu}{\int_0^\infty B(\nu,T)\,\mathrm{d}\nu} \\ &= \frac{15\gamma_a(x)}{\pi^4 T^3(x,t)}\,, \end{aligned} \tag{6.116}$$

and

$$\beta(x,t) = \frac{4aT^3(x,t)}{c_v(x)}\,. \tag{6.117}$$

6.6 Summary

In this chapter, we have derived the equations for the implicit and SBJ time-discretized, IMC linearized, linear discontinuous finite element S_N equations. We began in Section 6.1 by introducing the frequency-dependent, one-dimensional thermal radiation transport equations. Using these equations, we derived the grey thermal radiation transport equations in Section 6.2. In Section 6.3 we began by applying an IMC linearization and implicit time discretization, and then proceeded to discretize the angular variable using the S_N approximation and the spatial variable using the linear discontinuous finite element (LDFEM) method, resulting in the implicit IMC LDFEM equations. We also discussed the solution methodology for these equations. The SBJ discretization for the LDFEM equations was presented in Section 6.4. We also discussed restoring particle conservation using a rebalance scheme, and improving the accuracy of the method using iterations. Finally, in Section 6.5, we presented the material models that will be used to produce the numerical results we present in Chapter 7.

Chapter 7

Thermal Radiation Transport: Numerical Results

In this chapter, we consider three thermal radiation transport problems, to test the grey IMC SBJ transport method versus the traditional grey IMC implicit method. First, in Section 7.1 we consider the well-known Su-Olson benchmark problem. In Section 7.2, we examine the behavior of the grey IMC SBJ transport method and the grey IMC implicit method for a Marshak wave problem. Finally, in Section 7.3, we examine the behavior of the grey IMC SBJ transport method and the grey IMC implicit method for a cooling problem. In Section 7.4, we summarize our findings regarding the behavior of the grey SBJ TRT method. Throughout this chapter, we have scaled the problems such that $c = a = 1$.

7.1 TRT Problem 1: Su-Olson Problem

In this section, we consider the behavior of the grey SBJ transport method with the well-known Su-Olson benchmark [33]. Consider a slab 40 cm wide, divided into 4000 cells. We use the Su-Olson material model defined in Section 6.5.1, with $\sigma_P = 4$ cm^{-1} and $c_v = 1$ keV/(keV cm^3). We use an S_{16} quadrature set, impose a reflecting boundary on the left, a vacuum on the right, and set an initial scalar intensity and initial temperature of zero everywhere. We also impose an isotropic particle source of $Q_r = 1.0$ keV cm^{-3} s^{-1} in the first 0.5 cm on the left, which is turned on for the first 10 s of the simulation, and afterwards turned off. There is no particle source elsewhere, nor is there a temperature source.

Implicit IMC Results

Figures 7.1, 7.2, and 7.3 depict the radiation energy density $U_r(T)$ for the Su-Olson problem, using the implicit method, with time steps of length $\Delta t = 0.1$ s, 0.01 s, and 0.001 s, at times $t = 0.1$ s, 1 s, and 10 s, respectively. Figures 7.4, 7.5, and 7.6 depict the scalar intensity

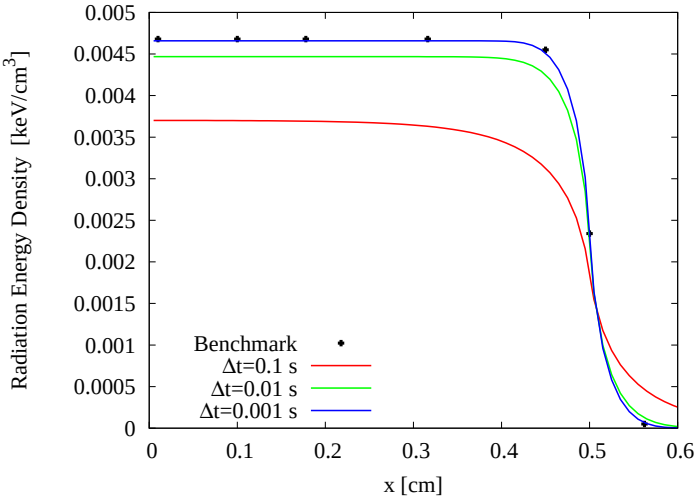

Figure 7.1 TRT Problem 1: Radiation Energy Density for the Implicit Method at $t = 0.1$ s

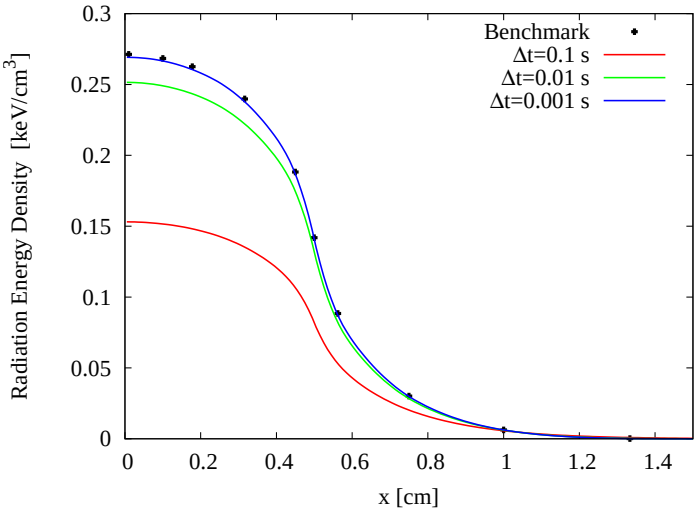

Figure 7.2 TRT Problem 1: Radiation Energy Density for the Implicit Method at $t = 1$ s

calculated using the implicit method, again with time steps of length $\Delta t = 0.1$ s, 0.01 s, and 0.001 s, at times $t = 0.1$ s, 1 s, and 10 s, respectively. Examining these results, we observe that the implicit method successfully converges to the Su-Olson benchmark results as Δt

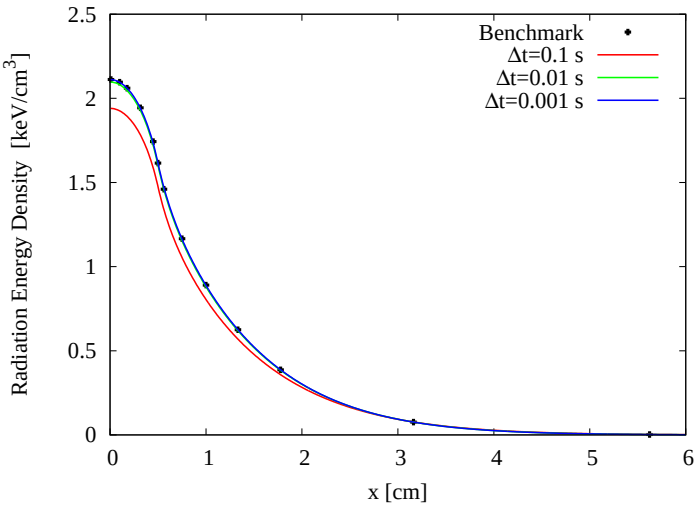

Figure 7.3 TRT Problem 1: Radiation Energy Density for the Implicit Method at $t = 10$ s

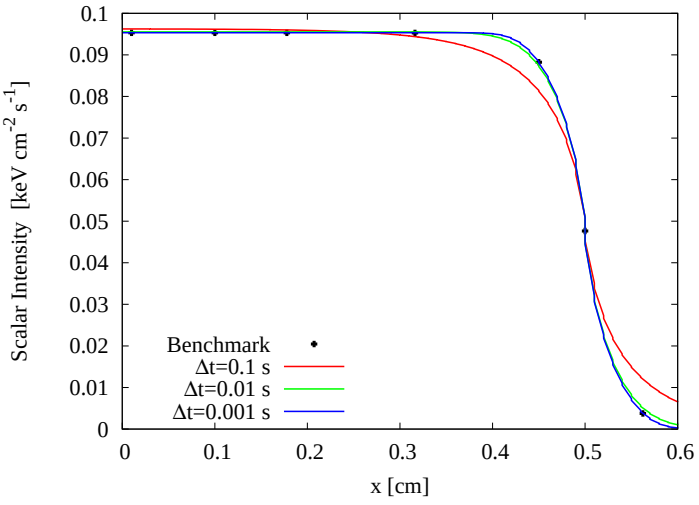

Figure 7.4 TRT Problem 1: Scalar Intensity for the Implicit Method at $t = 0.1$ s

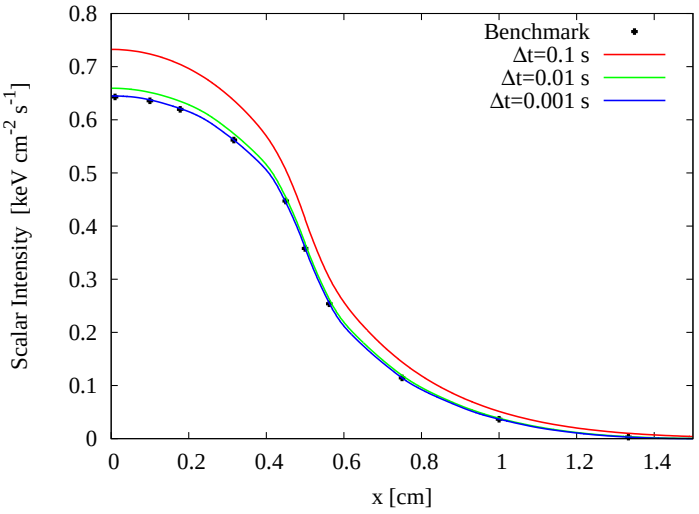

Figure 7.5 TRT Problem 1: Scalar Intensity Density for the Implicit Method at $t = 1$ s

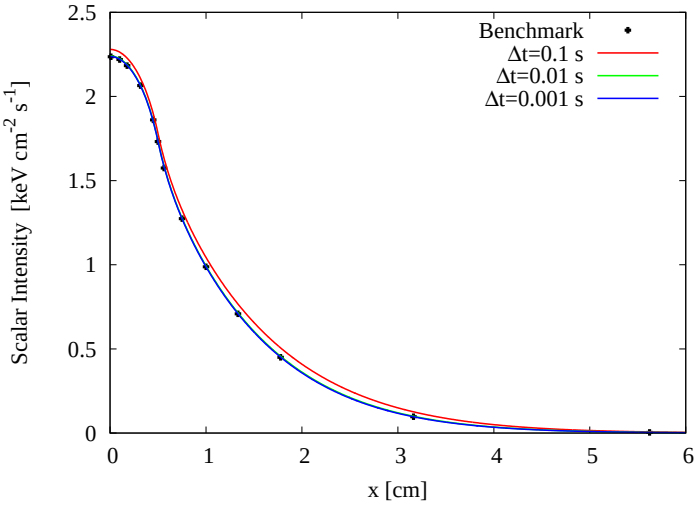

Figure 7.6 TRT Problem 1: Scalar Intensity Density for the Implicit Method at $t = 10$ s

becomes smaller. Moreover, we see a time step length of about $\Delta t = 0.001$ s is necessary before the numerical results begin to match the benchmark results. Coarser time steps lead to inaccurate solutions, particularly for early times. Examining the coarse time step results, we see that the implicit method tends to move particles too deeply into the slab. This conforms with the behavior observed for the linear implicit method in Chapter 5.

Plain SBJ IMC Results

Figures 7.7, 7.8, and 7.9 show the radiation energy density for the plain SBJ TRT method at times $t = 0.1$ s, 1 s, and 10 s, respectively, with time steps of length $\Delta t = 0.1$ s, 0.01 s, and 0.001 s. Figures 7.10, 7.11, and 7.12 show the scalar intensity for the plain SBJ method,

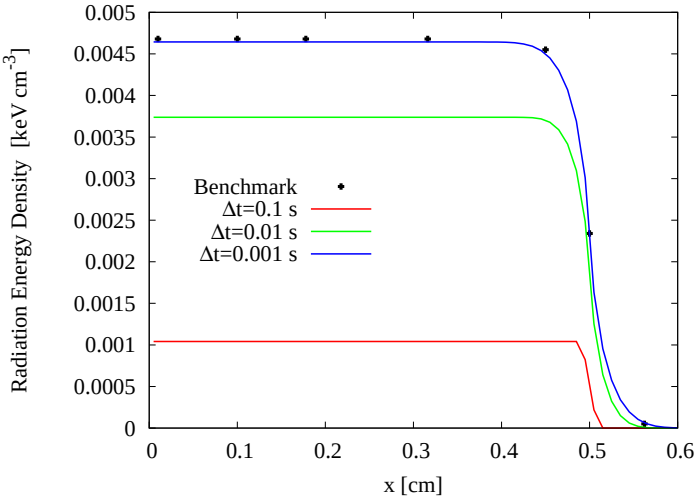

Figure 7.7 TRT Problem 1: Radiation Energy Density for the Plain SBJ Method at $t = 0.1$ s

again at times $t = 0.1$ s, 1 s, and 10 s, respectively. Examining the plain SBJ results, we see that, like the implicit method, the SBJ method does not converge to the benchmark results until we reduce the time step length to $\Delta t = 0.001$ s. For coarser time steps, the plain SBJ method is less accurate than the implicit method, though it does converge to the benchmark solutions at the same time step length. In contrast to the implicit method, which tends to push particles too deeply into the slab, the plain SBJ method tends to artificially slow the particle wave speed. This conforms with the results we obtained for the linear SBJ transport method in Chapter 5.

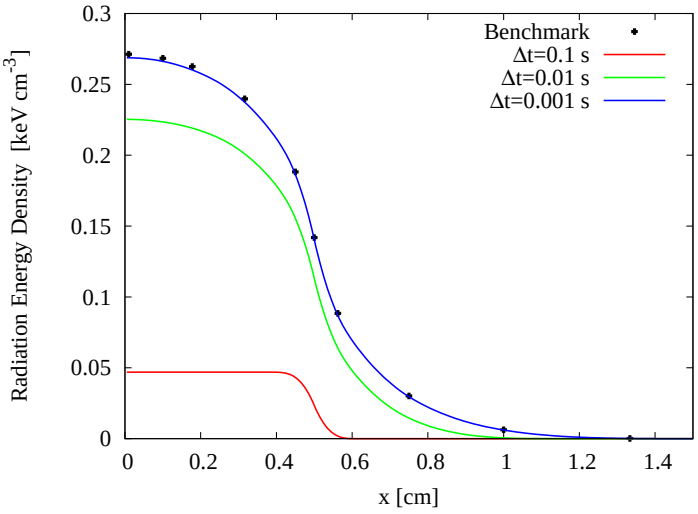

Figure 7.8 TRT Problem 1: Radiation Energy Density for the Plain SBJ Method at $t = 1$ s

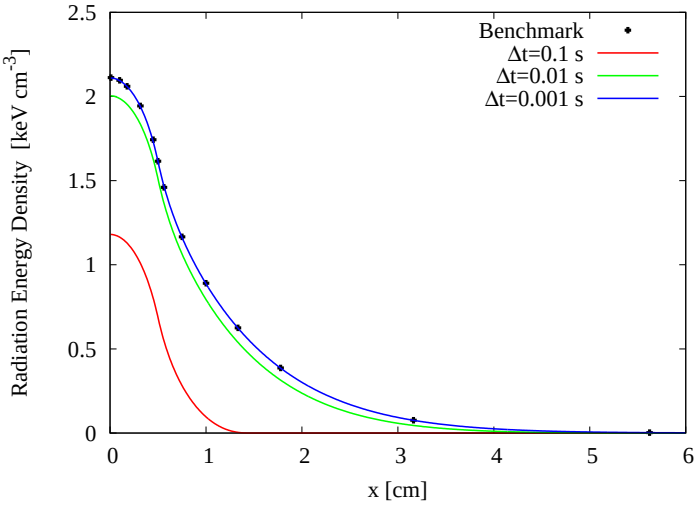

Figure 7.9 TRT Problem 1: Radiation Energy Density for the Plain SBJ Method at $t = 10$ s

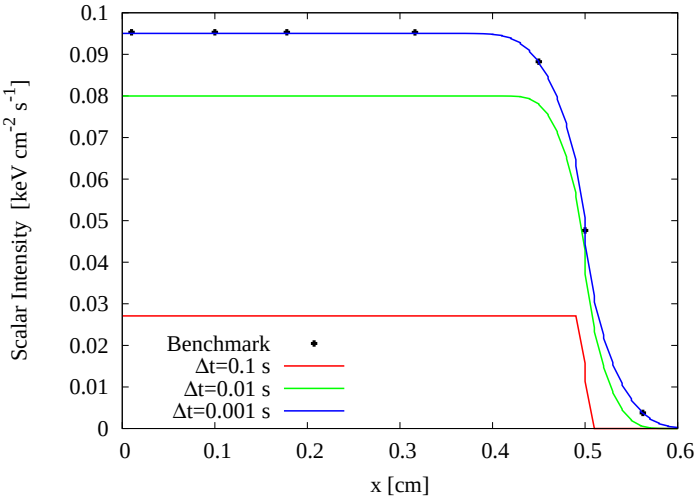

Figure 7.10 TRT Problem 1: Scalar Intensity for the Plain SBJ Method at $t = 0.1$ s

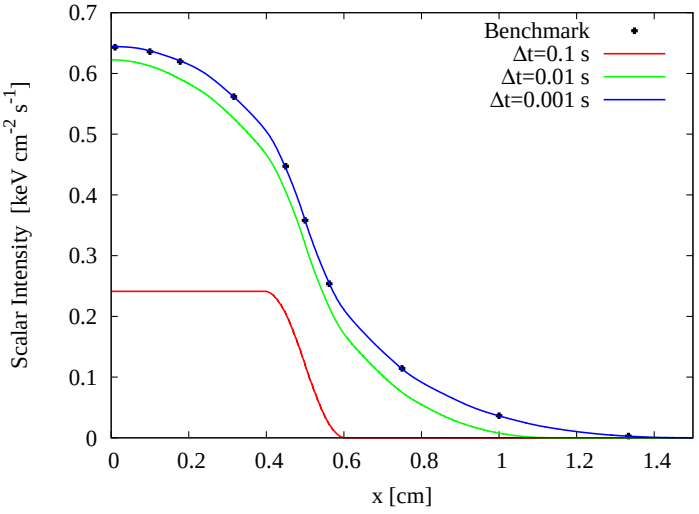

Figure 7.11 TRT Problem 1: Scalar Intensity for the Plain SBJ Method at $t = 1$ s

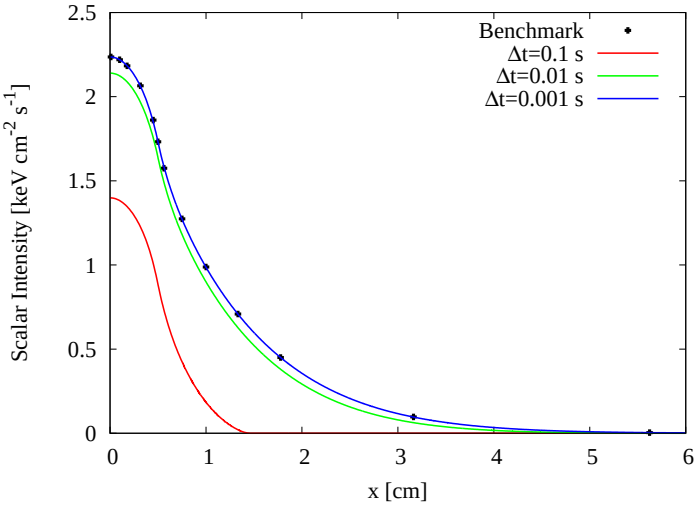

Figure 7.12 TRT Problem 1: Scalar Intensity for the Plain SBJ Method at $t = 10$ s

Conservative SBJ Results

Figures 7.13, 7.14, and 7.15 show the radiation energy density for the conservative SBJ method at times $t = 0.1$ s, 1 s, and 10 s, respectively, with time steps of length $\Delta t = 0.1$ s, 0.01 s, and 0.001 s. Figures 7.16, 7.17, and 7.18 show the scalar intensity for the conser-

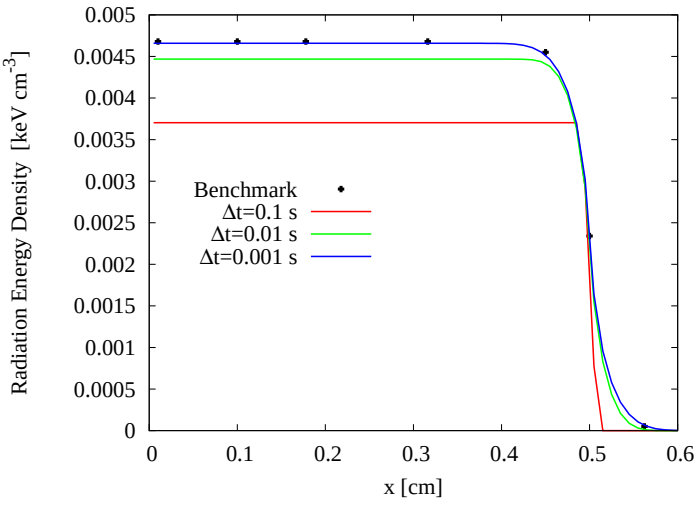

Figure 7.13 TRT Problem 1: Radiation Energy Density for the Conservative SBJ Method at $t = 0.1$ s

vative SBJ method at times $t = 0.1$ s, 1 s, and 10 s, respectively, with time steps of length $\Delta t = 0.1$ s, 0.01 s, and 0.001 s. Examining the results for the conservative SBJ method, we

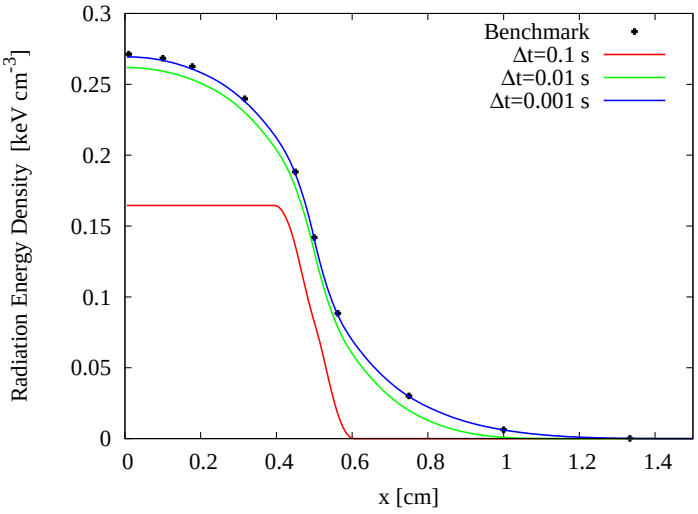

Figure 7.14 TRT Problem 1: Radiation Energy Density for the Conservative SBJ Method at $t = 1$ s

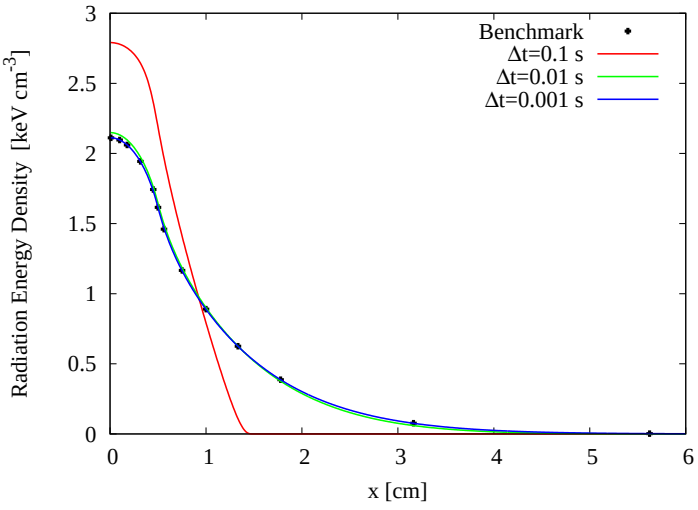

Figure 7.15 TRT Problem 1: Radiation Energy Density for the Conservative SBJ Method at $t = 10$ s

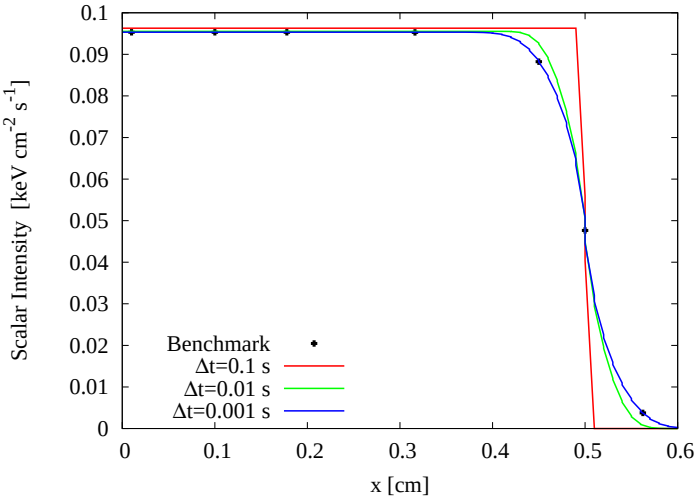

Figure 7.16 TRT Problem 1: Scalar Intensity for the Conservative SBJ Method at $t = 0.1$ s

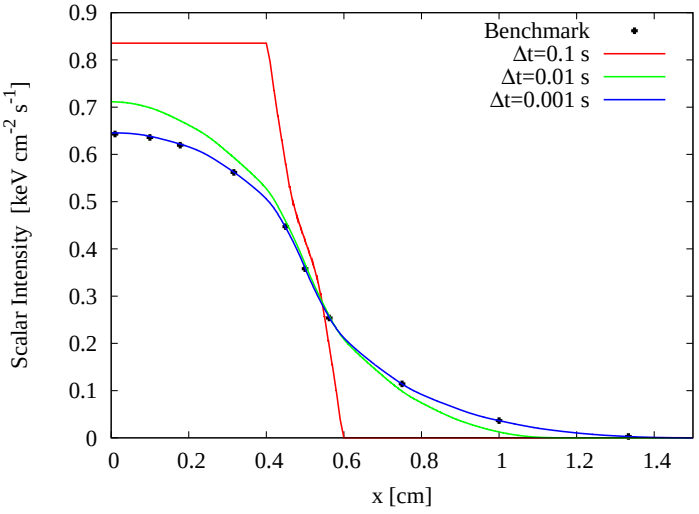

Figure 7.17 TRT Problem 1: Scalar Intensity for the Conservative SBJ Method at $t = 1$ s

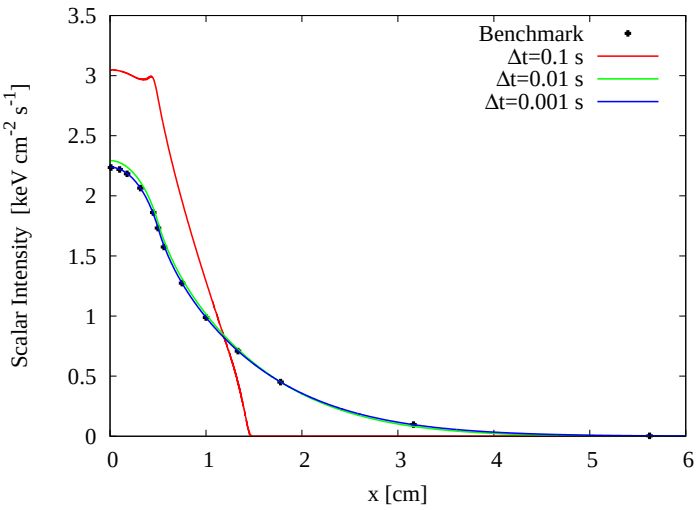

Figure 7.18 TRT Problem 1: Scalar Intensity for the Conservative SBJ Method at $t = 10$ s

see that the particle conservation enables the SBJ method to produce much more accurate results for coarse time steps, although the results still do not converge to the benchmark results until the time step is reduced to $\Delta t = 0.001$ s, and the results are still less accurate than the implicit method at every time step length.

Iterative Results

We next consider the iterative SBJ TRT method, with and without rebalance. Figures 7.19, 7.20, and 7.21 show the number of iterations required to converge the implicit and SBJ methods to an L_2 convergence criterion of 10^{-8} for time step lengths of $\Delta t = 0.1$ s, 0.01 s, and 0.001 s, respectively.

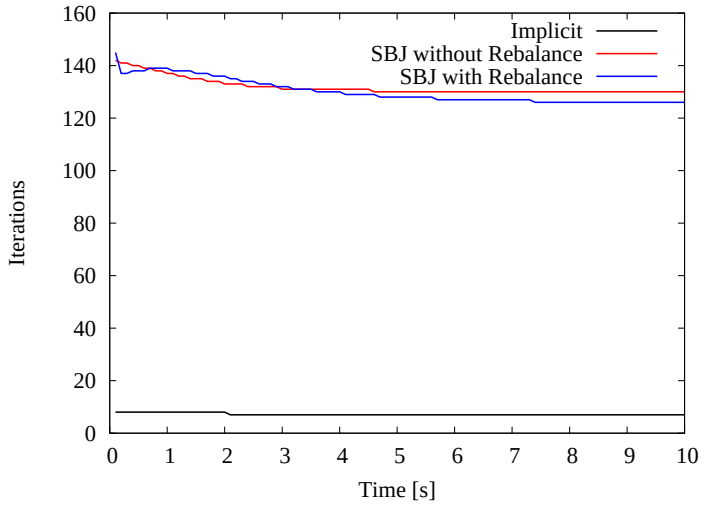

Figure 7.19 TRT Problem 1: Iterations for the Implicit and SBJ Methods with $\Delta t = 0.1$ s

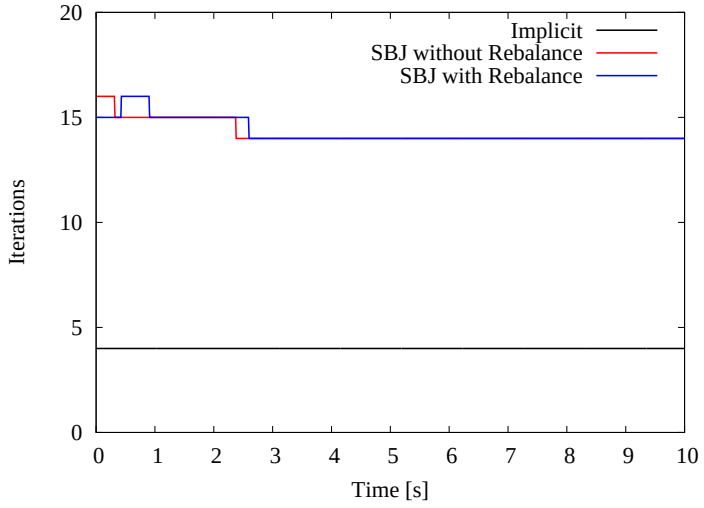

Figure 7.20 TRT Problem 1: Iterations for the Implicit and SBJ Methods with $\Delta t = 0.01$ s

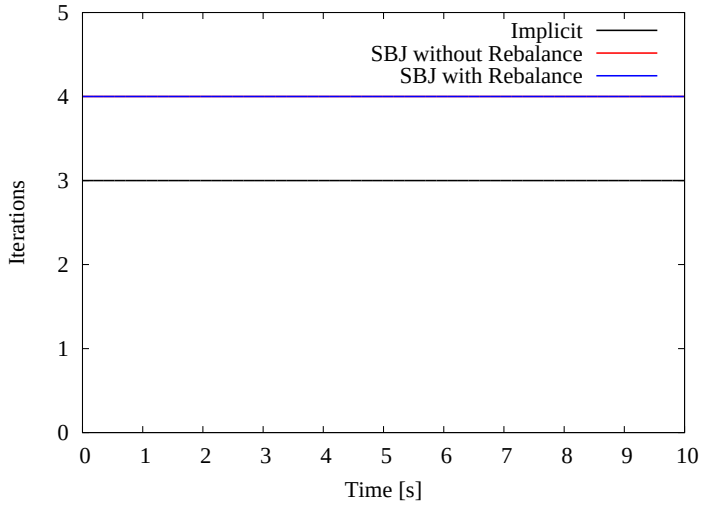

Figure 7.21 TRT Problem 1: Iterations for the Implicit and SBJ Methods with $\Delta t = 0.001$ s

Overall, we see that both the plain SBJ and conservative SBJ methods are less accurate for every time step length than the implicit method. However, if we choose a time step length such that the implicit method produces accurate answers (in comparison to the Su-Olson benchmark results), then the SBJ methods produce accurate answers as well. For coarse time step lengths, the implicit method tends to move particles too deeply into the slab. The plain SBJ method, by contrast, tends to not move particles sufficiently deep into the slab. This is mitigated somewhat by adding particle conservation. Examining the number of iterations required to converge the implicit and SBJ methods, we see that, for coarse time steps, the SBJ method requires many more iterations than the implicit method. However, for these coarse time steps, the SBJ method converges to an inaccurate implicit result. If we refine the time step length such that the results are accurate, the number of iterations required by the SBJ methods are modest.

In addition to the Su-Olson problems shown here, we also tested the code using the Marshak wave problem given in Section 4.5.3 in Ref. [36]. Though we do not show the results here, we were able to reproduce Wollaber's solutions with both the implicit and iterative SBJ methods.

7.2 TRT Problem 2: Marshak Wave Problem

For our second TRT problem, we consider a Marshak wave problem. Consider a slab 10 cm wide, divided into 100 cells. We set the Planck cross section as $\sigma_P = \frac{1}{T^3}$ cm^{-1}, and

use $c_v = 1$ keV/(keV cm^3). The slab is initially cold and in equilibrium, with an initial temperature of $T^i = 0.1$ keV. We set a temperature on the left boundary of $T_L = 1$ keV, and a temperature on the right boundary of $T_R = 0.1$ keV, and we use an S_{16} quadrature set. There is no internal radiation source or heat source.

Implicit IMC Results

Figures 7.22 and 7.23, depict the implicit IMC results for the Marshak wave problem at times $t = 5$ s, 25 s, 75 s, 150 s, and 300 s, for time steps of length $\Delta t = 1$ s and 0.1 s, respectively. In Figure 7.22, we see that the temperature at time $t = 5$ s spikes well above

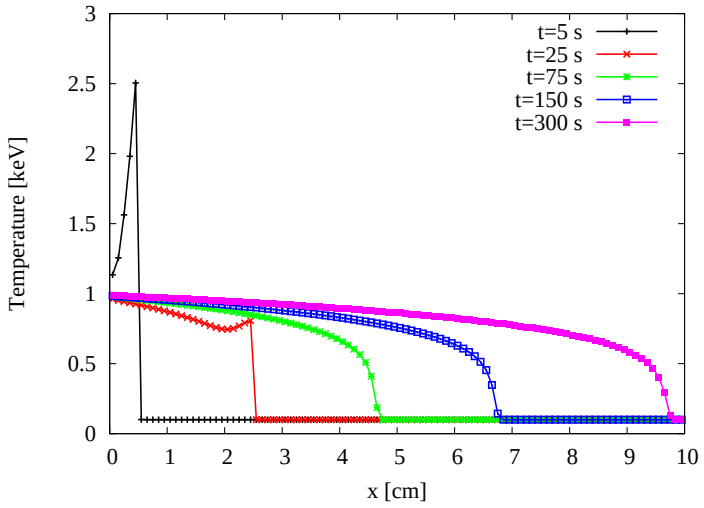

Figure 7.22 TRT Problem 2: Implicit IMC Solution with $\Delta t = 1$ s

the boundary temperature of $T_L = 1$ keV. This non-physical result violates the "maximum principle," which dictates, for this problem, that the temperature may not exceed 1 keV anywhere in the slab at any time (since the temperature source on the left boundary is 1 keV). The violation of the maximum principle is caused by time steps that are too large. If the time step is reduced to $\Delta t = 0.1$ s, as in Figure 7.23, we obtain physically-valid results. Therefore, time steps of $\Delta t = 1$ s are not permitted for this problem.

Figures 7.24 and 7.25 show the implicit solution at $t = 25$ s, for time steps of length $\Delta t = 1$ s, 0.1 s, 0.01 s, and 0.005 s. Figure 7.25 shows a close-up view of the wave front. Examining these figures, we see that the implicit solution does not converge until the time step is decreased to $\Delta t = 0.01$ s.

Figures 7.26 and 7.27 show the implicit solution at $t = 300$ s, for time steps of length $\Delta t = 1$ s, 0.1 s, 0.01 s, and 0.005 s. Figure 7.27 shows a close-up view of the wave front.

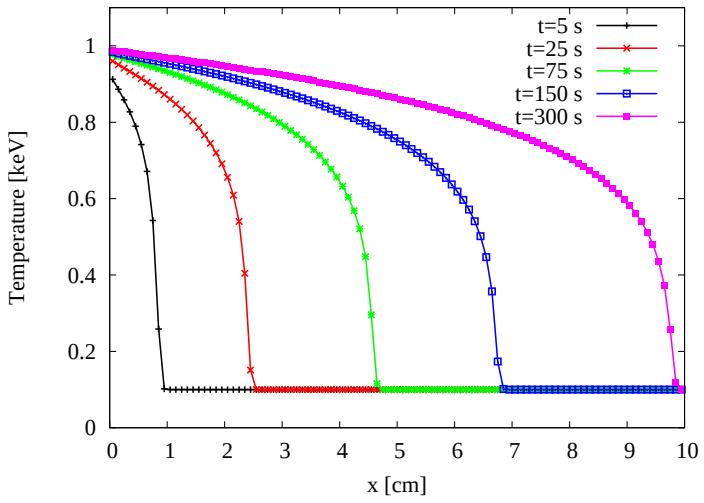

Figure 7.23 TRT Problem 2: Implicit IMC Solution with $\Delta t = 0.1$ s

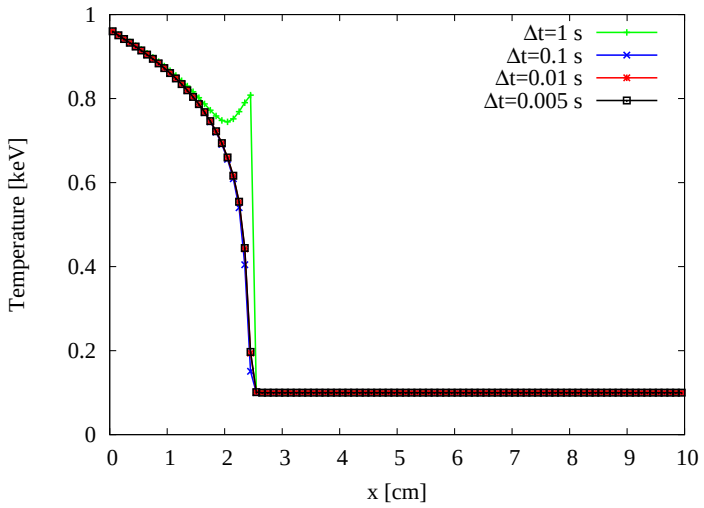

Figure 7.24 TRT Problem 2: Implicit IMC Solution at $t = 25$ s

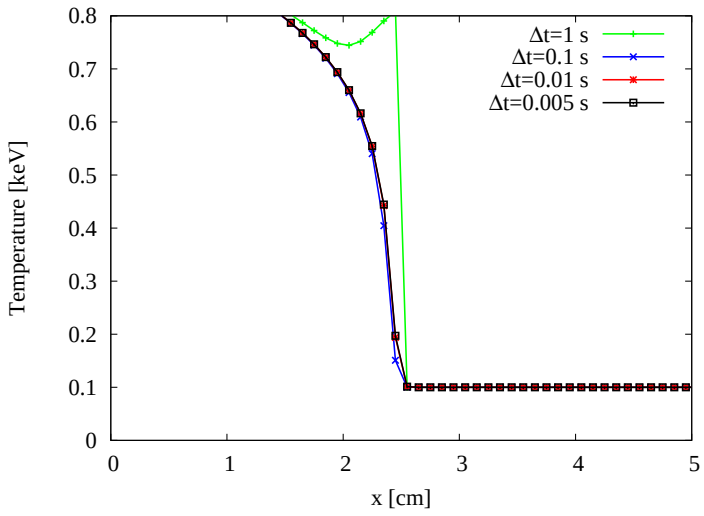

Figure 7.25 TRT Problem 2: Detailed View of the Wave Front for the Implicit IMC Solution at $t = 25$ s

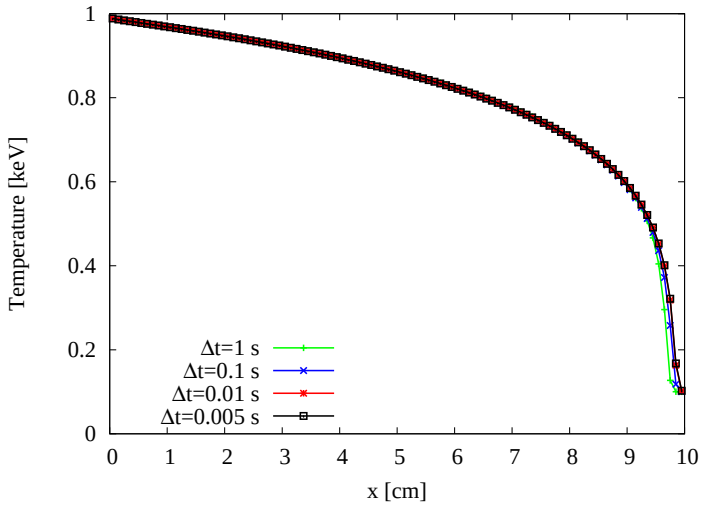

Figure 7.26 TRT Problem 2: Implicit IMC Solution at $t = 300$ s

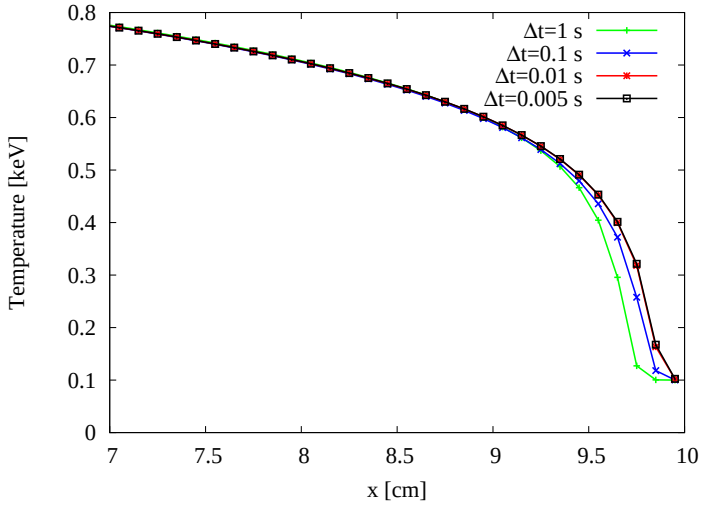

Figure 7.27 TRT Problem 2: Detailed View of the Wave Front for the Implicit IMC Solution at $t = 300$ s

Again, we see that the implicit method is not converged until the time step is decreased to $\Delta t = 0.01$ s.

Plain SBJ IMC Results

Figures 7.28 and 7.29 show the results for the plain SBJ TRT method, at times $t = 5$ s, 25 s, 75 s, 150 s, and 300 s, for time step lengths of $\Delta t = 1$ s and $\Delta t = 0.1$ s. Examining

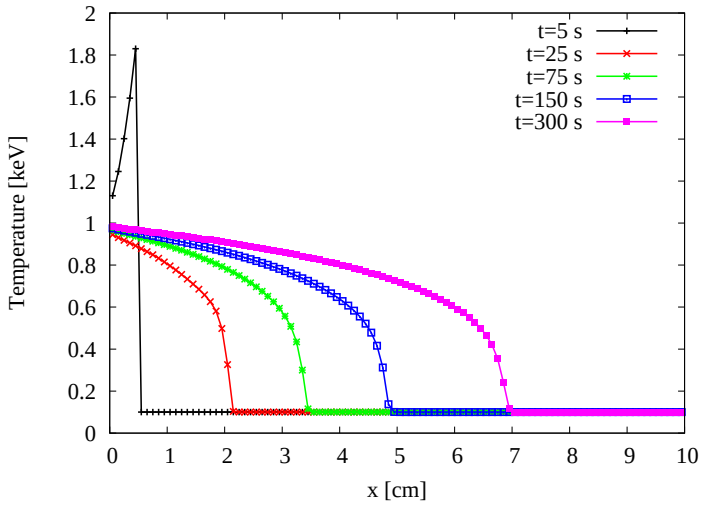

Figure 7.28 TRT Problem 2: Plain SBJ Solution with $\Delta t = 1$ s

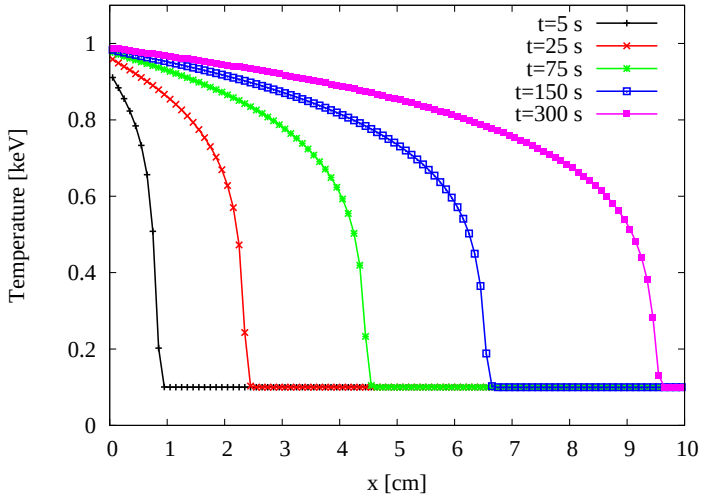

Figure 7.29 TRT Problem 2: Plain SBJ Solution with $\Delta t = 0.1$ s

Figure 7.28, we see that the SBJ IMC method also produces non-physical results if the time step length is too large, which is expected since both the implicit and SBJ IMC methods use the same IMC linearization. In Figure 7.29, we have reduced the time step length to $\Delta t = 0.1$ s, thereby eliminating the violation of the maximum principle, just as with the implicit IMC results. Comparing Figure 7.29 with Figure 7.23, we see that at every time, the wave front has not advanced as far as it should. This is consistent with the previous results.

Figures 7.30 and 7.31 show the results for the plain SBJ IMC method at time $t = 25$ s and $t = 300$ s. Examining these results, we see that the plain SBJ IMC method converges

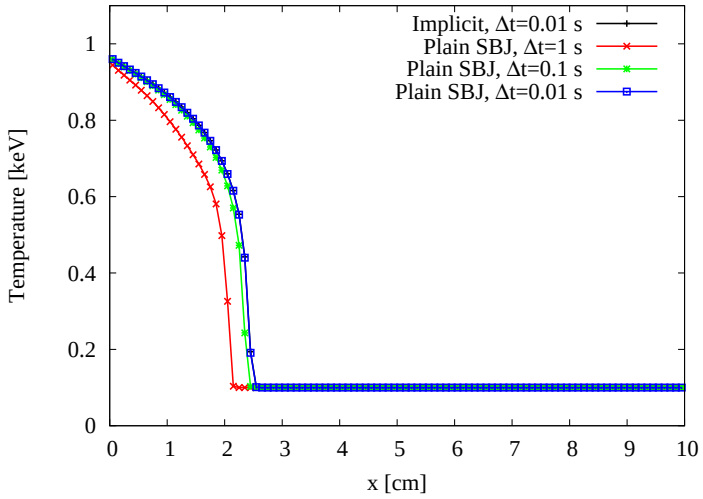

Figure 7.30 TRT Problem 2: Plain SBJ Solution for Various Time Step Lengths at $t = 25$ s

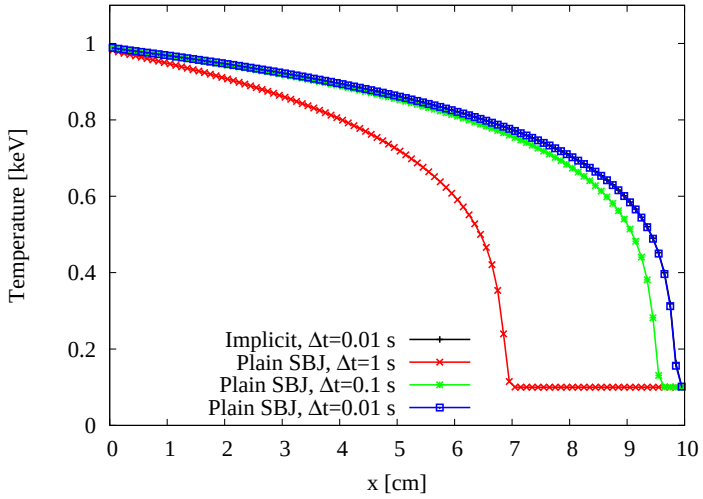

Figure 7.31 TRT Problem 2: Plain SBJ Solution for Various Time Step Lengths at $t = 300$ s

to the implicit IMC results for a time step length of $\Delta t = 0.001$ s. Comparing these results to Figures 7.24 and 7.26, we see that the plain SBJ method is less accurate than the implicit method for coarse time steps, but converges at about the same time step length. However, we also see that, unlike with the implicit IMC method, we can not see from these results that the maximum principle has been violated. It appears that a cancellation of errors has masked the maximum principle violation.

Conservative SBJ IMC Results

Figure 7.32 shows the results for the conservative SBJ TRT method, at times $t = 5$ s, 25 s, 75 s, 150 s, and 300 s, for a time step length of $\Delta t = 0.1$ s. Examining these results, and comparing them to the implicit IMC results in Figures 7.23, we see that, unlike the plain SBJ IMC method, the conservative SBJ IMC method advances the wave front at nearly the correct speed.

Figures 7.33 and 7.34 show the results for the conservative SBJ method at time $t = 25$ s and $t = 300$ s. Examining these results, we see that the conservative SBJ IMC method, at time steps of length $\Delta t = 0.1$ s, is much closer to the correct solution, which the conservative SBJ IMC method converges to at $\Delta t = 0.01$ s, just like the plain SBJ IMC and the implicit IMC methods. For time steps of length $\Delta t = 1$ s, we see symptoms indicative of a maximum principle violation, which were not apparent with the plain SBJ IMC method.

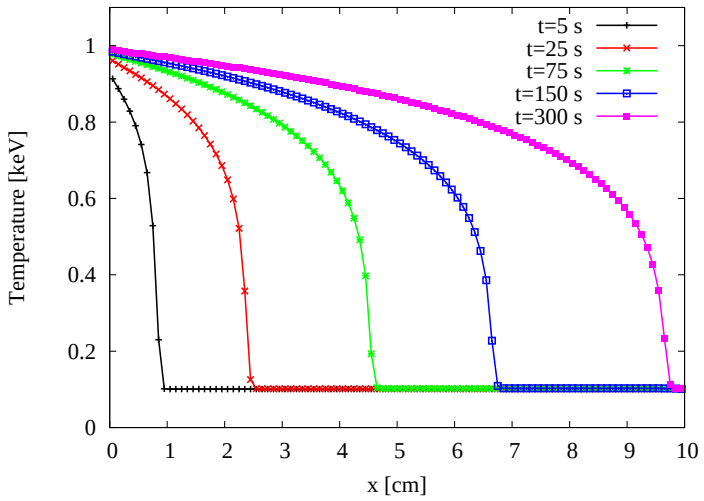

Figure 7.32 TRT Problem 2: Conservative SBJ Solution with $\Delta t = 0.1$ s

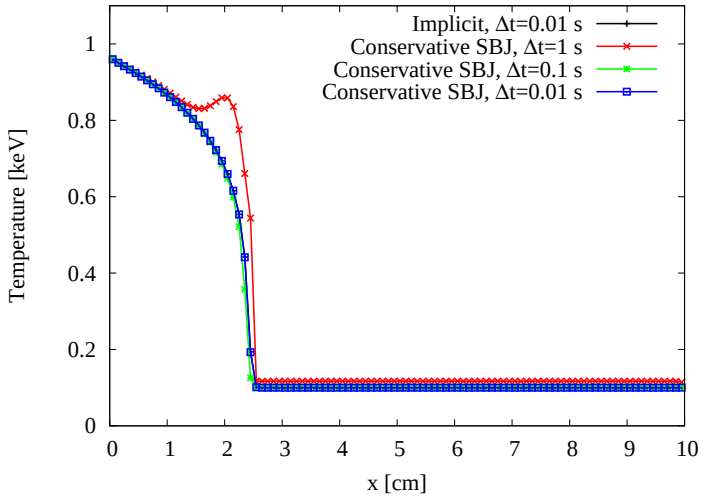

Figure 7.33 TRT Problem 2: Conservative SBJ Solution for Various Time Step Lengths at $t = 25$ s

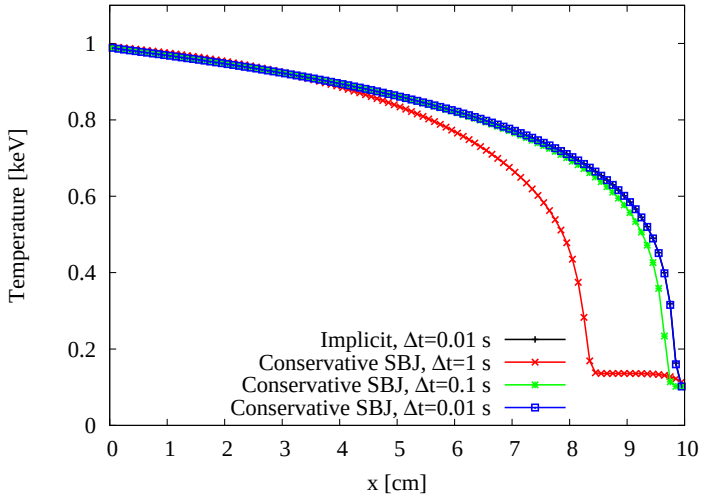

Figure 7.34 TRT Problem 2: Conservative SBJ Solution for Various Time Step Lengths at $t = 300$ s

Iterative Results

In Figures 7.35, 7.36, and 7.37, we show the number of iterations required to converge the iterative SBJ methods and the implicit method to an L_2 convergence criterion of 10^{-7} for time steps of length $\Delta t = 1$ s, 0.1 s, and 0.01 s, respectively. Here we see results similar to those of the Su-Olson problem in Section 7.1, namely, that when we reduce the time step length such that we converge to an accurate answer (i.e., $\Delta t = 0.01$ s for this problem), we also find that the number of iterations required by the SBJ IMC methods are modest.

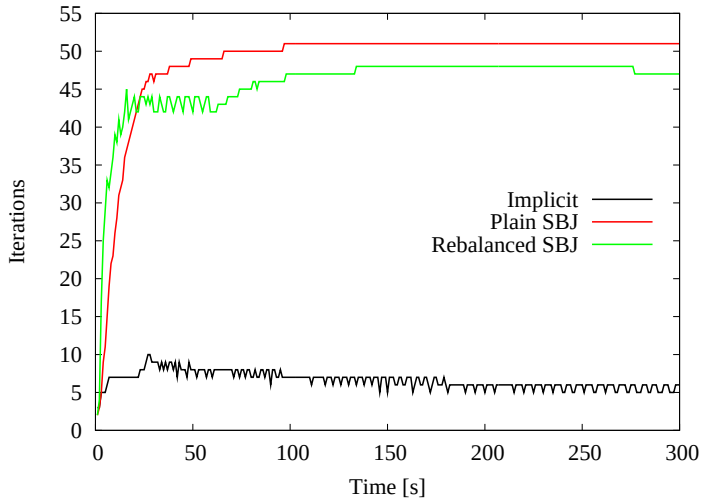

Figure 7.35 TRT Problem 2: Number of Iterations Required for Convergence with $\Delta t = 1$ s

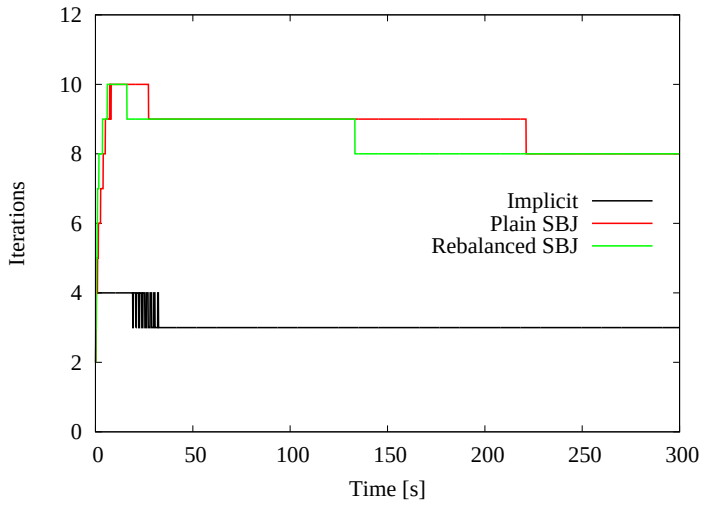

Figure 7.36 TRT Problem 2: Number of Iterations Required for Convergence with $\Delta t = 0.1$ s

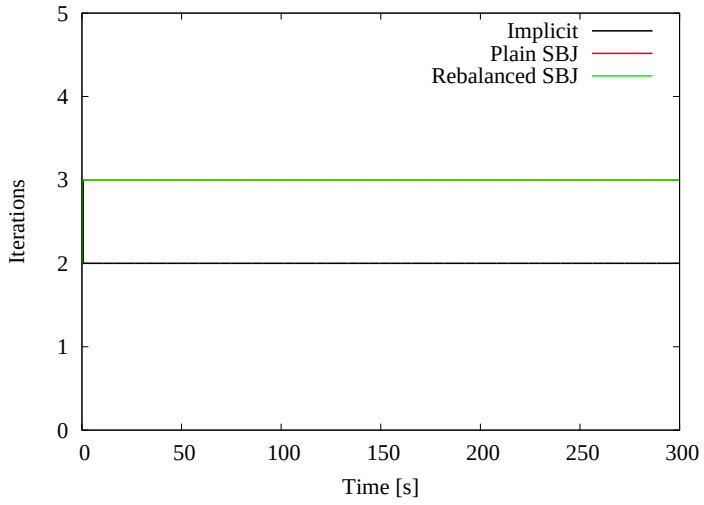

Figure 7.37 TRT Problem 2: Number of Iterations Required for Convergence with $\Delta t = 0.01$ s

We also see that as the Marshak wave proceeds to move through the problem, the number of iterations required to converge the SBJ IMC methods increases. This is because the slab becomes increasingly dominated by optically-thin regions, and the SBJ IMC methods require more iterations to converge optically-thin problems than optically-thick problems, just like the linear SBJ transport method we considered in Chapter 5. We also see that the global rebalance generally reduces the number of iterations required to converge.

Overall, the SBJ IMC methods perform well for the Marshak wave problem, converging to the correct solution for about the same time step length as the implicit IMC method, although the error in the solution is larger for the SBJ IMC methods than for the implicit IMC for coarse time steps. Large time steps that violate the maximum principle are sometimes masked by the plain SBJ method, although much less so by the conservative SBJ method. Obviously, the iterative SBJ methods will converge to the same solution as the implicit IMC methods. For coarse time steps the number of iterations can be fairly large, particularly as the slab becomes hot. However, if the time step length is reduced such that the implicit or iterative SBJ IMC methods produce accurate solutions, then the number of time steps is modest, even when the slab is hot.

7.3 TRT Problem 3: Cooling Problem

We now wish to investigate the behavior of the SBJ method in a hot, cooling slab. Consider a slab of material 10 cm wide divided into 100 cells, with opacity $\sigma_P = \frac{1}{T^3}$ cm^{-1} and heat capacity $c_v = 1$ keV/(keV cm^3). We begin with the slab in thermal equilibrium at $T^i = 1$ keV. We place a reflecting boundary on the left, and a $T_R = 0.1$ boundary on the right, and use an S_{16} quadrature set. We impose no internal particle source or heat source.

Implicit IMC Results

In Figure 7.38, we show the results for the implicit IMC method, with a time step length of $\Delta t = 1$ s, for times $t = 25$ s, 75 s, 150 s, 300 s, 500 s, and 1000 s. Here we see that the results conform to our physical intuitions: the slab gradually cools, starting on the right side.

Now we examine the implicit solution at $t = 10$ s and $t = 1000$ s, to determine what time step length is required to converge. In Figures 7.39 and 7.40, we show the temperature in the slab at time $t = 10$ s. Here we see that the slab is just beginning to cool. Figure 7.40 shows a closeup view of the region where cooling has begun. Here we see that the implicit IMC solution is almost converged at $\Delta t = 1$ s, and is essentially completely converged at

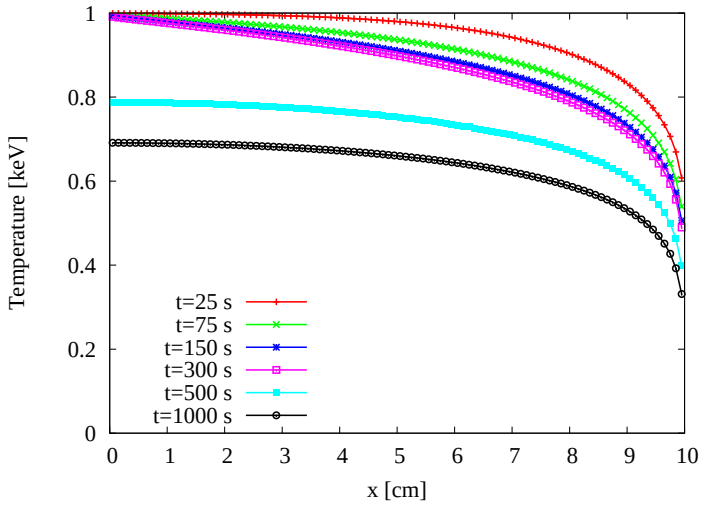

Figure 7.38 TRT Problem 3: Implicit IMC Solution at Various Times with $\Delta t = 1$ s

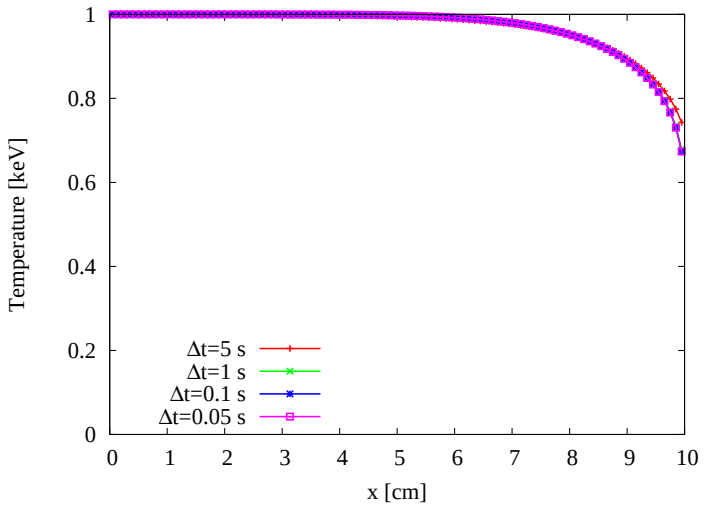

Figure 7.39 TRT Problem 3: Implicit IMC Solution at $t = 10$ s

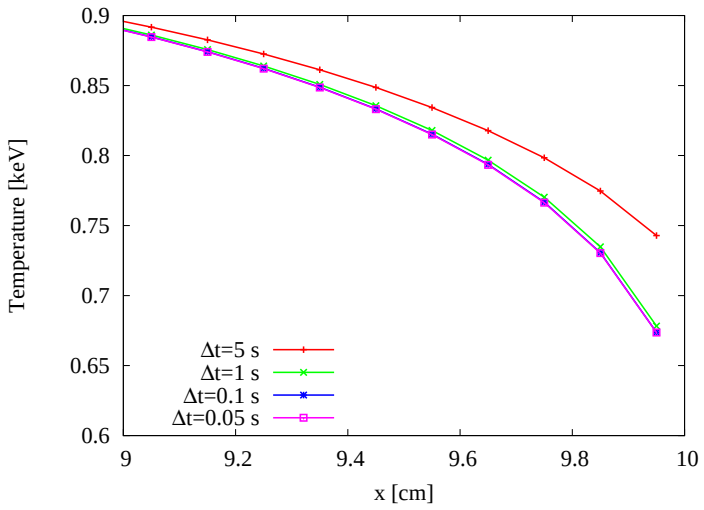

Figure 7.40 TRT Problem 3: Detailed View of the Implicit IMC Solution at $t = 10$ s

$\Delta t = 0.1$ s. In Figures 7.41 and 7.42, we show the temperature in the slab at time $t = 1000$ s. Here we see that the slab has cooled significantly. Figure 7.42 shows a detailed view of the right boundary, where the cooling is most significant. In Figure 7.42, we again see that the implicit IMC solution converges for a time step length of $\Delta t = 0.1$ s.

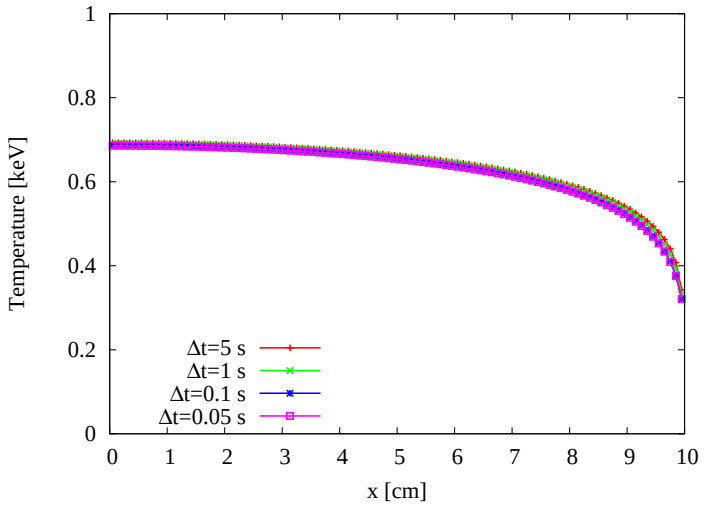

Figure 7.41 TRT Problem 3: Implicit IMC Solution at $t = 1000$ s

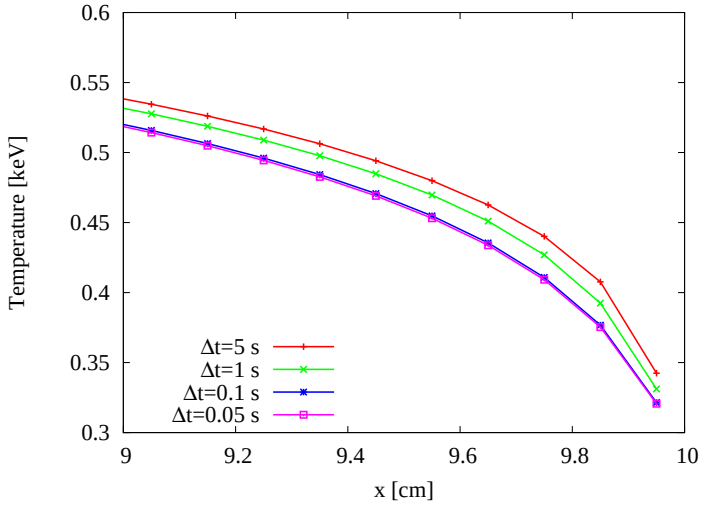

Figure 7.42 TRT Problem 3: Detailed View of the Implicit IMC Solution at $t = 1000$ s

Plain SBJ IMC Results

We now wish to examine the accuracy of the plain SBJ IMC method for this problem. Figure 7.43 shows results obtained with the plain SBJ method for a time step length of $\Delta t = 1$ s, at times $t = 25$ s, 75 s, 150 s, 300 s, 500 s, and 1000 s. Here we see that the plain

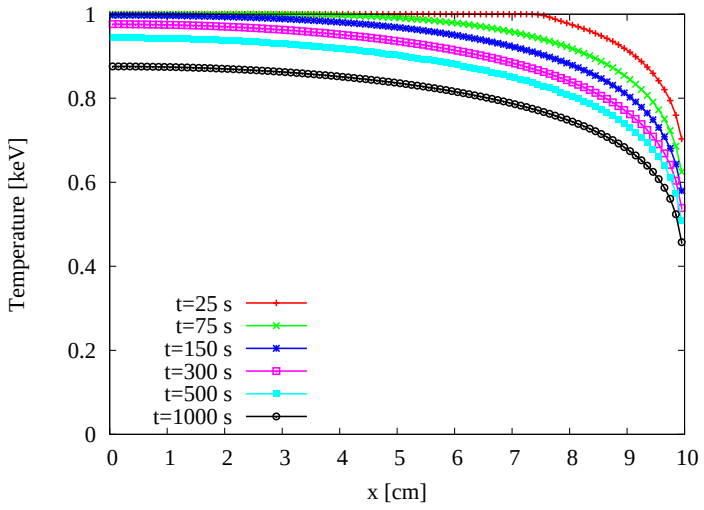

Figure 7.43 TRT Problem 3: Plain SBJ Solution at Various Times with $\Delta t = 1$ s

SBJ IMC method fails to cool the slab at the proper rate. Instead, the slab cools much too slowly. This is consistent with previous results, where we have found that the SBJ method tends to artificially slow the rate at which the problem evolves.

In Figures 7.44 and 7.45 we see the results for the plain SBJ method at time $t = 10$ s at various time step lengths. In Figure 7.45, we see a close up view of the solution near the right boundary. Here we see that at a time step length of $\Delta t = 0.1$ s, the plain SBJ is

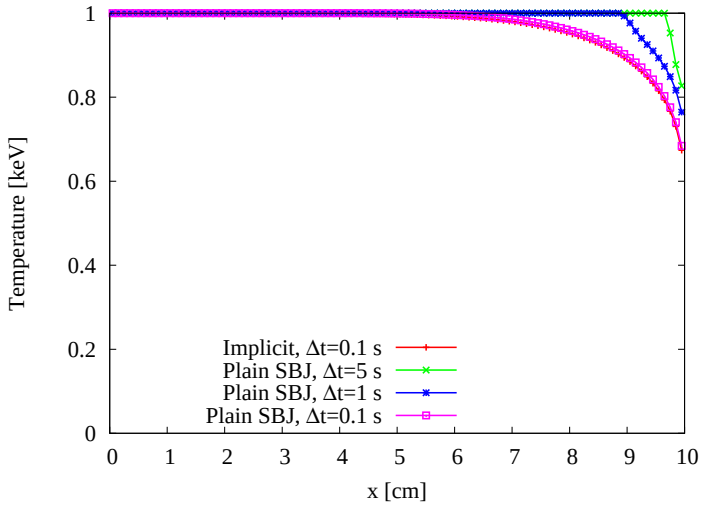

Figure 7.44 TRT Problem 3: Plain SBJ Solution at $t = 10$ s

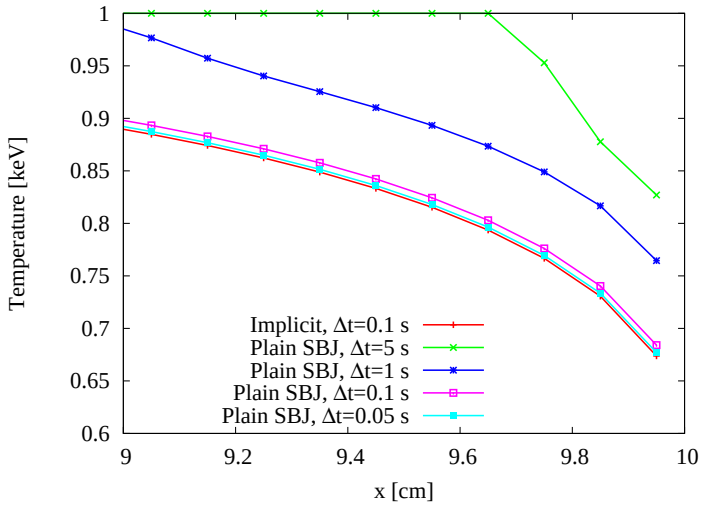

Figure 7.45 TRT Problem 3: Detailed View of the Plain SBJ IMC Solution at $t = 10$ s

nearly converged to the implicit solution, but not quite. Reducing the time step length to $\Delta t = 0.05$ s converges the plain SBJ solution to the implicit solution.

In Figures 7.46 and 7.47, we see the results for the plain SBJ method at time $t = 1000$ s at various time step lengths. Again, we observe that the plain SBJ IMC method requires a time step length of $\Delta t = 0.05$ s to converge to the implicit IMC results for this problem.

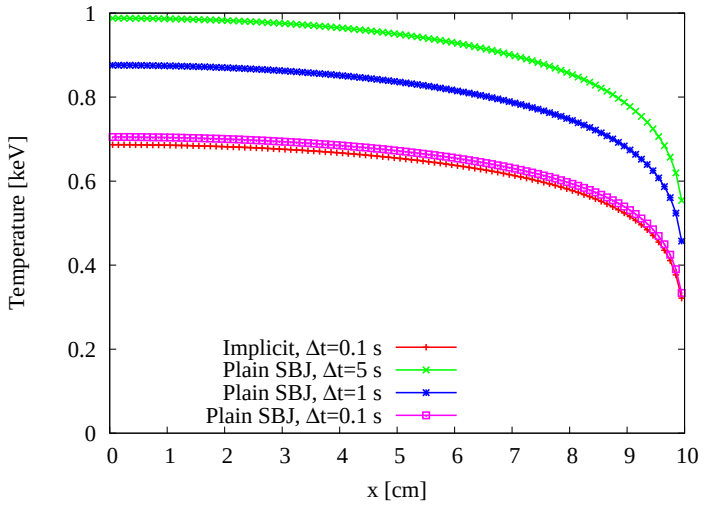

Figure 7.46 TRT Problem 3: Plain SBJ Solution at $t = 1000$ s

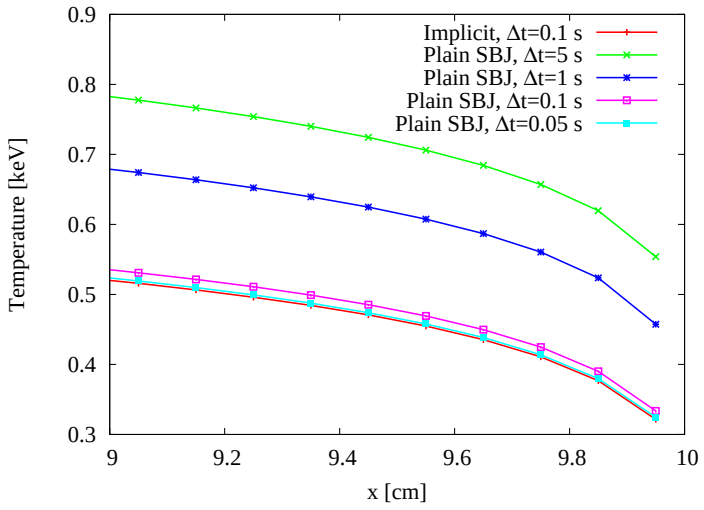

Figure 7.47 TRT Problem 3: Detailed View of the Plain SBJ Solution at $t = 1000$ s

Conservative SBJ IMC Results

We now examine the accuracy of the conservative SBJ method for this problem. Figure 7.48 shows results obtained with the conservative SBJ method for a time step length of $\Delta t = 1$ s, at times $t = 25$ s, 75 s, 150 s, 300 s, 500 s, and 1000 s. Observe that the conservative

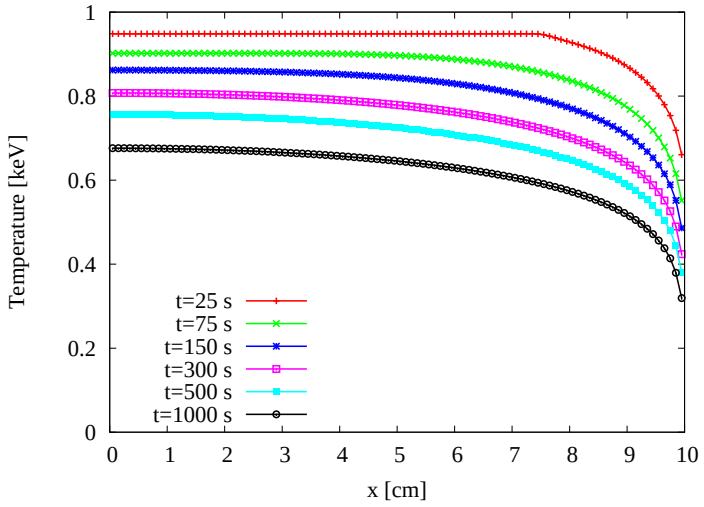

Figure 7.48 TRT Problem 3: Conservative SBJ IMC Solution at Various Times with $\Delta t = 1$ s

SBJ method, for this coarse time step length, has failed to maintain the correct equilibrium solution on the left side of the slab.

Figures 7.49 and 7.50 show the results for the conservative SBJ method at time $t = 10$ s at various time step lengths. In Figure 7.50, we see a detailed view of the solution near the right boundary. Again, we see that the conservative SBJ IMC method fails to maintain the correct equilibrium temperature on the left side of the slab, which should not have begun cooling significantly at this early time. As the time step is decreased, the conservative SBJ IMC solution converges to the the implicit IMC solution. Like the plain SBJ IMC method, a time step length of $\Delta t = 0.05$ s is required to converge the conservative SBJ IMC method, although the solution at $\Delta t = 0.01$ s is more accurate than it was for the plain SBJ IMC method.

Figures 7.51 and 7.52 show the results for the conservative SBJ method at time $t = 1000$ at various time step lengths. Like the results at time $t = 10$ s, we see that a time step length of $\Delta t = 0.05$ s is required to converge the conservative SBJ IMC method to the implicit IMC results.

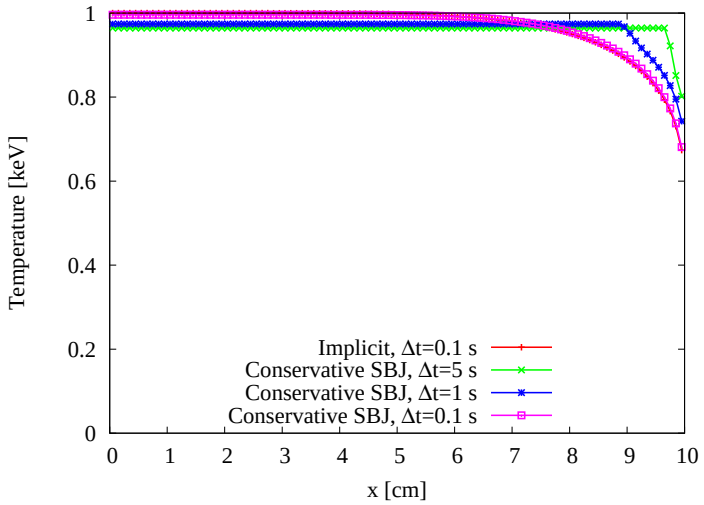

Figure 7.49 TRT Problem 3: Conservative SBJ IMC Solution at $t = 10$ s

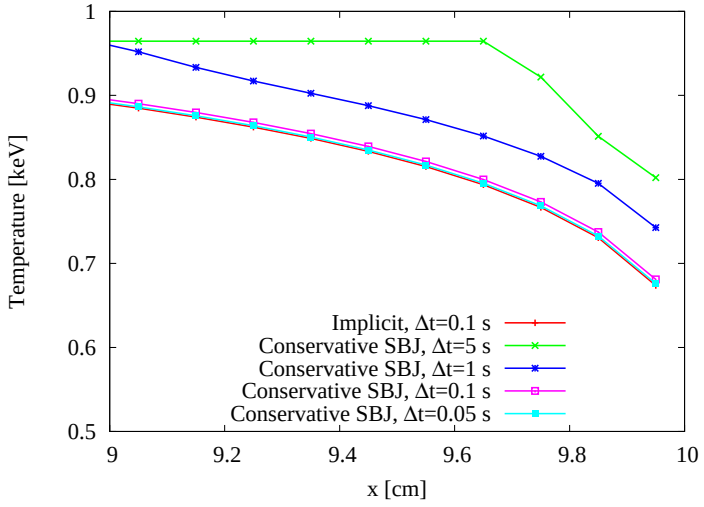

Figure 7.50 TRT Problem 3: Detailed View of the Conservative SBJ IMC Solution at $t = 10$ s

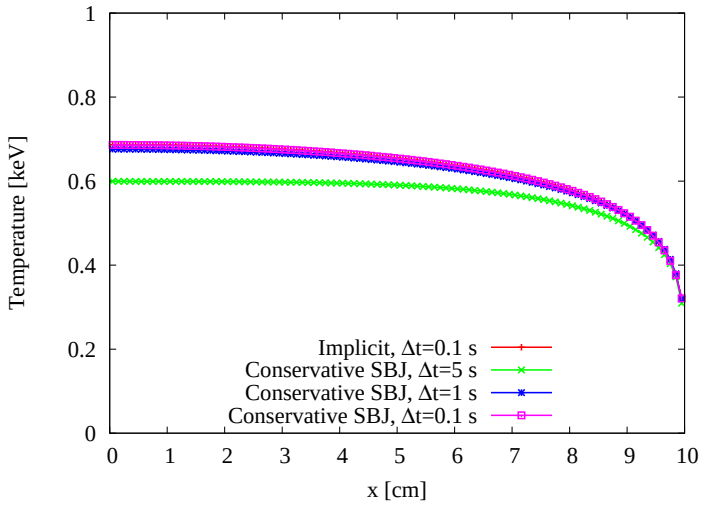

Figure 7.51 TRT Problem 3: Conservative SBJ Solution at $t = 1000$ s

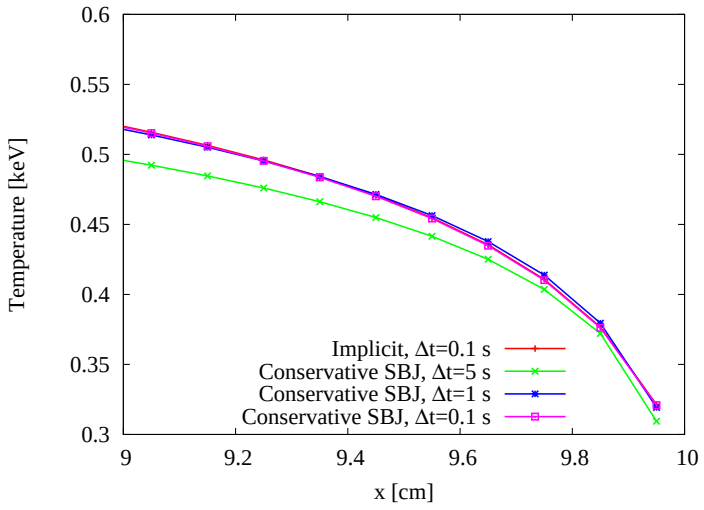

Figure 7.52 TRT Problem 3: Close-Up View of the Conservative SBJ Solution at $t = 1000$ s

Iterative Results

Figures 7.53, 7.54, and 7.55 show the number of iterations required to converge the implicit, plain SBJ, and conservative SBJ IMC methods to an L_2 convergence criterion of 10^{-7} for time steps of length $\Delta t = 5$ s, 1 s, and 0.1 s, respectively. Just as in the Su-Olson problems

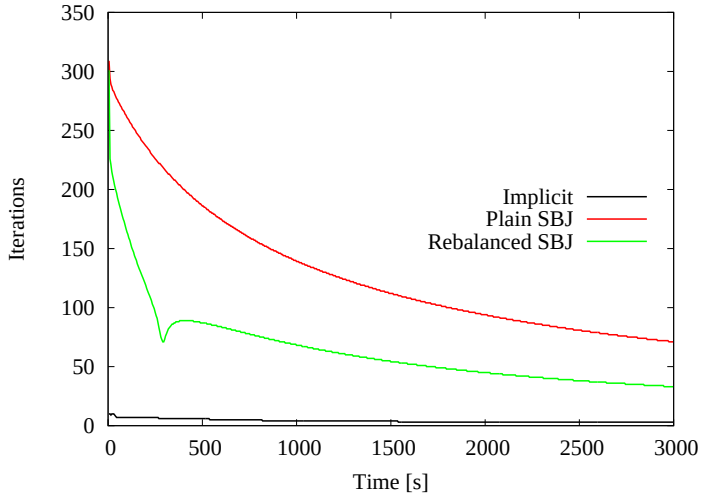

Figure 7.53 TRT Problem 3: Iterations Required for Convergence with $\Delta t = 5$ s

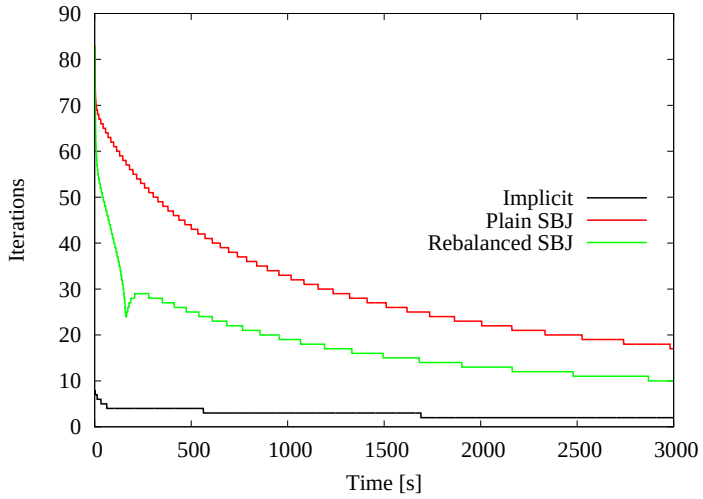

Figure 7.54 TRT Problem 3: Iterations Required for Convergence with $\Delta t = 1$ s

in Section 7.1, and the Marshak wave problems in Section 7.2, we see that if a time step is chosen such that the implicit IMC method converges to an accurate solution, then the number of SBJ iterations required to converge to this solution is modest. We see that the number of iterations decreases as the slab cools, which is to be expected, since the slab

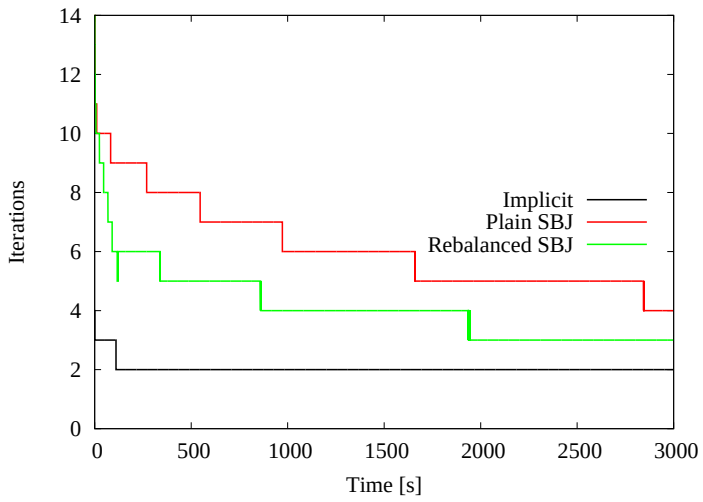

Figure 7.55 TRT Problem 3: Iterations Required for Convergence with $\Delta t = 0.1$ s

becomes increasingly optically-thick as the temperature is reduced. We also see that the global rebalance contributes significantly to reducing the number of iterations required for larger time steps.

7.4 Summary

In summary, we have found that the SBJ IMC method can produce accurate solutions for small time steps. For large time steps, the SBJ method produces less accurate solutions than the implicit method, but tends to converge to the correct solution at about the same time step length, or perhaps slightly smaller, than the implicit method requires for accurate solutions. Moreover, we have found, for the iterative SBJ method, that if a time step length is chosen such that the method will converge to an accurate solution, then the number of time steps required to converge to that solution is small.

Overall, the SBJ method works well with the IMC linearization. This linearization produces $O(\Delta t)$ errors [12], as does the SBJ method. Therefore, we would expect that time steps that produce accurate solutions with the implicit IMC method will also produce accurate and quickly convergent solutions with the SBJ IMC method.

Chapter 8

Conclusions and Future Work

We began our study of unconditionally stable, local radiation transport methods in Chapter 2 by first considering the diffusion equation. We examined four different time discretizations: the well-known implicit and fully-explicit methods, the semi-explicit method, and the new Staggered-Block Jacobi (SBJ) diffusion method. A stability analysis revealed that the implicit method is unconditionally stable. However, this method couples the solution throughout the spatial domain. Therefore, it is not local, and lacks the trivial parallelization that local methods possess. The fully-explicit method, by contrast, is local, and therefore trivial to parallelize. However, it is not unconditionally stable. We also analyzed a semi-explicit method. This method has the same locality as the fully-explicit method, but improved stability properties. Nevertheless, it still lacks unconditional stability. Finally, we investigated the new SBJ diffusion method. This method has both unconditional stability and locality. These properties come at the cost of a loss of particle conservation. We can restore global particle conservation using a global rebalance method. However, we can also iterate using the SBJ diffusion method. Upon convergence, the SBJ diffusion method produces the implicit solution, which satisfies cell-wise particle balance. For problems where the particle wave advances a fraction of a cell per time step, the non-iterative SBJ diffusion method produces accurate solutions, and the iterative SBJ diffusion method is quickly convergent. When the particle wave advances many cells per time step, the non-iterative SBJ diffusion method does not produce accurate solutions, and the iterative SBJ diffusion method requires a large number of iterations to converge.

In Chapter 3, we derived the well-known implicit and fully-explicit linear discontinuous finite element S_N transport methods. We noted that while the fully-explicit method is local, the implicit equations must be solved using mesh sweeps; therefore, the implicit method is not local, and cannot be trivially parallelized. We also derived a local semi-explicit transport method analogous to the semi-explicit diffusion method we investigated in Chapter 2.

Additionally, in Chapter 3, we described the SBJ transport method. Like the SBJ diffusion method, the SBJ transport method lacks particle conservation. We therefore derived a global rebalance method to restore global particle conservation. Also like the SBJ diffusion method, we derived an iterative form of the SBJ transport method. This method converges to the implicit transport solution, and therefore satisfies cell-wise particle balance. From the results obtained for the SBJ diffusion method in Chapter 2, we hypothesized that the SBJ transport method would be inefficient in optically-thin problems. The sweep-based approach used by the implicit method, by contrast, is efficient for optically-thin (or purely absorbing) problems, but is inefficient for optically-thick problems. Therefore, the traditional sweep-based method and the new SBJ transport method are complementary. We attempted to exploit this complementarity by using a sweep as an initial guess for the SBJ transport iterations. This reduces the number of iterations required for optically-thin problems, but is less effective for intermediate thickness problems. We therefore investigated stretching the transport sweeps and applying an angular redistribution to the angular flux produced by the stretched sweeps.

In Chapter 4, we conducted an asymptotic analysis on the implicit, fully-explicit, semi-explicit, and SBJ transport methods. We found that the implicit and fully-explicit methods both limit to the node-centered implicit and fully-explicit diffusion methods we investigated in Chapter 2. Therefore, we know that the fully-explicit transport method is not unconditionally stable in the thick diffusion limit, and it does not satisfy the stability and locality conditions that we seek. As a result, we did not consider the fully-explicit transport method further. The semi-explicit transport method did not limit to the semi-explicit diffusion method, but instead limited to a diffusion discretization even less stable than the fully-explicit transport method. For this reason, we also chose not to investigate the semi-explicit transport method either. Finally, we conducted an asymptotic analysis of the SBJ transport method. The results we obtained in Chapter 2 indicated that an unconditionally stable and local transport discretization should limit to the SBJ diffusion discretization in the diffusion limit. The SBJ transport method we described in Chapter 3 did limit to the SBJ diffusion method investigated in Chapter 2. We concluded that the SBJ transport method is unconditionally stable in the thick diffusion limit. We also believe, based on our numerical results, that the SBJ transport method is unconditionally stable away from the diffusion limit.

In Chapter 5 we presented several numerical results illustrating the behavior of the SBJ transport method in comparison to the implicit method. The SBJ transport method behaves analogously to the SBJ diffusion method investigated in Chapter 2. When the particle wave advances a fraction of a cell per time step, the SBJ transport method is accurate, and the iterative SBJ method is quickly convergent. When the particle wave advances more than a

cell per time step, the method becomes increasingly inaccurate, and the iterative SBJ method requires many more iterations to converge to the implicit solution. Adding mesh sweeps to the SBJ transport method helps reduce the number of iterations required for optically-thin problems. Applying the stretching and angular redistribution methods derived in Chapter 3 to the mesh sweeps generally reduces the number of iterations required for intermediate thickness problems. Overall, the SBJ method is accurate and efficient whenever the wave advances less than a cell width per time step, i.e., where the time step length is small or the problem is optically-thick. The iterative SBJ method will converge to the implicit method even for large time steps or optically-thin problems. However, it requires a large number of iterations to do so. Therefore, iteration acceleration techniques may be necessary for the SBJ transport method for these problems.

In Chapter 6, we applied the SBJ transport method to the nonlinear thermal radiation transport (TRT) equations. We derived the grey equations from the frequency-dependent TRT equations, and then we applied the well-known IMC linearization to these equations. The IMC equations were time-discretized using both the well-known implicit method and the new SBJ transport method. Similarly to the linear SBJ transport method, the SBJ IMC transport method does not satisfy energy conservation. Therefore, we derived a global rebalance to restore global energy conservation. We also described an iterative SBJ IMC transport method that converges to the implicit IMC results.

Finally, in Chapter 7, we demonstrated the implicit and SBJ IMC transport methods on the Su-Olson benchmark problem, a Marshak wave problem, and a cooling problem. In each case, we found that the SBJ IMC transport method was less accurate than the implicit IMC transport method. However, because the IMC linearization is $O(\Delta t)$, and the SBJ approximation is also $O(\Delta t)$, if we reduce the time step length such that the implicit IMC transport method produces accurate results, then the SBJ IMC transport method also produces accurate results, and the iterative SBJ IMC transport method is quickly convergent. For this reason, we believe that the SBJ transport method will likely be superior to the implicit method for most TRT problems on massively parallel machines.

8.1 Future Work

In this dissertation, we have limited the investigation to one-dimensional, mono-energetic radiation transport. However, most problems of interest must be modeled using two or three spatial dimensions over a broad range of particle energies. Therefore, in Section 8.1.1, we extrapolate from the results presented in this dissertation to hypothesize about the behavior

of the SBJ method in higher spatial dimensions and in a multigroup energy discretization. We have also found that, for some problems, SBJ iterations are slow to converge. In this dissertation, the only iterative acceleration we have attempted is a global rebalance. In Section 8.1.2, we will propose more advanced acceleration techniques that we believe may work well with the SBJ method.

8.1.1 SBJ Transport in Larger Phase Spaces

Moving to Higher Spatial Dimensions

We believe that extending the SBJ transport method to higher spatial dimensions should be straightforward. In one dimension, an SBJ block is composed of two cells. The angular fluxes incident on the block are lagged to the beginning of the time step. The unknown scalar fluxes are calculated inside the block. Afterwards, the angular fluxes within the block are calculated. The scalar fluxes and angular fluxes adjacent to the block boundary are discarded, while all other scalar fluxes and angular fluxes adjacent to the block interior are retained. This is described in Section 3.4.

For two-dimensional and three-dimensional problems, this space-time stencil can be naturally extended. Now a block is defined as all cells adjacent to a particular node. Again, the incident angular fluxes on the block are lagged to the beginning of the time step, and the unknown scalar fluxes and angular fluxes within the block are calculated. The scalar fluxes and angular fluxes adjacent to the block boundary are discarded, while the rest are retained. The space-time stencil for the angular fluxes on a two-dimensional block composed of rectangular cells is illustrated in Figure 8.1. The incident angular fluxes, shown in red, are evaluated at time t_k. The angular fluxes are calculated within the four-cell block. The angular fluxes adjacent to the block boundary, shown in green, are discarded, while the angular fluxes adjacent to the interior node, shown in blue, are retained. An analogous space-time stencil can be constructed for any block shape. The advantage of the SBJ transport method over sweep-based methods, in addition to the improvements in parallelism, is that it is not necessary to calculate complicated sweep orderings for more complex grids, such as three-dimensional grids composed of arbitrary polyhedron.

Multigroup Method

It is likely that the efficiency of the SBJ transport method relative to the implicit method will improve as the number of energy groups increases. The reason is that the iterations

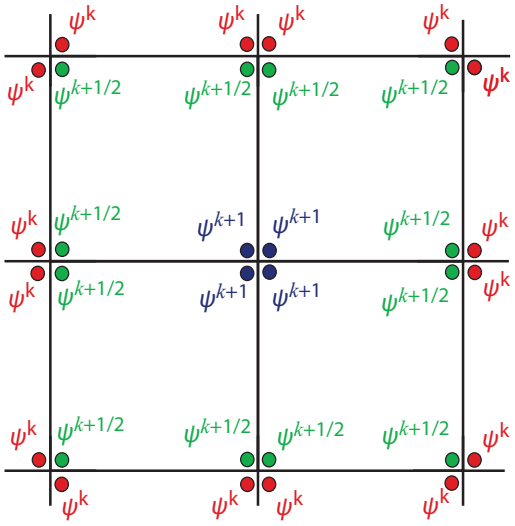

Figure 8.1 Space-Time Stencil for the 2D SBJ Method on a Rectangular Grid

over the energy groups becomes an inner iteration rather than an outer iteration. Consider Figure 8.2, where a schematic of an implicit multigroup algorithm is shown. The blue rectangles represent fast groups, and the red rectangles represent thermal groups, where upscattering must be considered. In the implicit method, the algorithm begins with group 1, and the mesh is swept until the scattering source is converged. The method then proceeds to solve for group 2, and so forth until group G. Since there is upscattering among the thermal groups, there may be iterations between these groups until all of the energy groups are converged. Therefore, many sweeps may be necessary to find the multigroup solution during the time step.

Now consider the schematic of an SBJ multigroup algorithm, shown in Figure 8.3. In this case, all of the groups for a single block can be solved at once. This makes upscattering much less expensive. After all of the group fluxes have been calculated, the incident angular fluxes for all groups are updated from the neighboring blocks. This continues until the method converges. If we consider a problem with 100 groups, and assume that it takes the implicit solution, on average, 6 iterations to converge (which may be unrealistically low), then a total of 600 sweeps (in every angle) must be performed per time step. If we assume that it takes 300 iterations to converge the optically-thinnest group (which may be unrealistically high), then the SBJ method will still be twice as fast than the implicit method, if a single SBJ iteration takes the same amount of time as a mesh sweep (although, more than likely, a single SBJ iteration would be significantly faster than a mesh sweep). We also note that the SBJ multigroup algorithm is likely more cache efficient as well.

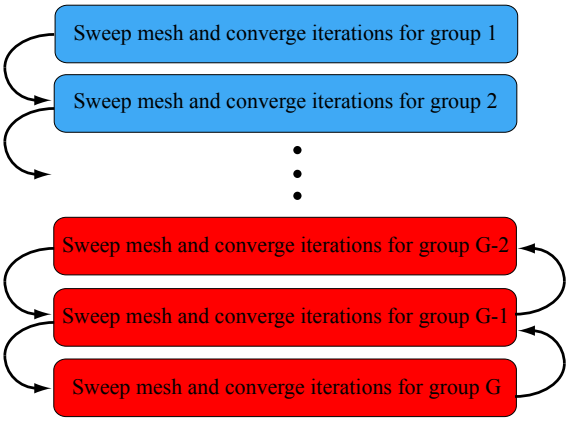

Figure 8.2 Schematic of the Implicit Multigroup Algorithm

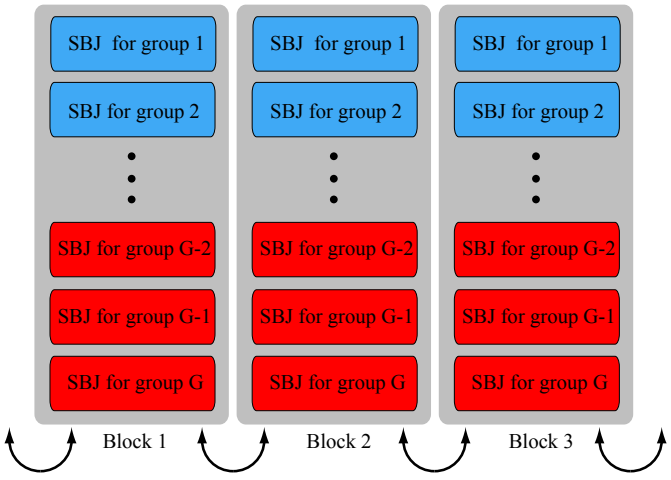

Figure 8.3 Schematic of the SBJ Multigroup Algorithm

8.1.2 Acceleration

We found in Chapter 5 that the number of iterations required for optically-thin problems can become large. We also found that the global rebalance method, while useful in reducing the number of iterations for thick and intermediate problems, is less effective, or even detrimental, in optically-thin problems. Therefore, in order to extend the SBJ transport method to optically-thin problems, more advanced acceleration techniques are required.

The simplest and most direct extrapolation from the work performed here would be to use a coarse-mesh rebalance instead of a global rebalance. Work has been done on coarse-mesh rebalance applied to the acceleration of source iteration [11], and likely much of that work could be applied to the SBJ method as well. Alternatively, a multigrid method may be useful. Since the SBJ method is efficient in optically-thick problems, the mesh could be coarsened until all cells are optically-thick. After the solution has been calculated on the coarse mesh, the mesh could be successively refined, until the solution is found on the original fine mesh.

Appendices

Appendix A

Calculating the Particle Wave Location

Because the SBJ diffusion and transport methods are local, we expect that they will be accurate for problems in which the particle wave advances a fraction of a cell width per time step. In this appendix, we derive the equations to calculate an estimate of the particle wave location. In this context, we are defining the wave location estimate as

$$d_{RMS}(t) = \sqrt{\frac{\int_{-\infty}^{\infty} x^2 \phi(x,t)\,\mathrm{d}x}{\int_{-\infty}^{\infty} \phi(x,t)\,\mathrm{d}x}} \tag{A.1}$$

$$= \text{root-mean-squared distance photons travel from the boundary (at } x = 0).$$

Note that because the wave location is averaged over the problem domain, this estimate will tend to underestimate the location of the wavefront, especially for later times. Nevertheless, we have found that this estimate of the wave location can provide a helpful guide in predicting when the non-iterative SBJ method will be accurate, or when the iterative SBJ method will be rapidly convergent. (See the numerical results in Chapters 2, 5, and 7 for details.) In Section A.1, we derive the equations necessary to calculate the particle wave location for the diffusion equation, and in Section A.2, we derive the equations necessary to calculate the particle wave location for the transport equation.

A.1 Calculating the Diffusion Wave Location

Consider the following diffusion problem:

$$\frac{1}{v}\frac{\partial}{\partial t}\phi(x,t) - D\frac{\partial^2}{\partial x^2}\phi(x,t) + \Sigma_a\phi(x,t) = Q\delta(x)\,, \tag{A.2a}$$

$$\phi(x,0) = 0\,, \tag{A.2b}$$

$$\lim_{x\to\infty}\phi(x,t) = \phi(-x,t) = 0\,. \tag{A.2c}$$

Eqs. (A.2) describe an infinite, homogeneous diffusion problem with a delta source at $x = 0$ and an initial condition of zero. Operating on Eq. (A.2a) by $\int_{-\infty}^{\infty} x^n(\cdot)\,\mathrm{d}x$, and defining

$$\phi_n(t) = \int_{-\infty}^{\infty} x^n(\cdot)\,\phi(x,t)\,\mathrm{d}x\,, \tag{A.3}$$

we find, for $n = 0$,

$$\frac{1}{v}\frac{\mathrm{d}}{\mathrm{d}t}\phi_0(t) + \Sigma_a\phi_0(t) = Q\,, \tag{A.4}$$

and, for $n = 2$

$$\frac{1}{v}\frac{\mathrm{d}}{\mathrm{d}t}\phi_2(t) - 2D\phi_0(t) + \Sigma_a\phi_2(t) = 0\,. \tag{A.5}$$

In the general case, the solution to Eqs. (A.4) and (A.5) are

$$\phi_0(t) = \frac{Q}{\Sigma_a}\left(1 - \mathrm{e}^{-\Sigma_a vt}\right)\,, \tag{A.6a}$$

$$\phi_2(t) = \frac{2DQ}{\Sigma_a}\left(\frac{1-\mathrm{e}^{-\Sigma_a vt}}{\Sigma_a} - vt\mathrm{e}^{-\Sigma_a vt}\right)\,. \tag{A.6b}$$

Therefore, we calculate the wave location as

$$d_{RMS}(t) = \sqrt{\frac{\phi_2(t)}{\phi_0(t)}} = \sqrt{2D\left(\frac{1}{\Sigma_a} - \frac{vt}{\mathrm{e}^{\Sigma_a vt} - 1}\right)}\,. \tag{A.7}$$

In the case of a purely scattering ($\Sigma_a = 0$) problem, the solutions to Eqs. (A.4) and (A.5) are

$$\phi_0(t) = Qvt\,, \tag{A.8a}$$

$$\phi_2(t) = DQv^2t^2\,, \tag{A.8b}$$

and the wave location is

$$d_{RMS}(t) = \sqrt{Dvt}\,. \tag{A.9}$$

A.2 Calculating the Transport Wave Location

We next calculate an estimate of the particle wave location for the transport equation. In Section A.2.1, we calculate the transport wave location in the general case, and in Section A.2.2, we calculate the transport wave location in the purely scattering case.

A.2.1 Calculating the Transport Wave Location in the General Case

Consider the following transport problem:

$$\frac{1}{v}\frac{\partial}{\partial t}\psi(x,\mu,t) + \mu\frac{\partial}{\partial x}\psi(x,\mu,t) + \Sigma_t\psi(x,\mu,t) = \frac{\Sigma_s}{2}\int_{-1}^{1}\psi(x,\mu',t)\,\mathrm{d}\mu' + \frac{Q}{2}\delta(x)\,, \tag{A.10a}$$

$$\psi(x,\mu,0) = 0\,, \tag{A.10b}$$

$$\lim_{x\to\infty}\psi(x,\mu,t) = \psi(-x,\mu,0) = 0\,. \tag{A.10c}$$

Eqs. (A.10) describe an infinite homogeneous transport problem with an isotropic delta source at $x = 0$ and an initial condition of zero. Operating on Eq. (A.10a) by $\int_{-\infty}^{\infty}\int_{-1}^{1} x^n\mu^m\psi(x,\mu,t)\,\mathrm{d}\mu\,\mathrm{d}x$ and defining

$$\psi_{n,m}(t)\int_{-\infty}^{\infty} x^n\mu^m\psi(x,\mu,t)\,\mathrm{d}\mu\,\mathrm{d}x\,, \tag{A.11}$$

we obtain

$$\begin{aligned}\frac{1}{v}\frac{\mathrm{d}}{\mathrm{d}t}\psi_{n,m}(t) + \int_{-\infty}^{\infty}\int_{-1}^{1} x^n\mu^{m+1}\frac{\partial}{\partial x}\psi(x,\mu,t)\,\mathrm{d}\mu\,\mathrm{d}x + \Sigma_t\psi_{n,m}(t)& \\ = \Sigma_s\left(\int_{-\infty}^{\infty} x^n\int_{-1}^{1}\psi(x,\mu,t)\,\mathrm{d}\mu\,\mathrm{d}x\right)\left(\frac{1}{2}\int_{-1}^{1}\mu^m\,\mathrm{d}\mu\right)& \\ + Q\left(\int_{-\infty}^{\infty} x^n\delta(x)\,\mathrm{d}x\right)\left(\frac{1}{2}\int_{-1}^{1}\mu^m\,\mathrm{d}\mu\right)\,.&\end{aligned} \tag{A.12}$$

Defining

$$\frac{1}{2}\int_{-1}^{1}\mu^m\,\mathrm{d}\mu = \begin{cases} 1, & m=0, \\ 0, & m=1, \\ \dfrac{1}{3}, & m=2, \end{cases}$$
$$= a_m\,, \tag{A.13a}$$

and

$$\int_{-\infty}^{\infty} x^n\delta(x)\,\mathrm{d}x = \begin{cases} 1, & n=0, \\ 0, & n>0, \end{cases}$$
$$= b_n\,, \tag{A.13b}$$

and using

$$\int_{-\infty}^{\infty}\int_{-1}^{1} x^n\mu^{m+1}\frac{\partial}{\partial x}\psi(x,\mu,t)\,\mathrm{d}\mu\,\mathrm{d}x = -n\int_{-\infty}^{\infty}\int_{-1}^{1} x^{n-1}\mu^{m+1}\psi(x,\mu,t)\,\mathrm{d}\mu\,\mathrm{d}x$$
$$= -n\psi_{n-1,m+1}(t)\,, \tag{A.14}$$

we can write Eq. (A.12) as

$$\frac{1}{v}\frac{\mathrm{d}}{\mathrm{d}t}\psi_{n,m}(t) - n\psi_{n-1,m+1}(t) + \Sigma_t\psi_{n,m}(t) = \Sigma_s a_m\psi_{n,0}(t) + Qa_m b_n\,. \tag{A.15}$$

Evaluating Eq. (A.15) for $n=2$ and $m=0$, we obtain

$$\frac{1}{v}\frac{\mathrm{d}}{\mathrm{d}t}\psi_{2,0}(t) - 2\psi_{1,1}(t) + \Sigma_a\psi_{2,0}(t) = 0\,. \tag{A.16}$$

Evaluating Eq. (A.15) for $n=1$ and $m=1$, we find

$$\frac{1}{v}\frac{\mathrm{d}}{\mathrm{d}t}\psi_{1,1}(t) - \psi_{0,2}(t) + \Sigma_t\psi_{1,1}(t) = 0\,. \tag{A.17}$$

Evaluating Eq. (A.15) for $n=0$ and $m=2$, we have

$$\frac{1}{v}\frac{\mathrm{d}}{\mathrm{d}t}\psi_{0,2}(t) + \Sigma_t\psi_{0,2}(t) = \frac{\Sigma_s}{3}\psi_{0,0}(t) + \frac{Q}{3}\,. \tag{A.18}$$

Finally, evaluating Eq. (A.15) for $n = 0$ and $m = 0$, we obtain

$$\frac{1}{v}\frac{\mathrm{d}}{\mathrm{d}t}\psi_{0,0}(t) + \Sigma_a \psi_{0,0}(t) = Q\,. \tag{A.19}$$

Solving this coupled system of ordinary differential equations, with the initial conditions given by Eq. (A.10b), we obtain

$$\psi_{0,0}(t) = \frac{Q}{\Sigma_a}\left(1 - \mathrm{e}^{-\Sigma_a vt}\right), \tag{A.20a}$$

$$\psi_{0,2}(t) = \frac{Q}{3\Sigma_a}\left(1 - \mathrm{e}^{-\Sigma_a vt}\right), \tag{A.20b}$$

$$\psi_{1,1}(t) = \frac{Q}{3\Sigma_a\Sigma_s\Sigma_t}\left[\Sigma_a + \left(\Sigma_s \mathrm{e}^{\Sigma_a vt} - \Sigma_t\right)\mathrm{e}^{\Sigma_s vt}\right]\mathrm{e}^{-\Sigma_t vt}, \tag{A.20c}$$

$$\psi_{2,0}(t) = \frac{2Q}{3\Sigma_a^2\Sigma_s^2\Sigma_t}\left(\Sigma_s^2 - \Sigma_s^2\left(1 + \Sigma_a vt\right)\mathrm{e}^{-\Sigma_a vt} + \Sigma_a^2\left[\left(1 - \Sigma_s vt\right)\mathrm{e}^{-\Sigma_a vt} - \mathrm{e}^{-\Sigma_t vt}\right]\right). \tag{A.20d}$$

Finally, we calculate the estimate of the particle wave location as

$$d_{RMS} = \sqrt{\frac{\psi_{2,0}(t)}{\psi_{0,0}(t)}}\,. \tag{A.21}$$

A.2.2 Calculating the Transport Wave Location in the Purely Scattering Case

In this section, we calculate the transport wave location in the case of a purely scattering ($\Sigma_a = 0$) material. Writing Eqs. (A.16)–(A.19) for $\Sigma_a = 0$ and $\Sigma_s = \Sigma_t$, we obtain

$$\frac{1}{v}\frac{\mathrm{d}}{\mathrm{d}t}\psi_{2,0}(t) - 2\psi_{1,1}(t) = 0\,, \tag{A.22a}$$

$$\frac{1}{v}\frac{\mathrm{d}}{\mathrm{d}t}\psi_{1,1}(t) - \psi_{0,2}(t) + \Sigma_t \psi_{1,1}(t) = 0\,, \tag{A.22b}$$

$$\frac{1}{v}\frac{\mathrm{d}}{\mathrm{d}t}\psi_{0,2}(t) + \Sigma_t \psi_{0,2}(t) = \frac{\Sigma_t}{3}\psi_{0,0}(t) + \frac{Q}{3}\,, \tag{A.22c}$$

$$\frac{1}{v}\frac{\mathrm{d}}{\mathrm{d}t}\psi_{0,0}(t) = Q\,. \tag{A.22d}$$

The solutions to this coupled set of ordinary differential equations are

$$\psi_{0,0}(t) = Qvt\,, \tag{A.23a}$$

$$\psi_{0,2}(t) = \frac{Qvt}{3}, \tag{A.23b}$$

$$\psi_{1,1}(t) = \frac{Q}{3\Sigma_t^2}\left(\mathrm{e}^{-v\Sigma_t t} + \Sigma_t vt - 1\right), \tag{A.23c}$$

$$\psi_{2,0}(t) = \frac{Q}{3\Sigma_t^3}\left[2\left(1 - \mathrm{e}^{-\Sigma_t vt}\right) + \Sigma_t vt\left(\Sigma_t vt - 2\right)\right]. \tag{A.23d}$$

The particle wave location estimate may then be calculated as

$$d_{RMS} = \sqrt{\frac{\psi_{2,0}(t)}{\psi_{0,0}(t)}}. \tag{A.24}$$

For large t, this result simplifies to

$$d_{RMS} = \sqrt{D\left(vt - \frac{2}{\Sigma_t}\right)} + O(\mathrm{e}^{-v\Sigma_t t}), \tag{A.25}$$

which agrees rather closely with the diffusion result given in Eq. (A.9).

Appendix B

Linear Modified Four-Step Diffusion Synthetic Acceleration

In this appendix, we present the Modified Four-Step diffusion synthetic acceleration (DSA) method [3] applied to the one-dimensional, time-dependent transport equation with isotropic scattering. To do this, let us consider the continous transport equation with a source iteration scheme:

$$\frac{1}{v}\frac{\partial}{\partial t}\psi^{(l+1/2)}(x,\mu,t)+\mu\frac{\partial}{\partial x}\psi^{(l+1/2)}(x,\mu,t)+\Sigma_t(x)\psi^{(l+1/2)}(x,\mu,t) = \frac{\Sigma_s(x)}{2}\phi^{(l)}(x,t)+Q(x,\mu,t)\,, \quad \text{(B.1a)}$$

$$\phi^{(l+1/2)}(x,t)=\int_{-1}^{1}\psi^{(l+1/2)}(x,\mu,t)\,\mathrm{d}\mu\,, \quad \text{(B.1b)}$$

$$\phi^{(l+1)}(x,t)=\phi^{(l+1/2)}(x,t)\,, \quad \text{(B.1c)}$$

where l is the iteration index. The source iteration scheme is known to converge with a spectral radius of

$$\rho_{SI}=\frac{\Sigma_s}{\Sigma_t}\,, \quad \text{(B.2)}$$

in an infinite homogeneous medium [2]. Therefore, in optically thick and diffusive problems, the source iteration method can converge slowly. Diffusion synthetic acceleration schemes accelerate this iterative process by using an additive correction to the scalar flux at iteration $l+1$ in Eq. (B.1c). The additive correction is calculated using a diffusion equation. This acceleration scheme is called diffusion synthetic acceleration (DSA).

One popular DSA scheme is the Modified Four-Step DSA method. The Modified Four-Step DSA method is so named because the derivation takes place in four steps, and is modified from the original Four-Step DSA scheme proposed by Larsen [21]. The original

four-step algorithm, which we have taken from [3], is as follows:

1a. Take zeroth angular moment of discretized transport equation

1b. Take first angular moment of discretized transport equation

2. Change iteration indices to $l+1$ except on second and higher moment terms

3. Subtract acceleration equations from unaccelerated equations to reduce algebraic complexity

4. Eliminate first moments from resulting system, leaving a discretized diffusion equation for the scalar fluxes. May not be possible given high-order discretization schemes in two or three dimensions.

With the original Four-Step DSA algorithm, it is not always possible to eliminate the first moments from the diffusion system, in order to find the needed discretized diffusion equation. This motivated the development of the Modified Four-Step DSA method. In this method, step 2 is modified, in that certain terms in the zeroth- and first-moment equations are not updated to $l+1$. This makes it possible to always eliminate the first moment terms and acquire a discretized diffusion equation. In Ref. [3], the method is applied to the time-independent transport equation. Here, we apply this method to the time-dependent transport equation.

In Section B.1, we derive the Modified Four-Step DSA equations for the implicitly time-discretized, spatially- and angularly-continuous transport equation, to demonstrate the derivation in a simplified case. In Section B.2, we derive the Modified Four-Step DSA equations for the implicit, linear discontinuous finite element transport discretization. This derivation is adapted from the derivation of the Modified Four-Step DSA method derived in Ref. [3] for the steady-state transport equation. Finally, in Section B.3 we derive the Modified Four-Step DSA equations for the implicit, linear discontinuous finite element grey IMC equations.

B.1 Derivation of the Time-Discretized Modified Four-Step Diffusion Synthetic Acceleration Equations

We first demonstrate the modified four-step diffusion synthetic acceleration (DSA) derivation on the implicitly time-discretized, spatially- and angularly-continuous transport equation.

The source iteration scheme for this equation is

$$\frac{1}{v\Delta t_{k+1}}\left[\psi^{k+1,(l+1/2)}(x,\mu)-\psi^{k}(x,\mu)\right]+\mu\frac{\partial}{\partial x}\psi^{k+1,(l+1/2)}(x,\mu) + \Sigma_t(x)\psi^{k+1,(l+1/2)}(x,\mu)=\frac{\Sigma_s(x)}{2}\phi^{k+1,(l)}(x)+Q^{k+1}(x,\mu)\,, \quad \text{(B.3a)}$$

$$\phi^{k+1,(l+1/2)}(x)=\int_{-1}^{1}\psi^{k+1,(l+1/2)}(x,\mu)\,\mathrm{d}\mu\,, \quad \text{(B.3b)}$$

$$\phi^{k+1,(l+1)}(x)=\phi^{k+1,(l+1/2)}(x)\,. \quad \text{(B.3c)}$$

As stated earlier, this iterative scheme is known to converge slowly for optically-thick and diffusive problems. The convergence of this scheme can be accelerated using an additive correction to the new scalar flux iterate in Eq. (B.3c), where the additive correction comes from the solution of a diffusion equation. The derivation of this diffusion equation proceeds in four steps.

The first step of the Modified Four-Step DSA derivation is to calculate the zeroth and first angular moments of Eq. (B.3a). The zeroth moment is

$$\frac{1}{v\Delta t_{k+1}}\left[\phi^{k+1,(l+1/2)}(x)-\phi^{k}(x)\right]+\frac{\mathrm{d}}{\mathrm{d}x}J^{k+1,(l+1/2)}(x)+\Sigma_t(x)\phi^{k+1,(l+1/2)}(x) = \Sigma_s(x)\phi^{k+1,(l)}(x)+\int_{-1}^{1}Q^{k+1}(x,\mu)\,\mathrm{d}\mu\,, \quad \text{(B.4)}$$

where

$$J^{k+1,(l+1/2)}(x)=\int_{-1}^{1}\psi^{k+1,(l+1/2)}(x,\mu)\,\mathrm{d}\mu\,, \quad \text{(B.5)}$$

is the current. The first angular moment of Eq. (B.3a) is

$$\frac{1}{v\Delta t_{k+1}}\left[J^{k+1,(l+1/2)}(x)-J^{k}(x)\right]+\frac{\mathrm{d}}{\mathrm{d}x}\int_{-1}^{1}\mu^2\psi^{k+1,(l+1/2)}(x,\mu)\,\mathrm{d}\mu+\Sigma_t(x)J^{k+1,(l+1/2)}(x) = \int_{-1}^{1}\mu Q^{k+1}(x,\mu)\,\mathrm{d}\mu\,. \quad \text{(B.6)}$$

We modify the spatial derivative term in Eq. (B.6) as

$$\begin{aligned}\frac{\mathrm{d}}{\mathrm{d}x}\int_{-1}^{1}\mu^2\psi^{k+1,(l+1/2)}(x,\mu)\,\mathrm{d}\mu &= \frac{2}{3}\frac{\mathrm{d}}{\mathrm{d}x}\int_{-1}^{1}\frac{1}{2}\Big(3\mu^2-1\Big)\psi^{k+1,(l+1/2)}(x,\mu)\,\mathrm{d}\mu \\ &\quad+\frac{1}{3}\frac{\mathrm{d}}{\mathrm{d}x}\int_{-1}^{1}\psi^{k+1,(l+1/2)}(x,\mu)\,\mathrm{d}\mu \\ &= \frac{2}{3}\frac{\mathrm{d}}{\mathrm{d}x}\Phi^{k+1,(l+1/2)}(x)+\frac{1}{3}\frac{\mathrm{d}}{\mathrm{d}x}\phi^{k+1,(l+1/2)}(x)\,, \qquad \text{(B.7)}\end{aligned}$$

where

$$\Phi^{k+1,(l+1/2)}(x)=\int_{-1}^{1}\frac{1}{2}\Big(3\mu^2-1\Big)\psi^{k+1,(l+1/2)}(x,\mu)\,\mathrm{d}\mu\,, \qquad \text{(B.8)}$$

is a second-moment flux term. Substituting Eq. (B.7) into Eq. (B.6), we obtain

$$\begin{aligned}&\frac{1}{v\Delta t_{k+1}}\Big[J^{k+1,(l+1/2)}(x)-J^{k}(x)\Big]+\frac{2}{3}\frac{\mathrm{d}}{\mathrm{d}x}\Phi^{k+1,(l+1/2)}(x)+\frac{1}{3}\frac{\mathrm{d}}{\mathrm{d}x}\phi^{k+1,(l+1/2)}(x) \\ &\qquad+\Sigma_t(x)J^{k+1,(l+1/2)}(x)=\int_{-1}^{1}\mu Q^{k+1}(x,\mu)\,\mathrm{d}\mu\,. \qquad \text{(B.9)}\end{aligned}$$

The second step in the derivation of the Modified Four-Step DSA equations is to update the iteration indices to $l+1$ in certain terms of Eqs. (B.4) and (B.9) to obtain

$$\begin{aligned}&\frac{1}{v\Delta t_{k+1}}\Big[\phi^{k+1,(l+1)}(x)-\phi^{k}(x)\Big]+\frac{\mathrm{d}}{\mathrm{d}x}J^{k+1,(l+1)}(x)+\Sigma_t(x)\phi^{k+1,(l+1)}(x) \\ &\qquad=\Sigma_s(x)\phi^{k+1,(l+1)}(x)+\int_{-1}^{1}Q^{k+1}(x,\mu)\,\mathrm{d}\mu\,, \qquad \text{(B.10a)}\end{aligned}$$

$$\begin{aligned}&\frac{1}{v\Delta t_{k+1}}\Big[J^{k+1,(l+1)}(x)-J^{k}(x)\Big]+\frac{2}{3}\frac{\mathrm{d}}{\mathrm{d}x}\Phi^{k+1,(l+1/2)}(x)+\frac{1}{3}\frac{\mathrm{d}}{\mathrm{d}x}\phi^{k+1,(l+1)}(x) \\ &\qquad+\Sigma_t(x)J^{k+1,(l+1)}(x)=\int_{-1}^{1}\mu Q^{k+1}(x,\mu)\,\mathrm{d}\mu\,. \qquad \text{(B.10b)}\end{aligned}$$

The third step in the Modified Four-Step DSA derivation is to subtract Eq. (B.4) from Eq. (B.10a), and Eq. (B.9) from Eq. (B.10b), and define

$$F_0^{k+1,(l+1)}(x)=\phi^{k+1,(l+1)}(x)-\phi^{k+1,(l+1/2)}(x)\,, \qquad \text{(B.11a)}$$

$$F_1^{k+1,(l+1)}(x)=J^{k+1,(l+1)}(x)-J^{k+1,(l+1/2)}(x)\,. \qquad \text{(B.11b)}$$

We obtain

$$\frac{1}{v\Delta t_{k+1}}F_0^{k+1,(l+1)}(x)+\frac{\mathrm{d}}{\mathrm{d}x}F_1^{k+1,(l+1)}(x)+\Sigma_a(x)F_0^{k+1,(l+1)}(x) = \Sigma_s(x)\left[\phi^{k+1,(l+1/2)}(x)-\phi^{k+1,(l)}(x)\right], \quad \text{(B.12a)}$$

$$\frac{1}{v\Delta t_{k+1}}F_1^{k+1,(l+1)}(x)+\frac{1}{3}\frac{\mathrm{d}}{\mathrm{d}x}F_0^{k+1,(l+1)}(x)+\Sigma_t(x)F_1^{k+1,(l+1)}(x)=0\,. \quad \text{(B.12b)}$$

The fourth step is to eliminate the current correction $F_1^{k+1,(l+1)}(x)$ from Eq. (B.12a). Solving Eq. (B.12b) for $F_1^{k+1,(l+1)}(x)$, we find

$$F_1^{k+1,(l+1)}(x)=-D^{k+1}(x)\frac{\mathrm{d}}{\mathrm{d}x}F_0^{k+1,(l+1)}(x)\,, \quad \text{(B.13)}$$

where

$$D^{k+1}(x)=\frac{v\Delta t_{k+1}}{3\left[1+\Sigma_t(x)v\Delta t_{k+1}\right]}\,. \quad \text{(B.14)}$$

Substituting Eq. (B.13) into Eq. (B.12a), we have the time-discretized, spatially- and angularly-continuous, Modified Four-Step DSA equation

$$\frac{1}{v\Delta t_{k+1}}F_0^{k+1,(l+1)}(x)-\frac{\mathrm{d}}{\mathrm{d}x}D^{k+1}(x)\frac{\mathrm{d}}{\mathrm{d}x}F_0^{k+1,(l+1)}(x)+\Sigma_a(x)F_0^{k+1,(l+1)}(x) = \Sigma_s(x)\left[\phi^{k+1,(l+1/2)}(x)-\phi^{k+1,(l)}(x)\right]. \quad \text{(B.15)}$$

Therefore, the Modified Four-Step iterative scheme for the time-discretized, angularly- and spatially-continuous transport equation is

$$\frac{1}{v\Delta t_{k+1}}\left[\psi^{k+1,(l+1/2)}(x,\mu)-\psi^{k}(x,\mu)\right]+\mu\frac{\partial}{\partial x}\psi^{k+1,(l+1/2)}(x,\mu) +\Sigma_t(x)\psi^{k+1,(l+1/2)}(x,\mu)=\frac{\Sigma_s(x)}{2}\phi^{k+1,(l)}(x)+Q^{k+1}(x,\mu)\,, \quad \text{(B.16a)}$$

$$\phi^{k+1,(l+1/2)}(x)=\int_{-1}^{1}\psi^{k+1,(l+1/2)}(x,\mu)\,\mathrm{d}\mu\,, \quad \text{(B.16b)}$$

$$\frac{1}{v\Delta t_{k+1}}F_0^{k+1,(l+1)}(x)-\frac{\mathrm{d}}{\mathrm{d}x}D^{k+1}(x)\frac{\mathrm{d}}{\mathrm{d}x}F_0^{k+1,(l+1)}(x)+\Sigma_a(x)F_0^{k+1,(l+1)}(x) = \Sigma_s(x)\left[\phi^{k+1,(l+1/2)}(x)-\phi^{k+1,(l)}(x)\right], \quad \text{(B.16c)}$$

$$\phi^{k+1,(l+1)}(x)=\phi^{k+1,(l+1/2)}(x)+F_0^{k+1,(l+1)}(x)\,. \quad \text{(B.16d)}$$

B.2 Deriving the Fully-Discretized Modified Four-Step Diffusion Synthetic Acceleration Equations

In this section we derive the Modified Four-Step DSA equations for the implicitly discretized, linear discontinuous finite element transport equation, derived in Chapter 3, using the methodology outlined in Ref. [3]. The source iteration scheme for this equation is

$$\frac{1}{v\Delta t_{k+1}}\underline{\underline{M}}_i\left(\underline{\psi}_{n,i}^{k+1,(l+1/2)}-\underline{\psi}_{n,i}^{k}\right)+\mu_n\underline{\underline{L}}_i^{surf}\underline{\psi}_{n,i}^{k+1,(l+1/2),surf}-\mu_n\underline{\underline{L}}_i\underline{\psi}_{n,i}^{k+1,(l+1/2)}$$
$$+\Sigma_{t,i}\underline{\underline{M}}_i\underline{\psi}_{n,i}^{k+1,(l+1/2)}=\frac{\Sigma_{s,i}}{2}\underline{\underline{M}}_i\underline{\phi}_i^{k+1,(l)}+\underline{\underline{M}}_i\underline{Q}_{n,i}^{k+1}\,, \quad \text{(B.17a)}$$

$$\underline{\phi}_i^{k+1,(l+1/2)}=\sum_{n=1}^{N}\underline{\psi}_{n,i}^{k+1,(l+1/2)}\,\Delta_n\,, \quad \text{(B.17b)}$$

$$\underline{\phi}_i^{k+1,(l+1)}=\underline{\phi}_i^{k+1,(l+1/2)}\,, \quad \text{(B.17c)}$$

where l indicates the iteration index, and the other terms in Eqs. (B.17) are defined in Chapter 3. As stated earler, the source iteration scheme is known to converge slowly for optically-thick and diffusive problems.

We begin the derivation of the modified DSA equations with Eq. (3.17), modified to assume an implicit time discretization and constant cross sections within each cell. We have also assumed an iterative scheme, with l signifying the iteration index. Therefore, we have

$$\frac{1}{v\Delta t_{k+1}}\int_{x_{i-1/2}}^{x_{i+1/2}}w_{i,p}(x)\left[\psi_n^{k+1,(l+1/2)}(x)-\psi_n^{k}(x)\right]\mathrm{d}x$$
$$+\mu_n\left[w_{i,p}(x_{i+1/2})\psi_n^{k+1,(l+1/2)}(x_{i+1/2})-w_{i,p}(x_{i-1/2})\psi_n^{k+1,(l+1/2)}(x_{i-1/2})\right]$$
$$-\mu_n\int_{x_{i-1/2}}^{x_{i+1/2}}\psi_n^{k+1,(l+1/2)}(x)\frac{\mathrm{d}}{\mathrm{d}x}w_{i,p}(x)\,\mathrm{d}x+\Sigma_{t,i}\int_{x_{i-1/2}}^{x_{i+1/2}}w_{i,p}(x)\psi_n^{k+1,(l+1/2)}(x)\,\mathrm{d}x$$
$$=\frac{\Sigma_{s,i}}{2}\int_{x_{i-1/2}}^{x_{i+1/2}}w_{i,p}(x)\phi^{k+1,(l)}(x)\,\mathrm{d}x+\int_{x_{i-1/2}}^{x_{i+1/2}}w_{i,p}(x)Q_n^{k+1}(x)\,\mathrm{d}x\,. \quad \text{(B.18)}$$

B.2.1 Step 1a: Calculate Zeroth Moment

We first calculate the zeroth angular moment of Eq. (B.18). Operating on Eq. (B.18) by $\sum_{n=1}^{N}(\cdot)\Delta_n$, we have

$$\begin{aligned}
&\frac{1}{v\Delta t_{k+1}}\int_{x_{i-1/2}}^{x_{i+1/2}} w_{i,p}(x)\left[\phi^{k+1,(l+1/2)}(x)-\phi^{k}(x)\right]\mathrm{d}x \\
&\quad+\sum_{n=1}^{N}\mu_n\left[w_{i,p}(x_{i+1/2})\psi_n^{k+1,(l+1/2)}(x_{i+1/2})-w_{i,p}(x_{i-1/2})\psi_n^{k+1,(l+1/2)}(x_{i-1/2})\right]\Delta_n \\
&\qquad-\int_{x_{i-1/2}}^{x_{i+1/2}} J^{k+1,(l+1/2)}(x)\frac{\mathrm{d}}{\mathrm{d}x}w_{i,p}(x)\,\mathrm{d}x+\Sigma_{t,i}\int_{x_{i-1/2}}^{x_{i+1/2}} w_{i,p}(x)\phi^{k+1,(l+1/2)}(x)\,\mathrm{d}x \\
&\qquad\quad=\Sigma_{s,i}\int_{x_{i-1/2}}^{x_{i+1/2}} w_{i,p}(x)\phi^{k+1,(l)}(x)\,\mathrm{d}x+\int_{x_{i-1/2}}^{x_{i+1/2}} w_{i,p}(x)\sum_{n=1}^{N}Q_n^{k+1}(x)\,\Delta_n\,\mathrm{d}x. \quad \text{(B.19)}
\end{aligned}$$

Splitting the surface term in Eq. (B.19) into incident and outgoing partial currents, and noting that the current on a reflecting boundary is zero, we obtain

$$\begin{aligned}
&\frac{1}{v\Delta t_{k+1}}\int_{x_{1/2}}^{x_{3/2}} w_{1,p}(x)\left[\phi^{k+1,(l+1/2)}(x)-\phi^{k}(x)\right]\mathrm{d}x \\
&\qquad\quad+\left(w_{1,p}(x_{3/2})\left[J^{k+1,out,(l+1/2)}(x_{3/2})-J^{k+1,inc,(l+1/2)}(x_{3/2})\right]\right) \\
&\qquad-\int_{x_{1/2}}^{x_{3/2}} J^{k+1,(l+1/2)}(x)\frac{\mathrm{d}}{\mathrm{d}x}w_{1,p}(x)\,\mathrm{d}x+\Sigma_{t,1}\int_{x_{1/2}}^{x_{3/2}} w_{1,p}(x)\phi^{k+1,(l+1/2)}(x)\,\mathrm{d}x \\
&\qquad\quad=\Sigma_{s,1}\int_{x_{1/2}}^{x_{3/2}} w_{1,p}(x)\phi^{k+1,(l)}(x)\,\mathrm{d}x+\int_{x_{1/2}}^{x_{3/2}} w_{1,p}(x)\sum_{n=1}^{N}Q_n^{k+1}(x)\,\Delta_n\,\mathrm{d}x, \\
&\qquad\qquad\qquad\qquad\qquad\qquad\qquad\qquad\text{left reflecting boundary}, \quad \text{(B.20a)}
\end{aligned}$$

$$\begin{aligned}
&\frac{1}{v\Delta t_{k+1}}\int_{x_{i-1/2}}^{x_{i+1/2}} w_{i,p}(x)\left[\phi^{k+1,(l+1/2)}(x)-\phi^{k}(x)\right]\mathrm{d}x \\
&\qquad\quad+\Bigg(w_{i,p}(x_{i+1/2})\left[J^{k+1,out,(l+1/2)}(x_{i+1/2})-J^{k+1,inc,(l+1/2)}(x_{i+1/2})\right] \\
&\qquad\qquad\qquad-w_{i,p}(x_{i-1/2})\left[J^{k+1,inc,(l+1/2)}(x_{i-1/2})-J^{k+1,out,(l+1/2)}(x_{i-1/2})\right]\Bigg) \\
&\qquad-\int_{x_{i-1/2}}^{x_{i+1/2}} J^{k+1,(l+1/2)}(x)\frac{\mathrm{d}}{\mathrm{d}x}w_{i,p}(x)\,\mathrm{d}x+\Sigma_{t,i}\int_{x_{i-1/2}}^{x_{i+1/2}} w_{i,p}(x)\phi^{k+1,(l+1/2)}(x)\,\mathrm{d}x \\
&\qquad\quad=\Sigma_{s,i}\int_{x_{i-1/2}}^{x_{i+1/2}} w_{i,p}(x)\phi^{k+1,(l)}(x)\,\mathrm{d}x+\int_{x_{i-1/2}}^{x_{i+1/2}} w_{i,p}(x)\sum_{n=1}^{N}Q_n^{k+1}(x)\,\Delta_n\,\mathrm{d}x, \\
&\qquad\qquad\qquad\qquad\qquad\qquad\qquad\qquad\text{interior and incident boundaries}, \quad \text{(B.20b)}
\end{aligned}$$

$$\frac{1}{v\Delta t_{k+1}}\int_{x_{I-1/2}}^{x_{I+1/2}} w_{I,p}(x)\left[\phi^{k+1,(l+1/2)}(x)-\phi^{k}(x)\right]\mathrm{d}x$$
$$-\left(w_{I,p}(x_{I-1/2})\left[J^{k+1,inc,(l+1/2)}(x_{I-1/2})-J^{k+1,out,(l+1/2)}(x_{I-1/2})\right]\right)$$
$$-\int_{x_{I-1/2}}^{x_{I+1/2}} J^{k+1,(l+1/2)}(x)\frac{\mathrm{d}}{\mathrm{d}x}w_{I,p}(x)\,\mathrm{d}x+\Sigma_{t,I}\int_{x_{I-1/2}}^{x_{I+1/2}} w_{I,p}(x)\phi^{k+1,(l+1/2)}(x)\,\mathrm{d}x$$
$$=\Sigma_{s,I}\int_{x_{I-1/2}}^{x_{I+1/2}} w_{I,p}(x)\phi^{k+1,(l)}(x)\,\mathrm{d}x+\int_{x_{I-1/2}}^{x_{I+1/2}} w_{I,p}(x)\sum_{n=1}^{N} Q_n^{k+1}(x)\,\Delta_n\,\mathrm{d}x\,,$$
right reflecting boundary. (B.20c)

The incident partial currents in Eqs. (B.20) are defined as

$$J^{k+1,inc,(l+1/2)}(x_{1/2})=\sum_{\mu_n>0}\mu_n\psi_{n,L}^{b,k+1}\Delta_n\,,\qquad\text{left incident boundary}\,,\tag{B.21a}$$

$$J^{k+1,inc,(l+1/2)}(x_{i-1/2})=\sum_{\mu_n>0}\mu_n\psi_{n}^{k+1,(l+1/2)}(x_{i-1/2}^{+})\Delta_n\,,\qquad 2\le i\le I\,,\tag{B.21b}$$

and

$$J^{k+1,inc,(l+1/2)}(x_{i+1/2})=\sum_{\mu_n<0}|\mu_n|\psi_{n}^{k+1,(l+1/2)}(x_{i+1/2}^{+})\Delta_n\,,\qquad 1\le I\le I-1\,,\tag{B.22a}$$

$$J^{k+1,inc,(l+1/2)}(x_{I+1/2})=\sum_{\mu_n<0}|\mu_n|\psi_{n,R}^{b,k+1}\Delta_n\,,\qquad\text{right incident boundary}\,,\tag{B.22b}$$

and the outgoing partial currents as

$$J^{k+1,out,(l+1/2)}(x_{i-1/2})=\sum_{\mu_n<0}|\mu_n|\psi_{n}^{k+1,(l+1/2)}(x_{i-1/2}^{-})\Delta_n\,,\tag{B.23}$$

$$J^{k+1,out,(l+1/2)}(x_{i+1/2})=\sum_{\mu_n>0}\mu_n\psi_{n}^{k+1,(l+1/2)}(x_{i+1/2}^{-})\Delta_n\,,\tag{B.24}$$

where $x_{i-1/2}^{+}$ and $x_{i+1/2}^{+}$ reside just outside cell i on the left and right cell boundaries, respectively, and $x_{i-1/2}^{-}$ and $x_{i+1/2}^{-}$ reside just inside cell i on the left and right cell boundaries, respectively. To proceed, we expand the angular flux evaluated on the cell boundaries in

terms of the first two angular moments

$$\psi_n^{k+1,(l+1/2)}(x_{i-1/2}) = \frac{1}{2}\phi^{k+1,(l+1/2)}(x_{i-1/2}) + \frac{3\mu_n}{2}J^{k+1,(l+1/2)}(x_{i-1/2}) + O^{k+1,(l+1/2)}(\mu_n^2), \quad \text{(B.25a)}$$

$$\psi_n^{k+1,(l+1/2)}(x_{i+1/2}) = \frac{1}{2}\phi^{k+1,(l+1/2)}(x_{i+1/2}) + \frac{3\mu_n}{2}J^{k+1,(l+1/2)}(x_{i+1/2}) + O^{k+1,(l+1/2)}(\mu_n^2), \quad \text{(B.25b)}$$

where $O^{k+1,(l+1/2)}(\mu_n^2)$ refers to order μ_n^2 and higher terms. Substituting Eqs. (B.25) into Eqs. (B.21) and Eqs. (B.22), we find, for the incident partial currents

$$J^{k+1,inc,(l+1/2)}(x_{1/2}) = \sum_{\mu_n>0}\mu_n\psi_{n,L}^{b,k+1}\Delta_n, \qquad \text{left incident boundary}, \quad \text{(B.26a)}$$

$$J^{k+1,inc,(l+1/2)}(x_{i-1/2}) = \frac{\rho}{2}\phi^{k+1,(l+1/2)}(x_{i-1/2}^+) + \frac{1}{2}J^{k+1,(l+1/2)}(x_{i-1/2}^+) + O^{k+1,(l+1/2)}(\mu_n), \qquad 2 \le i \le I, \quad \text{(B.26b)}$$

and

$$J^{k+1,inc,(l+1/2)}(x_{i+1/2}) = \frac{\rho}{2}\phi^{k+1,(l+1/2)}(x_{i+1/2}^+) - \frac{1}{2}J^{k+1,(l+1/2)}(x_{i+1/2}^+) + O^{k+1,(l+1/2)}(\mu_n), \qquad 1 \le i \le I-1, \quad \text{(B.27a)}$$

$$J^{k+1,inc,(l+1/2)}(x_{I+1/2}) = \sum_{\mu_n<0}|\mu_n|\psi_{n,R}^{b,k+1}\Delta_n, \qquad \text{right incident boundary}, \quad \text{(B.27b)}$$

where

$$\rho = \sum_{\mu_n>0}\mu_n\Delta_n = -\sum_{\mu_n<0}\mu_n\Delta_n \approx \frac{1}{2}. \quad \text{(B.28)}$$

For the outgoing partial currents, we substitute Eqs. (B.25) into Eqs. (B.23) and (B.24), and find

$$J^{k+1,out,(l+1/2)}(x_{i-1/2}) = \frac{\rho}{2}\phi^{k+1,(l+1/2)}(x_{i-1/2}^-) - \frac{1}{2}J^{k+1,(l+1/2)}(x_{i-1/2}^-) + O^{k+1,(l+1/2)}(\mu_n), \quad \text{(B.29)}$$

and

$$J^{k+1,out,(l+1/2)}(x_{i+1/2}) = \frac{\rho}{2}\phi^{k+1,(l+1/2)}(x^-_{i+1/2}) + \frac{1}{2}J^{k+1,(l+1/2)}(x^-_{i+1/2}) + O^{k+1,(l+1/2)}(\mu_n)\,. \quad \text{(B.30)}$$

Now Eqs. (B.20) can be written as

$$\begin{aligned}
&\frac{1}{v\Delta t_{k+1}}\int_{x_{1/2}}^{x_{3/2}} w_{1,p}(x)\left[\phi^{k+1,(l+1/2)}(x) - \phi^k(x)\right]\mathrm{d}x \\
&\quad + \left(w_{1,p}(x_{3/2})\left[\frac{\rho}{2}\phi^{k+1,(l+1/2)}(x^-_{3/2}) + \frac{1}{2}J^{k+1,(l+1/2)}(x^-_{3/2}) - \frac{\rho}{2}\phi^{k+1,(l+1/2)}(x^+_{3/2}) \right.\right. \\
&\qquad \left.\left. + \frac{1}{2}J^{k+1,(l+1/2)}(x^+_{3/2}) + O^{k+1,(l+1/2)}(\mu_n)\right]\right) \\
&\quad - \int_{x_{1/2}}^{x_{3/2}} J^{k+1,(l+1/2)}(x)\frac{\mathrm{d}}{\mathrm{d}x}w_{1,p}(x)\,\mathrm{d}x + \Sigma_{t,1}\int_{x_{1/2}}^{x_{3/2}} w_{1,p}(x)\phi^{k+1,(l+1/2)}(x)\,\mathrm{d}x \\
&\qquad = \Sigma_{s,1}\int_{x_{1/2}}^{x_{3/2}} w_{1,p}(x)\phi^{k+1,(l)}(x)\,\mathrm{d}x + \int_{x_{1/2}}^{x_{3/2}} w_{1,p}(x)\sum_{n=1}^{N} Q_n^{k+1}(x)\,\Delta_n\,\mathrm{d}x\,,
\end{aligned}$$

left reflecting boundary, (B.31a)

$$\begin{aligned}
&\frac{1}{v\Delta t_{k+1}}\int_{x_{1/2}}^{x_{3/2}} w_{1,p}(x)\left[\phi^{k+1,(l+1/2)}(x) - \phi^k(x)\right]\mathrm{d}x \\
&\quad + \left(w_{1,p}(x_{3/2})\left[\frac{\rho}{2}\phi^{k+1,(l+1/2)}(x^-_{3/2}) + \frac{1}{2}J^{k+1,(l+1/2)}(x^-_{3/2}) - \frac{\rho}{2}\phi^{k+1,(l+1/2)}(x^+_{3/2}) \right.\right. \\
&\qquad \left. + \frac{1}{2}J^{k+1,(l+1/2)}(x^+_{3/2}) + O^{k+1,(l+1/2)}(\mu_n)\right] \\
&\qquad - w_{1,p}(x_{1/2})\left[\sum_{\mu_n>0}\mu_n\psi^{b,k+1}_{n,L}\,\Delta_n - \frac{\rho}{2}\phi^{k+1,(l+1/2)}(x^-_{1/2}) + \frac{1}{2}J^{k+1,(l+1/2)}(x^-_{1/2}) \right. \\
&\qquad \left.\left. + O^{k+1,(l+1/2)}(\mu_n)\right]\right) \\
&\quad - \int_{x_{1/2}}^{x_{3/2}} J^{k+1,(l+1/2)}(x)\frac{\mathrm{d}}{\mathrm{d}x}w_{1,p}(x)\,\mathrm{d}x + \Sigma_{t,1}\int_{x_{1/2}}^{x_{3/2}} w_{1,p}(x)\phi^{k+1,(l+1/2)}(x)\,\mathrm{d}x \\
&\qquad = \Sigma_{s,1}\int_{x_{1/2}}^{x_{3/2}} w_{1,p}(x)\phi^{k+1,(l)}(x)\,\mathrm{d}x + \int_{x_{1/2}}^{x_{3/2}} w_{1,p}(x)\sum_{n=1}^{N} Q_n^{k+1}(x)\,\Delta_n\,\mathrm{d}x\,,
\end{aligned}$$

left incident boundary, (B.31b)

$$
\begin{aligned}
&\frac{1}{v\Delta t_{k+1}}\int_{x_{i-1/2}}^{x_{i+1/2}} w_{i,p}(x)\left[\phi^{k+1,(l+1/2)}(x)-\phi^{k}(x)\right]\mathrm{d}x \\
&\quad+\Bigg(w_{i,p}(x_{i+1/2})\left[\frac{\rho}{2}\phi^{k+1,(l+1/2)}(x_{i+1/2}^{-})+\frac{1}{2}J^{k+1,(l+1/2)}(x_{i+1/2}^{-})\right. \\
&\qquad\qquad-\frac{\rho}{2}\phi^{k+1,(l+1/2)}(x_{i+1/2}^{+})+\frac{1}{2}J^{k+1,(l+1/2)}(x_{i+1/2}^{+}) \\
&\qquad\qquad\left.+O^{k+1,(l+1/2)}(\mu_n)\right] \\
&\qquad-w_{i,p}(x_{i-1/2})\left[\frac{\rho}{2}\phi^{k+1,(l+1/2)}(x_{i-1/2}^{+})+\frac{1}{2}J^{k+1,(l+1/2)}(x_{i-1/2}^{+})\right. \\
&\qquad\qquad-\frac{\rho}{2}\phi^{k+1,(l+1/2)}(x_{i-1/2}^{-})+\frac{1}{2}J^{k+1,(l+1/2)}(x_{i-1/2}^{-}) \\
&\qquad\qquad\left.+O^{k+1,(l+1/2)}(\mu_n)\right]\Bigg) \\
&\quad-\int_{x_{i-1/2}}^{x_{i+1/2}} J^{k+1,(l+1/2)}(x)\frac{\mathrm{d}}{\mathrm{d}x}w_{i,p}(x)\,\mathrm{d}x+\Sigma_{t,i}\int_{x_{i-1/2}}^{x_{i+1/2}} w_{i,p}(x)\phi^{k+1,(l+1/2)}(x)\,\mathrm{d}x \\
&\qquad=\Sigma_{s,i}\int_{x_{i-1/2}}^{x_{i+1/2}} w_{i,p}(x)\phi^{k+1,(l)}(x)\,\mathrm{d}x+\int_{x_{i-1/2}}^{x_{i+1/2}} w_{i,p}(x)\sum_{n=1}^{N} Q_n^{k+1}(x)\,\Delta_n\,\mathrm{d}x, \\
&\qquad\qquad 2\le i\le I-1\,, \quad \text{(B.31c)}
\end{aligned}
$$

$$
\begin{aligned}
&\frac{1}{v\Delta t_{k+1}}\int_{x_{I-1/2}}^{x_{I+1/2}} w_{I,p}(x)\left[\phi^{k+1,(l+1/2)}(x)-\phi^{k}(x)\right]\mathrm{d}x \\
&\quad+\Bigg(w_{I,p}(x_{I+1/2})\left[\frac{\rho}{2}\phi^{k+1,(l+1/2)}(x_{I+1/2}^{-})+\frac{1}{2}J^{k+1,(l+1/2)}(x_{I+1/2}^{-})\right. \\
&\qquad\qquad\left.-\sum_{\mu_n<0}|\mu_n|\psi_{n,R}^{b,k+1}\,\Delta_n+O^{k+1,(l+1/2)}(\mu_n)\right] \\
&\qquad-w_{I,p}(x_{I-1/2})\left[\frac{\rho}{2}\phi^{k+1,(l+1/2)}(x_{I-1/2}^{+})+\frac{1}{2}J^{k+1,(l+1/2)}(x_{I-1/2}^{+})\right. \\
&\qquad\qquad-\frac{\rho}{2}\phi^{k+1,(l+1/2)}(x_{I-1/2}^{-})+\frac{1}{2}J^{k+1,(l+1/2)}(x_{I-1/2}^{-}) \\
&\qquad\qquad\left.+O^{k+1,(l+1/2)}(\mu_n)\right]\Bigg) \\
&\quad-\int_{x_{I-1/2}}^{x_{I+1/2}} J^{k+1,(l+1/2)}(x)\frac{\mathrm{d}}{\mathrm{d}x}w_{I,p}(x)\,\mathrm{d}x+\Sigma_{t,I}\int_{x_{I-1/2}}^{x_{I+1/2}} w_{I,p}(x)\phi^{k+1,(l+1/2)}(x)\,\mathrm{d}x \\
&\qquad=\Sigma_{s,I}\int_{x_{I-1/2}}^{x_{I+1/2}} w_{I,p}(x)\phi^{k+1,(l)}(x)\,\mathrm{d}x+\int_{x_{I-1/2}}^{x_{I+1/2}} w_{I,p}(x)\sum_{n=1}^{N} Q_n^{k+1}(x)\,\Delta_n\,\mathrm{d}x, \\
&\qquad\qquad\text{right incident boundary}\,, \quad \text{(B.31d)}
\end{aligned}
$$

$$\frac{1}{v\Delta t_{k+1}}\int_{x_{I-1/2}}^{x_{I+1/2}} w_{I,p}(x)\left[\phi^{k+1,(l+1/2)}(x)-\phi^{k}(x)\right]\mathrm{d}x$$
$$-\Bigg(w_{I,p}(x_{I-1/2})\Bigg[\frac{\rho}{2}\phi^{k+1,(l+1/2)}(x^{+}_{I-1/2})+\frac{1}{2}J^{k+1,(l+1/2)}(x^{+}_{I-1/2})$$
$$-\frac{\rho}{2}\phi^{k+1,(l+1/2)}(x^{-}_{I-1/2})+\frac{1}{2}J^{k+1,(l+1/2)}(x^{-}_{I-1/2})$$
$$+O^{k+1,(l+1/2)}(\mu_n)\Bigg]\Bigg)$$
$$-\int_{x_{I-1/2}}^{x_{I+1/2}} J^{k+1,(l+1/2)}(x)\frac{\mathrm{d}}{\mathrm{d}x}w_{I,p}(x)\,\mathrm{d}x+\Sigma_{t,I}\int_{x_{I-1/2}}^{x_{I+1/2}} w_{I,p}(x)\phi^{k+1,(l+1/2)}(x)\,\mathrm{d}x$$
$$=\Sigma_{s,I}\int_{x_{I-1/2}}^{x_{I+1/2}} w_{I,p}(x)\phi^{k+1,(l)}(x)\,\mathrm{d}x+\int_{x_{I-1/2}}^{x_{I+1/2}} w_{I,p}(x)\sum_{n=1}^{N}Q_n^{k+1}(x)\,\Delta_n\,\mathrm{d}x,$$
$$\text{right reflecting boundary}. \quad \text{(B.31e)}$$

B.2.2 Step 1b: Calculate First Moment

Next we calculate the first angular moment of Eq. (B.18). Operating by $\sum_{n=1}^{N}\mu_n(\cdot)\,\Delta_n$, we find

$$\frac{1}{v\Delta t_{k+1}}\int_{x_{i-1/2}}^{x_{i+1/2}} w_{i,p}(x)\left[J^{k+1,(l+1/2)}(x)-J^{k}(x)\right]\mathrm{d}x$$
$$+\Bigg[w_{i,p}(x_{i+1/2})\sum_{n=1}^{N}\mu_n^2\psi_n^{k+1,(l+1/2)}(x_{i+1/2})\,\Delta_n$$
$$-w_{i,p}(x_{i-1/2})\sum_{n=1}^{N}\mu_n^2\psi_n^{k+1,(l+1/2)}(x_{i-1/2})\,\Delta_n\Bigg]$$
$$-\int_{x_{i-1/2}}^{x_{i+1/2}}\sum_{n=1}^{N}\mu_n^2\psi_n^{k+1,(l+1/2)}(x)\,\Delta_n\frac{\mathrm{d}}{\mathrm{d}x}w_{i,p}(x)\,\mathrm{d}x+\Sigma_{t,i}\int_{x_{i-1/2}}^{x_{i+1/2}} w_{i,p}(x)J^{k+1,(l+1/2)}(x)\,\mathrm{d}x$$
$$=\int_{x_{i-1/2}}^{x_{i+1/2}} w_{i,p}(x)\sum_{n=1}^{N}\mu_n Q_n^{k+1}(x)\,\Delta_n\,\mathrm{d}x. \quad \text{(B.32)}$$

The in-cell gradient term in Eq. (B.32) can be manipulated using integration by parts to obtain

$$
\begin{aligned}
&-\int_{x_{i-1/2}}^{x_{i+1/2}} \sum_{n=1}^{N} \mu_n^2 \psi_n^{k+1,(l+1/2)}(x)\,\Delta_n \frac{\mathrm{d}}{\mathrm{d}x} w_{i,p}(x)\,\mathrm{d}x \\
&\quad = -\sum_{n=1}^{N} \mu_n^2 \left[w_{i,p}(x)\,\psi_n^{k+1,(l+1/2)}(x) \right]_{x_{i-1/2}}^{x_{i+1/2}} \Delta_n \\
&\qquad\qquad + \int_{x_{i-1/2}}^{x_{i+1/2}} w_{i,p}(x) \frac{\mathrm{d}}{\mathrm{d}x} \left[\sum_{n=1}^{N} \mu_n^2 \psi_n^{k+1,(l+1/2)}(x)\,\Delta_n \right] \mathrm{d}x \\
&\quad = -w_{i,p}(x_{i+1/2}) \sum_{n=1}^{N} \mu_n^2 \psi_n^{k+1,(l+1/2)}(x_{i+1/2})\,\Delta_n \\
&\qquad\qquad + w_{i,p}(x_{i-1/2}) \sum_{n=1}^{N} \mu_n^2 \psi_n^{k+1,(l+1/2)}(x_{i-1/2})\,\Delta_n \\
&\qquad\qquad + \frac{2}{3} \int_{x_{i-1/2}}^{x_{i+1/2}} w_{i,p}(x) \frac{\mathrm{d}}{\mathrm{d}x} \Phi^{k+1,(l+1/2)}(x)\,\mathrm{d}x \\
&\qquad\qquad\qquad + \frac{1}{3} \int_{x_{i-1/2}}^{x_{i+1/2}} w_{i,p}(x) \frac{\mathrm{d}}{\mathrm{d}x} \phi^{k+1,(l+1/2)}(x)\,\mathrm{d}x\,,
\end{aligned}
\tag{B.33}
$$

where

$$
\Phi^{k+1,(l+1/2)}(x) = \frac{2}{3} \sum_{n=1}^{N} \frac{1}{2} \left(3\mu_n^2 - 1 \right) \psi_n^{k+1,(l+1/2)}(x)\,\Delta_n\,, \tag{B.34}
$$

is a second-moment flux term. Now Eq. (B.32) can be written as

$$
\begin{aligned}
&\frac{1}{v\Delta t_{k+1}} \int_{x_{i-1/2}}^{x_{i+1/2}} w_{i,p}(x) \left[J^{k+1,(l+1/2)}(x) - J^{k}(x) \right] \mathrm{d}x \\
&\quad + \frac{2}{3} \int_{x_{i-1/2}}^{x_{i+1/2}} w_{i,p}(x) \frac{\mathrm{d}}{\mathrm{d}x} \Phi^{k+1,(l+1/2)}(x)\,\mathrm{d}x + \frac{1}{3} \int_{x_{i-1/2}}^{x_{i+1/2}} w_{i,p}(x) \frac{\mathrm{d}}{\mathrm{d}x} \phi^{k+1,(l+1/2)}(x)\,\mathrm{d}x \\
&\quad + \Sigma_{t,i} \int_{x_{i-1/2}}^{x_{i+1/2}} w_{i,p}(x) J^{k+1,(l+1/2)}(x)\,\mathrm{d}x = \int_{x_{i-1/2}}^{x_{i+1/2}} w_{i,p}(x) \sum_{n=1}^{N} \mu_n Q_n^{k+1}(x)\,\Delta_n\,\mathrm{d}x\,.
\end{aligned}
\tag{B.35}
$$

B.2.3 Step 2: Update the Indices

The second step in the Modified Four-Step DSA derivation is to update the iteration indexes in certain terms of the zeroth and first moment equations to $l+1$. Therefore, updating

Eqs. (B.31), the zeroth moment equations, we obtain

$$\begin{aligned}
&\frac{1}{v\Delta t_{k+1}}\int_{x_{1/2}}^{x_{3/2}} w_{1,p}(x)\Big[\phi^{k+1,(l+1)}(x)-\phi^{k}(x)\Big]\,\mathrm{d}x \\
&\quad+\Bigg(w_{1,p}(x_{3/2})\Bigg[\frac{\rho}{2}\phi^{k+1,(l+1)}(x_{3/2}^{-})+\frac{1}{2}J^{k+1,(l+1)}(x_{3/2}^{-})-\frac{\rho}{2}\phi^{k+1,(l+1)}(x_{3/2}^{+}) \\
&\qquad\qquad+\frac{1}{2}J^{k+1,(l+1)}(x_{3/2}^{+})+O^{k+1,(l+1/2)}(\mu_n)\Bigg]\Bigg) \\
&\qquad-\int_{x_{1/2}}^{x_{3/2}} J^{k+1,(l+1)}(x)\frac{\mathrm{d}}{\mathrm{d}x}w_{1,p}(x)\,\mathrm{d}x+\Sigma_{t,1}\int_{x_{1/2}}^{x_{3/2}} w_{1,p}(x)\phi^{k+1,(l+1)}(x)\,\mathrm{d}x \\
&\qquad\qquad=\Sigma_{s,1}\int_{x_{1/2}}^{x_{3/2}} w_{1,p}(x)\phi^{k+1,(l+1)}(x)\,\mathrm{d}x+\int_{x_{1/2}}^{x_{3/2}} w_{1,p}(x)\sum_{n=1}^{N} Q_n^{k+1}(x)\,\Delta_n\,\mathrm{d}x\,,
\end{aligned}$$

left reflecting boundary , (B.36a)

$$\begin{aligned}
&\frac{1}{v\Delta t_{k+1}}\int_{x_{1/2}}^{x_{3/2}} w_{1,p}(x)\Big[\phi^{k+1,(l+1)}(x)-\phi^{k}(x)\Big]\,\mathrm{d}x \\
&\quad+\Bigg(w_{1,p}(x_{3/2})\Bigg[\frac{\rho}{2}\phi^{k+1,(l+1)}(x_{3/2}^{-})+\frac{1}{2}J^{k+1,(l+1)}(x_{3/2}^{-})-\frac{\rho}{2}\phi^{k+1,(l+1)}(x_{3/2}^{+}) \\
&\qquad\qquad+\frac{1}{2}J^{k+1,(l+1)}(x_{3/2}^{+})+O^{k+1,(l+1/2)}(\mu_n)\Bigg] \\
&\qquad-w_{1,p}(x_{1/2})\Bigg[\sum_{\mu_n>0}\mu_n\psi_{n,L}^{b,k+1}\Delta_n-\frac{\rho}{2}\phi^{k+1,(l+1)}(x_{1/2}^{-})+\frac{1}{2}J^{k+1,(l+1)}(x_{1/2}^{-}) \\
&\qquad\qquad+O^{k+1,(l+1/2)}(\mu_n)\Bigg]\Bigg) \\
&\qquad-\int_{x_{1/2}}^{x_{3/2}} J^{k+1,(l+1)}(x)\frac{\mathrm{d}}{\mathrm{d}x}w_{1,p}(x)\,\mathrm{d}x+\Sigma_{t,1}\int_{x_{1/2}}^{x_{3/2}} w_{1,p}(x)\phi^{k+1,(l+1)}(x)\,\mathrm{d}x \\
&\qquad\qquad=\Sigma_{s,1}\int_{x_{1/2}}^{x_{3/2}} w_{1,p}(x)\phi^{k+1,(l+1)}(x)\,\mathrm{d}x+\int_{x_{1/2}}^{x_{3/2}} w_{1,p}(x)\sum_{n=1}^{N} Q_n^{k+1}(x)\,\Delta_n\,\mathrm{d}x\,,
\end{aligned}$$

left incident boundary , (B.36b)

$$
\begin{aligned}
&\frac{1}{v\Delta t_{k+1}}\int_{x_{i-1/2}}^{x_{i+1/2}} w_{i,p}(x)\left[\phi^{k+1,(l+1)}(x)-\phi^{k}(x)\right]\mathrm{d}x \\
&\quad+\Bigg(w_{i,p}(x_{i+1/2})\left[\frac{\rho}{2}\phi^{k+1,(l+1)}(x_{i+1/2}^{-})+\frac{1}{2}J^{k+1,(l+1)}(x_{i+1/2}^{-})\right. \\
&\qquad\qquad-\frac{\rho}{2}\phi^{k+1,(l+1)}(x_{i+1/2}^{+})+\frac{1}{2}J^{k+1,(l+1)}(x_{i+1/2}^{+}) \\
&\qquad\qquad\qquad\left.+O^{k+1,(l+1/2)}(\mu_n)\right] \\
&\qquad-w_{i,p}(x_{i-1/2})\left[\frac{\rho}{2}\phi^{k+1,(l+1)}(x_{i-1/2}^{+})+\frac{1}{2}J^{k+1,(l+1)}(x_{i-1/2}^{+})\right. \\
&\qquad\qquad-\frac{\rho}{2}\phi^{k+1,(l+1)}(x_{i-1/2}^{-})+\frac{1}{2}J^{k+1,(l+1)}(x_{i-1/2}^{-}) \\
&\qquad\qquad\qquad\left.+O^{k+1,(l+1/2)}(\mu_n)\right]\Bigg) \\
&\quad-\int_{x_{i-1/2}}^{x_{i+1/2}} J^{k+1,(l+1)}(x)\frac{\mathrm{d}}{\mathrm{d}x}w_{i,p}(x)\,\mathrm{d}x+\Sigma_{t,i}\int_{x_{i-1/2}}^{x_{i+1/2}} w_{i,p}(x)\phi^{k+1,(l+1)}(x)\,\mathrm{d}x \\
&\qquad=\Sigma_{s,i}\int_{x_{i-1/2}}^{x_{i+1/2}} w_{i,p}(x)\phi^{k+1,(l+1)}(x)\,\mathrm{d}x+\int_{x_{i-1/2}}^{x_{i+1/2}} w_{i,p}(x)\sum_{n=1}^{N}Q_n^{k+1}(x)\,\Delta_n\,\mathrm{d}x, \\
&\qquad\qquad 2\le i\le I-1\,, \quad \text{(B.36c)}
\end{aligned}
$$

$$
\begin{aligned}
&\frac{1}{v\Delta t_{k+1}}\int_{x_{I-1/2}}^{x_{I+1/2}} w_{I,p}(x)\left[\phi^{k+1,(l+1)}(x)-\phi^{k}(x)\right]\mathrm{d}x \\
&\quad+\Bigg(w_{I,p}(x_{I+1/2})\left[\frac{\rho}{2}\phi^{k+1,(l+1)}(x_{I+1/2}^{-})+\frac{1}{2}J^{k+1,(l+1)}(x_{I+1/2}^{-})\right. \\
&\qquad\qquad\left.-\sum_{\mu_n<0}|\mu_n|\psi_{n,R}^{b,k+1}\,\Delta_n+O^{k+1,(l+1/2)}(\mu_n)\right] \\
&\qquad-w_{I,p}(x_{I-1/2})\left[\frac{\rho}{2}\phi^{k+1,(l+1)}(x_{I-1/2}^{+})+\frac{1}{2}J^{k+1,(l+1)}(x_{I-1/2}^{+})\right. \\
&\qquad\qquad-\frac{\rho}{2}\phi^{k+1,(l+1)}(x_{I-1/2}^{-})+\frac{1}{2}J^{k+1,(l+1)}(x_{I-1/2}^{-}) \\
&\qquad\qquad\qquad\left.+O^{k+1,(l+1/2)}(\mu_n)\right]\Bigg) \\
&\quad-\int_{x_{I-1/2}}^{x_{I+1/2}} J^{k+1,(l+1)}(x)\frac{\mathrm{d}}{\mathrm{d}x}w_{I,p}(x)\,\mathrm{d}x+\Sigma_{t,I}\int_{x_{I-1/2}}^{x_{I+1/2}} w_{I,p}(x)\phi^{k+1,(l+1)}(x)\,\mathrm{d}x \\
&\qquad=\Sigma_{s,I}\int_{x_{I-1/2}}^{x_{I+1/2}} w_{I,p}(x)\phi^{k+1,(l+1)}(x)\,\mathrm{d}x+\int_{x_{I-1/2}}^{x_{I+1/2}} w_{I,p}(x)\sum_{n=1}^{N}Q_n^{k+1}(x)\,\Delta_n\,\mathrm{d}x, \\
&\qquad\qquad\text{right incident boundary}\,, \qquad \text{(B.36d)}
\end{aligned}
$$

$$\frac{1}{v\Delta t_{k+1}}\int_{x_{I-1/2}}^{x_{I+1/2}} w_{I,p}(x)\left[\phi^{k+1,(l+1)}(x)-\phi^{k}(x)\right]\mathrm{d}x$$
$$-\Bigg(w_{I,p}(x_{I-1/2})\Bigg[\frac{\rho}{2}\phi^{k+1,(l+1)}(x^{+}_{I-1/2})+\frac{1}{2}J^{k+1,(l+1)}(x^{+}_{I-1/2})$$
$$-\frac{\rho}{2}\phi^{k+1,(l+1)}(x^{-}_{I-1/2})+\frac{1}{2}J^{k+1,(l+1)}(x^{-}_{I-1/2})$$
$$+O^{k+1,(l+1/2)}(\mu_n)\Bigg]\Bigg)$$
$$-\int_{x_{I-1/2}}^{x_{I+1/2}} J^{k+1,(l+1)}(x)\frac{\mathrm{d}}{\mathrm{d}x}w_{I,p}(x)\,\mathrm{d}x+\Sigma_{t,I}\int_{x_{I-1/2}}^{x_{I+1/2}} w_{I,p}(x)\phi^{k+1,(l+1)}(x)\,\mathrm{d}x$$
$$=\Sigma_{s,I}\int_{x_{I-1/2}}^{x_{I+1/2}} w_{I,p}(x)\phi^{k+1,(l+1)}(x)\,\mathrm{d}x+\int_{x_{I-1/2}}^{x_{I+1/2}} w_{I,p}(x)\sum_{n=1}^{N}Q_n^{k+1}(x)\,\Delta_n\,\mathrm{d}x\,,$$
$$\text{right reflecting boundary}\,. \qquad \text{(B.36e)}$$

Updating Eq. (B.35), the first moment equation, we find

$$\frac{1}{v\Delta t_{k+1}}\int_{x_{i-1/2}}^{x_{i+1/2}} w_{i,p}(x)\left[J^{k+1,(l+1)}(x)-J^{k}(x)\right]\mathrm{d}x$$
$$+\frac{2}{3}\int_{x_{i-1/2}}^{x_{i+1/2}} w_{i,p}(x)\frac{\mathrm{d}}{\mathrm{d}x}\Phi^{k+1,(l+1/2)}(x)\,\mathrm{d}x+\frac{1}{3}\int_{x_{i-1/2}}^{x_{i+1/2}} w_{i,p}(x)\frac{\mathrm{d}}{\mathrm{d}x}\phi^{k+1,(l+1)}(x)\,\mathrm{d}x$$
$$+\Sigma_{t,i}\int_{x_{i-1/2}}^{x_{i+1/2}} w_{i,p}(x)J^{k+1,(l+1)}(x)\,\mathrm{d}x=\int_{x_{i-1/2}}^{x_{i+1/2}} w_{i,p}(x)\sum_{n=1}^{N}\mu_n Q_n^{k+1}(x)\,\Delta_n\,\mathrm{d}x\,. \qquad \text{(B.37)}$$

B.2.4 Step 3: Subtract Step 2 Equations from Step 1 Equations

The third step in the Modified Four-Step DSA derivation is to subtract the equations obtained in step 1 from the equations obtained in step 2. Therefore, we subtract Eqs. (B.31) from Eqs. (B.36), and Eq. (B.35) from Eq. (B.37), and define

$$F_0^{k+1,(l+1)}(x)=\phi^{k+1,(l+1)}(x)-\phi^{k+1,(l+1/2)}(x)\,, \qquad \text{(B.38a)}$$

$$F_1^{k+1,(l+1)}(x)=J^{k+1,(l+1)}(x)-J^{k+1,(l+1/2)}(x)\,. \qquad \text{(B.38b)}$$

Now the zeroth moment equations are

$$\begin{aligned}
&\frac{1}{v\Delta t_{k+1}}\int_{x_{1/2}}^{x_{3/2}} w_{1,p}(x)F_0^{k+1,(l+1)}(x)\,\mathrm{d}x \\
&\quad+\left(w_{1,p}(x_{3/2})\left[\frac{\rho}{2}F_0^{k+1,(l+1)}(x_{3/2}^-)+\frac{1}{2}F_1^{k+1,(l+1)}(x_{3/2}^-)-\frac{\rho}{2}F_0^{k+1,(l+1)}(x_{3/2}^+)\right.\right. \\
&\qquad\left.\left.+\frac{1}{2}F_1^{k+1,(l+1)}(x_{3/2}^+)\right]\right) \\
&\quad-\int_{x_{1/2}}^{x_{3/2}} F_1^{k+1,(l+1)}(x)\frac{\mathrm{d}}{\mathrm{d}x}w_{1,p}(x)\,\mathrm{d}x+\Sigma_{a,1}\int_{x_{1/2}}^{x_{3/2}} w_{1,p}(x)F_0^{k+1,(l+1)}(x)\,\mathrm{d}x \\
&\qquad=\Sigma_{s,1}\int_{x_{1/2}}^{x_{3/2}} w_{1,p}(x)\left[\phi^{k+1,(l+1/2)}(x)-\phi^{k+1,(l)}(x)\right]\mathrm{d}x,
\end{aligned}$$

left reflecting boundary, (B.39a)

$$\begin{aligned}
&\frac{1}{v\Delta t_{k+1}}\int_{x_{1/2}}^{x_{3/2}} w_{1,p}(x)F_0^{k+1,(l+1)}(x)\,\mathrm{d}x \\
&\quad+\left(w_{1,p}(x_{3/2})\left[\frac{\rho}{2}F_0^{k+1,(l+1)}(x_{3/2}^-)+\frac{1}{2}F_1^{k+1,(l+1)}(x_{3/2}^-)-\frac{\rho}{2}F_0^{k+1,(l+1)}(x_{3/2}^+)\right.\right. \\
&\qquad\left.+\frac{1}{2}F_1^{k+1,(l+1)}(x_{3/2}^+)\right] \\
&\qquad\left.-w_{1,p}(x_{1/2})\left[-\frac{\rho}{2}F_0^{k+1,(l+1)}(x_{1/2}^-)+\frac{1}{2}F_1^{k+1,(l+1)}(x_{1/2}^-)\right]\right) \\
&\quad-\int_{x_{1/2}}^{x_{3/2}} F_1^{k+1,(l+1)}(x)\frac{\mathrm{d}}{\mathrm{d}x}w_{1,p}(x)\,\mathrm{d}x+\Sigma_{a,1}\int_{x_{1/2}}^{x_{3/2}} w_{1,p}(x)F_0^{k+1,(l+1)}(x)\,\mathrm{d}x \\
&\qquad=\Sigma_{s,1}\int_{x_{1/2}}^{x_{3/2}} w_{1,p}(x)\left[\phi^{k+1,(l+1/2)}(x)-\phi^{k+1,(l)}(x)\right]\mathrm{d}x,
\end{aligned}$$

left incident boundary, (B.39b)

$$
\begin{aligned}
&\frac{1}{v\Delta t_{k+1}}\int_{x_{i-1/2}}^{x_{i+1/2}} w_{i,p}(x)F_0^{k+1,(l+1)}(x)\,\mathrm{d}x \\
&\quad+\Bigg(w_{i,p}(x_{i+1/2})\left[\frac{\rho}{2}F_0^{k+1,(l+1)}(x_{i+1/2}^-)+\frac{1}{2}F_1^{k+1,(l+1)}(x_{i+1/2}^-)\right.\\
&\qquad\qquad\left.-\frac{\rho}{2}F_0^{k+1,(l+1)}(x_{i+1/2}^+)+\frac{1}{2}F_1^{k+1,(l+1)}(x_{i+1/2}^+)\right]\\
&\qquad-w_{i,p}(x_{i-1/2})\left[\frac{\rho}{2}F_0^{k+1,(l+1)}(x_{i-1/2}^+)+\frac{1}{2}F_1^{k+1,(l+1)}(x_{i-1/2}^+)\right.\\
&\qquad\qquad\left.-\frac{\rho}{2}F_0^{k+1,(l+1)}(x_{i-1/2}^-)+\frac{1}{2}F_1^{k+1,(l+1)}(x_{i-1/2}^-)\right]\Bigg)\\
&\quad-\int_{x_{i-1/2}}^{x_{i+1/2}} F_1^{k+1,(l+1)}(x)\frac{\mathrm{d}}{\mathrm{d}x}w_{i,p}(x)\,\mathrm{d}x+\Sigma_{a,i}\int_{x_{i-1/2}}^{x_{i+1/2}} w_{i,p}(x)F_0^{k+1,(l+1)}(x)\,\mathrm{d}x\\
&=\Sigma_{s,i}\int_{x_{i-1/2}}^{x_{i+1/2}} w_{i,p}(x)\left[\phi^{k+1,(l+1/2)}(x)-\phi^{k+1,(l)}(x)\right]\mathrm{d}x, \qquad 2\le i\le I-1\,, \qquad \text{(B.39c)}
\end{aligned}
$$

$$
\begin{aligned}
&\frac{1}{v\Delta t_{k+1}}\int_{x_{I-1/2}}^{x_{I+1/2}} w_{I,p}(x)F_0^{k+1,(l+1)}(x)\,\mathrm{d}x\\
&\quad+\Bigg(w_{I,p}(x_{I+1/2})\left[\frac{\rho}{2}F_0^{k+1,(l+1)}(x_{I+1/2}^-)+\frac{1}{2}F_1^{k+1,(l+1)}(x_{I+1/2}^-)\right]\\
&\qquad-w_{I,p}(x_{I-1/2})\left[\frac{\rho}{2}F_0^{k+1,(l+1)}(x_{I-1/2}^+)+\frac{1}{2}F_1^{k+1,(l+1)}(x_{I-1/2}^+)\right.\\
&\qquad\qquad\left.-\frac{\rho}{2}F_0^{k+1,(l+1)}(x_{I-1/2}^-)+\frac{1}{2}F_1^{k+1,(l+1)}(x_{I-1/2}^-)\right]\Bigg)\\
&\quad-\int_{x_{I-1/2}}^{x_{I+1/2}} F_1^{k+1,(l+1)}(x)\frac{\mathrm{d}}{\mathrm{d}x}w_{I,p}(x)\,\mathrm{d}x+\Sigma_{a,I}\int_{x_{I-1/2}}^{x_{I+1/2}} w_{I,p}(x)F_0^{k+1,(l+1)}(x)\,\mathrm{d}x\\
&\qquad\qquad=\Sigma_{s,I}\int_{x_{I-1/2}}^{x_{I+1/2}} w_{I,p}(x)\left[\phi^{k+1,(l+1/2)}(x)-\phi^{k+1,(l)}(x)\right]\mathrm{d}x,\\
&\qquad\qquad\qquad\qquad\text{right incident boundary}\,, \qquad \text{(B.39d)}
\end{aligned}
$$

$$\frac{1}{v\Delta t_{k+1}}\int_{x_{I-1/2}}^{x_{I+1/2}} w_{I,p}(x)F_0^{k+1,(l+1)}(x)\,\mathrm{d}x$$
$$-\left(w_{I,p}(x_{I-1/2})\left[\frac{\rho}{2}F_0^{k+1,(l+1)}(x_{I-1/2}^+)+\frac{1}{2}F_1^{k+1,(l+1)}(x_{I-1/2}^+)\right.\right.$$
$$\left.\left.-\frac{\rho}{2}F_0^{k+1,(l+1)}(x_{I-1/2}^-)+\frac{1}{2}F_1^{k+1,(l+1)}(x_{I-1/2}^-)\right]\right)$$
$$-\int_{x_{I-1/2}}^{x_{I+1/2}} F_1^{k+1,(l+1)}(x)\frac{\mathrm{d}}{\mathrm{d}x}w_{I,p}(x)\,\mathrm{d}x+\Sigma_{a,I}\int_{x_{I-1/2}}^{x_{I+1/2}} w_{I,p}(x)F_0^{k+1,(l+1)}(x)\,\mathrm{d}x$$
$$=\Sigma_{s,I}\int_{x_{I-1/2}}^{x_{I+1/2}} w_{I,p}(x)\left[\phi^{k+1,(l+1/2)}(x)-\phi^{k+1,(l)}(x)\right]\mathrm{d}x,$$
$$\text{right reflecting boundary}. \qquad \text{(B.39e)}$$

The first moment equation is

$$\frac{1}{v\Delta t_{k+1}}\int_{x_{i-1/2}}^{x_{i+1/2}} w_{i,p}(x)F_1^{k+1,(l+1)}(x)\,\mathrm{d}x+\frac{1}{3}\int_{x_{i-1/2}}^{x_{i+1/2}} w_{i,p}(x)\frac{\mathrm{d}}{\mathrm{d}x}F_0^{k+1,(l+1)}(x)\,\mathrm{d}x$$
$$+\Sigma_{t,i}\int_{x_{i-1/2}}^{x_{i+1/2}} w_{i,p}(x)F_1^{k+1,(l+1)}(x)\,\mathrm{d}x=0. \qquad \text{(B.40)}$$

Before proceeding to step 4, we wish to rewrite Eqs. (B.39) and (B.40) in matrix form. Thus far, we have made no assumptions regarding the specifics of the finite element discretization being used. We now assume the linear discontinuous Galerkin weight and basis functions discussed in Section 3.3, and we assume that the unknown scalar flux and current corrections can be approximated as a superposition of basis functions:

$$F_0^{k+1,(l+1)}(x)=F_{0,i,L}^{k+1,(l+1)}b_{i,L}(x)+F_{0,i,R}^{k+1,(l+1)}b_{i,R}(x), \qquad x_{i-1/2}<x<x_{i+1/2}, \qquad \text{(B.41a)}$$

$$F_1^{k+1,(l+1)}(x)=F_{1,i,L}^{k+1,(l+1)}b_{i,L}(x)+F_{1,i,R}^{k+1,(l+1)}b_{i,R}(x), \qquad x_{i-1/2}<x<x_{i+1/2}. \qquad \text{(B.41b)}$$

We also apply the upstream closures, such that the scalar flux correction $F_0^{k+1,(l+1)}(x)$ evaluated on the cell edges is

$$F_0^{k+1,(l+1)}(x_{i-1/2}^-)=F_{0,i,L}^{k+1,(l+1)}, \qquad \text{(B.42a)}$$

$$F_0^{k+1,(l+1)}(x_{i+1/2}^-)=F_{0,i,R}^{k+1,(l+1)}, \qquad \text{(B.42b)}$$

and

$$F_0^{k+1,(l+1)}(x_{i-1/2}^+)=F_{0,i-1,R}^{k+1,(l+1)}, \qquad \text{(B.43a)}$$

$$F_0^{k+1,(l+1)}(x_{i+1/2}^+) = F_{0,i+1,L}^{k+1,(l+1)}\,, \tag{B.43b}$$

and the current correction on the cell edges is evaluated as

$$F_1^{k+1,(l+1)}(x_{i-1/2}^-) = F_{1,i,L}^{k+1,(l+1)}\,, \tag{B.44a}$$

$$F_1^{k+1,(l+1)}(x_{i+1/2}^-) = F_{1,i,R}^{k+1,(l+1)}\,, \tag{B.44b}$$

and

$$F_1^{k+1,(l+1)}(x_{i-1/2}^+) = F_{1,i-1,R}^{k+1,(l+1)}\,, \tag{B.45a}$$

$$F_1^{k+1,(l+1)}(x_{i+1/2}^+) = F_{1,i+1,L}^{k+1,(l+1)}\,. \tag{B.45b}$$

Now, using the matrices defined in Section 3.3, and defining the vectors

$$\underline{F}_{0,i}^{k+1,(l+1)} = \begin{bmatrix} F_{0,i,L}^{k+1,(l+1)} & F_{0,i,R}^{k+1,(l+1)} \end{bmatrix}^T\,, \tag{B.46a}$$

and

$$\underline{F}_{1,i}^{k+1,(l+1)} = \begin{bmatrix} F_{1,i,L}^{k+1,(l+1)} & F_{1,i,R}^{k+1,(l+1)} \end{bmatrix}^T\,, \tag{B.46b}$$

we can write Eqs. (B.39) as

$$\begin{aligned} &\frac{1}{v\Delta t_{k+1}}\underline{\underline{M}}_1\underline{F}_{0,1}^{k+1,(l+1)} + \underline{\underline{G}}_{b,L}\underline{F}_{0,1}^{k+1,(l+1)} + \underline{\underline{H}}_{b,L}\underline{F}_{1,1}^{k+1,(l+1)} + \underline{\underline{G}}_R\underline{F}_{0,2}^{k+1,(l+1)} + \underline{\underline{H}}_R\underline{F}_{1,2}^{k+1,(l+1)} \\ &\qquad - \underline{\underline{L}}_1\underline{F}_{1,1}^{k+1,(l+1)} + \Sigma_{a,1}\underline{\underline{M}}_1\underline{F}_{0,1}^{k+1,(l+1)} = \Sigma_{s,1}\underline{\underline{M}}_1\left(\underline{\phi}_1^{k+1,(l+1/2)} - \underline{\phi}_1^{k+1,(l)}\right), \\ &\qquad\qquad\qquad\qquad\qquad\qquad\qquad\qquad\qquad\qquad \text{left reflecting boundary}\,, \end{aligned} \tag{B.47a}$$

$$\begin{aligned} &\frac{1}{v\Delta t_{k+1}}\underline{\underline{M}}_1\underline{F}_{0,1}^{k+1,(l+1)} + \underline{\underline{G}}\underline{F}_{0,1}^{k+1,(l+1)} + \underline{\underline{H}}\underline{F}_{1,1}^{k+1,(l+1)} + \underline{\underline{G}}_R\underline{F}_{0,2}^{k+1,(l+1)} + \underline{\underline{H}}_R\underline{F}_{1,2}^{k+1,(l+1)} \\ &\qquad - \underline{\underline{L}}_1\underline{F}_{1,1}^{k+1,(l+1)} + \Sigma_{a,1}\underline{\underline{M}}_1\underline{F}_{0,1}^{k+1,(l+1)} = \Sigma_{s,1}\underline{\underline{M}}_1\left(\underline{\phi}_1^{k+1,(l+1/2)} - \underline{\phi}_1^{k+1,(l)}\right), \\ &\qquad\qquad\qquad\qquad\qquad\qquad\qquad\qquad\qquad\qquad \text{left incident boundary}\,, \end{aligned} \tag{B.47b}$$

$$\begin{aligned} &\frac{1}{v\Delta t_{k+1}}\underline{\underline{M}}_i\underline{F}_{0,i}^{k+1,(l+1)} + \underline{\underline{G}}\underline{F}_{0,i}^{k+1,(l+1)} + \underline{\underline{H}}\underline{F}_{1,i}^{k+1,(l+1)} + \underline{\underline{G}}_L\underline{F}_{0,i-1}^{k+1,(l+1)} + \underline{\underline{H}}_L\underline{F}_{1,i-1}^{k+1,(l+1)} \\ &\qquad + \underline{\underline{G}}_R\underline{F}_{0,i+1}^{k+1,(l+1)} + \underline{\underline{H}}_R\underline{F}_{1,i+1}^{k+1,(l+1)} - \underline{\underline{L}}_i\underline{F}_{1,i}^{k+1,(l+1)} + \Sigma_{a,i}\underline{\underline{M}}_i\underline{F}_{0,i}^{k+1,(l+1)} \\ &\qquad\qquad = \Sigma_{s,i}\underline{\underline{M}}_i\left(\underline{\phi}_i^{k+1,(l+1/2)} - \underline{\phi}_i^{k+1,(l)}\right), \qquad 2 \le i \le I-1\,, \end{aligned} \tag{B.47c}$$

$$\frac{1}{v\Delta t_{k+1}}\underline{\underline{M}}_I\underline{F}_{0,I}^{k+1,(l+1)}+\underline{\underline{G}}\underline{F}_{0,I}^{k+1,(l+1)}+\underline{\underline{H}}\underline{F}_{1,I}^{k+1,(l+1)}+\underline{\underline{G}}_L\underline{F}_{0,I-1}^{k+1,(l+1)}+\underline{\underline{H}}_L\underline{F}_{1,I-1}^{k+1,(l+1)}$$
$$-\underline{\underline{L}}_I\underline{F}_{1,I}^{k+1,(l+1)}+\Sigma_{a,I}\underline{\underline{M}}_I\underline{F}_{0,I}^{k+1,(l+1)}=\Sigma_{s,I}\underline{\underline{M}}_I\left(\underline{\phi}_I^{k+1,(l+1/2)}-\underline{\phi}_I^{k+1,(l)}\right),$$
right incident boundary, (B.47d)

$$\frac{1}{v\Delta t_{k+1}}\underline{\underline{M}}_I\underline{F}_{0,I}^{k+1,(l+1)}+\underline{\underline{G}}_{b,R}\underline{F}_{0,I}^{k+1,(l+1)}+\underline{\underline{H}}_{b,R}\underline{F}_{1,I}^{k+1,(l+1)}+\underline{\underline{G}}_L\underline{F}_{0,I-1}^{k+1,(l+1)}+\underline{\underline{H}}_L\underline{F}_{1,I-1}^{k+1,(l+1)}$$
$$-\underline{\underline{L}}_I\underline{F}_{1,I}^{k+1,(l+1)}+\Sigma_{a,I}\underline{\underline{M}}_I\underline{F}_{0,I}^{k+1,(l+1)}=\Sigma_{s,I}\underline{\underline{M}}_I\left(\underline{\phi}_I^{k+1,(l+1/2)}-\underline{\phi}_I^{k+1,(l)}\right),$$
right reflecting boundary, (B.47e)

where matrices $\underline{\underline{M}}_i$ and $\underline{\underline{L}}_i$ are defined in Section 3.3, and we have defined

$$\underline{\underline{G}}=\begin{bmatrix}\frac{\rho}{2} & 0\\ 0 & \frac{\rho}{2}\end{bmatrix}, \tag{B.48a}$$

$$\underline{\underline{G}}_L=\begin{bmatrix}0 & -\frac{\rho}{2}\\ 0 & 0\end{bmatrix}, \tag{B.48b}$$

$$\underline{\underline{G}}_R=\begin{bmatrix}0 & 0\\ -\frac{\rho}{2} & 0\end{bmatrix}, \tag{B.48c}$$

$$\underline{\underline{G}}_{b,L}=\begin{bmatrix}0 & 0\\ 0 & \frac{\rho}{2}\end{bmatrix}, \tag{B.48d}$$

$$\underline{\underline{G}}_{b,R}=\begin{bmatrix}\frac{\rho}{2} & 0\\ 0 & 0\end{bmatrix}, \tag{B.48e}$$

and

$$\underline{\underline{H}}=\begin{bmatrix}-\frac{1}{2} & 0\\ 0 & \frac{1}{2}\end{bmatrix}, \tag{B.49a}$$

$$\underline{\underline{H}}_L = \begin{bmatrix} 0 & -\frac{1}{2} \\ 0 & 0 \end{bmatrix}, \tag{B.49b}$$

$$\underline{\underline{H}}_R = \begin{bmatrix} 0 & 0 \\ \frac{1}{2} & 0 \end{bmatrix}, \tag{B.49c}$$

$$\underline{\underline{H}}_{b,L} = \begin{bmatrix} 0 & 0 \\ 0 & \frac{1}{2} \end{bmatrix}, \tag{B.49d}$$

$$\underline{\underline{H}}_{b,R} = \begin{bmatrix} -\frac{1}{2} & 0 \\ 0 & 0 \end{bmatrix}. \tag{B.49e}$$

We can write Eq. (B.40) in matrix form as

$$\frac{1}{v\Delta t_{k+1}}\underline{\underline{M}}_i \underline{F}_{1,i}^{k+1,(l+1)} + \frac{1}{3}\underline{\underline{B}}_i \underline{F}_{0,i}^{k+1,(l+1)} + \Sigma_{t,i}\underline{\underline{M}}_i \underline{F}_{1,i}^{k+1,(l+1)} = 0\,, \tag{B.50}$$

where we have defined the matrix $\underline{\underline{B}}_i$ as

$$\left[\underline{\underline{B}}_i\right]_{p,s} = \int_{x_{i-1/2}}^{x_{i+1/2}} w_{i,p}(x)\frac{\mathrm{d}}{\mathrm{d}x}b_{i,s}(x)\,\mathrm{d}x\,. \tag{B.51}$$

Using the linear basis and weight functions defined in Section 3.3, we evaluate this matrix as

$$\underline{\underline{B}}_i = \begin{bmatrix} -\frac{1}{2} & \frac{1}{2} \\ -\frac{1}{2} & \frac{1}{2} \end{bmatrix}. \tag{B.52}$$

B.2.5 Step 4: Eliminate the First Moment Corrections

In the final step of our Four-Step DSA derivation, we will use Eq. (B.50) to eliminate the first moment correction $\underline{F}_{1,i}^{k+1,(l+1)}$ from Eqs. (B.47). Solving Eq. (B.50) for $\underline{F}_{1,i}^{k+1,(l+1)}$, we find

$$\underline{F}_{1,i}^{k+1,(l+1)} = -D_i^{k+1}\underline{\underline{M}}_i^{-1}\underline{\underline{B}}_i \underline{F}_{0,i}^{k+1,(l+1)}\,, \tag{B.53}$$

where

$$D_i^{k+1} = \frac{v\Delta t_{k+1}}{3\left(1+\Sigma_{t,i} v\Delta t_{k+1}\right)}. \tag{B.54}$$

Substituting Eq. (B.53) into Eqs. (B.47), we obtain

$$\begin{aligned}
&\frac{1}{v\Delta t_{k+1}}\underline{\underline{M}}_1\underline{F}_{0,1}^{k+1,(l+1)} + \underline{\underline{G}}_{b,L}\underline{F}_{0,1}^{k+1,(l+1)} - D_1^{k+1}\underline{\underline{H}}_{b,L}\underline{\underline{M}}_1^{-1}\underline{\underline{B}}_1\underline{F}_{0,1}^{k+1,(l+1)} + \underline{\underline{G}}_R\underline{F}_{0,2}^{k+1,(l+1)} \\
&\quad - D_2^{k+1}\underline{\underline{H}}_R\underline{\underline{M}}_2^{-1}\underline{\underline{B}}_2\underline{F}_{0,2}^{k+1,(l+1)} + D_1^{k+1}\underline{\underline{L}}_1\underline{\underline{M}}_1^{-1}\underline{\underline{B}}_1\underline{F}_{0,1}^{k+1,(l+1)} + \Sigma_{a,1}\underline{\underline{M}}_1\underline{F}_{0,1}^{k+1,(l+1)} \\
&\qquad = \Sigma_{s,1}\underline{\underline{M}}_1\left(\underline{\phi}_1^{k+1,(l+1/2)} - \underline{\phi}_1^{k+1,(l)}\right), \qquad \text{left reflecting boundary}, \quad \text{(B.55a)}
\end{aligned}$$

$$\begin{aligned}
&\frac{1}{v\Delta t_{k+1}}\underline{\underline{M}}_1\underline{F}_{0,1}^{k+1,(l+1)} + \underline{\underline{G}}\underline{F}_{0,1}^{k+1,(l+1)} - D_1^{k+1}\underline{\underline{H}}\underline{\underline{M}}_1^{-1}\underline{\underline{B}}_1\underline{F}_{0,1}^{k+1,(l+1)} + \underline{\underline{G}}_R\underline{F}_{0,2}^{k+1,(l+1)} \\
&\quad - D_2^{k+1}\underline{\underline{H}}_R\underline{\underline{M}}_2^{-1}\underline{\underline{B}}_2\underline{F}_{0,2}^{k+1,(l+1)} + D_1^{k+1}\underline{\underline{L}}_1\underline{\underline{M}}_1^{-1}\underline{\underline{B}}_1\underline{F}_{0,1}^{k+1,(l+1)} + \Sigma_{a,1}\underline{\underline{M}}_1\underline{F}_{0,1}^{k+1,(l+1)} \\
&\qquad = \Sigma_{s,1}\underline{\underline{M}}_1\left(\underline{\phi}_1^{k+1,(l+1/2)} - \underline{\phi}_1^{k+1,(l)}\right), \qquad \text{left incident boundary}, \quad \text{(B.55b)}
\end{aligned}$$

$$\begin{aligned}
&\frac{1}{v\Delta t_{k+1}}\underline{\underline{M}}_i\underline{F}_{0,i}^{k+1,(l+1)} + \underline{\underline{G}}\underline{F}_{0,i}^{k+1,(l+1)} - D_i^{k+1}\underline{\underline{H}}\underline{\underline{M}}_i^{-1}\underline{\underline{B}}_i\underline{F}_{0,i}^{k+1,(l+1)} + \underline{\underline{G}}_L\underline{F}_{0,i-1}^{k+1,(l+1)} \\
&\quad - D_{i-1}^{k+1}\underline{\underline{H}}_L\underline{\underline{M}}_{i-1}^{-1}\underline{\underline{B}}_{i-1}\underline{F}_{0,i-1}^{k+1,(l+1)} + \underline{\underline{G}}_R\underline{F}_{0,i+1}^{k+1,(l+1)} - D_{i+1}^{k+1}\underline{\underline{H}}_R\underline{\underline{M}}_{i+1}^{-1}\underline{\underline{B}}_{i+1}\underline{F}_{0,i+1}^{k+1,(l+1)} \\
&\quad + D_i^{k+1}\underline{\underline{L}}_i\underline{\underline{M}}_i^{-1}\underline{\underline{B}}_i\underline{F}_{0,i}^{k+1,(l+1)} + \Sigma_{a,i}\underline{\underline{M}}_i\underline{F}_{0,i}^{k+1,(l+1)} = \Sigma_{s,i}\underline{\underline{M}}_i\left(\underline{\phi}_i^{k+1,(l+1/2)} - \underline{\phi}_i^{k+1,(l)}\right), \\
&\qquad\qquad 2 \le i \le I-1, \quad \text{(B.55c)}
\end{aligned}$$

$$\begin{aligned}
&\frac{1}{v\Delta t_{k+1}}\underline{\underline{M}}_I\underline{F}_{0,I}^{k+1,(l+1)} + \underline{\underline{G}}\underline{F}_{0,I}^{k+1,(l+1)} - D_I^{k+1}\underline{\underline{H}}\underline{\underline{M}}_I^{-1}\underline{\underline{B}}_I\underline{F}_{0,I}^{k+1,(l+1)} + \underline{\underline{G}}_L\underline{F}_{0,I-1}^{k+1,(l+1)} \\
&\quad - D_{I-1}^{k+1}\underline{\underline{H}}_L\underline{\underline{M}}_{I-1}^{-1}\underline{\underline{B}}_{I-1}\underline{F}_{0,I-1}^{k+1,(l+1)} + D_I^{k+1}\underline{\underline{L}}_I\underline{\underline{M}}_I^{-1}\underline{\underline{B}}_I\underline{F}_{0,I}^{k+1,(l+1)} + \Sigma_{a,I}\underline{\underline{M}}_I\underline{F}_{0,I}^{k+1,(l+1)} \\
&\qquad = \Sigma_{s,I}\underline{\underline{M}}_I\left(\underline{\phi}_I^{k+1,(l+1/2)} - \underline{\phi}_I^{k+1,(l)}\right), \qquad \text{right incident boundary}, \quad \text{(B.55d)}
\end{aligned}$$

$$\begin{aligned}
&\frac{1}{v\Delta t_{k+1}}\underline{\underline{M}}_I\underline{F}_{0,I}^{k+1,(l+1)} + \underline{\underline{G}}_{b,R}\underline{F}_{0,I}^{k+1,(l+1)} - D_I^{k+1}\underline{\underline{H}}_{b,R}\underline{\underline{M}}_I^{-1}\underline{\underline{B}}_I\underline{F}_{0,I}^{k+1,(l+1)} + \underline{\underline{G}}_L\underline{F}_{0,I-1}^{k+1,(l+1)} \\
&\quad - D_{I-1}^{k+1}\underline{\underline{H}}_L\underline{\underline{M}}_{I-1}^{-1}\underline{\underline{B}}_{I-1}\underline{F}_{0,I-1}^{k+1,(l+1)} + D_I^{k+1}\underline{\underline{L}}_I\underline{\underline{M}}_I^{-1}\underline{\underline{B}}_I\underline{F}_{0,I}^{k+1,(l+1)} + \Sigma_{a,I}\underline{\underline{M}}_I\underline{F}_{0,I}^{k+1,(l+1)} \\
&\qquad = \Sigma_{s,I}\underline{\underline{M}}_I\left(\underline{\phi}_I^{k+1,(l+1/2)} - \underline{\phi}_I^{k+1,(l)}\right), \qquad \text{right reflecting boundary}. \quad \text{(B.55e)}
\end{aligned}$$

We can rearrange and simplify Eqs. (B.55) by defining

$$\underline{\underline{A}}_1^{k+1} = \left(\frac{1}{v\Delta t_{k+1}} + \Sigma_{a,1}\right)\underline{\underline{M}}_1 + \underline{\underline{G}}_{b,L} + D_1^{k+1}\left(\underline{\underline{L}}_1 - \underline{\underline{H}}_{b,L}\right)\underline{\underline{M}}_1^{-1}\underline{\underline{B}}_1\,,$$

left reflecting boundary, (B.56a)

$$\underline{\underline{A}}_i^{k+1} = \left(\frac{1}{v\Delta t_{k+1}} + \Sigma_{a,i}\right)\underline{\underline{M}}_i + \underline{\underline{G}} + D_i^{k+1}\left(\underline{\underline{L}}_i - \underline{\underline{H}}\right)\underline{\underline{M}}_i^{-1}\underline{\underline{B}}_i\,,$$

interior and incident boundaries, (B.56b)

$$\underline{\underline{A}}_I^{k+1} = \left(\frac{1}{v\Delta t_{k+1}} + \Sigma_{a,I}\right)\underline{\underline{M}}_I + \underline{\underline{G}}_{b,R} + D_I^{k+1}\left(\underline{\underline{L}}_I - \underline{\underline{H}}_{b,R}\right)\underline{\underline{M}}_I^{-1}\underline{\underline{B}}_I\,,$$

right reflecting boundary, (B.56c)

and

$$\underline{\underline{C}}_{i,L}^{k+1} = \underline{\underline{G}}_L - D_i^{k+1}\underline{\underline{H}}_L\underline{\underline{M}}_i^{-1}\underline{\underline{B}}_i\,, \tag{B.57a}$$

$$\underline{\underline{C}}_{i,R}^{k+1} = \underline{\underline{G}}_R - D_i^{k+1}\underline{\underline{H}}_R\underline{\underline{M}}_i^{-1}\underline{\underline{B}}_i\,. \tag{B.57b}$$

Now we write the time dependent modified four-step DSA equations in a form appropriate for implementation on a computer. Noting that $\underline{\underline{C}}_{i,L}^{k+1}$ has only zeroes in its second row, and $\underline{\underline{C}}_{i,R}^{k+1}$ has only zeroes in its first row, we obtain a banded system of equations:

$$\left[\underline{\underline{A}}_1^{k+1}\right]_{1,1} F_{0,1,L}^{k+1,(l+1)} + \left[\underline{\underline{A}}_1^{k+1}\right]_{1,2} F_{0,1,R}^{k+1,(l+1)} = \Sigma_{s,1}\left[\underline{\underline{M}}_1\right]_{1,1}\left(\phi_{1,L}^{k+1,(l+1/2)} - \phi_{1,L}^{k+1,(l)}\right) + \Sigma_{s,1}\left[\underline{\underline{M}}_1\right]_{1,2}\left(\phi_{1,R}^{k+1,(l+1/2)} - \phi_{1,R}^{k+1,(l)}\right)\,, \tag{B.58a}$$

$$\left[\underline{\underline{A}}_1^{k+1}\right]_{2,1} F_{0,1,L}^{k+1,(l+1)} + \left[\underline{\underline{A}}_1^{k+1}\right]_{2,2} F_{0,1,R}^{k+1,(l+1)} + \left[\underline{\underline{C}}_{2,R}^{k+1}\right]_{2,1} F_{0,2,L}^{k+1,(l+1)} + \left[\underline{\underline{C}}_{2,R}^{k+1}\right]_{2,2} F_{0,2,R}^{k+1,(l+1)} = \Sigma_{s,1}\left[\underline{\underline{M}}_1\right]_{2,1}\left(\phi_{1,L}^{k+1,(l+1/2)} - \phi_{1,L}^{k+1,(l)}\right) + \Sigma_{s,1}\left[\underline{\underline{M}}_1\right]_{2,2}\left(\phi_{1,R}^{k+1,(l+1/2)} - \phi_{1,R}^{k+1,(l)}\right)\,, \tag{B.58b}$$

$$\left[\underline{\underline{C}}_{i-1,L}^{k+1}\right]_{1,1} F_{0,i-1,L}^{k+1,(l+1)} + \left[\underline{\underline{C}}_{i-1,L}^{k+1}\right]_{1,2} F_{0,i-1,R}^{k+1,(l+1)} + \left[\underline{\underline{A}}_i^{k+1}\right]_{1,1} F_{0,i,L}^{k+1,(l+1)} + \left[\underline{\underline{A}}_i^{k+1}\right]_{1,2} F_{0,i,R}^{k+1,(l+1)} = \Sigma_{s,i}\left[\underline{\underline{M}}_i\right]_{1,1}\left(\phi_{i,L}^{k+1,(l+1/2)} - \phi_{i,L}^{k+1,(l)}\right) + \Sigma_{s,i}\left[\underline{\underline{M}}_i\right]_{1,2}\left(\phi_{i,R}^{k+1,(l+1/2)} - \phi_{i,R}^{k+1,(l)}\right)\,, \qquad 2 \le i \le I-1\,, \tag{B.58c}$$

$$\left[\underline{\underline{A}}_i^{k+1}\right]_{2,1} F_{0,i,L}^{k+1,(l+1)} + \left[\underline{\underline{A}}_i^{k+1}\right]_{2,2} F_{0,i,R}^{k+1,(l+1)} + \left[\underline{\underline{C}}_{i+1,R}^{k+1}\right]_{2,1} F_{0,i+1,L}^{k+1,(l+1)}$$
$$+ \left[\underline{\underline{C}}_{i+1,R}^{k+1}\right]_{2,2} F_{0,i+1,R}^{k+1,(l+1)} = \Sigma_{s,i} \left[\underline{\underline{M}}_i\right]_{2,1} \left(\phi_{i,L}^{k+1,(l+1/2)} - \phi_{i,L}^{k+1,(l)}\right)$$
$$+ \Sigma_{s,i} \left[\underline{\underline{M}}_i\right]_{2,2} \left(\phi_{i,R}^{k+1,(l+1/2)} - \phi_{i,R}^{k+1,(l)}\right), \qquad 2 \le i \le I-1, \quad \text{(B.58d)}$$

$$\left[\underline{\underline{C}}_{I-1,L}^{k+1}\right]_{1,1} F_{0,I-1,L}^{k+1,(l+1)} + \left[\underline{\underline{C}}_{I-1,L}^{k+1}\right]_{1,2} F_{0,I-1,R}^{k+1,(l+1)} + \left[\underline{\underline{A}}_I^{k+1}\right]_{1,1} F_{0,I,L}^{k+1,(l+1)}$$
$$+ \left[\underline{\underline{A}}_I^{k+1}\right]_{1,2} F_{0,I,R}^{k+1,(l+1)} = \Sigma_{s,I} \left[\underline{\underline{M}}_I\right]_{1,1} \left(\phi_{I,L}^{k+1,(l+1/2)} - \phi_{I,L}^{k+1,(l)}\right)$$
$$+ \Sigma_{s,I} \left[\underline{\underline{M}}_I\right]_{1,2} \left(\phi_{I,R}^{k+1,(l+1/2)} - \phi_{I,R}^{k+1,(l)}\right), \quad \text{(B.58e)}$$

$$\left[\underline{\underline{A}}_I^{k+1}\right]_{2,1} F_{0,I,L}^{k+1,(l+1)} + \left[\underline{\underline{A}}_I^{k+1}\right]_{2,2} F_{0,I,R}^{k+1,(l+1)} = \Sigma_{s,I} \left[\underline{\underline{M}}_I\right]_{2,1} \left(\phi_{I,L}^{k+1,(l+1/2)} - \phi_{I,L}^{k+1,(l)}\right)$$
$$+ \Sigma_{s,I} \left[\underline{\underline{M}}_I\right]_{2,2} \left(\phi_{I,R}^{k+1,(l+1/2)} - \phi_{I,R}^{k+1,(l)}\right). \quad \text{(B.58f)}$$

Eqs. (B.58) represent a sparse, banded system of equations that can be solved using traditional linear algebra techniques.

Finally, the implicit linear discontinuous finite element transport scheme with DSA is

$$\frac{1}{v\Delta t_{k+1}} \underline{\underline{M}}_i \left(\underline{\psi}_{n,i}^{k+1,(l+1/2)} - \underline{\psi}_{n,i}^{k}\right) + \mu_n \underline{\underline{L}}_i^{surf} \underline{\psi}_{n,i}^{k+1,(l+1/2),surf} - \mu_n \underline{\underline{L}}_i \underline{\psi}_{n,i}^{k+1,(l+1/2)}$$
$$+ \Sigma_{t,i} \underline{\underline{M}}_i \underline{\psi}_{n,i}^{k+1,(l+1/2)} = \frac{\Sigma_{s,i}}{2} \underline{\underline{M}}_i \underline{\phi}_i^{k+1,(l)} + \underline{\underline{M}}_i \underline{Q}_{n,i}^{k+1}, \quad \text{(B.59a)}$$

$$\underline{\phi}_i^{k+1,(l+1/2)} = \sum_{n=1}^{N} \underline{\psi}_{n,i}^{k+1,(l+1/2)} \Delta_n, \quad \text{(B.59b)}$$

$$\underline{\phi}_i^{k+1,(l+1)} = \underline{\phi}_i^{k+1,(l+1/2)} + \underline{F}_{0,i}^{k+1,(l+1)}, \quad \text{(B.59c)}$$

where $\underline{F}_{0,i}^{k+1,(l+1)}$ in Eq. (B.59c) is calculated using Eqs. (B.58). This scheme is known to be quickly convergent regardless of the optical thickness of the transport problem.

B.3 Deriving the Grey IMC Modified Four-Step Diffusion Synthetic Acceleration Equations

In this section, we derive the Modified Four-Step DSA scheme for the grey, IMC linearized, implicit linear discontinuous finite element equations. The source iteration scheme for this

method is

$$\frac{1}{c\Delta t_{k+1}}\underline{\underline{M}}_i\left(\underline{\psi}_{n,i}^{k+1,(l+1/2)}-\underline{\psi}_{n,i}^{k}\right)+\mu_n\underline{\underline{L}}_i^{surf}\underline{\psi}_{n,i}^{k+1,(l+1/2),surf}-\mu_n\underline{\underline{L}}_i\underline{\psi}_{n,i}^{k+1,(l+1/2)}$$
$$+\sigma_{P,i}^{k}\underline{\underline{M}}_i\underline{\psi}_{n,i}^{k+1,(l+1/2)}=\frac{\sigma_{P,i}^{k}}{2}\left[1-f_i^k\right]\underline{\underline{M}}_i\underline{\phi}_i^{k+1,(l)}+\frac{c}{2}f_i^k\sigma_{P,i}^{k}\underline{\underline{M}}_i\underline{U}_{r,i}^{k}+\left[\frac{1-f_i^k}{2}\right]\underline{\underline{M}}_i\underline{Q}_{m,i}^{k+1}$$
$$+\underline{\underline{M}}_i\underline{Q}_{r,n,i}^{k+1}\,, \quad \text{(B.60a)}$$

$$\underline{\phi}_i^{k+1,(l+1/2)}=\sum_{n=1}^{N}\underline{\psi}_{n,i}^{k+1,(l+1/2)}\,\Delta_n\,, \quad \text{(B.60b)}$$

$$\underline{\phi}_i^{k+1,(l+1)}=\underline{\phi}_i^{k+1,(l+1/2)}\,, \quad \text{(B.60c)}$$

where l is the iteration index, and the other terms are defined in Chapter 6. The source iteration method for the thermal radiation equations is known to converge slowly for large time steps. The Modified Four-Step diffusion synthetic acceleration method uses a diffusion equation to accelerate the source iteration scheme. To derive the Modified Four-Step DSA equations, we begin with the spatially-discretized transport and radiative energy equations in integral form, from Eq. (6.57):

$$\frac{1}{c\Delta t_{k+1}}\left[\int_{x_{i-1/2}}^{x_{i+1/2}}w_{i,p}(x)\,\psi_n^{k+1,(l+1/2)}(x)\,\mathrm{d}x-\int_{x_{i-1/2}}^{x_{i+1/2}}w_{i,p}(x)\,\psi_n^{k}(x)\,\mathrm{d}x\right]$$
$$+\mu_n\left[w_{i,p}(x_{i+1/2})\,\psi_n^{k+1,(l+1/2)}(x_{i+1/2})-w_{i,p}(x_{i-1/2})\,\psi_n^{k+1,(l+1/2)}(x_{i-1/2})\right]$$
$$-\mu_n\int_{x_{i-1/2}}^{x_{i+1/2}}\psi_n^{k+1,(l+1/2)}(x)\frac{\mathrm{d}}{\mathrm{d}x}w_{i,p}(x)\,\mathrm{d}x+\sigma_{P,i}^{k}\int_{x_{i-1/2}}^{x_{i+1/2}}w_{i,p}(x)\,\psi_n^{k+1,(l+1/2)}(x)\,\mathrm{d}x$$
$$=\frac{1}{2}\sigma_{P,i}^{k}\left[1-f_i^k\right]\int_{x_{i-1/2}}^{x_{i+1/2}}w_{i,p}(x)\,\phi^{k+1,(l)}(x)\,\mathrm{d}x+\frac{c}{2}f_i^k\sigma_{P,i}^{k}U_{r,i}^{k}\int_{x_{i-1/2}}^{x_{i+1/2}}w_{i,p}(x)\,\mathrm{d}x$$
$$+\left[\frac{1-f_i^k}{2}\right]Q_{m,i}^{k+1}\int_{x_{i-1/2}}^{x_{i+1/2}}w_{i,p}(x)\,\mathrm{d}x+\int_{x_{i-1/2}}^{x_{i+1/2}}w_{i,p}(x)Q_{r,n}^{k+1}(x)\,\mathrm{d}x\,. \quad \text{(B.61)}$$

B.3.1 Step 1: Calculate Zeroth and First Moments

The first step of the Modified Four-Step DSA method is to calculate the zeroth and first angular moments of the implicit, grey IMC transport equation, Eq. (B.61). We omit the details, which are presented for the linear transport method in Section B.2, and simply report

the final result. The equations for the zeroth angular moment of Eq. (B.61) are

$$\begin{aligned}
&\frac{1}{c\Delta t_{k+1}}\int_{x_{1/2}}^{x_{3/2}} w_{1,p}(x)\Big[\phi^{k+1,(l+1/2)}(x)-\phi^{k}(x)\Big]\mathrm{d}x \\
&\quad+\Bigg(w_{1,p}(x_{3/2})\Bigg[\frac{\rho}{2}\phi^{k+1,(l+1/2)}(x_{3/2}^{-})+\frac{1}{2}J^{k+1,(l+1/2)}(x_{3/2}^{-})-\frac{\rho}{2}\phi^{k+1,(l+1/2)}(x_{3/2}^{+}) \\
&\qquad\qquad+\frac{1}{2}J^{k+1,(l+1/2)}(x_{3/2}^{+})+O^{k+1,(l+1/2)}(\mu_n)\Bigg]\Bigg) \\
&\qquad-\int_{x_{1/2}}^{x_{3/2}} J^{k+1,(l+1/2)}(x)\frac{\mathrm{d}}{\mathrm{d}x}w_{1,p}(x)\,\mathrm{d}x+\sigma_{P,1}^{k}\int_{x_{1/2}}^{x_{3/2}} w_{1,p}(x)\phi^{k+1,(l+1/2)}(x)\,\mathrm{d}x \\
&\qquad\quad=\sigma_{P,1}^{k}\Big[1-f_1^{k}\Big]\int_{x_{1/2}}^{x_{3/2}} w_{1,p}(x)\phi^{k+1,(l)}(x)\,\mathrm{d}x+cf_1^{k}\sigma_{P,1}^{k}U_{r,1}^{k}\int_{x_{1/2}}^{x_{3/2}} w_{1,p}(x)\,\mathrm{d}x \\
&\qquad\qquad+\Big[1-f_1^{k}\Big]Q_{m,1}^{k+1}\int_{x_{1/2}}^{x_{3/2}} w_{1,p}(x)\,\mathrm{d}x+\int_{x_{1/2}}^{x_{3/2}} w_{1,p}(x)\sum_{n=1}^{N}Q_{r,n}^{k+1}(x)\,\Delta_n\,\mathrm{d}x,
\end{aligned}$$

left reflecting boundary, (B.62a)

$$\begin{aligned}
&\frac{1}{c\Delta t_{k+1}}\int_{x_{1/2}}^{x_{3/2}} w_{1,p}(x)\Big[\phi^{k+1,(l+1/2)}(x)-\phi^{k}(x)\Big]\mathrm{d}x \\
&\quad+\Bigg(w_{1,p}(x_{3/2})\Bigg[\frac{\rho}{2}\phi^{k+1,(l+1/2)}(x_{3/2}^{-})+\frac{1}{2}J^{k+1,(l+1/2)}(x_{3/2}^{-})-\frac{\rho}{2}\phi^{k+1,(l+1/2)}(x_{3/2}^{+}) \\
&\qquad\qquad+\frac{1}{2}J^{k+1,(l+1/2)}(x_{3/2}^{+})+O^{k+1,(l+1/2)}(\mu_n)\Bigg] \\
&\qquad-w_{1,p}(x_{1/2})\Bigg[\sum_{\mu_n>0}\mu_n\psi_{n,L}^{b,k+1}\Delta_n-\frac{\rho}{2}\phi^{k+1,(l+1/2)}(x_{1/2}^{-})+\frac{1}{2}J^{k+1,(l+1/2)}(x_{1/2}^{-}) \\
&\qquad\qquad+O^{k+1,(l+1/2)}(\mu_n)\Bigg]\Bigg) \\
&\qquad-\int_{x_{1/2}}^{x_{3/2}} J^{k+1,(l+1/2)}(x)\frac{\mathrm{d}}{\mathrm{d}x}w_{1,p}(x)\,\mathrm{d}x+\sigma_{P,1}^{k}\int_{x_{1/2}}^{x_{3/2}} w_{1,p}(x)\phi^{k+1,(l+1/2)}(x)\,\mathrm{d}x \\
&\qquad\quad=\sigma_{P,1}^{k}\Big[1-f_1^{k}\Big]\int_{x_{1/2}}^{x_{3/2}} w_{1,p}(x)\phi^{k+1,(l)}(x)\,\mathrm{d}x+cf_1^{k}\sigma_{P,1}^{k}U_{r,1}^{k}\int_{x_{1/2}}^{x_{3/2}} w_{1,p}(x)\,\mathrm{d}x \\
&\qquad\qquad+\Big[1-f_1^{k}\Big]Q_{m,1}^{k+1}\int_{x_{1/2}}^{x_{3/2}} w_{1,p}(x)\,\mathrm{d}x+\int_{x_{1/2}}^{x_{3/2}} w_{1,p}(x)\sum_{n=1}^{N}Q_{r,n}^{k+1}(x)\,\Delta_n\,\mathrm{d}x,
\end{aligned}$$

left incident boundary, (B.62b)

$$
\begin{aligned}
&\frac{1}{c\Delta t_{k+1}} \int_{x_{i-1/2}}^{x_{i+1/2}} w_{i,p}(x) \Big[\phi^{k+1,(l+1/2)}(x) - \phi^{k}(x) \Big] \mathrm{d}x \\
&\quad + \Bigg(w_{i,p}(x_{i+1/2}) \Bigg[\frac{\rho}{2} \phi^{k+1,(l+1/2)}(x_{i+1/2}^{-}) + \frac{1}{2} J^{k+1,(l+1/2)}(x_{i+1/2}^{-}) \\
&\qquad\qquad - \frac{\rho}{2} \phi^{k+1,(l+1/2)}(x_{i+1/2}^{+}) + \frac{1}{2} J^{k+1,(l+1/2)}(x_{i+1/2}^{+}) \\
&\qquad\qquad\qquad + O^{k+1,(l+1/2)}(\mu_n) \Bigg] \\
&\qquad - w_{i,p}(x_{i-1/2}) \Bigg[\frac{\rho}{2} \phi^{k+1,(l+1/2)}(x_{i-1/2}^{+}) + \frac{1}{2} J^{k+1,(l+1/2)}(x_{i-1/2}^{+}) \\
&\qquad\qquad - \frac{\rho}{2} \phi^{k+1,(l+1/2)}(x_{i-1/2}^{-}) + \frac{1}{2} J^{k+1,(l+1/2)}(x_{i-1/2}^{-}) \\
&\qquad\qquad\qquad + O^{k+1,(l+1/2)}(\mu_n) \Bigg] \Bigg) \\
&\quad - \int_{x_{i-1/2}}^{x_{i+1/2}} J^{k+1,(l+1/2)}(x) \frac{\mathrm{d}}{\mathrm{d}x} w_{i,p}(x) \, \mathrm{d}x + \sigma_{P,i}^{k} \int_{x_{i-1/2}}^{x_{i+1/2}} w_{i,p}(x) \phi^{k+1,(l+1/2)}(x) \, \mathrm{d}x \\
&\qquad = \sigma_{P,i}^{k} \Big[1 - f_i^k \Big] \int_{x_{i-1/2}}^{x_{i+1/2}} w_{i,p}(x) \phi^{k+1,(l)}(x) \, \mathrm{d}x + c f_i^k \sigma_{P,i}^{k} U_{r,i}^{k} \int_{x_{i-1/2}}^{x_{i+1/2}} w_{i,p}(x) \, \mathrm{d}x \\
&\qquad\qquad + \Big[1 - f_i^k \Big] Q_{m,i}^{k+1} \int_{x_{i-1/2}}^{x_{i+1/2}} w_{i,p}(x) \, \mathrm{d}x + \int_{x_{i-1/2}}^{x_{i+1/2}} w_{i,p}(x) \sum_{n=1}^{N} Q_{r,n}^{k+1}(x) \Delta_n \, \mathrm{d}x, \\
&\qquad\qquad\qquad\qquad 2 \leq i \leq I-1 , \quad \text{(B.62c)}
\end{aligned}
$$

$$
\begin{aligned}
&\frac{1}{c\Delta t_{k+1}}\int_{x_{I-1/2}}^{x_{I+1/2}} w_{I,p}(x)\Big[\phi^{k+1,(l+1/2)}(x)-\phi^{k}(x)\Big]\,\mathrm{d}x\\
&\quad+\Bigg(w_{I,p}(x_{I+1/2})\Bigg[\frac{\rho}{2}\phi^{k+1,(l+1/2)}(x_{I+1/2}^{-})+\frac{1}{2}J^{k+1,(l+1/2)}(x_{I+1/2}^{-})\\
&\qquad\qquad-\sum_{\mu_n<0}|\mu_n|\psi_{n,R}^{b,k+1}\Delta_n+O^{k+1,(l+1/2)}(\mu_n)\Bigg]\\
&\qquad-w_{I,p}(x_{I-1/2})\Bigg[\frac{\rho}{2}\phi^{k+1,(l+1/2)}(x_{I-1/2}^{+})+\frac{1}{2}J^{k+1,(l+1/2)}(x_{I-1/2}^{+})\\
&\qquad\qquad-\frac{\rho}{2}\phi^{k+1,(l+1/2)}(x_{I-1/2}^{-})+\frac{1}{2}J^{k+1,(l+1/2)}(x_{I-1/2}^{-})\\
&\qquad\qquad+O^{k+1,(l+1/2)}(\mu_n)\Bigg]\Bigg)\\
&\quad-\int_{x_{I-1/2}}^{x_{I+1/2}}J^{k+1,(l+1/2)}(x)\frac{\mathrm{d}}{\mathrm{d}x}w_{I,p}(x)\,\mathrm{d}x+\sigma_{P,I}^{k}\int_{x_{I-1/2}}^{x_{I+1/2}}w_{I,p}(x)\phi^{k+1,(l+1/2)}(x)\,\mathrm{d}x\\
&\qquad=\sigma_{P,I}^{k}\Big[1-f_I^{k}\Big]\int_{x_{I-1/2}}^{x_{I+1/2}}w_{I,p}(x)\phi^{k+1,(l)}(x)\,\mathrm{d}x+cf_I^{k}\sigma_{P,I}^{k}U_{r,I}^{k}\int_{x_{I-1/2}}^{x_{I+1/2}}w_{I,p}(x)\,\mathrm{d}x\\
&\qquad\quad+\Big[1-f_I^{k}\Big]Q_{m,I}^{k+1}\int_{x_{I-1/2}}^{x_{I+1/2}}w_{I,p}(x)\,\mathrm{d}x+\int_{x_{I-1/2}}^{x_{I+1/2}}w_{I,p}(x)\sum_{n=1}^{N}Q_{r,n}^{k+1}(x)\Delta_n\,\mathrm{d}x,\\
&\qquad\qquad\text{right incident boundary},\qquad\text{(B.62d)}
\end{aligned}
$$

$$
\begin{aligned}
&\frac{1}{v\Delta t_{k+1}}\int_{x_{I-1/2}}^{x_{I+1/2}} w_{I,p}(x)\Big[\phi^{k+1,(l+1/2)}(x)-\phi^{k}(x)\Big]\,\mathrm{d}x\\
&\quad-\Bigg(w_{I,p}(x_{I-1/2})\Bigg[\frac{\rho}{2}\phi^{k+1,(l+1/2)}(x_{I-1/2}^{+})+\frac{1}{2}J^{k+1,(l+1/2)}(x_{I-1/2}^{+})\\
&\qquad\qquad-\frac{\rho}{2}\phi^{k+1,(l+1/2)}(x_{I-1/2}^{-})+\frac{1}{2}J^{k+1,(l+1/2)}(x_{I-1/2}^{-})\\
&\qquad\qquad+O^{k+1,(l+1/2)}(\mu_n)\Bigg]\Bigg)\\
&\quad-\int_{x_{I-1/2}}^{x_{I+1/2}}J^{k+1,(l+1/2)}(x)\frac{\mathrm{d}}{\mathrm{d}x}w_{I,p}(x)\,\mathrm{d}x+\sigma_{P,I}^{k}\int_{x_{I-1/2}}^{x_{I+1/2}}w_{I,p}(x)\phi^{k+1,(l+1/2)}(x)\,\mathrm{d}x\\
&\qquad=\sigma_{P,I}^{k}\Big[1-f_I^{k}\Big]\int_{x_{I-1/2}}^{x_{I+1/2}}w_{I,p}(x)\phi^{k+1,(l)}(x)\,\mathrm{d}x+cf_I^{k}\sigma_{P,I}^{k}U_{r,I}^{k}\int_{x_{I-1/2}}^{x_{I+1/2}}w_{I,p}(x)\,\mathrm{d}x\\
&\qquad\quad+\Big[1-f_I^{k}\Big]Q_{m,I}^{k+1}\int_{x_{I-1/2}}^{x_{I+1/2}}w_{I,p}(x)\,\mathrm{d}x+\int_{x_{I-1/2}}^{x_{I+1/2}}w_{I,p}(x)\sum_{n=1}^{N}Q_{r,n}^{k+1}(x)\Delta_n\,\mathrm{d}x,\\
&\qquad\qquad\text{right reflecting boundary}.\qquad\text{(B.62e)}
\end{aligned}
$$

In Eqs. (B.62), we have defined the scalar intensity

$$\phi^{k+1,(l+1/2)}(x) = \sum_{n=1}^{N} \psi_n^{k+1,(l+1/2)}(x)\,\Delta_n\,, \tag{B.63a}$$

and the radiative flux

$$J^{k+1,(l+1/2)}(x) = \sum_{n=1}^{N} \mu_n \psi_n^{k+1,(l+1/2)}(x)\,\Delta_n\,. \tag{B.63b}$$

We have also defined $x_{i-1/2}^{-}$ and $x_{i+1/2}^{-}$ as points just inside the left and right boundaries of cell i, respectively, and $x_{i-1/2}^{+}$ and $x_{i+1/2}^{+}$ as points just outside the left and right boundaries of cell i, respectively.

The first angular moment of Eq. (B.61) is

$$\begin{aligned}
&\frac{1}{c\Delta t_{k+1}} \int_{x_{i-1/2}}^{x_{i+1/2}} w_{i,p}(x) \left[J^{k+1,(l+1/2)}(x) - J^{k}(x) \right] \mathrm{d}x \\
&\quad + \frac{2}{3} \int_{x_{i-1/2}}^{x_{i+1/2}} w_{i,p}(x) \frac{\mathrm{d}}{\mathrm{d}x} \Phi^{k+1,(l+1/2)}(x)\,\mathrm{d}x + \frac{1}{3} \int_{x_{i-1/2}}^{x_{i+1/2}} w_{i,p}(x) \frac{\mathrm{d}}{\mathrm{d}x} \phi^{k+1,(l+1/2)}(x)\,\mathrm{d}x \\
&\quad + \sigma_{P,i}^{k} \int_{x_{i-1/2}}^{x_{i+1/2}} w_{i,p}(x) J^{k+1,(l+1/2)}(x)\,\mathrm{d}x = \int_{x_{i-1/2}}^{x_{i+1/2}} w_{i,p}(x) \sum_{n=1}^{N} \mu_n Q_{r,n}^{k+1}(x)\,\Delta_n\,\mathrm{d}x\,,
\end{aligned} \tag{B.64}$$

where

$$\Phi^{k+1,(l+1/2)}(x) = \frac{2}{3} \sum_{n=1}^{N} \frac{1}{2} \left(3\mu_n^2 - 1 \right) \psi_n^{k+1,(l+1/2)}(x)\,\Delta_n\,, \tag{B.65}$$

is a second-moment intensity term.

B.3.2 Step 2: Update the Indices

The second step of the Modified Four-Step DSA derivation is to update the iteration indices in certain terms of Eqs. (B.62) and (B.64) to $l+1$. The updated zeroth moment equations

are

$$\begin{aligned}
&\frac{1}{c\Delta t_{k+1}}\int_{x_{1/2}}^{x_{3/2}} w_{1,p}(x)\left[\phi^{k+1,(l+1)}(x)-\phi^{k}(x)\right]\mathrm{d}x \\
&\quad+\left(w_{1,p}(x_{3/2})\left[\frac{\rho}{2}\phi^{k+1,(l+1)}(x_{3/2}^{-})+\frac{1}{2}J^{k+1,(l+1)}(x_{3/2}^{-})-\frac{\rho}{2}\phi^{k+1,(l+1)}(x_{3/2}^{+})\right.\right. \\
&\qquad\left.\left.+\frac{1}{2}J^{k+1,(l+1)}(x_{3/2}^{+})+O^{k+1,(l+1/2)}(\mu_n)\right]\right) \\
&\quad-\int_{x_{1/2}}^{x_{3/2}} J^{k+1,(l+1)}(x)\frac{\mathrm{d}}{\mathrm{d}x}w_{1,p}(x)\,\mathrm{d}x+\sigma_{P,1}^{k}\int_{x_{1/2}}^{x_{3/2}} w_{1,p}(x)\phi^{k+1,(l+1)}(x)\,\mathrm{d}x \\
&\qquad=\sigma_{P,1}^{k}\left[1-f_1^{k}\right]\int_{x_{1/2}}^{x_{3/2}} w_{1,p}(x)\phi^{k+1,(l+1)}(x)\,\mathrm{d}x+cf_1^{k}\sigma_{P,1}^{k}U_{r,1}^{k}\int_{x_{1/2}}^{x_{3/2}} w_{1,p}(x)\,\mathrm{d}x \\
&\qquad\quad+\left[1-f_1^{k}\right]Q_{m,1}^{k+1}\int_{x_{1/2}}^{x_{3/2}} w_{1,p}(x)\,\mathrm{d}x+\int_{x_{1/2}}^{x_{3/2}} w_{1,p}(x)\sum_{n=1}^{N}Q_{r,n}^{k+1}(x)\,\Delta_n\,\mathrm{d}x,
\end{aligned}$$

left reflecting boundary, (B.66a)

$$\begin{aligned}
&\frac{1}{c\Delta t_{k+1}}\int_{x_{1/2}}^{x_{3/2}} w_{1,p}(x)\left[\phi^{k+1,(l+1)}(x)-\phi^{k}(x)\right]\mathrm{d}x \\
&\quad+\left(w_{1,p}(x_{3/2})\left[\frac{\rho}{2}\phi^{k+1,(l+1)}(x_{3/2}^{-})+\frac{1}{2}J^{k+1,(l+1)}(x_{3/2}^{-})-\frac{\rho}{2}\phi^{k+1,(l+1)}(x_{3/2}^{+})\right.\right. \\
&\qquad\left.+\frac{1}{2}J^{k+1,(l+1)}(x_{3/2}^{+})+O^{k+1,(l+1/2)}(\mu_n)\right] \\
&\qquad-w_{1,p}(x_{1/2})\left[\sum_{\mu_n>0}\mu_n\psi_{n,L}^{b,k+1}\,\Delta_n-\frac{\rho}{2}\phi^{k+1,(l+1)}(x_{1/2}^{-})+\frac{1}{2}J^{k+1,(l+1)}(x_{1/2}^{-})\right. \\
&\qquad\left.\left.+O^{k+1,(l+1/2)}(\mu_n)\right]\right) \\
&\quad-\int_{x_{1/2}}^{x_{3/2}} J^{k+1,(l+1)}(x)\frac{\mathrm{d}}{\mathrm{d}x}w_{1,p}(x)\,\mathrm{d}x+\sigma_{P,1}^{k}\int_{x_{1/2}}^{x_{3/2}} w_{1,p}(x)\phi^{k+1,(l+1)}(x)\,\mathrm{d}x \\
&\qquad=\sigma_{P,1}^{k}\left[1-f_1^{k}\right]\int_{x_{1/2}}^{x_{3/2}} w_{1,p}(x)\phi^{k+1,(l+1)}(x)\,\mathrm{d}x+cf_1^{k}\sigma_{P,1}^{k}U_{r,1}^{k}\int_{x_{1/2}}^{x_{3/2}} w_{1,p}(x)\,\mathrm{d}x \\
&\qquad\quad+\left[1-f_1^{k}\right]Q_{m,1}^{k+1}\int_{x_{1/2}}^{x_{3/2}} w_{1,p}(x)\,\mathrm{d}x+\int_{x_{1/2}}^{x_{3/2}} w_{1,p}(x)\sum_{n=1}^{N}Q_{r,n}^{k+1}(x)\,\Delta_n\,\mathrm{d}x,
\end{aligned}$$

left incident boundary, (B.66b)

$$
\begin{aligned}
&\frac{1}{c\Delta t_{k+1}} \int_{x_{i-1/2}}^{x_{i+1/2}} w_{i,p}(x) \Big[\phi^{k+1,(l+1)}(x) - \phi^{k}(x) \Big] \mathrm{d}x \\
&\quad + \Bigg(w_{i,p}(x_{i+1/2}) \Bigg[\frac{\rho}{2} \phi^{k+1,(l+1)}(x_{i+1/2}^{-}) + \frac{1}{2} J^{k+1,(l+1)}(x_{i+1/2}^{-}) \\
&\qquad\qquad - \frac{\rho}{2} \phi^{k+1,(l+1)}(x_{i+1/2}^{+}) + \frac{1}{2} J^{k+1,(l+1)}(x_{i+1/2}^{+}) \\
&\qquad\qquad\qquad + O^{k+1,(l+1/2)}(\mu_n) \Bigg] \\
&\qquad - w_{i,p}(x_{i-1/2}) \Bigg[\frac{\rho}{2} \phi^{k+1,(l+1)}(x_{i-1/2}^{+}) + \frac{1}{2} J^{k+1,(l+1)}(x_{i-1/2}^{+}) \\
&\qquad\qquad - \frac{\rho}{2} \phi^{k+1,(l+1)}(x_{i-1/2}^{-}) + \frac{1}{2} J^{k+1,(l+1)}(x_{i-1/2}^{-}) \\
&\qquad\qquad\qquad + O^{k+1,(l+1/2)}(\mu_n) \Bigg] \Bigg) \\
&\quad - \int_{x_{i-1/2}}^{x_{i+1/2}} J^{k+1,(l+1)}(x) \frac{\mathrm{d}}{\mathrm{d}x} w_{i,p}(x) \, \mathrm{d}x + \sigma_{P,i}^{k} \int_{x_{i-1/2}}^{x_{i+1/2}} w_{i,p}(x) \phi^{k+1,(l+1)}(x) \, \mathrm{d}x \\
&\qquad = \sigma_{P,i}^{k} \Big[1 - f_i^k \Big] \int_{x_{i-1/2}}^{x_{i+1/2}} w_{i,p}(x) \phi^{k+1,(l+1)}(x) \, \mathrm{d}x + c f_i^k \sigma_{P,i}^{k} U_{r,i}^{k} \int_{x_{i-1/2}}^{x_{i+1/2}} w_{i,p}(x) \, \mathrm{d}x \\
&\qquad\qquad + \Big[1 - f_i^k \Big] Q_{m,i}^{k+1} \int_{x_{i-1/2}}^{x_{i+1/2}} w_{i,p}(x) \, \mathrm{d}x + \int_{x_{i-1/2}}^{x_{i+1/2}} w_{i,p}(x) \sum_{n=1}^{N} Q_{r,n}^{k+1}(x) \Delta_n \, \mathrm{d}x \,, \\
&\qquad\qquad\qquad\qquad 2 \leq i \leq I-1 \,, \quad \text{(B.66c)}
\end{aligned}
$$

$$
\begin{aligned}
&\frac{1}{c\Delta t_{k+1}}\int_{x_{I-1/2}}^{x_{I+1/2}} w_{I,p}(x)\Big[\phi^{k+1,(l+1)}(x)-\phi^{k}(x)\Big]\,\mathrm{d}x\\
&\quad+\Bigg(w_{I,p}(x_{I+1/2})\Bigg[\frac{\rho}{2}\phi^{k+1,(l+1)}(x_{I+1/2}^{-})+\frac{1}{2}J^{k+1,(l+1)}(x_{I+1/2}^{-})\\
&\qquad\qquad-\sum_{\mu_n<0}|\mu_n|\psi_{n,R}^{b,k+1}\Delta_n+O^{k+1,(l+1/2)}(\mu_n)\Bigg]\\
&\qquad-w_{I,p}(x_{I-1/2})\Bigg[\frac{\rho}{2}\phi^{k+1,(l+1)}(x_{I-1/2}^{+})+\frac{1}{2}J^{k+1,(l+1)}(x_{I-1/2}^{+})\\
&\qquad\qquad-\frac{\rho}{2}\phi^{k+1,(l+1)}(x_{I-1/2}^{-})+\frac{1}{2}J^{k+1,(l+1)}(x_{I-1/2}^{-})\\
&\qquad\qquad+O^{k+1,(l+1/2)}(\mu_n)\Bigg]\Bigg)\\
&\quad-\int_{x_{I-1/2}}^{x_{I+1/2}}J^{k+1,(l+1)}(x)\frac{\mathrm{d}}{\mathrm{d}x}w_{I,p}(x)\,\mathrm{d}x+\sigma_{P,I}^{k}\int_{x_{I-1/2}}^{x_{I+1/2}}w_{I,p}(x)\phi^{k+1,(l+1)}(x)\,\mathrm{d}x\\
&\qquad=\sigma_{P,I}^{k}\Big[1-f_I^{k}\Big]\int_{x_{I-1/2}}^{x_{I+1/2}}w_{I,p}(x)\phi^{k+1,(l+1)}(x)\,\mathrm{d}x+cf_I^{k}\sigma_{P,I}^{k}U_{r,I}^{k}\int_{x_{I-1/2}}^{x_{I+1/2}}w_{I,p}(x)\,\mathrm{d}x\\
&\qquad\quad+\Big[1-f_I^{k}\Big]Q_{m,I}^{k+1}\int_{x_{I-1/2}}^{x_{I+1/2}}w_{I,p}(x)\,\mathrm{d}x+\int_{x_{I-1/2}}^{x_{I+1/2}}w_{I,p}(x)\sum_{n=1}^{N}Q_{r,n}^{k+1}(x)\Delta_n\,\mathrm{d}x,\\
&\qquad\qquad\qquad\text{right incident boundary},\qquad\text{(B.66d)}
\end{aligned}
$$

$$
\begin{aligned}
&\frac{1}{v\Delta t_{k+1}}\int_{x_{I-1/2}}^{x_{I+1/2}} w_{I,p}(x)\Big[\phi^{k+1,(l+1)}(x)-\phi^{k}(x)\Big]\,\mathrm{d}x\\
&\quad-\Bigg(w_{I,p}(x_{I-1/2})\Bigg[\frac{\rho}{2}\phi^{k+1,(l+1)}(x_{I-1/2}^{+})+\frac{1}{2}J^{k+1,(l+1)}(x_{I-1/2}^{+})\\
&\qquad\qquad-\frac{\rho}{2}\phi^{k+1,(l+1)}(x_{I-1/2}^{-})+\frac{1}{2}J^{k+1,(l+1)}(x_{I-1/2}^{-})\\
&\qquad\qquad+O^{k+1,(l+1/2)}(\mu_n)\Bigg]\Bigg)\\
&\quad-\int_{x_{I-1/2}}^{x_{I+1/2}}J^{k+1,(l+1)}(x)\frac{\mathrm{d}}{\mathrm{d}x}w_{I,p}(x)\,\mathrm{d}x+\sigma_{P,I}^{k}\int_{x_{I-1/2}}^{x_{I+1/2}}w_{I,p}(x)\phi^{k+1,(l+1)}(x)\,\mathrm{d}x\\
&\qquad=\sigma_{P,I}^{k}\Big[1-f_I^{k}\Big]\int_{x_{I-1/2}}^{x_{I+1/2}}w_{I,p}(x)\phi^{k+1,(l+1)}(x)\,\mathrm{d}x+cf_I^{k}\sigma_{P,I}^{k}U_{r,I}^{k}\int_{x_{I-1/2}}^{x_{I+1/2}}w_{I,p}(x)\,\mathrm{d}x\\
&\qquad\quad+\Big[1-f_I^{k}\Big]Q_{m,I}^{k+1}\int_{x_{I-1/2}}^{x_{I+1/2}}w_{I,p}(x)\,\mathrm{d}x+\int_{x_{I-1/2}}^{x_{I+1/2}}w_{I,p}(x)\sum_{n=1}^{N}Q_{r,n}^{k+1}(x)\Delta_n\,\mathrm{d}x,\\
&\qquad\qquad\qquad\text{right reflecting boundary}.\qquad\text{(B.66e)}
\end{aligned}
$$

The updated first moment equation is

$$\frac{1}{c\Delta t_{k+1}}\int_{x_{i-1/2}}^{x_{i+1/2}} w_{i,p}(x)\left[J^{k+1,(l+1)}(x)-J^{k}(x)\right]\mathrm{d}x$$
$$+\frac{2}{3}\int_{x_{i-1/2}}^{x_{i+1/2}} w_{i,p}(x)\frac{\mathrm{d}}{\mathrm{d}x}\Phi^{k+1,(l+1/2)}(x)\,\mathrm{d}x+\frac{1}{3}\int_{x_{i-1/2}}^{x_{i+1/2}} w_{i,p}(x)\frac{\mathrm{d}}{\mathrm{d}x}\phi^{k+1,(l+1)}(x)\,\mathrm{d}x$$
$$+\sigma_{P,i}^{k}\int_{x_{i-1/2}}^{x_{i+1/2}} w_{i,p}(x)J^{k+1,(l+1)}(x)\,\mathrm{d}x=\int_{x_{i-1/2}}^{x_{i+1/2}} w_{i,p}(x)\sum_{n=1}^{N}\mu_n Q_{r,n}^{k+1}(x)\,\Delta_n\,\mathrm{d}x. \quad \text{(B.67)}$$

B.3.3 Step 3: Subtract Step 2 Equations from Step 1 Equations

The third step in the Modified Four-Step DSA derivation is to subtract the equations we derived in step 1 from the equations we found in step 2. Subtracting Eqs. (B.62) from Eqs. (B.66), and defining

$$F_0^{k+1,(l+1)}(x)=\phi^{k+1,(l+1)}(x)-\phi^{k+1,(l+1/2)}(x), \quad \text{(B.68a)}$$

$$F_1^{k+1,(l+1)}(x)=J^{k+1,(l+1)}(x)-J^{k+1,(l+1/2)}(x), \quad \text{(B.68b)}$$

we obtain

$$\frac{1}{c\Delta t_{k+1}}\int_{x_{1/2}}^{x_{3/2}} w_{1,p}(x)F_0^{k+1,(l+1)}(x)\mathrm{d}x$$
$$+\left(w_{1,p}(x_{3/2})\left[\frac{\rho}{2}F_0^{k+1,(l+1)}(x_{3/2}^{-})+\frac{1}{2}F_1^{k+1,(l+1)}(x_{3/2}^{-})-\frac{\rho}{2}F_0^{k+1,(l+1)}(x_{3/2}^{+})\right.\right.$$
$$\left.\left.+\frac{1}{2}F_1^{k+1,(l+1)}(x_{3/2}^{+})\right]\right)$$
$$-\int_{x_{1/2}}^{x_{3/2}} F_1^{k+1,(l+1)}(x)\frac{\mathrm{d}}{\mathrm{d}x}w_{1,p}(x)\,\mathrm{d}x+\sigma_{P,1}^{k}f_1^{k}\int_{x_{1/2}}^{x_{3/2}} w_{1,p}(x)F_0^{k+1,(l+1)}(x)\,\mathrm{d}x$$
$$=\sigma_{P,1}^{k}\left[1-f_1^{k}\right]\int_{x_{1/2}}^{x_{3/2}} w_{1,p}(x)\left[\phi^{k+1,(l+1/2)}(x)-\phi^{k+1,(l)}(x)\right]\mathrm{d}x,$$

left reflecting boundary, (B.69a)

$$
\begin{aligned}
&\frac{1}{c\Delta t_{k+1}}\int_{x_{1/2}}^{x_{3/2}} w_{1,p}(x)F_0^{k+1,(l+1)}(x)\mathrm{d}x \\
&\quad+\Bigg(w_{1,p}(x_{3/2})\left[\frac{\rho}{2}F_0^{k+1,(l+1)}(x_{3/2}^-)+\frac{1}{2}F_1^{k+1,(l+1)}(x_{3/2}^-)-\frac{\rho}{2}F_0^{k+1,(l+1)}(x_{3/2}^+)\right.\\
&\qquad\qquad\left.+\frac{1}{2}F_1^{k+1,(l+1)}(x_{3/2}^+)\right]\\
&\qquad-w_{1,p}(x_{1/2})\left[-\frac{\rho}{2}F_0^{k+1,(l+1)}(x_{1/2}^-)+\frac{1}{2}F_1^{k+1,(l+1)}(x_{1/2}^-)\right]\Bigg)\\
&\qquad-\int_{x_{1/2}}^{x_{3/2}}F_1^{k+1,(l+1)}(x)\frac{\mathrm{d}}{\mathrm{d}x}w_{1,p}(x)\,\mathrm{d}x+\sigma_{P,1}^k f_1^k\int_{x_{1/2}}^{x_{3/2}}w_{1,p}(x)F_0^{k+1,(l+1)}(x)\,\mathrm{d}x\\
&\qquad=\sigma_{P,1}^k\left[1-f_1^k\right]\int_{x_{1/2}}^{x_{3/2}}w_{1,p}(x)\left[\phi^{k+1,(l+1/2)}(x)-\phi^{k+1,(l)}(x)\right]\mathrm{d}x,
\end{aligned}
$$

left incident boundary, (B.69b)

$$
\begin{aligned}
&\frac{1}{c\Delta t_{k+1}}\int_{x_{i-1/2}}^{x_{i+1/2}} w_{i,p}(x)F_0^{k+1,(l+1)}(x)\mathrm{d}x \\
&\quad+\Bigg(w_{i,p}(x_{i+1/2})\left[\frac{\rho}{2}F_0^{k+1,(l+1)}(x_{i+1/2}^-)+\frac{1}{2}F_1^{k+1,(l+1)}(x_{i+1/2}^-)\right.\\
&\qquad\qquad\left.-\frac{\rho}{2}F_0^{k+1,(l+1)}(x_{i+1/2}^+)+\frac{1}{2}F_1^{k+1,(l+1)}(x_{i+1/2}^+)\right]\\
&\qquad-w_{i,p}(x_{i-1/2})\left[\frac{\rho}{2}F_0^{k+1,(l+1)}(x_{i-1/2}^+)+\frac{1}{2}F_1^{k+1,(l+1)}(x_{i-1/2}^+)\right.\\
&\qquad\qquad\left.-\frac{\rho}{2}F_0^{k+1,(l+1)}(x_{i-1/2}^-)+\frac{1}{2}F_1^{k+1,(l+1)}(x_{i-1/2}^-)\right]\Bigg)\\
&\qquad-\int_{x_{i-1/2}}^{x_{i+1/2}}F_i^{k+1,(l+1)}(x)\frac{\mathrm{d}}{\mathrm{d}x}w_{i,p}(x)\,\mathrm{d}x+\sigma_{P,i}^k f_i^k\int_{x_{i-1/2}}^{x_{i+1/2}}w_{i,p}(x)F_0^{k+1,(l+1)}(x)\,\mathrm{d}x\\
&\qquad=\sigma_{P,i}^k\left[1-f_i^k\right]\int_{x_{i-1/2}}^{x_{i+1/2}}w_{i,p}(x)\left[\phi^{k+1,(l+1/2)}(x)-\phi^{k+1,(l)}\right]\mathrm{d}x,
\end{aligned}
$$

$2 \le i \le I-1$, (B.69c)

$$\frac{1}{c\Delta t_{k+1}}\int_{x_{I-1/2}}^{x_{I+1/2}} w_{I,p}(x)F_0^{k+1,(l+1)}(x)\mathrm{d}x$$
$$+\left(w_{I,p}(x_{I+1/2})\left[\frac{\rho}{2}F_0^{k+1,(l+1)}(x_{I+1/2}^-)+\frac{1}{2}F_1^{k+1,(l+1)}(x_{I+1/2}^-)\right]\right.$$
$$-w_{I,p}(x_{I-1/2})\left[\frac{\rho}{2}F_0^{k+1,(l+1)}(x_{I-1/2}^+)+\frac{1}{2}F_1^{k+1,(l+1)}(x_{I-1/2}^+)\right.$$
$$\left.\left.-\frac{\rho}{2}F_0^{k+1,(l+1)}(x_{I-1/2}^-)+\frac{1}{2}F_1^{k+1,(l+1)}(x_{I-1/2}^-)\right]\right)$$
$$-\int_{x_{I-1/2}}^{x_{I+1/2}} F_I^{k+1,(l+1)}(x)\frac{\mathrm{d}}{\mathrm{d}x}w_{I,p}(x)\,\mathrm{d}x+\sigma_{P,I}^k\int_{x_{I-1/2}}^{x_{I+1/2}} w_{I,p}(x)F_0^{k+1,(l+1)}(x)\,\mathrm{d}x$$
$$=\sigma_{P,I}^k\left[1-f_I^k\right]\int_{x_{I-1/2}}^{x_{I+1/2}} w_{I,p}(x)\left[\phi^{k+1,(l+1/2)}(x)-\phi^{k+1,(l)}(x)\right]\mathrm{d}x\,,$$

right incident boundary, (B.69d)

$$\frac{1}{v\Delta t_{k+1}}\int_{x_{I-1/2}}^{x_{I+1/2}} w_{I,p}(x)F_0^{k+1,(l+1)}(x)\mathrm{d}x$$
$$-\left(w_{I,p}(x_{I-1/2})\left[\frac{\rho}{2}F_0^{k+1,(l+1)}(x_{I-1/2}^+)+\frac{1}{2}F_1^{k+1,(l+1)}(x_{I-1/2}^+)\right.\right.$$
$$\left.\left.-\frac{\rho}{2}F_0^{k+1,(l+1)}(x_{I-1/2}^-)+\frac{1}{2}F_1^{k+1,(l+1)}(x_{I-1/2}^-)\right]\right)$$
$$-\int_{x_{I-1/2}}^{x_{I+1/2}} F_1^{k+1,(l+1)}(x)\frac{\mathrm{d}}{\mathrm{d}x}w_{I,p}(x)\,\mathrm{d}x+\sigma_{P,I}^k f_I^k\int_{x_{I-1/2}}^{x_{I+1/2}} w_{I,p}(x)F_0^{k+1,(l+1)}(x)\,\mathrm{d}x$$
$$=\sigma_{P,I}^k\left[1-f_I^k\right]\int_{x_{I-1/2}}^{x_{I+1/2}} w_{I,p}(x)\left[\phi^{k+1,(l+1/2)}-\phi^{k+1,(l)}\right]\mathrm{d}x\,,$$

right reflecting boundary. (B.69e)

Subtracting Eq. (B.64) from Eq. (B.67), we obtain the updated first moment equation

$$\frac{1}{c\Delta t_{k+1}}\int_{x_{i-1/2}}^{x_{i+1/2}} w_{i,p}(x)F_1^{k+1,(l+1)}(x)\mathrm{d}x+\frac{1}{3}\int_{x_{i-1/2}}^{x_{i+1/2}} w_{i,p}(x)\frac{\mathrm{d}}{\mathrm{d}x}F_0^{k+1,(l+1)}(x)\,\mathrm{d}x$$
$$+\sigma_{P,i}^k\int_{x_{i-1/2}}^{x_{i+1/2}} w_{i,p}(x)F_1^{k+1,(l+1)}(x)\,\mathrm{d}x=0\,. \quad \text{(B.70)}$$

Before proceeding to step 4, we will recast Eqs. (B.69) and (B.70) into matrix form. We assume linear discontinuous Galerkin weight and basis functions, such that

$$F_0^{k+1,(l+1)}(x)=F_{0,i,L}^{k+1,(l+1)}b_{i,L}(x)+F_{0,i,R}^{k+1,(l+1)}b_{i,R}(x)\,,\qquad x_{i-1/2}<x<x_{i+1/2}\,, \quad \text{(B.71a)}$$

$$F_1^{k+1,(l+1)}(x)=F_{1,i,L}^{k+1,(l+1)}b_{i,L}(x)+F_{1,i,R}^{k+1,(l+1)}b_{i,R}(x)\,,\qquad x_{i-1/2}<x<x_{i+1/2}\,. \quad \text{(B.71b)}$$

We also apply the upstream closures, such that the scalar intensity correction $F_0^{k+1,(l+1)}(x)$ evaluated on the cell edges is

$$F_0^{k+1,(l+1)}(x_{i-1/2}^-) = F_{0,i,L}^{k+1,(l+1)}, \tag{B.72a}$$

$$F_0^{k+1,(l+1)}(x_{i+1/2}^-) = F_{0,i,R}^{k+1,(l+1)}, \tag{B.72b}$$

and

$$F_0^{k+1,(l+1)}(x_{i-1/2}^+) = F_{0,i-1,R}^{k+1,(l+1)}, \tag{B.73a}$$

$$F_0^{k+1,(l+1)}(x_{i+1/2}^+) = F_{0,i+1,L}^{k+1,(l+1)}, \tag{B.73b}$$

and the first moment correction on the cell edges is evaluated as

$$F_1^{k+1,(l+1)}(x_{i-1/2}^-) = F_{1,i,L}^{k+1,(l+1)}, \tag{B.74a}$$

$$F_1^{k+1,(l+1)}(x_{i+1/2}^-) = F_{1,i,R}^{k+1,(l+1)}, \tag{B.74b}$$

and

$$F_1^{k+1,(l+1)}(x_{i-1/2}^+) = F_{1,i-1,R}^{k+1,(l+1)}, \tag{B.75a}$$

$$F_1^{k+1,(l+1)}(x_{i+1/2}^+) = F_{1,i+1,L}^{k+1,(l+1)}. \tag{B.75b}$$

Defining the vectors

$$\underline{F}_{0,i}^{k+1,(l+1)} = \begin{bmatrix} F_{0,i,L}^{k+1,(l+1)} & F_{0,i,R}^{k+1,(l+1)} \end{bmatrix}^T, \tag{B.76a}$$

and

$$\underline{F}_{1,i}^{k+1,(l+1)} = \begin{bmatrix} F_{1,i,L}^{k+1,(l+1)} & F_{1,i,R}^{k+1,(l+1)} \end{bmatrix}^T, \tag{B.76b}$$

we can write Eqs. (B.69) as

$$\begin{aligned} &\frac{1}{c\Delta t_{k+1}} \underline{\underline{M}}_1 \underline{F}_{0,1}^{k+1,(l+1)} + \underline{\underline{G}}_{b,L} \underline{F}_{0,1}^{k+1,(l+1)} + \underline{\underline{H}}_{b,L} \underline{F}_{1,1}^{k+1,(l+1)} + \underline{\underline{G}}_R \underline{F}_{0,2}^{k+1,(l+1)} + \underline{\underline{H}}_R \underline{F}_{1,2}^{k+1,(l+1)} \\ &\quad - \underline{\underline{L}}_1 \underline{F}_{1,1}^{k+1,(l+1)} + \sigma_{P,1}^k f_1^k \underline{\underline{M}}_1 \underline{F}_{0,1}^{k+1,(l+1)} = \sigma_{P,1}^k \left[1 - f_1^k\right] \underline{\underline{M}}_1 \left(\underline{\phi}_1^{k+1,(l+1/2)} - \underline{\phi}_1^{k+1,(l)} \right), \\ &\qquad\qquad\qquad\qquad\qquad\qquad\qquad\qquad\qquad\qquad\qquad\qquad \text{left reflecting boundary}, \end{aligned} \tag{B.77a}$$

$$\frac{1}{c\Delta t_{k+1}}\underline{\underline{M}}_1\underline{F}_{0,1}^{k+1,(l+1)}+\underline{\underline{G}}\underline{F}_{0,1}^{k+1,(l+1)}+\underline{\underline{H}}\underline{F}_{1,1}^{k+1,(l+1)}+\underline{\underline{G}}_R\underline{F}_{0,2}^{k+1,(l+1)}+\underline{\underline{H}}_R\underline{F}_{1,2}^{k+1,(l+1)}$$
$$-\underline{\underline{L}}_1\underline{F}_{1,1}^{k+1,(l+1)}+\sigma_{P,1}^k f_1^k\underline{\underline{M}}_1\underline{F}_{0,1}^{k+1,(l+1)}=\sigma_{P,1}^k\left[1-f_1^k\right]\underline{\underline{M}}_1\left(\underline{\phi}_1^{k+1,(l+1/2)}-\underline{\phi}_1^{k+1,(l)}\right),$$
left incident boundary, (B.77b)

$$\frac{1}{c\Delta t_{k+1}}\underline{\underline{M}}_i\underline{F}_{0,i}^{k+1,(l+1)}+\underline{\underline{G}}\underline{F}_{0,i}^{k+1,(l+1)}+\underline{\underline{H}}\underline{F}_{1,i}^{k+1,(l+1)}+\underline{\underline{G}}_L\underline{F}_{0,i-1}^{k+1,(l+1)}+\underline{\underline{H}}_L\underline{F}_{1,i-1}^{k+1,(l+1)}$$
$$+\underline{\underline{G}}_R\underline{F}_{0,i+1}^{k+1,(l+1)}+\underline{\underline{H}}_R\underline{F}_{1,i+1}^{k+1,(l+1)}-\underline{\underline{L}}_i\underline{F}_{1,i}^{k+1,(l+1)}+\sigma_{P,i}^k f_i^k\underline{\underline{M}}_i\underline{F}_{0,i}^{k+1,(l+1)}$$
$$=\sigma_{P,i}^k\left[1-f_i^k\right]\underline{\underline{M}}_i\left(\underline{\phi}_i^{k+1,(l+1/2)}-\underline{\phi}_i^{k+1,(l)}\right),\qquad 2\le i\le I-1,\quad\text{(B.77c)}$$

$$\frac{1}{c\Delta t_{k+1}}\underline{\underline{M}}_I\underline{F}_{0,I}^{k+1,(l+1)}+\underline{\underline{G}}\underline{F}_{0,I}^{k+1,(l+1)}+\underline{\underline{H}}\underline{F}_{1,I}^{k+1,(l+1)}+\underline{\underline{G}}_L\underline{F}_{0,I-1}^{k+1,(l+1)}+\underline{\underline{H}}_L\underline{F}_{1,I-1}^{k+1,(l+1)}$$
$$-\underline{\underline{L}}_I\underline{F}_{1,I}^{k+1,(l+1)}+\sigma_{P,I}^k f_I^k\underline{\underline{M}}_I\underline{F}_{0,1}^{k+1,(l+1)}=\sigma_{P,I}^k\left[1-f_I^k\right]\underline{\underline{M}}_I\left(\underline{\phi}_I^{k+1,(l+1/2)}-\underline{\phi}_I^{k+1,(l)}\right),$$
right incident boundary, (B.77d)

$$\frac{1}{c\Delta t_{k+1}}\underline{\underline{M}}_I\underline{F}_{0,I}^{k+1,(l+1)}+\underline{\underline{G}}_{b,R}\underline{F}_{0,I}^{k+1,(l+1)}+\underline{\underline{H}}_{b,R}\underline{F}_{1,I}^{k+1,(l+1)}+\underline{\underline{G}}_L\underline{F}_{0,I-1}^{k+1,(l+1)}+\underline{\underline{H}}_L\underline{F}_{1,I-1}^{k+1,(l+1)}$$
$$-\underline{\underline{L}}_I\underline{F}_{1,I}^{k+1,(l+1)}+\sigma_{P,I}^k f_I^k\underline{\underline{M}}_1\underline{F}_{0,1}^{k+1,(l+1)}=\sigma_{P,I}^k\left[1-f_I^k\right]\underline{\underline{M}}_I\left(\underline{\phi}_I^{k+1,(l+1/2)}-\underline{\phi}_I^{k+1,(l)}\right),$$
right reflecting boundary, (B.77e)

where the matrices are defined in Section B.2.

We can write Eq. (B.70) in matrix form as

$$\frac{1}{c\Delta t_{k+1}}\underline{\underline{M}}_i\underline{F}_{1,i}^{k+1,(l+1)}+\frac{1}{3}\underline{\underline{B}}_i\underline{F}_{0,i}^{k+1,(l+1)}+\sigma_{P,i}^k\underline{\underline{M}}_i\underline{F}_{1,i}^{k+1,(l+1)}=0,\qquad\text{(B.78)}$$

where matrix $\underline{\underline{B}}_i$ is also defined in Section B.2.

B.3.4 Step 4: Eliminate the First Moment Corrections

The final step in the Modified Four-Step DSA derivation is to use Eq. (B.78) to eliminate the first order correction $F_{1,i}^{k+1,(l+1)}$ from Eqs. (B.77). Solving Eq. (B.78) for $F_{1,i}^{k+1,(l+1)}$, we obtain

$$\underline{F}_{1,i}^{k+1,(l+1)}=-D_i^{k+1}\underline{\underline{M}}_i^{-1}\underline{\underline{B}}_i\underline{F}_{0,i}^{k+1,(l+1)},\qquad\text{(B.79)}$$

where

$$D_i^{k+1} = \frac{c\Delta t_{k+1}}{3\left(1+\sigma_{P,i}^k c\Delta t_{k+1}\right)}. \tag{B.80}$$

Substituting Eq. (B.79) into Eqs. (B.77), we obtain

$$\begin{aligned}
&\frac{1}{c\Delta t_{k+1}}\underline{\underline{M}}_1\underline{F}_{0,1}^{k+1,(l+1)} + \underline{\underline{G}}_{b,L}\underline{F}_{0,1}^{k+1,(l+1)} - D_1^{k+1}\underline{\underline{H}}_{b,L}\underline{\underline{M}}_1^{-1}\underline{\underline{B}}_1\underline{F}_{0,1}^{k+1,(l+1)} + \underline{\underline{G}}_R\underline{F}_{0,2}^{k+1,(l+1)} \\
&\quad - D_2^{k+1}\underline{\underline{H}}_R\underline{\underline{M}}_2^{-1}\underline{\underline{B}}_2\underline{F}_{0,2}^{k+1,(l+1)} + D_1^{k+1}\underline{\underline{L}}_1\underline{\underline{M}}_1^{-1}\underline{\underline{B}}_1\underline{F}_{0,1}^{k+1,(l+1)} + \sigma_{P,1}^k f_1^k\underline{\underline{M}}_1\underline{F}_{0,1}^{k+1,(l+1)} \\
&\quad = \sigma_{P,1}^k\left[1-f_1^k\right]\underline{\underline{M}}_1\left(\underline{\phi}_1^{k+1,(l+1/2)} - \underline{\phi}_1^{k+1,(l)}\right), \qquad \text{left reflecting boundary}, \quad \text{(B.81a)}
\end{aligned}$$

$$\begin{aligned}
&\frac{1}{c\Delta t_{k+1}}\underline{\underline{M}}_1\underline{F}_{0,1}^{k+1,(l+1)} + \underline{\underline{G}}\underline{F}_{0,1}^{k+1,(l+1)} - D_1^{k+1}\underline{\underline{H}}\underline{\underline{M}}_1^{-1}\underline{\underline{B}}_1\underline{F}_{0,1}^{k+1,(l+1)} + \underline{\underline{G}}_R\underline{F}_{0,2}^{k+1,(l+1)} \\
&\quad - D_2^{k+1}\underline{\underline{H}}_R\underline{\underline{M}}_2^{-1}\underline{\underline{B}}_2\underline{F}_{0,2}^{k+1,(l+1)} + D_1^{k+1}\underline{\underline{L}}_1\underline{\underline{M}}_1^{-1}\underline{\underline{B}}_1\underline{F}_{0,1}^{k+1,(l+1)} + \sigma_{P,1}^k f_1^k\underline{\underline{M}}_1\underline{F}_{0,1}^{k+1,(l+1)} \\
&\quad = \sigma_{P,1}^k\left[1-f_1^k\right]\underline{\underline{M}}_1\left(\underline{\phi}_1^{k+1,(l+1/2)} - \underline{\phi}_1^{k+1,(l)}\right), \qquad \text{left incident boundary}, \quad \text{(B.81b)}
\end{aligned}$$

$$\begin{aligned}
&\frac{1}{c\Delta t_{k+1}}\underline{\underline{M}}_i\underline{F}_{0,i}^{k+1,(l+1)} + \underline{\underline{G}}\underline{F}_{0,i}^{k+1,(l+1)} - D_i^{k+1}\underline{\underline{H}}\underline{\underline{M}}_i^{-1}\underline{\underline{B}}_i\underline{F}_{0,i}^{k+1,(l+1)} + \underline{\underline{G}}_L\underline{F}_{0,i-1}^{k+1,(l+1)} \\
&\quad - D_{i-1}^{k+1}\underline{\underline{H}}_L\underline{\underline{M}}_{i-1}^{-1}\underline{\underline{B}}_{i-1}\underline{F}_{0,i-1}^{k+1,(l+1)} + \underline{\underline{G}}_R\underline{F}_{0,i+1}^{k+1,(l+1)} - D_{i+1}^{k+1}\underline{\underline{H}}_R\underline{\underline{M}}_{i+1}^{-1}\underline{\underline{B}}_{i+1}\underline{F}_{0,i+1}^{k+1,(l+1)} \\
&\qquad + D_i^{k+1}\underline{\underline{L}}_i\underline{\underline{M}}_i^{-1}\underline{\underline{B}}_i\underline{F}_{0,i}^{k+1,(l+1)} + \sigma_{P,i}^k f_i^k\underline{\underline{M}}_i\underline{F}_{0,i}^{k+1,(l+1)} \\
&\qquad = \sigma_{P,i}^k\left[1-f_i^k\right]\underline{\underline{M}}_i\left(\underline{\phi}_i^{k+1,(l+1/2)} - \underline{\phi}_i^{k+1,(l)}\right), \qquad 2\le i\le I-1, \quad \text{(B.81c)}
\end{aligned}$$

$$\begin{aligned}
&\frac{1}{c\Delta t_{k+1}}\underline{\underline{M}}_I\underline{F}_{0,I}^{k+1,(l+1)} + \underline{\underline{G}}\underline{F}_{0,I}^{k+1,(l+1)} - D_I^{k+1}\underline{\underline{H}}\underline{\underline{M}}_I^{-1}\underline{\underline{B}}_I\underline{F}_{0,I}^{k+1,(l+1)} + \underline{\underline{G}}_L\underline{F}_{0,I-1}^{k+1,(l+1)} \\
&\quad - D_{I-1}^{k+1}\underline{\underline{H}}_L\underline{\underline{M}}_{I-1}^{-1}\underline{\underline{B}}_{I-1}\underline{F}_{0,I-1}^{k+1,(l+1)} + D_I^{k+1}\underline{\underline{L}}_I\underline{\underline{M}}_I^{-1}\underline{\underline{B}}_I\underline{F}_{0,I}^{k+1,(l+1)} + \sigma_{P,I}^k f_I^k\underline{\underline{M}}_I\underline{F}_{0,I}^{k+1,(l+1)} \\
&\quad = \sigma_{P,I}^k\left[1-f_I^k\right]\underline{\underline{M}}_I\left(\underline{\phi}_I^{k+1,(l+1/2)} - \underline{\phi}_I^{k+1,(l)}\right), \qquad \text{right incident boundary}, \quad \text{(B.81d)}
\end{aligned}$$

$$\begin{aligned}
&\frac{1}{c\Delta t_{k+1}}\underline{\underline{M}}_I\underline{F}_{0,I}^{k+1,(l+1)} + \underline{\underline{G}}_{b,R}\underline{F}_{0,I}^{k+1,(l+1)} - D_I^{k+1}\underline{\underline{H}}_{b,R}\underline{\underline{M}}_I^{-1}\underline{\underline{B}}_I\underline{F}_{0,I}^{k+1,(l+1)} + \underline{\underline{G}}_L\underline{F}_{0,I-1}^{k+1,(l+1)} \\
&\quad - D_{I-1}^{k+1}\underline{\underline{H}}_L\underline{\underline{M}}_{I-1}^{-1}\underline{\underline{B}}_{I-1}\underline{F}_{0,I-1}^{k+1,(l+1)} + D_I^{k+1}\underline{\underline{L}}_I\underline{\underline{M}}_I^{-1}\underline{\underline{B}}_I\underline{F}_{0,I}^{k+1,(l+1)} + \sigma_{P,I}^k f_I^k\underline{\underline{M}}_I\underline{F}_{0,I}^{k+1,(l+1)} \\
&\quad = \sigma_{P,I}^k\left[1-f_I^k\right]\underline{\underline{M}}_I\left(\underline{\phi}_I^{k+1,(l+1/2)} - \underline{\phi}_I^{k+1,(l)}\right), \qquad \text{right reflecting boundary}. \quad \text{(B.81e)}
\end{aligned}$$

We can rearrange and simplify Eqs. (B.81) by defining

$$\underline{\underline{A}}_1^{k+1} = \left(\frac{1}{c\Delta t_{k+1}} + \sigma_{P,1}^k f_1^k\right)\underline{\underline{M}}_1 + \underline{\underline{G}}_{b,L} + D_1^{k+1}\left(\underline{\underline{L}}_1 - \underline{\underline{H}}_{b,L}\right)\underline{\underline{M}}_1^{-1}\underline{\underline{B}}_1\,,$$

left reflecting boundary, (B.82a)

$$\underline{\underline{A}}_i^{k+1} = \left(\frac{1}{c\Delta t_{k+1}} + \sigma_{P,i}^k f_i^k\right)\underline{\underline{M}}_i + \underline{\underline{G}} + D_i^{k+1}\left(\underline{\underline{L}}_i - \underline{\underline{H}}\right)\underline{\underline{M}}_i^{-1}\underline{\underline{B}}_i\,,$$

interior and incident boundaries, (B.82b)

$$\underline{\underline{A}}_I^{k+1} = \left(\frac{1}{c\Delta t_{k+1}} + \sigma_{P,I}^k f_I^k\right)\underline{\underline{M}}_I + \underline{\underline{G}}_{b,R} + D_I^{k+1}\left(\underline{\underline{L}}_I - \underline{\underline{H}}_{b,R}\right)\underline{\underline{M}}_I^{-1}\underline{\underline{B}}_I\,,$$

right reflecting boundary, (B.82c)

and

$$\underline{\underline{C}}_{i,L}^{k+1} = \underline{\underline{G}}_L - D_i^{k+1}\underline{\underline{H}}_L\underline{\underline{M}}_i^{-1}\underline{\underline{B}}_i\,, \tag{B.83a}$$

$$\underline{\underline{C}}_{i,R}^{k+1} = \underline{\underline{G}}_R - D_i^{k+1}\underline{\underline{H}}_R\underline{\underline{M}}_i^{-1}\underline{\underline{B}}_i\,. \tag{B.83b}$$

Now we write the time dependent, grey IMC, Modified Four-Step DSA equations in a form appropriate for implementation on a computer. Noting that $\underline{\underline{C}}_{i,L}^{k+1}$ has only zeroes in its second row, and $\underline{\underline{C}}_{i,R}^{k+1}$ has only zeroes in its first row, we obtain a banded system of equations:

$$\begin{aligned}\left[\underline{\underline{A}}_1^{k+1}\right]_{1,1} F_{0,1,L}^{k+1,(l+1)} + \left[\underline{\underline{A}}_1^{k+1}\right]_{1,2} F_{0,1,R}^{k+1,(l+1)} \\ = \sigma_{P,1}^k\left[1-f_1^k\right]\left[\underline{\underline{M}}_1\right]_{1,1}\left(\phi_{1,L}^{k+1,(l+1/2)} - \phi_{1,L}^{k+1,(l)}\right) \\ + \sigma_{P,1}^k\left[1-f_1^k\right]\left[\underline{\underline{M}}_1\right]_{1,2}\left(\phi_{1,R}^{k+1,(l+1/2)} - \phi_{1,R}^{k+1,(l)}\right)\,,\end{aligned} \tag{B.84a}$$

$$\begin{aligned}\left[\underline{\underline{A}}_1^{k+1}\right]_{2,1} F_{0,1,L}^{k+1,(l+1)} + \left[\underline{\underline{A}}_1^{k+1}\right]_{2,2} F_{0,1,R}^{k+1,(l+1)} + \left[\underline{\underline{C}}_{2,R}^{k+1}\right]_{2,1} F_{0,2,L}^{k+1,(l+1)} \\ + \left[\underline{\underline{C}}_{2,R}^{k+1}\right]_{2,2} F_{0,2,R}^{k+1,(l+1)} = \sigma_{P,1}^k\left[1-f_1^k\right]\left[\underline{\underline{M}}_1\right]_{2,1}\left(\phi_{1,L}^{k+1,(l+1/2)} - \phi_{1,L}^{k+1,(l)}\right) \\ + \sigma_{P,1}^k\left[1-f_1^k\right]\left[\underline{\underline{M}}_1\right]_{2,2}\left(\phi_{1,R}^{k+1,(l+1/2)} - \phi_{1,R}^{k+1,(l)}\right)\,,\end{aligned} \tag{B.84b}$$

$$\left[\underline{\underline{C}}_{i-1,L}^{k+1}\right]_{1,1} F_{0,i-1,L}^{k+1,(l+1)} + \left[\underline{\underline{C}}_{i-1,L}^{k+1}\right]_{1,2} F_{0,i-1,R}^{k+1,(l+1)} + \left[\underline{\underline{A}}_{i}^{k+1}\right]_{1,1} F_{0,i,L}^{k+1,(l+1)}$$
$$+ \left[\underline{\underline{A}}_{i}^{k+1}\right]_{1,2} F_{0,i,R}^{k+1,(l+1)} = \sigma_{P,i}^{k}\left[1-f_i^k\right]\left[\underline{\underline{M}}_i\right]_{1,1}\left(\phi_{i,L}^{k+1,(l+1/2)} - \phi_{i,L}^{k+1,(l)}\right)$$
$$+ \sigma_{P,i}^{k}\left[1-f_i^k\right]\left[\underline{\underline{M}}_i\right]_{1,2}\left(\phi_{i,R}^{k+1,(l+1/2)} - \phi_{i,R}^{k+1,(l)}\right), \qquad 2 \le i \le I-1, \quad \text{(B.84c)}$$

$$\left[\underline{\underline{A}}_{i}^{k+1}\right]_{2,1} F_{0,i,L}^{k+1,(l+1)} + \left[\underline{\underline{A}}_{i}^{k+1}\right]_{2,2} F_{0,i,R}^{k+1,(l+1)} + \left[\underline{\underline{C}}_{i+1,R}^{k+1}\right]_{2,1} F_{0,i+1,L}^{k+1,(l+1)}$$
$$+ \left[\underline{\underline{C}}_{i+1,R}^{k+1}\right]_{2,2} F_{0,i+1,R}^{k+1,(l+1)} = \sigma_{P,i}^{k}\left[1-f_i^k\right]\left[\underline{\underline{M}}_i\right]_{2,1}\left(\phi_{i,L}^{k+1,(l+1/2)} - \phi_{i,L}^{k+1,(l)}\right)$$
$$+ \sigma_{P,i}^{k}\left[1-f_i^k\right]\left[\underline{\underline{M}}_i\right]_{2,2}\left(\phi_{i,R}^{k+1,(l+1/2)} - \phi_{i,R}^{k+1,(l)}\right), \qquad 2 \le i \le I-1, \quad \text{(B.84d)}$$

$$\left[\underline{\underline{C}}_{I-1,L}^{k+1}\right]_{1,1} F_{0,I-1,L}^{k+1,(l+1)} + \left[\underline{\underline{C}}_{I-1,L}^{k+1}\right]_{1,2} F_{0,I-1,R}^{k+1,(l+1)} + \left[\underline{\underline{A}}_{I}^{k+1}\right]_{1,1} F_{0,I,L}^{k+1,(l+1)}$$
$$+ \left[\underline{\underline{A}}_{I}^{k+1}\right]_{1,2} F_{0,I,R}^{k+1,(l+1)} = \sigma_{P,I}^{k}\left[1-f_I^k\right]\left[\underline{\underline{M}}_I\right]_{1,1}\left(\phi_{I,L}^{k+1,(l+1/2)} - \phi_{I,L}^{k+1,(l)}\right)$$
$$+ \sigma_{P,I}^{k}\left[1-f_I^k\right]\left[\underline{\underline{M}}_I\right]_{1,2}\left(\phi_{I,R}^{k+1,(l+1/2)} - \phi_{I,R}^{k+1,(l)}\right), \quad \text{(B.84e)}$$

$$\left[\underline{\underline{A}}_{I}^{k+1}\right]_{2,1} F_{0,I,L}^{k+1,(l+1)} + \left[\underline{\underline{A}}_{I}^{k+1}\right]_{2,2} F_{0,I,R}^{k+1,(l+1)}$$
$$= \sigma_{P,I}^{k}\left[1-f_I^k\right]\left[\underline{\underline{M}}_I\right]_{2,1}\left(\phi_{I,L}^{k+1,(l+1/2)} - \phi_{I,L}^{k+1,(l)}\right)$$
$$+ \sigma_{P,I}^{k}\left[1-f_I^k\right]\left[\underline{\underline{M}}_I\right]_{2,2}\left(\phi_{I,R}^{k+1,(l+1/2)} - \phi_{I,R}^{k+1,(l)}\right). \quad \text{(B.84f)}$$

Eqs. (B.84) represent a sparse, banded system of equations that can be efficiently solved using traditional linear algebra techniques.

Finally, the implicit grey IMC linear discontinuous finite element transport scheme with DSA is

$$\frac{1}{c\Delta t_{k+1}}\underline{\underline{M}}_i\left(\underline{\psi}_{n,i}^{k+1,(l+1/2)} - \underline{\psi}_{n,i}^{k}\right) + \mu_n \underline{\underline{L}}_i^{surf}\underline{\psi}_{n,i}^{k+1,(l+1/2),surf} - \mu_n \underline{\underline{L}}_i\underline{\psi}_{n,i}^{k+1,(l+1/2)}$$
$$+ \sigma_{P,i}^{k}\underline{\underline{M}}_i\underline{\psi}_{n,i}^{k+1,(l+1/2)} = \frac{\sigma_{P,i}^{k}}{2}\left[1-f_i^k\right]\underline{\underline{M}}_i\underline{\phi}_i^{k+1,(l)} + \frac{c}{2}f_i^k\sigma_{P,i}^{k}\underline{\underline{M}}_i\underline{U}_{r,i}^{k} + \left[\frac{1-f_i^k}{2}\right]\underline{\underline{M}}_i\underline{Q}_{m,i}^{k+1}$$
$$+ \underline{\underline{M}}_i\underline{Q}_{r,n,i}^{k+1}, \quad \text{(B.85a)}$$

$$\underline{\phi}_i^{k+1,(l+1/2)} = \sum_{n=1}^{N}\underline{\psi}_{n,i}^{k+1,(l+1/2)}\Delta_n, \quad \text{(B.85b)}$$

$$\underline{\phi}_i^{k+1,(l+1)} = \underline{\phi}_i^{k+1,(l+1/2)} + \underline{F}_{0,i}^{k+1,(l+1)}, \quad \text{(B.85c)}$$

where $\underline{F}_{0,i}^{k+1,(l+1)}$ in Eq. (B.85c) is calculated using Eqs. (B.84). This scheme is known to be quickly convergent.

Bibliography

[1] M. L. Adams. Discontinuous Finite Element Transport Solutions in Thick Diffusive Problems. *Nuclear Science and Engineering*, 137:298–333, 2001.

[2] M. L. Adams and E. W. Larsen. Fast Iterative Methods for Discrete-Ordinates Particle Transport Calculations. *Progress in Nuclear Energy*, 40(1):3–159, 2002.

[3] M. L. Adams and W. R. Martin. Diffusion Synthetic Acceleration of Discontinuous Finite Element Transport Iterations. *Nuclear Science and Engineering*, 111:145–167, 1992.

[4] M. L. Adams and P. F. Nowak. Asymptotic Analysis of a Computational Method for Time- and Frequency-Dependent Radiative Transfer. *Journal of Computational Physics*, 146(1):366–403, 1998.

[5] R. E. Alcouffe and R. S. Baker. Time-Dependent Deterministic Transport on Parallel Architectures using PARTISN. In *1998 Radiation Protection and Shielding Division*, 1998.

[6] Y. Azmy. Challenges in High Performance Computing: Case of the Method of Discrete Ordinates for Particle Transport Problems. *Transaction of the American Nuclear Society*, 91, 2004.

[7] T. Bailey, November 2009. Personal Communication.

[8] C. L. Bentley, S. Goluoglu, M. E. Dunn, L. S. Paschal, R. E. Pevey, and H. L. Dodds. Progress in Time-Dependent, Three-Dimensional Neutron Transport Methods Development. In *PHYSOR96 International Conference on the Physics of Reactors, Breakthrough of Nuclear Energy by Reactor Physics*, 1996.

[9] L. Boltzmann. Weitere Studien über das Wärmegleichgewicht unter Gasmolekülen. *Wiener Beichte*, 66:275-370:25, 1872.

[10] A. Brandt. Multi-Level Adaptive Solutions to Boundary-Value Problems. *Mathematics of Computation*, 31:333–390, 1977.

[11] G. R. Cefus and E. W. Larsen. Stability Analysis of Coarse-Mesh Rebalance. *Nuclear Science and Engineering*, 105:31–39, 1990.

[12] J. R. Cheatham. *Truncation Analysis and Numerical Method Improvements for the Thermal Radiation Transfer Equations*. PhD thesis, University of Michigan, 2009.

[13] J. J. Duderstadt and L. J. Hamilton. *Nuclear Reactor Analysis*. Wiley, New York, 1976.

[14] S. Dulla, E. Mund, and P. Ravetto. The Quasi-Static Method Revisited. *Progress in Nuclear Energy*, 50:908–920, 2008.

[15] J. A. Fleck and J. D. Cummings. An Implicit Monte Carlo Scheme for Calculating Time and Frequency Dependent Nonlinear Radiation Transport. *Journal of Computational Physics*, 8(3):313–42, 1971.

[16] S. L. Graham, M. Snir, and C. A. Patterson, editors. *Getting Up to Speed: The Future of Supercomputing*. National Research Council of the National Academies, Washington, DC, 2005.

[17] T. Hill and W. Reed. TIMEX: A Time-Dependent Explicit Discret Ordinates Program for the Solution of Multigroup Transport Equations with Delayed Neutrons. Technical Report LA-6201-MS, Los Alamos National Laboratory, 1976.

[18] D. Johnston. NNSA Awards IBM Contract to Build Next Generation Supercomputer. Lawrence Livermore News Release, 2008.

[19] K. Koch. Roadrunner Platform Overview. Slides for Road Runner Technical Seminar Series, 2008.

[20] K. Koch, R. Baker, and R. Alcouffe. Solution of the First-Order Form of the 3-D Discrete Ordinates Equations on a Massively Parellel Machine. *Transactions of the American Nuclear Society*, 65(198), 1992.

[21] E. W. Larsen. Unconditionally Stable Diffusion-Synthetic Acceleration Methods for the Slab Geometry Discrete Ordinates Equations. Part 1: Theory. *Nuclear Science and Engineering*, 82:47–63, 1982.

[22] E. W. Larsen. A Grey Transport Acceleration Method for Time-Dependent Radiative Transfer Problems. *Journal of Computational Physics*, 78(2):459–480, 1988.

[23] K. Lathrop. Ray Effects in Discrete Ordinates Equations. *Nuclear Science and Engineering*, 32:357–368, 1968.

[24] S. J. Leon. *Linear Algebra with Applications*. Pearson Prentice Hall, Upper Saddle River, NJ, seventh edition, 2006.

[25] R. LeVeque. *Finite Difference Methods for Ordinary and Partial Differential Equations*. SIAM, Philadelphia, 2007.

[26] E. Lewis and W. Miller. *Computational Methods of Neutron Transport*. John Wiley and Sons, Inc., New York, NY, 1984.

[27] R. G. McClarren. *Spherical Harmonics Methods for Thermal Radiation Transport*. PhD thesis, University of Michigan, 2007.

[28] R. G. McClarren and R. B. Lowrie. Effects of the Temperature Discretization on Numerical Methods for Thermal Radiation Transport. In *International Conference on Mathematics, Computational Methods & Reactor Physics*, Saratoga Springs, New York, 2009.

[29] K. S. Oh and J. P. Holloway. Nonlinear P_1 Closure for Rapid Transients in Radiation Transport. *Transactions of the American Nuclear Society*, 2009. To Appear.

[30] S. Pautz. An Algorithm for Parallel S_N Sweeps on Unstructured Meshes. *Nuclear Science and Engineering*, 140:111–136, 2002.

[31] G. Pomraning. *The Equations of Radiation Hydrodynamics*. Dover Publications, Inc., Mineola, NY, 1973.

[32] SC09 Conference. Portland, OR. Online at http://scyourway.supercomputing.org/conference/view/pan125, November 2009.

[33] B. Su and G. L. Olson. An Analytical Benchmark for Non-Equilibrium Radiative Transfer in an Isotropically Scattering Medium. *Annals of Nuclear Energy*, 24(13):1035–1055, 1997.

[34] Top 500. Online at http://top500.org, November 2009.

[35] T. Warsaw, November 2009. Personal Communication.

[36] A. B. Wollaber. *Advanced Monte Carlo Methods for Thermal Radiation Transport*. PhD thesis, University of Michigan, 2008.